Calendar of forthcoming meetings

6–12 January 2008
Temecula, CA, USA
2008 Winter Conference on Plasma Spectrochemistry.
Contact: Ramon Barnes, ICP Information Newsletter, Inc., PO Box 666, Hadley, MA 01003-0666, USA.
Tel.: (+1-413) 256-8942;
Fax: (+1-413) 256-3747;
E-mail: wc2006@chem.umass.edu;
URL: http://www-unix.oit.umass.edu/~wc2006

30 March – 2 April 2008
Dublin, Ireland
Europtrode IX: Ninth International Conference on Optical Chemical Sensors and Biosensors.
URL: www.europtrodeIX.eu

19–21 May 2008
Egmond aan Zee, The Netherlands
EuroResidue VI Conference on Residues of Veterinary Drugs in Food.
Contact: EuroResidue, PO Box 18, 5298 ZG Liempde, The Netherlands.
Tel. (+31-411) 611-199;
E-mail: euroresidue@congresservice.nl;
URL: www.euroresidue.nl

25–29 May 2008
Neuherberg, Germany
4th International Conference on Trace Element Speciation in Biomedical, Nutritional and Environmental Sciences.
URL: http://www.gsf.de/spec

30 June – 4 July 2008
Montpellier, France
CAC 2008: 11th Conference on Chemometrics in Analytical Chemistry.
Contact: Dr Jean-Michel Roger, Cemagraf, 361 rue J.F. Breton, BP 5095, F-34196 Montpellier, France.
Tel. (+33-4) 6704-6383;
Fax: (+33-4) 6704-6306;
E-mail: contact@cac2008.org;
URL: http://cac2008.teledetection.fr

7–11 September 2008
Bologna, Italy
ISLS 2008: XIIIth International Symposium on Luminescence Spectrometry.
Contact: Professor Aldo Roda, Department of Pharmaceutical Sciences, Faculty of Pharmacy, Unviersity of bologna, Italy.
Tel. (+39-051) 343-398;
Fax: (+39-051) 343-398;
E-mail: isls2008@unibo.it;
URL: http://www.isls2008.unibo.it

2–5 November 2008
Kaohsiung, Taiwan
APCE 2008: 8th Asia-Pacific International Symposium on Microscale Separations and Analysis.
URL: http://www.tl.ntu.edu.tw/apce2008

6–10 September 2009
Innsbruck, Austria
Euroanalysis 2009.
Contact: Euroanalysis 2009 Symposium Office, PCO Tyrol Congress, c/o Ina Kaehler, Rennweg 3, 6020 Innsbruck, Austria.
Tel. (+43-512) 575-600; Fax: (+43-512) 575-607;
E-mail: euroanalysis09@come-innbruck.at;
URL: www.euroanalysis2009.at

doi:10.1016/S0039-9140(07)00698-4

Talanta

The International Journal of Pure and Applied Analytical Chemistry

Publication information: *Talanta* (ISSN 0039-9140). For 2007, volumes 71–73 are scheduled for publication. Subscription prices are available upon request from the Publisher or from the Regional Sales Office nearest you or from this journal's website (http://www.elsevier.com/locate/talanta). Further information is available on this journal and other Elsevier products through Elsevier's website: (http://www.elsevier.com). Subscriptions are accepted on a prepaid basis only and are entered on a calendar year basis. Issues are sent by standard mail (surface within Europe, air delivery outside Europe). Priority rates are available upon request. Claims for missing issues should be made within six months of the date of dispatch.

Orders, claims, and journal enquiries: please contact the Customer Service Department at the Regional Sales Office nearest you:
Orlando: Elsevier, Customer Service Department, 6277 Sea Harbor Drive, Orlando, FL 32887-480 USA; phone: (+1) (877) 8397126 [toll free number for US customers], or (+1) (407) 3454020 [customers outside US]; fax: (+1) (407) 3631354; e-mail: usjcs@elsevier.com
Amsterdam: Elsevier, Customer Service Department, PO Box 211, 1000 AE Amsterdam, The Netherlands; phone: (+31) (20) 4853757; fax: (+31) (20) 4853432; e-mail: nlinfo-f@elsevier.com
Tokyo: Elsevier, Customer Service Department, 4F Higashi-Azabu, 1-Chome Bldg, 1-9-15 Higashi-Azabu, Minato-ku, Tokyo 106-0044, Japan; phone: (+81) (3) 5561 5037; fax: (+81) (3) 5561 5047; e-mail: jp.info@elsevier.com
Singapore: Elsevier, Customer Service Department, 3 Killiney Road, #08-01 Winsland House I, Singapore 239519; phone: (+65) 63490222; fax: (+65) 67331510; e-mail: asiainfo@elsevier.com

USA mailing notice: *Talanta* (ISSN 0039-9140) is published monthly by Elsevier B.V. (P.O. Box 211, 1000 AE Amsterdam, The Netherlands). Annual subscription price in the USA US$ 3,818 (valid in North, Central and South America), including air speed delivery. Application to mail at periodical postage rate is paid at Rathway, NJ and additional mailing offices.
USA POSTMASTER: Send address changes to *Talanta*, Publications Expediting Inc., 200 Meacham Avenue, Elmont, NY 11003.
AIRFREIGHT AND MAILING in the USA by Publications Expediting Inc., 200 Meacham Avenue, Elmont, NY 11003.

Available online at www.sciencedirect.com
ScienceDirect
Talanta 73 (2007) 906–912
Talanta
www.elsevier.com/locate/talanta

A flow-batch analyzer with piston propulsion applied to automatic preparation of calibration solutions for Mn determination in mineral waters by ET AAS

Luciano F. Almeida [a], Maria G.R. Vale [b], Morgana B. Dessuy [b], Márcia M. Silva [b], Renato S. Lima [c,1], Vagner B. Santos [c,1], Paulo H.D. Diniz [c,1], Mário C.U. Araújo [c,*]

[a] *Universidade Federal de Pernambuco, CCEN, Departamento de Química Fundamental, Brazil*
[b] *Universidade Federal do Rio Grande do Sul, Instituto de Química, Brazil*
[c] *Universidade Federal da Paraíba, CCEN, Departamento de Química, P.O. Box 5093, 58051-970 João Pessoa, PB, Brazil*

Received 1 February 2007; received in revised form 2 May 2007; accepted 11 May 2007
Available online 21 May 2007

Abstract

The increasing development of miniaturized flow systems and the continuous monitoring of chemical processes require dramatically simplified and cheap flow schemes and instrumentation with large potential for miniaturization and consequent portability. For these purposes, the development of systems based on flow and batch technologies may be a good alternative. Flow-batch analyzers (FBA) have been successfully applied to implement analytical procedures, such as: titrations, sample pre-treatment, analyte addition and screening analysis. In spite of its favourable characteristics, the previously proposed FBA uses peristaltic pumps to propel the fluids and this kind of propulsion presents high cost and large dimension, making unfeasible its miniaturization and portability. To overcome these drawbacks, a low cost, robust, compact and non-propelled by peristaltic pump FBA is proposed. It makes use of a lab-made piston coupled to a mixing chamber and a step motor controlled by a microcomputer. The piston-propelled FBA (PFBA) was applied for automatic preparation of calibration solutions for manganese determination in mineral waters by electrothermal atomic-absorption spectrometry (ET AAS). Comparing the results obtained with two sets of calibration curves (five by manual and five by PFBA preparations), no significant statistical differences at a 95% confidence level were observed by applying the paired *t*-test. The standard deviation of manual and PFBA procedures were always smaller than 0.2 and 0.1 $\mu g\,L^{-1}$, respectively. By using PFBA it was possible to prepare about 80 calibration solutions per hour.

Keywords: Flow-batch analyzer; Automatic preparation of calibration solutions; ET AAS; Manganese; Mineral water analysis

1. Introduction

The minimization of human interaction in analytical procedures is an exhaustively persecuted target by the modern instrumental analytical chemistry studies, mainly when a large number of samples are involved [1,2]. In general, the automated procedures are independent of errors caused by the operator and provide high repeatability [3]. Several flow analyzers (FA) [4] have been developed in order to automate and to simplify analytical procedures [5–16]. However, even with the successful application of FA for automation and simplification of analytical methodologies, their flexibility and versatility are still limited. The FA manifolds require significant changes in their physical assemblies when it is necessary to analyze samples with a large variation of analyte concentration and/or physical–chemical properties.

Automated micro batch (AMBA) and flow-batch analyzers (FBA) proposed by Sweileh and Dasgupta [17,18] and Honorato et al. [19], respectively, are systems more flexible and versatile (multi-task characteristic). In these analyzers, it is possible to work in any analyte concentration range as well as to implement different analytical processes. It may be accomplished just by changing the operational parameters in their control software, without significant alterations on the physical configurations of the analyzer. AMBA and FBA combine favourable

* Corresponding author. Tel.: +55 83 3216 7438; fax: +55 83 3216 7438.
E-mail address: laqa@quimica.ufpb.br (M.C.U. Araújo).
[1] Tel.: +55 83 3216 7438; fax: +55 83 3216 7438.

0039-9140/$ – see front matter © 2007 Elsevier B.V. All rights reserved.
doi:10.1016/j.talanta.2007.05.009

characteristics of both flow and batch analyzers (BA). As in FA, the transportation of reagents, samples or other solutions are carried out in a flow mode, and, as in BA, the sample processing is carried out into a mixing chamber (MC). In AMBA, an injecting loop is used on the sampling stage (as in FA), while in FBA the sample amounts are added into the MC by controlling the ON switching time of one solenoid valve.

As most of the FA, FBA and AMBA also present good precision and accuracy, high sample throughput and low contamination, consumption, manipulation of reagents and samples, cost per analysis and waste liberation for the environment, etc. They have been used to implement several analytical procedures such as: titrations [19,20], analyte addition [21,22], internal standard [23], screening analysis [24], exploitation of concentration gradients [25], on line matching of pH [26] and salinity [27], liquid–liquid extraction [17], distillation of volatile analyte [17], sample digestion [28] and kinetic approach [18].

In general, FBA and AMBA present the following characteristics: the use of solenoid valves and MC; highly precise fluid aliquots can be delivered by microcomputer controlling the ON valves switching times; high sensitivity because the physical and chemical equilibria inherent to the analytical processes may be attained and the dispersion and/or dilution of the samples may be negligible; the analytical signal measurements can be performed in flow cells or directly inside MC and the multicommutation [29,30] may be used in order to manipulate the fluids in a simultaneous and/or in an intermittent way.

In spite of their favourable characteristics, the previously proposed FBA and AMBA make use of a peristaltic pump and/or pneumatically pressurized reservoirs to propel the fluids. These kinds of propulsion result in manifolds with large dimensions, making their miniaturization and portability unfeasible. To overcome these drawbacks, a low cost, robust, compact flow-batch analyzer based on piston propulsion is proposed. This new approach to accomplish automatic analysis was designed to add a new study prospect in the present flow-batch technique. It was named as the piston propelled flow-batch analyzer (PFBA) because it uses a step motor-controlled piston coupled to the MC. To illustrate the feasibility of PFBA, it was applied to prepare calibration solutions for determination of manganese in mineral waters by electrothermal atomic absorption spectrometry (ET AAS). It is worth noting that the most critical and time-consuming steps of an analytical methodology, during which errors may be introduced, are the sample pre-treatment and the preparation of calibration solutions. The proposed system is a good alternative to perform these tasks.

2. Experimental

2.1. Reagents and solutions

The 1000 mg L^{-1} Mn stock solution was prepared from a Titrisol (Merck, Germany) ampoule in 0.5% (v/v) bidistilled HNO_3 (Merck, Germany). Calibration solutions were prepared by dilution of Mn stock solution in 0.5% (v/v) HNO_3. A 0.5% (v/v) bidistilled HNO_3 was used as the blank solution.

Table 1
Graphite furnace heating program of the Shimadzu AA6800 for determination of Mn in mineral water samples. The optimized pyrolisis and atomization temperatures were 2100 and 700 °C respectively

Step	Temperature (°C)	Time (s)		Gas flow rate (mL min^{-1})
		Ramp	Hold	
Drying 1	110	10	15	500
Drying 2	250	7	15	500
Pyrolysis 1	700	45	10	500
Pyrolysis 2	700	0	10	500
Atomization[a]	2100	0	5	0
Clean-out	2300	0	3	500

[a] The signal reading is performed in this step.

For the measurements of minimum times for switching ON valves, the dye solution was composed of 0.1 mol L^{-1} acetic acid/sodium acetate buffer, a 1000 mg L^{-1} Fe(II) in medium of 0.5 mol L^{-1} HCl prepared from a Titrisol (Merck, Germany) ampoule and the chromogenic reagent was a 0.25% (w/v) 1,10-phenantroline solution prepared in medium of 0.05 mol L^{-1} HCl.

All solutions were prepared with chemicals of analytical grade and freshly distilled-deionized water from a Millipore Milli-Q device. The mineral water samples were purchased in local supermarkets and analyzed without any previous treatment.

2.2. Instrumental parameters and operation of the spectrometer

A Shimadzu AA6800 furnished with a longitudinally heated graphite tube atomizer was used for all atomic absorption measurements and pyrolytic-coated graphite tubes were used. Samples were delivered to the furnace using a Shimadzu ASC-6100 auto sampler and stored in acid washed polypropylene cups prior to injection. The lamp used was a Mn hollow cathode lamp (Hamamatsu Photonics) operated at 10 mA; the wavelength at 279.5 nm was used with a slit-width of 0.2 nm. The inert gas used was argon (99.999%). Dilutions were carried out with calibrated Eppendorf pneumatic pipettes. The graphite furnace heating program is given in Table 1. The volumes taken of all solutions were always 20 μL.

2.3. The piston propelled flow-batch analyzer (PFBA)

The proposed analyzer is shown in Fig. 1a. Four Cole Parmer three-way solenoid valves were used: V_B and V_{CS} to direct the blank and work calibration solution or sample towards MC, respectively; $V_{D/S}$ to seal the MC outlet during the preparation of calibration solutions or to discharge these solutions or diluted samples of MC and $V_{A/W}$ to direct these solutions into the cup of the spectrometer auto sampler or towards waste.

A Pentium 550 MHz microcomputer was used to control PFBA, the spectrometer and to acquire and treat the analytical data. Software written in Labview® 5.1 with a friendly interface and easy operation was developed to manage PFBA. An electronic actuator (EA) was used to increase the power of the

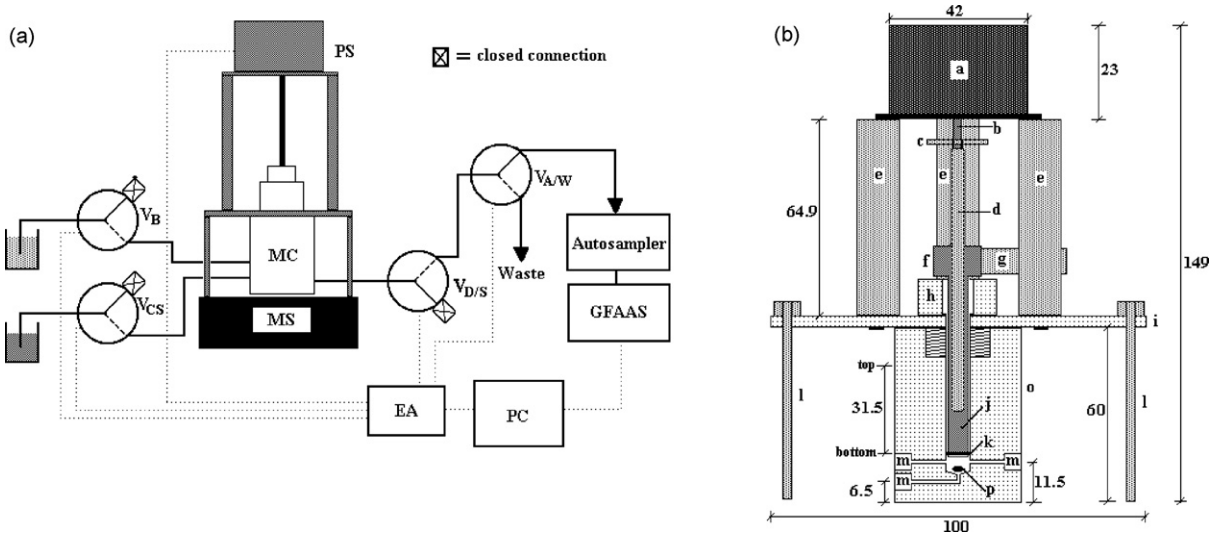

Fig. 1. (a) Schematic diagram of PFBA at starting configuration: MC = mixing chamber (the dimensions of MC are described elsewhere [16,17]); MS = magnetic stirrer; EA = electronic actuator; PS = propulsion system and PC = microcomputer, V_B, V_{CS}, $V_{D/S}$ and $V_{A/W}$ = blank, work calibration solution, MC discharge/sealing and auto sampler/waste three-way solenoid valves, respectively. Note that the valves V_B, V_{CS} and $V_{D/S}$ present one of its outlets completely sealed in order to minimize any internal pressure variation. (b) A transversal view of MC-piston assembly at starting configuration: a = step motor; b = motor axis; c = connection pin; d = screw; e = motor support columns; f = piston head; g = guide bar of the piston; h = connection between the MC and the motor set; i = support of the motor set; j = piston body; k = rubber o-ring; l = system support columns; m = solenoid valves connections; o = MC and p = magnetic bar. The piston course edges are indicated by top and bottom marks. The air volume into MC with the piston at bottom position is 210 mm^3, taking account the magnetic bar volume (about 40 mm^3). The dimensions are expressed in millimetres.

signal sent by the parallel port of the microcomputer in order to control the solenoid valves and the step motor. The 378 and 37A hexadecimal addresses were used to control the ON switching times of the solenoid valves and to send the activation pulses to the step motor, respectively.

A transversal view of PFBA is shown in Fig. 1b. The lab-made propulsion system (PS) comprises a brass piston connected mechanically to a dot-matrix printer step motor through a screw. This system is coupled to the MC so that the MC-PS assembly works similarly to an automatic syringe. A rubber o-ring placed at the extremity of the piston is used for internal sealing of MC. The full-step motor operation was chosen in order to provide an enough torque to displace the piston. In this operation mode, two coils are simultaneously activated, generating a stronger magnetic field than the yielded by one coil activation.

The transmission lines were constructed with 0.8 mm i.d. PTFE tubing. The 2.0 mL laboratory-made MC was also constructed in Teflon®.

2.4. Procedure

The preparation of each calibration solution is always initialized with all the valves switched OFF and the piston placed on the bottom position (Fig. 1b). After that, 48 pulses (see Section 3.1) are applied to the step motor with all the valves switched OFF in order to displace the piston towards the top position, yielding a slight lower pressure inside the MC regarding to the atmospheric pressure. Afterwards, the V_{CS} valve and the piston are simultaneously switched ON during a previously defined time interval t_{CS}, promoting the aspiration of an aliquot of work calibration solution (CS) towards MC. It occurs due to the internal pressure variation inside MC caused by the piston displacement. In the sequence, the same procedure is applied to the V_B valve, which is switched ON during a time interval t_B and an aliquot of blank (B) is aspirated towards the MC. Soon afterwards, the valve $V_{D/S}$ and the piston are simultaneously switched ON during 6 s in order to displace the piston to the top position. This step is accomplished in order to insert enough air inside the MC to transport the prepared mixture into the cup of the spectrometer auto sampler and to empty completely the MC and analytical path. This transport is always carried out by ON switching the $V_{D/S}$ valve and the piston during 16 s with reversal piston displacement (top to bottom).

All calibration solutions are prepared by using the same procedure, however, with t_{CS} increasing (1–9 s), t_B decreasing (9–1 s) and $t_{CS} + t_B = 10$ s.

If a dilution of the sample (S) is needed in order to obtain an analytical signal into the linear range of calibration curve, it can be carried out by replacing CS from the sample and by accomplishing the same procedure of calibration solution preparation with the appropriated time intervals for t_S and t_B regarding to the required dilution.

Among the preparations of calibration solutions or sample dilutions, a cleaning step may be carried out by using only the blank solution and the same procedure described above. However, it was unnecessary to perform this step because no carryover was observed, owing to the hydrophobic property of PTFE used in the MC, valves and transmission lines of the PFBA manifold.

The magnetic stirrer was always activated during the insertion of the fluids aliquots into MC in order to assure a good homogenization of the solutions.

2.5. Theoretical

In the automatic preparation of calibration curves with PFBA, the analytical response may be directly related to the switching ON time, t_{CS}, of the V_{CS} valve as demonstrated below.

In PFBA, since $v = Qt$ (where Q is the channel flow-rate), the valve timing courses, t, define the volumes, v_{CS} and v_B, added into MC. So, $t_{CS}(i)$ and $t_B(i)$ can be used instead of $v_B(i)$ and $v_{CS}(i)$. Moreover, if significant statistical differences do not occur among the flow-rates of the channels ($Q_{CS} = Q_B = Q$), the following expression is valid:

$$R_{CS}(i) = KC^0_{CS}\left(\frac{t_{CS}(i)}{t_{CS}(i) + t_B(i)}\right) \quad (i = 1, 2, 3, \ldots, n) \qquad (1)$$

where $R_{CS}(i)$ is the ith analytical responses for the ith concentration of a prepared work calibration solution, C^0_{CS} and n is the number of points of the calibration curve.

In order to simplify the mathematical model, the total time of switching ON valves $t_{Total} = t_{CS}(i) + t_B(i)$ in a given calibration set is maintained constant, and Eq. (1) assumes the form below:

$$R_{CS}(i) = \left(\frac{KC^0_{CS}}{t_{Total}}\right) t_{CS}(i) \qquad (2)$$

that can be rewritten as:

$$R_{CS}(i) = K' t_{CS}(i) \qquad (3)$$

where K' is the angular coefficient of the curve $R_{CS}(i)$ versus $t_{CS}(i)$.

Therefore, it is demonstrated that a linear relation between the analytical responses, $R_{CS}(i)$, and the switching ON time of the calibration solution valve, $t_{CS}(i)$, is obtained from Eq. (3) for the constructed calibration curve with PFBA. However, the calibration curves used in analysis by ET AAS are usually constructed by plotting the integrated absorbance data versus analyte mass (nanograms, in general). The $t_{CS}(i)$ values may be transformed in analyte mass values, $m_{CS}(i)$, of each prepared calibration solution with PFBA, by using the expression below:

$$m_{CS}(i) = \left(\frac{v_{AS}C^0_{CS}}{t_{Total}}\right) t_{CS}(i) \qquad (4)$$

where v_{AS} is the inserted volume into the graphite tube by the auto sampler of the spectrometer.

Substituting Eq. (4) in (3), the following equation is obtained:

$$R_{CS}(i) = K\left(\frac{1}{v_{AS}}\right) m_{CS}(i) \qquad (5)$$

making $\theta = K(1/v_{AS})$ Eq. (5) can be rewritten as:

$$R_{CS}(i) = \theta m_{CS}(i) \qquad (6)$$

Finally, if a sample dilution is carried out with PFBA, the analyte concentration in the sample flask, C^0_S, can be calculated by Eq. (6) below:

$$C^0_S = \left(\frac{t_{CS} + t_B}{t_{CS}}\right)\frac{R_S}{\theta} \qquad (7)$$

where t_{CS} and t_B are the switching ON time V_{CS} and V_B valves, respectively, during the sample measurement, R_S, and θ is the angular coefficient of Eq. (6) estimated by linear least-squares regression fitting.

3. Results and discussion

3.1. The effect of the air elasticity inside the MC

The amounts of blank and work calibration (or sample) solutions inserted into the MC depend on the ON switching time of the V_B or V_{CS} valves when the piston is displaced towards the top position (Fig. 1b). However, the air elasticity inside the MC impairs the instantaneous transmission of movement to the fluids when the piston starts its displacement. In order to compensate this effect, the piston must be initially displaced to a suitable position by applying an adequate velocity of piston displacement towards the top position. To find this position and velocity, it was investigated the number and the frequency of pulses to be applied to the step motor. It was verified that the application of 48 pulses with a frequency of 50 Hz was enough to compensate the air elasticity inside the MC.

3.2. The flow-rate of channels

The flow-rates of the blank and work calibration solution channels were estimated by aspirating water into the MC during interval times from 1 to 5 s and by weighting the sampled water aliquots. The water into the MC has always been aspirated after the air elasticity compensation (48 pulses at 50 Hz). By using the well known density values of the water at monitored temperature (21–23 °C), the volumes were calculated and the flow-rates for different pulse frequencies (50–200 Hz) applied to the step motor were estimated from the volume versus time curves (Fig. 2).

No significant statistical difference was observed at a 95% confidence level between the flow-rates of the blank and work calibration solution channels for each different pulse frequencies applied to the step motor (Table 2). Thus, the condition $Q_B = Q_{CS} = Q$, proposed in the PFBA mathematical modelling is valid.

3.3. The choice of the pulse frequency applied to the step motor

To elect the pulse frequency to be applied to the step motor in fluids sampling stage (f_S), both the accuracy and the analytical velocity inherent to each studied frequency were taken into account. At 50 Hz or less, PFBA provides a good precision, although significant losses in analytical velocity may occur. At larger f_S values (above 100 Hz), PFBA provides higher analytical velocities. However, the sampling is more susceptible to errors due to the uncertainty in the valves timing control. Even with the rigorous controlling furnished by the control software, slight timing variations (0.05–0.1 s) may occur, propagating, thus, significant errors in calibration solutions preparation and/or sample dilutions. The pulse frequency of 100 Hz has been cho-

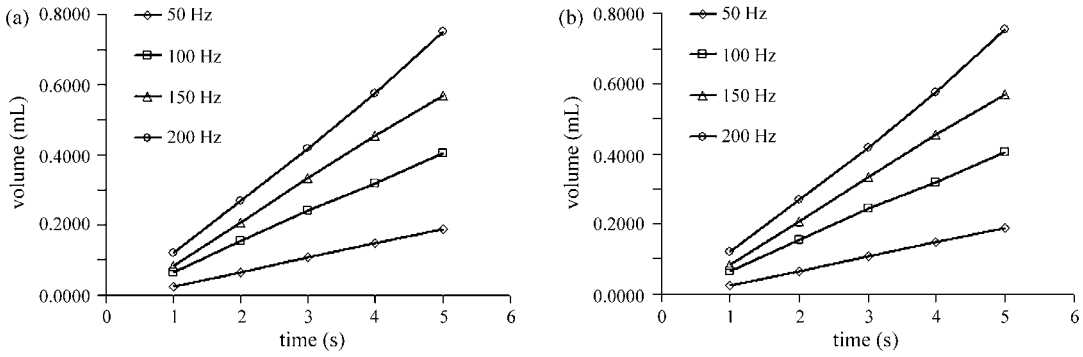

Fig. 2. The volume vs. time curves for different pulse frequencies applied to the step motor used to estimate the flow-rates (Table 2) of the blank (a) and work calibration solution (b) channels.

Table 2
Estimated equations from the curves of volume vs. time (Fig. 2). Volume and time are expressed in mL and seconds, respectively

Pulses frequency (Hz)	Channels			
	Blank		Work calibration solution	
	Equations	R^{2a}	Equations	R^{2a}
50	$v = 0.0417t - 0.0199$	1.0000	$v = 0.0417t - 0.02$	0.9999
100	$v = 0.0846t - 0.0173$	0.9992	$v = 0.0847t - 0.0179$	0.9998
150	$v = 0.1217t - 0.0357$	0.9998	$v = 0.1217t - 0.0355$	0.9993
200	$v = 0.1578t - 0.0463$	0.9984	$v = 0.1575t - 0.0459$	0.9990

[a] Correlation coefficient.

sen as the better compromise between precision and analytical velocity.

3.4. PFBA dilution capability

The available internal volume of the MC (v_{ma}) used in this work is about 1.583 mm^3 and it is limited by the piston displacement course (about 31.5 mm). A portion corresponding to 2/3 v_{ma} was adopted as the maximum work volume (v_{mw}) to be inserted into the MC of the blank plus the work calibration solution in order to guarantee an enough amount of air to expel the fluids and empty the MC and the analytical path completely.

As described in Section 2.5, the ON switching valves times can be used instead of volumes, thus, the volume v_{mw} is corresponding to the work total time of piston displacement course, t_{Total}. Since the pulse frequency of 100 Hz has been elected for PFBA operation, a $t_{Total} = 16$ s was determined.

Other parameter that must be taken into account to determine the PFBA dilution capability is the minimum valve switching ON time (t_{min}) necessary to delivery a fluid volume into the MC without significant impairing of the analytical precision. Thereby, $t_{min} = 0.2$ s was found. By using t_{min} and t_{Total} values above, the PFBA dilution capability can be determined by $t_{Total}/t_{min} = 16/0.2 = 80$.

3.5. Analysis by manual and PFBA procedures

For comparison purposes, five calibration curves into 0.2–0.5 μg L^{-1} Mn range were constructed using the calibration standard solutions prepared by manual and PFBA procedures. The same working calibration solution (5.0 μg L^{-1} Mn) was utilized in both procedures. The absorbance measurements were always carried out in triplicate. The parameters of the constructed curves are shown in Table 3.

The angular coefficients of the curves built from the application of both procedures were very similar. It can be attested by a simple comparison between the mean values of this parameter for the manual (8.566 ± 0.4038) and PBFA (8.369 ± 0.3371) procedures. No significant statistical differences at a 95% confidence level were observed by applying the paired t-test. The

Table 3
Angular (b) and correlation (R^2) coefficients and characteristic mass (m_0), limits of detection (LOD = $3s_{blank}/b$) and quantification (LOQ = $10s_{blank}/b$) obtained by PFBA and manual procedures. LOD and LOQ values were calculated based on the blank standard deviation, s_{blank} ($n = 10$)

Method[a]	b (ng^{-1})	R^2	LOD (ng)	LOQ (ng)	m_0 (pg)
M-1	8.798	0.9982	0.0014	0.0045	0.51
M-2	7.907	0.9954	0.0015	0.0050	0.51
M-3	8.750	0.9986	0.0014	0.0045	0.51
M-4	8.463	0.9974	0.0014	0.0047	0.50
M-5	8.912	0.9982	0.0013	0.0044	0.50
P-1	8.566	0.9954	0.0014	0.0046	0.51
P-2	8.514	0.9979	0.0014	0.0047	0.52
P-3	7.768	0.9968	0.0015	0.0051	0.50
P-4	8.495	0.9849	0.0014	0.0047	0.51
P-5	8.502	1.0000	0.0014	0.0047	0.44

[a] M and P represent the manual and PFBA preparations, respectively.

Table 4
Results (expressed in $\mu g\,L^{-1}$) of Mn determinations in 10 mineral water samples by using the PFBA and manual procedures. Volumes taken by spectrometer auto sampler were always 20 μL

Samples	Manual procedure						PFBA procedure					
	1	2	3	4	5	Mean ± S.D.	1	2	3	4	5	Mean ± S.D.
1	0.8	0.7	0.8	0.7	0.5	0.7 ± 0.1	0.7	0.8	0.6	0.7	0.7	0.7 ± 0.1
2	1.9	1.9	1.8	1.8	1.5	1.8 ± 0.2	1.8	1.8	1.8	1.8	1.8	1.8 ± 0.0
3	1.8	1.8	1.8	1.8	1.5	1.7 ± 0.1	1.8	1.8	1.7	1.7	1.8	1.7 ± 0.1
4	0.9	0.8	0.9	0.9	0.6	0.8 ± 0.1	0.9	0.9	0.7	0.8	0.8	0.8 ± 0.1
5	1.0	0.9	0.9	0.9	0.6	0.8 ± 0.2	0.9	0.9	0.7	0.8	0.8	0.8 ± 0.1
6	0.8	0.7	0.8	0.8	0.5	0.7 ± 0.1	0.8	0.8	0.6	0.7	0.7	0.7 ± 0.1
7	2.1	2.2	2.1	2.1	1.8	2.1 ± 0.2	2.1	2.1	2.1	2.1	2.1	2.1 ± 0.0
8	1.2	1.1	1.2	1.1	0.9	1.1 ± 0.1	1.1	1.1	1.0	1.1	1.1	1.1 ± 0.0
9	1.0	0.9	1.0	0.9	0.7	0.9 ± 0.1	0.9	0.9	0.8	0.9	0.9	0.9 ± 0.0
10	1.1	1.0	1.1	1.0	0.8	1.0 ± 0.1	1.0	1.0	0.9	1.0	1.0	1.0 ± 0.0

same statistical test was also applied to evaluate the mean values of LOD, LOQ and characteristic mass obtained from both procedures and no statistical differences were observed among the manual ($LOQ = 0.0014 \pm 0.0001$; $LOD = 0.0046 \pm 0.0002$; $m_0 = 0.51 \pm 0.0055$) and PBFA ($LOQ = 0.0014 \pm 0$; $LOD = 0.0048 \pm 0.0002$; $m_0 = 0.50 \pm 0.0321$) procedures. Good linearity was obtained for all curves (the correlation coefficients, $R^2 \sim 1.0000$) and no systematic errors were observed.

In Table 4 the obtained results are shown by using the parameters of calibration curves presented in Table 3.

The sample measurements ($n = 3$) were always accomplished at the same day of the calibration curves construction, thereby, no corrections of the analytical signals were necessary.

As can be observed in Table 4, the use of PFBA to prepare the calibration solutions has provided a slightly better precision than the manual procedure. Besides, with PFBA is possible to carry out the preparation of one calibration solution or a sample dilution at about 45 s by using a pulse frequency of 100 Hz applied to the step motor.

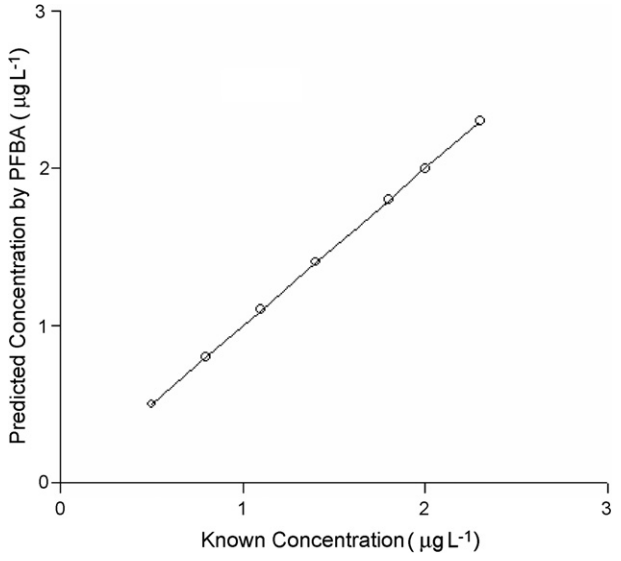

Fig. 3. Predicted concentration using an automatically prepared calibration curve by PFBA vs. known concentration for Mn in manually prepared test samples (0.5, 0.8, 1.1, 1.4, 1.8, 2.0 and 2.3 $\mu g\,L^{-1}$).

In order to provide a more complete validation, test samples were manually prepared and their manganese concentrations were determined by using an automatically prepared calibration curve (Fig. 3).

As can be seen in Fig. 3, a good agreement among the predicted concentration using an automatically prepared calibration curve by PFBA and known concentration of manganese in manually prepared test samples. The results lie near the ideal line (bisectrix), indicating no evidence problems with prepared concentrations by PFBA (i.e. there is no systematic errors).

4. Conclusions

The PFBA strategy for automatic preparation of calibration solutions was successfully applied to manganese determination in mineral waters by ET AAS. Carry-over and pulsation effects were not observed. All operations are totally controlled by the PFBA control software. Its portability is feasible to be implemented by allying its compact dimensions and its low weight with the use of PIC microcontrollers for PFBA control, making the use of the microcomputer, unnecessary. A new PFBA manifold suitable for this aim is under investigation at the present time.

PFBA uses only one calibration solution per analyte to carry out the whole preparation procedure. In addition, its operation requires a complete sealing of the MC, allowing to process hazardous and volatile matrix samples or any reagents that demand special care in its processing.

Other techniques and procedures may be implemented without alterations in PFBA physical configurations, being enough to modify operational parameters in the control software. The flexibility, versatility, robustness, compactness and universal applicability, turn the PFBA into an attractive and powerful tool for routine analysis laboratories and analysis *in situ*, also due to its easy operation, very low acquisition and maintenance cost, high throughput rate and portable capability.

Acknowledgements

The authors gratefully acknowledge the support of CNPq/Brazil (Proc. no. 479341/20010). The research

fellowships granted by the Brazilian Agencies CNPq and CAPES are gratefully acknowledged. The authors also thank Carlos Menezes for his collaboration in the translation of the text.

References

[1] M. Valcárcel, M.D. Luque de Castro, Automatic Methods of Analysis, Elsevier, Amsterdam, 1988.
[2] M. Trojanowicz, Flow Injection Analysis: Instrumentation and Applications, World Scientific, Singapore, 2000.
[3] J.L. Burguera, M. Burguera, Spectrochim. Acta Part B 56 (2001) 1801.
[4] B. Karlberg, G.E. Pacey, Flow Injection Analysis. A Practical Guide, Elsevier, Amsterdam, 1989.
[5] S. Martinez-Barrachina, M. del Valle, Microchem. J. 83 (2006) 48.
[6] L. Agui, A. Guzman, M. Pedrero, P. Yanez-Sedeno, J.M. Pingarron, Electroanalysis 15 (2003) 601.
[7] L.G. Shaidarova, L.N. Davietshina, G.K. Budnikov, J. Anal. Chem. 61 (2006) 502.
[8] R.C. Matos, L. Angnes, M.C.U. Araujo, T.C.B. Saldanha, Analyst 125 (2000) 2011.
[9] B.C. Xue, T. Wang, E.B. Liu, Spectrosc. Spec. Anal. 26 (2006) 816.
[10] Y. Rodriguez, J.F. Tyson, J. Anal. At. Spectrom. 21 (2006) 757.
[11] M. Burguera, J.L. Burguera, P. Carrero, C. Rondon, Talanta 58 (2002) 1157.
[12] J.L. Burguera, M. Burguera, C. Rondon, Talanta 58 (2002) 1167.
[13] P. Carrero, L. Gutiérrez, C. Rondón, J.L. Burguera, M. Burguera, Y.P. de Pena, Talanta 64 (2004) 1309.
[14] G. Tao, Z. Fang, J. Baasner, B. Welz, Anal. Chim. Acta 481 (2003) 273.
[15] A. Gutés, F. Céspedes, S. Alegret, M. del Valle, Talanta 66 (2005) 1187.
[16] L. Bordera, V. Hernandis, A. Canals, Fresenius J. Anal. Chem. 355 (1996) 112.
[17] J.A. Sweileh, P.K. Dasgupta, Anal. Chim. Acta 214 (1988) 107.
[18] J.A. Sweileh, J.L. Lopez, P.K. Dasgupta, Rev. Sci. Instrum. 59 (1988) 2609.
[19] R.S. Honorato, M.C.U. Araújo, R.A.C. Lima, E.A.G. Zagatto, R.A.S. Lapa, J.L.F. Costa Lima, Anal. Chim. Acta 396 (1999) 91.
[20] R.S. Honorato, M.C.U. Araújo, R.A.C. Lima, E.A.G. Zagatto, Anal. Chim. Acta 416 (2000) 231.
[21] L.F. Almeida, V.L. Martins, E.C. Silva, P.N.T. Moreira, M.C.U. Araújo, Anal. Chim. Acta 486 (2003) 143.
[22] L.F. Almeida, V.L. Martins, E.C. Silva, P.N.T. Moreira, M.C.U. Araújo, J. Braz. Chem. Soc. 14 (2003) 249.
[23] J.E. da Silva, F.A. da Silva, M.F. Pimentel, R.S. Honorato, V.L. da Silva, B.S.M. Montenegro, A.N. Araújo, Talanta 70 (2006) 522.
[24] R.A.C. Lima, S.R.B. Santos, R.S. Costa, G.P.S. Marcone, R.S. Honorato, V.B. Nascimento, M.C.U. Araújo, Anal. Chim. Acta 518 (2004) 25.
[25] E.P. Medeiros, E.C.L. Nascimento, A.C.D. Medeiros, J.G.V. Neto, E.C. da Silva, M.C.U. Araújo, Anal. Chim. Acta 511 (2004) 113.
[26] R.S. Honorato, J.M.T. Carneiro, E.A.G. Zagatto, Anal. Chim. Acta 441 (2001) 309.
[27] J.M.T. Carneiro, A.C.B. Dias, R.S. Honorato, E.A.G. Zagatto, Anal. Chim. Acta 455 (2002) 327.
[28] R.S. Honorato, M.T. Carneiro, E.A.G. Zagatto, Fresenius J. Anal. Chem. 368 (2000) 496.
[29] B.F. Reis, M.F. Giné, E.A.G. Zagatto, J.L.F.C. Lima, R.A. Lapa, Anal. Chim. Acta 293 (1994) 129.
[30] P.C.A. Jerônimo, A.N. Araújo, M.C.B.S.M. Montenegro, C. Pasquini, I.M. Raimundo, Anal. Bioanal. Chem. 380 (2004) 108.

Available online at www.sciencedirect.com
ScienceDirect
Talanta 73 (2007) 878–885
Talanta
www.elsevier.com/locate/talanta

Synthesis of *N*,*N*′-dimethyl-*N*,*N*′-dibutyl malonamide functionalized polymer and its sorption affinities towards U(VI) and Th(IV) ions

S.A. Ansari, P.K. Mohapatra, V.K. Manchanda *

Radiochemistry Division, Bhabha Atomic Research Centre, Mumbai 400085, India

Received 14 March 2007; received in revised form 3 May 2007; accepted 9 May 2007
Available online 18 May 2007

Abstract

A novel chelating polymeric material was synthesized by chemical anchoring of *N*,*N*′-dimethyl-*N*,*N*′-dibutyl malonamide (DMDBMA) with chloromethylated polystyrene-divinyl benzene polymer. The polymeric material thus prepared was characterized by ^{13}C NMR, FT-IR spectroscopy and CHN elemental analysis. The fabricated polymeric material exhibited superior binding for hexa-valent and tetra-valent metal ions such as U(VI) and Th(IV). Various physico-chemical properties of the functionalized polymer like phase adsorption kinetics, metal sorption mechanism and metal sorption capacity was studied in the static method. Adsorption kinetics studies show that <20 min was sufficient for >99.99% adsorption of Th(IV) and U(VI). The kinetics for adsorption of U(VI) and Th(IV) was found to follow the first order Lagergren rate kinetics. Adsorption of U(VI) on the malonamide functionalized polymer followed the Langmuir adsorption isotherm. The Langmuir monolayer adsorption phenomenon was also confirmed by the theoretical approach calculated based on the adsorption kinetics. The metal sorption capacities for uranium and thorium were found to be 18.78 ± 1.53 mg and 15.74 ± 1.59 mg/g of the chelating polymer at 3 M HNO_3, respectively.

Keywords: Functionalized polymer; Malonamide; Actinides; Separation; Pre-concentration

1. Introduction

Actinides are the toxic heavy metals which, if ingested or swallowed, can stay inside the human body for long period of time leading to acute chemical as well as radio toxic effects [1]. As compared to the naturally occurring actinides such as U and Th, man made trans-uranides, viz. Pu, Np and Am are of greater concern from environmental point of view due to their higher dose factors for ingestion [2]. Therefore, actinide ions need to be monitored in various waste streams emanating from the nuclear facilities. The long half-life and radiotoxicity coupled with the favourable migration behaviour of some of the actinides have necessitated their strict monitoring in the dischargeable streams [3]. The monitoring requires efficient pre-concentration methods followed by their analysis using a suitable analytical method. Moreover, the extraction and pre-concentration of actinide ions from the waste solutions are extremely important not only from the point of view of their various possible uses, but also to reduce their quantum for disposal as radioactive waste [3]. Hence, there is increased awareness in preventing these radiotoxic metal ions by means of various reprocessing methods for effective recycling. Various analytical methods developed for this purpose include solvent extraction and ion-exchange methods which operate under different feed conditions.

Extractants such as tri-*n*-butyl phosphate (TBP), di(2-ethylhexyl) phosphoric acid (HD2EHP), di-isodecyl phosphoric acid (DIDPA), trialkyl phosphine oxides (TRPO), *N*,*N*,*N*′,*N*′-dimethyldibutyl tetradecyl malonamide (DMDBTDMA), *N*,*N*,*N*′,*N*′-tetraoctyl diglycolamide (TODGA), etc. can effectively separate uranium from various process solutions by liquid–liquid extraction technique utilizing hydrocarbon diluents [4–9]. The generation of secondary waste containing hydrolytic and radiolytic degradation products of organic compounds might affect the back extraction of the metal ions in liquid–liquid extraction process [10]. On the other hand, solid phase extraction has been increasingly used for the

* Corresponding author. Fax: +91 22 25505151.
E-mail address: vkm@barc.gov.in (V.K. Manchanda).

0039-9140/$ – see front matter © 2007 Elsevier B.V. All rights reserved.
doi:10.1016/j.talanta.2007.05.007

pre-concentration of trace as well as ultra trace amounts of inorganic species from complex matrices [11,12]. Chelating polymers have been frequently used for solid phase extraction as they provide good stability, high sorption capacity for the metal ions and good flexibility in the working conditions. There are two methodologies which are frequently adopted for designing such chelating polymers. The first involves the physical sorption of chelating ligands on the polymeric solid support. The other is based on co-valent coupling of the ligands with the polymer backbone through certain functional groups such as –N=N– or $–CH_2–$ groups. The latter approach renders a more stable resin which can be recycled over long periods.

'Green reagents' such as substituted monoamides/diamide have shown good metal extraction behaviour, high radiolytic stability and complete incinerability [13,14]. The present work deals with the synthesis and characterization of a novel malonamide grafted polymer using DMDBMA as chelating ligand and polystyrene-divinyl benzene polymer as the support backbone. The positive features of this functionalized polymer towards the adsorption of uranium and thorium is being reported in this communication.

2. Materials and methods

2.1. Chemicals and radionuclides

Chloromethylated Merrifield polymer [chloromethylated polystyrene-divinyl benzene polymer containing ~5.5 mmol of Cl/g of polymer, 16–50 mesh] obtained from Fluka Chemicals was purified by successive washing with methanol and water followed by vacuum drying before use. Dimethyl formamide was vacuum distilled at 50 °C after refluxing with calcium hydride at 60 °C before use. Standard solutions of uranium and thorium were prepared by dissolving requisite amounts of $UO_2(NO_3)_2{\cdot}6H_2O$ and $Th(NO_3)_4{\cdot}5H_2O$ in acidified de-ionized water. All the other reagents used were of analytical reagent grade and were used without further purifications. ^{233}U tracer was purified by anion exchange in HCl medium and it's purity was confirmed by α-spectrometry [15]. ^{234}Th was obtained by selective extraction of the latter U from HCl medium using Aliquat-336. Finally, ^{234}Th tracer was purified by extraction with 0.01 M solution of 3-phenyl-4-benzoyl-5-isoxazolone (HPBI) in xylene at 0.5 M HNO_3 followed by stripping with 7 M HNO_3.

2.2. Synthesis of DMDBMA functionalized polymer

For chemical anchoring of the chelating ligand, 5 g of vacuum dried chloromethylated polystyrene-divinyl benzene polymer was reacted with 30 mmol of *N*,*N*′-dimethyl-*N*,*N*′-dibutyl malonamide (DMDBMA) and 30 mmol of NaH in ~50 mL of dried dimethyl formamide (DMF). The reaction mixture was refluxed on an oil bath at 60 °C for 16 h. The final product was purified from the excess reactants by repeated washing with methanol and water. The resultant modified polymer was vacuum dried to constant weight. The synthesis scheme for the anchoring of amide moiety on the polymeric matrix is represented in Scheme 1.

2.3. Metal sorption studies

The sorption of metal ions was determined by equilibrating a known volume of aqueous phase (1 mL) containing radiotracer at given acidity with a known quantity of chelating polymer (~25 mg) in stoppered glass tubes. Agitation of the two phases was carried out in a thermostated water bath maintained at 25 ± 0.1 °C for 45 min. Subsequently, the tubes were centrifuged and suitable aliquots of the aqueous phase were taken before and after equilibration for assaying radiometrically. Assay of ^{234}Th was carried out by gamma counting in a well type NaI(Tl) scintillation counter interphased with a multichannel analyzer. Alpha counting for ^{233}U was carried out by liquid scintillation counter employing a toluene-based scintillator containing 10% (v/v) di(2-ethylhexyl) phosphoric acid (HD2EHP), 0.7% (w/v) 2,5-diphenyloxazole (PPO), 0.03% (w/v) 1,4-di-[2-(5-phenyloxazoyl)]-benzene (POPOP). The distribution coefficient (K_d) of metal ions on the solid matrix was calculated by employing the following formula:

$$K_d = \frac{C_0 - C}{C}\frac{V}{W}(\text{mL/g}) \quad (1)$$

where C_0 and C are the concentrations of metal ions (in counts per unit time per unit volume) before and after equilibration, V the volume of aqueous phase used (mL) and W is the weight of the polymer material employed (g). Similarly, the amount of metal ions adsorbed on the solid matrix (Q_t) was calculated as follows:

$$Q_t = (C_0 - C_t)\frac{V}{W}(\text{mg/g}) \quad (2)$$

where C_0 and C_t are the concentrations of metal ions in the aqueous phase at initial time ($t = 0$) and at time t, respectively, V the volume of aqueous phase used (mL) and W is the weight of the chelating polymer employed (g). All the experiments were carried out in duplicate and the error limit was within the relative standard deviation of 5%.

3. Results and discussion

3.1. Characterization of DMDBMA functionalized polymer

The characterization of the grafted polymer was carried out by solid state NMR, FT-IR spectroscopy as well as by elemental analysis. Solid-state ^{13}C NMR spectra of the chloromethylated polystyrene-divinyl benzene polymer exhibited a resonance signal at 40.1 ppm, corresponding to alkyl group ($–CH_2–Cl$), was shifted to 48.4 ppm in the DMDBMA functionalized polymer due to the substitution of malonamide moiety. The presence of lateral methyl group ($–CH_3$) of the malonamide was confirmed by the resonance signal at 14.2 ppm. In addition, a broad resonance signal of carbonyl carbon (>C=O) of malonamide in the grafted polymer was observed at 169.5 ppm, which was absent in the non-functionalized polymer, suggesting the successful

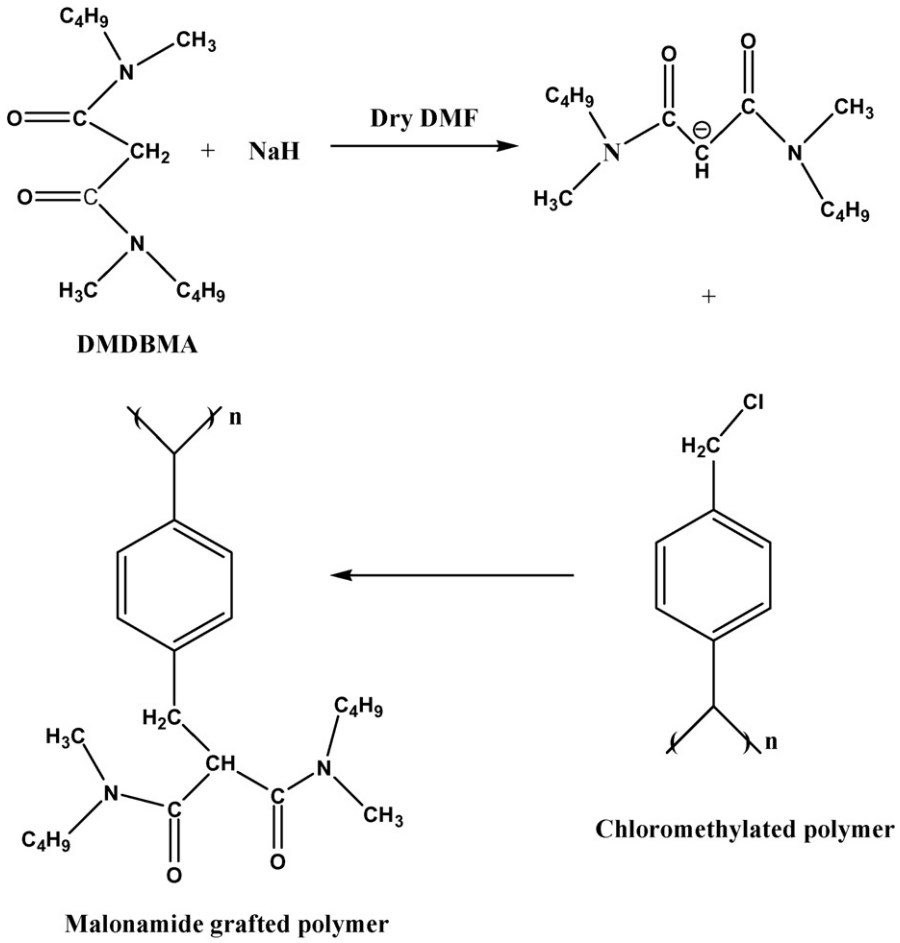

Scheme 1. Synthesis of malonamide functionalized polymer.

anchoring of the chelating ligand. The solid state ^{13}C NMR spectra of the functionalized and non-functionalized polymer are shown in Fig. 1.

FT-IR spectra of the functionalized polymer exhibited enhanced stretching vibrations between 3000 and 2800 cm^{-1} corresponding to =CH–, $–CH_2–$ and $–CH_3$ groups. Appearance of characteristics band of carbonyl group (>C=O) at 1645 cm^{-1}, in addition to a band at 1390 cm^{-1} due to C–N stretching vibration, suggested the presence of amide moiety on the grafted polymer. Similarly, disappearance of vibrational band at 673 cm^{-1}, which corresponded to $–CH_2Cl$ group in the non-functionalized polymer, confirmed the chemical modification of the Merrifield polymer. The FT-IR spectra of the modified and the non-modified polymer are shown in Fig. 2. Similarly, the CHN elemental analysis of the functionalized polymer yielded 6.58% of nitrogen against 7.23% of the theoretical value, suggesting >91% anchoring of the malonamide moiety on the polymeric support. This nitrogen content corresponded to 60% (w/w) loading of the ligand on the polymeric support.

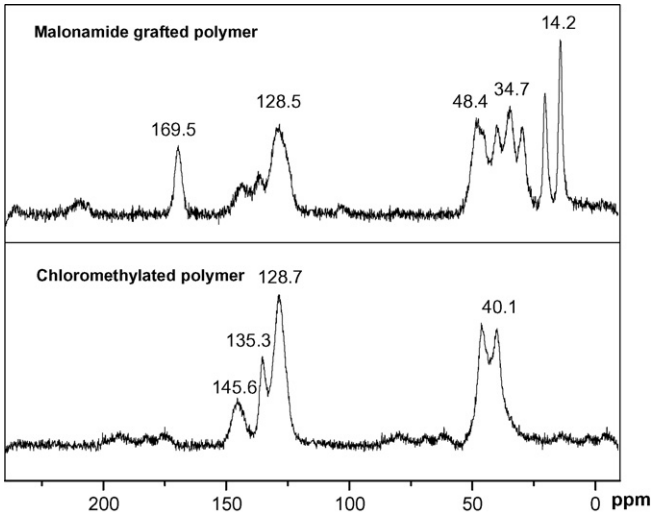

Fig. 1. ^{13}CNMR spectra of non-functionalized and malonamide functionalized polymer.

3.2. Adsorption kinetics

The rate of transfer of U(VI) and Th(IV) ions from aqueous phase to the solid phase was studied at 3 M HNO_3 by equilibrating the malonamide functionalized polymer with aqueous solution containing metal ions tracer for different periods. The phase adsorption kinetics was monitored in terms of fractional

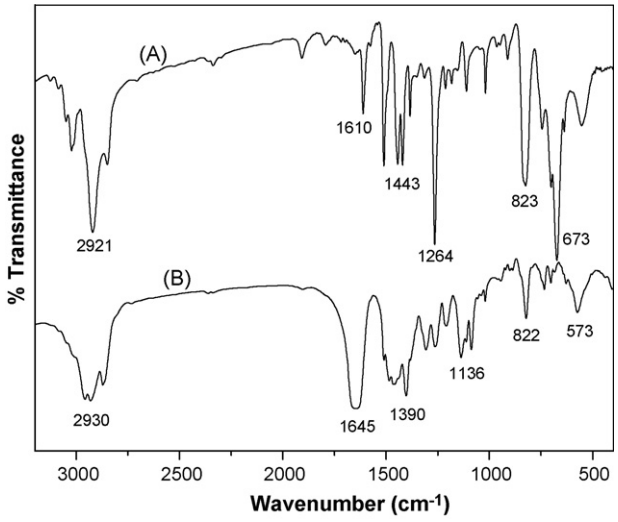

Fig. 2. FT-IR spectra of non-functionalized and malonamide functionalized polymer. (A) Choloromethylated polymer and (B) DMDBMA-grafted polymer.

attainment of the equilibrium expressed as follows [16]:

$$F = \frac{[M^R]_t}{[M^R]_{eq}} \quad (3)$$

where $[M^R]_t$ and $[M^R]_{eq}$ are the metal ions concentration on the solid phase at time 't' and at equilibrium, respectively. The kinetics data were plotted in terms of $(1 - F)$ values as a function of equilibration time and are shown in Fig. 3. It is evident from the figure that the equilibrium condition reached within 20 min for both the metal ions. The kinetics for adsorption of U(VI) and Th(IV) on DMDBMA functionalized polymer was found to follow the first order rate expression given by Lagergren as

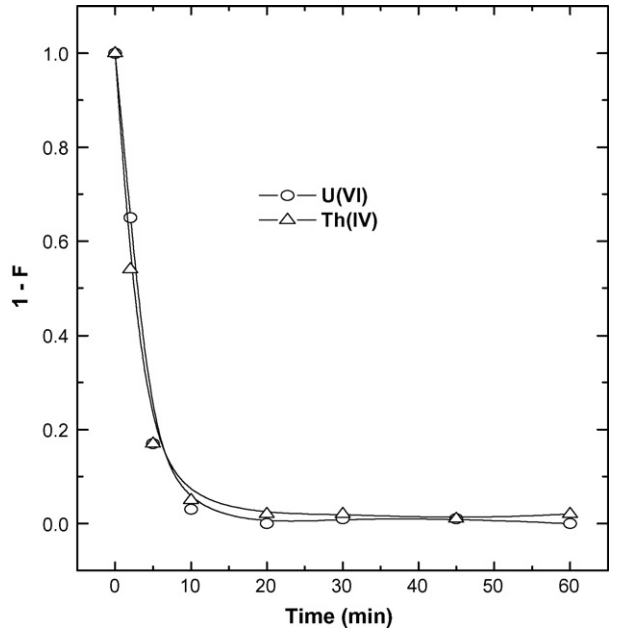

Fig. 3. Kinetics for the sorption of U(VI) and Th(IV) ions on malonamide functionalized polymer at 3 M HNO_3; temperature: 25 °C.

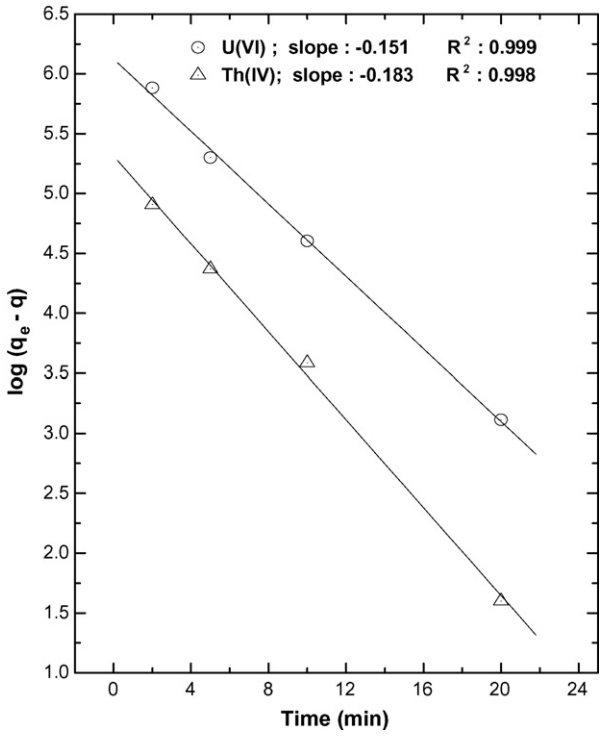

Fig. 4. Lagergren plots for the adsorption of metal ions on malonamide functionalized polymer at 3 M HNO_3; temperature: 25 °C.

follows [17]:

$$\log(q_e - q) = \log\, q_e - \left(\frac{K_{ads}}{2.303}\right) t \quad (4)$$

where q and q_e are the amount of metal ions adsorbed per gram of chelating polymer at time 't' and at equilibrium, respectively, and K_{ads} is the adsorption rate constant. The linear plots of $\log(q_e - q)$ versus 't' at 3 M HNO_3 (Fig. 4) suggested the applicability of the above equation for adsorption of U(VI) and Th(IV) on the malonamide functionalized polymer. The K_{ads} values calculated from the slope of the plot were 0.421 ± 0.015 and $0.348 \pm 0.011\ min^{-1}$ for Th(IV) and U(VI), respectively. Higher adsorption rate constant for Th(IV) as compared to U(VI) reflected the stronger complexation of tetravalent metal ions due to higher ionic potential.

3.3. Adsorption isotherms

The sorption studies of uranium on the malonamide functionalized polymer were conducted and the sorption data were tested to several types of isotherms such as Dubinin-Rodushkevich (D-R), Langmuir and Freundlich adsorption isotherms. Langmuir isotherm is the most simple for the adsorption of adsorbate on to the adsorbent, which is based on the following assumptions [18]: (i) only one monolayer of an adsorbing molecule can be sorbed on the surface of the adsorbent, (ii) all sites of adsorbent are equivalent, (iii) the ability of a molecule to adsorb at a given site is independent of the nature of the neighbouring sites, and (iv) the enthalpy of adsorption is constant. Though Langmuir adsorption isotherm was developed for the adsorption of gases

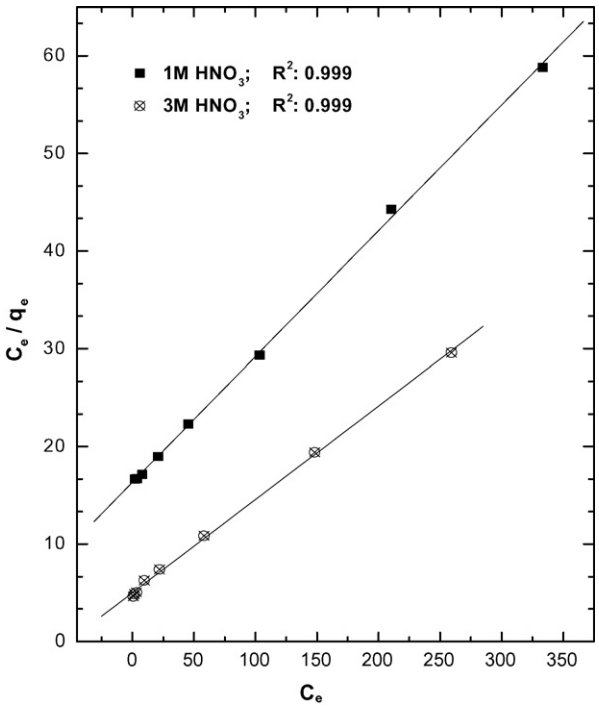

Fig. 5. Langmuir isotherm for the adsorption of uranium on the malonamide functionalized polymer; temperature: 25 °C.

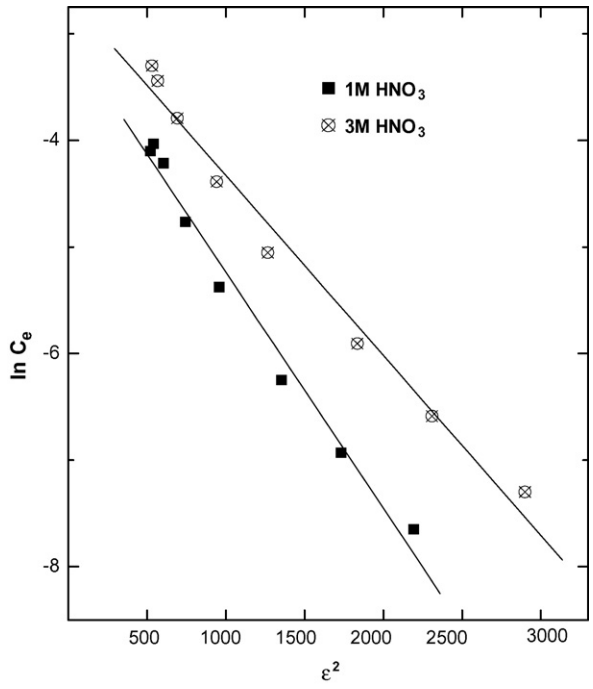

Fig. 6. D-R isotherm for the adsorption of uranium on the malonamide functionalized polymer; temperature: 25 °C.

on the solid surface, it could also be applied for the liquid phase. The Langmuir adsorption isotherm in the liquid phase can be represented by the following equation [19]:

$$\frac{C_e}{q_e} = \frac{1}{q_0 b} + \frac{C_e}{q_0} \tag{5}$$

where C_e is the equilibrium concentration of metal ions in the aqueous phase, q_e the amount of metal ions adsorbed on the solid phase at equilibrium; q_0 and b are the Langmuir constant related to adsorption capacity of the metal ions and energy of adsorption, respectively. As shown in Fig. 5, the linear plot of C_e/q_e versus C_e suggested that the adsorption of uranium on malonamide grafted polymer obeys Langmuir adsorption model. The correlation coefficients for the linear fits of the plot were found to be 0.999 for both, at 1 and 3 M HNO_3. The Langmuir constant q_0 determined from the slope of the plot were found to be 32.6 ± 0.33 and 43.9 ± 0.65 μmol of uranium per gram of the polymeric material at 1 and 3 M HNO_3, respectively. Similarly, the values of 'b' calculated from the intercept were $(1.9 \pm 0.1) \times 10^3$ and $(4.5 \pm 0.1) \times 10^3$ L/mol at 1 and 3 M HNO_3, respectively. The maximum sorption capacity (q_0) represents the monolayer coverage of metal ions on the malonamide grafted polymer and 'b' represents the enthalpy of adsorption.

The sorption data were also examined on the following linearized form of D-R isotherm [20,21]:

$$\ln\ q_e = \ln\ X_m - \beta\varepsilon^2 \tag{6}$$

where q_e is the amount of metal ions adsorbed on the solid matrix at equilibrium, X_m the maximum sorption capacity, β the activity coefficient which is related to the mean sorption energy, and ε is Polanyi potential [21]which is given as

$$\varepsilon = RT\ \ln\left(1 + \frac{1}{C_e}\right) \tag{7}$$

where C_e is the equilibrium concentration of metal ions in the aqueous phase, R the gas constant (kJ/mol) and T is the absolute temperature. The saturation limit (X_m) may represent the total specific active sites on the polymer. The plot of $\ln q_e$ versus ε^2 is a straight line as shown in Fig. 6. From the slope of plot the value of β was calculated as -0.0022 ± 0.0002 and -0.0017 ± 0.0002 mol^2/kJ^2 at 1 and 3 M HNO_3, respectively. Similarly, the value of X_m was calculated from the intercept as 30.2 ± 1.1 and 49.9 ± 1.7 μmol/g at 1 and 3 M HNO_3, respectively. The sorption energy (E) was worked out using the following relationship:

$$E = \frac{1}{(-2\beta)^{1/2}} \tag{8}$$

The value of E for the present system was estimated to be 15.08 ± 0.65 and 17.15 ± 0.93 kJ/mol at 1 and 3 M HNO_3, respectively.

Similarly, the Freundlich adsorption isotherm was also applied to the present system, which assumes that the enthalpy of adsorption varies logarithmically with gas pressure (or initial concentration of metal ions in liquid phase). The Freundlich adsorption isotherm in the liquid phase is given by the following equation [22,23]:

$$\log\left(\frac{x}{m}\right) = \log\ K_f + \left(\frac{1}{n}\right)\ \log\ C_e \tag{9}$$

where C_e is the concentration of metal ions in the aqueous phase at equilibrium, x/m the concentration of metal ions adsorbed per

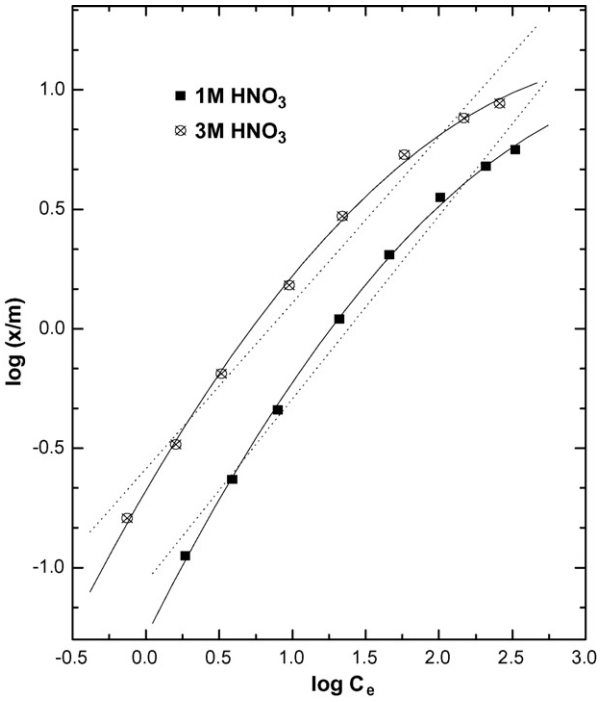

Fig. 7. Freundlich isotherm for the adsorption of uranium on the malonamide functionalized polymer; temperature: 25 °C.

unit mass of the polymer, K_f and n are the constant related to the adsorption capacity and adsorption intensity, respectively. The Freundlich plot of $\log(x/m)$ versus $\log C_e$ for sorption of uranium at 1 and 3 M HNO_3 is presented in Fig. 7. As can be seen from the figure, the observed points do not fit on the theoretical line (dotted line) and coefficients of the linear regression fits were 0.981 and 0.979 at 1 and 3 M HNO_3, respectively. This observation reflected the non-applicability of Freundlich isotherm, confirming the absence of multilayer adsorption of uranium on the malonamide functionalized polymer. On the other hand, better linear fits for Langmuir model were observed as the coefficients for linear fits were 0.999 for both the systems (Fig. 5). Since the Langmuir model represents monolayer chemisorption on a set of well-defined localized adsorption sites, better fitting of the present data to the Langmuir model is an evidence for the presence of monolayer adsorption. However, to confirm the presence of monolayer adsorption of U(VI), a theoretical model based on adsorption kinetics was applied to the present system.

3.4. Adsorption mechanism

On the basis of Langmuir and Freundlich adsorption isotherms model described above, we might conclude that the sorption of uranium on the malonamide functionalized polymer was a monolayer adsorption process. However, to deeply understand the adsorption mechanism we followed the adsorption model described by Zang et al. [24]. If one assumes that the adsorption of U(VI) on the DMDBMA functionalized polymer was monolayer process, then the adsorption rate would increase with the available concentration of U(VI) introduced to the polymer $(C_0 - C_t)$; and the effect of contact time is not significant on the rate of adsorption [24]. Then the adsorption equation can be expressed as follows:

$$\frac{dC_t}{dt} = K(C_0 - C_t) \tag{10}$$

Eq. (10) can be written as follows:

$$\int_{C_0}^{C_t} \frac{dC_t}{C_0 - C_t} = \int_0^t K\,dt \tag{11}$$

$$-\ln\left[\frac{C_0 - C_t}{C_0}\right] = K\,t \tag{12}$$

$$-\ln\left[1 - \frac{C_t}{C_0}\right] = K\,t \tag{13}$$

where C_0 and C_t represent the adsorbed amount of U(VI) at equilibrium and at time t, respectively, and K is the adsorption constant for monolayer adsorption. According to the above model, the plot of $-\ln[1 - (C_t/C_0)]$ versus time 't' should be a straight line with slope K. The adsorption of U(VI) on malonamide grafted polymer was investigated as a function of time at 3 M HNO_3 and Eq. (13) was plotted in Fig. 8. The linearity of the plot of $-\ln[1 - (C_t/C_0)]$ versus time 't' was an evidence that the adsorption of U(VI) followed the monolayer mechanism. The correlation coefficient of the linear regression fit was observed to be 0.999, i.e. ~1. This observation confirmed that our prediction for the Langmuir monolayer adsorption isotherm was correct for the present system.

Similarly, if one assumes that adsorption of U(VI) on the grafted polymer was multilayer molecule adsorption, then the rate of U(VI) adsorption on the polymer usually increased with the available concentration of U $(C_0 - C_t)$ and decreased with

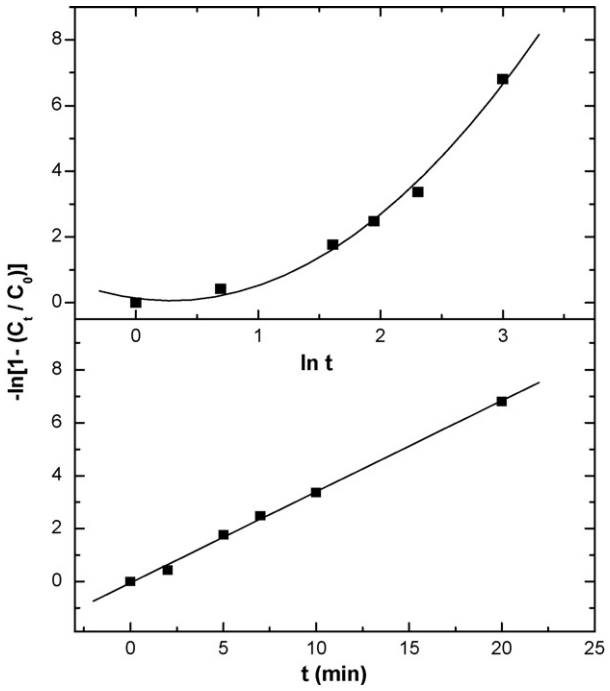

Fig. 8. Relationship between $-\ln[1 - (C_t/C_0)]$ and t as well as $-\ln[1 - (C_t/C_0)]$ and $\ln t$ for sorption of uranium at 3 M HNO_3; temperature: 25 °C.

Table 1
Desorption of uranium from DMDBTDMA grafted polymer

Equilibrating solution	% Desorption		
	I stage	II stage	III stage
0.01 M HNO_3	49.27	82.12	98.45
0.01 M EDTA	55.38	88.25	99.47
0.25 M oxalic acid	89.62	96.02	99.28
0.25 M Na_2CO_3	93.46	98.08	99.23

the contact time [24]. Then the adsorption equation can be expressed as follows:

$$\frac{dC_t}{dt} = \frac{K_m(C_0 - C_t)}{t} \quad (14)$$

Eq. (14) can be written as follows:

$$\int_{C_0}^{C_t} \frac{dC_t}{C_0 - C_t} = \int_0^t \frac{K_m\, dt}{t} \quad (15)$$

$$-\ln\left[\frac{C_0 - C_t}{C_0}\right] = K_m \ln t \quad (16)$$

$$-\ln\left[1 - \frac{C_t}{C_0}\right] = K_m \ln t \quad (17)$$

where K_m is the adsorption constant for multilayer adsorption. From the above equation one should also get a straight line of the plot $-\ln[1-(C_t/C_0)]$ versus $\ln t$ with slope K_m, if the assumption for multilayer adsorption was correct. However, non-linearity of the plot of $-\ln[1-(C_t/C_0)]$ versus $\ln t$ (Fig. 8) suggested that the assumption for multilayer adsorption of U(VI) was incorrect. Similar observation was also exhibited by Freundlich adsorption isotherm where nonlinearity of the plot suggested the absence of multilayer adsorption mechanism. This observation confirmed that the adsorption of U(VI) on the malonamide functionalized polymer followed the monolayer Langmuir adsorption isotherm instead of Freundlich multilayer isotherm.

3.5. Desorption studies

Desorption studies on uranium from the activity loaded malonamide functionalized polymer were conducted employing various strippant solutions such as 0.01 M HNO_3, 0.01 M EDTA, 0.25 M Na_2CO_3 and 0.25 M oxalic acid. As reported in Table 1, though near quantitative desorption of uranyl ion was possible with all the four reagents after three stages, maximum desorption of uranium (>93%) was observed in the first stage itself with Na_2CO_3. It is well known that the strong complexation of UO_2^{2+} with CO_3^{2-} ion ($\log \beta_3 = 21.54$) makes the latter an effecting eluting agent involving ion exchange separations [25].

3.6. Effect of acidity on metal ion sorption

The roles of acid concentration and the nature of mineral acid such as HNO_3, HCl and $HClO_4$ on the sorption behaviour of uranium were investigated and the data are represented in Fig. 9.

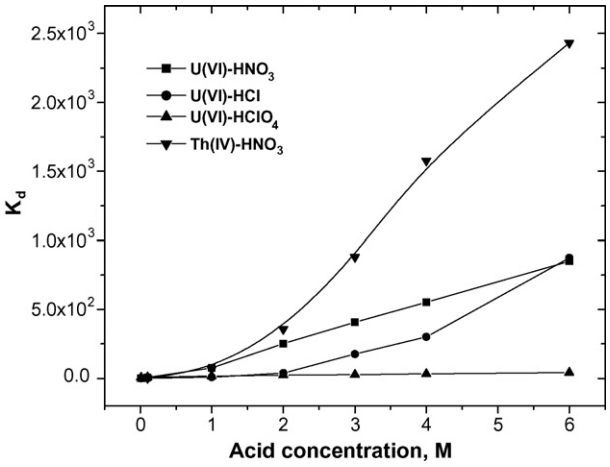

Fig. 9. Distribution coefficient (K_d) of metal ions from various mineral acid solutions; temperature: 25 °C.

The sorption behaviour of Th(IV) from HNO_3 medium was also included for comparison purpose. As shown in the figure, the distribution coefficient (K_d) of U(VI) was minimal from $HClO_4$ medium which is ascribed to the weak complexing ability of the ClO_4^- ions. On the other hand, the K_d value was very good at higher acid concentration in both, HCl as well as HNO_3 medium. The K_d value of Th(IV) as compared to U(VI) increased sharply at nitric acid concentration >2 M. This is due to a much higher nitrate ion concentration dependency for Th(IV) as compared to that for U(VI) as indicated in the following sorption equilibrium:

$$Th^{4+} + 4NO_3^- + 3L\text{-}R \rightleftharpoons Th(NO_3)_4 \cdot 3L\text{-}R \quad (18)$$

$$UO_2^{2+} + 2NO_3^- + 2L\text{-}R \rightleftharpoons UO_2(NO_3)_2 \cdot 2L\text{-}R \quad (19)$$

where L-R is the malonamide moiety attached to the resin. It appears that though Th(IV) exhibited very high K_d values (Fig. 9), the loading may be lower than U(VI) as the former requires higher number of malonamide moieties as compared to the latter. The K_d values observed at 3 M HNO_3 were 880 and 410 for Th(IV) and U(VI), respectively, suggesting the good extraction properties of malonamide grafted polymer for these metal ions.

3.7. Analytical applications

The maximum metal loading capacity of uranium and thorium by DMDBMA functionalized polymer was determined at 1 and 3 M HNO_3 by equilibrating 100 mg of polymeric material with 5 mL of individual solution of U and Th (1 mg/mL for each metal ions) for 24 h. Suitable aliquots of the aqueous phases were removed before and after equilibration for the estimation of uranium and thorium. The analyte solutions were diluted accordingly in the calibration range and estimated spectrophotometrically using Arsenazo-III as the chromophoric agent. The calibration curve for Th(IV) was plotted in the concentration range of 1×10^{-6} to 1×10^{-5} M giving a molar extinction coefficient value of $1.0 \times 10^5\ M^{-1}\ cm^{-1}$. Similarly, calibration curve for U(VI) was constructed between the concentration range of 1×10^{-5} to 5×10^{-5} M, which yielded

a molar extinction coefficient value of $2.0 \times 10^4\ M^{-1}\ cm^{-1}$. The metal sorption capacities were found to be 9.06 ± 0.53 and 6.66 ± 1.02 mg at 1 M HNO_3; and 18.78 ± 1.53 and 15.74 ± 1.59 mg at 3 M HNO_3/g of polymer for U and Th, respectively. Though the kinetics for sorption of Th(IV) was higher, the polymer exhibited higher loading capacity for U(VI). Higher loading of U(VI) as compared to Th(IV) could be explained on the basis of stoichiometry of the extracted species where two ligand molecules were involved for the extraction of uranium as compared to thorium (Eqs. (18) and (19)). On the other hand, increase in the loading of metal ions with the acidity can be explained by law of mass action where the equilibrium reactions (18) and (19) were favoured at higher nitrate concentration. High loading capacities for uranium and thorium by DMDBMA functionalized polymer reflect its possible use in the pre-concentration of these metal ions from their dilute acidic solutions.

4. Conclusions

A chelating polymeric material containing *N*,*N*′-dimethyl-*N*,*N*′-dibutyl malonamide (DMDBMA) anchored with chloromethylated polystyrene-divinyl benzene polymer was successfully synthesized for the solid phase extraction of U(VI) and Th(IV). The metal sorption kinetics for the adsorption of U(VI) and Th(IV) followed the Lagergren first order rate kinetics. The adsorption rate constant at 25 °C were 0.421 ± 0.015 and $0.348 \pm 0.011\ min^{-1}$ for Th(IV) and U(VI), respectively. The adsorption isotherm studies reflected that the adsorption of U(VI) on the malonamide functionalized polymer followed the monolayer adsorption mechanism. The metal sorption capacity at 3 M HNO_3 was found to be 18.78 ± 1.53 mg and 15.74 ± 1.59 mg/g of chelating polymer for U and Th, respectively. High loading capacity of uranium at 3 M HNO_3 suggested the possible use of malonamide functionalized polymer in the nuclear fuel reprocessing.

Acknowledgements

The authors thank Dr. K.V. Chetty and Dr. V. Sudarshan for help rendered during the recording of FT-IR and NMR spectra, respectively.

References

[1] J.J. Katz, G.T. Seaborg, L.R. Morss, The Chemistry of the Actinide Elements, vol. I, 2nd ed., Chapman and Hall, New York, 1986.
[2] C. Madic, M.J. Hudson, European Commission Report, EUR18038EN, 1998, p. 5.
[3] G.R. Choppin, A. Morgenstern, J. Radioanal. Nucl. Chem. 243 (2000) 45–51.
[4] W.D. Bond, in: W.W. Schulz, L.L. Burger, J.D. Navratil, K.P. Bender (Eds.), Science and Technology of Tributyl Phosphate, Application of Tributyl Phosphate in Nuclear Fuel Reprocessing, vol. III, CRC Press, Boca Raton, Florida, 1990, p. 225.
[5] F.J. Hurst, Trans. Soc. Min. Eng. AIME 262 (1977) 240–248.
[6] Y. Morita, I. Yamaguchi, Y. Kondo, K. Shirahashi, I. Yamagishi, T. Fujirawa, M. Kubota, Safety and Environmental Aspects of Partitioning and Transmutation of Actinides and Fission Products, IAEA-TECDOC-783, IAEA, Vienna, 1995, p. 93.
[7] G.R. Mahajan, D.R. Prabhu, V.K. Manchanda, L.P. Badheka, Waste Manage. 18 (1998) 125–133.
[8] S.A. Ansari, P.N. Pathak, M. Husain, A.K. Prasad, V.S. Parmar, V.K. Manchanda, Solv. Extr. Ion Exch. 23 (2005) 463–479.
[9] Y. Sasaki, Y. Sugo, S. Suzuki, S. Tachimori, Solv. Extr. Ion Exch. 19 (2001) 91–103.
[10] C. Cuillerdier, C. Musikas, P. Hoel, L. Nigond, X. Vitart, Sep. Sci. Technol. 26 (1991) 1229–1244.
[11] V. Camel, Spectrochim. Acta Part B 58 (2003) 1177–1233.
[12] N. Masque, R.M. Marce, F. Borull, Trends Anal. Chem. 17 (1998) 384–395.
[13] K.K. Gupta, V.K. Manchanda, M.S. Subramanian, R.K. Singh, Solv. Extr. Ion Exch. 18 (2000) 273–292.
[14] C. Cuillerdier, C. Musikas, L. Nigond, Sep. Sci. Technol. 28 (1993) 155–175.
[15] P.K. Mohapatra, Studies on the complexation of actinides with some macrocyclic ligands, PhD Thesis, University of Bombay, 1993.
[16] R. Chiarizia, E.P. Horwitz, S.D. Alexandratos, Solv. Extr. Ion Exch. 12 (1994) 211–237.
[17] D.B. Singh, G. Prasad, D.C. Rupainwar, V.N. Singh, Water, Air Soil Pollut. 42 (1988) 373–386.
[18] I.J. Langmuir, J. Am. Chem. Soc. 40 (1918) 1361–1365.
[19] P. Metilda, K. Sanghamitra, J.M. Gladis, G.R.K. Naidu, T.P. Rao, Talanta 65 (2005) 192–200.
[20] M.M. Dubininn, L.V. Raushkevich, Proc. Acad. Sci. USSR, Phys. Chem. Sect. 55 (1947) 331.
[21] M. Polanyi, Trans. Faraday Soc. 28 (1932) 316–320.
[22] G. McKay, H.S. Blair, J.R. Garden, J. Appl. Polym. Sci. 27 (1982) 3043–3057.
[23] P.W. Atkins, Physical Chemistry, 5th ed., Oxford University press, Oxford, 1994.
[24] A. Zhang, Y. Wei, M. Kumagai, React. Funct. Polym. 61 (2004) 191–202.
[25] J.J. Katz, G.T. Seaborg, L.R. Morss, The Chemistry of the Actinide Elements, vol. II, 2nd ed., Chapman and Hall, New York, 1986 (Chapter 21).

Available online at www.sciencedirect.com
ScienceDirect
Talanta 73 (2007) 962–964
Talanta
www.elsevier.com/locate/talanta

Short communication

Hydrogen peroxide in basic media for whole blood sample dissolution for determination of its lead content by electrothermal atomization atomic absorption spectrometry

Juliany Biasino, José Ramón Domínguez, José Alvarado *

Departamento de Química, Universidad Simón Bolívar, Laboratorio de Espectroscopia Atómica, Caracas 1080-A, Venezuela

Received 10 May 2007; received in revised form 13 May 2007; accepted 14 May 2007
Available online 21 May 2007

Abstract

Hydrogen peroxide in basic media is proposed as a means for dissolving whole blood samples to be analyzed by electrothermal atomization atomic absorption spectrometry, ET AAS. Approximately 2 g of the whole blood sample were directly weighed in a 150 mL volumetric flask; 3 mL of a NaOH 0.2 mol L^{-1} solution, two drops of 1-octanol, as an antifoaming agent, and 1 mL of 30% volume hydrogen peroxide were added to the flask to promote oxidation. The solution was then manually shaken and after approximately three minutes of shaking, a clear solution, with no apparent suspended solids or greasy layers, was obtained. Distilled-deionized water was used to complete the volume. Ten μL of the resulting solution along with 10 μL of a solution containing 5000 mg L^{-1} of $NH_4H_2PO_4$ and 300 mg L^{-1} of $Mg(NO_3)_2$ as a modifier, were injected into transversely heated graphite tubes for lead determination. Both aqueous standards and standard addition calibration curves produced results not significantly different at a 95% confidence limit level. Accuracy of the measurements was assessed by analysis of the IAEA A-13 (*concentration of trace and minor elements in freeze dried animal blood*) standard reference material containing 0.18 mg L^{-1} lead on a dry basis and by means of recovery tests. Analysis of the IAEA A-13 standard produced 0.17 ± 0.02 mg L^{-1} lead on a dry basis; recovery tests afforded values from 95 to 105%. Ten consecutive measurements of a 5 ppb lead solution gave a characteristic mass of 47.2 pg and a (3S) detection limit of 1.77 μg L^{-1} Pb. Results obtained from analysis of whole blood samples of volunteer donors covered a lead concentration range between 8 and 21 μg L^{-1} with a mean value of 11.9 ± 4.7 μg L^{-1}.

Keywords: Whole blood; Basic media sample treatment; Lead determination; Atomic absorption

1. Introduction

Lead is probably one of the most studied analytes especially in biological samples. The interest in this element comes from its toxicity and ubiquity. Lead stands out as one of the poisonous elements practically ever-present in our environment [1]. In places like Venezuela were leaded gasoline was vastly used; lead poisoning could become a public health risk [2]. Lead determination in biological fluids such as blood constitutes an appropriate means to estimate lead burden in the organism [3–6]. Electrothermal atomization atomic absorption spectrometry has been widely used for analysis of this type of samples [7–9]. The requirement of liquid samples for analysis imposed by ET AAS makes it necessary to develop sample treatments capable of rendering the samples in solution with minimum risks of analyte losses or sample contamination. A rapid and simple dissolution method, performed at ambient temperature and involving few reagents, could easily comply with the above requirements. The aim of this paper is to describe a whole blood sample dissolution method which produces clear blood solutions by simply adding hydrogen peroxide in basic media, with no need for sample heating. The method was tested on the dissolution of blood samples collected by vein puncture from gas station workers. The dissolved samples were analyzed for lead by electrothermal atomization atomic absorption spectrometry as part of a larger study undertaken to assess the possible reduction of lead contamination as a consequence of introduction of unleaded gasoline in the Venezuelan market by the end of 1999.

* Corresponding author. Tel.: +58 212 906 3981; fax: +58 212 906 3981.
E-mail address: jalvar@usb.ve (J. Alvarado).

0039-9140/$ – see front matter © 2007 Elsevier B.V. All rights reserved.
doi:10.1016/j.talanta.2007.05.020

2. Experimental

2.1. Instrumentation

A Perkin-Elmer model 5100 ZL atomic absorption spectrometer with transversely heated electrothermal atomization, longitudinal Zeeman background correction and an AS-71 autosampler was used for lead determination at the 283.3 nm line.

2.2. Reagents

Sodium hydroxide (Prolabo, 98% purity) and hydrogen peroxide (Riedel de Häen, 30%, v/v purity) were used for sample dissolution. Octanol (Aldrich Chemical Company Inc., 99% purity) was used as an antifoaming agent. A 1000 mg L^{-1} (Merck Titrisol®) Pb solution was used for standard preparation. Dibasic ammonium phosphate ($NH_4H_2PO_4$) (J.T. Baker), $Mg(NO_3)_2{\cdot}6H_2O$ (Riedel de Häen, 99% purity) and nitric acid (p.a., Riedel de Häen, 65%) were used to prepare a solution containing 5000 mg L^{-1} $NH_4H_2PO_4$, 300 mg L^{-1} $Mg(NO_3)_2$ and 0.2% HNO_3 to be used as a modifier. Distilled-deionized water from a Milli-Q system (Millipore, Bedford, MA) with 18 MΩ resistivity was used throughout.

2.3. Samples

Blood samples were collected from gas station workers by vein puncture in vacutainer® tubes containing EDTA as an anticoagulant. After collection, the tubes were capped, manually shaken for distribution of the anticoagulant in the mass of blood and kept refrigerated at 4 °C until analysis.

2.4. Sample, standards and blank preparation

Approximately 2 g of the whole blood samples were exactly weighed in a 150 mL volumetric flask; 3 mL of NaOH 0.2 mol L^{-1} solution and two drops of octanol were added, followed by the addition of 1 mL of hydrogen peroxide. The flask was manually shaken to promote oxidation of the sample and then taken to volume by addition of distilled-deionized water. For aqueous standard calibration lead standard solutions were prepared by convenient dilution of a 1000 mg L^{-1} lead Titrisol® solution. For calibration using the method of standard addition 1300 μL of each blood sample solution were thoroughly mixed in autosampler vials with 200 μL of solutions containing 5, 20, 50 and 100 μg L^{-1} lead. A solution containing hydrogen peroxide, 1-octanol and distilled-deionized water in the same proportions as the samples, was used as a blank.

3. Results and discussion

3.1. Sample preparation

Addition of H_2O_2 to the basic whole blood samples resulted in massive foam formation which could be difficult to control. Amounts of blood larger than 0.75 g could easily spill out of the sample container on addition of hydrogen peroxide. This inconvenience was overcome by the addition of two drops of octanol prior to the addition of the oxidant. Production of gaseous oxygen and CO_2 species during oxidation of the sample could account for the foaming. Addition of the antifoaming alcohol reduces the surface tension of the solution, thus inhibiting foam formation. This sample preparation procedure produced clear solutions, with no apparent undissolved particles or greasy layers, in approximately 3 min without need for heating. This rapid dissolution procedure is thus amenable for preparing samples to be analyzed for volatile elements such as Pb and Hg.

3.2. Atomization conditions

Lead was thermally stabilized by addition of 10 μL of the modifier solution already described. No attempt was made to optimize the default heating program proposed for lead in the PE 5100 ZL software, except for the introduction of a second drying step and, for the first measurements, an extension of the cleaning step time. The second drying step was needed to improve precision of the results. Increasing the cleaning step in the first measurements was necessary to get rid of carbon residues observed in the graphite platform after a few atomization cycles. In the following measurements, carbon residue formation was avoided by addition of 10 μL of a 1:1 water–methanol solution as proposed by Trzcinka-Ochoka [10]. The final temperature program used is shown in Table 1.

3.3. Figures of merit

Under the analytical conditions stated In Table 1, a (3S) detection limit of 1.77 μg L^{-1}, a characteristic mass of 47.2 pg and a relative standard deviation of 7.92%, were achieved.

3.4. Determination of lead in whole blood samples

Lead was determined by ET AAS in seven whole blood samples, brought into solution by the method proposed here. The samples were collected by vein puncture from male and female volunteer donors, aged 19–39 years, working in gas stations located in Caracas, Venezuela, and surrounding areas. Comparison of aqueous standards and standard addition calibration curves showed no significant difference at the 95% confidence limit level. This is an indication of efficient sample matrix destruction by the dissolution method employed. Therefore, aqueous standards were used for preparation of calibration

Table 1
Temperature program for lead determination by ET AAS in whole blood samples dissolved using Na OH and H_2O_2

Step	T (°C)	Ramp (s)	Hold (s)	Ar flow (mL/min)
Drying	110	5	20	250
Drying	130	5	30	250
Ashing	850	10	20	250
Atomization	1500	0	5	0
Cleaning	2400	5	5	250

Table 2
Comparison of the proposed method with some literature procedures commonly used for sample preparation for determination of blood metal by atomic absorption

Procedure	Sample amount (g)	Reagents used	Instrumentation	Solution stability	Time needed (min)	Ref.
APDC complexation and MIBK extraction	5.0	APDC, MIBK, Triton X-100	Centrifuge	Unstable, must be used within 1 h after preparation	20	[11]
Acid dilution	2.0	HNO_3, Triton X-100	Mechanical shaker	Stable for at least 24 h	60	[7]
Microwave assisted acid digestion	1.0	Nitric acid	Microwave oven	Idem	45	[13]
Microwave assisted acid digestion	1.0	Nitric acid/hydrogen peroxide	Microwave oven	Idem	45	[12]
Hydrogen peroxide in basic media dissolution	2.0	$NaOH/H_2O_2$/1-octanol	None	Idem	3	This work

graphs. Lead concentration in the samples analyzed ranged from 8 to 21 $\mu g\,L^{-1}$ with an average value of $11.9 \pm 4.7\,\mu g\,L^{-1}$. Accuracy of these results was assessed by analysis of the IAEA A-13 (*concentration of trace and minor elements in freeze dried animal blood*) containing $0.18\,mg\,L^{-1}$ lead and by means of recovery tests. Analysis of the IAEA standard indicated a lead content of $0.17\,mg\,L^{-1}$. Recovery tests produced results from 95 to 105%. Since these results are part of a larger study aimed at elucidating the effect of introduction of unleaded gasoline in the Venezuelan market, their interpretation is not within the scope of this paper.

3.5. Comparison with other blood dissolution methods

The hydrogen peroxide in basic media procedure for blood dissolution proposed in this work has been compared in Table 2, with some other methods commonly reported in the literature. As seen in this table, the main asset of the method is speed of analysis. Blood samples can be dissolved in approximately 3 min. Additionally, the method does not require heating nor especial instrumentation and uses common and inexpensive reagents.

4. Conclusions

Basic attack of the blood sample by NaOH followed by addition of two drops of 1-octanol and hydrogen peroxide can be considered as an efficient, convenient, fast and easy to perform dissolution procedure to produce whole blood sample solutions amenable to analysis by ET AAS. Treatment of whole blood samples as proposed in this paper renders clear solutions, without heating, with no apparent suspended particles and no greasy layers, in approximately 3 min. The procedure effectively decomposes the whole blood matrix allowing for analysis using comparison with aqueous calibration graphs.

Acknowledgments

This research was carried out with the financial support of the Fondo Nacional de Ciencia, Innovación y Tecnología, FONACIT, de la República Bolivariana de Venezuela, through grant S1-2000000558.

Authors thank Lic. Ivelin Morales for dealing with the manuscript.

References

[1] World Health Organization, International Programme on Chemical Safety, Environmental Health Criteria 3, Geneva, 1977.
[2] J. Alvarado, R. Jaffe, H. Carrero, A. Cabrera, Water, Air Soil 71 (1992) 293–313.
[3] M. Ikeda, Z. Zhang, S. Shimbo, T. Watanabe, H. Nakatsuka, C. Moon, N. Matsuda-Inoguchi, K. Higashikawa, Sci. Total Environ. 249 (2000) 373–384.
[4] C. Marvelias, S. Athansaleis, A. Dona, C. Priftis, A. Chatzioanou, A. Koutselinis, Arch. Environ. Health 6 (53) (1998) 424–426.
[5] P.C. Kao, I. Schloegel, R. Cyr, Y.S. Leung, K. Dees, Clin. Chem. 7 (43) (1997) 1251–1252.
[6] H.T. Delves, Analyst 95 (1970) 431–438.
[7] C.C. Yen, W.K. Chen, C.C. Hu, B.L. Wei, C. Chung, S.S. Kuo, At. Spectrosc. 18 (1997) 64–69.
[8] K.S. Subramanian, At. Spectrosc. 8 (1981) 7–11.
[9] Y. Zhou, P.J. Parsons, K.M. Aldous, P. Brockman, W. Slavin, J. Anal. At. Spectrom. 16 (2001) 82–89.
[10] M. Trzcinka-Ochocka, G. Razniewska, M. Jakubowki, Trace Elem. Electrolyt. 3 (2000) 147–153.
[11] E. Ramirez, C. Sanchez, R. Pajuelo, Ciencia e Investigación 5 (2002) 34–37.
[12] A. Prange, H. Böddeker, W. Michaelis, Fresenius Z. Anal. Chem. 335 (1989) 914–918.
[13] H. Matusiewicz, R. Sturgeon, S. Berman, J. Anal. At. Spectrom. 4 (1989) 323–327.

Available online at www.sciencedirect.com
ScienceDirect
Talanta 73 (2007) 948–952
Talanta
www.elsevier.com/locate/talanta

Removal of interferences in the speciation of chromium using an octopole reaction system in ion chromatography with inductively coupled plasma mass spectrometry

ZuLiang Chen [a,*], Mallavarapu Megharaj [a], Ravendra Naidu [a,b]

[a] *Centre for Environmental Risk Assessment and Remediation, University of South Australia, Mawson Lakes, SA 5095, Australia*
[b] *Cooperative Research Centre for Contamination Assessment and Remediation of Environments, Mawson Lakes Boulevard, Mawson Lakes, SA 5095, Australia*

Received 12 March 2007; received in revised form 14 May 2007; accepted 15 May 2007
Available online 24 May 2007

Abstract

When inductively coupled plasma mass spectrometry (ICP-MS) is used for the detection of ^{52}Cr (83.8%) species in ion chromatography (IC), interference from polyatomic ions such as $^{40}Ar^{12}C^{+}$ and $^{35}Cl^{16}O^{1}H^{+}$, often occurs due to their mass at *m*/*z* 52. To address the issue, an octopole reaction system (ORS) in ICP-MS, including He and H_2 modes, was used to determine whether the background and interference from polyatomic ions could be reduced in the detection of ^{52}Cr. Compared to standard mode, the polyatomic ions were reduced by either He or H_2; for example, more than 97 and 98% of ^{35}Cl was removed using a He and H_2 tune, respectively. However, the detection sensitivity for ^{52}Cr was decreased, for example, the sensitivity was 27.95 and 67.02% of the standard mode for $Cr(EDTA)_2^{-}$ using a He and H_2 tune, respectively. The H_2 tune is recommended for the detection of ^{52}Cr at a flow rate of 2.0 mL/min with detection limits in the range of 0.2–0.4 μg/L. The developed method was used to measure chromium speciation in waters containing high concentration of chloride.

Keywords: Chromium speciation; Collision reaction cell; IC–ICPMS; Contaminated water

1. Introduction

High performance liquid chromatography (HPLC) combined with inductively coupled plasma mass spectrometry (ICP-MS) is often used for speciation analysis since ICP-MS offers high selectivity and sensitivity [1,2]. HPLC is a convenient technique for simultaneous separation of Cr(III) and Cr(VI) species [3]. Various HPLC separation modes, including reversed-phase chromatography (RPC) [4,5], ion chromatography (IC) [6–11], ion-pairing liquid chromatography (IPLC) [12] have been used for the separation of chromium species, and detected by ICP-MS for quantization. These methods are useful for chromium speciation analysis.

As ^{52}Cr is more abundant (83.8%), it is the isotope preferentially analysed by ICP-MS to give the highest sensitivity. However, when matrices containing high levels of Cl or C are introduced into an ICP-MS, polyatomic ions such as $^{35}Cl^{16}OH^{+}$, $^{40}Ar^{12}C^{+}$ and $^{37}Cl^{14}NH^{+}$, are formed either in the plasma or in the reaction cell [13,14]. These polyatomic ions may significantly interfere with the detection of ^{52}Cr due to the ions having the same mass. To reduce such interferences, several approaches have been explored. One of the approaches is based on the separation of nitrogen, chlorine, sulfur, and carbon-based interferences from chromium species by chromatography prior to detection with ICP-MS [6,7], or using a high-resolution ICP-MS instrument to specifically attenuate the chloride-based interference [10]. Another approach is the development of a procedure based on a point-by-point mathematical correction along the chromatogram to overcome the polyatomic interferences in HPLC–ICP-MS. This approach was successfully used in speciation of chromium by size exclusion chromatography (SEC)–ICP-MS [15].

ICP-MS equipped with a reaction/collision cell has been developed as an alternative technique to remove polyatomic

* Corresponding author. Fax: +61 8 83023057.
E-mail address: zuliang.chen@unisa.edu.au (Z. Chen).

0039-9140/$ – see front matter © 2007 Elsevier B.V. All rights reserved.
doi:10.1016/j.talanta.2007.05.030

interferences [16,17]. In collision/reaction cell techniques, various gases can be efficiently employed to eliminate polyatomic ions. In the He cell mode, helium gas is introduced into the collision/reaction cell and can reduce or even eliminate polyatomic interferences by either collisionally induced dissociation (CID) or kinetic energy discrimination (KED). Both of these mechanisms are non-reactive and, therefore, no new polyatomic ionic species are formed [16,17]. In the H_2 reaction mode, the octopole reaction cell is pressurized using a small flow of pure hydrogen, which removes interfering polyatomic ions by chemical reaction with hydrogen [16,17] or other mechanism [18] even the mechanisms using H_2 tune has not been full understanding. Reactive gases that preferentially react with the polyatomic ions rather than with the elements of interest are selected. Thus, in the H_2 mode, ion–molecule reactions are employed to chemically remove interferences away from the targeted analyte mass. To date, there are a few reports on the use of a reaction/collision cell to reduce polyatomic interferences in HPLC–ICP-MS system for the detection of chromium. One report concerns the dynamic reaction cell (DRC) used in IPLC–ICP-MS, which has proven to be an effective technique to reduce such interferences in ICP-MS [12]. Polyatomic ions such as $^{35}Cl^{16}OH^+$, $^{40}Ar^{12}C^+$ and $^{37}Cl^{14}NH^+$ were reduced in intensity by approximately three orders of magnitude by using 0.65 mL/min NH_3 as a reaction cell gas for determining chromium speciation [12]. Recently, a collision/reaction cell system has been used to reduce chloride-based polyatomic ions interfering in high-performance chelation IC–ICP-MS, and this technique has successfully been used for the chromatographic analysis of samples in an incubation medium containing Cr(VI) incubated with cell nuclei [19].

Ion-exchange chromatography is often used for the separation of chromium species in most of the applications [6–11]. This paper presents an alternative technique for determining chromium speciation [20] using an octopole collision/reaction cell to reduce chloride based interference during chromium speciation after separation by anion-exchange chromatography. A comparison of chromium detection obtained using standard (no cell gas), He and H_2 modes is included and the developed technique was applied to the determination of chromium species in high chloride matrix samples.

2. Experimental

2.1. Chemicals and solutions

All chemicals used in this study were analytical grade reagents from Sigma and Aldrich (Sydney, Australia). Milli-Q water (18.2 MΩ/cm, Milli-Q Plus system, Millipore, Bedford, MA, USA) was used for preparing all solutions and standards. Standard solutions ($K_2Cr_2O_7$ and $CrCl_3{\cdot}6H_2O$) were prepared daily from 10 mM aqueous stock solutions. The complexation of Cr(III) with EDTA was achieved by adding the appropriate amounts of Cr(III), EDTA and water into 15 mL polypropylene tubes and heating the tubes in a water bath set at 80 °C for 20 min. IC–ICP-MS mobile phases were prepared by dissolution of the appropriate amount of ammonium salts in Milli-Q water, pH-adjusted with 0.1 M ammonium hydroxide, filtered through a disposable 0.45 μm cellulose acetate membrane filter (Millipore) and degassed in an ultrasonic bath prior to use. Chromium contaminated wastewater was also filtered through a 0.45 m membrane filter.

2.2. IC–ICP-MS conditions

An Agilent 1100 liquid chromatography module (Aglient, Tokyo, Japan) equipped with a guard column (G3154A/102) and a separation column (G3154A/101) were used, and it was based on a porous polymethacrylate resin with 10 μm particle size and had an exchange capacity of 50 μequiv./g. The column temperature was set at 30 °C. Samples were injected using an 1100 autosampler, with an injection volume of 50 μL. The mobile phase used for separation of chromium species was 20 mM NH_4NO_3 at pH 5.9; with a flow-rate set at 1.0 mL/min. The outlet of the separation column was connected directly to the Babington nebulizer of an Agilent 7500c ICP-MS by use of a 50 cm length of PEEK tubing. The conditions used for ICP-MS were: RF power 1450W, plasma gas (Ar) flow 15 L/min, auxiliary gas (Ar) flow 1.0 L/min, carrier gas (Ar) flow 1.15 L/min, sampling depth 7.5 mm, integration time 1 s and dwell time 0.5 s. The optimized flow rate for He and H_2 was 2.5 and 2.0 mL/min, respectively. The parameters for cell analyser were set as octopoole bias at −15 V, cell exit lens at −18 V, quadrupole entrance lens at −40 and quadrupole at −20 V. Chromium was detected at m/z 52. The IC–ICP-MS system was controlled and data processed using Agilent's Chemstation software package.

3. Results and discussion

3.1. ICP-MS detection

Since radio frequency (RF) forward power and carrier gas flow rate are usually the most significant parameters affecting the background and analytical signals in standard tune (without adding gas), these parameters were adjusted to obtain an optimal signal to noise ratio. In a preliminary study, 20 mM NH_4NO_3 (pH 5.9) test solutions spiked with 10 μg/L Cr, were aspirated into the nebulizer and then into the plasma. The intensities of the blank and spike solution increased with increasing carrier gas flow rate in the range 1.1–1.25 L/min, and they also increased with increasing RF power in the range 1300–1500 W. The best conditions using direct detection of ^{52}Cr were forward power of 1450 W and carrier gas flow rate of 1.15 L/min.

In addition, the flow rate of He or H_2 into the collision/reaction cell also affected the background and analytical samples. Therefore, the reaction gas flow rate was varied from 0 to 5 mL/min, and the background and ^{52}Cr signal were subsequently monitored. When He was added to the collision cell, an increase in He flow rate produced a decrease in ^{52}Cr and background signals. The desired reduction of the interference by either collision induced dissociation (CID) or kinetic energy discrimination (KED) was significant, with the maximum difference between ^{52}Cr and background observed at a He flow rate of 2.5 mL/min. An increase in H_2 flow rate, also used as a reac-

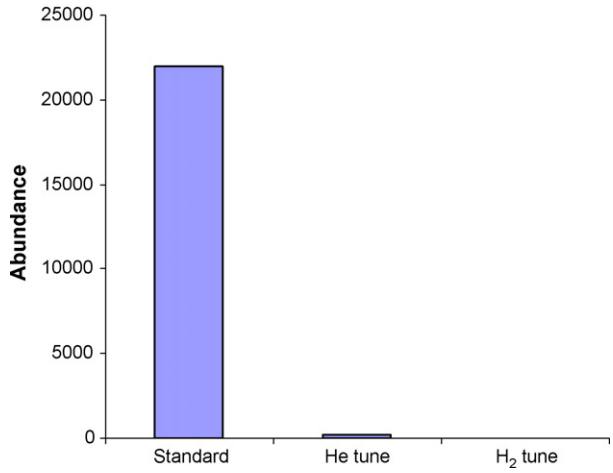

Fig. 1. Comparison of the background signal obtained from three tunes.

tion gas, was found to reduce the background and ^{52}Cr signals. However, a more pronounced decrease in the background signal relative to the ^{52}Cr signal was observed for H_2. A maximum difference between background and ^{52}Cr signals was obtained when H_2 flow rate was 2.0 mL/min, which yielded an acceptable detection limit of 0.2 μg/L.

As shown in Fig. 1, compared with the standard tune the background signal was significantly reduced using either a He or H_2 tune, with the background intensity (abundance) reduced to 0.81 and 0.22% using He (2.5 mL/min) and H_2 (2.0 mL/min), respectively. This was due to polyatomic ions $^{35}Cl^{16}OH^+$, $^{40}Ar^{12}C^+$ and $^{37}Cl^{14}NH^+$ were removed in the collision/reaction cell. It is concluded that an octopole system in ICP-MS is a viable alternative to remove polyatomic interferences for ICP-MS detection of ^{52}Cr.

3.2. Evaluation of three tunes to remove the interferences

Fig. 2 shows the chromatograms obtained using IC–ICP-MS with standard (no gas), H_2 and He tunes when a mixture of 1000 mg/L Cl^- and 100 μg/L $[Cr(EDTA)]^-$ and Cr(VI) was injected into the IC–ICP-MS system. Separation of the chromium species and chloride ions was preformed on an anion-exchange column with a mobile phase containing 20 mM NH_4NO_3 (pH 5.9). The sensitivity for the detection of ^{52}Cr, as indicated by the counts obtained, decreased in the order: standard > H_2 > He. This indicates that the introduction of H_2 or He gas to the cell decreased the sensitivity, while the standard tune gave greatest sensitivity. When normalised to the standard tune, the relative sensitivity expressed as a percent was in the order of standard $[Cr(EDTA)]^-$, 100%; Cr(VI), 100%] > H_2 ($Cr[EDTA]^-$, 67.02%; Cr(VI), 63.17%) > He ($Cr[EDTA]^{1-}$, 27.95%; Cr(VI), 26.95%). The background noise decreased in the order: standard > He > H_2. The removal or reduction of $^{40}Ar^{12}C^+$, $^{35}Cl^{16}OH^+$ and $^{37}Cl^{14}NH^+$ from plasma source can be contributed to a number of different mechanisms. For example, in hydrogen reaction mode, various mechanism could be involved to remove the polyatomic ions using H_2 tune [16–18], while helium collision mode can reduce or eliminate polyatomic interferences by one of two mechanisms such as either CID or KED [16,17].

In addition, as shown in Fig. 3, Cl^- was reduced by 98.8% relative to the standard tune, when H_2 was added to the reaction cell, while the use of He only reduced about 97.2% of the Cl^- relative to the standard tune. This was most likely due to the fact that hydrogen reacts with $[ClOH]^+$ (m/z 52) to form $[ClOH_2]^+$ (m/z 53) with the loss of water [14,15]. As a result, a lower Cl^- signal was observed, due to H_2 reacting with polyatomic interferences containing Cl^- [16,17]. In contrast, a higher Cl^- signal, relative to hydrogen, was obtained when He was used as a collision gas because of its non-reactive mechanisms for eliminating polyatomic interferences [16,17]. On this basis, we conclude

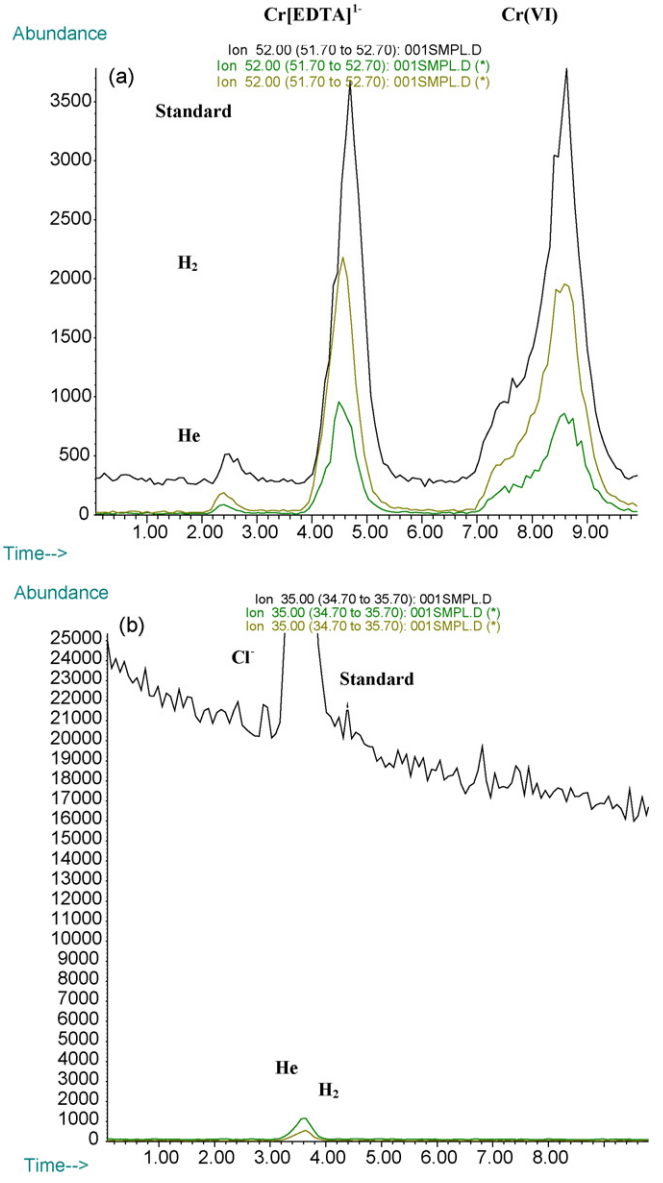

Fig. 2. Comparison of standard (nor reaction gas), He (2.5 mL/min) and H_2 (2.0 mL/min) tunes for the detection of chromium (a) and Cl^- (b). A mixture containing 1000 mg/L Cl^- and 100 μg/L $[Cr(EDTA)]^{1-}$ and Cr(VI); mobile phase: 20 mM NH_4NO_3 at pH 5.9.

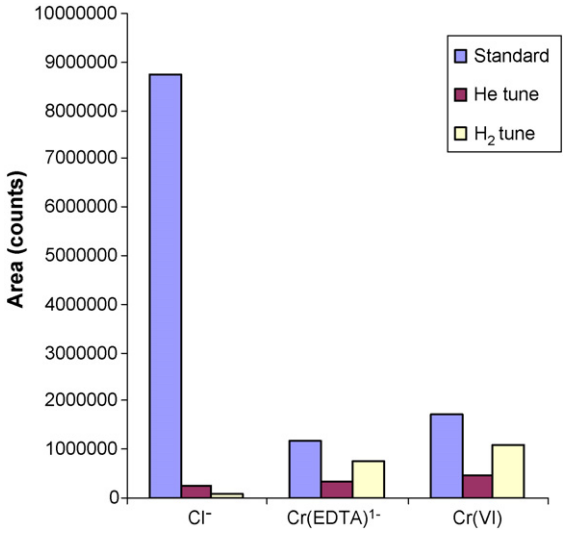

Fig. 3. Comparison of three tunes to remove the polyatomic ions based on chloride, and the effecting of three tunes on the sensitivity for the chromium species.

that Cl^- matrix interferences can be significantly reduced by using H_2 as a reaction gas, with some associated loss of the ^{52}Cr signal, it could be resulted in the H_2 reacting with Cr and consequently reduced Cr signal [16,17]. Fig. 4 clearly exhibits the comparison of three tunes used for the detection of ^{52}Cr in matrices containing high concentrations of Cl^-, and for the reducing the polyatomic interferences based on chloride. For this reason, the H_2 or He reaction technique has recently been used for the determination of trace elements in matrices containing high Cl^- matrix such as sea water [21] and food [22].

3.3. Analysis of real samples

The proposed method was used to detect chromium species in real samples. The chromatogram shown in Fig. 4 is a typical example where the sample contained a high concentration of Cl^- (1425 mg/L). A higher background and noise level, as well as a large Cl^- peak, were obtained using a standard tune (Fig. 4). In addition, a larger Cl^- peak overlapped with $Cr[EDTA]_2^-$, and, consequently, it interfered with the detection of $Cr[EDTA]_2^-$. In contrast, Fig. 4 (b) shows that a chromatogram obtained using a H_2 tune, has a significantly reduced background, noise and Cl^- peaks. Also, Cl^- did not interfere with the detection of $Cr[EDTA]_2^-$ since there is little overlap between the peaks. However, detection sensitivity was lost in this case. The chromium contaminated water was found to contain Cr(III) = 22.2 ± 1.3 μg/L (n = 3) and Cr(VI) = 31.69 ± 1.8 μg/L (n = 3).

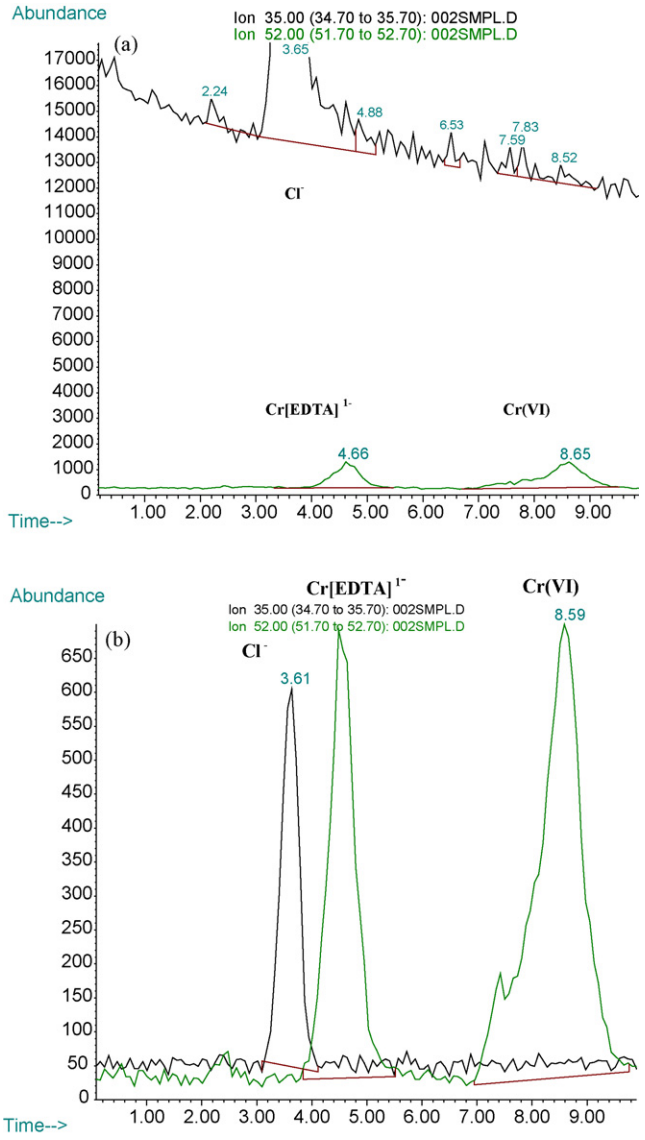

Fig. 4. Typical chromatograms obtained from chromium contaminated water samples with high Cl concentrations (a) standard tune mode (b) H_2 tune mode. Others conditions as in Fig. 2.

Calibration curves for quantification were obtained by plotting peak area versus the concentration of the corresponding target anion. All calibrations were linear over a concentration range of 1–500 μg/L, with correlation coefficients greater than 0.999 when 20 μg/L standards were injected. Detection limits (S/N = 3) ranged from 0.2 to 0.4 μg/L. The reproducibility from injection of a 20 μg/L standard solution containing a mixture of $[Cr(EDTA)]^{1-}$ and Cr(VI) (n = 5) showed that the RSD was <2.8%. In order to test the applicability of the method for the

Table 1
The analytical characteristics for chromium species using the proposed method

Species (μg/L)	LDR (μg/L)	Coefficient	DL (μg/L)	RSD (n = 5)	Lake water (spiked with 20 μg/L, n = 5, %)	Seawater (spiked with 20 μg/L, n = 5, %)
Cr(III)	1.0–500	1.000	0.3	1.9	98.5 ± 2.3	92.3 ± 3.2
Cr(VI)	1.0–500	0.999	0.4	2.8	94.5 ± 2.7	91.1 ± 2.9

DL = detection limit (signal/noise = 3), LDR = linear dynamic range, and RSD = relative standard deviation.

Table 2
The data from different methods

Species	The propose method		The previous method	
	Lake water (20 μg/L, $n=5$, %)	Seawater (20 μg/L, $n=5$, %)	Lake water (20 μg/L, $n=5$, %)	Seawater (20 μg/L, $n=5$, %)
Cr(III)	19.70 ± 0.05	18.46 ± 0.06	19.84 ± 0.04	18.92 ± 0.05
Cr(VI)	18.90 ± 0.05	18.22 ± 0.05	19.42 ± 0.04	19.01 ± 0.05

Cr speciation, lake water samples were spiked with a mixture of 20 μg/L mixed standards, and recoveries for $[Cr(EDTA)]^{1-}$ and Cr(VI) were 98.5 ± 2.3% and 94.5 ± 2.7% ($n=5$), respectively. In addition, the seawater diluted with 10-fold and spiked with 20 μg/L $[Cr(EDTA)]^{1-}$ and Cr(V) were further tested, Cr(VI) were 92.3 ± 3.2% and 91.1 ± 2.9% ($n=5$), respectively, because of the seawater containing a higher concentration of chloride as listed in Table 1. Furthermore, the concentration of Cr(III) and Cr(V) in the lake water and seawater spiked with 20 μg/L were validated using previous method [20], and the data was in agreement with that obtained from the proposed method as listed Table 2.

4. Conclusion

An octopole reaction system can be used to reduce interference by polyatomic ions, formed from Cl^-, for the detection of ^{52}Cr by either a He or H_2 tune. However, the H_2 tune was more efficient in eliminating the polyatomic ions. Also, background noise was significantly reduced using an octopole reaction system compared to the background noise obtained from a standard tune. The separation of chromium species was performed within 10 min and the proposed method was demonstrated for the separation and detection of chromium species by IC–ICP-MS.

References

[1] M. Montes-Bayon, K. DeNicola, J.A. Caruso, J. Chromatogr. A 1000 (2003) 457–476.
[2] B. Michalke, Trends Anal. Chem. 21 (2002) 142–153.
[3] C. Sarzanini, M.C. Bruzzoniti, Trends Anal. Chem. 20 (2001) 304–310.
[4] G.K. Zooro, J.A. Caruso, J. Chroamtogr. A 773 (1997) 157–162.
[5] C.M. Andrle, K. Jakubowski, J.A.C. Broekaert, Spectrochim. Acta B 52 (1997) 189–200.
[6] I. Inoue, T. Sakai, H. Kumagai, J. Chroamtogr. A 706 (1997) 127–136.
[7] M. Pantsarkallio, P.K.G. Manine, J. Chroamtogr. A 750 (1996) 88–95.
[8] F.A. Byrdy, L.L. Olson, N.P. Vela, J.A. Caruson, J. Chroamtogr. A 712 (1995) 311–320.
[9] C. Barnowski, N. Jakubowski, D. Stuewer, J.A.C. Broekaert, J. Anal. Atom. Spectrom. 12 (1997) 1155–1161.
[10] F. Vanhaecke, S. Saverwybs, G. De Wannemacker, L. Moens, R. Dams, Anal. Chim. Acta 419 (2000) 55–64.
[11] H. Gurleyuk, D. Wallschlager, J. Anal. Atom. Spectrom. 16 (2001) 926–930.
[12] Y.L. Chang, S.J. Jiang, J. Anal. Atom. Spectrom. 16 (2001) 858–862.
[13] N. Yamada, J. Takahashi, K. Sakata, J. Anal. Atom. Spectrom. 17 (2002) 1213–1222.
[14] M.A. Dexter, H.J. Reid, B. Sharp, J. Anal. Atom. Spectrom. 17 (2002) 676–681.
[15] F. Laborda, M.P. Gorriz, E. Bolea, J.R. Castillo, Spectrochim. Acta B 61 (2006) 433–437.
[16] S.D. Tanner, V.I. Baranov, D.R. Bandura, Spectrochim. Acta B 57 (2002) 1361–1452.
[17] E. McCurdy, G. Woods, J. Anal. Atom. Spectrom. 19 (2004) 607–615.
[18] V. Chrastny, M. Komarek, M. Mihaljevic, J. Stichvo, Anal. Bioanal. Chem. 385 (2006) 962–970.
[19] A.P. Vonderheide, J. Meija, K. Tepperman, A. Puga, A.R. Pinhas, J.C. States, J.A. Caruso, J. Chroamtogr. A 1024 (2004) 129–137.
[20] Z.L. Chen, M. Megharaj, R. Naid, Talanta 72 (2007) 394–400.
[21] P. Leonhard, R. Pepelnik, A. Prange, N. Yamada, T. Yamada, J. Anal. Atom. Spectrom. 17 (2002) 189–196.
[22] V. Dufailly, L. Noel, T. Guerin, Anal. Chim. Acta 565 (2006) 214–221.

Available online at www.sciencedirect.com
ScienceDirect
Talanta 73 (2007) 899–905
Talanta
www.elsevier.com/locate/talanta

Use of CdSe/ZnS core-shell quantum dots as energy transfer donors in sensing glucose

Hong Dinh Duong, Jong Il Rhee *

Department of Material and Biochemical Engineering, School of Applied Chemical Engineering, Research Center for Biophotonics, Chonnam National University, Yong-Bong dong 300, 500-757 Gwangju, Republic of Korea

Received 6 April 2007; received in revised form 3 May 2007; accepted 9 May 2007
Available online 18 May 2007

Abstract

In the present work, CdSe/ZnS core-shell quantum dots were synthesized and conjugated with enzymes, glucose oxidase (GOD) and horseradish peroxidase (HRP). The complex of enzyme-conjugated QDs was used as QD-FRET-based probes to sense glucose. The QDs were used as an electron donor, whereas GOD and HRP were used as acceptors for the oxidation/reduction reactions involved in oxidizing glucose to gluconic acid. Electron transfer between the redox enzymes and the electrochemical reduction of H_2O_2 (or O_2) occurred rapidly, resulting in an increase of the turnover rate of the electron exchange between the substrates (e.g. glucose, H_2O_2 and O_2) and the enzymes (GOD, HRP), as well as between the QDs and the enzymes. The transfer of non-radiative energy from the QDs to the enzymes resulted in the fluorescence quenching of the QDs, corresponding to the increase in the concentration of glucose. The linear detection ranges of glucose concentrations were 0–5.0 g/l ($R = 0.992$) for the volume ratios of 10/5/5, 0.2–5.0 g/l ($R = 0.985$) for the volume ratios of 10/5/3 and 1.0–5.0 g/l ($R = 0.982$) for the volume ratios of 10/5/0. Temperature (29–37 °C), pH (6–10) and some ions (NH_4^+, NO_3^-, Na^+, Cl^-) had no interference effect on the glucose measurement.

Keywords: Glucose detection; Glucose oxidase; Horseradish peroxidase; Quantum dots; CdSe/ZnS

1. Introduction

Semiconductor nanoparticle quantum dots (QDs) are luminescent inorganic fluorophores that can be excited for multicolor emission with a single light source [1]. They are attractive in the area of biosensors due to their long-term photostability, allowing real-time and continuous monitoring. However, the application of QDs in this field is still limited because the photoluminescence quantum yield of the QDs decreases significantly when they are transformed from the hydrophobic to hydrophilic form or when they are conjugated with other materials. Recently, scientists have concentrated on developing sensors for some target analytes, wherein QDs are used as electron donors for fluorescence resonance energy transfer (FRET) between the QDs (donor) and an acceptor molecule [2–7]. Besides FRET, many advantageous properties of QDs have been exploited for the development of sensors based on the change in the emission wavelength [8], voltage [9] or fluorescence intensity [10,11].

Glucose is an important nutrient source for microorganisms in biotechnological processes. The measurement of glucose concentrations is always useful in controlling various food and biotechnological processes, as well as in diagnosing many metabolic disorders, especially in the diagnosis and therapy of diabetes. Many methods have been used for the detection of glucose, such as amperometric [12,13], spectrophotometric [14], fluorometric methods [15,16], but none of the methods developed so far have used QDs for glucose detection.

In this study we describe the use of hydrophilic CdSe/ZnS core-shell QDs to sense glucose. The fluorescence quenching of the QDs was used to measure the concentrations of glucose in aqueous solution. The quenching process was based on the transfer of electrons from the QDs to enzymes (glucose oxidase (GOD), peroxidase (HRP)), which catalyze the oxidation/reduction reactions of glucose and all of the components involved in the process. The QDs were able to be used to detect glucose by introducing them directly into the glucose solution

* Corresponding author. Tel.: +82 62 530 1847; fax: +82 62 530 0846.
E-mail address: jirhee@chonnam.ac.kr (J.I. Rhee).

0039-9140/$ – see front matter © 2007 Elsevier B.V. All rights reserved.
doi:10.1016/j.talanta.2007.05.011

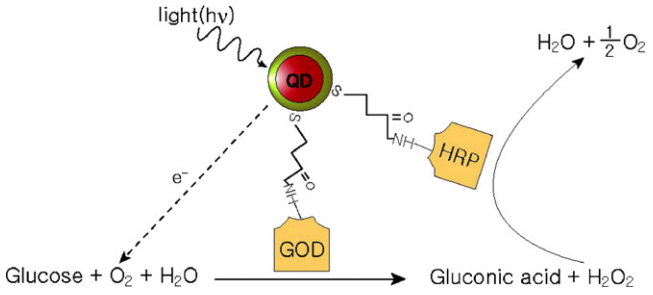

Fig. 1. Reaction scheme of glucose oxidation to gluconic acid using GOD/HRP conjugated to CdSe/ZnS quantum dots (QDs).

after their conjugation with the enzymes (Fig. 1). The more glucose was added the more fluorescence quenching of the QDs was observed.

2. Materials and methods

2.1. Materials

Cadmium acetate, selenium, zinc acetate, hexamethyldisilathiane ($(TMS)_2S$), trioctylphosphine oxide (TOPO), trioctylphosphine (TOP), mercaptopropionic acid (MPA), 4-dimethylamino pyridine (DMAP), 1-hexadecylamine, (stearic?) acid, glucose oxidase (GOD), horseradish peroxidase (HRP) and ABTS (diammonium 2,2′-azino-bis(3-ethylbenzothiazoline-6-sulfonate)) were purchased from Sigma–Aldrich Chemical Co.(Seoul, Korea). *N*,*N*-dimethylformamide (DMF), methanol, and chloroform were obtained from Honeywell International Inc./Burdick & Jackson (USA). All other chemicals, such as sodium phosphate, sodium chloride, etc., used for the preparation of the phosphate buffer saline were of analytical grade and used without further purification.

2.2. Synthesis of CdSe/ZnS core-shell quantum dots (QDs)

The synthesis of the CdSe/ZnS core-shell QDs was based on a modified version of the existing methods. Firstly, CdSe nanoparticles were synthesized using a modified version of the methods of Qu and Peng [17] and Gaunt et al. [18]. Cadmium acetate dehydrate (0.6 mM, 147 mg) and stearic acid (2.13 mM, 607 mg) were loaded into a 50 ml three-neck flask and heated to 150 °C under vacuum conditions until a colorless liquid was obtained. Hexadecylamine (1.94 g) and TOPO (2.2 g) were added to the flask after cooling to room temperature. The mixture was then degassed with a pump and heated to 120–150 °C under vacuum. The reaction vessel was then filled with nitrogen gas and heated to 310–320 °C and, at this point, a solution of selenium (211 mg) in TOP (2.5 ml) was rapidly injected into the vigorously stirred reaction mixture. The solution was heated for 25 s before removing the flask from the heating mantle and then allowing it to cool to room temperature. The resulting CdSe nanoparticles were purified by dissolving the reaction mixture in chloroform, followed by precipitation with an equal volume of methanol. In the next step, these purified CdSe particles were used to synthesize the CdSe/ZnS core-shell QDs (CZ-QDs). A mixture of hexadecylamine (2 g) and TOPO (2.5 g) were loaded into a 50 ml three-neck flask and then degassed and heated to 180 °C. At 180 °C, the purified CdSe particles dispersed in 2.0 ml chloroform were added to this solution. After the chloroform was completely pumped out, the flask was filled with nitrogen gas. The temperature of the reaction was then increased to 180–185 °C. A mixture of zinc acetate (54 mg) and $(TMS)_2S$ (0.05 ml) dissolved in 1.0 ml TOP was then injected dropwise for 5–10 min. After the injection, the mixture was stirred for 1 h at 180–185 °C.

2.3. Synthesis of hydrophilic surfactant capped CdSe/ZnS core-shell QDs

The synthesized CZ-QDs were coated with MPA using a slightly modified version of the protocols reported in the literature [19–21]. Two hundred milligrams of CZ-QDs in TOP-TOPO-hexadecylamine were purified by dissolution and precipitation in anhydrous chloroform and methanol, respectively. The wet precipitate was then dispersed in a mixture of 2 ml of DMF and 0.25 ml of 3-mercaptopropionic acid. The mixture was sonicated for about 30 min until it became transparent and then stored for 1 week at room temperature. In the next step, 0.5–0.7 ml of DMAP dissolved in DMF was added (50 mg DMAP/1.0 ml DMF) and the solution centrifuged for 30 min at 5000 rpm. The supernatant was discarded, while the precipitate was dried in a desiccator and then dissolved in 10 mM phosphate buffer saline. The resultant MPA-coated CdSe/ZnS core-shell QDs (MPA-QDs) were used for glucose sensing.

2.4. Optical characterization of QDs and their bioconjugation

The absorption and emission spectra of CdSe nanoparticles, MPA-QDs and enzyme-conjugated MPA-QDs were determined using a Multiskan Spectrum (Thermo electron corporation, Finland) and Fluorescence Spectrophotometer (Model: F-4500, Hitachi Co., Japan), respectively. A fixed amount of enzymes was mixed with different volumes of MPA-QDs or a given volume of the MPA-QDs was added to various amounts of the enzymes. The evaluation of their conjugation and interactions was performed after 3–24 h of incubation. The conjugation of the MPA-QDs and enzymes was also determined by gel electrophoresis (2% agarose). A voltage of 100 V was applied along the gel for 1 h. The enzyme activity of the GOD-conjugated or -unconjugated MPA-QDs was determined using ABTS as a peroxidase substrate in the presence of 0.5 g/l glucose. This substrate produces a soluble end product that is green in color and can be read spectrophotometrically at 405 nm. A microtiter plate reader (Wallac Victor 2, Perkin-Elmer Co., USA) was used for measuring the absorbance.

$$H_2O_2 + \text{reduced ABTS}\cdots(\text{HRP}) \rightarrow H_2O + 0.5O_2 + \text{oxidized ABTS}$$

2.5. Measurement of glucose concentrations

Glucose was also measured using a mixture of MPA-QDs, GOD and HRP. The enzymes (GOD, HRP) and MPA-QDs were added to the wells which included 100 μl of various concentrations of glucose solution. Mixtures of the MPA-QDs, GOD and HRP at ratios of 10:10:10, 10:5:5, 10:5:3, and 10:5:0 (μl/well) were used. The microtiter plate was then immediately inserted into the measurement chamber of the plate reader (Wallac Victor 2, Perkin-Elmer Co., USA), and the fluorescence intensity at an excitation/emission wavelength of 485/525 nm was measured 40 times at 3 min intervals.

2.6. Effects of pH and temperature

The effects of pH and temperature on the glucose sensing were investigated by using a mixture of GOD, HRP and MPA-QDs. The universal buffer used in this work contained 0.1 M Na_2SO_4, 0.04 M NaOAc, 0.04 M H_3BO_3, and 0.04 M NaH_2PO_4, whose pH was adjusted with 3N NaOH and 3 M HCl, and measured using a pH meter (Metrohm Co., Switzerland) to obtain the pH range of 4.0–11.0. A 100 μl of 1 g/l glucose solution prepared in universal buffer at a given pH and 20 μl of the mixture of GOD, HRP and MPA-QDs (volume ratio of QDs/GOD/HRP: 10/5 μl (10^4 U GOD)/5 μl(10^3 U HRP)) were introduced into a well and then the fluorescence intensity was measured. To investigate the interference effect of temperature on the measurements, 120 μl of the reaction mixture solution at a glucose concentration of 1.0 g/l in the well was incubated at temperatures between 23 and 37 °C, and the fluorescence intensity was then measured at an excitation/emission wavelength of 485/525 nm.

2.7. Interference study

The concentration range of the various ions (NH_4^+, NO_3^-, Na^+, Cl^-, CO_3^{2-}, Fe^{3+}) tested in this work was from 0.01 to 200 mM. A 100 μl of the ion solution was added to a well of a microtiter plate and mixed with 10 g/l glucose to obtain a final glucose concentration of 1 g/l. Each solution of ions at the different concentrations was prepared on a microtiter plate in the form of a duplicate and control sample (without any ions) as well. Thereafter, 20 μl of the MPA-QDs were introduced into each well containing 1 g/l glucose solution at different ion concentrations, and the fluorescence intensity was then measured. Afterwards, the enzyme mixture (GOD/HRP: 30/3 U, respectively) was added to these samples and their fluorescence intensity was measured for the second time. The difference in the fluorescence intensity of the samples and control sample before and after adding the enzymes was statistically assessed by one-way analysis of variance (ANOVA) using Instat software [25].

3. Results and discussion

3.1. Optical characteristics of QDs

The CdSe/ZnS core-shell QDs synthesized herein had a high fluorescence intensity with a quantum yield (QY) of 64% (QY calculation based on the theory of Sondy et al. [22]) and their particle size ranged from 2 to 4.5 nm (from the TEM analysis). Fig. 2(a) shows the absorption spectra of the QDs, i.e. the CdSe particles, CZ-QDs and MPA-QDs. Their broad absorption spectra allows for the efficient excitation of multiple QD-based fluorophores with a single light source. That is, easy tuning with the excitation filter of a microplate reader or excitation at a short wavelength that does not directly excite the acceptor are possible. In Fig. 2(b), the emission wavelength of the QDs (e.g. MPA-QDs) was 590 nm with a FWHM (full width at half maximum of the emission spectrum) of 40 nm, which overlapped with the absorption band of GOD and HRP (Fig. 2(c)). This interesting property was exploited in order to utilize the QDs for glucose sensing via the electron transfer from the QDs to the enzymes. The quantum yield of the QDs after covering the carboxyl groups (MPA) on their surface was decreased to about 50% of its initial value.

In the 2D fluorescence spectra of the mixture of MPA-QDs and enzymes (HRP and GOD) in solution (data not shown), it was observed that the fluorescence intensity of the enzymes changed in the excitation wavelength range of 260–320/445 nm and in the emission wavelength range of 280–450/525 nm, while the QDs changed in the fluorescence intensity range of 280–550 nm for excitation and 580–610 nm for emission. That is, the fluorescence intensities of the QDs and enzymes are changed by their conjugation and interaction, their activities and the amount of each component involved.

The clear binding of the QDs and enzymes was observed in the photo images of Fig. 3. The amine groups of the enzymes are easily bound to the carboxyl groups on the surface of the QDs, even though no carbodiimide was used as a coupling agent. The sizes of the QD increased after their conjugation with the enzymes, and increasing the amount of GOD resulted in an increase in the amount of the enzymes bound to the binding sites of the QD surface (photo image of Fig. 3(a)). Their movement in the gel plate was slower than that of the enzyme-conjugated MPA-QDs (Enz-QDs) containing a lesser amount of enzymes and, therefore, their migration distances in the gel were slightly shorter than those of the MPA-QDs containing a smaller amount of GOD. The same tendency was observed when increasing the QD concentrations, which were mixed with a given amount of enzymes (photo image of Fig. 3(b)), in which more quantum dots were conjugated with the enzymes and their movement was slower. In the photos, the bands of the QDs were not clear, perhaps because the aggregation of the QDs under basic conditions leads to only a small amount of the QDs moving to the positive pole. Increasing or decreasing the amounts of enzymes or QDs leads to a change in the fluorescence intensity of both the enzymes and QDs. Fig. 3(a) also shows the fluorophore quenching of the QDs at an emission wavelength of 590 nm when the amount of GOD is increased. As mentioned above, the enzymes were able to receive energy from the excited QDs, resulting in an increase in their fluorescence intensity. An increase in the fluorescence intensity of the enzymes was also observed at an emission wavelength of 525 nm. This is associated with the increase in the amount of enzymes and the fluorescence resonance energy transfer (FRET) from the QDs to

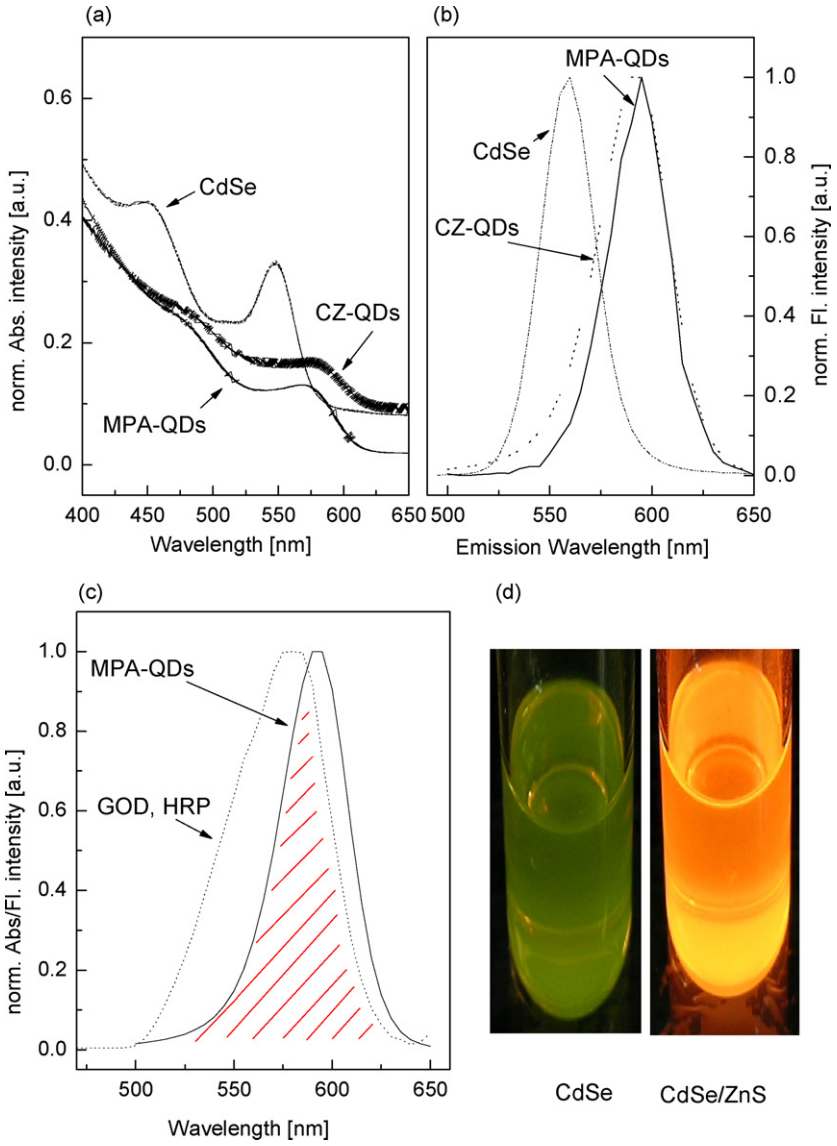

Fig. 2. (a) Absorption spectra of quantum dots, CdSe (550 nm), CZ-QDs (580 nm), and MPA-QDs (580 nm); (b) emission spectra of QDs, i.e. CdSe (560 nm), CZ-QDs (590 nm), and MPA-QDs (590 nm) at excitation wavelength of 480 nm; (c) overlap of absorption and emission spectra of the enzymes (GOD, HRP) and QDs; (d) image of CdSe (left) and CdSe/ZnS (right) under UV light.

the enzymes. The FRET is also shown in Fig. 3(b), since the use of a given amount of GOD conjugated with different concentrations of QDs resulted in an increase in the fluorescence intensity of the enzymes and a decrease in the fluorescence intensity of the QDs, as compared with the enzyme conjugated QDs.

3.2. *Effects of MPA-QDs on enzyme activity*

GOD, a structurally rigid glycoprotein of 160,000 Da, has a hydrodynamic radius of about 43 Å and consists of two identical polypeptide chains. The rigidity and ruggedness of GOD are derived in part from the polysaccharide that forms its outer hydrophilic envelope [23]. Provided the electrons are transferred between the redox enzyme and the electrochemically reduced form of H_2O_2, which is generated upon the O_2-biocatalyzed oxidation of the glucose, the turnover rate of the electron exchange between the substrates (e.g. glucose, H_2O_2, O_2) and the biocatalyst (GOD and HRP), as well as between the QDs and enzymes, is rapidly increased. Hence, the transduced physical energy of the QDs associated with the quenched fluorophores reflects the substrate concentration in the system.

As shown in Fig. 4, the fluorescence emission of the enzymes and their activities were considerably changed after their conjugation with the MPA-QDs. After the incubation of GOD and HRP with the MPA-QDs for 3 or 12 h, the fluorescence intensity at 445 nm (ex)/525 nm (em) increased to about 30 or 43% of its original value, respectively. In the case where only GOD was incubated with the MPA-QDs for 3 or 12 h, the fluorescence intensity of GOD decreased rapidly to 20 or 41% of its original value, respectively. This means that the functional groups on the MPA-QD surface inhibited the enzyme activities, whereas those enzymes which retained their activity received a large amount of energy from the excited QDs, leading to their fluorescence emission being stronger than that of the intact enzymes. In addition,

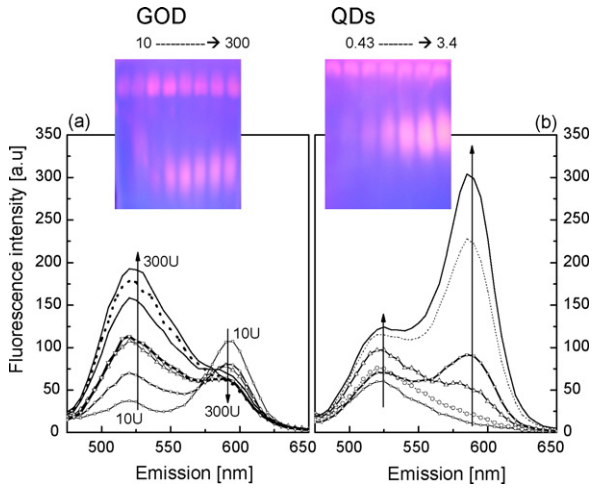

Fig. 3. (a) Photo image of gel electrophoresis (2% agarose) for Enz-QDs containing different amounts of GOD (GOD = 10, 50, 100, 150, 200, 250 and 300 U, increase of GOD amount from left to right) and their emission spectra with a fixed amount of QDs (3.145 mg/ml) and HRP (10 U) at an excitation wavelength of 445 nm in 0.5 g/l glucose solution, (b) photo image of gel electrophoresis (2% agarose) of Enz-QDs at different concentrations of QDs (QD = 0.4309, 0.8622, 1.7254, 2.5872 and 3.445 mg/ml, increase of QDs amount from left to right) and their emission spectra with a fixed amount of GOD (200 U) and HRP (10 U) at an excitation wavelength of 445 nm in 0.5 g/l glucose solution.

the fluorescence emission of the MPA-QDs was decreased after a long period of incubation (data not shown).

3.3. Effects of pH and temperature

As shown in Fig. 5, the temperature and pH had only a slight effect on the glucose measurement. The change in the fluorescence intensity was different at low or high pH (4–5 or 11). Although the fluorescence intensity at low or high pH seems to be higher than that at neutral pH, in practice the QD nanoparticles could not be used under strong acidic or basic conditions since they became aggregated and precipitated. Based on another published paper dealing with the effect of pH on the fluorescence intensity of QDs [26], in which the photoluminescence intensity increased with increasing pH from 8 to 11.5, this pH range can be taken as the region of stability of the MPA-QDs toward changes in the environment. The pH range of 6–10 is a stable environment for measurement. It is well known that increasing the temperature results in the decrease of the reaction time. Indeed, the reaction time was decreased by 60% at temperatures above 26 °C. However, the fluorescence intensity decreased rapidly at these temperatures, due to the self-fluorescence quenching of the QDs and no significant difference in the fluorescence intensity was observed over the temperature range of 29–37 °C.

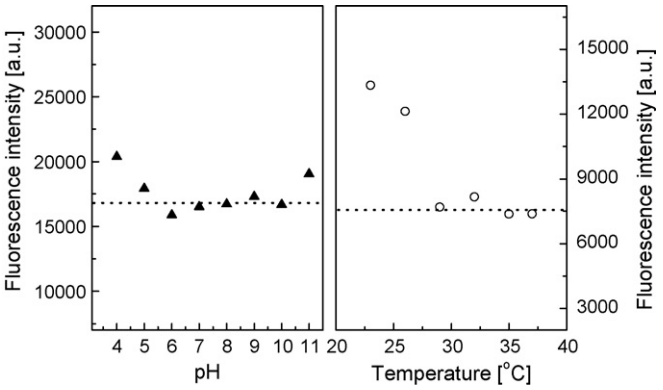

Fig. 5. Effect of pH and temperature of reaction solution during glucose measurements.

3.4. Glucose detection using QD-FRET-based probes

As indicated in the theoretical works on this subject, the direct electrical activation of enzymes, particularly redox enzymes, represents a general approach to the stimulation of the bioelectrocatalyzed oxidation (or reduction) of the enzyme substrates [24]. Fig. 6 shows the effect of the volume ratios of the MPA-QDs, GOD and HRP in the glucose solutions and the ratio between the enzymes and MPA-QDs on the output signals of

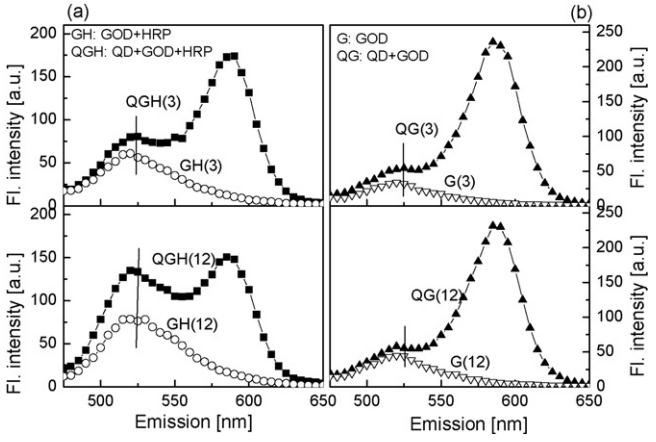

Fig. 4. Emission spectra of enzymes in the presence and absence of MPA-QDs (445 nm (ex)/525 nm (em)). The measurements were performed in 0.5 g/l glucose solution after a given period of conjugation with the MPA-QDs; (a) both GOD and HRP conjugated with MPA-QDs (volume ratio of QDs/GOD/HRP: 10/3/3) or kept alone for 3 or 12 h and (b) only GOD conjugated with MPA-QDs (volume ratio of QDs/GOD: 10/3) and non-conjugation with QDs for 3 or 12 h.

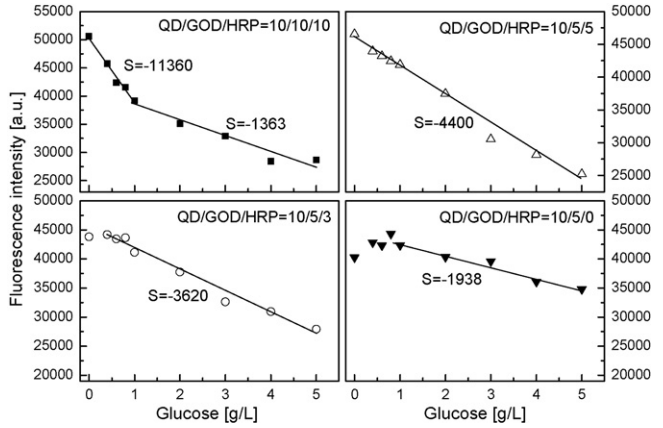

Fig. 6. Change in fluorescence intensities of the QD-FRET-based probes at different glucose concentrations and various volume ratios of QDs/GOD/HRP added to glucose solution; 10/10/10, 10/5/5, 10/5/3, 10/5/0.

the QD-FRET-based probes after exposing them to various concentrations of glucose.

With the volume ratios of the three components set to 10/10/10, the fluorescence intensity changed significantly in the low range of glucose concentrations. The sensitivity (slope value) was very high ($S = -11{,}360$) in the linear concentration range of 0–1.0 g/l with $R = 0.990$. With the volume ratios of the three components set to 10/5/5, 10/5/3 or 10/5/0, the sensitivity or reaction efficiency of the QD-FRET-based probes decreased with decreasing amount of HRP used. Furthermore, the fluorescence intensities in the low range of glucose concentrations (0.2–1.0 g/l) became smaller with decreasing amount of HRP used. That is, the linear detection ranges of glucose concentrations were 0–5.0 ($R = 0.992$) for the volume ratio of 10/5/5, 0.2–5.0 ($R = 0.985$) for the volume ratio of 10/5/3 and 1.0–5.0 ($R = 0.982$) for the volume ratio of 10/5/0. The pathway of electron transfer from the excited QDs to the hydrogen peroxide (H_2O_2) reduction reaction was influenced (e.g. depression or prevention). Hence, a decrease of the electron numbers resulted in a decrease of the turnover rate of the electron exchange reflecting the lower photoluminescence quenching of the QDs and lower sensitivity to glucose.

The reaction time of the QD-FRET-based probes to obtain signal stability was 30 min. This is slower than that of the other glucose sensing systems reported in our previous studies [25], however, it is difficult to compare them, since their fabrication and operation are totally different. The low response time of the present probes could be due to the low diffusion of the molecules in the free environment, leading to inhomogeneity of the running of the components in the reactions. However, this application demonstrates the potential of the QDs for use as QD-FRET-based probes in the detection of glucose in solution.

The low response time and stability of the mixture solution of QDs and enzymes in glucose sensing could be improved by immobilizing the QDs and enzymes into a sol–gel layer of 3-glycidoxypropyltrimethoxysilane (GPTMS) and 3-aminopropyltrimethoxysilane (APTMS) [27].

3.5. Interferences

The various ions that were tested, viz. NH_4^+, NO_3^-, Na^+, Cl^-, in the concentration range of 0.01–200 mM had no significant effect on the fluorescence intensity of the MPA-QDs which were taking part in the glucose reaction. All of their p values (probabilities) were larger than 0.05 when comparing their fluorescence intensities with the fluorescence intensity of the control sample (solution with no ions tested in this work) before and after adding enzymes to the glucose solution ($p_{NH_4,NO_3} = 0.5487$, $p_{Na,Cl} = 0.0564$ in the absence of enzymes; $p_{NH_4,NO_3} = 0.873$, $p_{Na,Cl} = 0.2271$ in the presence of enzymes).

Table 1
Interference effect of ions (CO_3^{2-}, Fe^{3+}) on glucose sensing

Ions (mM)	CO_3^{2-}		Fe^{3+}	
	No enzyme	Enzyme	No enzyme	Enzyme
0.01	ns	ns	ns	ns
0.1	ns	ns	*	ns
0.5	ns	ns	***	***
1.0	ns	ns	***	***
10	ns	ns	***	ns
50	ns	ns	***	**
100	ns	ns	***	***
200	*	ns	***	***

Note: ns means no significance, *$p < 0.05$; **$p < 0.01$; ***$p < 0.001$.

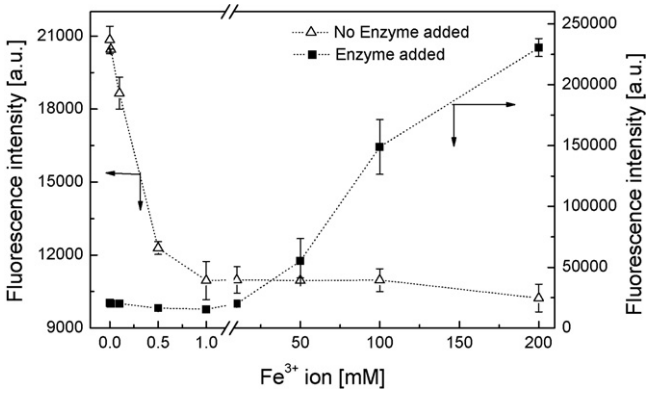

Fig. 7. Effect of Fe^{3+} ions on the fluorescence emission of MPA-QDs during the measurement of 1 g/l glucose solution.

For the CO_3^{2-} ions, only the concentration of 200 mM had a weak effect on the fluorescence intensity of the MPA-QDs ($p < 0.05$) before adding the enzymes to the glucose solution (Table 1). From the results in Table 1, it can be seen that the Fe^{3+} ion had a strong effect ($p < 0.01$ or 0.001) on the fluorescence emission of the MPA-QDs in the glucose oxidation.

Before adding the enzymes to the glucose solution, the fluorescence emission of the MPA-QDs was quenched at an Fe^{3+} ion concentration of 0.1 mM and absolutely quenched at higher concentrations (>0.5 mM) (Fig. 7). After adding the enzymes, the fluorescence intensity of the MPA-QDs decreased at low concentrations of Fe^{3+} (0.5 and 1.0 mM), but considerably increased at high concentrations. In theory, the Fe^{3+} ion acts as a mediator, which has appropriate oxidation potentials, to replace oxygen in the glucose oxidation. Therefore, the response of the signal after adding the enzyme was too fast and a 10-fold higher fluorescence intensity was observed at high concentrations of Fe^{3+} ions.

4. Conclusion

Use of CdSe/ZnS nanoparticles in sensing glucose is a new method and a good prospect in the field of biosensor. They showed the sensitive characteristics of the new biosensor over a large range of glucose detection (0.0–5.0 g/l) with minor effects of interferences (temperature, pH, ions). The tune in conjugating carboxyl groups attached on the surface of QDs and amine groups of enzymes in a normal condition as well as the high potential of QDs for electron transfer to neighbor molecules led to high efficiency of the applied technique, FRET. From these data, the application of CdSe/ZnS QDs in sensing glucose could replace the fluorescent dyes (ruthenium complex, etc.), which are normally used in the conventional methods, in the simple approach.

Acknowledgments

This work was supported by grant No. RTI04-03-03 from the Regional Technology Program of the Ministry of Commerce, Industry and Energy (MOCIE) and also in part by the BK21 program of the Ministry of Education & Human Resources Development, Republic of Korea.

References

[1] R.E. Bailey, A.M. Smith, S. Nie, Physica E 25 (2004) 1–12.
[2] D.M. Willard, L.L. Carillo, J. Jung, A.V. Orden, Nano Lett. 1 (2001) 469–474.
[3] M.L. Curri, A. Agostiano, G. Leo, A. Mallardi, P. Cosma, M.D. Monica, Mater. Sci. Eng. C 22 (2002) 449–452.
[4] E.R. Goldman, I.L. Medintz, J.L. Whitley, A. Hayhurst, A.R. Clapp, H.T. Uyeda, J.R. Deschamps, M.E. Lassman, H. Mattoussi, J. Am. Chem. Soc. 127 (2005) 6744–6751.
[5] P.T. Tran, E.R. Goldman, G.P. Anderson, J.M. Mauro, H. Mattoussi, Phys. Status Solidi (b) 229 (2002) 427–432.
[6] A.R. Clapp, I.L. Medintz, J.M. Mauro, B.R. Fisher, M.G. Bawendi, H. Mattoussi, J. Am. Chem. Soc. 126 (2004) 301–310.
[7] P.T. Snee, R.C. Somers, G. Nair, J.P. Zimmer, M.G. Bawendi, D.G. Nocera, J. Am. Chem. Soc. 128 (2006) 13320–13321.
[8] A.S. Susha, A.M. Javier, W.J. Parak, A.L. Rogach, Colloid Surf. A: Physicochem. Eng. Aspects 281 (2006) 40–43.
[9] Z. Dai, A.-N. Kawde, Y. Xiang, J.T. la Belle, J. Gerlach, V.P. Bhavanandan, L. Joshi, J. Wang, J. Am. Chem. Soc. 128 (2006) 10018–10019.
[10] S. Ding, J. Chen, H. Jiang, J. He, W. Shi, W. Zhao, J. Shen, J. Agric. Food Chem. 54 (2004) 6139–6142.
[11] S. Aoyagi, M. Kudo, Biosens. Bioelectron. 20 (2005) 1680–1684.
[12] C.M.C.M. Couto, A.N. Araujo, M.C.B.S.M. Montenegro, J. Rohwedder, I. Raimindo, C. Pasquini, Talanta 56 (2002) 997–1003.
[13] Q. Yang, P. Atanasov, E. Wilkins, Sens. Actuators B 46 (1998) 249–256.
[14] H. Ukeda, Y. Fujita, M. Ohira, M. Sawamura, J. Agric. Food Chem. 44 (1996) 3858–3963.
[15] M. Lepore, M. Portaccio, E.D. Tommasi, P.D. Luca, U. Bencivenga, P. Maiuri, D.G. Mita, J. Mol. Catal. B: Enzym. 31 (2004) 151–158.
[16] X.J. Wu, M.M.F. Choi, Anal. Chim. Acta 514 (2004) 219–226.
[17] L. Qu, X. Peng, J. Am. Chem. Soc. 124 (2002) 2049–2051.
[18] J.A. Gaunt, A.E. Knight, S.A. Windsor, V. Chechik, J. Colloid Interf. Sci. 290 (2005) 437–443.
[19] D. Gerion, F. Pinaud, S.C. Williams, W.J. Parak, D. Zanchet, S. Weiss, A.P. Alivisatos, J. Phys. Chem. B 105 (2001) 8861–8871.
[20] C.C. Chen, C.P. Yet, H.N. Wang, C.Y. Chao, Langmuir 15 (1999) 6845–6850.
[21] J. Aldana, Y.A. Wang, X. Peng, J. Am. Chem. Soc. 123 (2001) 8844–8850.
[22] I. Sondi, O. Siiman, E. Matijevic, J. Colloid Interf. Sci. 275 (2004) 503–507.
[23] Y. Degani, A. Heller, J. Phys. Chem. 91 (1987) 1285–1289.
[24] A. Heller, J. Phys. Chem. 96 (1992) 3579–3587.
[25] H.D. Duong, J.I. Rhee, Talanta 72 (2007) 1275–1282.
[26] C.P. Huang, Y.K. Li, T.M. Chen, Biosens. Bioelectron. 22 (2007) 1835–1838.
[27] H.D. Duong, J.I. Rhee, Proceedings of the International Conference on NanoScience, NanoTechn., Korea, 2006, p. 285.

Available online at www.sciencedirect.com
ScienceDirect
Talanta 73 (2007) 803–811
Talanta
www.elsevier.com/locate/talanta

Ni^{2+} selective sensors based on meso-tetrakis-{4-[tris-(4-allyl dimethylsilyl-phenyl)-silyl]-phenyl}porphyrin and $(sal)_2$trien in poly(vinyl chloride) matrix

Vinod Kumar Gupta [a,*], Ajay Kumar Jain [a], Zakariyya Ishtaiwi [b], Heinrich Lang [b], Gaurav Maheshwari [a]

[a] *Department of Chemistry, Indian Institute of Technology Roorkee, Roorkee 247667, Uttaranchal, India*
[b] *Technische Universität Chemnitz, Fakultät für Naturwissenschaften, Institut für Chemie, Lehrstuhl für Anorganische Chemie, Straße der Nationen 62, 09111 Chemnitz, Germany*

Received 27 March 2007; received in revised form 26 April 2007; accepted 27 April 2007
Available online 10 May 2007

Abstract

PVC-based membranes of meso-tetrakis-{4-[tris-(4-allyl dimethylsilyl-phenyl)-silyl]-phenyl}porphyrin (**I**) and $(sal)_2$trien (**II**) as electroactive material with dioctylphthalate (DOP), tri-*n*-butylphosphate (TBP), chloronapthalene (CN), dibutylphthalate (DBP) and dibutyl(butyl) phosphonate (DBBP) as plasticising solvent mediators have been found to act as Ni^{2+} selective sensor. The best performance was obtained with the sensor having a membrane of composition of **I**: sodium tetraphenyl borate: PVC in the ratio 5:5:150. The sensor exhibits Nernstian response in the activity range 2.5×10^{-6} to 1.0×10^{-1} M, performs satisfactorily over wide pH range (2–5.5) with a fast response time (∼8 s). The sensor was found to work satisfactorily in partially non-aqueous media up to 20% (v/v) content of methanol or ethanol and acetone and could be used over a period of 4 months. Potentiometric selectivity coefficients determined by matched potential method (MPM) indicate excellent selectivity for Ni^{2+} ions. The sensors could be used successfully in the estimation of nickel in different brand of chocolates and also as an indicator electrode in potentiometric titration.

Keywords: Poly(vinyl chloride) (PVC); Nernstian slope; Nickel ion sensor; Porphyrin; Schiff base

1. Introduction

Nickel is widely used in electroplating, manufacture of Ni–Cd batteries, rods for arc welding, pigments for paints, ceramics, surgical and dental prostheses, magnetic tapes of computers and as catalysts. Its widespread use results in its presence normally at low concentration level in raw meats, chocolates, hydrogenated oils, milk and milk products, canned food, etc. and in various industrial and domestic effluents. Nickel is a moderately toxic element and is known to cause cancer of respiratory system [1], skin disorder known as nickel-eczema [2], acute pneumonitis, asthma and increase in blood cells. Thus, it is important to know its concentration in various samples. A number of methods such as flow injection spectrometry, flame and graphite furnace atomic absorption spectrometry, ICP-AES and flame photometry are used for its determination. These methods provide accurate results but are not very appropriate for analysis of large number of environmental samples because they require expertise and good infrastructure. On the other hand, selective ion sensors are very useful for the monitoring of heavy metals in large number of samples as they are convenient, fast, easy to operate, generally require no sample pre-treatment, suitable for online monitoring and cost little. Therefore, a number of nickel sensors based on heterogeneous membranes of porphyrins [3,4], crownethers [5–8], cyclams [9–11], ion exchangers [12,13], pentacyclooctaaza [14], 2,5-thiophenylbis(5-tertbutyl-1,3-benzexazole) [15], dioxime derivative [16] and Schiff bases [17–19] in PVC, nickel phosphate [20] in paraffin and silicone rubber and nickel complex of 1,4,8,11-tetraazacyclotetradecane [21] in araldite have been reported. However, their performance is poor with regard to one or more sensor characteristics, i.e., working activity range, selectivity, response time, pH range and lifetime. In addition to these solid membrane sensors, liquid membrane sensors have also been investigated [22–24].

* Corresponding author. Tel.: +91 1332 285801; fax: +91 1332 273560.
E-mail address: vinodfcy@iitr.ernet.in (V.K. Gupta).

0039-9140/$ – see front matter © 2007 Elsevier B.V. All rights reserved.
doi:10.1016/j.talanta.2007.04.049

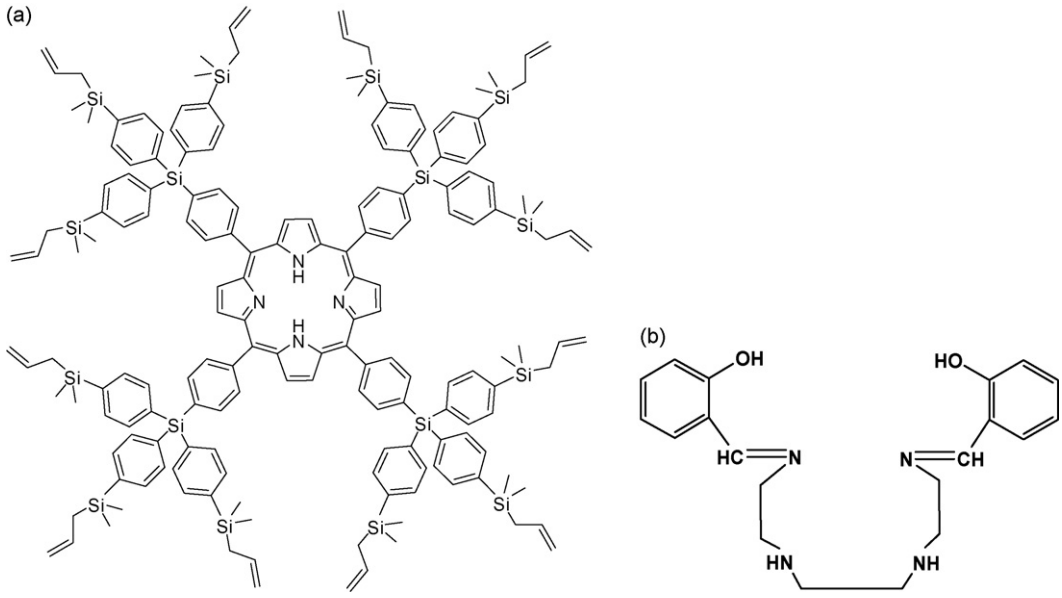

Fig. 1. (a) Structure formula of meso-tetrakis-{4-[tris-(4-allyl dimethylsilyl-phenyl)-silyl]-phenyl}porphyrin (**I**). (b) Structure formula of $(sal)_2$trien (**II**).

However, they are of limited use in view of attrition of liquid membrane during experimentation. In order to achieve wider applicability, these limitations need to be removed. Efforts in this direction are on using different materials for preparation of membranes. The main requirement to impart selectivity to the ion sensor is to use membranes of a material which shows strong affinity for a particular metal ion and poor to others. The main problem in the development of a good sensor is that such materials are not easily available. Thus, newer materials synthesized are continuously being examined for such roles. Continuing efforts in this direction, we have recently synthesized diverse porphyrin and studied their membranes in PVC matrix as Ni^{2+} selective sensors. Besides this, Schiff bases with N and O donor atoms are well known to from strong complexes with transition metal ions. Some of the Schiff bases are reported to from strong complexes with a specific ion due to geometric factors [25,26]. As a result, Schiff base complexes have attracted increasing attention in solvent extraction [27,28], ion exchangers [29,30] and catalytic studies [31,32]. Thus, Schiff bases offer a good possibility to be used as Ni^{2+} selective ionophores. Therefore, PVC based membranes of meso-tetrakis-{4-[tris-(4-allyl dimethylsilyl-phenyl)-silyl]-phenyl}porphyrin (**I**) and $(sal)_2$trien (**II**) (Fig. 1a and b) have been studied as Ni^{2+} selective sensors and the results reported in the present communication show that they perform well and could be used for its selective quantification.

2. Experimental

2.1. Reagents

All the reagents used for synthesis were obtained from Aldrich (Germany). High molecular weight polyvinyl chloride (PVC) Aldrich (USA); sodium tetraphenyl borate (NaTBP) BDH (UK); dioctylphthalate (DOP) Riedel (India); tri-*n*-butylphosphate (TBP) BDH (England), chloronapthalene (CN), dibutylphthalate (DBP) and dibutyl(butyl) phosphonate (DBBP), Mobil (USA) were used as obtained. 0.5 M stock solutions were prepared by dissolving AR grade metal nitrates solution in double distilled water and standardized wherever necessary. The working solutions of different concentrations were prepared by diluting the stock solutions.

2.2. Apparatus and potential measurements

IR spectra were recorded with a Perkin-Elmer FTIR1000 Spectrometer as films between NaCl discs. ^{1}H, $^{13}C\{^{1}H\}$ NMR and $^{29}Si\{^{1}H\}$ spectra were recorded on a Bruker Advance 250 spectrometer operating in the Fourier transform mode. ^{1}H NMR spectra recorded at 250.130 MHz (internal standard relative to $CDCl_3$, $\delta = 7.26$ ppm); $^{13}C\{^{1}H\}$ NMR spectra were recorded at 67.890 MHz (internal standard relative to $CDCl_3$, $\delta = 77.0$ ppm); $^{29}Si\{^{1}H\}$ NMR spectra were recorded at 49.692 Hz (extenal standard relative to $SiMe_4$, $\delta = 0.0$ ppm); chemical shifts are reported in δ units (ppm) downfield from tetra methyl silane. The potential measurements were carried out at $25 \pm 0.1\,^{\circ}C$ with a digital potentiometer (Model 5652 A, ECIL, India) and microvoltmeter, model CVM 301, Century (India) by setting up the following cell assembly.

External reference electrode (SCE)	Solution 2 (Test solution)	Membrane	Solution 1 (Internal solution) 0.1 M Ni^{2+}	Internal reference electrode (SCE)

2.2.1. Synthesis of porphyrin *I*

Meso-tetrakis-[4-{tris(4-allyl dimethyl silyl) phenyl}silyl phenyl] porphyrin (**I**) was synthesized according to the reported procedure [33] as follows.

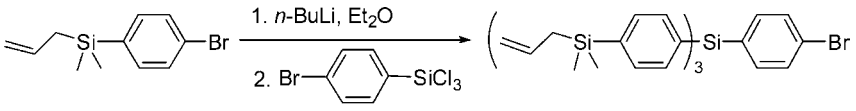

*2.2.1.1. Synthesis of 4-[tris-(4-allyldimethylsilyl-phenyl)-silyl]-bromobenzene (**b**).* *n*-BuLi in *n*-hexane (2.5 M, 27.02 mmol, 10.80 mL) was added drop-wise to **a** (27.02 mmol, 6.890 g) dissolved in diethyl ether (100 mL) at −30 °C. The reaction solution was stirred below −10 °C for 30 min, then TMEDA (40.53 mmol, 4.710 g, 6.101 mL) was added and stirring was continued for 5 min. A solution of 4-trichlorosilyl-bromobenzene (8.58 mmol, 2.492 g) in diethyl ether (40 mL) was added and the reaction solution was stirred for 30 min at the same temperature and 24 h at 25 °C. The reaction was quenched with water (50 mL) and the resulting mixture was extracted with diethyl ether (100 mL). The organic layer was dried over magnesium sulfate and all volatiles were removed under vacuum. The crude product was purified by silica gel column chromatography (*n*-hexane: 4 cm × 35 cm) to afford **b** (5.04 mmol, 3.58 g, 59%, mp = 99.6–102.3 °C).

IR ν (cm^{-1}) (KBr disc): 3070 (w), 3048 (w), 2989 (w), 2953 (w), 2908 (w), 2885 (w), 1629 (m, C=C), 1249 (m, CH_3 bending), 1133 (m), 836 (s, Si–C), 802 (s, Si–C).

^{1}H NMR δ (ppm) ($CDCl_3$): 0.29 (s, 18 H, $SiCH_3$), 1.77 (dt, 8.05 Hz, 1.06 Hz, 6 H, $SiC\underline{H}_2CH{=}CH_2$), 4.86 (ddt, 10.37 Hz, 2.69 Hz 1.06 Hz, 3 H, $SiCH_2CH{=}C\underline{H}_2$), 4.88 (ddt, 16.65 Hz, 2.69 Hz, 1.06 Hz, 3 H, $SiCH_2CH{=}C\underline{H}_2$), 5.79 (ddt, 16.65 Hz, 10.37 Hz, 8.06 Hz, 3 H, $SiCH_2C\underline{H}{=}CH_2$), 7.43 (dt, 8.33 Hz, 1.74 Hz, 2 H, C_6H_4), 7.53 (dt, 8.33 Hz, 1.74 Hz, 2 H, C_6H_4), 7.53 (s, 12 H, C_6H_4).

^{13}C{^{1}H} NMR δ (ppm) ($CDCl_3$): −3.6 (6 C, $SiCH_3$), 23.5 (3 C, $Si\underline{C}H_2CH{=}CH_2$), 113.5 (3 C, $SiCH_2CH{=}\underline{C}H_2$), 124.7 (1 C), 131.1 (2 C), 133.0 (6 C), 133.1 (1 C), 134.2 (3 C), 134.5 (3 C, $SiC\underline{H}_2CH{=}CH_2$), 135.5 (6 C), 137.9 (2 C), 140.5 (3 C).

^{29}Si{^{1}H} NMR δ (ppm) ($CDCl_3$): −14.6 (1 Si, $Si(C_6H_4)_4$), −4.6 (3 Si, $SiCH_2CH{=}CH_2$).

ESI-TOF *m/z* (rel. intensity): 749.19 (100) $[M+K]^+$.

Anal. Calcd. for $C_{39}H_{49}BrSi_4$ (710.05): C, 65.97; H, 6.96. Found: C, 65.81; H, 6.72.

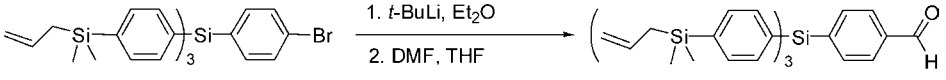

2.2.1.2. Synthesis of 4-[tris-(4-allyldimethylsilyl-phenyl)-silyl]-benzaldeyde (c). ^{t}BuLi in *n*-pentane (1.7 M, 8.00 mmol, 4.71 mL) was added drop-wise to a solution of **b** (4.00 mmol, 2.836 g) in diethyl ether (18 mL) at −78 °C. The reaction solution was stirred at this temperature for 1 h. The resulting solution was drop-wise transferred via canula to DMF (12 mmol, 0.877 g, 0.93 mL) in tetrahydrofuran (12 mL) at 0 °C and kept at this temperature for 15 min. The reaction solution was further stirred at room temperature for 2 h and was then quenched with HCl (3 N, 20 mL). The product was extracted with diethyl ether (100 mL) and the organic layer was washed with water (2 mL × 60 mL), saturated $NaHCO_3$ (60 mL) and brine (60 mL). The organic layer was dried over $MgSO_4$ and then all volatile materials were removed under oil-pump vacuum. The crude product was purified by column chromatography (*n*-hexane—20% dichloromethane/hexane) to afford **c** as colorless oil (8.872 mmol, 1.813 g, 87%) which solidified on cooling (3.676 mmol, 2.423 g, 92%, mp = 87.5–89.7 °C).

IR ν (cm^{-1}) (KBr disc): 3074 (w), 2048 (w), 2995 (w), 2953 (w), 2910 (w), 2890 (w), 2818 (w, CHO), 2726 (w, CHO), 1703 (s, C=O), 1629 (w, C=C), 1248 (w, CH_3 bending), 1133 (m), 836 (s, Si–C), 802 (m, Si–C).

^{1}H NMR δ (ppm) ($CDCl_3$): 0.29 (s, 18 H, $SiCH_3$), 1.77 (dt, 8.13 Hz, 1.10 Hz, 6 H, $SiC\underline{H}_2CH{=}CH_2$), 4.87 (ddt, 10.38 Hz, 2.14 Hz, 1.10 Hz, 3 H, $SiCH_2CH{=}C\underline{H}_2$), 4.88 (ddt, 17.10 Hz, 2.14 Hz, 1.10 Hz, 3 H, $SiCH_2CH{=}C\underline{H}_2$), 5.79 (ddt, 17.10 Hz, 10.38, 8.14 Hz, 3 H, $SiCH_2C\underline{H}{=}CH_2$), 7.54 (brs, 12 H, C_6H_4), 7.77 (brd, 8.08 Hz, 2 H, C_6H_4), 7.87 (brd, 8.08 Hz, 2 H, C_6H_4), 10.06 (s, 1 H, CHO).

^{13}C{^{1}H} NMR δ (ppm) ($CDCl_3$): −3.6 (6 C, $SiCH_3$), 23.5 (3 C, $Si\underline{C}H_2CH{=}CH_2$), 113.5 (3 C,=$CH_2$, $SiCH_2CH{=}\underline{C}H_2$), 128.6 (2 C), 132.9 (1 C), 133.1 (6 C), 133.7 (3 C), 134.4 (3 C, $SiCH_2\underline{C}H{=}CH_2$), 135.5.(6 C), 136.9 (2 C), 140.8 (3 C), 143.0 (1 C), 192.6 (1 C, CHO).

^{29}Si{^{1}H} NMR δ (ppm) ($CDCl_3$): −14.7 (1 Si, $Si(C_6H_4)_4$), −4.5 (3 Si, $SiCH_2CH{=}CH_2$).

ESI-TOF *m/z* (rel. intensity): 697.29 (100) $[M+K]^+$ (calcd. 697.26).

Anal. Calcd. for $C_{40}H_{50}OSi_4$ (659.17): C, 72.88; H, 7.65. Found: C, 72.96; H, 7.64.

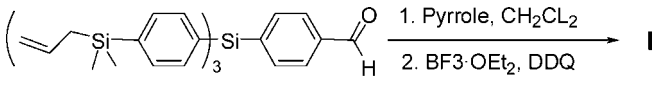

*2.2.1.3. Synthesis of meso-tetrakis-{4-[tris-(4-allyldimethylsilyl-phenyl)-silyl]-phenyl}-porphyrin (**I**).* To a solution of **c** (2.42 mmol, 1.595 g) and pyrrole (2.42 mmol, 0.157 g, 0.168 mL) in dichloromethane (242 mL), $BF_3{\cdot}OEt_2$ (0.242 mmol, 0.0344 g, 0.030 mL) was added. The mixture was stirred for 2 h and then 2,3-dichloro-5,6-dicyanobenzoquinone

Table 1
Composition of PVC membranes of I and performance characteristics of Ni^{2+} selective sensors based on them

Sensor no.	Components in membranes (w/w; mg)							Working activity range (M)	Slope (±0.1 mV/decade of activity)	Response time (s)
	I	NaTPB	TBP	CN	DBBP	DOP	PVC			
1	5	5	150	–	–	–	150	3.2×10^{-4} to 1.0×10^{-1}	33.0	20
2	5	5	–	150	–	–	150	8.9×10^{-5} to 1.0×10^{-1}	30.6	18
3	5	5	–	–	200	–	150	7.9×10^{-5} to 1.0×10^{-1}	34.4	14
4	5	5	–	–	–	150	150	7.9×10^{-6} to 1.0×10^{-1}	29.4	9
5	5	5	–	–	–	–	150	2.5×10^{-6} to 1.0×10^{-1}	29.5	8

(1.815 mmol, 0.412 g) was added and stirring was continued for 1 h. The reaction mixture was washed with saturated $NaHCO_3$ (40 mL) and water (3 mL × 40 mL). The organic layer was filtered over silica gel band and then all volatile materials were removed under vacuum. The crude product was purified by column chromatography (*n*-hexane—20% dichloromethane/hexane) to afford **I** as dark red solid (0.224 mmol, 0.633 g, 37%).

IR ν (cm^{-1}) (KBr disc): 3321 (S, NH), 3066 (w), 3048 (w), 2993 (w), 2952 (w), 2917 (w), 2851 (w), 1628 (m, C=C), 1250 (m, CH_3 bending), 1132 (m), 835 (s, Si–C), 801 (s, Si–C).

^{1}H NMR δ (ppm) ($CDCl_3$): −2.75 (s, 2 H, NH), 0.35 (s, 72 H, $SiCH_3$), 1.83 (dt, 8.06 Hz, 1.04 Hz, 24 H, $SiC\underline{H}_2CH{=}CH_2$), 4.89 (ddt, 10.12 Hz, 2.14 Hz, 1.04 Hz, 12 H, $SiCH_2CH{=}C\underline{H}_2$), 4.92 (ddt, 16.82 Hz, 2.14 Hz, 1.04 Hz, 12 H, $SiCH_2CH{=}C\underline{H}_2$), 5.85 (ddt, 16.82 Hz, 10.12 Hz, 8.06 Hz, 12 H, $SiCH_2C\underline{H}{=}CH_2$), 7.67 (brd, 7.99 Hz, 24 H, C_6H_4), 7.81 (brd, 7.99 Hz, 24 H, C_6H_4), 7.98 (brd, 8.00 Hz, 8 H, C_6H_4), 8.25 (brd, 8.00 Hz, 8 H, C_6H_4), 8.92 (s, 8 H, β-pyrrole).

^{13}C{^{1}H} NMR δ (ppm) ($CDCl_3$): −3.5 (24 C, $SiCH_3$), 23.6 (12 C, $Si\underline{C}H_2CH{=}CH_2$), 113.5 (12 C, $SiCH_2CH{=}\underline{C}H_2$), 120.1 (4 C, meso-C), 133.2 (24 C), 133.4 (4 C), 134.2 (8 C), 134.6 (12 C, $SiCH_2\underline{C}H{=}CH_2$), 134.7 (8 C), 134.8 (12 C), 135.8 (24 C), 140.5 (12 C), 143.4 (4 C).

^{29}Si{^{1}H} NMR δ (ppm) ($CDCl_3$): −14.2 (4 Si, $Si(C_6H_4)_4$), −4.5 (12 Si, $SiCH_2CH{=}CH_2$).

Anal. Calcd. for $C_{176}H_{206}N_4Si_{16}$ (2826.97): C, 74.78; H, 7.34, N, 1.98. Found: C, 74.45; H, 7.46; N, 1.89.

2.2.2. Synthesis of Schiff base [(sal)$_2$trien; *II*]

$(Sal)_2$trien was prepared by the reported method [34]. According to this, a cooled methanolic solution (10 mL) of triethylenetetramine (0.84 g, 5.65 mmol) was added dropwise to a solution of 2-hydroxybenzaldehyde (1.38 g, 11.28 mmol) in methanol (15 mL) at 0 °C and stirred for 1 h. The yellow powder formed was then dried under vacuum. $(Sal)_2$trien (**II**) was obtained as a yellow precipitate. Yield = 1.71 g; mp 107 °C. Elemental analysis % calculated for $C_{20}H_{26}N_4O_2$, C = 67.74, H = 7.35, N = 15.80 and observed % was C = 67.10, H = 7.34, N = 15.25.

2.3. Preparation of membranes

The PVC based membranes were prepared by dissolving appropriate amounts of **I** or **II**, anion excluder (NaTPB), solvent mediators (tri-*n*-butylphosphate (TBP), 1-chloro naphthalene (CN), dibutyl(butyl) phosphonate (DBBP) and dioctyl phthalate (DOP)) and PVC in THF (5–10 mL). After complete dissolution of all the components and thorough mixing, the resulting mixture was poured into polyacrylates ring placed on a smooth glass plate and was allowed to evaporate. The transparent membranes of 0.4 mm thickness formed were removed carefully from the glass plate. A 5 mm diameter piece was cut out and glued to one end of a "Pyrex" glass tube. The membranes thus prepared were equilibrated for 8 days in 0.1 M Ni^{2+} solution. Membranes of different composition were prepared and investigated and those, which gave reproducible results and better performance characteristics, were selected for further studies. The optimum composition of membranes for best performance is given in Tables 1 and 2. The activity coefficient (γ), of metal ions was calculated from the modified form of the Debye–Hückel equation [35].

2.4. Dissolution of chocolate samples

A 20 g chocolate sample was charred in silica crucible for 6 h on a hot plate. The charred material was kept in a muffle furnace for 12 h at 350 °C. The residue was cooled and further 5 mL concentrated nitric acid was added and again kept in the furnace for 2 h to ensure that no carbon remained. In this residue 1 mL of concentrated hydrochloric acid and 5 mL of 70% per-

Table 2
Composition of PVC membranes of II and performance characteristics of Ni^{2+} selective sensors based on them

Sensor no.	Components in membranes (w/w; mg)							Working activity range (M)	Slope (±0.1 mV/decade of activity)	Response time (s)
	II	NaTPB	TBP	DOP	DBBP	CN	PVC			
6	5	5	150	–	–	–	150	1.2×10^{-4} to 1.0×10^{-1}	30.0	22
7	5	5	–	150	–	–	150	5.6×10^{-5} to 1.0×10^{-1}	30.6	20
8	5	5	–	–	200	–	150	2.8×10^{-5} to 1.0×10^{-1}	36.4	15
9	5	5	–	–	–	150	150	5.0×10^{-6} to 1.0×10^{-1}	29.5	10
10	5	5	–	–	–	–	150	1.0×10^{-5} to 1.0×10^{-1}	29.1	25

chloric acid were added and evaporated to fumes so that all the nickel metal changes to ionic form. The dried residue was dissolved in water and made up to 25 mL. The pH was maintained at ~5. Ni^{2+} was estimated in four different varieties of chocolates to obtain representative values. The concentration of nickel ions in this solution was estimated with atomic absorption spectrophotometer (AAS) (Perkin-Elmer model 8440) and inductively coupled plasma atomic emission spectrometer (ICP-AES) (Labtam, Australia).

3. Results and discussion

3.1. Working activity range and slope

The potential generated across the membranes of **I** and **II** was investigated as a function of Ni^{2+} activity in the range 5.0×10^{-7} to 1.0×10^{-1} M and the results obtained are shown in Fig. 2. In order to achieve good selectivity, it is essential that no significant amount of other ions should enter the membrane phase. Tetraphenylborate was added to all prepared membranes to reduce the interference from anions, optimize sensing selectivity and reduce bulk membrane impedance [36]. It is seen from Fig. 2(a) that the sensor no. 5 having the membrane of porphyrin **I** without plasticizer exhibits maximum activity range (linear response) of 2.5×10^{-6} to 1.0×10^{-1} M with Nernstian slope of 29.5 mV/decade of activity. Four plasticizers namely TBP, CN, DBBP and DOP were added in an attempt to improve the performance of the sensors and the results obtained are also shown in Fig. 2(a). All performance characteristics of the sensors determined from this Figure are compiled in Table 1. It is seen that the addition of plasticizers to the membranes (sensor nos. 1–4) does not improve the performance of membranes. It appears that the ionophore **I** itself acts as a good plasticizer due to the presence of the 4-[bis-(4-allyl dimethyl-silyl-phenyl)-silyl]-phenyl substituent. The potential response of membranes of **II** is shown in Fig. 2(b) and performance characteristics there by evaluated are compiled in Table 2. The membrane without plasticizer (sensor no. 10) shows limited working activity range of 1.0×10^{-5} to 1.0×10^{-1} M with a slope of 29.1 mV/decade of activity. As compared to membrane of **I**, the performance of membrane of **II** is significantly affected by the addition of plasticizers. TBP, DOP and DBBP adversely affect the performance as working activity range is shortened, whereas CN improves the performance as the membrane (sensor no. 9) exhibits widest working activity range 5.0×10^{-6} to 1.0×10^{-1} M with Nernstain slope of 29.5 mV/decade of activity. Repeated monitoring of potential (15 measurements) at the same activity (1.0×10^{-3} M) gave a standard deviation of ±0.05 mV. The performance of the membranes without ionophores (dummy membranes) was also investigated and it was found that they generated no potential.

3.2. Response and lifetime

The response time of the sensor has been determined by measuring the time required to achieve a steady potential for 1.0×10^{-4} M solution, when Ni^{2+} ion activity was rapidly increased 10-fold from 1.0×10^{-5} to 1.0×10^{-4} M. The response time of the membrane without plasticizer is found to be 8 s (Table 1). The low response time of the sensor no. 5 is most probably due to the fast exchange of Ni^{2+} between ionophore and the bulk solution occurring at the membrane interface. Amongst the membranes of **II**, the membranes with CN plasticizer exhibited a minimum response time (10 s) (Table 2). The main factor responsible for limited lifetime of a sensor is believed to be the loss of one or more of its components while contacting with aqueous solution. The loss of ionophore from the membrane

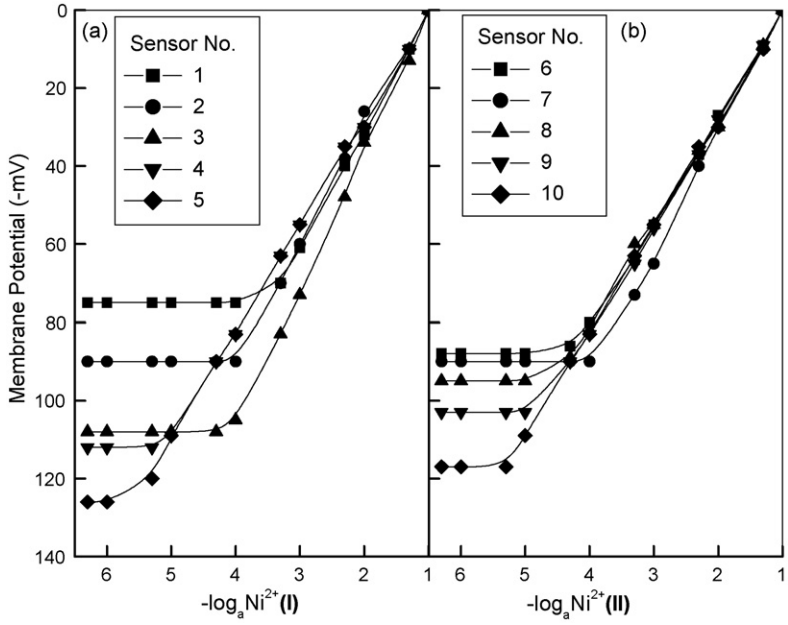

Fig. 2. (a) Variation of membrane potential with activity of Ni^{2+} ions for PVC based membranes of (**I**) with plasticizers, TBP (1), CN (2), DBBP (3), DOP (4) and without plasticizer (5). (b) Variation of membrane potential with activity of Ni^{2+} ions for PVC based membranes of (**II**) with plasticizers, TBP (6), DOP (7), DBBP (8), CN (10) and without plasticizer (9).

Table 3
Effect of partially non-aqueous medium on the working of Ni^{2+} sensor (no. 5)

Non-aqueous content (%, v/v)	Slope (±0.1 mV/decade of activity)	Working activity range (M)
0	29.5	2.5×10^{-6} to 1.0×10^{-1}
Methanol		
10	29.5	2.5×10^{-6} to 1.0×10^{-1}
20	29.2	4.0×10^{-6} to 1.0×10^{-1}
25	28.7	1.2×10^{-5} to 1.0×10^{-1}
Ethanol		
10	29.5	2.5×10^{-6} to 1.0×10^{-1}
20	29.2	4.4×10^{-6} to 1.0×10^{-1}
25	28.0	1.8×10^{-5} to 1.0×10^{-1}
Acetone		
10	29.5	2.5×10^{-6} to 1.0×10^{-1}
20	29.5	2.5×10^{-6} to 1.0×10^{-1}
25	30.5	4.5×10^{-5} to 1.0×10^{-1}

Table 4
Effect of partially non-aqueous medium on the working of Ni^{2+} sensor (no. 9)

Non-aqueous content (%, v/v)	Slope (±0.1 mV/decade of activity)	Working activity range (M)
0	29.5	5.0×10^{-6} to 1.0×10^{-1}
Methanol		
10	29.5	5.0×10^{-6} to 1.0×10^{-1}
20	29.5	5.6×10^{-6} to 1.0×10^{-1}
25	28.3	2.8×10^{-5} to 1.0×10^{-1}
Ethanol		
10	29.5	5.0×10^{-6} to 1.0×10^{-1}
20	29.3	6.0×10^{-6} to 1.0×10^{-1}
25	28.5	4.8×10^{-5} to 1.0×10^{-1}
Acetone		
10	29.4	5.0×10^{-6} to 1.0×10^{-1}
20	29.1	5.1×10^{-6} to 1.0×10^{-1}
25	28.7	5.0×10^{-5} to 1.0×10^{-1}

phase is less if it has high lipophilicity. The membrane of porphyrin (sensor no. 5) possesses high lipophilicity due to the presence of substituent and thus shows a significant long life of 4 months whereas the membrane of **II** (sensor no. 9) having less lipophilicity, shows shorter life time (2 months). It is important to mention here that membranes were stored in 0.5 M solution when not in use. After this shelf lifetime membrane started showing less reproducibility and cracks also started developing in the membrane. As sensor nos. 5 and 9 exhibit best performance, all further studies were done with them only.

3.3. Effect of solvents

The effect of non-aqueous content on their performance was looked into and results shown in Tables 3 and 4 for methanol–water, ethanol–water and acetone–water mixtures. It is seen from these tables that the performance of the two sensors remains unaffected in partially non-aqueous mixtures having up to 20% (v/v) methanol, ethanol and acetone. However, above this non-aqueous content performance is affected as the working activity range of both the sensors is significantly reduced.

3.4. Effect of pH

The effect of pH on the performance of two sensors was also seen at two Ni^{2+} activities of 1.0×10^{-3} and 1.0×10^{-4} M. The potential of the two sensors (Fig. 3a and b) remains constant over a pH range of 2.0–5.5. This can be taken as the useful pH working range. The deviation in potential at pH below 2 appears

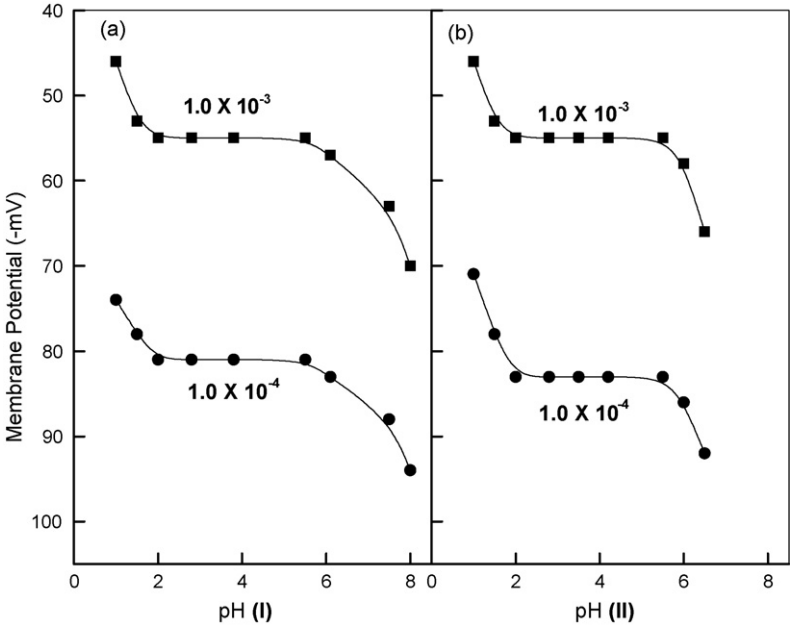

Fig. 3. (a) Effect of pH on potential of sensor no. 5 at $[Ni^{2+}] = 1.0 \times 10^{-3}$ M and 1.0×10^{-4} M. (b) Effect of pH on potential of sensor no. 9 at $[Ni^{2+}] = 1.0 \times 10^{-3}$ M and 1.0×10^{-4} M.

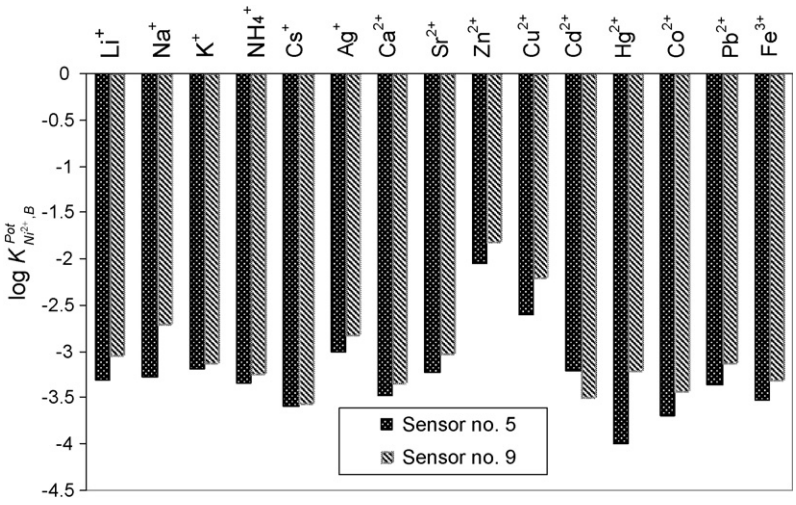

Fig. 4. Comparison of selectivity coefficient values of different metal ions for sensor nos. 5 and 9.

due to H^+ ion interference and above 5.5 due to hydrolysis of Ni^{2+}.

3.5. Potentiometric selectivity

The selectivity is the most important characteristics, as it determines the extent of utility of a sensor in real sample measurement. The selectivity coefficient values were determined by matched potential method (MPM), which was proposed by Gadzekpo and Christian [37] to overcome difficulties in obtaining selectivity coefficient values when ions of unequal charges are involved. In this procedure, the selectivity coefficient $K^{\mathrm{Pot}}_{\mathrm{Ni}^{2+},\mathrm{B}}$ is calculated by the expression

$$K^{\mathrm{Pot}}_{\mathrm{Ni}^{2+},\mathrm{B}} = \frac{a'_{\mathrm{Ni}^{2+}} - a_{\mathrm{Ni}^{2+}}}{a_{\mathrm{B}}} = \frac{\Delta a_{\mathrm{Ni}^{2+}}}{a_{\mathrm{B}}}$$

and is therefore determined by measuring the change in potential upon increasing by a definite amount the primary ion activity from an initial values of $a_{\mathrm{Ni}^{2+}}$ to $a'_{\mathrm{Ni}^{2+}}$ and a_{B} represents the activity of interfering ion (B) added to the same reference solution of activity $a_{\mathrm{Ni}^{2+}}$ which causes the same potential change. The values of $a_{\mathrm{Ni}^{2+}}$ and $a'_{\mathrm{Ni}^{2+}}$ were taken to be 1×10^{-3} M and 5×10^{-3} M, whereas the values of a_{B} were experimentally determined. The values determined by MPM are given in Table 3 and Fig. 4. It is seen that the selectivity coefficients are much smaller than 1.0 showing that both the sensors are sufficiently selective over all the interfering ions studied. A critical comparison of potentiometric selectivity data of Table 5 and Fig. 4 shows that the sensor based on **I** is more selective for Ni^{2+} ions as compared to the sensor of **II**. Hence, this sensor can be used for Ni^{2+} estimation in presence of these metal ions.

Table 5
Selectivity coefficient [$K^{\mathrm{Pot}}_{\mathrm{Ni}^{2+},\mathrm{B}}$] values for Ni^{2+} selective sensors (no. 5 and 9) by the matched potential method

Interfering ions (B)	Selectivity coefficient (I) (sensor no. 5)	Selectivity coefficient (II) (sensor no. 9)
Li^+	5.0×10^{-4}	9.1×10^{-4}
Na^+	5.2×10^{-4}	2.0×10^{-3}
K^+	6.5×10^{-4}	7.5×10^{-4}
NH_4^+	4.5×10^{-4}	5.8×10^{-4}
Cs^+	2.5×10^{-4}	2.8×10^{-4}
Ag^+	1.0×10^{-3}	1.5×10^{-3}
Ca^{2+}	3.4×10^{-4}	4.6×10^{-4}
Sr^{2+}	5.9×10^{-4}	9.3×10^{-4}
Zn^{2+}	9.0×10^{-3}	1.5×10^{-2}
Cu^{2+}	2.5×10^{-3}	6.3×10^{-3}
Cd^{2+}	6.3×10^{-4}	3.2×10^{-4}
Hg^{2+}	1.0×10^{-4}	6.3×10^{-4}
Co^{2+}	2.0×10^{-4}	3.8×10^{-4}
Pb^{2+}	4.4×10^{-4}	7.6×10^{-4}
Fe^{3+}	3.0×10^{-4}	5.0×10^{-4}

4. Analytical applications

4.1. Potentiometric titration

The analytical application of the sensor no. 5 was tested and so it was used as an indicator electrode to determine the end

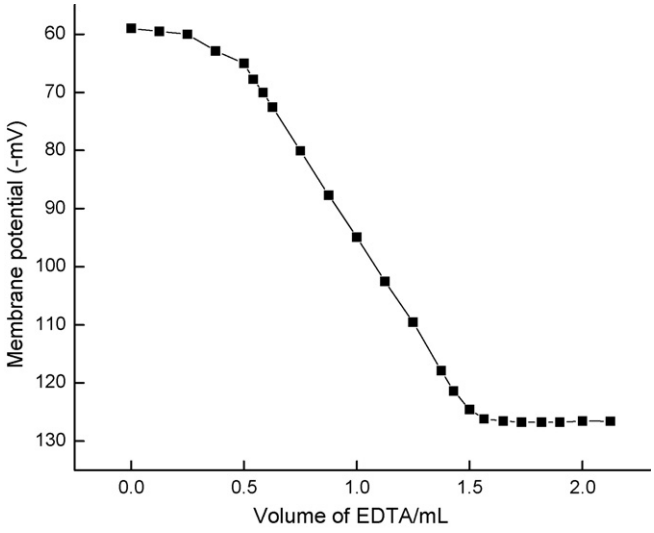

Fig. 5. Potentiometric titration plot of 1.0×10^{-3} M Ni^{2+} solution (10 mL) with EDTA (1.0×10^{-2} M).

Table 6
Results for Ni (II) concentration determined in chocolates by AAS, ICP-AES and the sensor no. 5

Chocolates	Ni^{2+} concentration as determined by AAS (mg/kg) ±0.01	Ni^{2+} concentration as determined by ICP-AES (mg/kg) ±0.01	Ni^{2+} concentration as determined by sensor no. 5 (mg/kg) ±0.01
Fruit and nut	0.89	0.88	0.86
Five star	0.80	0.86	0.84
Gold	0.83	0.83	0.81
Classic	0.87	0.87	0.83

Table 7
Comparison of the selectivity coefficients of different Ni^{2+} selective sensors

Reference	Selectivity coefficient, $K^{Pot}_{Ni^{2+},B}$									
	Na^+	K^+	Ag^+	Ca^{2+}	Cu^{2+}	Hg^{2+}	Cd^{2+}	Co^{2+}	Zn^{2+}	Fe^{3+}
[3]	6.0×10^{-1}	2.2×10^{-2}	NM	1.0×10^{-3}	2.2×10^{-3}	1.2×10^{-3}	2.0×10^{-3}	7.3×10^{-2}	1.8×10^{-3}	6.5×10^{-3}
[4]	8.2×10^{-2}	2.0×10^{-2}	NM	1.2×10^{-3}	1.8×10^{-3}	1.4×10^{-3}	2.4×10^{-3}	4.8×10^{-1}	2.6×10^{-3}	6.5×10^{-3}
[5]	NM	8.8×10^{-1}	NM	NM	3.8×10^{-2}	2.7×10^{-2}	5.9×10^{-2}	3.6×10^{-2}	4.0×10^{-2}	6.5×10^{-2}
[8]	6.0×10^{-1}	1.0×10^{-1}	1.1×10^{-1}	2.4×10^{-1}	7.0×10^{-1}	1.0×10^{-1}	2.0×10^{-1}	1.3×10^{-1}	2.3×10^{-1}	1.7×10^{-1}
[9]	8.0×10^{-1}	3.0×10^{-2}	2.5×10^{-2}	1.8×10^{-3}	2.5×10^{-3}	1.4×10^{-3}	1.1×10^{-3}	2.5×10^{-3}	NM	6.5×10^{-3}
[10]	5.0×10^{-1}	3.1×10^{-2}	2.3×10^{-2}	1.3×10^{-3}	8.2×10^{-2}	2.3×10^{-3}	3.2×10^{-3}	1.2×10^{-3}	8.6×10^{-3}	6.5×10^{-3}
[11]	6.8×10^{-1}	5.4×10^{-2}	1.3×10^{-2}	1.1×10^{-3}	8.9×10^{-2}	2.3×10^{-3}	2.9×10^{-3}	1.7×10^{-3}	4.7×10^{-3}	6.5×10^{-3}
[14]	1.7×10^{-3}	1.6×10^{-3}	6.1×10^{-3}	9.0×10^{-3}	8.1×10^{-4}	NM	9.6×10^{-3}	5.1×10^{-3}	9.3×10^{-3}	NM
[16]	2.1×10^{-1}	1.4×10^{-1}	5.2×10^{-1}	2.6×10^{-3}	6.2×10^{-2}	3.0×10^{-3}	3.1×10^{-3}	4.7×10^{-2}	1.1×10^{-3}	3.7×10^{-3}
[17]	6.3×10^{-6}	3.1×10^{-5}	1.0×10^{-1}	5.0×10^{-5}	6.3×10^{-4}	3.1×10^{-2}	3.1×10^{-4}	1.5×10^{-4}	8.0×10^{-5}	NM
[18]	6.3×10^{-4}	6.5×10^{-4}	1.7×10^{-3}	7.0×10^{-4}	8.7×10^{-4}	1.5×10^{-3}	9.0×10^{-4}	2.9×10^{-3}	9.7×10^{-4}	8.5×10^{-4}
[19]	1.4×10^{-2}	1.7×10^{-2}	1.3×10^{-2}	2.5×10^{-3}	8.8×10^{-3}	3.8×10^{-3}	5.0×10^{-3}	6.4×10^{-3}	4.7×10^{-3}	NM
Proposed sensor	5.2×10^{-4}	6.5×10^{-4}	1.0×10^{-3}	3.4×10^{-4}	2.5×10^{-3}	1.0×10^{-4}	6.3×10^{-4}	2.0×10^{-4}	9.0×10^{-3}	3.0×10^{-4}

NM, not mentioned.

point in the potentiometric titration of Ni^{2+} with EDTA. 10 mL of a 1.0×10^{-3} M Ni^{2+} solution was titrated against a 1.0×10^{-2} EDTA solution at pH 5.0. The plot obtained (Fig. 5) is of sigmoid shape, the sharp inflexion point observed corresponds to the stoichiometry of the Ni (II)-EDTA complex. Thus, Ni^{2+} can be successfully determined potentiometrically by using this sensor.

4.2. Estimation of Ni^{2+} in chocolate samples

Quantitative estimation of Ni^{2+} was done in some Indian brand chocolates by using this sensor and the results were found comparable to those obtained by AAS and ICP-AES (Table 6). These estimations show the utility of the sensor.

4.3. Comparison of sensor (no. 5) with other reported sensors

The performance of this sensor is comparable to the reported sensors in terms of working activity range, pH range and response time. Besides this, another most important parameter which is used to evaluate a sensor is selectivity coefficient. On this score, when the present sensor is compared with reported sensors in Table 7, it is found that it shows better selectivity (smaller values of $K^{Pot}_{Ni^{2+},B}$) as compared to most reported sensors. Thus, this sensor is an important addition to the family of Ni^{2+} selective sensors.

5. Conclusions

The studies on membranes of meso-tetrakis-{4-[tris-(4-allyl dimethylsilyl-phenyl)-silyl]-phenyl}porphyrin **(I)** and $(sal)_2$trien **(II)** have shown that they act as Ni^{2+} selective sensors. Of the two sensors, sensor no. 5 of ionophore **I** is better as it exhibits wider working activity range, low response time, better selectivity and long shelf life. The sensor can be used for Ni^{2+} estimation in diverse samples by direct potentiometry.

Acknowledgement

Financial support to one of the authors (G.M.) from Human Resource Development (MHRD), New Delhi, India is gratefully acknowledged.

References

[1] D. Templeton, Biological Monitoring of Chemical Exposure in the Workplace, World Health Organization, Geneva, 1990.
[2] J. Kristiansen, J.M. Christensen, T. Henriksen, N.H. Nielsen, T. Menne, Anal. Chim. Acta 403 (2000) 265.
[3] V.K. Gupta, A.K. Jain, L.P. Singh, U. Khurana, Anal. Chim. Acta 355 (1997) 33.
[4] L.P. Singh, J.M. Bhatnager, Sensors 3 (2003) 393.
[5] M.F. Mousavi, N. Alizadeh, M. Shamsipur, N. Zohari, Sens. Actuat. B 66 (2000) 98.
[6] M. Shamsipur, S.Y. Kazemi, Electroanalysis 12 (2000) 1472.
[7] M.D. Hampton, C.A. Peters, L.A. Wellington, Anal. Chim. Acta 194 (1987) 171.

[8] V.K. Gupta, R.N. Goyal, S. Agarwal, P. Kumar, N. Bachheti, Talanta 71 (2007) 795.
[9] A.K. Jain, V.K. Gupta, R.D. Singh, U. Khurana, L.P. Singh, Sens. Actuat. B 40 (1997) 15.
[10] V.K. Gupta, R. Prasad, P. Kumar, R. Mangla, Anal. Chim. Acta 420 (2000) 19.
[11] V.K. Gupta, R. Prasad, A. Kumar, Sensors 2 (2002) 384.
[12] G.N. Rao, S. Srivastava, S.K. Srivastava, M. Singh, Talanta 43 (1996) 1821.
[13] I.O. Gyrdasova, V.L. Volkov, J. Anal. Chem. 52 (1997) 764.
[14] M. Mazloum, M. Niassary, M.K. Amini, Sens. Actuat. B 82 (2002) 259.
[15] M. Shamsipur, T. Poursaberi, A.R. Karami, M. Hosseini, A. Momeni, A. Alizadeh, M. Yousefi, M.R. Ganjali, Anal. Chim. Acta 501 (2004) 55.
[16] A. Yari, S. Azizi, A. Kakanejadifard, Sens. Actuat. B 119 (2006) 167.
[17] H. Mashhadiazadeh, I. Sheikhshoaie, S. Saeid-Nia, Sens. Actuat. B 94 (2003) 241.
[18] A.K. Jain, V.K. Gupta, P.A. Ganeshpure, J. Raisoni, Anal. Chim. Acta 553 (2005) 177.
[19] K.G. Kumar, R. Poduval, S. John, P. Augustine, Microchim. Acta 156 (2007) 283.
[20] B. Buchanan, Anal. Chem. 40 (1968) 517.
[21] U.S. Lal, M.C. Chattopadhyaya, A.K. Dey, J. Ind. Chem. Soc. 59 (1982) 493.
[22] C. Luca, M. Pleniceanu, N. Muresan, Rev. Chim. 27 (1976) 1088.
[23] M. Pleniceanu, M. Isvoranu, C. Spinu, J. Ind. Chem. Soc. 79 (2002) 884.
[24] M. Pleniceanu, M. Isvoranu, C. Spinu, Seria Chim. 30 (2001) 9.
[25] J. Reglinski, S. Morris, D.E. Stevenson, Polyhedron 21 (2002) 2175.
[26] S. Yamada, Coord. Chem. Rev. 190 (1999) 537.
[27] S. Memon, M. Yilmaz, J. Macromol, Sci. Pure Appl. Chem. 39 (2002) 63.
[28] Z. Cimerman, N. Galic, B. Bosner, Anal. Chim. Acta 343 (1997) 145.
[29] W.B. Gurnule, P.K. Rahangadale, L.J. Paliwal, R.B. Kharat, Ult. Sci. Phys. Sci. 15 (2003) 89.
[30] J. Sima, P. Fodran, J. Hledik, A. Kotocova, D. Valigura, Inorg. Chim. Acta 81 (1984) 143.
[31] Y.N. Belokon, N.B. Bespalova, D.T. Churkina, I. Cisarova, M.G. Ezernitskaya, R.S. Harutyunyan, R. Hrdina, H.B. Kagan, P. Kocovsky, K.A. Kochetkov, O.V. Larionov, K.A. Lyssenko, M. North, M. Polasek, A.S. Peregudov, V.V. Prisyazhnyuk, S. Vyskocil, J. Am. Chem. Soc. 125 (2003) 12860.
[32] P.G. Cozzi, Chem. Soc. Rev. 33 (2004) 410.
[33] Z. Ishtawi, Ph.D. Thesis, Technical University of Chemnitz, Germany, 2006.
[34] M.F. Tweedle, L.J. Wilson, J. Am. Chem. Soc. 98 (1976) 4824.
[35] G.D. Christian, Analytical Chemistry, sixth ed., John Wiley & Sons, Inc., NJ, 2003, p. 212 (Chapter 6).
[36] P.M. Gehring, W.E. Morf, M. Welti, E. Pretsch, W. Simon, Helv. Chim. Acta 73 (1990) 203.
[37] V.P. Gadzekpo, G.D. Christian, Anal. Chim. Acta 164 (1984) 279.

Available online at www.sciencedirect.com
ScienceDirect
Talanta 73 (2007) 886–892
Talanta
www.elsevier.com/locate/talanta

A competitive immunochromatographic assay for testosterone based on electrochemical detection

Kumi Inoue, Pascal Ferrante, Yu Hirano, Tomoyuki Yasukawa *, Hitoshi Shiku, Tomokazu Matsue **

Graduate School of Environmental Studies, Tohoku University, 6-6-11 Aoba, Aramaki, Aoba, Sendai 980-8579, Japan

Received 16 March 2007; received in revised form 7 May 2007; accepted 9 May 2007
Available online 18 May 2007

Abstract

An immunochromatographic assay using nitrocellulose membrane was combined with electrochemical detection using an electrode chip in order to quantitatively detect testosterone as a model analyte. The electrode chip consisted of a gold working electrode, a counter electrode and a pseudo-reference electrode, all fabricated on the bottom of a 3.2 mm × 3.2 mm well. Competitive immunoreactions on the membrane were initiated by flowing a solution containing testosterone and horseradish peroxidase (HRP)-labeled testosterone (a competitor) over the membrane. Prepared membrane was placed in a solution containing ferrocenemethanol (FcOH) and H_2O_2 in the well of the electrode chip, and the enzyme reaction was detected by amperometry. Labeled HRP captured on the membrane catalyzed the oxidation of FcOH to the oxidized form $FcOH^+$, which was reduced electrochemically by the electrode chip. The electrochemical response of the reduction current decreased with increasing concentration of testosterone over the range 1–625 ng/ml.

Keywords: Immunochromatography; Testosterone; Nitrocellulose membrane; Amperometry; Competitive-ELISA

1. Introduction

Porous polymer membranes with high absorption capacities for biomolecules are widely used as platforms for analytical detection. In immunochromatographic assays, porous membrane strips are indispensable as immunosorbent materials in point-of-care-testing (POCT) systems. These systems are generally simple self-test kits used at home or first-sign screening kits used to diagnose specific diseases in clinics. Lateral flow-type immunochromatographic tests have been used to detect hormones [1], allergens [2] and viral [3] or bacterial [4] infections. The most successful commercially available application is a pregnancy test kit based on the detection of human chorionic gonadotropin (HCG) hormone in urine. The success of this kit is due to its short assay time, easy handling for sensing (one-step), low consumption of sample solution, portable size and high cost performance. In many immunochromatographic tests, nitrocellulose membrane is used as the test strip due to its high absorption capacity for antibodies, and the ease with which solutions flow across the surface by capillary action. However, a significant disadvantage of present tests is that they are qualitative, since the colorimetric signal is detected with the naked eye. Therefore, a combination of quantitative analysis systems with immunochromatographic tests is required for the reliable and valuable sensing of target analytes.

In a typical immunochromatographic assay, a molecule that recognizes a specific analyte, such as an antibody or antigen, is immobilized on the nitrocellulose membrane. The sample solution containing the target analytes flows over this membrane test strip via capillary action. Quantitative detection of immuno-complexes formed on test strips has been studied by detecting the reflectance of gold particles [5], the fluorescence of labeled proteins [6,7] and by detecting photons from phosphor particles [8,9] and quantum dots [10]. Compact test strip readers using CCD photo sensors [11] or fluorometers [12] have also been developed to quantitatively detect analytes captured on

* Corresponding author. Tel.: +81 22 795 7281; fax: +81 22 795 6167.
** Corresponding author. Tel.: +81 22 795 7209; fax: +81 22 795 7209.
E-mail addresses: yasu@bioinfo.che.tohoku.ac.jp (T. Yasukawa), matsue@bioinfo.che.tohoku.ac.jp (T. Matsue).

0039-9140/$ – see front matter © 2007 Elsevier B.V. All rights reserved.
doi:10.1016/j.talanta.2007.05.008

test lines. In addition, electrochemistry-based detection, where electrochemical detection systems are incorporated into the test strip, has been investigated [13]. Such electrochemical systems would be advantageous as on-site quantitative detection tools with excellent properties of original immunochromatography. Lee et al. developed a liposome immunosensor which used a redox species encapsulated in labeled liposomes as an electrochemical signal source [14]. In addition, stripping voltammetry was used to detect silver deposits on captured gold nanoparticles on a membrane [15].

We describe here an electrochemical immunochromatographic assay using testosterone as a model analyte. The concentration of testosterone in blood is an important indicator for prostate cancer [16]. Moreover, low testosterone levels in elderly men increases the risk of depression [17]. The reference range of serum total testosterone in male adults was reported by Iwamoto et al. and showed to be 2.01–7.50 ng/ml [18]. In this study, we fabricated an electrode chip consisting of three electrodes patterned in a single 3.2 mm × 3.2 mm chamber by photolithography. The electrochemical behavior of the chip was characterized by cyclic voltammetry (CV) in 2.0 mM ferrocenemethanol (FcOH). Then, we investigated this electrochemical detection system in combination with membrane immunoassay using nitrocellulose membrane. Testosterone was quantitatively determined by competitive-type enzyme-linked immunosorbent assay (ELISA) using horseradish peroxidase (HRP)-labeled testosterone as the competitor. The activity of the captured HRP was detected with the electrode chip. This quantitative immunochromatographic assay indicates the potential usefulness of the present method for the rapid and facile detection of various analytes.

2. Materials and methods

2.1. Materials and reagents

Monoclonal mouse anti-testosterone IgG antibody (Testosterone-3, clone number: M021812) was purchased from Fitzgerald Industries International, Inc. (USA). Testosterone and bovine serum albumin (BSA) were purchased from Wako Pure Chemical Industries, Ltd. (Japan). HRP-labeled testosterone, used as a competitor, was obtained from BiosPacific, Inc. (USA). Blocking reagent N-101 (NOF Corporation, Japan) was diluted 1:4 with deionized water to prevent non-specific binding of proteins to the membranes. For electrochemical measurements, ferrocenemethanol (FcOH, 97%, Sigma–Aldrich Co., USA), and hydrogen peroxide (Kanto Chemical Co. Inc., Japan) were used without further purification. All other chemicals used were analytical reagents or laboratory grade. Aqueous solutions were prepared using high-purity distilled and deionized water from a Milli-Q filtration system (Millipore Corporation, USA). Four different buffers were used in this work and were prepared as follows:

PBS: Phosphate buffer saline for immunoreactions between antigens and antibodies; 8.1 mM Na_2HPO_4, 1.5 mM KH_2PO_4, 2.7 mM KCl and 137 mM NaCl, pH 7.6.

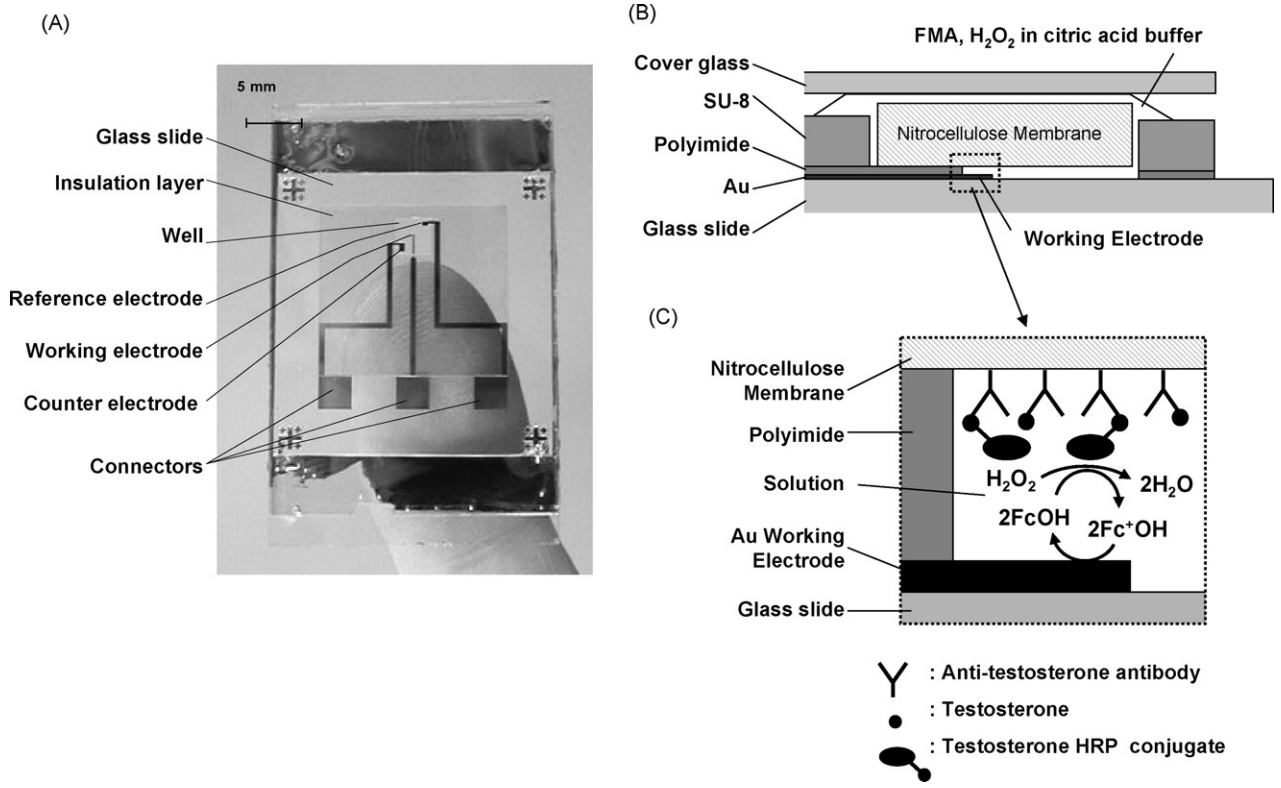

Fig. 1. (A) Photograph of the electrode chip; (B) cross-sectional view of the electrode chip with the membrane in the well; (C) principles behind the enzymatic reaction and the electrochemical detection assay.

PBS-T: Buffer for washing; PBS containing 0.05% (v/v) Tween 20.
PBS-G: Buffer to immobilize antibodies on the nitrocellulose membrane; PBS containing 10% (v/v) glycerol, 1 μg/ml sodium dodecyl sulfate (SDS) and 50 ng/ml BSA [19].
Citric acid buffer: Buffer for electrochemical measurements; 200 mM citric acid, 340 mM NaOH and 100 mM KCl, pH 4.5.

2.2. Fabrication of the electrode chip

The electrode chip incorporating the three gold electrodes, and the well for accommodating the membrane, were fabricated by conventional photolithography. Fig. 1A shows a fabricated electrode chip. A positive photoresist (OFPR5000, 50 cp; Tokyo Ohka Kogyo Co. Ltd., Japan) was spin-coated on a cleaned glass slide at 4000 rpm for 30 s. After baking 10 min at 90 °C, the slide was exposed to UV light through a photomask with a mask aligner (MA-20; Mikasa Co. Ltd., Japan) and developed in NMD-W (Tokyo Ohka Kogyo Co. Ltd.). An Au film (200 nm) with a Ti adhesive layer was then deposited on the photoresist-patterned slide by sputtering (L-332S-FH; Anelva Corp., Japan). Finally, removal of the remaining photoresist with acetone (lift-off) completed the formation of the gold electrode pattern on the chip.

A thin polyimide insulation layer (~8 μm thick) was fabricated by a similar method using photosensitive pre-polyimide (UR-Photoneece 3140, Toray Industries Inc., Japan). The polyimide film served as an insulator to define the electrode area exposed to the solution. The effective size of the working electrode was 200 μm × 200 μm. Finally, the 3.4 mm × 3.4 mm well (depth ~60 μm) was fabricated using a negative photoresist (SU-8 2050, MicroChem Corp., USA).

2.3. Immunoassay using nitrocellulose membrane as an antibody support

A 3 mm × 3 mm piece of nitrocellulose membrane (pore size: 0.2 μm, Bio-Rad Laboratories, Inc., USA) was used as the antibody support in the electrochemical/membrane immunoassay detection system. The clean nitrocellulose membrane pieces were immersed individually in 200 μl of 5.0 μg/ml anti-testosterone IgG antibody solution in PBS-G and incubated for 90 min at room temperature. The membranes were then washed three times in PBS-T and incubated in 500 μl of blocking solution for 90 min at 4 °C to prevent non-specific adsorption of proteins during subsequent steps. After again washing three times with PBS-T, the membranes were immersed in 400 μl of PBS containing testosterone, 500 ng/ml HRP-labeled testosterone (about 12.5 nM) and 50 ng/ml BSA. Competitive immunoreaction was allowed to proceed for 30 min at 37 °C with mixing every 5 min. This resulted in the formation of antibody–antigen complexes on the membrane pieces. Finally, the membranes were washed five times in PBS-T to remove unbound molecules, dried on soft absorbent paper, and then air was blown over the membranes to prepare them for use in electrochemical assay.

2.4. Equipment and methods for electrochemical measurements

Cyclic voltammetry (CV) was carried out using a potentiostat (HA1010mM8; Hokuto Denko Corp., Tokyo, Japan) in order to characterize the electrochemical behavior and basic performance of the electrochemical chip. There were three gold electrodes in the well: the working electrode, the counter electrode and the pseudo-reference electrode. The potential of the working electrode at the center of the well was scanned at 100 mV/s between −0.5 and +0.3 V *versus* the pseudo-reference electrode. During these scans, the well was filled with 20 μl citric acid buffer containing 2.0 mM FcOH and 2.0 mM H_2O_2. After 8 CV cycles, HRP-labeled testosterone was added (final concentration: 1 μg/ml) and then an additional 8 CV cycles were measured. Each cycle was separated by an 84-s waiting interval during which no potential was applied.

To detect the activity of labeled HRP bound to the membranes, individual membrane pieces were put in wells defined by the thin polyimide layer on the electrode chip. Fig. 1B depicts a cross-sectional view of the center of a well to show the arrangement of the components in detail. Citric acid buffer (2 μl) containing 2.0 mM FcOH and 2.0 mM H_2O_2 was dropped on the membrane with a laboratory pipette. A glass slide was used to push the membrane against the bottom of the well in order to ensure a reproducible membrane-electrode distance, then amperometric measurements were carried out 6 min after addition of the buffered solution. The potential was held at −0.3 V *versus* the pseudo-reference electrode. This allowed the reduction current from the oxidized form of FcOH (Fc^+OH), which is generated by the reaction of labeled HRP captured on the nitrocellulose membrane, to be detected. The amperometric response signal was taken to be the average amperometric response between 10 and 20 s after application of the potential.

The enzymatic reaction of labeled HRP and the electrochemical detection of reduction currents for Fc^+OH are illustrated schematically in Fig. 1C. In the presence of H_2O_2, HRP catalyzes the oxidation of FcOH to Fc^+OH as follows:

$$2FcOH + H_2O_2 + 2H^+ \rightarrow 2Fc^+OH + 2H_2O$$

(*HRP catalyzed on the membrane*)

The enzymatically generated Fc^+OH diffuses to the surface of the working electrode and is reduced back to FcOH at the electrode, which is held at −0.3 V *versus*. the pseudo-reference potential. The resulting reduction current is monitored (amperometric measurements):

$$Fc^+OH + e^- \rightarrow FcOH \qquad \text{(at the electrode)}$$

Thus, the reduction current serves as an indicator of the quantity of captured HRP-labeled testosterone and, consequently, of the concentration of testosterone in the sample.

2.5. Immunochromatographic assay for testosterone

Anti-testosterone antibody in PBS-G (2.0 mg/ml) was spotted on nitrocellulose membrane (8 μm pore size, Pure Bind G-R,

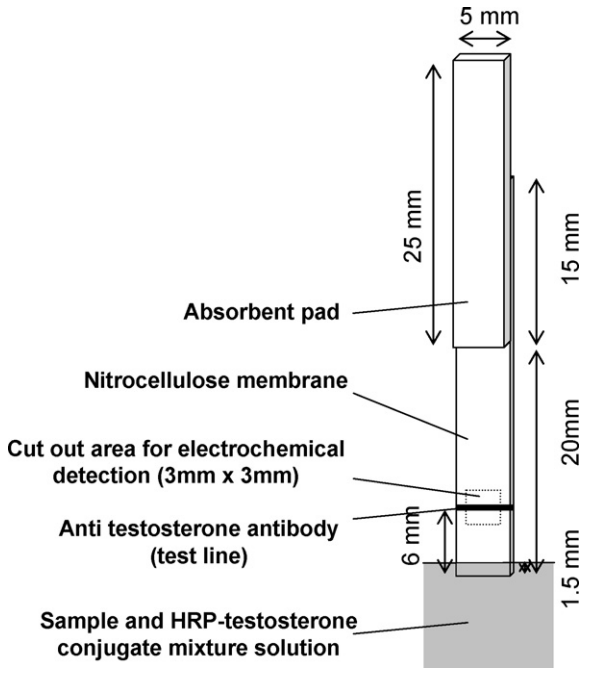

Fig. 2. Structure of the immunochromatographic test strip.

Whatman, Germany) using an arrayer (BioChip-Arrayer, Filgen, Inc., Japan) with a spot pin (diameter: 400 μm, TeleChem International, Inc., USA). The antibody spots were deposited in a line at 600 μm intervals to produce a test line 6 mm from the edge of the immunochromatographic test strips (5 mm × 35 mm) (Fig. 2). The strips were incubated in blocking solution for 90 min at 4 °C. After washing three times in PBS-T, the strips were dried in a desiccant dry box (Super dry SD-302-02, TOYO Living, Japan) at room temperature. An absorbent pad (5 mm × 25 mm; CFSP203000 cellulose fiber sample pads, Millipore, USA) was then positioned to overlap the strips by 15 mm. A 1.5 mm portion of the prepared test strips was dipped into 500 μl of PBS-T containing testosterone and 500 ng/ml HRP-labeled testosterone for 30 min, permitting the solution to flow up the strips by capillary action and form the immuno-complex at the test line. After washing the test strips, a 3 mm × 3 mm piece was cut from the nitrocellulose membrane as shown in Fig. 2, and the HRP activity of the resultant immuno-complex was electrochemically detected.

2.6. Equipment and methods for chemiluminescence detection

Chemiluminescence measurement was used to estimate the optimum concentration of immobilized anti-testosterone antibodies for immunochromatography. Various concentrations of anti-testosterone antibodies in PBS-G were spotted on nitrocellulose membranes (pore size: 0.2 μm, Bio-Rad Laboratories, Inc., USA) using an arrayer with a spot pin (diameter: 400 μm). After the blocking treatment, the membranes were immersed for 30 min in PBS solution containing various concentrations of testosterone and 500 ng/ml HRP-labeled testosterone. A luminal substrate with enhancer and H_2O_2 (ECL Western Blotting Detection Reagents, General Electric Company, USA) was used to detect the chemiluminescence signal. The detection reagent solution (0.125 ml/cm^2) was dropped on the membrane in a dark room. After a 5 min incubation at room temperature, chemiluminescence images were taken (exposure time: 10 s) with a highly sensitive CCD camera coupled to intensifiers (PI-MAX, Princeton Instruments, USA).

3. Results and discussion

3.1. Electrochemical characterization of the electrode chip

The electrode chip was characterized by CV using citric acid buffer containing 2.0 mM FcOH and 2.0 mM H_2O_2, in the presence or absence of 1 μg/ml HRP-labeled testosterone. Since the pseudo-reference electrode employed in this system was made of a gold thin layer, it was especially important to characterize the electrochemical behavior of the chip and, in particular, its ability to detect enzyme activities by amperometry. Fig. 3 shows the cyclic voltammograms obtained from repeated CV measurements. In the absence of labeled HRP (Fig. 3b), the oxidation and reduction current peaks for the FcOH/Fc$^+$OH redox couple were observed in the positive potential region, and the formal potential remained almost unchanged during eight consecutive scans (+0.096 V). Since the potential, determined by the Nernst equation, is dependent on the concentration ratio of FcOH/Fc$^+$OH at the surface of the pseudo-reference electrode, the FcOH solution used in the measurements was calculated to contain approximately 2.3% Fc$^+$OH. There were no changes in the shape of the voltammograms during eight consecutive voltage scan between −0.5 and +0.3 V (12 min). These results indicate that the pseudo-reference electrode system based on the gold electrode is sufficiently stable, at least under the present experimental conditions without HRP. The increase in the reduc-

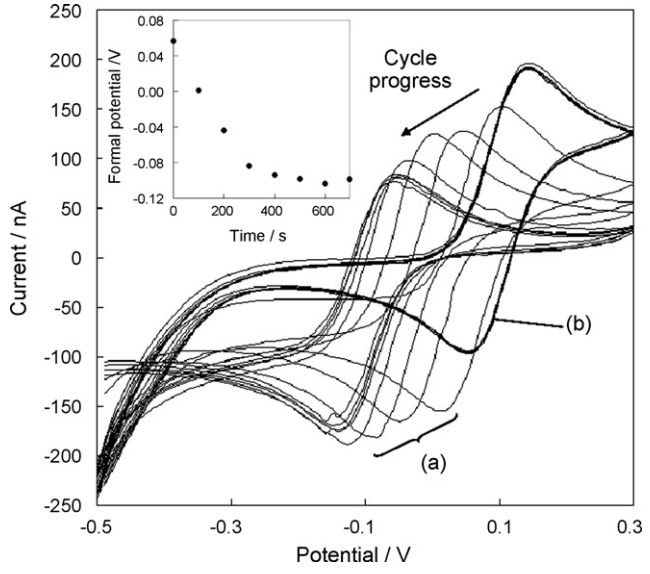

Fig. 3. Cyclic voltammograms measured in citric acid buffer containing 2.0 mM FcOH and 2.0 mM H_2O_2 in (a) presence and (b) absence of 1.0 μg/ml HRP-labeled testosterone. Scan rate: 100 mV/s. The inset shows the time-course of the shift of the apparent formal potential in the presence of HRP.

tion current in the negative scan, where the potential is below −0.3 V, is due to reduction of both oxygen and H_2O_2.

In contrast, the cyclic voltammetric behavior of the chip in the presence of labeled HRP was markedly different (Fig. 3a). The apparent formal potential significantly shifted in consecutive voltammograms, together with changes in the voltammetric peaks. The inset in Fig. 3 shows the time-course of the shift of the apparent formal potential. These changes are caused by increases in the concentration of Fc^+OH due to enzymatic reaction of HRP and the resulting decrease of the $FcOH/Fc^+OH$ concentration ratio. The decreasing ratio gradually shifts the apparent formal potential *versus* the pseudo-reference electrode in the negative direction. However, after five consecutive scans, the formal potential remained constant at −0.099 V since most of the FeOH molecules in the solution had been oxidized by the HRP-catalyzed reaction, and the $FcOH/Fc^+OH$ concentration ratio around the reference electrode reached 0.021. Because this potential shift affects amperometric measurements, the potential of the working electrode must be set to ensure that Fe^+OH remains diffusion-controlled. Therefore, we set the potential of the working electrode at −0.3 V *versus* the pseudo-reference electrode for the amperometric measurements.

3.2. Electrochemical detection of testosterone captured on nitrocellulose membrane

Calibration of both antibody adsorption on nitrocellulose membrane and of the concentration of the competitor (HRP-labeled testosterone) was carried out in order to characterize and optimize the immunoassay. The membrane was treated with various concentrations of anti-testosterone antibody (2.5–20 μg/ml) in PBS-G in order to immobilize the antibody on the membrane. After the blocking treatment, membranes with immobilized antibody were reacted with 20 μg/ml HRP-labeled testosterone for 30 min. After washing, the enzymatic activity of HRP immobilized on each membrane was evaluated using the electrode chip from the Fc^+OH reduction currents. The amperometric responses linearly increased with increasing antibody concentration used for immobilization, up to 5.0 μg/ml. However, at antibody concentrations above 5.0 μg/ml, the response gradually became saturated. Therefore, we used a solution containing 5.0 μg/ml anti-testosterone antibody for producing the membrane-immobilized antibody. Next, the concentration of HRP-labeled testosterone was optimized using this antibody-immobilized nitrocellulose membrane. The current responses increased linearly with increasing concentration of HRP-labeled testosterone up to 500 ng/ml, but became saturated at higher concentrations. Thus, the 500 ng/ml HRP-labeled testosterone solution was used in the competition experiments.

Testosterone detection was demonstrated using the device described above. Following the membrane treatments outlined in Section 2.4, the membrane was laid on the electrode chip and used to detect the amperometric responses. Fig. 4A shows the amperometric responses obtained using membranes treated with different concentrations of testosterone after the potential was stepped to −0.3 V. The spike-like responses of the capacitive currents were observed immediately after the potential step; subsequently, the reduction currents decreased gradually to almost steady-state in 10–20 s. The average currents between 10 and 20 s were used as the amperometric responses for the calibration curve.

Fig. 4B shows these current responses normalized to currents obtained in the absence of testosterone. The results indicate that the response depends on testosterone concentration. The response decreased with increasing concentration of testosterone since testosterone and HRP-labeled testosterone in the solution competitively react with the anti-testosterone antibodies immobilized on the nitrocellulose membrane. Good correlation between the testosterone concentration and current response was obtained in the range 0.25–10 ng/ml (0.87–35 nM) testosterone.

3.3. Electrochemical detection of testosterone by an immunochromatographic method

We estimated the concentration of immobilized anti-testosterone antibodies on the membrane required for optimal immunochromatography. The antibodies (0.25, 0.5, 1.0 and 2.0 μg/ml) were spotted on 5 mm × 60 mm nitrocellulose mem-

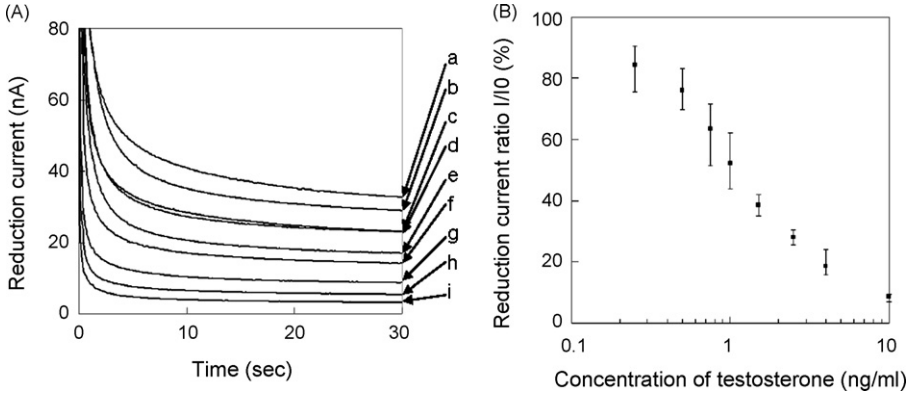

Fig. 4. (A) Amperometric responses based on the reduction current of Fc^+OH generated by the enzymatic reaction of labeled-HRP captured on a nitrocellulose membrane. Amperometric measurements were carried out at −0.3 V *vs.* the pseudo-reference electrode in 2.0 mM FeOH, 2.0 mM H_2O_2 in citric acid buffer, pH 4.5. The concentrations of testosterone; (a) 0, (b) 0.25, (c) 0.5, (d) 0.75, (e) 1.0, (f) 1.5, (g) 2.5, (h) 4.0 and (i) 10 ng/ml. (B) Calibration curves obtained upon competitive immunoreaction of a constant concentration of HRP-labeled testosterone (500 ng/ml) and increasing concentrations of analyte testosterone.

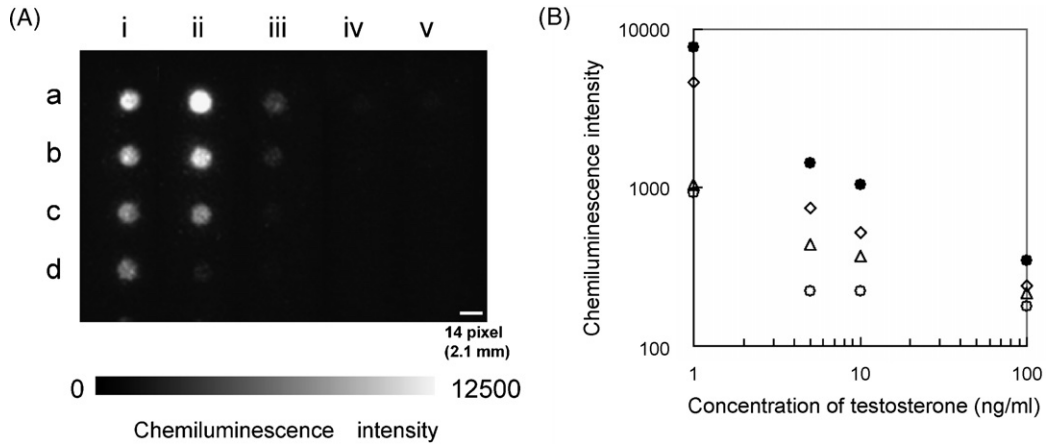

Fig. 5. (A) Chemiluminescence images of labeled HRP captured by the anti-testosterone antibody. Concentrations of anti-testosterone antibodies spotted on the membrane; (a) 2000, (b) 1000, (c) 500 and (d) 250 μg/ml. Concentrations of analyte testosterone; (i) 0, (ii) 1.0, (iii) 5.0, (iv) 10 and (v) 100 ng/ml. (B) Chemiluminescence intensities as a function of the concentration of testosterone. Averages of chemiluminescence intensities of 14 × 14 pixels in the center of each spot were plotted. Concentrations of anti-testosterone antibodies spotted on the membrane; ●: 2000, ◊: 1000, △: 500 and ◯: 250 μg/ml.

branes at 600 μm intervals to create the test line. Each membrane was treated with PBS solution containing various concentrations of testosterone (0, 1.0, 5.0, 10 and 100 ng/ml) and 500 ng/ml HRP-labeled testosterone. Fig. 5A shows the chemiluminescence signals from five membrane strips with four antibody-immobilized spots. Chemiluminescence was emitted from HRP-labeled testosterone captured on the antibody spots. Fig. 5B shows the chemiluminescence intensity as a function of testosterone concentration. The average chemiluminescence intensity from a 14 pixel × 14 pixel (2.1 mm × 2.1 mm) square in the center of each spot was plotted and showed that, in a single membrane strip, the signal intensity increases with increasing immobilized antibody concentration. On the other hand, the intensity decreases with increasing concentration of testosterone. Using a 2.0 μg/ml antibody solution for immobilization studies provided large signal differences in the concentration range investigated; therefore, we used 2.0 μg/ml anti-testosterone antibody solution for immobilizing the antibody on the membrane.

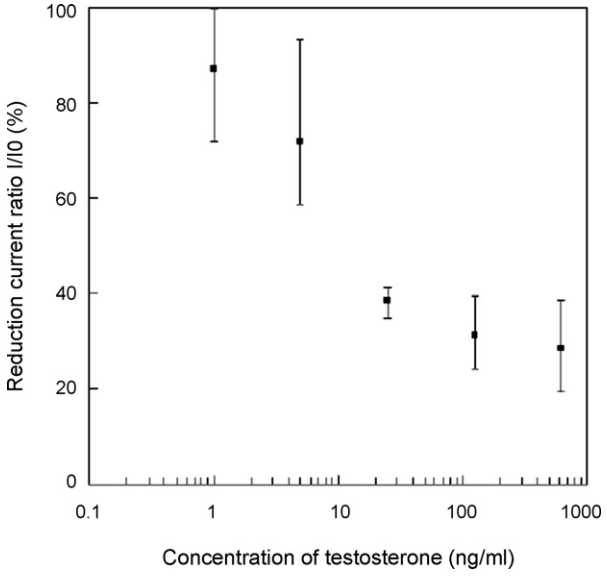

Fig. 6. Calibration curve obtained from the $Fc^{+}OH$ reduction current generated by the reaction of HRP-labeled testosterone captured on the test line. A 1.5-mm portion of the test strips was dipped for 30 min in PBS-T containing testosterone and 500 ng/ml HRP-labeled testosterone.

Finally, we performed preliminary immunochromatography experiments using the membrane strip immunosensor (Fig. 2). A 1.5 mm portion of the prepared nitrocellulose membrane strips was dipped into various concentrations of testosterone solution containing 500 ng/ml HRP-labeled testosterone. The fluid flow rate was essentially constant at 1.3 mm/min. After washing the test strips, a 3 mm × 3 mm piece was cut out and amperometric measurements were carried out. Fig. 6 shows the change in the current responses as a function of testosterone concentration. The responses decreased with increasing concentration of testosterone in the range 1–625 ng/ml which covers the concentration levels required to measure in serum samples. Further improvement in the reaction between HRP-labeled testosterone and the anti-testosterone antibody is necessary in order to minimize signal errors in the lower concentration range. The total measurement time required by this system (about 40 min, including the time for solution flow and the electrochemical measurement) is considerably shorter than that required for conventional ELIZA formats. We are presently in the process of developing a hybrid system which will incorporate the electrode chip into the immunochromatographic membrane.

4. Conclusion

In this study, we demonstrated a quantitative assay for testosterone which combines an immunochromatographic method with an electrochemical detection chip. Electrochemical detection was based on amperometric measurement of $Fc^{+}OH$ generated by a HRP-labeled antibody catalyzed reaction.

First, we fabricated the electrochemical detection chip, which incorporated a gold pseudo-reference electrode, and characterized its performance by CV. The redox potential of $FcOH/Fc^{+}OH$ shifted to negative potentials, and the shape of the CV scans changed upon repeated potential scanning. These

changes were caused by changes in the FcOH/Fc^+OH concentration ratio at the pseudo-reference electrode resulting from HRP-catalyzed oxidation of FcOH. Based on these results, we selected a potential of −0.3 V *versus* the pseudo-reference electrode in order to ensure the diffusion-controlled detection of Fc^+OH for amperometric measurements.

We showed that testosterone could be quantitatively detected using nitrocellulose membrane (3 mm × 3 mm pieces) as a platform for competitive immunoassay with detection by an electrochemical chip. Testosterone competitively reacted with horseradish peroxidase-labeled testosterone and was captured by the anti-testosterone antibody immobilized on the membrane. The activity of the labeled-HRP captured on the membrane was measured with amperometry, and it was found that the current decreased with increasing concentrations of analyte testosterone.

Finally, immunochromatographic assays combined with electrochemical detection performed in this study showed that testosterone concentrations between 1 and 625 ng/ml could be detected by the amperometric measurements. This method provides an on-site, rapid, easy to use and portable detection system for testosterone that combines immunochromatography and electrochemical detection for application in POCT measurements.

References

[1] K. Sananikone, M.J. Delwiche, R.H. BonDurant, C.J. Munro, Trans. ASAE 47 (2004) 1357.
[2] A. Puerta, J.C. Diez-Masa, M. de Frutos, Anal. Chim. Acta 53 (2005) 69.
[3] K. Patterson, B. Olsen, C. Thomas, D. Norn, M. Tam, C. Elkins, J. Clin. Microbiol. 40 (2002) 3694.
[4] R.A. Cole, H.M. Lu, Y.Z. Shi, J. Wang, T. De-Hua, A.T. Zhou, Tuber. Lung Dis. 77 (1996) 363.
[5] M. Müller-Bardorff, T. Rauscher, M. Kampmann, S. Schoolmann, F. Laufenberg, D. Mangold, R. Zerback, A. Remppis, H.A. Katus, Clin. Chem. 45 (1999) 1002.
[6] Y.M. Kim, S.W. Oh, S.Y. Jeong, D. Jinpyo, E.Y. Choi, Environ. Sci. Technol. 37 (2003) 1899.
[7] S. Choi, E.Y. Choi, D.J. Kim, J.H. Kim, T.S. Kim, S.W. Oh, Clin. Chim. Acta 339 (2004) 147.
[8] J. Hampl, M. Hall, N.A. Mufti, Y.M. Yao, D.B. MacQueen, W.H. Wright, D.E. Cooper, Anal. Biochem. 288 (2001) 176.
[9] R.S. Niedbala, H. Feindt, K. Kardos, T. Vail, J. Burton, B. Bielska, S. Li, D. Milunic, P. Bourdelle, R. Vallejo, Anal. Biochem. 293 (2001) 22.
[10] R.H. Daniels, A.R. Watson, U.S. Patent US 2002/0004246 A1 (2002).
[11] H. Kikuchi, A. Ohta, Y. Takahashi, A. Shibata, T. Ohtake, K. Watanabe, Clin. Chem. 49 (2003) 1709.
[12] S.W. Oh, J.D. Moon, S.Y. Park, H.J. Jang, J.H. Kim, K.B. Nahmd, E.Y. Choi, Clin. Chim. Acta 356 (2005) 172.
[13] C.H. Yoon, J.H. Cho, H. Oh, M.J. Kim, C.W. Lee, J.W. Choi, S.H. Paek, Biosens. Bioelectron. 19 (2003) 289.
[14] K.S. Lee, T.H. Kim, M.C. Shin, W.Y. Lee, J.K. Park, Anal. Chim. Acta 380 (1999) 17.
[15] F. Lu, K.H. Wang, Y. Lin, Analyst 130 (2005) 1513.
[16] P.Y. Liu, A.K. Death, D.J. Handelsman, Endocr. Rev. 24 (2003) 313.
[17] M.M. Shores, V.M. Moceri, K.L. Sloan, A.M. Matsumoto, D.R. Kivlahan, J. Clin. Psychiatry 66 (2005) 7.
[18] T. Iwamoto, T. Yanase, E. Koh, H. Horie, K. Baba, M. Namiki, H. Nawata, Int. J. Urol. 95 (2004) 751.
[19] T.O. Joos, M. Schrenk, P. Höpfl, K. Kröger, U. Chowdhury, D. Stoll, D. Schörner, M. Dürr, K. Herick, S. Rupp, K. Sohn, H. Hämmerle, Electrophoresis 21 (2000) 2641.

Available online at www.sciencedirect.com
ScienceDirect
Talanta 73 (2007) 926–931
Talanta
www.elsevier.com/locate/talanta

A rapid and sensitive immunonanogold resonance scattering spectral probe for complement 3

Zhiliang Jiang [a,b,*], Wenxin Huang [a], Aihui Liang [b], Bing Chen [a]

[a] School of Environment and Resource, Guangxi Normal University, Guilin 541004, China
[b] Department of Material and Chemical Engineering, Guilin University of Technology, Guilin 541004, China

Received 22 March 2007; received in revised form 12 May 2007; accepted 14 May 2007
Available online 24 May 2007

Abstract

Gold nanoparticles in size of about 10 nm was used to label goat anti-human complement 3 (anti-C3) to obtain a sensitive and selective immunoresonance scattering spectral probe for C3. It was based on the immune reaction between labeled anti-C3 and C3 in the pH 5.6 Na_2HPO_4–citric acid buffer solutions and in presence of polyethylene glycol (PEG). The resonance scattering (RS) intensity at 560 nm enhanced greatly with C3. Well linear relationships between the enhanced RS intensity ($\triangle I_{RS}$) and the C3 concentration in the range of 8.33–200 ng ml^{-1} were obtained, with a detection limit of 2.8 ng ml^{-1} and the limit of quantification 8.51 ng ml^{-1} for C3. The convenient and selective and sensitive assay was applied to quantification of C3 in human sera, with satisfactory results.

Keywords: Complement 3; Resonance scattering effect of colloidal gold; Immunonanogold resonance scattering spectral probe

1. Introduction

Low or high levels of human complement 3 (C3) are often associated with systemic lupus erythematosus (SLE), rheumatoid arthritis (RA) or acute inflammation and malignancy [1–4]. Therefore, the determination of C3 plays a critical role in clinic, which can provide good evidence for diagnosis of some diseases. Several assays for C3 has been reported, such as immunonephelometric assay (INA) [5], radial immunodiffusion (RID) [6], electroimmunodiffusion (EID) [7], radioimmunoassay (RIA) [8], enzyme-linked immunosorbent assay (ELISA) [9], electrochemical immunosensor [10,11]. INA and RID assays for analysis of C3 are simple, but they have drawbacks of low sensitivity [12]. EID assay is susceptible to many factors such as other plasma proteins, and detect less samples in each plate [13]. RIA assay is sensitive. However, this method is hampered by its complicated operation and using radioactive elements as tracer. ELISA assay is commonly used in routine clinical laboratory but it is easy to be influenced by apparatus, reaction temperature and the detection limit for human serum C3 only reached 1.2 μg ml^{-1} [14]. Electrochemical immunosensor can be directly detected antibody and antigen, but the immobilization of antibody is not very good and the renewability of immunosensor is restricted [10]. So establishment of rapid and selective assay is necessary for assay of C3.

Gold nanoparticles have been studied and applied due to its novel physical and chemical properties [11–16]. For example, gold nanoparticles are applied to analytical chemistry for developing biochips and biosensors [17–19], and detection of oligonucleotide [20–22], and proteins [23]. As we know, gold nanoparticle was a good labeling substance [24]. It can also be modified chemically by biomolecules, organic compounds, amino or mercapto groups [25]. At present, it has been used as probe for labeling antibody or antigen by non-covalent electrostatic adsorption [26]. This has become the fourth immuno-labeling technique. Recently, as a detection method, spectrophotometry has been applied in immuno-labeling technique. However, the sensitivity of spectrophotometry is low. Light scattering is a commonly phenomenon, and RS or resonance light scattering (RLS) is the resonance between the incident photon and the interface electron on the particle surface,

* Corresponding author at: School of Environment and Resource, Guangxi Normal University, Guilin 541004, China.
E-mail address: zljiang@mailbox.gxnu.edu.cn (Z. Jiang).

0039-9140/$ – see front matter © 2007 Elsevier B.V. All rights reserved.
doi:10.1016/j.talanta.2007.05.021

which cause the scattering signal enhanced greatly. RS analytical technique [27,28], with simple and high sensitivity, has been applied to analytical chemistry. However, most of their selectivity was not high. Because of the correlation of RS intensity with the size of the gold particles [29], recently, the combination of RS effect of gold nanoparticles and nanogold labeled immunoreaction has been applied to assay of trace apolipoprotein and fibrinogen [30], with high selectivity and sensitivity and simplicity. Here, we have developed a simple and sensitive immunonanogold resonance scattering spectral (IRSS) probe for C3, with rapidity, sensitivity, selectivity and no phase separation procedure.

2. Experimental

2.1. Apparatus

A RF-540 spectrofluorometer (Shimadzu, Japan) was used to record resonance scattering spectra and to measure the RSS intensity. A TU-1901 double beams UV–vis spectrophotometer (Puxi General Apparatus Limited Company, Beijing, China) was used to record the absorption spectra of colloidal gold and the labeled anti-C3 immune reaction. A 79-1 magnetic heat agitator (Zhongda Instrumental Plant, Jiangsu, China) was used for stirring when colloidal gold labeling anti-C3. A SK8200LH ultrasonic reactor (Kedao Ultrasonic Instrument Limited Company, Shanghai, China) was used to reduce incubation time and an H-600 transmission electron microscope (Electronic Stock Limited Company, Japan) was use to characterize gold particles and gold labeled anti-C3 particles and to measure their diameters.

2.2. Reagents

Goat anti-human C3 anti-serum and C3 standard reagents were all purchased from the Jiemen Biological Technology Cooperation Company, Shanghai, China. Anti-C3 and C3 was dissolved in de-ionized water to 1000.0 μg ml^{-1}, 15.0 μg ml^{-1}, respectively. Human sera were supplied by No.5 Hospital of Guilin. A 1.0% (w/w) $HAuCl_4$ solution (National Pharmaceutical Group Chemical Reagents Company, China) and a 1.0% (w/w) sodium citrate solution (Shanghai Chemical Reagent Plant, Shanghai, China) were used to prepare gold nanoparticles in size of 10 nm. Na_2HPO_4–NaH_2PO_4 (PB), Tris–HCl and Na_2HPO_4–citric acid buffer solution were prepared according to a certain volume ratio. The stock solution of KCl, K_2CO_3 were prepared with water at 100.0 mg ml^{-1} and 27.6 mg ml^{-1}. A 30% (w/w) PEG 4000, PEG 6000, PEG 10,000, PEG 20,000 was prepared with water. All the chemicals used were analytical grade and all aqueous solutions were prepared using de-ionized water.

2.3. Preparation and evaluation of colloidal gold

Au particles in size of 10 nm were prepared according to Ref. [31]. A typical solution of 10 nm gold nanoparticles exhibit a characteristic surface plasmon absorption band centered at 518 nm. Transmission electron microscopy (TEM) was used to measure the size. The TEM showed the gold particles with high dispersion and good distribution due to repelling force of double electrical layer of gold particles surface absorption citrate ions [32], the average size is about 10 nm.

2.4. Preparation of the immunoresonance spectral probe

2.4.1. Influence of pH on gold labeling anti-C3

The effect of different pH on the gold labeling anti-C3 was considered by RS procedure. A 1.0 ml colloidal gold solution was transferred to each calibration test tube, and regulated the pH from 4.0 to 8.5 by 27.6 mg ml^{-1} K_2CO_3 or 0.1 M HCl, then dropped 30.0 μl (1000.0 μg ml^{-1}) anti-C3 serum into each test tube. After 5 min at room temperature, 0.10 ml 100.0 mg ml^{-1} KCl was added into each test tube. Ten minutes later, diluted each calibration tube to 3.0 ml with water, and then recorded the $I_{560\,nm}$ on the spectrofluorometer. When the pH was less than 6.5, anti-C3 could not stabilize colloidal gold, the $I_{560\,nm}$ enhanced since gold nanoparticles were aggregated as drop of KCl. When the pH was in 6.5–7.5, the $I_{560\,nm}$ remained approximately constant. It could be interpreted that colloidal gold being coated by anti-C3 and KCl could not make them aggregate. Though the values of $I_{560\,nm}$ were minimum, when the pH exceeded 8.0, in fact colloidal gold had not labeled anti-C3, to some extent anti-C3 solution could only stabilize colloidal gold that the added KCl solution could not result in gold nanoparticles aggregation. A pH 7.5 of colloidal gold was considered to be suitable.

2.4.2. Selection of anti-C3 amount

A 0–30.0 μg anti-C3 was added to 1.0 ml pH 7.5 colloidal gold solutions, after 5 min, a 0.10 ml 100 mg ml^{-1} KCl solution was added and then shook the mixture. Ten minutes later, it was diluted to 3.0 ml. The $I_{560\,nm}$ was measured. Results shown that 20.0 μg anti-C3 was the minimum content for stabilizing 1.0 ml colloidal gold, and was chosen for use.

2.4.3. Preparation of gold labeling anti-C3

A 0.20 ml 3.0% PEG 20,000 (the end concentration was 0.03%) as stabilizer was added to 200.0 ml colloidal gold, the pH was adjusted to 7.5. Under the condition of magnetic stirring, 2.0 mg anti-C3 was slowly added to the above colloidal gold solution, controlling the dropping time 10 min. After stirring the solution 15 min, then stored them at 4 °C until assayed. When the gold labeled anti-C3, the surface plasmon absorption peak was at 519 nm. Because the colloidal gold was coated by anti-C3, the TEM of the gold particles (Fig. 1a) was not clear same as the colloidal gold.

2.5. Procedures

To a graduated test tube, 0.50 ml gold labeled goat anti-human C3 (labeled anti-C3), 0.20 ml of pH 5.6 Na_2HPO_4–citric acid

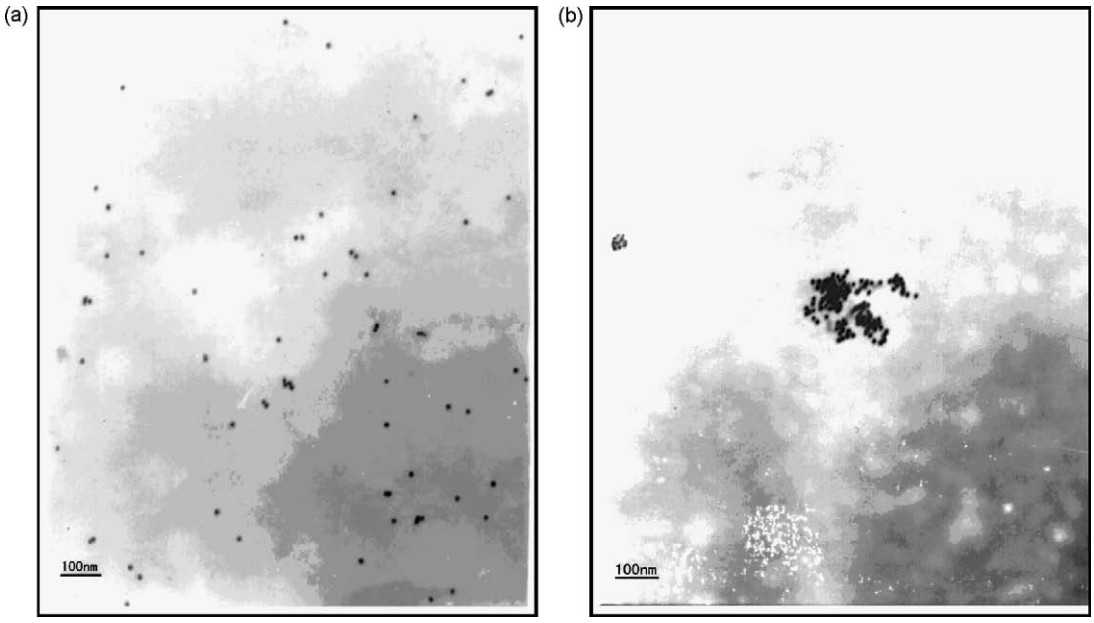

Fig. 1. Transmission electron microscopy of (a) gold labeled anti-C3, and (b) gold labeled anti-C3 and C3 system.

buffer, and a certain amount of C3 solution was added successively. The mixture was shook, then 0.60 ml 30% PEG 6000 solution was added, and then diluted it to 3.0 ml. Subsequently, placed these tubes to ultrasonic reactor for incubation 15 min at 37 °C. The $I_{560\,nm}$ was recorded. The blank $(I_{560\,nm})_b$ with no C3 was also measured. A value $\triangle I_{RS} = I_{560\,nm} - (I_{560\,nm})_b$ was obtained.

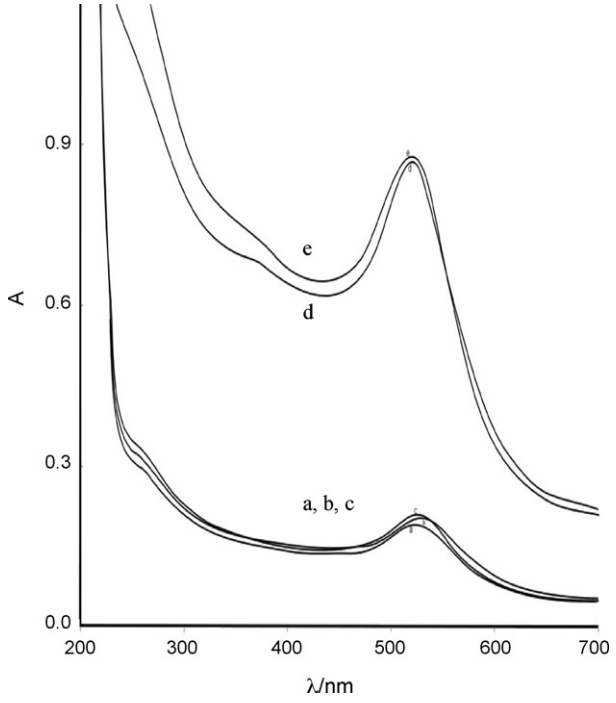

Fig. 2. UV spectra. (a) pH 5.6–9.65 μg ml^{-1} labeled anti-C3–0.050 μg ml^{-1} C3–60 mg ml^{-1} PEG 6000; (b) pH 5.6–9.65 μg ml^{-1} labeled anti-C3–0.10 μg ml^{-1} C3–60 mg ml^{-1} PEG 6000; (c) pH 5.6–9.65 μg ml^{-1} labeled anti-C3–0.150 μg ml^{-1} C3–60 mg ml^{-1} PEG 6000; (d) 57.9 μg ml^{-1} colloidal gold; (e) 57.9 μg ml^{-1} labeled anti-C3.

3. Results and discussion

3.1. UV absorption spectra

As can be seen from Fig. 2, colloidal gold and the labeled anti-C3 exhibited strong and narrow absorption peak at 518 and 519 nm. However, when the immunoreaction took place between labeled anti-C3 and different concentrations of C3, the absorption decreased and the absorption peaks shifted to red, about

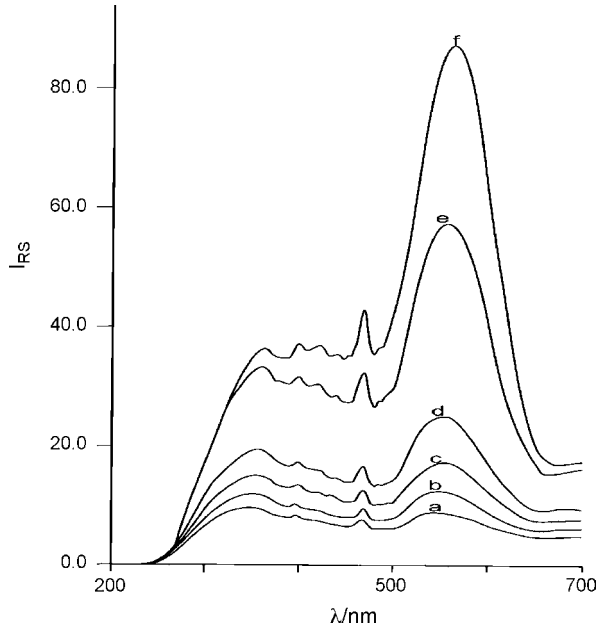

Fig. 3. RS spectra of labeled anti-C3 and C3 system. (a) pH 5.6–9.65 μg ml^{-1} labeled anti-C3–60 mg ml^{-1} PEG 6000; (b) (a)–0.0167 μg ml^{-1} C3; (c) (a)–0.033 μg ml^{-1} C3; (d) (a)–0.050 μg ml^{-1} C3; (e) (a)–0.10 μg ml^{-1} C3; (f) (a)–0.15 μg ml^{-1} C3.

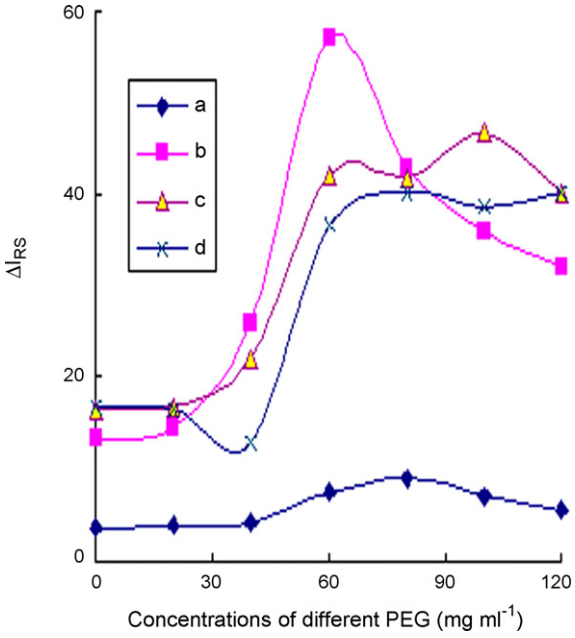

Fig. 4. Influence of different PEG and concentrations on $\triangle I_{RS}$. pH 5.6–9.65 μg ml^{-1} labeled anti-C3–0.067 μg ml^{-1} C3. (a) PEG 4000; (b) PEG 6000; (c) PEG 10,000; (d) PEG 20,000.

522 nm. This also indicated that there are aggregations in the system.

3.2. Resonance scattering spectra (RSS)

As Fig. 3 shows, anti-C3, C3 and their immunocomplex showed weak RS signals, and the system exhibited four resonance-scattering peaks at 360, 400, 420, and 560 nm, and a synchronous scattering peak at 470 nm that is owing to the maximum emission of the light source. And obviously, the 560 nm one is stronger than the others. Gold labeled anti-C3 could stably exist in the 60 mg ml^{-1} PEG 6000 solution. After the immune reaction took place between anti-C3 and C3 in the presence of PEG 6000, the gold particles would be aggregated and formed immunogold complex. It could be proved by transmission electron microscope (Fig. 1b). We can also see from Fig. 3 that in the addition of C3 concentration, the aggregated gold particles led the enhancement of RS at 560 nm greatly. A wavelength of 560 nm was selected.

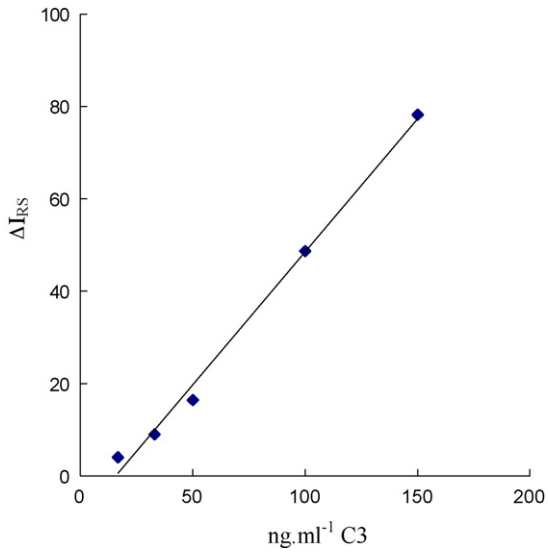

Fig. 5. Working curve.

3.3. Selection of pH, types and volume of buffer solutions

The effect of pH 5.8–8.0 Na_2HPO_4–NaH_2PO_4(PB), pH 7.0–8.4 Tris–HCl and pH 5.0–8.0 Na_2HPO_4–citric acid buffer solution on $\triangle I_{RS}$ were tested, respectively. Results showed the optimum buffer solution was pH 5.6 Na_2HPO_4–citric acids, and its volume was 0.20 ml.

3.4. Effect of different PEG concentrations

Low concentration of PEG could stabilize colloidal gold, but high concentration of PEG would lead aggregation of nanogold particles to enhance the RS signals. The effect of concentrations of PEG 4000, PEG 6000, PEG 10,000, PEG 20,000 on $\triangle I_{RS}$ were considered. As in Fig. 4 the four PEG could enhance the $\triangle I_{RS}$. However, 60 mg ml^{-1} of PEG 6000 was considered to be the most effective.

3.5. Effect of labeled anti-C3 concentrations

Our results showed that the immunoreaction between anti-C3 and C3 could be applied to assay of microamounts of C3. However, the used amount of precious anti-C3 was higher. These results demonstrated that the $\triangle I_{RS}$ increased with the

Table 1
Comparison analytical methods for C3

Methods	Detection samples	Linear range (μg ml^{-1})	Detection limits (μg ml^{-1})	Reference
Chronopotentiometry	Human sera	0.00012–0.117	0.00002	[10]
Electrostatic attraction immunosensor	Human plasma	0.0182–0.2925	0.0091	[35]
Sandwich SS-RTP-IA	Human serum	0.00625–0.100	0.00137	[36]
HPLC	Rat serum	0.0125–0.400	No	[37]
TrFIA	Cerebrospinal fluid	0.0007–3.65	0.0001	[38]
Immunonephelometry	Human milk	11.56–370	No	[39]
Laser nephelometry	Cerebrospinal fluid	80–12000	No	[40]
Turbidimetry method	Human serum	0.167–3.33	0.093	In our work
Gold labeled immunoresonance scattering	Human serum	0.00833–0.200	0.00280	In this paper

Table 2
Effects of coexistence substances on the determination of 0.13 μg ml^{-1} C3

Coexistence substance	Tolerance (μg ml^{-1})	Relative error (%)	Coexistence substances	Tolerance (μg ml^{-1})	Relative error (%)
L-Tyrosine	200	−4.1	HAS	20	+4.6
Glycine	500	−3.1	Polyaspartic acid	300	−2.8
Urea	400	−4.3	L-Arginine	22	+4.1
Histidine	300	+4.5	Tryptophan	270	−4.8
Folic acid	166	−5.0	Cane sugar	833	−2.0
Vb_2	16	−0.9	L-Cystine	280	−3.1
IgA	33	+4.1	IgG	46	+4.0
BSA	15	+3.9	Ascorbic acid	120	+3.5
$MnSO_4$	100	+4.3	$ZnSO_4$	120	−3.9
DL-Tryptophan	80	+2.9	IgM	18	+2.8
α-acid Glycoprotein	8	+4.6	DL-Methionine	120	+1.7

labeled anti-C3 in the range of 0–7.72 μg ml^{-1}. A 9.65 μg ml^{-1} of labeled anti-C3, giving a maximum $\triangle I_{RS}$, was chosen for use. The anti-C3 amount of this labeled assay reduced greatly.

3.6. Selection of ultrasonic incubation time

Results showed that the incubation time obviously shorted in an ultrasonic device. The $\triangle I_{RS}$ increased with the incubation time within 15 min. After 15 min the $\triangle I_{RS}$ tended to be stable. A 15 min incubation time at 37 °C was chosen for use.

3.7. Calibration curve

The calibration curve for C3 was constructed according to the procedure as above, as in Fig. 5. The RS intensities were obtained under the optimum conditions. The $\triangle I_{RS}$ was linear to the concentrations C in the range of 8.33–200 ng ml^{-1} for C3. The regression equation could be expressed as $\triangle I_{RS} = 0.575C - 8.98$, the correlation coefficient was 0.9938, and the detection limit (LOD) can be calculated according to the equation $L_D = 3S_b/K$ [33], where L_D represents detection limit, 3 is the factor at the 95% confidence level, S_b the standard deviation of the blank measurements ($n = 20$), and K is the slope of the calibration curve. The limit of detection reached at 2.8 ng ml^{-1}. According to the equation of quantification limit (LOQ) is given by $L_Q = 10\sigma_0$, where 10 is the IUPAC recommendation 1995 default value, σ_0 is the standard deviation of the estimated quantity (net signal or concentration) under the null hypothesis [34]. The quantification limit was 8.51 ng ml^{-1} C3. As shown in Table 1, compared with other methods of C3 [10,35–40], this method had the advantages of rapid and good selectivity.

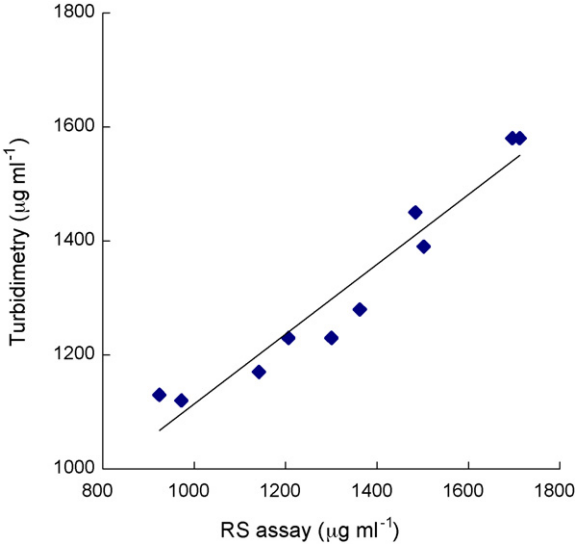

Fig. 6. Linear regression analysis.

3.8. Interference by coexisting foreign substances

Under optimum conditions, according to the procedure of Section 2.5, the influence of foreign coexisting substances on the determination of 0.13 μg ml^{-1} C3 was tested by pre-mixing 0.20 ml of pH 5.6 Na_2HPO_4–citric acid buffer and 0.50 ml gold labeled anti-C3 with foreign substances such as Table 2 listed. As results shown in Table 2, we could know under the permission of ±5% error, the tested substances can be present in relatively higher concentrations, which demonstrate the assay has good selectivity.

3.9. Assay of samples

Ten normal serum samples were drawn from hospital and diluted the serum (1:100) with PB buffer solution, and then a volume of 30.0 μl diluted samples were measured accord-

Table 3
Results of determination for C3 in human sera

Samples	Average found ($n = 5$, μg ml^{-1})	R.S.D. (%)	Reference method, turbidimetry ($n = 5$, μg ml^{-1})
1#	1206	3.4	1230
2#	924	2.9	1130
3#	1502	2.8	1390
4#	1142	5.6	1170
5#	1712	2.3	1580
6#	972	3.5	1120
7#	1484	2.4	1450
8#	1362	2.2	1280
9#	1696	2.8	1580
10#	1300	3.4	1230

ing to the procedure. As shown in Table 3, we analyzed 10 serum samples abstained from No. 5 People's Hospital, Guilin, China. The samples were also assayed by turbidimetry method (Fig. 6). The results obtained with both methods were consistent with published reference intervals for serum in the range of 900.0–1800.0 $\mu g\,ml^{-1}$ [41]. The confidence intervals for both assays were 95%.

4. Conclusions

In view of gold nanoparticle-labeled technique has the advantages of simplicity, accuracy and non-pollution, here we described a means to prepare IRRS probe with high specificity quantification of human serum C3. A rational assay was established with combination resonance scattering effect of nanogold particles with highly selective immune reaction. This approach of physically modified IRRS probes will be applied to a wide range in clinical chemistry.

Acknowledgements

This work was supported by the National Natural Scientific Foundation of China (20365001, 20667001) and the Foundation of New Century Ten-Hundred-Thousand Talents of Guangxi.

References

[1] M.A. Seelen, A. Roos, J. Wieslander, T.E. Mollnes, J. Immunol. Methods 296 (2005) 187.
[2] X. Shen, T. Li, Clinic Immunology and Immunology Test New Technology, People Military Medicine Press, Beijing, 2002.
[3] J.M. Wu, Practical Medicine Test Reference Values and Analysis for Abnormal Results, People Sanitation Press, Beijing, 1998.
[4] J.F. Zhen, Medical Immunology, 1st ed., People Sanitation Press, Beijing, 1991.
[5] S.R. Barnum, J.E. Volanakis, Molecules and Cells of Immunology, Karger Press, Basel, 1990.
[6] R. Vlaicu, H.G. Rus, F. Niculescu, A. Cristea, R.M. Rev, Med. Interne 23 (1985) 29.
[7] A. Fryden, P. Forsberg, H. Link, Acta Neurol. Scand. 68 (1983) 157.
[8] B.C.G. Dujardin, P.C. Driejijk, A.F.M. Roijers, T.A. Out, J. Immunol. Methods 80 (1985) 227.
[9] J. Zwirner, G. Dobos, O. Gotze, J. Immunol. Methods 186 (1995) 55.
[10] X. Chu, X. Fu, G.L. Shen, R.Q. Yu, Chem. Res. Chin. Univ. 26 (2005) 1637.
[11] J. Yguerabide, E. Yguerabide, Anal. Biochem. 262 (1998) 137.
[12] J. Yguerabide, E. Yguerabide, Anal. Biochem. 262 (1998) 157.
[13] K.L. Kelly, E. Coronado, L.L. Zhao, G.C. Schatz, J. Phys. Chem. B 107 (2003) 668.
[14] A. Henglein, J. Phys. Chem. B 97 (1993) 5457.
[15] A.A. Lazarides, G.C. Schatz, J. Phys. Chem. B 104 (2000) 460.
[16] G.L. Hornysk, C.J. Patdssi, C.R. Martin, J. Phys. Chem. B 101 (1997) 1548.
[17] W.M. Mullett, E.P. Lai, J.M. Yeung, Methods 22 (2000) 77.
[18] A. Kadir, R.L. Joseph, D.G. Chris, Anal. Chem. 77 (2005) 2007.
[19] R.A. Reynolds, C.A. Mirkin, R.L. Letsinger, J. Am. Chem. Soc. 122 (2000) 3795.
[20] C.A. Mirkin, R.L. Letsinger, R.C. Mucic, J.J. Storhoff, Nature 382 (1996) 607.
[21] W. Fritzsche, Rev. Mol. Biotechnol. 82 (2001) 37.
[22] P.C. Ray, A. Fortner, J. Griffin, Chem. Phys. Lett. 414 (2005) 259.
[23] R.B. Dickson, M.C. Willingham, I.H. Pastan, J. Biol. Chem. 256 (1981) 3454.
[24] X. Shen, D. Li, Clinical Immunology and New Immunological Technique, People Military Medicine Press, Beijing, 2002.
[25] S.P. Liu, Z. Yang, Z.F. Liu, L. Kong, Anal. Biochem. 353 (2006) 108.
[26] F. Daumas, H. Mazarguil, C. Millot, Biol. Biophy. Res. Commun. 295 (2002) 610.
[27] H. Zhong, J.J. Xu, H.Y. Chen, Talanta 67 (2005) 749.
[28] C.Z. Huang, Y.F. Li, Talanta 70 (2006) 609.
[29] Z.L. Jiang, Z.W. Feng, Y.S. Li, F. Li, Sci. Chin. Ser. B 31 (2001) 183.
[30] Z.L. Jiang, S.J. Sun, A.H. Liang, W.X. Huang, A.M. Qin, Clin. Chem. 52 (2006) 1389.
[31] M. Moeremans, G. Daneels, A. Van Dijck, G. Langanger, J. DeMey, J. Immunol. Methods 74 (1984) 353.
[32] W.G. Hou, D.J. Sun, C.G. Zhang, Application of Colloid Chemistry, Science Press, Beijing, 1998.
[33] Z.G. Chen, J.B. Liu, Y.L. Han, Talanta 71 (2007) 1246.
[34] L.A. Currie, Anal. Chim. Acta 391 (1999) 105.
[35] Z.S. Wu, J.S. Li, M.H. Luo, G.L. Shen, R.Q. Yu, Chem. Res. Chin. Univ 26 (2005) 441.
[36] Y.L. Wu, L.D. Li, J.M. Liu, G.H. Zhu, Anal. Chim. Acta 539 (2005) 271.
[37] M. Rajanikanth, R.C. Gupta, J. Pharm. Biomed. Anal. 26 (2001) 519.
[38] O. Gaillard, D. Meillet, M.C. Diemert, L. Musset, J. Delattre, E. Schuller, J. Galli, Clin. Chem. 39 (1993) 309.
[39] V. Tregoat, P. Montagne, M.L. Cuilliere, M.C. Bene, G. Faure, J. Clin. Immunol. 19 (1999) 300.
[40] D.D. Carl, W.M. Kameron, S.S. Richard, L.C. Robert, Clin. Chem. 22 (1976) 1465.
[41] M.E. Grevink, G. Horst, P.C. Limburg, C.G.M. Kallenberg, M. Bijl, J. Autoimmun. 24 (2005) 329.

Available online at www.sciencedirect.com
ScienceDirect
Talanta 73 (2007) 850–856
Talanta
www.elsevier.com/locate/talanta

Electrical conductivity and cation exchange kinetic studies on poly-*o*-toluidine Th(IV) phosphate nano-composite cation exchange material

Asif Ali Khan *, Anish Khan

Analytical and Polymer Research Laboratory, Department of Applied Chemistry, Faculty of Engineering and Technology, Aligarh Muslim University, Aligarh 202002, India

Received 9 March 2007; received in revised form 1 May 2007; accepted 1 May 2007
Available online 13 May 2007

Abstract

An advanced organic–inorganic cation exchange material poly-*o*-toluidine Th(IV) phosphate nano-composite was synthesized by a modified sol–gel technique by incorporating Th(IV) phosphate precipitate with the matrix of poly-*o*-toluidine. The material showed good ion-exchange behavior and used successfully in separation of metal ions. The conductivity of the composite was found within the range of 10^{-2} to 10^{-3} S/cm; measured by 4-in-line-probe dc electrical conductivity measuring technique. The conductivity is at the border of metallic and semiconductor region. Ion-exchange kinetics for few divalent metal ions was evaluated by particle diffusion-controlled ion-exchange phenomenon at four different temperatures. The particle diffusion mechanism is confirmed by the linear τ (dimensionless time parameter) versus t (time) plots. The exchange processes thus controlled by the diffusion within the exchanger particle for the systems studies herein. Some physical parameters like self-diffusion coefficient (D_0), energy of activation (E_a) and entropy of activation (ΔS^0) have been evaluated under conditions favoring a particle diffusion-controlled mechanism.

Keywords: Cation exchange kinetics; Poly-*o*-toluidine Th(IV) phosphate; Composite cation exchanger

1. Introduction

Poly-*o*-toluidine Th(IV) phosphate, a nano-composite cation exchange material has shown excellent ion-exchange properties and successfully used in analytical and electro analytical studies in our previous work [1]. However, ion-exchange mechanism of this material has yet to be reported in our present work. The mechanism of ion-exchange can be explained taking into account of ion-exchange equilibrium with respect to time and the phenomenon of ion-exchange is considered as diffusion of ion through particles of the exchanger and its adherent film. With the help of experimental data and mathematical computation some physical parameters like self-diffusion co-efficient (D_0), energy of activation (E_a) and entropy of activation (ΔS^0) are obtained.

Many types of electrically conducting materials classified as electrolytes or polymer ionics have been developed and characterized in recent years [2]. Composite materials composed of conducting polymers and polyvalent metal acid salt have generated interest in the field of synthetic metals. Composite systems having high conductivity at ambient and some ambient temperatures find unique applications such as rechargeable lithium batteries. Thus at present research work poly-*o*-toluidine Th(IV) phosphate, a composite material in the range of nano-particle size is selected for electrical conducting studies.

2. Experimental

2.1. Reagents and instruments

The main reagents used for the synthesis of the material were obtained from CDH, Loba Chemie, E-merck and Qualigens (India Ltd., used as received). All other reagents and chemicals were of analytical grade; an electronic balance (digital, Sartorius-21OS, Japan). A 4-in-line-probe electrical conductivity-measuring instrument, scientific Equipment (India), was used for measuring the dc electrical conductivity.

* Corresponding author. Tel.: +91 571 2720323.
E-mail address: asifkhan42003@yahoo.com (A.A. Khan).

0039-9140/$ – see front matter © 2007 Elsevier B.V. All rights reserved.
doi:10.1016/j.talanta.2007.05.003

A hydraulic pressure instrument was used for making pellets of sample material.

2.2. Preparation of poly-o-toluidine Th(IV) phosphate composite

As given in our previous work [1].

2.2.1. Synthesis of poly-o-toluidine

The polymerization of the monomer *ortho*-tolidine was initiated by the addition of oxidizing agent, i.e., ammonium persulphate in 1:1 ratio under constant stirring at room temperature for 2 h [3]. After two hours a brown color poly-*o*-toluidine polymer was obtained.

2.2.2. Synthesis of thorium(IV) phosphate

The method of preparation of the inorganic precipitate of Th(IV) phosphate ion-exchanger was very similar to that of Alberti Constantino with slight modification [4].

2.2.3. Synthesis of poly-o-toluidine Th(IV) phosphate

Electrically conducting composite was prepared by the sol–gel mixing of poly-*o*-toluidine into the inorganic precipitate of thorium(IV) phosphate. Similarly, a number of poly-*o*-toluidine thorium(IV) phosphate nano-composite cation exchanger samples were prepared and on the basis of Na^+ exchange capacity (I.E.C), percent of yield and physical appearance, sample S-3 [1] was selected for further studies.

2.3. Electrical conductivity measurements

The composite sample was treated with 1 M aqueous solution of HCl and washed with DMW to remove excess HCl. The sample material was dried completely at between 40 and 50 °C in an oven. Then 200 mg material was finely ground in a mortar pastel and pellets were made at room temperature with the help of a hydraulic pressure instrument at 25 KN pressure for 20 min. The thickness of pellet was measured by a micrometer. Four-probe electrical conductivity measurements with increasing temperatures (between 35 and 200 °C) for the composite samples were performed on pressed pellets by using a 4-in-line-probe dc electrical conductivity-measuring technique.

2.4. Kinetic measurements

The composite cation exchange material was treated with 1 M HNO_3 for 24 h at room temperature with occasional shaking. Intermittently the supernatant liquid was replaced with fresh acid to ensure the complete conversion to the H^+-form and the excess acid was removed after packing the material in column and washing with DMW. Then the dried ion-exchanger sample in the H^+-form was ground and then sieved to obtain particles of definite mesh sizes. From these, the particles of mean radii ~125 μm (50–70 mesh) were used to evaluate various kinetic parameters. The rate of exchange was determined by the limited bath technique as follows. Twenty milliliter fractions of the 0.03 M metal ion solutions (Mg, Ca, Sr, Ba, Ni, Cu, Mn and Zn) were shaken with 200 mg of the cation exchanger in H^+-form in several stoppered conical flasks at the desired temperatures [25, 40, 55 and 70 °C] for different time intervals (0.5, 1.0, 2.0, 3.0, 4.0 and 5.0 min). The supernatant liquid was removed immediately and determinations were made, usually by EDTA titration [5]. Each set was repeated four times and the mean value was taken for calculations.

3. Results and discussion

3.1. Electrical conducting behavior of poly-o-toluidine Th(IV) phosphate nano-composite

Electrical conductivities of the pellets of poly-*o*-toluidine Th(IV) phosphate composite samples were determined from the measurement of conductivity of the samples using the four-probe method [6] of conductivity measurement for semiconductors. This is the most satisfactory method as it overcomes difficulties which are encountered in conventional methods of conductivity measurement (i.e., two probe), e.g., the rectifying nature of the metal-semiconductor contacts and the injection of minority carriers by one of the current-carrying contacts, which affects the potential of the other contacts and modulates the conductance of the material, etc. The current–voltage data generated at increasing temperatures for the determination of electrical conductivity of the composite sample were processed for calculation of electrical conductivity using the following equation:

$$\rho = \frac{\rho_0}{G_7(W/S)} \tag{1}$$

where ρ is corrected resistivity (Ω cm), ρ_0 the uncorrected resistivity (Ω cm), $G_7(W/S)$ is the correction factor used for the case of a no conducting bottom surface, which is a function of W, the thickness of the sample under test (cm) and S, the probe spacing (cm); i.e.

$$G_7(W/S) = (2S/W)\ln 2 \tag{2}$$

$$\rho_0 = V/I \times 2\pi S, \tag{3}$$

$$\sigma = \frac{1}{\rho} \tag{4}$$

where I is the current (A), V the voltage (V) and σ is the dc electrical conductivity (s/cm). Although the electrical conductivity measurements were done under ambient conditions, the composite samples were thoroughly dried before making the pellets and performing the electrical conductivity measurements. Hence, the contribution of protonic conductivity to the total electrical conductivity due to the presence of moisture should be minimum and need not be taken into consideration.

The main constituent that makes the composite electrically conductive is poly-*o*-toluidine. The conducting properties depend on the percolation behavior of the conducting phase. The electrical conductivity of the composite is due to oxidized poly-*o*-toluidine maintained in its conductive state by poly-*o*-toluidine Th(IV) phosphate counter ions in excess. The variation of electrical conductivity (σ) of the composite samples prepared with 10 vol.% *o*-tolidine concentration, with increasing

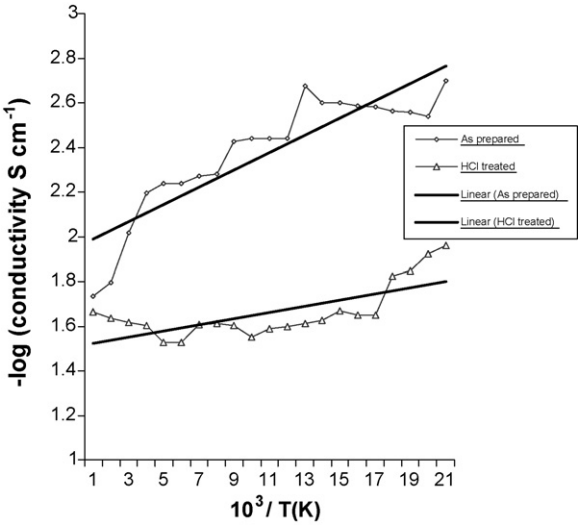

Fig. 1. Arrhenius plots for poly-*o*-toluidine Th(IV) phosphate nano-composite material.

temperatures (between 35 and 200 °C) was investigated. On examination, it was observed that the electrical conductivities of the samples increase with the increase in temperature and the values are of the order of 10^{-3} to 10^{-2} S cm^{-1}, i.e., in the borderline of conductor and semiconductor region. To determine the nature of the dependence of electrical conductivity on temperature, plots of $\log \sigma$ versus $1000/T$ (K) were drawn (Fig. 1) and they followed the Arrhenius equation similarly to other semiconductors [7].

The thermal stability of the composite material (HCl treated) in terms of dc electrical conductivity retention was studied under isothermal conditions (at 50, 80, 110 and 140 °C) using 4-probe-in-line dc electrical conductivity measurements at 30 °C intervals. The electrical conductivity measured with respect to the time of accelerated ageing is presented in Fig. 2. It was observed that the electrical conductivity is quite stable at 50, 80, 110 and 140 °C, which supports the fact that the dc electrical conductivity of the composites is sufficiently stable under ambient temperature conditions. The electrical conductivity decreases with time at 140 °C, which may be attributed to the loss of dopant and the chemical reaction of dopant with the material. The material was also observed to be a stable material, i.e., the room temperature conductivity is negligibly affected by short-term exposure to laboratory air as is evident from Fig. 3.

The conductivity (1.77×10^{-2} s/cm) of poly-*o*-toluidine Th(IV) phosphate nano-composite synthesized presently is higher compare to that of the homopolymer of poly(*o*-toluidine) prepared by chemical polymerization with ammonium persulfate as the oxidant at 0 °C (2.2×10^{-3} s/cm) [8] may be due to the electron donating property of the Th(IV) phosphate group. The conductivity of the composite by self doped polymerization (as prepared) increase by increasing temperature up to 120 °C. This increase in conductivity with increase in temperature is the characteristics of "Thermal activated behaviour" [9]. The increase conductivity could be due to the increase of efficiency of charge transfer between the composite chains and the dopant with increase in the temperature [10]. It is also possible that the

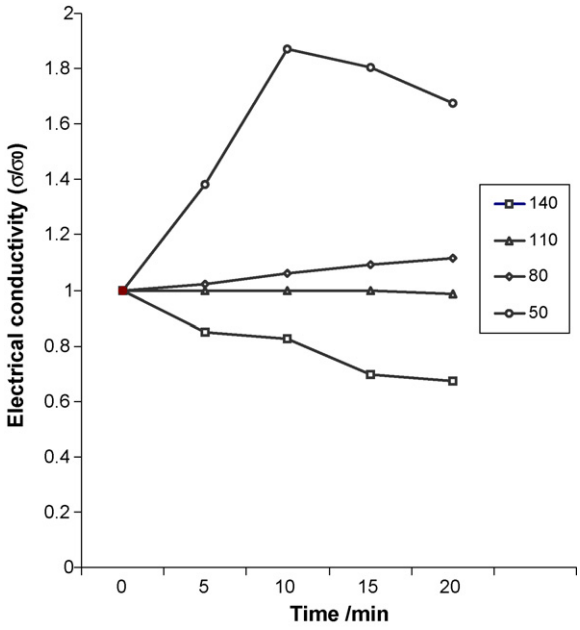

Fig. 2. Isothermal stability of poly-*o*-toluidine Th(IV) phosphate nano-composite in terms of dc electrical conductivity with respect to time at 50, 80, 110 and 140 °C.

thermal curing affects of the chain alignment of the polymeric inorganic composite, which leads to the increase of conjugation length and that brings about the increase of conductivity.

3.2. *Ion-exchange kinetics of poly-o-toluidine Th(IV) phosphate nano-composite*

Kinetic measurements were made under conditions favoring a particle diffusion-controlled ion-exchange phenomenon for the exchange of Mg(II)–H(I), Ca(II)–H(I), Sr(II)–H(I), Ba(II)–H(I), Ni(II)–H(I), Cu(II)–H(I), Mn(II)–H(I) and Zn(II)–H(I). The particle diffusion controlled phenomenon is favoured by a high metal ion concentration, a relatively large particle size of the exchanger and vigorous shaking of the exchanging mixture. The infinite time of exchange is the time necessary to obtain

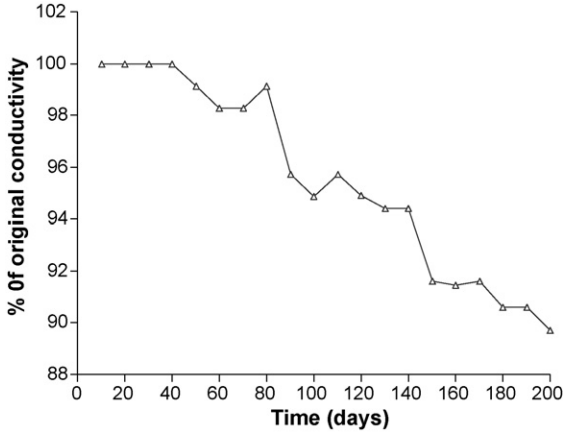

Fig. 3. Conductivity with time on exposure to laboratory air for poly-*o*-toluidine Th(IV) phosphate nano-composite material (HCl treated).

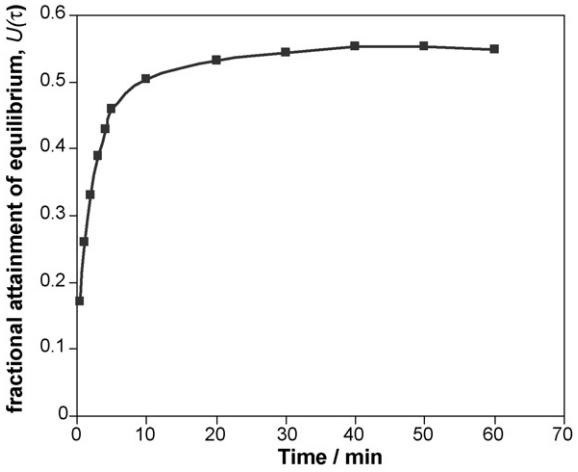

Fig. 4. A plot of $U(\tau)$ vs. t for M(II)–H(I) exchanges at 40 °C on a poly-*o*-toluidine Th(IV) phosphate nano-composite cation exchanger for the determination of infinite time.

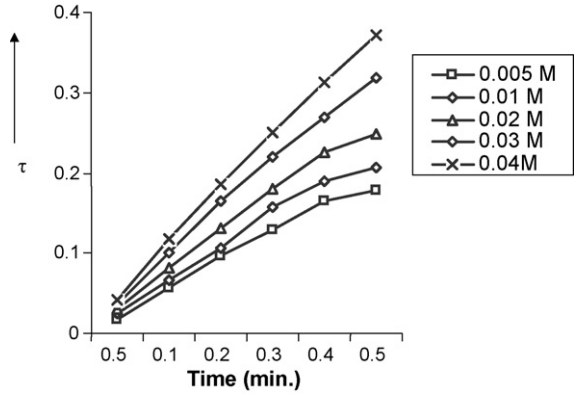

Fig. 5. A plot of τ vs. t (time) for M(II)–H(I) exchanges at 40 °C on a poly-*o*-toluidine Th(IV) phosphate nano-composite cation exchanger using different metal solution concentration.

equilibrium in an ion-exchange process. The ion-exchange rate becomes independent of time after this interval. Fig. 4. shows that 40 min were required for the establishment of equilibrium at 40 °C for Mg^{2+}–H^+ exchange. Similar behavior was observed for Ca^{2+}–H^+, Sr^{2+}–H^+, Ba^{2+}–H^+, Ni^{2+}–H^+, Cu^{2+}–H^+, Mn^{2+}–H^+ and Zn^{2+}–H^+ exchanges. Therefore, 40 min was assumed to be the infinite time of exchange for the system. A study of the concentration effect on the rate of exchange at 40 °C showed that the initial rate of exchange was proportional to the metal ion concentration at and above 0.03 M (Fig. 5). Below the concentration of 0.03 M, film diffusion control was

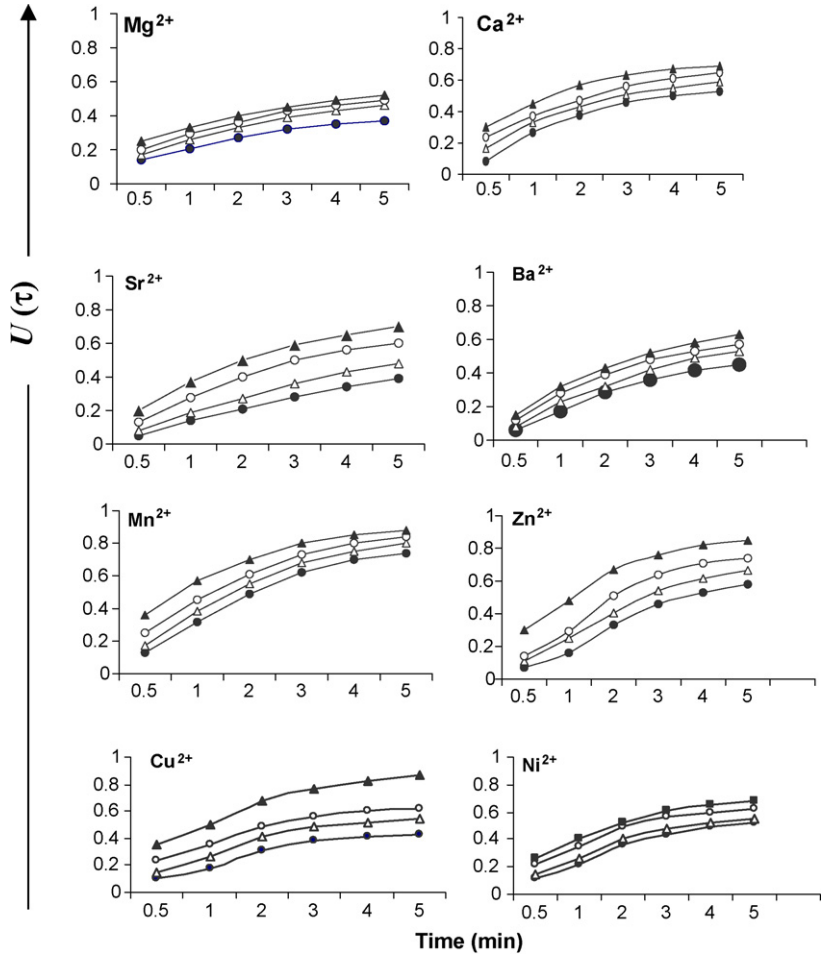

Fig. 6. Plots of $U(\tau)$ vs. t (time) for different M(II)–H(I) exchanges at different temperature: (●) 25 °C; (△) 40 °C; (◯) 55 °C; (▲) 70 °C on a poly-*o*-toluidine Th(IV) phosphate nano-composite cation exchanger.

more prominent. The results are expressed in terms of the fractional attainment of equilibrium, $U(\tau)$ with time according to the equation:

$$U(\tau) = \frac{\text{the amount of exchange at time '}t\text{'}}{\text{the amount of exchange at infinite time}}. \quad (5)$$

Plots of $U(\tau)$ versus t (min), for all metal ions (Fig. 6) indicated that the fractional attainment of equilibrium was faster at a higher temperature suggesting that the mobility of the ions increased with an increase in temperature and the uptake decreased with time. Each value of $U(\tau)$ will have a corresponding value of τ, a dimensionless time parameter. On the basis of the Nernst–Planck equation, the numerical results can be expressed by explicit approximation [11–13]:

$$U(\tau) = \{1 - \exp[\pi^2(f_1(\alpha)\dot{\tau} + f_2(\alpha)\tau^2 + f_3(\alpha)\tau^3)]\}^{1/2} \quad (6)$$

where τ is the half time of exchange $= \bar{D}_{H^+}t/r_0^2$, α the mobility ratio $= \bar{D}_{H^+}/\bar{D}_{M^{2+}}$, r_0 the particle radius, $\bar{D}_{H^+}$ and $\bar{D}_{M^{2+}}$ are the inter diffusion coefficients of counter ions H^+ and M^{2+}, respectively in the exchanger phase. The three functions $f_1(\alpha)$, $f_2(\alpha)$ and $f_3(\alpha)$, depend upon the mobility ratio (α) and the charge ratio ($Z_{H^+}/Z_{M^{2+}}$) of the exchanging ions. Thus they have different expressions as given below. When the exchanger is taken in the H^+ form and the exchanging ion is M^{2+}, for $1 \leq \alpha \leq 20$, as in

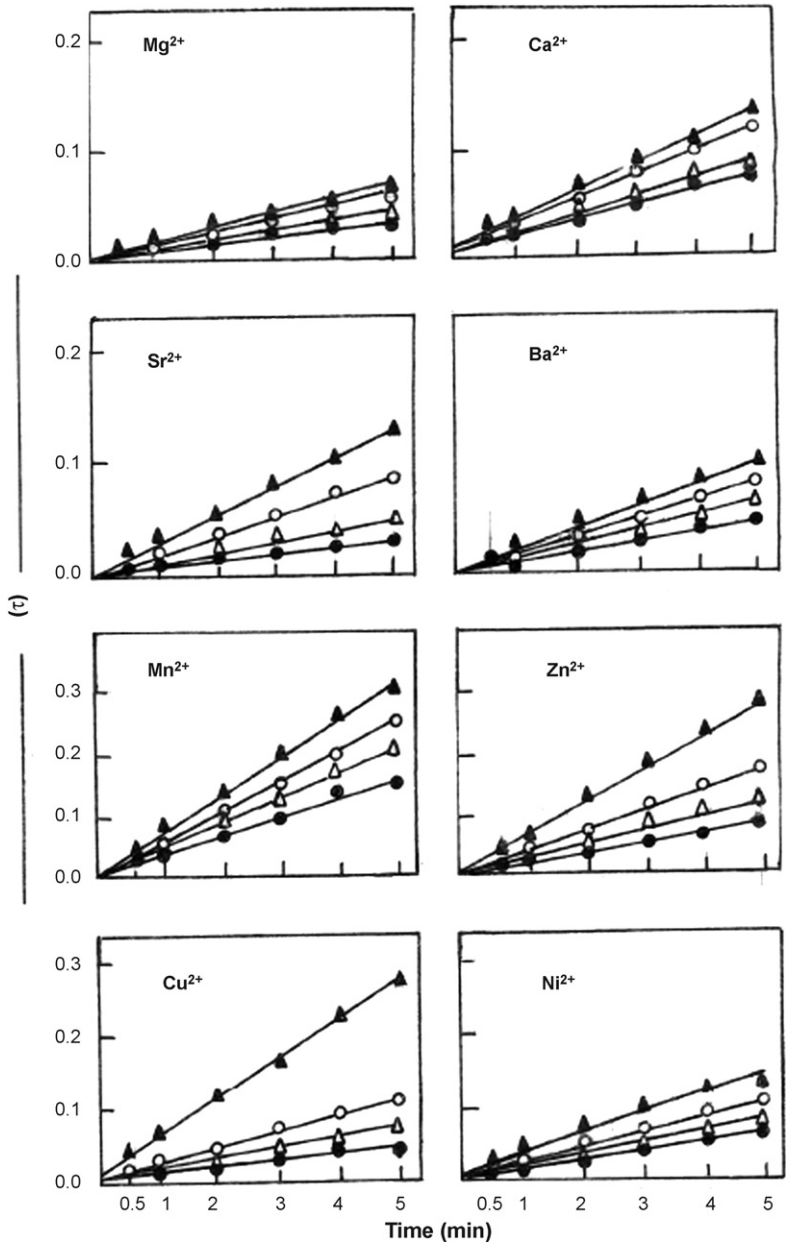

Fig. 7. Plots of τ vs. t (time) for different M(II)–H(I) exchanges at different temperature: (●) 25 °C; (△) 40 °C; (◯) 55 °C; (▲) 70 °C on a poly-*o*-toluidine Th(IV) phosphate nano-composite cation exchanger.

the present case, the three functions have the values:

$$f_1(\alpha) = -\frac{1}{0.64 + 0.36\alpha^{0.668}}, \quad (7)$$

$$f_2(\alpha) = -\frac{1}{0.96 - 2.0\alpha^{0.4635}}, \quad (8)$$

$$f_3(\alpha) = -\frac{1}{0.27 + 0.09\alpha^{1.140}}, \quad (9)$$

The value of τ is obtained on solving Eq. (6) using a computer. The plots of τ versus time (t) at the four temperatures, as shown in Fig. 7 are straight lines passing through the origin, confirming the particle diffusion control phenomenon for M(II)–H(I) exchanges at a metal ion concentration of 0.03 M. The slopes (S values) of various τ versus time (t) plots are given in Table 1. The S values are related to $\bar{D}_{H^+}$ as follows:

$$S = \frac{\bar{D}_{H^+}}{r_0^2} \quad (10)$$

The values of $-\log \bar{D}_{H^+}$ obtained by using Eq. (10) plotted against $1/T$ are straight lines as shown in Fig. 8, thus verifying the validity of the Arrhenius relation;

$$\log \bar{D}_{H^+} = D_0 \exp(-E_a/RT). \quad (11)$$

D_0 is obtained by extrapolating these lines and using the intercepts at the origin. The activation energy (E_a) is then calculated with the help of the Eq. (11), putting the value of $\bar{D}_{H^+}$ at 273 K.

Table 1
Slopes of various τ vs. time (t) plots on poly-*o*-toluidine Th(IV) phosphate nano-composite cation exchanger at different temperatures

Migrating ions	10^4 S (s^{-1})			
	25 °C	40 °C	55 °C	70 °C
Mg(II)	2.35	2.77	3.86	4.30
Ca(II)	1.00	1.55	1.83	2.11
Sr(II)	1.00	1.48	2.78	4.15
Ba(II)	1.30	1.91	2.42	3.05
Cu(II)	1.43	2.50	3.48	8.82
Ni(II)	2.15	2.50	3.58	4.50
Zn(II)	4.92	6.58	7.98	10.15
Mn(II)	2.55	3.65	5.40	8.90

The entropy of activation (ΔS°) was then calculated by substituting D_0 in Eq. (12)

$$D_0 = 2.72d^2(kT/h)\exp(\Delta S^\circ/R) \quad (12)$$

where d is the ionic jump distance taken as 5 Å [14], k the Boltzmann constant, R the gas constant, h the Plank's constant and T is the taken as 273 K. The values of the diffusion coefficient (D_0), energy of activation (E_a) and entropy of activation (ΔS°) thus obtained are summarized in Table 2. The kinetic study reveals that equilibrium is attained faster at a higher temperature (Fig. 6.), probably because of a higher diffusion rate of ions through the thermally enlarged interstitial positions of the ion-exchange matrix. The particle diffusion phenomenon is evident from the straight lines passing through the origin for the τ versus

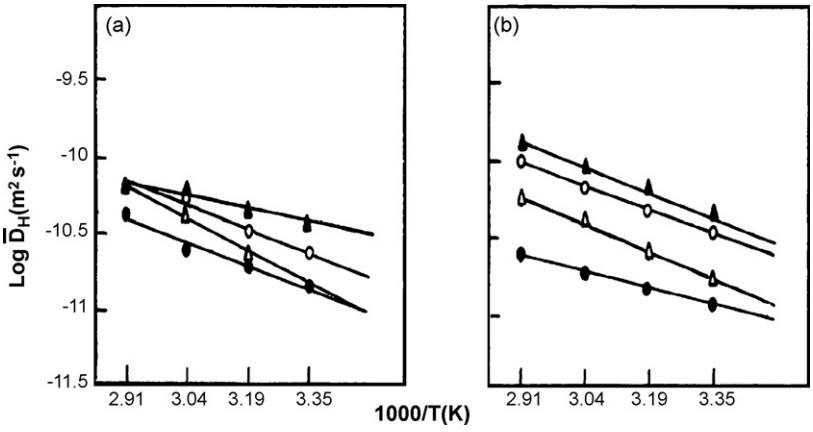

Fig. 8. Plots of $-\log \bar{D}_{H^+}$ vs. 1000/T (K) for (a) Mg(II): ▲, Ca(II): ◯, Ba(II) △, Sr(II)● and (b) Mn(II): ▲, Cu(II): ◯, Ni(II): △ and Zn(II) ● on poly-*o*-toluidine Th(IV) phosphate nano-composite cation exchanger.

Table 2
Values of D_0, E_a and ΔS° for the exchange of H(I) with some metal ions on poly-*o*-toluidine Th(IV) phosphate nano-composite cation exchanger

Metal ion exchange with H(I)	10^9 ionic mobility ($m^2\ V^{-1}\ s^{-1}$)	10^2 ionic radii (nm)	10^{10} D_0 ($m^2\ s^{-1}$)	E_a (k Jmol^{-1})	ΔS° (J K^{-1} mol^{-1})
Mg(II)	55	7.8	10.06	8.12	145.60
Ca(II)	62	10.6	9.99	8.14	145.15
Sr(II)	62	12.7	9.93	8.16	145.21
Ba(II)	66	14.3	10.26	8.08	144.80
Cu(II)	57	7.0	6.65	9.06	148.51
Ni(II)	52	7.8	7.07	8.93	157.99
Zn(II)	56	8.3	6.72	9.04	148.41
Mn(II)	55	9.1	8.16	8.59	146.82

time (t) plots, as shown in Fig. 7. Negative values of the entropy of activation suggest a greater degree of order achieved during the forward ion-exchange in M(II)–H(I) process. From the Table 2 it is observed that the self-diffusion co-efficient is highest for Ba^{2+} ion. As ionic radii of Ba^{2+} ion is greater, the Ba^{2+} ion is least hydrated and therefore its self-diffusion co-efficient is higher.

According to the value of self-diffusion co-efficient, the selectivity order of metal ions is $Ba^{2+} > Mg^{2+} > Ca^{2+} > Sr^{2+} > Mn^{2+} > Ni^{2+} > Zn^{2+} > Cu^{2+}$. Further, it is observed that E_a values of metal ion are in the order $Ba^{2+} < Mg^{2+} < Ca^{2+} < Sr^{2+} < Mn^{2+} < Ni^{2+} < Zn^{2+} < Cu^{2+}$ indicate the order of exchange process of metal ion. Lower the activation energy (E_a) stronger the preference for metal ion by the exchanger site. Similarly smaller the standard entropy change (ΔS°) values indicate the preference of more active exchangeable site in the exchanger and strong preference for that metal ions [15].

4. Conclusion

Poly-*o*-toluidine Th(IV) phosphate exhibit good ion-exchange capacity, thermal and chemical resistivity. Inorganic precipitate of Th(IV) phosphate modified by incorporation of poly-*o*-toluidine behaves as an electrically conducting composite cation exchanger. The electrical borderline semi-conducting behavior of this organic-inorganic composite material can be employed as a semiconductor in electrical and electronic devices. The mechanism of ion-exchange suggest the particle diffusion as confirmed by the linear τ (dimensionless time parameter) versus t (time) plots. Further, various kinetic parameters like self-diffusion coefficient (D_0), Energy of activation (E_a) and entropies of activation (ΔS°) have been evaluated under condition favoring a particle diffusion-controlled mechanism. The above studies thus reveal the promising use of poly-*o*-toluidine Th(IV) phosphate as a cation exchanger. The chemical, thermal and mechanical strength of this electro-active material can make the material more important for the electro analytical purpose.

Acknowledgements

The authors are thankful to the Chairman, Department of Applied Chemistry, Z.H. College of Engineering and Technology, A.M.U. (Aligarh) and also to the U.G.C. funded research project for providing financial assistance.

References

[1] A.A. Khan, A. Khan, Inamuddin, Talanta 72 (2007) 69.
[2] F. Corce, G. Gerace, G. Dautzenberg, G.P. Passerini, Appetecchi, B. Scrosati, Electrochim. Acta 39 (1994) 2187.
[3] Xin-Guili, Mei-Rong Hung, Rui Liu, React. Funct. Polym. 2 (2005) 285.
[4] A.A. Khan, Inamuddin, M.M. Alam, Mat. Res. Bull. 40 (2005) 289.
[5] C.N. Reilly, R.W. Schmidt, F.S. Sadek, J. Chem. Edu. 36 (1959) 555.
[6] Instruction Manual, Scientific Equipment and Services, Roorkee, India (2000).
[7] F. Mohammad, in: H.S. Nalwa (Ed.), Handbook of Advanced Electronic and Photonic Materials and Devices, Academic Press, New York, 2000, p. 321.
[8] P.S. Raw, D.N. Sathyanarayana, Synth. Met. 138 (2003) 519.
[9] F. Zuo, M. Angelopoulos, A.G. MacDiarmid, A.J. Epstein, Phys. Riv. B. 36 (1987) 3475.
[10] A. Kobayashi, H. Ishikawa, K. Amano, M. Satoh, E. Hasegawa, J. Appl. Phys. (I) 74 (1993) 296.
[11] T. Vermeulen, Ind. Eng. Chem. 45 (1953) 1664.
[12] F. Helfferich, M.S. Plesset, J. Chem. Phys. 28 (1958) 418.
[13] M.S. Plesset, F. Helfferich, J.N. Franklin, J. Chem. Phys. 29 (1958) 1064.
[14] R.M. Barrer, R.F. Bertholomew, L.V.C. Rees, Phys. Chem. Solids 21 (1961) 12.
[15] K.G. Varshney, U. Gupta, S.M. Maheshwari, React. Kinet. Catal. Lett. 61 (1997) 127.

Available online at www.sciencedirect.com
ScienceDirect
Talanta 73 (2007) 838–844
Talanta
www.elsevier.com/locate/talanta

DNA sensor based on an *Escherichia coli lac Z* gene probe immobilization at self-assembled monolayers-modified gold electrodes

Óscar A. Loaiza, Susana Campuzano, María Pedrero, José M. Pingarrón *

Departamento de Química Analítica, Facultad de Ciencias Químicas, Universidad Complutense de Madrid, E-28040 Madrid, Spain

Received 7 March 2007; received in revised form 25 April 2007; accepted 30 April 2007
Available online 13 May 2007

Abstract

A novel approach to construct an electrochemical DNA sensor based on immobilization of a 25 base single-stranded probe, specific to *E. coli lac Z* gene, onto a gold disk electrode is described. The capture probe is covalently attached using a self-assembled monolayer of 3,3′-dithiodipropionic acid di(*N*-succinimidyl ester) (DTSP) and mercaptohexanol (MCH) as spacer. Hybridization of the immobilized probe with the target DNA at the electrode surface was monitored by square wave voltammetry (SWV), using methylene blue (MB) as electrochemical indicator. Variables involved in the sensor performance, such as the DTSP concentration in the modification solution, the self-assembled monolayers (SAM) formation time, the DNA probe drying time atop the electrode surface and the amount of probe immobilized, were optimized.

A good stability of the single- and double-stranded oligonucleotides immobilized on the DTSP-modified electrode was demonstrated, and a target DNA detection limit of 45 nM was achieved without signal amplification. Hybridization specificity was checked with non-complementary and mismatch oligonucleotides. A single-base mismatch oligonucleotide gave a hybridization response only $7 \pm 3\%$, higher than the signal obtained for the capture probe before hybridization. The possibility of reusing the electrochemical genosensor was also tested.

Keywords: *E. coli*; Genosensor; Electrochemical; Self-assembled monolayers; Methylene blue

1. Introduction

The efficient immobilization of single-stranded nucleic acid probes on a suitable electrode support is an important issue in the fabrication of reliable electrochemical genosensors [1]. Gold and glassy carbon surfaces [2,3] have demonstrated to be suitable platforms for the covalent immobilization of oligonucleotides. This immobilization method allows the nucleic acid probes retaining their hybridization function and bioaffinity properties. Moreover, self-assembled monolayers (SAMs) have resulted as powerful tools to immobilize biomolecules, including enzymes and probe oligonucleotides [4–10], on a variety of substrates. In fact, nowadays, SAMs play an important role in the development of DNA sensors.

Escherichia coli (*E. coli*) is a dangerous human pathogen that can produce life-threatening complications ranging from bloody diarrhoea to renal failure [11]. Conventional culture tests for determining coliforms and faecal coliforms are time-consuming and bacterial identification requires from days to weeks to be completed. Several rapid methods for *E. coli* have been developed [12], some of them based on the measurement of enzyme activities, such as β-galactosidase [13]. A DNA electrochemical hybridization biosensor for the detection of DNA sequences from the *E. coli* pathogen was described by Wang et al. [11]. It was based on the immobilization of the probe onto a carbon screen-printed carbon electrode and $Co(bpy)_3^{3+}$ was used as the hybridization indicator. Modification of *E. coli* single-stranded DNA binding protein with gold nanoparticles has been used for the electrochemical detection of DNA hybridization with a detection limit of 2.17 pM target DNA [14]. Recently, a flow-through piezoelectric quartz crystal (PQC) DNA biosensor system has been described which combines sequential flow polymerase reaction products denaturing and PQC detection via hybridization of ss-DNA for *E. coli* detection leading to an improvement in repeatability and sensitivity as compared to an existing manual method [15]. Moreover, Elsholz et al. have developed low-density electrical 16S rRNA specific oligonucleotide microarrays together with an automated analysis system

* Corresponding author.
E-mail address: pingarro@quim.ucm.es (J.M. Pingarrón).

0039-9140/$ – see front matter © 2007 Elsevier B.V. All rights reserved.
doi:10.1016/j.talanta.2007.04.059

leading to a limit of detection of *E. coli* total RNA of 0.5 ng μL^{-1} [16].

This article describes a sequence-specific electrochemical biosensor based on the immobilization of a 25 base single-stranded probe, specific to the *E. coli lac Z* gene, onto a gold disk electrode via covalent binding. Methylene blue (MB), an electrochemical indicator widely used to monitor the DNA hybridization processes [9,17–22], was thus used as the hybridization indicator. In this context, we have reported recently the construction of a reliable calf-thymus DNA sensor based on self-assembled monolayers for denaturalisation and hybridization detection [9]. This DNA sensor was constructed by covalent immobilization of calf thymus DNA on a self-assembled 3-mercaptopropionic acid (MPA) monolayer by using water soluble *N*-3-(dimethylaminopropyl)-*N*′ethylcarbodiimide hydrochloride (EDC) and *N*-hydroxisulfosuccinimide (NHSS) as linkers.

The *E. coli* sequence-specific electrochemical biosensor described in this paper is based on the development of a simple DNA immobilization strategy using a novel approach to form a 3,3′-dithiodipropionic acid di(*N*-succinimidyl ester) (DTSP) SAM without derivatization. This approach has been very scarcely used for DNA sensors and only in combination with optical and piezoelectric methodologies [23,24]. However, in our knowledge, this is the first time that this DNA immobilization strategy is coupled with electrochemical hybridization detection. The efficiency of the hybridization process is enhanced employing 6-mercapto-1-hexanol (MCH) for the displacement of non-specifically adsorbed oligonucleotide molecules.

2. Experimental

2.1. Apparatus and electrodes

Voltammetric measurements were carried out with an ECO Chemie Autolab PSTAT 10 potentiostat using the software package General Purpose Electrochemical System (GPES 4.9). A P-Selecta Digiterm 100 thermostatic bath, a P-Selecta ultrasonic bath, a IKAMAG® RET heating plate and a P-Selecta Agimatic magnetic stirrer were also used.

A Metrohm 6.1204.020 gold disk electrode (3 mm Ø) was used as electrode substrate to be coated with the respective SAMs: DTSP and MPA and further covalent immobilization of the probe oligonucleotide. A BAS MF-2063 Ag|AgCl|KCl 3 M reference electrode and a Pt wire counter electrode were also employed. A 10-mL glass electrochemical cell was used.

2.2. Reagents and solutions

Methylene blue (MB) was purchased from Sigma. Stock solutions of MB (1 mM) were prepared in a 50 mM Tris–HCl, 20 mM NaCl buffer solution (pH 7.2). More dilute solutions were prepared by suitable dilution with the same buffer solution.

The tested oligomers were synthetized by Sigma Genosys. Their base sequences were as follows:

- 25-mer probe (EC1PROBE): 5′ CAG GAT ATG TGG CGG ATG AGC GGC A-3′;
- 25-mer target DNA (EC1COMP): 5′ TGC CGC TCA TCC GCC ACA TAT CCT G-3′;
- 25-mer one-base mismatch (EC1COMPF): 5′ TGC CGC TCA TC<u>A</u> GCC ACA TAT CCT G-3′;
- 25-mer non-complementary (EC1NCOMP): 5′ GGC CAT CGT TGA AGA TGC CTC TGC C-3′.

25-mer one-base mismatch (EC1COMPF) is a mutant of the 25-mer target DNA (EC1COMP), with one base changed (as underlined).

DNA oligonuleotide stock solutions (nominally 1000 $\mu g\,mL^{-1}$) were prepared in a TE buffer solution containing 10 mM Tris–HCl, and 1 mM EDTA (pH 8.0) and kept frozen. More dilute solutions of the oligomers were prepared in a 50 mM Tris–HCl and 20 mM NaCl buffer solution (pH 7.2).

For the covalent probe immobilization on the gold electrode, a 4 mM 3,3′-dithiodipropionic acid di(*N*-succinimidyl ester) (DTSP) (Fluka) solution, prepared in dimethylsulfoxide (DMSO) (Scharlau) was used.

For the probe immobilization onto the MPA-SAM, a 5 mM *N*-hydroxysulfosuccinimide (NHSS) sodium salt (Fluka) and 2 mM 1-(3-dimethylaminopropyl)-3-ethylcarbodiimide (EDC) (Sigma) solution, prepared in 0.05 M phosphate buffer (pH 5.5) were used.

A 40 mM mercaptopropionic acid (MPA) (Research Chemicals Ltd.) solution, prepared in a 75/25% (v/v) ethanol/water mixture, was employed for the formation of the monolayer.

Other solutions employed, prepared in deionized water were a 50 mM Tris-(hydroxymethyl)aminomethane–HCl (Tris–HCl) (Aldrich) buffer solution containing 20 mM NaCl (Scharlau) (pH 7.2), as supporting electrolyte; a 10 mM Tris–HCl (Sigma) buffer solution containing 1 mM EDTA (pH 8.0). Ethanol (absolute, Scharlau), acetone (Scharlau) and a 25% (v/v) glutaraldehyde solution (Scharlau) were also used. All chemicals used were of analytical-reagent grade, and deionized water was obtained from a Millipore Milli-Q purification system.

2.3. Procedures

2.3.1. Pretreatment of the gold electrode (AuE)

Before carrying out the deposition of the SAMs, the gold disk electrode (AuE) was pretreated as described previously [4]. The AuE was polished with 3-μm diamond powder (BAS MF-2059) for 1 min. Then, it was sonicated in deionized water for 1 min, and immersed for 1 h in a hot 2 M KOH (Scharlau) solution. Next, the electrode was rinsed with water, immersed in concentrated H_2SO_4 (Scharlau) for 10 min, rinsed with water, immersed in concentrated HNO_3 (Scharlau) for 10 min and rinsed again with deionized water. Finally the electrode was dried thoroughly under a N_2 flow.

2.3.2. Preparation of the MPA-modified AuE

MPA-SAMs were formed by immersion of the pretreated AuE in a 40 mM MPA solution in EtOH/H_2O (75/25, v/v) for at least 15 h. Then, the modified electrode was rinsed with deionized water. Under these conditions, a surface coverage of $\theta = 0.95$ was calculated by electrochemical impedance spectroscopy, indicating a high electrode coverage by the alkanethiol SAM.

2.3.3. Preparation of the DTSP-modified AuE

DTSP-SAMs were formed by immersion of the clean AuE in a 4 mM DTSP solution in DMSO for 1 h. Then, the modified electrode was rinsed with acetone.

2.3.4. Probe immobilization

A versatile method for covalently attaching the probe was used. It finally consisted in using the DTSP linking reaction as shown in Scheme 1. Briefly, DTSP adsorbs onto the gold electrode through the disulfide group. The terminal succinimidyl groups become exposed to the solution allowing covalent immobilization of amine-residues of the oligonucleotide. Accordingly, a 2.5 μL drop of a 1000 mg L^{-1} DNA probe solution was pipetted onto the DTSP-AuE, let to dry either at room temperature for at least 12 h or under a N_2 atmosphere for 1 h and finally soaked in deionized water for 2 h to remove unbound oligonucleotides.

For comparison purposes, monolayers of MPA were also used, where DNA was immobilized either by covalent attachment using NHSS/EDC, or by cross-linking with glutaraldehyde (GA). In the first case, the MPA-AuE was activated by immersion for 1 h at room temperature (in dark condition) in a solution formed with 2 mM EDC and 5 mM NHSS (in 50 mM phosphate buffer solution, pH 5.5). Subsequently, a 2.5 μL drop of a 1000 mg L^{-1} ss-probe solution was deposited on the linker/MPA/AuE, let to dry at room temperature for at least 24 h and finally soaked in water for 2 h to remove any unbound ss-probe. A similar procedure was followed in the second option: 2.5 μL of a 1000 mg L^{-1} ss-oligonucleotide were deposited on the MPA-AuE and let to dry at ambient temperature. Next the modified electrode was immersed in a 25% glutaraldehyde solution for 1 h at 4 °C.

The probe immobilization step was followed in every case by post-treatment with MCH for the displacement of non-specifically adsorbed oligonucleotide molecules [7]. A 10 μL drop of a 1 mmol L^{-1} aqueous solution of MCH was placed onto the probe SAM-modified gold electrode surface for 1 h in a N_2 atmosphere, and the modified electrode was finally soaked in a 50 mM Tris–HCl, 20 mM NaCl buffer solution (pH 7.2) for 10 seconds to remove any unbound ss-probe.

2.3.5. MB accumulation onto the DNA-modified electrodes

The DNA-modified electrodes were stirred in a 50 mM Tris–HCl and 20 mM NaCl buffer solution (pH 7.2) containing 10 μM MB for 1 min at open circuit.

2.3.6. Voltammetric transduction

After accumulation of MB, the DNA-modified electrodes were washed with the supporting electrolyte for 5 s to remove the non-specifically bound MB and transferred into the blank buffer solution (50 mM Tris–HCl + 20 mM NaCl, pH 7.2) for the voltammetric measurements. The oxidation signal of the accumulated MB was measured using square wave stripping voltammetry (SWSV) by scanning the potential from −0.50 to +0.10 V with amplitude of 30 mV and a step potential of 5 mV at 100 Hz. All experiments were conducted at room temperature (unless otherwise stated, 25 ± 0.5°C).

The electrodes were electrochemically cleaned in-between stripping voltammetric measurements to assure the complete stripping of the previously accumulated redox label. This was accomplished by applying successive potential SW scans between −0.5 and 0.1 V during 5 min in the blank buffer solution.

2.3.7. Hybridization

The hybridization protocol was performed by pipetting 2.5 μL of different concentrations of target DNA onto the probe-modified electrodes. This process was left to progress for at least 40 min in a N_2 atmosphere. The electrode surface was then washed with ultrapure water for 1 min to remove the unbound oligonucleotides. The same protocol was applied to the Probe-DTSP-AuE in order to test the hybridization reactions of the probe with a one-base mismatch oligomer and also with non-complementary oligonucleotide sequences.

2.3.8. Denaturing

In order to denaturing the ds-DNA immobilized onto the modified AuE, the sensor was immersed in 5 mL of a 10 mM Tris–HCl and 1 mM EDTA buffer solution (pH 8.0) at 100 °C for 5 min, followed by cooling in an ice bath for 30 min [9,25].

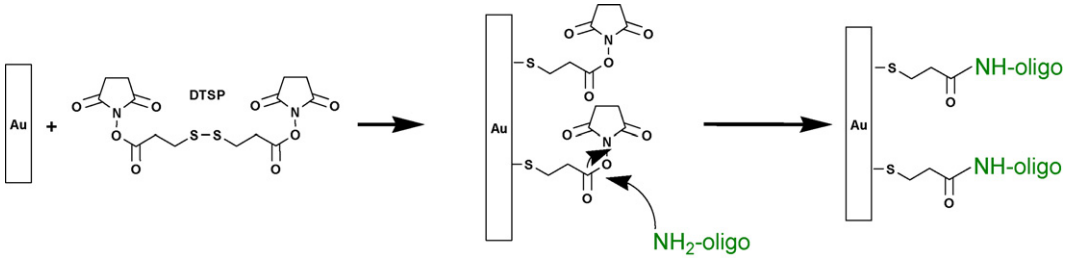

Scheme 1. Covalent attachment of DNA probes to a DTSP-modified Au electrode.

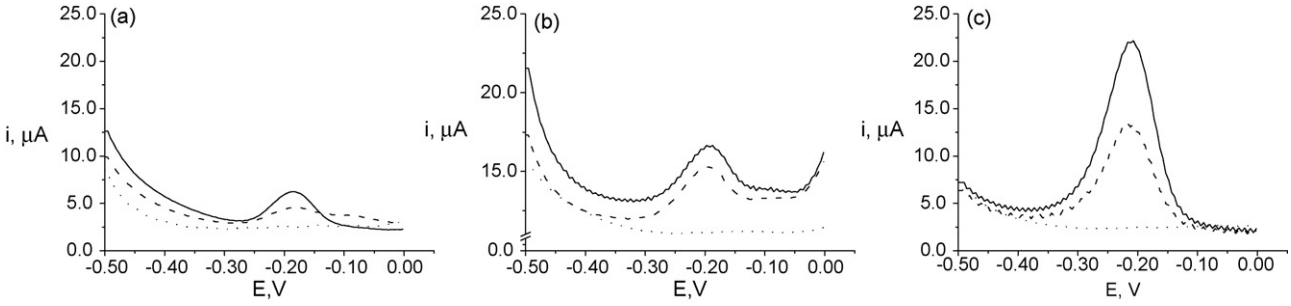

Fig. 1. Stripping square wave voltammograms obtained after accumulation of MB before (- - -) and after (—) the hybridization process, for different immobilization strategies: (a) MCH-Probe-NHSS/EDC-MPA-AuE; (b) GA-MCH-Probe-MPA-AuE; (c) MCH-Probe-DTSP-AuE. Supporting electrolyte: 50 mM Tris–HCl, 20 mM NaCl (pH 7.2) (. . . in figures). Accumulation conditions: [MB] = 10 μM, t_{acc} = 1 min, open circuit. Measurement conditions: E_{sw} = 30 mV, f = 100 Hz, v = 500 mV s^{-1}.

3. Results and discussion

3.1. Optimization studies

In a first approach, several probe immobilization strategies atop the electrode were evaluated. Three electrode configurations were tested and the signals produced compared. As described in the Section 2, two of them involved modification of the gold electrode with an MPA-SAM, the DNA probe being attached using EDC/NHSS or cross-linking with glutaraldehyde. The third electrode configuration tested used a DTSP monolayer.

In all cases, MB was used as hybridization indicator. This molecule produces different voltammetric signals in the presence of ss-DNA or ds-DNA [9]. Thus, Kelley et al. [17,20] concluded that MB shows high affinity for immobilized ds-DNA and that MB binding sites are localized mainly to the solution-accessible periphery of the monolayer. Therefore, the difference between the obtained MB voltammetric signals in the presence of the single-stranded DNA probe, and after the hybridization process, was employed as indicator of the extent of this process. Furthermore, the use of this electroactive indicator shows the advantage of the relatively low potential where its electrochemical reaction occurs (oxidation at −0.20 V versus Ag/AgCl in the experimental conditions used), allowing minimization of potential electroactive interferences. Fig. 1 shows SW stripping voltammograms of MB obtained before and after the hybridization process for each one of the immobilization strategies checked. As can be seen, the signals obtained after the hybridization process were always higher than those obtained in the presence of the single-stranded DNA probe. This behaviour can be attributed to the interaction of MB with two guanine bases in the ss-DNA [26,27], as well as to the intercalation of MB in the DNA double helix, if there are at least two G–C base pairs [28]. Moreover, it was observed that the increment in the signal at the target-MCH-Probe-DTSP-AuE was the greatest of the three immobilization methods investigated. Thus, this electrode configuration was chosen for further studies taking also into account the shorter electrode preparation time needed in this case, given that the DTSP monolayer is readily formed in only 1 h (as opposed to the at least 15 h needed for obtaining the MPA-SAM). The use of DTSP-SAMs for the DNA probe immobilization also has the advantage that it does not require the previous modification of the oligonucleotide probe.

Optimization studies were carried out to obtain reproducible signals with high sensitivity. The employed concentration of MB was optimized by checking the sensor response between 2 and 20 μM. An increase in the response was observed up to 10 μM MB with a level off for higher concentrations. Accordingly, a 10 μM MB concentration was selected for further work, while an accumulation time of 1 min at open circuit was used [9].

The influence of the DTSP concentration in the modification solution and of the SAM formation time was therefore investigated. The DTSP concentration was varied between 2 and 8 mM (Fig. 2a), the peak current increase being levelled off from 4 mM, which was chosen as DTSP concentration for further measurements. DTSP concentrations higher than 4 mM

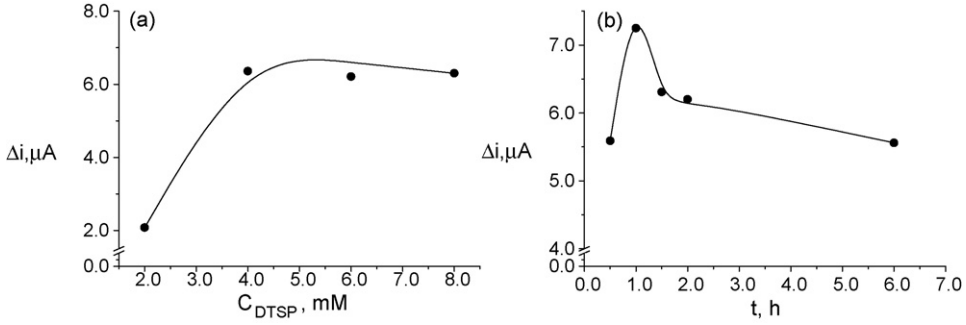

Fig. 2. Effect of the DTSP concentration in the modification solution (a), and of the formation time of the DTSP-SAM (b) on the MB anodic stripping SW peak current increment between the target-MCH-Probe-DTSP-AuE and the MCH-Probe-DTSP-AuE. Supporting electrolyte: 50 mM Tris–HCl, 20 mM NaCl (pH 7.2). Accumulation conditions: [MB] = 10 μM, t_{acc} = 1 min, open circuit. Measurement conditions: E_{sw} = 30 mV, f = 100 Hz, v = 500 mV s^{-1}.

showed no significant increase in the voltammetric signal, thus indicating that this was the necessary concentration to reach saturation of binding sites on the electrode surface. Concerning the monolayer formation time (Fig. 2b), a higher peak current increment was obtained for 1 h, which was chosen as the period of time to complete the formation and reorganization of the DTSP monolayer.

Experimental variables, such as the effect of the DNA probe drying time atop the modified electrode, and the amount of probe immobilized were also evaluated. Thus, the effect of the drying time in the range 2–12 h at room temperature on the MB SW stripping peak currents was checked. Under these conditions, at least 12 h were needed to assure an adequate covalent binding between the succinimidyl groups in the DTSP-AuE and the DNA probe. However, when the immobilization process was carried out under a nitrogen atmosphere, the drying time needed showed a significant decrease, from 12 to 1 h (data not shown). Taking these results into account, the drying under a N_2 stream for 1 h method was chosen for further studies.

On the other hand, the probe amount immobilized on the DTSP-AuE greatly affected the MB accumulation process at the modified electrode. As it can be seen in Fig. 3, the redox label SW stripping peak current increased linearly (slope, $4.9 \pm 0.5\ \mu A\ \mu g^{-1}$; intercept, $1.2 \pm 0.4\ \mu A$; $r = 0.994$) in the 0–1.25 μg probe range, for a constant amount of complementary DNA. This fact would allow the possibility of DNA probe quantification in unknown samples. Above 1.25 μg, the stripping signal decreased sharply, probably due to the blocking of the electrode surface by the great amount of immobilized probe. Thus, 1.25 μg of DNA probe was selected for the fabrication of the sensor.

3.2. Stability and analytical characteristics

Different aspects regarding the stability of the DNA-modified MCH-DTSP-AuE before and after the hybridization process, as a previous step before studying the oligonucleotides denaturing and re-hybridization processes at the sensors surface, were evaluated.

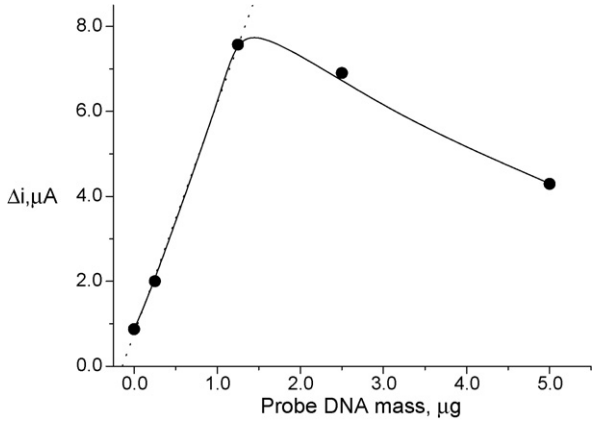

Fig. 3. Effect of the DNA probe amount immobilized at the MCH-Probe-DTSP-AuE on the increment in the MB stripping SW oxidation peak current obtained after the hybridization process with the complementary sequence (25 ng). Other experimental conditions as in Fig. 2.

Firstly, the repeatability of the electrochemical responses was checked. Thus, five successive SWSV measurements for 10 μM MB were performed with one single DNA sensor. The electrode was cleaned in-between measurements as described in Section 2.3.6. In these conditions, relative standard deviations (R.S.D.s) of 5.7 and 5.0% were obtained for the stripping peak currents of MB at the electrode before and after the hybridization (25 ng target) process, respectively. These results indicate a good stability of the single and double-stranded oligonucleotides immobilized on the DTSP-modified electrode.

Secondly, the reproducibility of the DNA sensors preparation procedure was tested. Results for MB stripping peak currents at five independently probe-modified electrodes constructed in the same manner yielded a R.S.D. of 8.7%, while for five modified electrodes after the hybridization process at a 25 ng target level, a R.S.D. of 9.0% was obtained. These results demonstrated that the fabrication procedure of the DNA sensor was reliable, thus allowing reproducible electroanalytical responses to be obtained with different sensors.

The response for the oxidation of accumulated MB after hybridization with increasing amounts of the target oligonucleotide is displayed in Fig. 4. As can be seen, the increment in the MB oxidation peak current increased with increasing target concentration. The response leveled off at ca. 50.0 ng, which suggests that all the available immobilized probes on the electrode surface were then involved in hybridization. A linear calibration graph was obtained over the 3.1–50.0 ng target DNA range ($r = 0.999$, slope $= (6.5 \pm 0.1) \times 10^{-2}\ \mu A\ ng^{-1}$, intercept $= (2.7 \pm 3.1) \times 10^{-2}\ \mu A$). The limit of detection was calculated according to the $3s_b/m$ criteria, where m is the slope of the calibration plot and s_b was estimated as the standard deviation ($n = 10$) of the voltamperometric signals obtained for 3.1 ng of target DNA. Thus, the detection limit was 0.85 ng (45 nM) of oligonucleotide target sequence, which means an acceptable sensitivity taking into account that no signal amplification was employed. Enzyme-amplified sensing is under study to improve sensitivity.

3.3. Hybridization specificity of the E. coli probe

Taking into account, the significant difference observed between the voltammetric signals of MB obtained before and

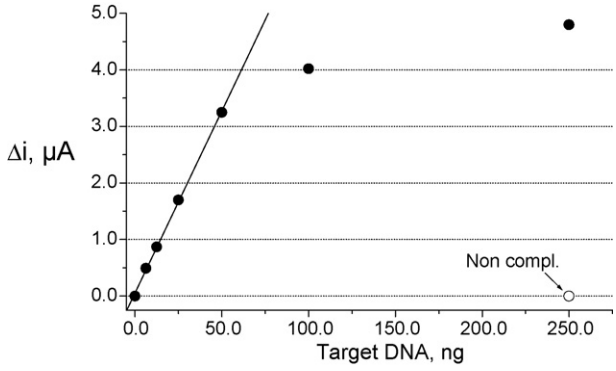

Fig. 4. Increment in the MB oxidation peak current obtained after the hybridization process with increasing amounts of target oligonuleotide. Other experimental conditions as in Fig. 2.

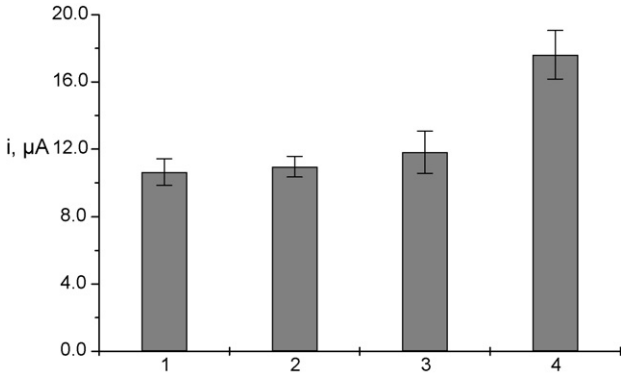

Fig. 5. Bar chart of stripping square wave voltammograms obtained after accumulation of MB on a MCH-Probe-DTSP-AuE (1) and after hybridization with the non-complementary sequence (25 ng) (2), a one mismatch sequence (25 ng) (3) and the complementary target sequence (25 ng) (4). Other experimental conditions as in Fig. 2.

after hybridization with the target oligonucleotide, the capture probe was investigated for the response of non-complementary and mismatch oligonucleotides. As can be seen in Fig. 5, no significant change was observed for the peak current when the capture probe-modified electrode was exposed to the non-complementary oligonucleotide. This implied that no change occurred at the capture probe electrode surface and hence hybridization had not been achieved. For the response of the single-base mismatch oligonucleotide, the voltammetric signal observed was just slightly higher, $7 \pm 3\%$, than the one observed for the capture probe before hybridization. This small increase can be attributed to a very little intercalation of MB, and showed a lower hybridization efficiency of single-base mistmatch DNA compared with complementary target DNA. Each experiment was repeated 10 times with a good reproducibility, as shown by the error bars in Fig. 5. Thus, MB can be considered as an efficient intercalator to distinguish between hybrids, non-complementary and mismatch oligonucleotides. The ability of sensitive detection of single-base mutation is of great importance to gene detection in diagnosis at early stage [29].

3.4. Reusability of the sensor

The possibility to use the developed DNA sensor in several successive hybridization/denaturing cycles was also tested. The electrodes modified with target oligonucleotides bound to the DNA probe sequence were denatured as described in Section 2.3.8. After denaturing, the peak current obtained for MB was similar as those obtained at the MCH-Probe-DTSP-AuE prior to hybridization. Thus, a decrease in the MB peak current of $17 \pm 5\%$ ($n = 3$) was obtained at the denaturalised/target-MCH-Probe-DTSP-AuE. This behaviour was shown to be reproducible when the denaturing process was repeated, and the signal kept constant after storing the denaturalised electrode at 4 °C in dry conditions for 24 h. Therefore, it could be concluded that no significant re-hybridization occurred after application of the denaturing procedure. The reusability of the developed sensor was tested by repetitive hybridization/denaturing cycles. No significant deterioration occurs on the anodic MB peak currents over three hybridization/denaturing cycles, thus indicating the possibility to reuse the developed *E. coli* DNA sensor in the analysis of more than one target samples.

4. Conclusions

The construction of an *E. coli* specific DNA biosensor using a DTSP-SAM-modified gold electrode, as described in this paper, allows the enhancement of the efficiency of the DNA hybridization process with the complementary target on the gold surface. The hybridization event is effectively detected by voltammetry of MB intercalated to hybridized DNA. The results obtained confirm that this detection approach provides a quick, sensitive, reusable and convenient methodology for the quantification of *E. coli*, which, moreover, allows the detection of mismatch oligonucleotides.

Acknowledgements

The financial support of the projects PETRI No. PTR95-0893.0.1.02.OP and BQU2003-00365 are gratefully acknowledged. Óscar A. Loaiza acknowledges a pre-PhD fellowship of the Universidad Complutense de Madrid.

References

[1] A.M. Chiorcea Paquim, V.C. Diculescu, T.S. Oretskaya, A.M. Oliveira Brett, Biosens. Bioelectron. 20 (2004) 933.
[2] M.I. Pividori, A. Merkoci, S. Alegret, Biosens. Bioelectron. 15 (2000) 291.
[3] F.H. Teh, H. Gong, X.D. Dong, X. Zeng, A.L.K. Tan, X. Yang, S.N. Tan, Anal. Chim. Acta 551 (2005) 23.
[4] S. Campuzano, B. Serra, M. Pedrero, F.J. Manuel de Villena, J.M. Pingarrón, Anal. Chim. Acta 494 (2003) 187.
[5] J. Gau Jr., H.E. Lan, B. Dunn, H. Chih-Ming, J.C.S. Woo, Biosens. Bioelectron. 16 (2001) 745.
[6] K. Kerman, D. Ozkan, P. Kara, B. Meric, J.J. Gooding, M. Ozsoz, Anal. Chim. Acta 462 (2002) 39.
[7] G. Carpini, F. Lucarelli, G. Marrazza, M. Mascini, Biosens. Bioelectron. 20 (2004) 167.
[8] F. Lucarelli, G. Marrazza, A.P.F. Turner, M. Mascini, Biosens. Bioelectron. 19 (2004) 515.
[9] O.A. Loaiza, S. Campuzano, M. López-Berlanga, M. Pedrero, J.M. Pingarrón, Sensors 5 (2005) 344.
[10] E. Nebling, T. Grunwald, J. Albers, P. Schafer, R. Hintsche, Anal. Chem. 76 (2004) 689.
[11] J. Wang, J. Rivas, X. Cai, Electroanalysis 9 (1997) 395.
[12] N.S. Hobson, I.E. Tothill, A.P.F. Turner, Biosens. Bioelectron. 11 (1996) 455.
[13] B. Serra, M.D. Morales, J. Zhang, A.J. Reviejo, E.H. Hall, J.M. Pingarron, Anal. Chem. 77 (2005) 8115.
[14] K. Kerman, Y. Morita, Y. Takamura, M. Ozsoz, E. Tamiya, Anal. Chim. Acta 510 (2004) 169.
[15] H. Sun, Y. Zang, Y. Fung, Biosens. Bioelectron. 22 (2006) 506.
[16] B. Elsholz, R. Wörl, L. Blohm, J. Albers, H. Feucht, T. Grunwald, B. Jürgen, T. Schweder, R. Hintsche, Anal. Chem. 78 (2006) 4794.
[17] O.S. Kelley, K.J. Barton, Bioconjugate Chem. 8 (1997) 31.
[18] A. Erdem, K. Kerman, B. Meric, U.S. Akarca, M. Ozsoz, Anal. Chim. Acta 422 (2000) 139.
[19] A. Tani, A.J. Thomson, J.N. Butt, Analyst 126 (2001) 1756.
[20] B.J. Taft, M. O'Keefe, J.T. Fourkas, S.O. Kelley, Anal. Chim. Acta 496 (2003) 81.
[21] R. Rohs, H. Sklenar, J. Biomol. Struct. Dyn. 21 (2004) 699.
[22] V. Dharuman, T. Grunwald, E. Nebling, J. Albers, L. Blohm, R. Hintsche, Biosens. Bioelectron. 21 (2005) 645.

[23] J.C. Feldner, M. Ostrop, O. Friedrichs, S. Sohn, D. Lipinsky, U. Gunst, H.F. Arlinghaus, App. Surf. Sci. 203–204 (2003) 722.
[24] K. Nakano, H. Matsunaga, K. Sai, N. Soh, T. Imato, Anal. Chim. Acta 578 (2006) 93.
[25] D.W. Pang, M. Zhang, Z.L. Wang, Y.P. Qi, J.K. Cheng, Z.Y. Liu, J. Electroanal. Chem. 403 (1996) 183.
[26] F. Yan, A. Erdem, B. Meric, K. Kerman, M. Ozsoz, O.A. Sadik, Electrochem. Commun. 3 (2001) 224.
[27] J. Gu, X. Lu, H. Ju, Electroanalysis 14 (2002) 949.
[28] G.S. Bang, S. Cho, B.G. Kim, Biosens. Bioelectron. 21 (2005) 863.
[29] Y. Jin, X. Yao, Q. Liu, J. Li, Biosens. Bioelectron. 22 (2007) 1126.

Available online at www.sciencedirect.com
ScienceDirect
Talanta 73 (2007) 893–898
Talanta
www.elsevier.com/locate/talanta

Cloud point extraction equilibrium of lanthanum(III), europium(III) and lutetium(III) using di(2-ethylhexyl)phosphoric acid and Triton X-100

Akira Ohashi *, Takuma Hashimoto, Hisanori Imura, Kousaburo Ohashi

Department of Environmental Sciences, Faculty of Science, Ibaraki University, Mito 310-8512, Japan

Received 2 April 2007; received in revised form 7 May 2007; accepted 9 May 2007
Available online 21 May 2007

Abstract

The cloud point extraction behaviors of lanthanoids(III) (Ln(III) = La(III), Eu(III) and Lu(III)) with and without di(2-ethylhexyl)phosphoric acid (HDEHP) using Triton X-100 were investigated. It was suggested that the extraction of Ln(III) into the surfactant-rich phase without added chelating agent was caused by the impurities contained in Triton X-100. The extraction percentage more than 91% for all Ln(III) metals was obtained using 3.0×10^{-5} mol dm^{-3} HDEHP and 2.0% (v/v) Triton X-100. From the equilibrium analysis, it was clarified that Ln(III) was extracted as $Ln(DEHP)_3$ into the surfactant-rich phase. The extraction constant of Ln(III) with HDEHP and 2.0% (v/v) Triton X-100 were also obtained.

Keywords: Cloud point extraction; Lanthanoids; Triton X-100; Di(2-ethylhexyl)phosphoric acid; Extraction constant

1. Introduction

Rare earth metals have been used in various industrial products such as a strong magnet, the magnetic embrocation, the solid metal hydride, the fluorescent materials, and the high temperature superconducting compounds, because they have useful and specific physical properties [1]. Therefore, the development of the separation and preconcentration method for rare earth metals is desired for the availability of them for industrial products. Solvent extraction is generally used as the separation method for rare earth metals [2–8]. However, this method has some problems, such as a large use of organic solvents that are toxic and flammable, slow extraction-speed, and low concentration efficiency for solute.

On the other hand, the homogeneous liquid–liquid extraction [9–12], cloud point extraction based on non-ionic surfactants [13–15] and ionic surfactants [16,17], and aqueous biphasic extraction [18,19] are simple, rapid and powerful preconcentration methods that extract the solutes existing in the homogeneous or pseudo-homogeneous aqueous solution into the water-immiscible phase after the phase separation. These methods are more inexpensive, lower toxicity, and smaller environmental pollution than the conventional liquid–liquid extraction.

The technique of cloud point extraction is based on the property that an aqueous solution of non-ionic surfactant becomes turbid above a temperature defined as the cloud point. Two phases separated are a surfactant-rich phase of small volume, composed almost of the surfactant, and an aqueous phase containing a surfactant at the concentration below, or equal to, a critical micelle concentration. An analyte interacting with micellar systems can be concentrated into the surfactant-rich phase of small volume. First application of cloud point extraction to the separation/concentration of metal ions was carried out by Miura et al. [20]. Thereafter, many studies on the cloud point extraction of metal ions have been reported [21–26]. There are a few reports on the cloud point extraction of lanthanoids (III) (Ln(III)) with various chelating agents such as 2-(3,5-dichloro-2-pyridylazo)-5-diethylaminophenol [27], 8-quinolinol [28], and calixarenes [29].

Acidic organophosphorus compounds, such as di(2-ethylhexyl)phosphoric acid (HDEHP), 2-ethylhexyl phosponic acid mono-2-ethylhexyl ester, and di(2,4,4′-hexylphosphoric, acid have been used as extractants for various metal ions containing rare earth metals in the conventional liquid–liquid extraction [2,3,30–33]. Many studies on the kinetics and mechanisms of

* Corresponding author. Tel.: +81 29 228 8704; fax: +81 29 228 8403.
E-mail address: oakira@mx.ibaraki.ac.jp (A. Ohashi).

0039-9140/$ – see front matter © 2007 Published by Elsevier B.V.
doi:10.1016/j.talanta.2007.05.012

metal extraction by acidic organophosphorus extractants have been performed. In most of these studies, HDEHP has been used as the extractant.

In this study, the cloud point extraction behavior of lanthanoids (Ln(III) = La(III), Eu(III) and Lu(III)) using HDEHP and Triton X-100 with was investigated. The dependencies of the experimental conditions, such as pH, the concentration of HDEHP, and ionic strength, on the cloud point extraction behavior, were also investigated. Moreover, the extraction constants of Ln(III) with HDEHP in cloud point extraction system were obtained.

2. Experimental

2.1. Reagents

Ln(III) stock solutions were prepared by dissolving high purity Ln(III) oxide, La_2O_3 (Spectrographically Standardized, Johnson Matthey Chemicals Ltd.), Eu_2O_3 (99.999%, Aldrich), and Lu_2O_3 (99.99%, Nippon Yttrium Co. Ltd.), in nitric acid, evaporating to dryness, and redissolving in perchloric acid. HDEHP (EP, Nacalai Tesque) was purified by precipitation method of copper(II) [34]. Polyethylene glycol mono-*p*-isooctylphenyl ether (liquid scintillation grade) was purchased from Nacali Tesque and is represented as Triton X-100 in this paper, because the ingredient of Triton X-100 is mainly polyethylene glycol mono-*p*-isooctylphenyl ether. Two bottles of Triton X-100 (lot no. 13112LB and 03615HC) were also purchased from Aldrich. They were used for only an experiment to compare with Triton X-100 purchased from Nacalai Tesque. Arsenazo-III (Dojindo Lab.) was used as purchased. Water was doubly distilled and further purified with Milli-Q (Millipore) equipment. All other chemicals were of analytical reagent grade.

2.2. Apparatus

The pH measurements were performed by a Radiometer PHM93 pH meter. The determinations of La(III), Eu(III), and Lu(III) in an aqueous solution were performed with an inductively coupled plasma atomic-emission spectrometer (ICP-AES, Nippon Jurrell Ash ICAP-575) at 408.692 nm, 412.974 nm, and 261.542 nm, respectively. The voltage of photomultiplier tube was set to 550 V for La(III), 500 V for Eu(III), and 650 V for Lu(III). The HPLC system used consisted of a Shimadzu DGU-12A degasser, a Shimadzu LC-10Ai pump, a Shimadzu CTO-10Avp column oven, a Jasco MD-1515 UV–vis detector, a Rheodyne 9125 loop injector equipped with a 20 mm^3 sample loop and a GL Sciences Inertsil ODS-2 column (4.0 mm × 100 mm). The Jasco-PDA soft was used to analyze the HPLC data.

2.3. Cloud point extraction procedure

An aqueous solution (20 ml) containing Ln(III), HDEHP and Triton X-100 was taken in a test tube with a glass stopper. After standing for 30 min, the solution was heated for 60 min in a thermostated water bath at 80 °C, which is higher than the cloud points of Triton X-100 (about 65 °C [35]). The resulting turbid solution was cooled at about −10 °C for 20 min in a freezer to enhance the viscosity of the surfactant-rich phase, and then the pH value of the aqueous phase was measured. Moreover, the aqueous phase (7 ml) was taken out, poured into a test tube, and diluted with 0.5 mol dm^{-3} perchloric acid aqueous solution to 10 ml. The resulting solution was utilized to determine the concentration of Ln(III) by ICP-AES. In the case of the cloud point extraction without added chelating agents, the surfactant-rich phase was diluted with water (5 ml) containing Arsenazo-III and the existence of La(III) in the surfactant-rich phase was confirmed spectrophotometrically.

The cloud point extraction of Ln(III) from micellar solutions was evaluated in terms of distribution ratio (D), extraction percentage ($\%E$), and the concentration factor (F) that are defined as follows:

$$D = \frac{C_s}{C_a} = \frac{C_i(V_s + V_a) - C_a V_a}{C_a V_s} \quad (1)$$

$$\%E = \frac{100D}{D + (V_a/V_s)} = \frac{C_i(V_s + V_a) - C_a V_a}{C_i(V_s + V_a)} \times 100 \quad (2)$$

$$F = \frac{C_s}{C_i} = \frac{C_i(V_s + V_a) - C_a V_a}{C_i V_s} \quad (3)$$

where C_s is the concentration of Ln(III) in the surfactant-rich phase after phase separation, C_a the concentration of Ln(III) in the aqueous phase after phase separation, C_i the initial concentration of Ln(III) in the micellar solution, V_s the volume of the surfactant-rich phase after phase separation, and V_a the volume of the aqueous phase after phase separation. The concentrations of Ln(III) was constant at 3.60×10^{-5} mol dm^{-3}. The concentrations of HDEHP and Triton X-100 were changed in the range of (0.5–5.0) × 10^{-3} mol dm^{-3} and 1.0–8.0% (v/v), respectively. The pH was changed in the range of 0.15–3.70 with (H, Na)ClO_4. The ionic strength was kept at 0.1 mol dm^{-3} (pH > 1) or 1.0 mol dm^{-3} (pH < 1) with (H, Na)ClO_4.

The volume of the surfactant-rich phase after the phase separation was measured by using a graduated cylinder instead of a test tube.

2.4. HPLC measurement

Standard solution of HDEHP was prepared by dissolving suitable amount in a mixture of 80% acetonitrile and 20% water. Calibration curve for HDEHP by HPLC was obtained in the range of 2.50×10^{-5} to 1.67×10^{-4} mol dm^{-3}. The cloud point extraction was carried out using 2.0% (v/v) Triton X-100 solutions containing 5.0×10^{-3} and 1.0×10^{-2} mol dm^{-3} HDEHP. The pH and ionic strength were constant at 2.3 and 0.1 mol dm^{-3}, respectively. The cloud point extraction procedure was same as the above. After the phase separation, the aqueous phase (0.5 ml) was taken off, poured into a 10-ml volumetric flask, and diluted with acetonitrile and water to 10 ml. The resulting solution was utilized to determine the concentration of HDEHP in the aqueous phase by HPLC. The equilibrium concentration of HDEHP in the surfactant-rich phase was calculated

from a mass balance using the concentration of HDEHP in the aqueous phase. The mobile phase consisted of a mixture of 80% acetonitrile and 20% water. Flow rate of the mobile phase was 0.5 ml min^{-1}. Temperature of ODS column was kept at 30 °C. A peak of HDEHP was detected at 258 nm.

3. Results and discussion

3.1. Volume of surfactant-rich phase after the phase separation

The effect of the Triton X-100 concentration on the volume (V_s, ml) of the surfactant-phase after the phase separation was investigated in the case of no HDEHP. The V_s linearly increased in the concentration of Triton X-100. The relationship of V_s with the Triton X-100 concentration was represented as

$$V_s = 0.700 \times [\text{Triton } X - 100]_T + 0.052 \quad |r| = 0.999 \qquad (4)$$

where $[\text{Triton X-100}]_T$ denotes the total Triton X-100 concentration (v/v %). The effects of pH and the HDEHP concentration on the volume of the surfactant-rich phase were also investigated at 2.0% (v/v) Triton X-100. The volume of the surfactant-rich phase was independent of pH and the HDEHP concentration in the range of 0.5–3.0 and 2.0×10^{-3}–5.0×10^{-3} mol dm^{-3}, respectively. However, the interface between the surfactant-rich and aqueous phases became obscure around pH 3.1 and disappeared above pH 3.7. This phenomenon was not observed without added HDEHP. The pK_a value of HDEHP is reported as 1.9 in the aqueous solution at 25 °C [30]. Although detailed mechanism is not understood, it is thought that anion species of HDEHP disturbs the phase separation. The cloud point extraction of Ln(III) with HDEHP was performed in pH < 3.1. The equilibrium volume of the surfactant-rich phase after the phase separation was obtained using Eq. (4) in the following experiments.

3.2. Extraction behavior of Ln(III) without added chelating agents

The cloud point extraction of Ln(III) without added chelating agents was carried out using a 2.0% (v/v) Triton X-100 solution. Comparison of the cloud point extraction behavior provided with Triton X-100 purchased from Nacalai Tesque with that with Triton X-100 purchased from Aldrich was carried out (Fig. 1). Surprisingly, in the case of Triton X-100 from Aldrich (lot no. 13112LB), La(III), Eu(III), and Lu(III) were almost quantitatively extracted without added chelating agents. The existence of La(III) in the surfactant-rich phase was spectrophotometrically confirmed using arsenazo-III. The extractability increased in the following order: Lu(III) < Eu(III) < La(III). This order is accordant with that obtained by the liquid–liquid extraction of Ln(III) with picric acid and 18-crown-6 as ion-pairs [36] and is different from that obtained by the liquid–liquid extraction of Ln(III)s with chelating agents such as β-diketones [6], 8-quinolinols [5] and acidic organophosphorus compounds [2,3]. Moreover, the cloud point extraction behavior was dependent on the anionic

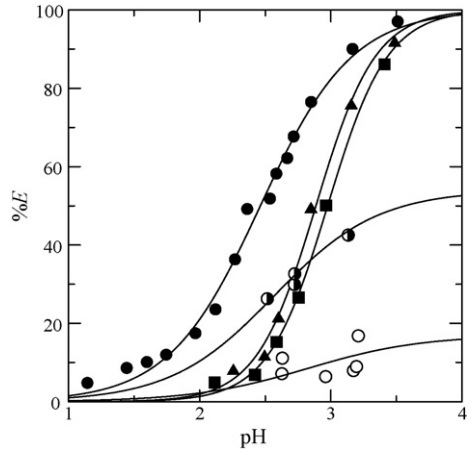

Fig. 1. Extraction percentage of La(III), Eu(III) and Lu(III) vs. pH without chelating agents. Circle, La(III); triangle, Eu(III); square, Lu(III); closed, Aldrich (lot no. 13112LB); half closed, Aldrich (lot no. 03615HC); open, Nacalai Tesque; Ln(III), 3.6×10^{-5} mol dm^{-3}; Triton X-100, 2.0% (v/v); $I = 0.01$ mol dm^{-3} (pH > 2.0) and 0.1 mol dm^{-3} (pH < 2.0) with (H, Na)ClO_4.

species: the extractability of La(III) with ClO_4^- was the highest among ClO_4^-, NO_3^-, and Cl^- (data not shown). From these results, it is suggested that Ln(III)s are extracted as ion-pairs into the surfactant-rich phase. On the other hand, the extraction percentages of Ln(III) with Triton X-100 from Aldrich (lot no. 03615HC) and Nacalai Tesque became lower than the ones with Triton X-100 from Aldrich (lot no. 13112LB). This result suggests that the cloud point extraction of Ln(III) without added chelating agents is caused by the impurities contained in Triton X-100. We expected that the impurities contained in Triton X-100 were like crown ether and tried to analyze the impurities in Triton X-100. However, we have not been able to make clear what the impurities contained in Triton X-100 are. Some studies on the cloud point extractions of metals without added chelating agents have been reported [29,37,38]. It is worried that the extractions of metals without added chelating agents in these papers were caused by the impurities contained in the commercial non-ionic surfactants.

3.3. Extraction behavior of Ln(III) with HDEHP

The extraction behavior of Ln(III) with HDEHP was investigated using Triton X-100 purchased from Nacalai Tesque, because there was hardly the influence of the impurities on the extraction of Ln(III). The effect of ionic strength (I) on the cloud point extraction of La(III) was investigated at $I = 0.01$, 0.1, and 1.0 mol dm^{-3}. The extractability of La(III) was hardly affected by the ionic strength. Fig. 2 shows the effect of pH on the cloud point extractions of La(III), Eu(III), and Lu(III) with 3.0×10^{-5} mol dm^{-3} HDEHP using 2.0% (v/v) Triton X-100 aqueous solutions. Relatively high extraction percentages were obtained for all Ln(III). The highest extraction percentages were observed as 91.8% at pH 3.01 for La(III), 91.7% at pH 2.45 for Eu(III), and 93.8% at pH 1.67 for Lu(III). The concentration factors for La(III), Eu(III), and Lu(III) were obtained as 12.4, 12.4, and 12.7, respectively. These values are listed in Table 1. The

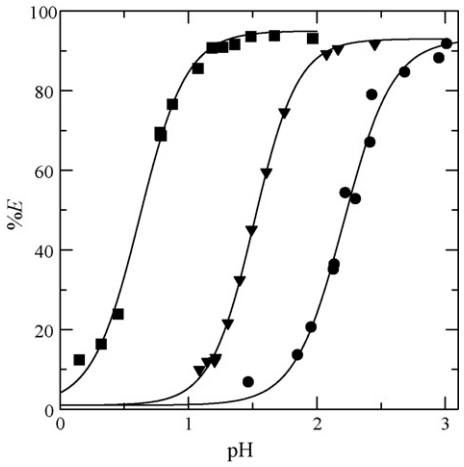

Fig. 2. Effect of pH on the cloud point extraction of Ln(III) with HDEHP. La(III) (●), Eu(III) (▲), Lu(III) (■); Ln(III), 3.6×10^{-5} mol dm^{-3}; HDEHP, 3.0×10^{-3} mol dm^{-3}; Triton X-100, 2.0% (v/v); $I = 0.1$ mol dm^{-3} (pH > 1) and 1.0 mol dm^{-3} (pH < 1) with (H, Na)ClO_4.

value of F may be improved by the decrease in the concentration of Triton X-100.

3.4. Extraction equilibrium of Ln(III) with HDEHP

The cloud point extraction equilibrium of La(III) with HDEHP was investigated using 2.0% (v/v) Triton X-100 solutions. In nonpolar diluents, HDEHP trends to associate by intermolecular hydrogen bonding and to form dimer. However, HDEHP may exist as monomer in the surfactant-rich phase, because polarity of the surfactant-rich phase is relatively high. Fig. 3 shows the effect of pH on the distribution ratio of La(III) between the surfactant-rich and the aqueous phases. In both cases of extraction of 3.0×10^{-3} and 5.0×10^{-3} mol dm^{-3} HDEHP, plots of log D versus pH gave straight lines with slopes of about 3. Fig. 4 shows the effect of the initial HDEHP concentration ($[HDEHP]_i$) on the distribution ratio of La(III). In both cases of pH 2.15 and 2.58, plots of log D versus log $[HDEHP]_i$ gave straight lines with slopes of about 3 in the high range of $[HDEHP]_i$. However, in the low range of $[HDEHP]_i$, the slope tends to decrease slightly. As shown in Fig. 1, La(III) was slightly extracted into the surfactant-rich phase without added chelating agents, causing the derivation from the straight lines with slopes of 3 in the low range of $[HDEHP]_i$. From the results obtained, it is suggested that three hydrogen ions and HDEHP molecules participate in the cloud point extraction of La(III) with HDEHP. The cloud point extraction equilibrium of Ln(III) with HDEHP is assumed to be

$$Ln(III) + 3HDEHP_s \overset{K_{ex}}{\rightleftharpoons} Ln(DEHP)_{3,s} + 3H^+ \quad (5)$$

Table 1
Highest extraction percentage, concentration factor and extraction constant of Ln(III) with HDEHP and 2.0% (v/v) Triton X-100

	pH	%E	F	log K_{ex}
La(III)	3.01	91.8	12.4	−1.15 ± 0.25
Eu(III)	2.45	91.7	12.4	0.94 ± 0.19
Lu(III)	1.67	93.8	12.7	3.52 ± 0.14

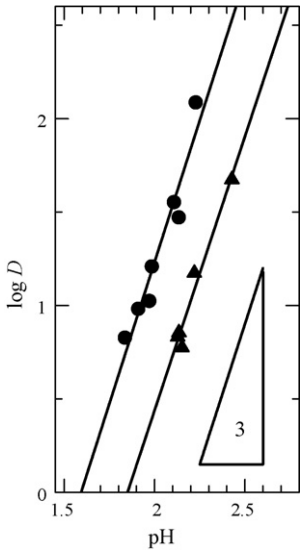

Fig. 3. Effect of pH on the distribution ratio of Ln(III). HDEHP 3.0×10^{-3} mol dm^{-3} (●), 5.0×10^{-3} mol dm^{-3} (▲); Ln(III), 3.6×10^{-5} mol dm^{-3}; Triton X-100, 2.0% (v/v); $I = 0.1$ mol dm^{-3} with (H, Na)ClO_4.

where subscript s represents the surfactant-rich phase. The extraction constant (K_{ex}) is expressed by

$$K_{ex} = \frac{[Ln(DEHP)_3]_s[H^+]^3}{[Ln(III)][HDEHP]_s^3} \quad (6)$$

When the existence of the Ln(III)-HDEHP chelates in the aqueous phase can be neglected, the following equation can be derived from Eq. (6) as

$$\log K_{ex} = \log D - 3\log [HDEHP]_s - 3pH \quad (7)$$

As seen in Eq. (7), the HDEHP concentration in the surfactant-rich phase is necessary to obtain the extraction con-

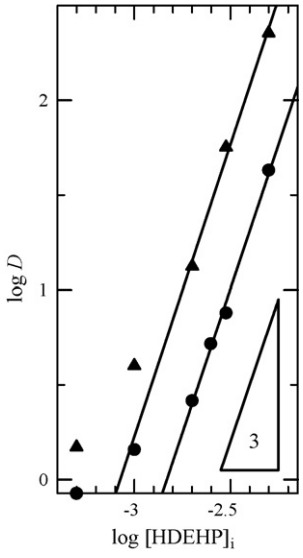

Fig. 4. Effect of the initial HDEHP concentration on the distribution ratio of Ln(III). pH 2.15 (●), 2.58 (▲); Ln(III), 3.6×10^{-5} mol dm^{-3}, Triton X-100, 2.0% (v/v), $I = 0.1$ mol dm^{-3} with (H, Na)ClO_4.

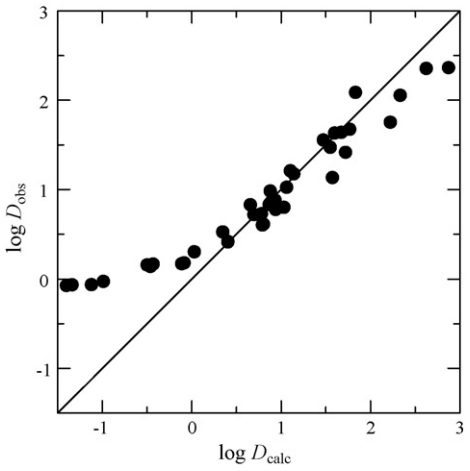

Fig. 5. Comparison of experimental results with calculated ones of distribution ratio of La(III) with HDEHP.

stant. The distribution ratio (D_{HDEHP}) of HDEHP between the surfactant-rich phase and the aqueous phase was measured by HPLC using 2.0% (v/v) Triton X-100 solutions at pH 2.3. The D_{HDEHP} value was independent of the initial concentration of HDEHP. From the HPLC measurement, the value of D_{HDEHP} was obtained as $10^{1.83\pm0.01}$. Since the pK_a value for HDEHP is 1.9, the value of log D_{HDEHP} is affected by pH. However, it is thought that the concentration of HDEHP in the surfactant-rich phase is hardly changed by pH, because most of HDEHP is distributed to the surfactant-rich phase. Therefore, the values of log $[HDEHP]_s$ in the all pH ranges was calculated from the D_{HDEHP} value obtained at pH 2.3.

From the plots in Figs. 2–4, the values of $\log K_{ex}$ for La(III), Eu(III), and Lu(III) were calculated by using Eq. (7) as -1.15 ± 0.25, 0.94 ± 0.19, and 3.52 ± 0.14, respectively. These values are listed in Table 1. Comparison of the distribution ratio obtained experimentally (D_{obs}) with the calculated one (D_{calc}) from the value of log K_{ex} was carried out for La(III). The result is shown in Fig. 5. The calculated values are good agreement with the experimental ones except for ones in the low range of D_{calc}. As mentioned above, it is suggested that the large derivation in the low range of D_{calc} is caused by the extraction without added chelating agents.

4. Conclusion

In the present work, we investigated the cloud point extraction behaviors of Ln(III) with and without HDEHP using Triton X-100 in detail. The results of this work show the utility and validity as separation/concentration method of Ln(III) of the proposed method. In the cloud point extraction of Ln(III) without HDEHP, the extraction behavior was different with Triton X-100 purchased from Aldrich and Nacalai Tesque. This result suggests that the cloud point extraction of Ln(III) without added chelating agents is caused by the impurities contained in Triton X-100. In the cloud point extraction of metals, the impurities contained in non-ionic surfactants should give serious influence to a result. The relative high extraction percentages of Ln(III) metals were obtained by the cloud point extraction with HDEHP. The composition of the complex extracted into the surfactant-rich phase was determined as $Ln(DEHP)_3$ from the slope analysis. The extraction constants of Ln(III) metals using HDEHP and 2.0% (v/v) Triton X-100 were also determined. Compared with the conventional liquid–liquid extraction, the equilibrium constants such as the extraction constant, distribution constants of metal chelates and chelating reagents and formation constant in the cloud point extraction are not yet clarified enough. The accumulation of the detail analysis will bring more development of the cloud point extraction.

References

[1] V.S. Sastri, J.-C. Bünzli, V.R. Rao, G.V.S. Rayudu, J.R. Perumareddi, Modern Aspects of Rare Earths and their Complexes, Elsevier, Amsterdam, 2003.
[2] D.F. Peppard, G.W. Mason, J.L. Maier, W.J. Driscoll, J. Inorg. Nucl. Chem. 4 (1957) 334.
[3] G.W. Mason, D.N. Metta, D.F. Peppard, J. Inorg. Nucl. Chem. 38 (1976) 2077.
[4] K. Ohto, K. Inoue, M. Goto, F. Nakashio, T. Nagasaki, Bull. Chem. Soc. Jpn. 66 (1993) 2528.
[5] J. Noro, T. Sekine, Bull. Chem. Soc. Jpn. 66 (1993) 2564.
[6] S. Satake, S. Tsukahara, N. Suzuki, Solvent Extr. Ion Exch. 17 (1999) 259.
[7] S. Nakamura, S. Takei, K. Akiba, Solvent Extr. Res. Dev. Jpn. 10 (2003) 103.
[8] A. Shimada, T. Yaita, H. Narita, S. Tachimori, T. Kimura, K. Okuno, Y. Nakano, Solvent Extr. Res. Dev. Jpn. 11 (2004) 1.
[9] Y. Takagai, S. Igarashi, Anal. Bioanal. Chem. 373 (2002) 87.
[10] R. Akiyama, Y. Takagai, S. Igarashi, Analyst 129 (2004) 396.
[11] A.R. Ghiasvand, E. Mohagheghzadeh, Anal. Sci. 20 (2004) 917.
[12] J. Fuchimukai, H. Yamaguchi, Y. Meguro, T. Kubota, S. Igarashi, Solvent Extr. Res. Dev. Jpn. 13 (2006) 139.
[13] C.D. Stalikas, Trends Anal. Chem. 21 (2002) 343.
[14] A. Ohashi, M. Ogiwara, R. Ikeda, H. Okada, K. Ohashi, Anal. Sci. 20 (2004) 1353.
[15] L. Wang, Y.-Q. Cai, B. He, C.-G. Yuan, D.-Z. Shen, J. Shao, G.-B. Jiang, Talanta 70 (2006) 47.
[16] B.K.-W. Man, M.H.-W. Lam, P.K.S. Lam, R.S.S. Wu, G. Shaw, Environ. Sci. Technol. 36 (2002) 3985.
[17] I.Y. Goryacheva, S.N. Shtykov, A.S. Loginov, I.V. Panteleeva, Anal. Bioanal. Chem. 382 (2005) 1413.
[18] S.T. Griffin, S.K. Spear, R.D. Rogers, J. Chromatogr. B 807 (2004) 151.
[19] S.T. Griffin, M. Dilip, S.K. Spear, J.G. Huddleston, R.D. Rogers, J. Chromatogr. B 844 (2006) 23.
[20] J. Miura, H. Ishii, H. Watanabe, Bunseki Kagaku 25 (1976) 808.
[21] H. Watanabe, T. Saitoh, T. Kamidate, K. Haraguchi, Mikrochim. Acta 106 (1992) 83.
[22] A.N. Tang, D.Q. Jiang, X.P. Yan, Anal. Chim. Acta 507 (2004) 199.
[23] M.F. Silva, L. Fernandez, R.A. Olsina, D. Stacchiola, Anal. Chim. Acta 342 (1997) 229.
[24] A. Ohashi, A. Tsuguchi, H. Imura, K. Ohashi, Anal. Sci. 20 (2004) 1091.
[25] A. Ohashi, H. Ito, C. Kanai, H. Imura, K. Ohashi, Talanta 65 (2005) 525.
[26] A.-N. Tang, G.-S. Ding, X.-P. Yan, Talanta 67 (2005) 942.
[27] C. Ortega, S. Cerutti, R.A. Olsina, M.F. Silva, L.D. Martinez, Anal. Bioanal. Chem. 375 (2003) 270.
[28] A. Favre-Réguillon, M. Draye, G. Lebuzit, S. Thomas, J. Foos, G. Cote, A. Guy, Talanta 63 (2004) 803.
[29] A. Mustafina, J. Elistratova, A. Burilov, I. Knyazeva, R. Zairov, R. Amirov, S. Solovieva, A. Konovalov, Talanta 68 (2006) 863.
[30] Y. Miyake, H. Matsuyama, M. Nishida, M. Nakai, N. Nagase, M. Teramoto, Hydrometallugy 23 (1990) 19.
[31] R.-S. Juang, S.-H. Lee, J. Chem. Technol. Biotechnol. 60 (1994) 61.

[32] K. Kondo, M. Matsumoto, Solvent Extr. Res. Dev. Jpn. 3 (1996) 178.
[33] R.K. Singh, P. Dhadke, J. Serb. Chem. Soc. 67 (2002) 41.
[34] J.A. Partridge, R.C. Jensen, J. Inorg. Nucl. Chem. 31 (1969) 2587.
[35] B.M. Cordero, J.R.P. Pavón, C.G. Pinto, M.E. Laespada, Talanta 40 (1993) 1703.
[36] Y. Inoue, K. Nakagawa, T. Hakushi, J. Chem. Soc., Dalton Trans. (1993) 1333.
[37] M.O. Luconi, M.F. Silva, R.A. Olsina, L.P. Fernández, Talanta 51 (2000) 123.
[38] A. Afkhami, T. Madrakian, H. Siampour, J. Hazard. Mater. 138 (2006) 269.

Available online at www.sciencedirect.com
ScienceDirect
Talanta 73 (2007) 862–869
Talanta
www.elsevier.com/locate/talanta

Method development for the determination of manganese, cobalt and copper in green coffee comparing direct solid sampling electrothermal atomic absorption spectrometry and inductively coupled plasma optical emission spectrometry

Nédio Oleszczuk [a], Jacira T. Castro [b], Márcia M. da Silva [a], Maria das Graças A. Korn [b], Bernhard Welz [b], Maria Goreti R. Vale [a,*]

[a] *Instituto de Química, Universidade Federal do Rio Grande do Sul, Av. Bento Gonçalves 9500, 91501-970 Porto Alegre, RS, Brazil*
[b] *Instituto de Química, Departamento de Química Analítica, Universidade Federal da Bahia, 40170-290 Salvador, BA, Brazil*

Received 20 April 2007; accepted 5 May 2007
Available online 13 May 2007

Abstract

A method has been developed for the determination of cobalt, copper and manganese in green coffee using direct solid sampling electrothermal atomic absorption spectrometry (SS-ET AAS). The motivation for the study was that only a few elements might be suitable to determine the origin of green coffee so that the multi-element techniques usually applied for this purpose might not be necessary. The three elements have been chosen as test elements as they were found to be significant in previous investigations. A number of botanical certified reference materials (CRM) and pre-analyzed samples of green coffee have been used for method validation, and inductively coupled plasma optical emission spectrometry (ICP OES) after microwave-assisted acid digestion of the samples as reference method. Calibration against aqueous standards could be used for the determination of Mn and Co by SS-ET AAS, but calibration against solid CRM was necessary for the determination of Cu. No significant difference was found between the results obtained with the proposed method and certified or independently determined values. The limits of detection for Mn, Cu and Co were 0.012, 0.006 and 0.004 μg g^{-1} using SS-ET AAS and 0.015, 0.13 and 0.10 μg g^{-1} using ICP OES. Seven samples of Brazilian green coffee have been analyzed, and there was no significant difference between the values obtained with SS-ET AAS and ICP OES for Mn and Cu. ICP OES could not be used as a reference method for Co, as essentially all values were below the limit of quantification of this technique.

Keywords: Electrothermal atomic absorption spectrometry; Inductively coupled plasma optical emission spectrometry; Solid sampling; Coffee; Cobalt; Copper; Manganese

1. Introduction

The vast majority of trace element determinations in food and beverage are carried out because of their nutritive importance and toxic effects [1,2]. The determination of trace elements in order to identify the geographic origin of food products is a relatively new, but increasingly active research area, driven by increasing demands on the agrifood industry from free-trade, globalization and changing technology. Financial incentives continue to drive retailers/resellers to misidentify the geographic origin of food products. Coffee is currently exported by more than 50 countries and on the international trade market ranks second only to petroleum, providing livelihood for over 100 million people worldwide [3]. With over 50 billion in US dollars in coffee retail sales [4], import/export, legal implications and financial concerns make determining country of origin for coffee important.

It is recognized that mineral and trace metal compositions of fruits and vegetables are a distorted reflection of the trace mineral composition of the soil and environment in which the plant grows [5]. Several authors have tried to differentiate geographic growing origins of coffee using elemental analysis – typically inductively coupled plasma optical emission spectrometry (ICP OES) – and statistical pattern recognition methods, such as

* Corresponding author. Tel.: +55 51 3308 6278; fax: +55 51 3308 7304.
E-mail address: mgrvale@iq.ufrgs.br (M.G.R. Vale).

0039-9140/$ – see front matter © 2007 Elsevier B.V. All rights reserved.
doi:10.1016/j.talanta.2007.05.005

principal component analysis (PCA), cluster analysis, discriminant function analysis and neural network modeling [6–10]. Fernandes et al. [9] determined 15 elements but did not succeed to correlate the metal content with the geographical origin of coffee. Martin et al. [6,7] determined 11 elements and found that Cu, Mn and P were the most discriminating variables. Anderson and Smith [8] investigated 18 elements and found that several geographic areas could be identified by their content of Al, Mn and Na, and better distinction could be obtained by adding the content of Cu and Fe. The most comprehensive study about the correlation between the trace element content of coffee and its origin was carried out by Krivan et al. [10] who determined 20 elements in coffee samples from 8 different countries using instrumental neutron activation analysis (INAA), electrothermal atomic absorption spectrometry (ET AAS), flame atomic absorption spectrometry (F AAS) and combustion elemental analysis. These authors found that among the investigated elements manganese was best suited as an indicator for the origin of coffee, but elements like Co, Cs, Na and Rb proved to be of interest too.

Inductively coupled plasma OES has been used in most of the above studies as the analytical technique because of its multi-element capability, its good sensitivity, wide linear dynamic range, relatively high freedom from non-spectral interferences and its precision [11]. Hence, ICP OES could offer considerable advantages for the quantitative analysis of food and has been applied repeatedly for the analysis of coffee [12–15]. Although instant coffee might be analyzed directly after appropriate dilution [15] or after solubilization with tetra methylammonium hydroxide [14], green or roasted coffee beans require an acid digestion before their analysis by ICP OES [9,12,13]. Microwave-assisted digestion in closed vessels using a combination of mineral acids is the technique of choice for sample preparation nowadays. A mixture of HNO_3 and H_2O_2 is preferred in many instances for the digestion of food samples since they are strong oxidizing agents and produce minimum matrix effects in ICP OES [16].

However, microwave-assisted acid digestion in closed vessels requires high-purity reagents in order to avoid sample contamination, and it is rather time consuming when a large number of samples have to be analyzed. Digestion inevitably also results in significant dilution, so that the concentration of trace elements in the final solution might be below the limit of quantification of ICP OES. In addition, in the studies carried out until now, it turned out that only a few elements are really useful in characterizing the geographic origin of coffee, hence a multi-element technique might not be necessary for this task. It could therefore be of interest to investigate alternate techniques for that purpose, and solid sampling ET AAS (SS-ET AAS) in a graphite tube furnace was considered a good approach, as it offers maximum sensitivity due to the absence of any dilution, a minimum risk of contamination or loss of analyte as no reagents and only a minimum of sample preparation is required, and calibration can often be carried out against aqueous standards, as has been shown in a recent review article [17]. Obviously, direct SS analysis also has some limitations, the most important one being the inferior precision, compared to solution analysis, due to the natural inhomogeneity of solid samples. However, a relative standard deviation (R.S.D.) of some 10% of an accurate result appears to be much more acceptable than a R.S.D. of 1–2% of a result that is affected by errors due to contamination or analyte loss in the sample preparation stage. It has been shown in several recent publications that SS-ET AAS could be applied successfully for the determination of elements such as cobalt [18], lead [19] and mercury [20] in various biological materials. However, SS-ET AAS has never been described for the direct determination of trace elements in green coffee.

The goal of this work was to develop a method for the determination of a few key elements in green coffee using direct SS-ET AAS and compare its performance with that of ICP OES after conventional acid digestion. Manganese was first choice, because it was found to be best suited to identify the origin of coffee in all related publications [6–8,10], followed by copper [6–8], and cobalt was added because of the results obtained by Krivan et al. [10]. The relative advantages and limitations of both techniques have been evaluated, including speed of analysis, sensitivity and accuracy of the results. As no certified reference material (CRM) for coffee is available, several coffee samples that have been pre-analyzed by several techniques [10] were used in this work in addition to a few botanical CRM. No attempt has been made to correlate the content of the above metals found in the samples of Brazilian coffee investigated here with their origin, as only one sample from each region has been analyzed, which does not allow any statistical evaluation. The goal has been to develop a fast and reliable routine method that could be used in future work to analyze a large number of samples for a few elements in order to establish a data basis for the determination of the origin of green coffee.

2. Experimental

2.1. Instrumentation

All SS-ET AAS measurements were carried out using an AAS 5EA atomic absorption spectrometer (Analytik Jena AG, Germany), equipped with a transversely heated graphite tube atomizer and deuterium background correction. Hollow cathode lamps (Narwa, Berlin, Germany) were used as the radiation source with a lamp current of 4.5, 3.0 and 3.5 mA for Co, Cu and Mn, respectively. The analytical lines at 240.7, 324.8 and 403.1 nm with a spectral bandpass of 0.2, 0.5 and 0.5 nm were used for Co, Cu and Mn, respectively. The graphite furnace temperature program is given in Table 1. The spectrometer was interfaced to an IBM PC/AT compatible computer. All experiments were carried out using pyrolytically coated SS graphite tubes without a dosing hole (Analytik Jena, Part No. 07-8130325) and SS graphite platforms (Analytik Jena, Part No. 407-A81.312). An M2P microbalance (Sartorius, Göttingen, Germany) was used for weighing the samples directly into the SS platforms. The sample weight was automatically transmitted to the instrument computer to calculate the normalized absorbance (integrated absorbance per milligram of sample) after each measurement. A pre-adjusted pair of tweezers, which is part of the SSA 5 manual solid sampling accessory (Analytik Jena) was

Table 1
Graphite furnace temperature program for the determination of manganese, cobalt and copper in green coffee

Stage	Temperature (°C)	Ramp (°C s^{-1})	Hold time (s)	Gas flow rate (L min^{-1})
Drying 1	90	10	10	2.0
Drying 2	120	10	10	2.0
Drying 3	150	10	10	2.0
Pyrolysis	900[a]; 1100[b]; 1400[c]	400	30	2.0
Atomization	1900[a]; 2100[b]; 2400[c]	1500	10	0.1[a]; 0[b,c]
Cleaning	2500	1000	4	2.0

[a] Conditions for Mn.
[b] Conditions for Cu.
[c] Conditions for Co.

used to transfer the SS platforms to the atomizer. Argon was used as the purge gas with a flow rate of 2.0 L min^{-1} during all stages, except during atomization, when the flow was stopped. Integrated absorbance (peak area) was used exclusively for all measurements. Standard reference materials were used to establish the optimum parameters for the graphite furnace temperature program in Table 1.

An inductively coupled plasma optical emission spectrometer with axially viewed configuration (VISTA PRO, Varian, Mulgrave, Australia) equipped with solid state detector, cyclonic spray chamber, and concentric nebulizer was employed for ICP OES determinations of Co, Cu and Mn. The operational parameters are described in Table 2.

A microwave oven, model Ethos EZ (Milestone, Sorisole, Italy), equipped with 100 mL Teflon PFA vessels and pressure sensor, was used for digestion of coffee samples for ICP OES analysis.

The samples for SS-ET AAS were ground in a Vibratory Micro-Mill "pulviresette 0" (Fritsch GmbH, Idar-Oberstein, Germany). During the grinding stage liquid nitrogen was used to facilitate the operation and to reach the desired granulometry. Different mesh-size polyester sieves were used in order to obtain four sets of particle sizes: (a) 250–150 μm; (b) 150–85 μm; (c) 85–45 μm; and (d) <45 μm.

The particle size analysis was carried out in an MS-17 particle size analyzer (Malvern Instruments, Malvern, UK).

2.2. Reagents and solutions

Analytical grade reagents were used throughout. Distilled, deionized water (DDW) with a specific resistivity of 18 MΩ cm, from a Millipore water purification system (Milli-Q, Millipore, Bedford, MA, USA), was used for the preparation of the samples and standards. The nitric acid (Merck, Germany) used to prepare the aqueous calibration standards was further purified by sub-boiling distillation in a quartz sub-boiling still (Kürner Analysentechnik, Rosenheim, Germany). All containers and glassware were soaked in 3.0 mol L^{-1} nitric acid for at least 24 h and rinsed three times with deionized water before use. Reference solutions were prepared by diluting stock solutions containing 1000 mg L^{-1} of each element (Tec-Lab, Hexis, São Paulo, SP, Brazil) with deionized water. The palladium nitrate and magnesium nitrate modifier solutions were from Merck, Germany, and Triton X-100 from Union Carbide.

Table 2
Operational parameters for the determination of Co, Cu and Mn using axial-view ICP OES

Instrumental parameter	
RF generator (MHz)	40
Power (kW)	1.3
Plasma gas flow (L min^{-1})	15.0
Auxiliary gas flow (L min^{-1})	1.5
Nebulizer gas flow (L min^{-1})	0.70
Analytical wavelengths (nm)	
Co(II)	230.786
Cu(I)	327.397
Mn(II)	257.611

2.3. Samples and reference materials

The description of the investigated samples of green coffee obtained from the Research and Test Unit of ICO (London, Great Britain), which have been pre-analyzed by Krivan et al. [10] and the Brazilian coffees obtained from the Coffee Market (Porto Alegre, Rio Grande do Sul, Brazil) are shown in Table 3. The samples were coffees of commercial types available on the international markets. All coffee samples, with one exception, were of the *Arabica* type.

The following certified reference materials (CRM) have been used in this work: NIST SRM 8433 Corn Bran, NIST SRM

Table 3
Investigated samples of green coffee

Country of origin	Type	Crop year
Colombia	Medellin excelso	1987/1988
Costa Rica	Strictly hard bean	1987/1988
Cuba	Crystal mountain	1987/1988
Mexico	Strictly hard bean	1987/1988
Nicaragua	A	1987/1988
Panamá	Chiriqui	1987/1988
Brazil	XX	2003/2004
Brazil (BA)	Planalto Cerrado	2004/2005
Brazil (ES)[a]	Robusta	2004/2005
Brazil (MG)	Cerrado Mineiro	2004/2005
Brazil (MG)	Sul de Minas	2004/2005
Brazil (PR)	Apucarana	2004/2005
Brazil (SP)	Mogiana	2004/2005

All samples except one were of *Arabic* species.
[a] *Robusta* species.

1568a Rice Flour, NIST SRM 1572 Citrus Leaves and NIST SRM 1515 Apples Leaves (all from National Institute of Standards and Technology, Gaithersburg, MD, USA) and NIES CRM 10a Rice Flour (National Institute for Environmental Studies, Japan Environment Agency, Yatabe-machi, Tsukuba, Ibaraki, Japan).

2.4. Microwave-assisted sample digestion

A mass of about 500 mg of coffee was directly weighed in a PTFE digestion vessel, 7 mL of HNO_3 conc. and 1 mL of H_2O_2 conc. were added, and the vessels were placed in a fume hood for 1 h for pre-digestion before they were placed on the turntable of the microwave system. The coffee samples were digested by a four-step temperature program. In the first step the temperature was linearly increased to 90 °C in 4 min with maximum power of the rotating magnetron of 1000 W. In the second step the temperature was kept at 90 °C for 2 min. In the third step the temperature was linearly increased to 180 °C in 4 min and in the fourth step the temperature was kept at 180 °C for 15 min. After digestion and cooling, which took about 3 h, each solution was diluted to 25 mL with deionized water in a volumetric flask and the analytes were determined by ICP OES. Matrix effect studies were carried out by spiking some of the original non-digested samples (accurately weighed different amounts) with variable amounts of standard solution of the metals. The spiked samples were then mineralized using the same digestion procedures as were applied to the non-spiked samples. All digestions were performed in triplicate.

2.5. Direct SS-ET AAS

The green coffee samples were dried to constant weight and kept in a closed plastic vial until they were analyzed. The sample mass weighed directly onto the SS platforms and introduced into the graphite furnace for SS-ET AAS was between 0.03 and 0.17 mg for the determination of Cu and Mn and between 0.3 and 0.5 mg for the determination of Co. As the actual sample mass was obviously different for each measurement the integrated absorbance obtained in each measurement was 'normalized' for a sample mass of 0.1 mg in the case of Cu and Mn, and 1.0 mg in the case of Co for better comparison.

3. Results and discussion

3.1. Digestion procedure for ICP OES analysis

As ICP OES was intended to be used as reference method it was necessary to verify first the accuracy of this technique, particularly with respect of the digestion procedure. Initially results obtained for digested samples using aqueous standards for calibration were biased low. It was suspected that there was some influence from the high nitric acid concentration in the digested samples on the analyte signal that had to be taken into consideration. Previous investigations have demonstrated that inorganic acids cause a decrease in signal intensity and plasma thermal characteristics are deteriorated compared to aqueous standards. Stewart and Olesik [21] studied the effect of nitric acid on the aerosol generation and transport processes and concluded that the higher the acid concentration the lower the aerosol liquid mass transported to the plasma. Hence, the slopes of the regression lines by plotting the emission intensities of aqueous standards versus the emission intensities of standard addition solutions were calculated and used for correction. Based on these results, calibration using the analyte addition technique is recommended for determination of trace elements in digested coffee samples to overcome or to eliminate most of the errors due to acid interference that causes low sensitivity.

The values that have been obtained for the three analytes in one CRM and in six pre-analyzed samples of green coffee are summarized in Table 4. There is no significant difference between the certified or reference values and those that have been obtained in this work according to a Student's *t*-test on a 95% confidence level for Mn and Cu. However, the results for Co were all below the limit of quantification (LOQ) of this technique, so that their accuracy is limited. Nevertheless, ICP OES after microwave-assisted acid digestion of the samples could be considered a reliable reference technique, at least for the determination of Mn and Cu in green coffee.

Table 4
Determination of manganese, copper and cobalt in NIST SRM 1569a rice flour and six pre-analyzed samples of green coffee using ICP OES after microwave-assisted acid digestion

Sample	Mn ($\mu g\,g^{-1}$)		Cu ($\mu g\,g^{-1}$)		Co ($\mu g\,g^{-1}$)	
	Reference value	Found	Reference value	Found	Reference value	Found
NIST SRM 1568a	20.0 ± 1.6[a]	19.5 ± 0.2	2.4 ± 0.3[a]	1.6 ± 0.01	0.018[b]	<LOD
Colombia	46.5	50.5 ± 0.6	13.7 ± 1.0	13.0 ± 0.04	0.13 ± 0.02	0.1[c]
Costa Rica	33.3 ± 6.5	29.4 ± 0.3	15.3 ± 1.1	14.5 ± 0.2	0.15 ± 0.02	0.2[c]
Cuba	42.4 ± 3.0	37.2 ± 0.4	14.0 ± 0.8	14.5 ± 0.2	0.095 ± 0.020	0.1[c]
Mexico	57.7 ± 4.0	44.0 ± 0.6	12.1 ± 0.9	10.7 ± 0.06	0.18 ± 0.02	0.1[c]
Nicaragua	18.0 ± 1.0	17.2 ± 0.4	19.8 ± 0.4	18.6 ± 0.2	0.10 ± 0.01	0.1[c]
Panama	19.4 ± 1.1	19.7 ± 0.1	15.0 ± 0.5	12.6 ± 0.2	0.064 ± 0.008	0.1[c]

Reference values are from Ref. [10].
[a] Certified value.
[b] Not certified.
[c] No S.D. reported; value below LOQ.

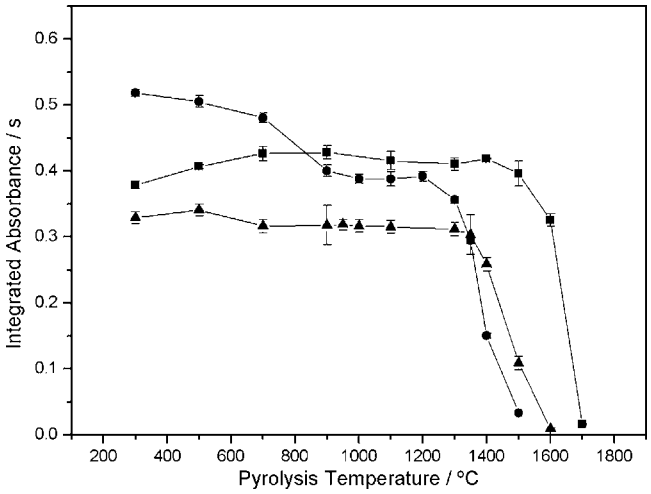

Fig. 1. Pyrolysis curves for manganese with and without modifier; atomization temperature 1900 °C; (●) 2.0 ng Mn aqueous standard without modifier; (■) 2.0 ng Mn aqueous standard with 5 μg Pd, 3 μg Mg and 5 μg Triton X-100 as modifier; (▲) Café Brasil, integrated absorbance normalized for 0.1 mg sample.

3.2. Method development for direct SS-ET AAS

Pyrolysis and atomization curves have been established for all three elements using both, aqueous standards and a sample of green coffee (Café Brasil). For cobalt and copper the pyrolysis and atomization curves established with aqueous standards and the coffee sample were essentially identical and are therefore not shown here. Pyrolysis temperatures of 1400 and 1100 °C could be used for Co and Cu, respectively, without adding a modifier, and the optimum atomization temperatures were 2400 and 2100 °C, respectively.

The only analyte that required some additional optimization was manganese, mostly because of the relatively high content of this element in coffee, which made it necessary to use the secondary analytical line at 403.1 nm. Although this line is about one order of magnitude less sensitive than the main resonance line at 279.5 nm, the sensitivity had to be further reduced by using a gas flow of 0.1 L min^{-1} during atomization in order to allow the introduction of reasonably high sample mass into the furnace—a pre-requirement for an acceptable precision. Another problem in the case of manganese was that the pyrolysis curves established with aqueous standards and the coffee sample were significantly different, as can be seen in Fig. 1. While manganese in the coffee sample was thermally stable up to 1300 °C, analyte losses from aqueous standards were observed already above 700 °C. Hence, the addition of a modifier was considered mandatory, and a mixture of 5 μg Pd, 3 μg Mg, both as the nitrates [22], and 5 μg Triton X-100 was found optimum, as it could stabilize the analyte in aqueous standards to a pyrolysis temperature of 1400 °C (see Fig. 1). The addition of a modifier to the solid samples was found to be not necessary, which simplified the procedure significantly. The optimum atomization temperature was determined to be 1900 °C.

Another very important issue in direct SS-ET AAS is particle size, as only small sample mass of the order of 1 mg can usually be introduced into the furnace, which has to be representative for the sample. One sample of green coffee (Mogiana Verde) was therefore ground and divided into four different granulometric fractions, >150 μm, 85–150 μm, 45–85 μm, and <45 μm, using sieves of different mesh size. The initial result was kind of surprising, because decreasing analyte content was found with decreasing particle size, as is shown in Table 5 for manganese. The source of the problem was found to be the hygroscopic nature of green coffee, which resulted in much more rapid adsorption of humidity from the environment for the fractions with small particle size, compared to the coarser fractions. This problem can be solved by drying the samples to constant weight just before analysis or to correct for humidity that has been determined in a separate sample aliquot, as can be seen in Table 5. The most important outcome of this experiment was that neither the analytical result nor the precision of the analysis appears to depend on the particle size, which means that the analyte must be distributed rather homogeneously in the coffee beans. This is important for two reasons, firstly, green coffee in contrast to roasted coffee is rather difficult to be ground to small particle size, and secondly, the problem of adsorption of humidity from the environment is minimized when the beans are not ground to small particle size.

Table 5
Influence of particle size of green coffee (Mogiana) on the normalized (for 0.1 mg of sample) integrated absorbance measured for manganese without and with correction for humidity

Particle size (μm)	Normalized integrated absorbance (s)	
	Without drying	Corrected for humidity
>150	0.590 ± 0.030	0.414 ± 0.037
85–150	0.537 ± 0.025	0.411 ± 0.017
45–85	0.386 ± 0.031	0.415 ± 0.032
<45	0.334 ± 0.024	0.435 ± 0.018

Average and standard deviation of $n = 5$ measurements.

3.3. Analysis of reference materials using SS-ET AAS

The next step was to analyze the six coffee reference materials and a number of botanical CRM using direct SS-ET AAS and aqueous standards for calibration. In order to test the validity of this approach we also established a linear correlation equation between the certified values of the CRM and the normalized integrated absorbance obtained by SS-ET AAS. The slope of this correlation curve was then used to calculate the analyte content in the coffee reference samples, and the results compared with those obtained by calibration against aqueous standards. For manganese and cobalt there was no significant difference between the two sets of data at a 95% confidence level according to a paired Student's *t*-test. Therefore only the values obtained by calibration against aqueous standards are shown in Table 6. The validity of using aqueous standards for calibration for these elements can also be deduced from the good agreement between the values obtained in this work and the certified or reference values, which showed no significant difference using the same test.

Table 6
Determination of manganese, copper and cobalt in certified reference materials and six pre-analyzed samples of green coffee using direct SS-ET AAS with calibration against aqueous standards, except for copper

Sample	Mn ($\mu g\,g^{-1}$)		Cu ($\mu g\,g^{-1}$)		Co ($\mu g\,g^{-1}$)	
	Reference value	Found	Reference value	Found[a]	Reference value	Found
NIST SRM 1568a	20.0 ± 1.6	19.3 ± 1.8	2.4 ± 0.3	n.d.[b]	0.018[c]	0.011 ± 0.002
NIST SRM 8433	2.55 ± 0.29	2.28 ± 0.2	2.47 ± 0.40	1.6 ± 0.5	0.006 ± 0.006	n.d.[b]
NIST SRM 1515	54 ± 3	57.7 ± 1.6	5.64 ± 0.24	3.1 ± 0.2	0.09[c]	0.071 ± 0.002
NIST SRM 1572	23 ± 2	n.d.[b]	16.5 ± 1.0	11.5 ± 1.4	0.02[c]	n.d.[b]
NIES CRM 10a	34.7 ± 1.8	30.3 ± 1.2	3.5 ± 0.3	2.3 ± 0.2	0.02	n.d.[b]
Colombia	46.5	49.4 ± 1.3	13.7 ± 1.0	13.3 ± 0.9	0.13 ± 0.02	0.18 ± 0.005
Costa Rica	33.3 ± 6.5	32.4 ± 1.4	15.3 ± 1.1	14.5 ± 0.8	0.15 ± 0.02	0.19 ± 0.005
Cuba	42.4 ± 3.0	39.6 ± 3.0	14.0 ± 0.8	15.5 ± 1.7	0.095 ± 0.020	0.082 ± 0.001
Mexico	57.7 ± 4.0	53.8 ± 6.0	12.1 ± 0.9	11.8 ± 1.2	0.18 ± 0.02	0.13 ± 0.005
Nicaragua	18.0 ± 1.0	19.8 ± 0.5	19.8 ± 0.4	17.2 ± 1.5	0.10 ± 0.01	0.11 ± 0.002
Panama	19.4 ± 1.1	22.1 ± 1.8	15.0 ± 0.5	12.7 ± 0.8	0.064 ± 0.008	0.066 ± 0.001

Reference values are from Ref. [10]. For identification of the CRM see Section 2.
[a] Correlation curve of the CRM was used for calibration of the coffee samples.
[b] n.d. = not determined.
[c] Non-certified value.

For copper, however, the above test exhibited a significant difference, which means that calibration with aqueous standards is not feasible for this element. This also becomes obvious from the results obtained for the CRM shown in Table 6, which are all biased low, indicating the existence of some interference. For this reason for copper only the results obtained by calibration using the correlation curve established with the CRM are shown for the coffee samples in Table 6. These values are in agreement with the reference values, as there is no significant difference between the two sets of data at a 95% confidence level according to a paired Student's *t*-test. This means that the matrix effect is the same not only for all the coffee samples, but actually for all the botanical CRM as well. The source of this interference could not be identified in this work, nor could it be eliminated.

3.4. Analysis of Brazilian green coffee samples comparing ICP OES and SS-ET AAS

Seven samples of green coffee from different growing areas of Brazil were analyzed comparing ICP OES after microwave-assisted acid digestion in closed vessels and direct SS-ET AAS. In the case of ICP OES calibration was against analytical curves established with aqueous standards and the results were corrected for the nitric acid interference as described in Section 3.1. In the case of SS-ET AAS calibration for Mn and Co was against analytical curves established with aqueous standards; only Cu had to be calibrated using a regression curve established with solid CRM, as described in the previous section. All results are shown in Table 7. According to a Student's *t*-test there was no significant difference at a 95% confidence level between the data obtained by the two techniques for Mn and Cu. The results obtained for Co with ICP OES could not be used as reference values for a statistical comparison, as all of them were below or very close to the LOQ. Direct SS-ET AAS is obviously better suited for the determination of very low Co concentrations because of its higher sensitivity and the absence of any sample preparation except grinding, which is also necessary for ICP OES prior to digestion.

3.5. Figures of merit

The most important figures of merit for both techniques, ICP OES and SS-ET AAS are summarized in Table 8. The limits of detection (LOD) for ICP OES were obtained using the back-

Table 7
Determination of manganese, copper and cobalt in green coffee samples from different regions in Brazil comparing ICP OES after microwave-assisted acid digestion and direct SS-ET AAS

Sample	Mn ($\mu g\,g^{-1}$)		Cu ($\mu g\,g^{-1}$)		Co ($\mu g\,g^{-1}$)	
	ICP OES	SS-ET AAS[a]	ICP OES	SS-ET AAS[b]	ICP OES	SS-ET AAS[a]
Café Brasil	32.0 ± 0.2	36.2 ± 6.7	13.4 ± 0.2	13.8 ± 1.1	0.1[c]	0.62 ± 0.02
Planalto Cerrado BA	15.7 ± 0.2	15.8 ± 0.5	10.1 ± 0.1	10.9 ± 0.2	0.1[c]	0.019 ± 0.001
Robusta ES	16.9 ± 0.1	19.1 ± 0.7	16.2 ± 0.1	16.0 ± 0.8	0.2[c]	0.36 ± 0.01
Cerrado Mineiro MG	18.7 ± 0.4	18.3 ± 0.3	13.4 ± 0.2	14.6 ± 0.1	0.1[c]	0.020 ± 0.002
Sul de Minas MG	28.6 ± 0.5	28.1 ± 0.9	13.9 ± 0.2	13.6 ± 0.6	0.3 ± 0.03	0.51 ± 0.02
Apucarana PR	30.5 ± 0.4	34.0 ± 0.8	13.4 ± 0.1	17.2 ± 1.1	0.3 ± 0.04	0.23 ± 0.01
Mogiana SP	27.2 ± 0.5	31.8 ± 2.2	10.8 ± 0.2	11.4 ± 0.8	0.3 ± 0.03	0.24 ± 0.01

[a] Calibration against aqueous standards.
[b] Calibration against solid CRM.
[c] No S.D. reported; value below LOQ.

Table 8
Figures of merit for the determination of Mn, Cu and Co in coffee using ICP OES after microwave-assisted acid digestion and direct SS-ET AAS

Technique	Parameter	Mn	Cu	Co
ICP OES	LOD ($\mu g\,L^{-1}$)	0.31	2.5	2.0
ICP OES	LOD[a] ($\mu g\,g^{-1}$)	0.015	0.13	0.10
SS-ET AAS	LOD[b] ($\mu g\,g^{-1}$)	0.012	0.006	0.004
ICP OES	LOQ[a] ($\mu g\,g^{-1}$)	0.050	0.42	0.33
SS-ET AAS	LOQ[b] ($\mu g\,g^{-1}$)	0.040	0.021	0.012
SS-ET AAS	m_0 (pg)	19	5.8	5.6

[a] Based on 500 mg sample in 25 mL of solution after digestion.
[b] Based on the introduction of 1 mg of sample into the graphite tube.

ground equivalent concentration (BEC) of the analyte, which was calculated from the ratio of 10 measurements of the blank and the inclination of the analytical curve. The LOD were calculated as three times the standard deviation of the blank. The LOD in the solid samples were calculated based on a mass of 500 mg of sample in 25 mL of solution after digestion and dilution. The LOD in SS-ET AAS was obtained according to the 'zero mass response' as proposed by Kurfürst [23], i.e., by inserting an empty solid sampling platform that only contains the modifier (if used) 10 times into the graphite tube and run a full atomization cycle. The LOD is then calculated as three times the standard deviation of the blank readings. The limit of quantification (LOQ) is based on the same measurements, using 10 times the standard deviation of the blank readings.

For manganese the LOD and LOQ in the original sample are comparable for the two techniques, but it has to be kept in mind that the sensitivity for SS-ET AAS has been reduced deliberately by choosing a less sensitive analytical line and by maintaining a gas flow through the tube in order to bring the absorbance signals within the working range of the spectrometer. For the other two analytes, for which the primary analytical lines could be used, the LOD and LOQ of SS-ET AAS are more than a factor of 20 better than the values for ICP OES, mostly because of the absence of any dilution with the former technique. This is not a problem in the case of copper, as the concentration of this element in essentially all of the investigated samples is more than an order of magnitude above the LOQ, which means that quantitative determination is possible with good precision. However, this is not the case for the determination of cobalt, as essentially all values for this analyte in the investigated samples are lower than the LOQ, which means that no quantitative determination is possible and only approximate values can be reported. This fact also explains the significant differences that have been observed in the values found for cobalt between SS-ET AAS and ICP OES.

The precision obtained with SS-ET AAS in this work for real samples, based on five replicates, with one exception (Mn in Café Brasil with an R.S.D. of ~20%) was typically better than 10% R.S.D., which is normal for direct solid sampling analysis, but frequently even better than 5% R.S.D. for all three analytes, indicating good homogeneity of analyte distribution in the samples. The precision obtained with ICP OES for the determination of Mn and Cu was typically better than 5% R.S.D. and often in the range of 2–3% R.S.D., which is within expectation for solution analysis. However, the question has to be raised if this improved precision is of importance in the present investigation. The natural heterogeneity in the trace element content of samples even from the same plantation area, and even more from the same region probably exceeds already 10%, so that an R.S.D. < 10% appears to be more than acceptable for the purpose. The only element that did not meet this criterion was cobalt when it was determined by ICP OES, as the imprecision at the LOD by definition is 33%.

The comparison of the time required for an analysis with ICP OES after microwave-assisted digestion and with SS-ET AAS could obviously be made only for the equipment and the experimental conditions used in this work. This includes that all digestions for ICP OES were carried out in triplicate, i.e., three samples could be digested per run, and that five independent sample portions were weighed and determined per element and sample for SS-ET AAS. The sample preparation for ICP OES including digestion and cooling takes about 270 min for three samples in triplicate; the measurement time with ICP OES is essentially negligible in this context. This means that the time required per element and per sample is about 30 min. The graphite furnace temperature program for SS-ET AAS takes about 90 s, followed by about 30 s of cooling and another 30 s for weighing and sample introduction, i.e., one measurement takes about 2.5 min and five repetitive measurements per element and sample take 12.5 min. This means that the sample throughput is more than a factor of 2 higher in the case of SS-ET AAS compared to the digestion approach.

4. Conclusion

Direct SS-ET AAS has been shown to be a powerful tool for the determination of selected trace elements in green coffee for the determination of its origin. The method has been validated by analyzing several botanical CRM and a number of pre-analyzed samples of green coffee, as well as by comparing the results with values obtained by ICP OES after microwave-assisted acid digestion as independent method. Manganese and cobalt could be determined using aqueous standards for calibration, but calibration with solid CRM was necessary for accurate determination of copper. The LOD for copper and cobalt were more than an order of magnitude better for SS-GF AAS due to the absence of any dilution, demonstrating the superiority of this technique for trace element determination. The multi-element capability of ICP OES appears to be of little advantage for this kind of application, as all papers on this subject agree that only a very few elements might be used to determine the origin of coffee, while the majority of the others does not contribute. Hence, a single-element technique that does not require any sample preparation besides grinding of the coffee beans appears to be an attractive alternative to the multi-element techniques that have been used up to now. The much better sensitivity if this technique is an additional advantage in the determination of trace elements such as cobalt and others that might be of importance.

Acknowledgements

The authors are grateful to Conselho Nacional de Desenvolvimento Científico e Tecnológico (CNPq) and to Fundação de Amparo à Pesquisa do Estado da Bahia (FAPESB) for financial support. M.G.A.K., M.M.S., M.G.R.V and J.T.C. have research scholarships from CNPq and B.W. has a research scholarship from FAPESB. The authors are also grateful to Analytik Jena AG for the donation of an atomic absorption spectrometer. The authors are particularly grateful to Prof. Viliam Krivan for the donation of the pre-analyzed samples of green coffee, which have been extremely useful in validating the proposed procedure.

References

[1] B.L. O'Dell, R.A. Sunde (Eds.), Handbook of Nutritionally Essential Mineral Elements, Marcel Dekker, New York, 1997.
[2] H.R. Roberts, Food Safety, Wiley, New York, 1981.
[3] International Coffee Organization, The Coffee Story, ICO Information Centre, London, 1989.
[4] International Coffee Organization, 2006, http://www.imf.org/external/np/sec/decdo/ico.htm.
[5] H. Esechie, J. Sci. Food Agric. 58 (1992) 435.
[6] M.J. Martin, F. Pablos, A.G. González, Anal. Chim. Acta 358 (1998) 177.
[7] M.J. Martin, F. Pablos, A.G. González, Food Chem. 66 (1999) 365.
[8] K.A. Anderson, B.W. Smith, J. Agric. Food Chem. 50 (2002) 2068.
[9] A.P. Fernandes, M.C. Santos, S.G. Lemos, M.M.C. Ferreira, A.R.A. Nogueira, J.A. Nobrega, Spectrochim. Acta Part B 60 (2005) 717.
[10] V. Krivan, P. Barth, A.F. Morales, Microchim. Acta 110 (1993) 217.
[11] A. Montaser, D.W. Golightly, Inductively Coupled Plasmas in Analytical Atomic Spectrometry, VCH Publishers, New York, 1992.
[12] K.R. Koch, M.A.B. Pougnet, S. de Villiers, Analyst 114 (1989) 911.
[13] E.J. Santos, E. Oliveira, J. Food Comp. Anal. 14 (2001) 523.
[14] A.S. Ribeiro, A.L. Moretto, M.A.S. Arruda, S. Cadore, Microchim. Acta 141 (2003) 149.
[15] A. Asfaw, G. Wibetoe, Anal. Bioanal. Chem. 382 (2005) 173.
[16] L.M. Costa, S.T. Gouveia, J.A. Nobrega, Anal. Sci. 18 (2002) 313.
[17] M.G.R. Vale, N. Oleszczuk, W.N.L. dos Santos, Appl. Spectrosc. Rev. 41 (2006) 377.
[18] A.S. Ribeiro, M.A. Vieira, A.F. da Silva, D.L.G. Borges, B. Welz, U. Heitmann, A.J. Curtius, Spectrochim. Acta Part B 60 (2005) 693.
[19] D.L.G. Borges, A.F. da Silva, B. Welz, A.J. Curtius, U. Heitmann, J. Anal. Atom. Spectrom. 21 (2006) 763.
[20] A.F. da Silva, F.G. Lepri, D.L.G. Borges, B. Welz, A.J. Curtius, U. Heitmann, J. Anal. Atom. Spectrom. 21 (2006) 1321.
[21] I.I. Stewart, J.W. Olesik, J. Anal. Atom. Spectrom. 13 (1998) 1249.
[22] G. Schlemmer, B. Welz, Spectrochim. Acta Part B 41 (1986) 1157.
[23] U. Kurfürst, in: U. Kurfürst (Ed.), Solid Sample Analysis, Springer, Berlin, 1998, pp. 115–116.

Available online at www.sciencedirect.com
ScienceDirect
Talanta 73 (2007) 959–961
Talanta
www.elsevier.com/locate/talanta

Short communication

Automatic determination of insolubles in lubricating oils by flow injection analysis employing an LED-photometer detector

Gustavo Pignalosa *, Alexandra Sixto, Moisés Knochen

Universidad de la República, Facultad de Química, Cátedra de Química Analítica, Av. Gral. Flores 2124, Casilla 1157, 11800 Montevideo, Uruguay

Received 5 February 2007; received in revised form 12 May 2007; accepted 14 May 2007
Available online 21 May 2007

Abstract

A flow injection system is presented for the determination of the insolubles content in used lubricating oil samples. The system is based on the injection of an aliquot of the sample in a stream of organic solvent where it is dispersed, and measurement of the scattered radiation (measured as apparent absorbance) in the visible range ($\lambda = 640$ nm). An LED-based photometer was used for this purpose. The whole system including sample injection and data acquisition was controlled by a personal computer. Calibration curves exhibited good linearity ($h = 0.415 \pm 0.016C + 0.00 \pm 0.03$, $r^2 = 0.9995$, confidence level of 95%) in the range up to 2.68% (insolubles in pentane). Detection and quantification limits were respectively 0.07% and 0.16% (w/w). The method was validated by analysis of 25 real samples by the proposed method and the FTIR method finding high correlation. Waste generation and reactive consumption is much less than in the official method (ASTM D-893). The proposed method employs 25 mL of kerosene per sample while the official method employs 200 mL of pentane.

Keywords: Insoluble determination; Lubricating analysis; Automation; LED-photometer

1. Introduction

The analysis of used lubricating oil is a widely used tool for the proactive maintenance of lubricated engines [1,2]. Insolubles determination is one of the parameters employed to evaluate the residual life of oil because a high content of it, is one of the majors factors in causing abrasive engine wear and also this contamination results in lubricant breakdown [3].

In a previous work [4], a flow injection method was presented for the determination of insolubles employing detection by absorption in the visible region. Despite its usefulness the method required manual loading of the injection valve, which reduced its sampling rate and required a dedicated operator.

In the present work, an automatic flow injection system for the determination of insolubles was developed. The system consists of a motorised six-port injection valve to introduce the sample through a loop into the solvent stream, a lab-built motorised syringe and a packed reactor that ensures the thorough mixing of the sample and the carrier (both already described elsewhere [5]), and a lab-made LED-photometer detector. A personal computer with a multipurpose board was used for the system control and data acquisition. The whole system was operated by means of a program written for this purpose and compiled in Quick-BASIC 4.0 (Microsoft).

The proposed method was compared against FTIR because is actually the most employed method for the insolubles determination [6].

2. Experimental

Flow injection determinations were carried out in the system schematically shown in Fig. 1.

The solvent stream was pumped by an eight-channel Dynamax RP-1 peristaltic pump (Rainin Instrument Co., Woburn, MA, USA) fitted with Viton® tubing. Sample injection was carried out by means of a motorised six-port injection valve (Valco, Houston, TX, USA, model C22-3186EH). The valve's loop (15 μL) was loaded by suction with a lab-built motorised syringe made from a gas tight 1-mL syringe (Hewlett–Packard, Palo Alto CA, USA) driven by a stepping motor and a three-way, 12 V solenoid valve (model 225T031, NResearch, West Calwell,

* Corresponding author.
E-mail address: gpigna@fq.edu.uy (G. Pignalosa).

0039-9140/$ – see front matter © 2007 Elsevier B.V. All rights reserved.
doi:10.1016/j.talanta.2007.05.017

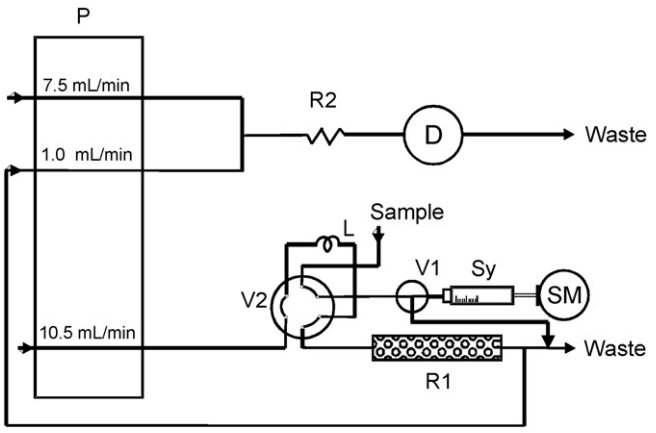

Fig. 1. Flow diagram. P: peristaltic pump, V1: solenoid valve, V2: injector valve, R1: packed reactor, R2: tubular reactor (40 cm), D: detector (LED-photometer), L: loop, Sy: syringe, and SM: stepping motor.

NJ, USA) which selects between the operations of loading and unloading the syringe.

The detection system comprised an LED, a flow cell with 10 mm optical length and 80 μL inner volume, and a photodiode assembled in a black acrylic block.

The whole system was controlled from an IBM-compatible PC.

The determination of insolubles by FTIR was carried out by means of a Nicolet Protege 460 spectrometer (Nicolet, Madison, WI, USA) with a 100-μm potassium bromide demountable transmission cell (PIKE Technologies, Madison, WI, USA, model 162-1100).

2.1. Reagents

Deodorised kerosene (ANCAP, Montevideo, Uruguay) was used as diluent.

Unused SAE-40 Diesel lubricating oil (Superdiesel 40, Ancap) was employed as a blank sample and diluent for standards.

Pentane 98% (Sigma, USA) was employed as diluent, *N*-butyl diethanolamine 99% (Fluka, Germany) and isopropyl alcohol 99.5% (Sigma, USA) were employed as coagulant for the centrifugation standard method.

2.2. Samples

Used lubricating oils for diesel engines were taken from cars, locomotives and buses.

3. Results and discussion

3.1. System development

A verification function implanted by means of an optical switch, which is actuated when the syringe reaches the "full" position, was designed to check that the syringe operates properly and to establish the zero position.

The oil sample and solvent streams were mixed by a 10-cm packed mixing reactor made of 2.48-mm i.d. PTFE tubing filled with small pieces of PTFE already described elsewhere [5].

System control and data acquisition, were carried out by means of an 80-MHz IBM-compatible 80486-based personal computer fitted with a multipurpose data acquisition and control board (CIO-DAS-08AOH, Measurement Computing Corp., Middleboro, MA, USA) installed on the ISA bus. The 12-bit analogue-to-digital converter (ADC) in the card was used to capture analogue data from the LED-photometer recorder output, while several of the digital input and output (I/O) ports were used for logic control of the stepper motor and the solenoid valve. Communication with the motorised injection valve was made through the RS232 serial port of the computer. The overall connection and signal flow schematic is depicted in Fig. 2, which also shows the photometer circuitry.

Software compiled in QuickBASIC 4.0 (Microsoft) was developed for the operation of the system and run under the MS-DOS 6.0 operating system.

The motorised syringe was used to load the loop (15 μL) and the motorised injection valve was used to insert the sample into the carrier solvent. A volume of 500 μL of the solvent was used to clean the loop and the syringe between different samples and 1.0 mL of sample was passed trough the loop before injection.

Before starting work, the LED-photometer was calibrated by means of an option in the software which executes the necessary data acquisition. Analogue data (mV) are acquired when the light beam was completely interrupted by an opaque block (I_0) and when the light beam passed through the cell with the carrier flowing (I_{100}). These data were memorized until a new calibration was necessary.

The transmittance was calculated by software using the formula $T = (I - I_0)/(I_{100} - I_0)$ where I is the acquired data in mV when the light beam passes through the sample. Absorbance was then calculated as $-\log T$.

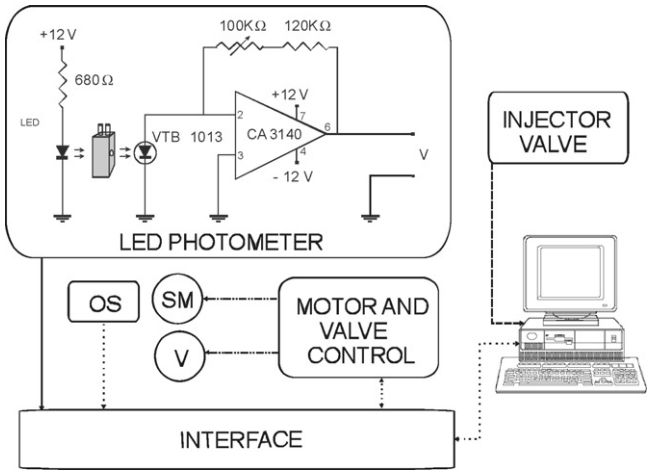

Fig. 2. Connections and signals diagram, and detector circuit scheme. SM: stepping motor V: solenoid valve, OS: optical switch. - - -, RS 232; —, analogic signal; · · ·, digital signal; and – · · –, power line.

Data acquisition was carried out by means of the ADC, the input of which was connected to the analogue output of the photometer, at a sampling rate of eight measurements per second. Raw data were transformed to true absorbance by a scaling process. An optional subroutine allowed smoothing of the data by a five-point moving average and finding peak-height values, which were displayed on screen. Unprocessed absorbance data were saved to the hard disk in ASCII format. Post run processing of the ASCII files was achieved by means of a chromatography program (Peak Simple II, Version 1.25, SRI Inc., Torrance, CA, USA).

3.2. Figures of merit

Calibration curves were constructed with five injections of the calibration samples (blank, 0.68, 1.34, 2.02 and 2.68% (w/w) of insolubles in pentane). Previous to analysis, the samples were homogenised with a wrist-action mechanical shaker.

Linear response of the proposed method was found up to 2.68% (w/w) of insolubles in pentane (ASTM D-893) [7].

Regression equation was $h = 0.415 \pm 0.016C + 0.00 \pm 0.03$ (confidence level of 95%), h being peak height (absorbance) and C concentration (% insolubles in pentane), with a regression coefficient $r^2 = 0.9995$.

For six injections of a calibration sample containing 2.68% insolubles in pentane a relative standard deviation (s_r,%) of 1.0% was found.

Detection and quantification limits (LD and LQ) were calculated respectively according to the 3σ and 10σ criteria. Values found were LD = 0.07% and LQ = 0.16% (w/w) insolubles in pentane.

The sampling frequency was about 45 samples h^{-1}.

3.3. Analysis of real samples

Twenty-five real samples were analysed by the FIA and FTIR methods. Results were compared by linear correlation analysis. Slope and intercept of the straight line were compared with the theoretical values of 1 and 0 by means of the joint-confidence ellipse F-test (H_0: $a = 1$ and $b = 0$, H_a: $a \neq 1$ and/or $b \neq 0$) [8]. The value of F_{exp} obtained was 3.322 and $F_{0.05}$ (2, 23) is 3.422, thus at the confidence level of 95% there is no evidence of significant difference between both methods.

The results suggest that the proposed method can be useful as a routine method for the automated determination of insolubles in lubricating oils. It requires simple instrumentation and provides a considerable reduction in analysis time when compared with the standard methods. With the appropriate modifications the system could be also made portable thus making it possible to carry out these field determinations of this critical parameter.

Acknowledgements

The authors thank UdelaR-CSIC and PEDECIBA-Química for financial support.

References

[1] M. Lukas, D.P. Anderson, Lubr. Eng. 54 (1998) 31.
[2] M. Lukas, D.P. Anderson, Lubr. Eng. 54 (1998) 19.
[3] S. George, S. Balla, V. Gautam, M. Gautam, Tribol. Int. 40 (2007) 809.
[4] M. Knochen, A. Sixto, G. Pignalosa, S. Domenech, S. Garrigues, M. de la Guardia, Talanta 64 (2004) 1359.
[5] G. Pignalosa, M. Knochen, Atom. Spectrosc. 22 (2001) 250.
[6] J.R. Powell, D.A.C. Compton, Lubr. Eng. 49 (1993) 233.
[7] Standard Test Method for Pentane Insolubles by Centrifugation, ASTM Standard D 893-97, American Society for Testing Materials, Philadelphia, 1997.
[8] J. Mandel, F. Linnig, Anal. Chem. 29 (1957) 743.

Available online at www.sciencedirect.com
ScienceDirect
Talanta 73 (2007) 953–958
Talanta
www.elsevier.com/locate/talanta

^{31}P NMR peak width in humate–phosphate complexes

Jeremy Riggle, Ray von Wandruszka *

University of Idaho, Department of Chemistry, P.O. Box 442343, Moscow, ID 83844-2343, USA

Received 22 March 2007; received in revised form 15 May 2007; accepted 15 May 2007
Available online 21 May 2007

Abstract

The mobility of inorganic phosphate (P) attached to solid humic acid (HA) and fulvic acid (FA) via a metal "anchor" was investigated by ^{31}P NMR spectroscopy. The peak width of the ^{31}P resonance was monitored as an indicator of the degree of attachment of the element to the humic matrix. The concept was demonstrated by contrasting peak widths of thoroughly dry M–HA–P complexes with those that had been allowed to absorb different amounts of moisture. It was shown that the presence of moisture, which enhances the mobility of P, results in a significant reduction of chemical shift peak width. The work was extended to comparisons between dry systems with and without metal anchors; systems with anchors consisting of different metals; systems comprising different humates and fulvates; and systems with different size fractions of a humate. It was shown that both the type of humate/fulvate, and the metal anchor used lead to different degrees of mobility within the humic matrix. It was also found that the effect of metal addition on ^{31}P peak width is greater with fulvates and smaller HA fractions than with the larger HA components.

Keywords: Humic substances; ^{31}P NMR; Peak broadening; P mobility/retention

1. Introduction

As an essential nutrient to both plants and animals, phosphorus (P) plays a vital role in the environment. It is often a limiting nutrient in crop production—5.7 billion ha of agricultural land are currently estimated to have sub-optimal P levels [1]. Complicating the obvious remedy – increased application – for limited P availability is the serious environmental problem of P enrichment of surface waters that this brings. The resulting eutrophication, leading to algae blooms and oxygen depletion, can have serious effects on water bodies. Advanced eutrophication results in severe problems for the use of these waters for fisheries, recreation, industry, and drinking [2]. Initially attributed to sewage discharge, it was later discovered that P loss from agricultural land contributed significantly to the overall P input to surface waters. The USEPA stipulates [3] that eutrophication can result from P concentrations as low as 0.02 mg/L, and recommends a P limit of 0.05 mg/L for streams feeding into lakes and 0.1 mg/L for other waters [4].

Especially in the case of calcareous soils, the retention and mobilization of P have proven to be complex processes. It is difficult to distinguish the nature of the interactions taking place and the soil components involved. Despite these difficulties, it has become clear that adsorption and precipitation of P are major factors in P retention and mobility. Much work has been done identifying the formation of P minerals with the focus being on the role played by inorganic soil constituents, especially $CaCO_3$, and iron oxides. It was found that, depending on the conditions, dicalcium phosphate (DCP), octacalcium phosphate (OCP) and hydroxyapatite (HAP) may all be formed to varying degrees [5–9]. What is less understood is the role played by organic soil components such as humic substances (HS) in the retention and mobilization of P.

HS, particularly humic acid (HA), represent a significant soil constituent that has relevance to the status of P in the soil. Being the breakdown products of the total biota in the environment HA is ubiquitous in all aquatic and terrestrial environments. It is involved in many processes in the soil, including nutrient cycling, soil weathering, pH buffering, trace metal mobility and toxicity, and transport of hydrophobic organic pollutants [10]. HA can be applied to agricultural land as a soil conditioner to increase crop yields, and its effect on plant growth and nutrition is well documented [11,12].

Previous work on P retention/mobility focused largely on the mineral components of soils. More recent investigations into the effect of the application of HA on the recovery of P from

* Corresponding author. Tel.: +1 208 8856552; fax: +1 208 8856173.
E-mail address: rvw@uidaho.edu (R. von Wandruszka).

0039-9140/$ – see front matter © 2007 Elsevier B.V. All rights reserved.
doi:10.1016/j.talanta.2007.05.018

soils found an increase in Olson-P recovery from all soils except those with very high Na content [13]. It was also found that strong interactions between P and HA are predicated on the presence of metal ions that act as "anchors," allowing anionic humates and phosphates to associate [14]. Stability constants for these metal–humate–P complexes were subsequently found to be moderately high, with log *K* values in the 4.87 (Zn anchor) to 5.92 (Mg anchor) range [15]. A recent report also noted that a large portion of native P associated with humates is not available for plant uptake [16]. The source of the humates was found to be the most important factor controlling this effect.

^{31}P NMR is the technique of choice for the identification of organic P species in soils [17–19]. This technique was initially thought to be limited somewhat by the presence of paramagnetic nuclei, such as Fe and Mn, that tend to cause line broadening. Shand et al. [20] later found that the resolution limitations of solid-state ^{31}P NMR spectra of HS are the result of multiple attachment sites for P in the humic medium, and the slow P exchange at these locations on the NMR timescale. ^{31}P magic angle spinning (MAS) NMR line widths have been identified as indicators of P mobility in lipid membrane structures [21]. In humic materials, Khalaf et al. used an analogous technique involving ^{19}F NMR, in which appreciable line broadening was attributed to an immobile fluorine species, and multiple sorption sites within HA were identified [22].

The objective of the present work was to evaluate the use of ^{31}P NMR data in assessing the degree of association between inorganic P and HA, including the role of calcium and other common soil cations.

2. Experimental

2.1. Humic substances

HA was isolated from a crude Leonardite humic acid (LHA) [23], obtained under the trade name Agri-Plus from Horizon Ag-Products (Kennewick, WA). This material was a dark brown powder, 40–50 mesh, with a density of 0.78 g/cm^3. It was reported by the purveyor to contain 80% humic acid, 5% fulvic acid, 15% clay, shale, gypsum, silica, and fossilized organic matter. The crude material was shaken with 0.1 M NaOH for 24 h, and centrifuged. The supernatant, containing both humic and fulvic acid, was decanted and acidified to precipitate the HA fraction. The precipitated HA was redissolved in 0.1 M NaOH, and the acidification process was repeated. Mineral impurities were removed by treatment with a 0.1 M HCl–0.3 M HF solution, and overnight shaking. The HA was again dissolved in 0.1 M NaOH and dialyzed against deionized water through a 500 Da cutoff membrane (Spectra/Por) to a negative Cl^- test. The extracted HA was freeze dried (Labconco) and stored in the solid state.

Waskish peat fulvic acid (WPFA) and Leonardite humic acid (LHA) were purchased from the International Humic Substances Society (IHSS) and used as received. $CaCl_2$, $CdCl_2$ (EM Scientific), $FeCl_3$ (J.T. Baker), $MgCl_2$, $ZnCl_2$, K_2HPO_4, NaOH, HF, HCl, and $AgNO_3$ (Fisher Scientific) were all used as received.

2.2. Fractionation

The isolated HA was separated into two molecular size fractions by ultrafiltration [24]. First, an alkaline solution of HA was filtered through a 0.2-μm membrane (Gelman Sciences), and the retentate was rinsed with DI water until the washings were colorless. The filtrate was then fractionated with a stirred-cell ultrafiltration apparatus (Amicon), using membranes with successively smaller MW cut-off values and 20 psi N_2 pressure. Two size fractions were isolated: 0.2 μm–100 kDa, and 1 kDa–500 Da. The material was freeze dried and stored in the dark.

2.3. Metal–HA complexes

Approximately 100 mg of the whole isolated, whole standard, or fractionated HA were dissolved using a minimum amount of 0.01 M NaOH and shaking. A 10.0-mL aliquot of 5.0×10^{-3} M metal solution was then added to the HA solution, and the mixture was again shaken vigorously. After an equilibration time of *ca.* 60 min, 10.0 mL of 2.0×10^{-3} M K_2HPO_4 was added. The material was freeze dried to isolate the solid metal–humate–P complex, which was thoroughly washed with DI water to remove uncomplexed P, dried again, and stored in a dessicator.

For the moisture studies, dry metal–humate–P complexes were wetted by: (i) exposing them to the ambient atmosphere in an open container for several hours; (ii) adding distilled water to *ca.* 40% paste saturation. Both types of samples maintained a dry appearance.

2.4. ^{31}P NMR measurements

^{31}P NMR spectra were obtained at room temperature using a Bruker Avance 500 Spectrometer, with a static field of 11.747 T. The Larmor frequency was 202.456 MHz. Chemical shifts were calibrated with liquid H_3PO_4 as an external standard. The experiments were performed under magic-angle spinning conditions with single pulse excitation and broadband cw H^1 decoupling. The relaxation delay was 5 s, the number of scans was between 500 and 1k, and the spinning rate was 12 kHz.

2.5. ^{13}C NMR measurements

Solid-state CPMAS ^{13}C NMR spectra of HA fractions were obtained using a Bruker Avance 500 spectrometer, operating at a frequency of 125.758 MHz, with a static field of 11.747 T. Approximately 100 mg dry weight per sample was placed in a 4-mm (o.d.) NMR rotor with Kel-F cap. A relaxation delay of 1 s, and CP contact time of 1.5 ms were used for all spectra. The number of scans was between 10k and 20k, and the spinning rate was 8 kHz. Chemical shifts were referenced to adamantane, an external standard. The Hartmann–Hahn condition was adjusted with solid adamantane prior to each experiment. The broadband ^{1}H decoupling was achieved with a two-pulse phase modulated (TPPM) pulse sequence. All experiments were performed at room temperature.

3. Results and discussion

A complete characterization of LHA isolated from LHACB has been reported previously [25]. Suffice it to note that its carbon distribution was that of a typical HS. Aliphatic, aromatic, and carboxyl carbons predominated in this material, while hetero-aliphatic, ester/amide, and ketonic carbons were relatively minor constituents. Comparison of this material with the Leonardite standard provided by the IHSS shows that aliphatic and hetero-aliphatic carbons were relatively more abundant in the isolated HA, while the aromatic content was somewhat lower.

3.1. The influence of moisture

To evaluate the relevance of the ^{31}P NMR peak width to the mobility of the element in the solid humic matrix, the spectra of thoroughly dry systems were compared with those that had been allowed to absorb moisture. Fig. 1A shows the ^{31}P resonance in dry solid Ca–LHA–P. It is immediately clear that the peak was broad (970 Hz), which, as noted above, indicates the existence of many different P-attachment sites with minimal exchange between them on the NMR timescale.

Conversely, Fig. 1B shows the same sample after exposure to ambient atmospheric conditions. The peak has narrowed notably (175 Hz peak width), due to absorption of moisture from the atmosphere by the humate. Water absorbed by humic materials in this manner typically amounts to *ca.* 5%, w/w, and this allowed the associated P sufficient mobility on a short time scale to produce a much narrower average signal.

Interestingly, when water was added to 40% paste saturation of the sample (Fig. 1C), no further peak narrowing was observed. The moisture absorbed from the atmosphere was evidently enough to give maximum P mobility in this solid.

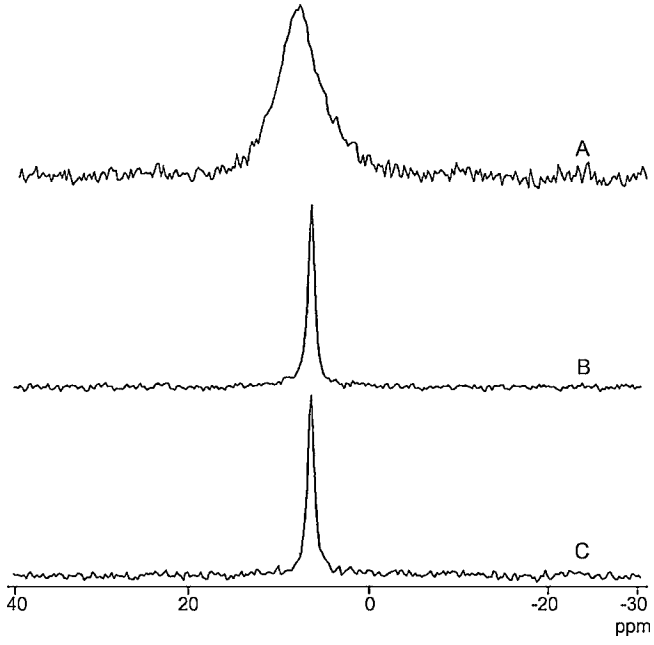

Fig. 1. ^{31}P NMR spectra for Ca–LHA–P: (A) dry, (B) H_2O absorbed from atmosphere, and (C) H_2O (40% paste saturation).

The results of this moisture study demonstrate that the ^{31}P NMR peak width is a reasonable metric for the mobility of P associated with humates. It opens the door to a series of relative studies in which the P-mobility in different humates is contrasted in this manner. It is also possible to vary the metal anchor (Ca in the above case), and thereby assess its influence on P mobility. In such work, cognizance must be taken of possible paramagnetic peak broadening by certain metals. Moreover, to make comparisons of this type meaningful, all systems were thoroughly dried, so that moisture was eliminated as a variable.

3.2. The metal anchor

The precept of a metal anchor in strong humate–phosphate interactions was discussed above. The absence of such an anchor should lead to a less associated system, which is expected to manifest itself in a relatively narrow ^{31}P resonance. Fig. 2 bears out this concept: the ^{31}P peak in a "clean" (metal-free) humic acid is much narrower (650 Hz) than the peak in the corresponding calcium humate (1050 Hz). The chemical shifts in the two cases are, however, identical.

The effects of some other common soil cations on the ^{31}P resonance peak width in HA complexes are illustrated in Fig. 3

In all cases the metal ions caused a broadening of the ^{31}P resonance, but they did so to different degrees. For the cations shown in Fig. 3 the order was: Fe < Ca < Mg < Zn < Cd. The res-

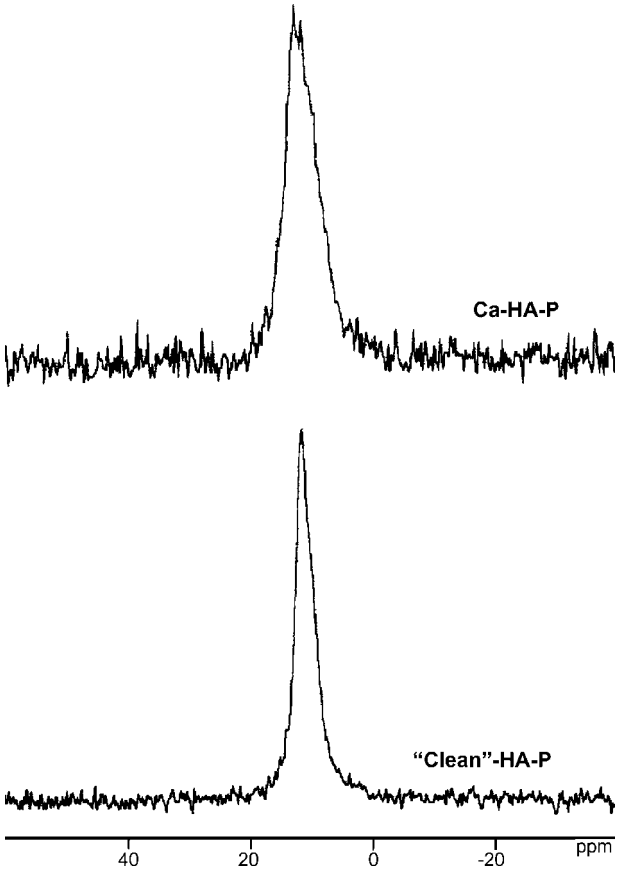

Fig. 2. ^{31}P NMR spectra for clean LHA–P and Ca–LHA–P.

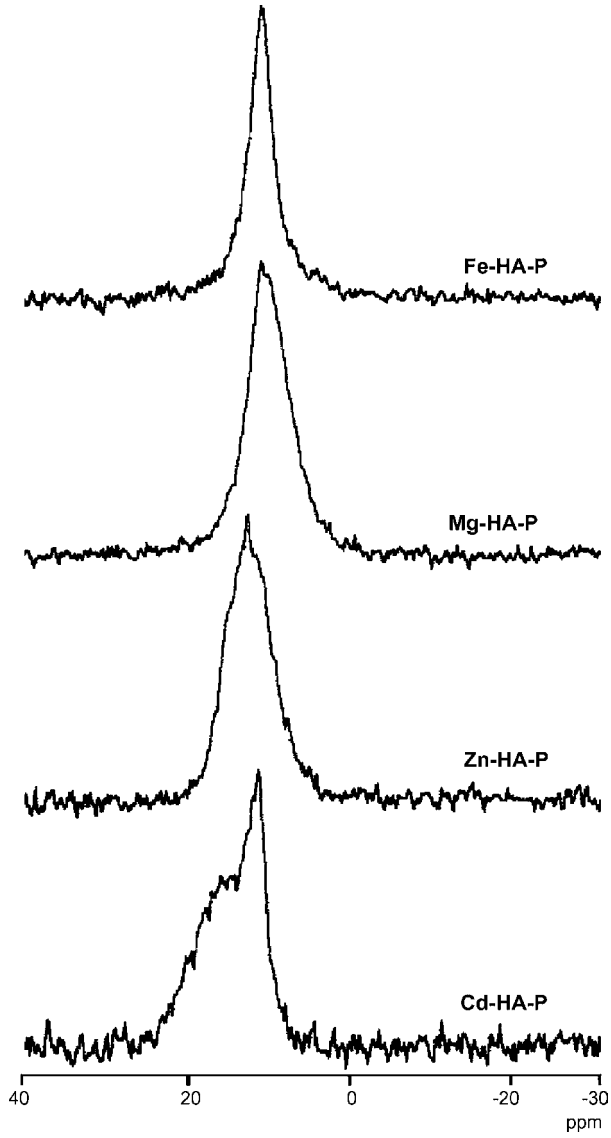

Fig. 3. ^{31}P NMR spectra for Fe, Mg, Zn, and Cd–LHA–P complexes.

onance peak widths were found to be 670, 1050, 1088, 1300, and 1800 Hz, respectively. The broadening of ^{31}P NMR peak can, in principle, have two causes: (i) the availability of more attachment sites, or (ii) stronger attachment at the available sites. In the present case, where the same humate was used for all complexes, the second scenario is more likely. It therefore suggests that the peak width ranking corresponds to the strength of the solid-state association in these systems.

Further studies were carried out on the IHSS standards LHA and WPFA (Fig. 4). It is interesting to note that in this LHA the ^{31}P peak width in the Ca humate is only 5% greater than in the metal-free material. This is notably less than was the case for LHA isolated from LHACB (18% broadening). In contrast, the increase for WPFA was 26%—a relatively large value. This observation may be related to the fact that WPFA is a fulvic acid, which tends to be smaller and more functionalized than HA. A fulvate can therefore offer more points of Ca (and hence P) attachment and consequently stronger complexes.

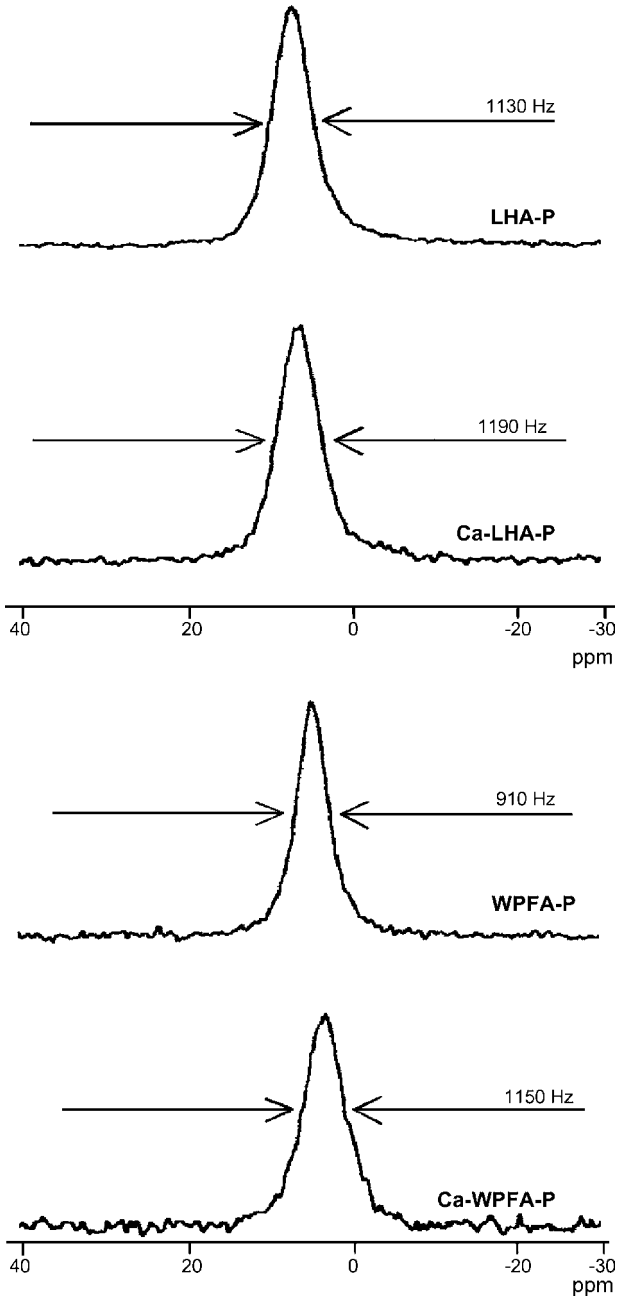

Fig. 4. ^{31}P NMR spectra for IHSS standard LHA, Ca–LHA, WPFA, and Ca–WPFA, following the addition of P. Peak widths are shown in Hz.

It should also be noted that the metal-free LHA–P complex displays a considerably larger peak width than the metal-free WPFA–P complex. Discounting the possibility that this may be due to different amounts of "left over" metals in the two IHSS products, it could be ascribed to the fact that the humate is larger than the fulvate and can sequester P more effectively (even in the absence of metals).

3.3. HA size fractions

In view of the apparent differences between P mobilities in different humate complexes, the effects of two size fractions of

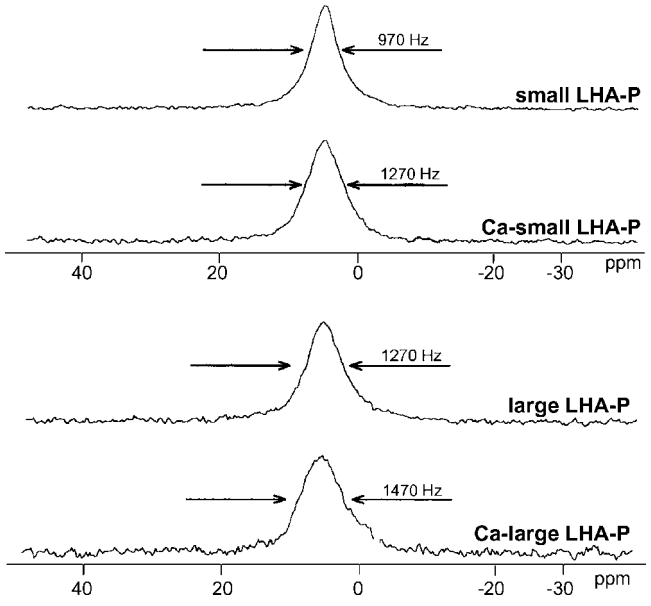

Fig. 5. ^{31}P NMR spectra for small and large HA size fractions, and their Ca complex counterparts. Peak widths are shown in Hz.

the same humate were investigated. Fig. 5 shows the ^{31}P NMR spectra of complexes with small and large fractions of LHA (isolated).

It can be seen that the increase in line broadening upon formation of the Ca–humate complex was 31% for the small LHA size fraction, and 16% for the large fraction. The behavior of the small LHA fraction was comparable to that of the FA described above, which is in line with similarities in size and functionality. The chief difference between the large and small fractions, as inferred from the ^{13}C NMR spectra (not shown), was that the former had a noticeably higher aliphatic content. These somewhat less functionalized moieties can account for relatively lower ability of the large LHA fraction to form strong Ca–P complexes.

Earlier work by Khalaf et al. [22], showed similar effects arising from a reduction in sample heterogeneity. The authors found that smaller HA size fractions exhibited multiple sorption sites for hexafluorobenzene, while larger fractions had only two. Despite the differences in processes, sorption *versus* complexation, it is clear that a reduction in HS heterogeneity is accompanied by an increase in functionality. In the present case, the moieties responsible for metal complexation were unequally distributed with the higher concentration being found in FA and small HA size fractions.

The variations in ^{31}P NMR peak width shown above make it clear that metal ions associated with the humates and fulvates has a major, but not exclusive, effect on the mobility of P in solid HS. It could be surmised that the varied roles of the metals simply arise from differences in solubility of the metal phosphate in question. In fact, the phosphates of all metals considered are extremely insoluble, with K_{sp} values ranging from 1.3×10^{-22} to 2.5×10^{-33}. It is highly improbable that values this small would produce a discernable difference in mobility. In contrast, both the mode and strength of association between the metal anchor and the humate may lead to such a differentiation. It is not possible, at this time, to assess this aspect quantitatively, since it involves differential attachment of the metal cation to functional groups that cannot be identified individually. What can be stated is that differences in metal connection to the humic matrix lead, in subsequently formed M–HA–P complexes, to different degrees of P mobility.

The nature of the interactions between inorganic P (specifically HPO_4^{2-}) and metal humate deserves special attention. As explained in Section 2, the complexes were formed by dissolving M–HA, adding K_2HPO_4, equilibration, and freeze drying. The resulting solid, after thorough washing to remove excess P, yielded the ^{31}P NMR spectra shown above.

In a modification of the procedure, the solid Ca–HA was formed (freeze dried) first, shaken with a solution of K_2HPO_4, filtered and washed, and then dried again The solid resulting from this process did not yield ^{31}P NMR spectra, indicating that once the metal was fully complexed with HA in the solid state, it did not function as an anchor for dissolved P.

Several mechanisms could be proposed for this observation – the surface hydrophobicity of freeze dried humate, and the lack of thorough wetting by aqueous K_2HPO_4 being one – but it does raise the possibility that the 'one-pot' creation of solid M–HA–P actually involved the formation of $MHPO_4$ microcrystallites during the freeze drying process, and that these were incorporated in the solid humic matrix. A consideration that militates against this arises from the fact that moisture adsorbed from the atmosphere was sufficient to narrow the ^{31}P NMR peak substantially. This is unlikely to be possible if crystalline phosphate were involved.

To further investigate this phenomenon, a dilute Ca–LHA solution and a metal-free LHA solution were titrated side-by-side with K_2HPO_4. The acid content of LHA was previously determined to be 4.1 mequiv./g [26], and as a 25 μg/mL solution of the humate was used, the carboxylate concentration was 1.0×10^{-4} M. The Ca concentration in the solution was 5.1×10^{-5} M, corresponding to an occupation of about half the carboxyl sites. Incremental addition of P did not result in $CaHPO_4$ precipitation in either solution ($K_{sp} = 1.0 \times 10^{-7}$), even when the P concentration reached 2.0×10^{-3} M. This observation supports the view that the Ca^{2+} ion is part of a dissolved HA complex and interacts with P in this form. As the chemical shift anisotropy data show, the presence of such a metal anchor is a condition for firm attachment of P in the M–HA–P complex.

It must be kept in mind that the observations described here pertain to dry M–HA–P complexes and that comparisons are made only with regard to motions of P that average the signal on the NMR timescale. No claim is made that this can be extrapolated to a heterogeneous natural setting. The work does, however, confirm that the attachment of P to a solid humic matrix is predicated on the presence of a metal anchor and depends on both the metal and the humate in question.

It was especially interesting to find that the formation of the M–HA–P complex proceeds effectively when dissolved metal humates interact with P and precipitate in its presence. Solid M–HA suspended in an aqueous phase does not appear to operate as a "phosphate-trap" that can immobilize dissolved P.

Acknowledgements

The authors would like to thank Dr. Alex Blumenfeld for performing the NMR experiments, as well as Inland Northwest Research Alliance (INRA) for financial support.

References

[1] P. Hinsinger, Plant Soil 237 (2001) 173.
[2] A.N. Sharpley, S. Rekolainen, in: H. Tunney, O.T. Canton, P.C. Brookes, A.E. Johnstone (Eds.), Phosphorus Loss from Soil to Water, CAB International, New York, 1997.
[3] USEPA, Clean Water Action Plan: Restoring and Protecting America's Waters, Washington DC, 1996.
[4] USEPA, Water Quality Criteria for Water, Rep. 440/5-86-001, Office of Water, Washington DC, 1986.
[5] C.V. Cole, S.R. Olsen, C.O. Scott, Soil Sci. Am. Proc. 17 (1953) 352.
[6] J.S. Clark, M. Peech, Soil Sci. Soc. Am. Proc. 19 (1955) 171.
[7] J.C. Arvieu, O. Bouvier, Sci Sol 74 (1974) 207.
[8] W. Stumm, J.O., Leckie, Proceedings of the 5th International Pollution Research Conference, San Francisco, 1970.
[9] J.S. Freemen, D.L. Rowell, J. Soil Sci. 32 (1981) 75084.
[10] F.J. Stevenson, Humic Chemistry: Genesis, Composition, Reactions, John Wiley & Sons, New York, 1982.
[11] F. Adani, P. Genevini, P. Zaccheo, G. Zocchi, J. Plant Nutr. 21 (1998) 561.
[12] R. Fernandez-Escobar, M. Benlloxh, D. Barranco, A. Duenas, J.A. Gutierrez-Ganan, Sci. Hortic. 66 (1996) 191.
[13] A. Delgado, A. Madrid, S. Kassem, L. Andreu, M. Campillo, Plant Soil 245 (2002) 277.
[14] K.H. Tan, Humic Matter in Soil and the Environment, Marcel Dekker, Inc., New York, 2003.
[15] J. Riggle, R. von Wandruszka, Talanta 66 (2003) 372.
[16] H. Zhongqi, O. Tsutomu, B.J. Cade-Menum, S.M. Erich, W.C. Honeycutt, Soil Sci. Soc. Am. J. 70 (2006) (1741).
[17] C.N. Bedrock, M.V. Cheshire, J.A. Chudek, A.R. Fraser, B.A. Goodman, C.A. Shand, Commun. Soil Sci. Plant Anal. 26 (1995) 1411.
[18] B.J. Cade-Menum, C.W. Liu, R. Nunlist, J.G. McColl, J. Environ. Qual. 31 (2002) 457.
[19] N. Mahieu, D.C. Olk, E.W. Randall, Eur. J. Soil Sci. 51 (2000) 391.
[20] C.A. Shand, M.V. Cheshire, C.N. Bedrock, P.J. Chapman, A.R. Fraser, J.A. Chudek, Plant Soil 214 (1999) 153.
[21] G.P. Holland, S.K. McIntyre, T.M. Alam, Biophys. J. 90 (2006) 4248.
[22] M. Khalaf, S.D. Kohl, E. Klumpp, J.A. Rice, E. Tombacz, Environ. Sci. Technol. 37 (2003) 2855.
[23] IHSS Product Literature, International Humic Substance Society, St. Paul, 1985.
[24] H.S. Shin, J.M. Monsallier, G.R. Choppin, Talanta 50 (1999) 641.
[25] J. Riggle, Fundamental chemistry relevant to the use of humic materials in pollution remediation, Masters Degree thesis, 2002.
[26] J. Riggle, R. von Wandruszka, Talanta 57 (2002) 519.

Available online at www.sciencedirect.com
ScienceDirect
Talanta 73 (2007) 845–849
Talanta
www.elsevier.com/locate/talanta

Evaluation of selenium behavior in thermospray flame furnace atomic absorption spectrometry

Fabiana Rosini [a], Clésia C. Nascentes [b], José Y. Neira [c], Joaquim A. Nóbrega [a,*]

[a] *Grupo de Análise Instrumental Aplicada, Departamento de Química, Universidade Federal de São Carlos, P.O. Box 676, 13560-970 São Carlos, SP, Brazil*
[b] *Departamento de Química, Instituto de Ciências Exatas, Universidade Federal de Minas Gerais, Belo Horizonte, MG, Brazil*
[c] *Departamento de Análisis Instrumental, Facultad de Farmácia, Universidad de Concepción, Concepción, Chile*

Received 22 March 2007; received in revised form 26 April 2007; accepted 30 April 2007
Available online 10 May 2007

Abstract

The behavior of selenium in thermospray flame furnace atomic absorption spectrometry (TS-FF-AAS) was studied and the developed procedure was applied for selenium determination in biological materials after microwave-assisted sample digestion. A sample volume of 600 μL was introduced into the hot metallic Ni tube at a flow rate of 0.4 mL min^{-1} using water as carrier. The limit of detection obtained for Se was 8.7 μg L^{-1} ($3s_{blank}$/slope, $n = 10$), which is 95-fold better than that typically obtained using FAAS. The applicability of the TS-FF-AAS procedure was evaluated for selenium determination in biological materials. Certified reference materials of pig kidney (BCR 186) and mussel (GBW 08571) were analyzed and a *t*-test had not shown any statistically significant difference at a 95% confidence level between determined and certified values for both materials. The procedure was successfully applied for determination of Se in pig kidney and shellfish. It was demonstrated that TS-FF-AAS improved the performance of FAAS (flame atomic absorption spectrometry) for determination of Se.

Keywords: Atomic absorption; Flame furnace; Thermospray; Selenium; Biological materials

1. Introduction

Selenium is an element that can be essential or toxic for human beings depending on its concentration and chemical form. In the past there was no information on irreversible chronic diseases or death caused by contamination with selenium or its compounds [1]. Nowadays, it is known that selenium deficiency causes the Keshan disease characterized by widening and aging of the heart with consequent cardiac insufficiency [2].

This element is found in the form of selenocysteine in the enzyme glutatione peroxidase, responsible for protecting the organism against oxidative processes degradation caused by lipoperoxides and hydrogen peroxide [3,4]. At low concentrations, it can prevent or cure some diseases, such as breast and gastrointestinal cancers [5].

However, the extreme ingestion of selenium can also cause gastrointestinal riots, dermatitis, modifications of the nervous system, loss of hair and nails, and tooth deterioration [2,6]. The exposition to Se occurs mainly through foods but also through water and air. Additionally, an important contribution is the air contamination by burning of fossil fuel, rubber, and urban garbage.

In human beings selenium contamination can occur mainly through the skin or by food ingestion from cultivated area with high concentrations of this element. Seafoods and animal organs, such as liver and kidney, also contain high concentrations of selenium. However, vegetal materials are the major selenium diet sources owing to their greatest consumption compared with animal sources [3]. On the other hand, selenium has anticancer action when present in selenocysteine form, and it can reduce breast tumors [5,7].

The determination of selenium is frequently difficult due to the low concentration of this analyte in most samples and therefore the use of techniques with high sensitivity and selectivity are necessary. Generally, the analytical techniques employed are electrothermal atomic absorption spectrometry with graphite tube and proper chemical modifiers (ETAAS) or hydride generation atomic absorption spectrometry (HGAAS) [8]. Inductively

* Corresponding author. Tel.: +55 16 3351 8088; fax: +55 16 3351 8350.
E-mail address: djan@power.ufscar.br (J.A. Nóbrega).

0039-9140/$ – see front matter © 2007 Elsevier B.V. All rights reserved.
doi:10.1016/j.talanta.2007.04.053

coupled plasma mass spectrometry could also be employed. All these techniques are sensitive but are affected by interferences. Selenium could also be determined by FAAS, however the sensitivity is poor due to the inefficient sample introduction by pneumatic nebulization and spectral interferences aggravated by the low wavelength (196.0 nm) usually employed to reach better sensitivity [9].

One alternative to overcome the sensitivity loss caused by sample introduction by pneumatic nebulization could be the use of TS-FF-AAS. This system consisted of a Ni tube positioned on the burner head of an air/acetylene flame with a ceramic capillary tube connected to it and heated by a flame. This technique was recently developed to improve the analytical performance of FAAS [10,11]. In this work the selenium behavior was evaluated by TS-FF-AAS and Se was determined in biological samples using the developed procedure. The sample was transported towards the capillary heated ceramic tube by action of a peristaltic pump. The aerosol generated is totally transferred to a Ni heated tube positioned on the flame. Sensitivity is improved due to both the complete introduction of the sample thermal aerosol and the greater residence time of the atomic cloud into the observation analytical zone inside the hot tube [10–12].

2. Experimental

2.1. Instrumentation

A Varian SpectrAA-640 flame atomic spectrometer (Varian, Mulgrave, Australia) equipped with a deuterium lamp background corrector was used. A hollow cathode ultralamp of Se (Varian) was used. Selenium was measured at the 196.0 nm wavelength. The instrumental parameters for Se determination were set according to the manual recommendations (Table 1) and others parameters were optimized.

A cryogenic mill (Spex Certiprep, Metuchen, NJ, USA) was used for grinding the commercial pig kidney sample.

A closed-vessel microwave digestion system (ETHOS-1600, Milestone, Italy) was used for sample digestion.

The TS-FF-AAS system was assembled according to Nascentes et al. [13]. Solutions were propelled using an eight-channel peristaltic pump (Ismatec, Labortechnik Analytik, Glattbrugg-Zurich, Switzerland) furnished with Tygon® tubes. The Ni tube contained six holes (o.d. 2 mm) in its bottom for flame gases entrance and one orifice at 90° for inserting the thermospray ceramic capillary (0.5 mm i.d., 2.0 mm o.d., and 100 mm of length). The Ni tube was inserted over the burner head after ignition of the flame in order to avoid an explosion caused by accumulation and expansion of flame gases during ignition.

Table 1
Instrumental parameters for selenium measurements by TS-FF-AAS

Parameter	Set value
Spectral resolution (nm)	1.0
Lamp current (mA)	15
Carrier flow rate (mL min^{-1})	0.4
Delay time (s)	30
Measurement time (s)	27[a]
Data acquisition	Peak area

[a] Measurement time for 150 μL.

2.2. Reagents and samples

All solutions were prepared using distilled and deionized water (18 MΩ cm, Millipore, Bedford, MA, USA). All glassware and plasticware was washed with soap, soaked in 10% (v/v) HNO_3 and rinsed with deionized water prior use.

Selenium reference solutions were prepared by diluting the standard stock solutions containing 1000 mg L^{-1} (Tec Lab, Hexis, São Paulo, Brazil) in deionized water.

Commercial pig kidney was bought in a local market. This sample was lyophilized (EC Apparatus, New York, NY, USA) and ground with a cryogenic mill. Shellfish sample was obtained in Chile.

Standard reference materials, mussel (GBW 08571, National Research Centre for Certified Reference Materials, Beijing, China) and pig kidney (BCR 186, Institute for Reference Materials and Measurements, Geel, Belgium) were used to check the accuracy of the method.

2.3. Optimization of the TS-FF-AAS parameters

A factorial design experiment (2^3) was applied for evaluating the effects caused by flame composition (oxidant and stoichiometric), carrier type (water and air), and observation height (0.3 and 1.5 cm over the burner head) on absorbance signals. A 4 mg L^{-1} Se solution prepared in 0.14 mol L^{-1} HNO_3 was used in this study.

Flame compositions utilized were 18.0 L min^{-1} of air and 2.0 L min^{-1} of C_2H_2 for oxidant flame and 13.5 L min^{-1} of air and 2.0 L min^{-1} of C_2H_2 for stoichiometric flame.

The effect of sample volume on sensitivity was also investigated adopting the optimized operating conditions. The introduced sample volumes were 150, 300, 600, and 900 μL. The effect caused by flow rate on sensitivity was also evaluated (0.30–0.50 mL min^{-1}). For both studies, a 100 μg L^{-1} Se solution was prepared in 0.14 mol L^{-1} HNO_3.

2.4. Interferences

In order to evaluate the effects caused by major concomitants usually present in biological samples, the behavior of Se was analyzed by TS-FF-AAS in the presence of Na, K, Ca, and Mg. Only these elements were studied because they are major components in biological samples.

The Se concentration was kept in 100 μg L^{-1} (0.14 mol L^{-1} HNO_3) and the concomitants concentrations were increased up to 10,000 μg L^{-1}.

For comparison purposes, the same study was carried out by FAAS. Owing to the poor sensitivity of this later technique, Se concentration was kept in 10 mg L^{-1} (0.14 mol L^{-1} HNO_3) and the concomitant concentrations were increased up

Table 2
Heating program used for microwave-assisted digestion of biological samples

Step	Power (W)	Time (min)	Temperature (°C)
1	200	2.0	150
2	0	2.0	165
3	300	3.0	180
4	450	3.0	240
5	520	3.0	240
Ventilation	0	5.0	–

to 1000 mg L^{-1}. The analyte/concomitant ratio was the same in both experiments.

2.5. Procedure

The established procedure was used for determination of Se in two certified reference materials (CRM's) and two biological samples. Calibration was based on the standard additions method (SAM) in order to correct for interferences caused by concomitants. Masses of CRM's and samples from 250 to 500 mg were weight and microwave-assisted digested using 3 mL of diluted HNO_3 (2 mol L^{-1}) and 1 mL of H_2O_2 (30%, w/v). The digestion using diluted nitric acid was employed because preliminary data had shown that higher concentrations of nitric acid caused a decrease in Se absorbance signals in TS-FF-AAS.

The digest was transferred to 15 mL polypropylene flasks and diluted to 10 or 12 mL with deionized water. Shellfish sample was digested in two separated digestion flasks (250 mg in each Teflon PFA® flask) and the digests were mixed and diluted to 10 mL. This strategy was adopted for avoiding sudden and uncontrolled increase of pressure during digestion of high sample masses. The SAM was applied to 1.5 mL aliquots of diluted digests. After addition of the stock solution, resulting solutions were diluted to 3.0 mL with water. The microwave-heating program was performed in six steps (Table 2). This program was applied for four digestion vessels simultaneously.

3. Results and discussion

3.1. Optimization of operating parameters

The Pareto's chart for evaluating the effect of operating parameters is shown in Fig. 1. All factors exerted a significant

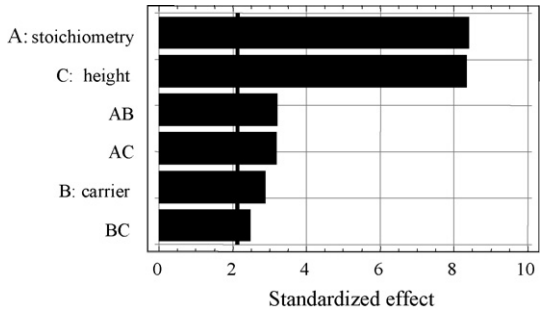

Fig. 1. Standardized Pareto's chart for selenium absorbance signals by TS-FF-AAS.

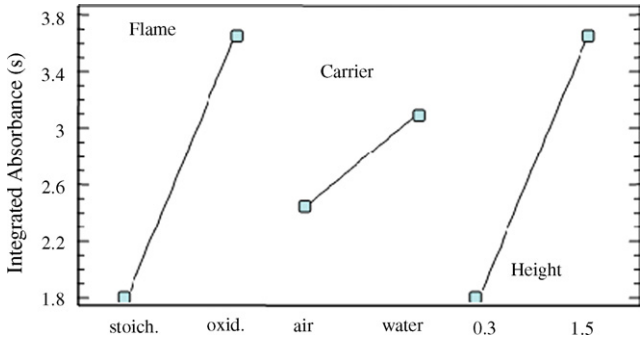

Fig. 2. Main effect plots for selenium absorbance signals by TS-FF-AAS.

effect on the absorbance signal at a 95% confidence level, but flame composition and observation height exerted the highest influences. Fig. 2 shows how each factor affected the analytical signal. It can be seen that best sensitivity was reached using an oxidant flame, water as sample carrier and an observation height of 1.5 cm. These conditions were adopted in all further studies.

It is well known that peak area is proportional to the sample volume because if a larger sample volume is introduced into the tube furnace the atom population in the absorption volume is greater [13]. The greatest transient signal was achieved when 900 μL of sample was introduced, but this volume affected negatively both, the analytical frequency and the repeatability of method. Then, the chosen volume was 600 μL.

The influence of the flow rate used for introducing the solution into the hot Ni tube was studied in the 0.30–0.50 mL min^{-1} range. The use of flow rates higher than 0.50 mL min^{-1} was not feasible because the residence time of the flowing liquid in the heated ceramic capillary was too short for proper evaporation and formation of the thermal aerosol [5,9]. On the other hand, when smaller flow rates were used, the transient signals were reduced because of the very erratic sample vaporization [12].

3.2. Figures of merit

The figures of merit for Se by TS-FF-AAS were compared with those reached by FAAS (Table 3). Calibration curves were obtained with reference solutions prepared in 0.14 mol L^{-1} HNO_3 for both methods. The limits of detection (LOD) and quantification (LOQ) were defined as the concentrations corresponding to 3 and 10 times, respectively, the standard deviations

Table 3
Analytical characteristics of Se determination by TS-FF-AAS and FAAS

Parameter	TS-FF-AAS	FAAS
Regression equation	$y = 0.0048x + 0.0071$	$y = 0.000002x + 0.0013$
R	0.9990	0.9980
Linear range (μg L^{-1})	28.9–1000	2700–80,000
LOD (μg L^{-1})[a]	8.70	830
LOQ (μg L^{-1})[b]	28.9	2700
R.S.D.[c]	3.0	2.0

[a] $3s_{blank}$/slope, $n = 10$.
[b] $10\sigma_{blank}$/slope, $n = 10$.
[c] Relative standard deviation, $n = 6$, 100 μg L^{-1} for TS-FF-AAS and $n = 6$, 10 mg L^{-1} for FAAS.

Table 4
Relative signal intensity for selenium in the presence of concomitant ions obtained by TS-FF-AAS and FAAS

Ion	TS-FF-AAS		FAAS	
	Concomitant concentration ($\mu g\,L^{-1}$)	Relative signal intensity[a]	Concomitant concentration ($mg\,L^{-1}$)	Relative signal intensity[b]
Na(I)	100	173	10	94
	1,000	162	100	72
	5,000	79	500	62
	10,000	65	1000	45
K(I)	100	56	10	99
	1,000	49	100	108
	5,000	34	500	115
	10,000	32	1000	125
Ca(II)	100	96	10	102
	1,000	80	100	109
	5,000	83	500	102
	10,000	69	1000	117
Mg(II)	100	103	10	107
	1,000	117	100	97
	5,000	117	500	107
	10,000	135	1000	106

The relative intensities (%) were calculated based on a Se signal obtained for a solution without any concomitant.
[a] Selenium concentration $100\,\mu g\,L^{-1}$.
[b] Selenium concentration $10\,mg\,L^{-1}$.

of the blank ($n = 10$) divided by the slopes of analytical curves [14].

For FAAS, the instrumental parameters utilized were set according to the manufacturer's recommendations, i.e. air and acetylene flame at 11.0 and $6.6\,L\,min^{-1}$ flow rates.

The LOD attained using TS-FF-AAS was 95 times lower than that attained by conventional FAAS. However, it should be mentioned that in both cases the measurement of LOD is critically affected by blank fluctuations caused by the low wavelength employed for Se measurements.

3.3. Interferences

The effects caused by Na(I), K(I), Ca(II), and Mg(II) on Se absorbance signals measured by TS-FF-AAS and FAAS were evaluated. Results are shown in Table 4. It can be seen that all concomitants affected significantly the analytical signals of Se generated by TS-FF-AAS. The observed effects were more intense than those observed for FAAS for all concomitants. This can be explained by the lower temperature inside the Ni tube due to the only partial penetration of the flame. This is a paradoxical situation frequently observed when working with spectrochemical techniques. Efforts are directed towards the introduction of a greater sample volume into the atomizer to obtain an improvement in sensitivity. However, this generally imply in a higher amount of concomitants being introduced together with the analyte and consequent deterioration of the selectivity.

The severe interference effects observed in TS-FF-AAS can be probably related to the relatively low temperature of the Ni tube atomizer and the great concentration of concomitants in the atomic cloud. Spectral interference effects can be circumvented by using a continuum source background corrector, but chemical effects require either a previous separation step during sample preparation as recently demonstrated for Co determination in biological samples by TS-FF-AAS [15] or a special strategy for calibration. Here the SAM was successfully adopted for Se determination in biological materials. However, it should be mentioned that most interferences were negative and consequently affected the sensitivity of the procedure.

3.4. Selenium determination in biological samples

Selenium was determined in two certified materials in order to evaluate the accuracy of the procedure. Results are shown in Table 5. It can be seen that the selenium contents in both certified reference materials were in good agreement with certified values. A *t*-test was applied and it was shown that there is no statistically significant difference at a 95% confidence level for pig kidney (BCR 186 with $p = 0.237$) and mussel (GBW 08571 with $p = 0.192$).

The developed procedure was applied for the determination of Se at $\mu g\,g^{-1}$ levels in a commercial pig kidney and in a shellfish sample. The Se content in the commercial pig kid-

Table 5
Determined and certified selenium contents in certified reference materials

CRM	Determined ($\mu g\,g^{-1}$)	Certified ($\mu g\,g^{-1}$)	*p*
Pig kidney BCR 186	9.8 ± 0.9	10.3 ± 0.5[a]	0.2267
Mussel GBW 08571	3.82 ± 0.21	3.65 ± 0.18	0.1921

[a] $(x \pm ts)/N^{1/2}$, $n = 3$.

ney sample was $9.94 \pm 1.20\ \mu g\ g^{-1}$ (mean ± S.D., $n = 3$) similar to that observed in the BCR 186. The selenium content in the Chilean shellfish was $2.32 \pm 0.59\ \mu g\ g^{-1}$ (mean ± S.D., $n = 3$).

The developed procedure can be successfully applied for samples containing relatively high concentrations of Se. The occurrence of interferences affected negatively the sensitivity but they can be circumvented by adopting the SAM for calibration. The microwave-assisted acid digestion must be carried out in a medium containing as low as possible nitric acid concentration because high acidities affected negatively the sensitivity.

4. Conclusions

The applicability of the TS-FF-AAS for Se determination in biological materials was demonstrated. The good sensitivity and the proper correction of interferences caused by concomitant ions allowed the selenium determination at $\mu g\ g^{-1}$ in digests of pig kidney and seafood samples. Alternatively, concomitants would be removed and Se would be extracted for improving both selectivity and sensitivity for samples containing lower concentrations of Se. The good repeatability demonstrated by relative standard deviations lower than 4% indicates that TS-FF-AAS is suitable for routine analysis of these biological materials. Compared to FAAS, TS-FF-AAS led to a better sensitivity due to the complete sample introduction, but this same aspect also caused a deterioration of selectivity as demonstrated for alkaline and alkaline-earth ions generally present as major concomitants in biological samples.

Acknowledgements

The authors are grateful to the Fundação de Amparo à Pesquisa do Estado de São Paulo by financial support (FAPESP, Grant 03/00326-1). The authors are also thankful to the Conselho Nacional de Desenvolvimento Científico e Tecnológico (CNPq) and the Coordenação de Aperfeiçoamento de Pessoal de Nível Superior (CAPES) for fellowships. The authors also express their gratitude to Dr. Carlos G. Bruhn (Universidad de Concepción, Concepción, Chile) for furnishing the seafood sample and Dr. Harald Berndt (ISAS, Dortmund, Germany) for providing ceramic capillaries. J.Y.N. is grateful to the Universidad of Concepción by his post-doctoral license and for providing funds for academic visit to Brazil.

References

[1] R.A. Passwater's, Selenium as Food and Medicine, Keats Publ., New Canaan, 1980.
[2] E.N. Whitney, S.R. Rolfes, Understanding Nutrition, West Publ., Saint Paul, 1996.
[3] D.G. Barceloux, J. Toxicol. Clin. Toxicol. 37 (1999) i2.
[4] H.G. Seiler, H. Sigel, A. Sigel, Handbook on Toxicities of Inorganic Compounds, Marcel Dekker, New York, 1988.
[5] P.D. Whanger, Br. J. Nutr. 91 (2004) 11.
[6] H.D. Revanasiddappa, T.K.K. Kumar, Anal. Sci. 17 (2001) 1309.
[7] L.H. Foster, S. Sumar, Food Chem. 56 (1996) 93.
[8] P.C. Aleixo, D.J. Santos, R.C.S. Müller, J.A. Nóbrega, Quim. Nova 23 (2000) 310.
[9] B. Welz, M. Sperling, Atomic Absorption Spectrometry, 3rd ed., Weinheim, VCH, 1999.
[10] J. Davies, H. Berndt, Anal. Chim. Acta 479 (2003) 215.
[11] A. Gáspar, H. Berndt, Spectrochim. Acta B 55 (2000) 215.
[12] J. Davies, H. Berndt, Anal. Chem. 72 (2000) 240.
[13] C.C. Nascentes, M.A.Z. Arruda, A.R.A. Nogueira, J.A. Nóbrega, Talanta 64 (2004) 912.
[14] Analytical Methods Committee, Analyst 112 (1987) 199.
[15] G.L. Donati, C.C. Nascentes, A.R.A. Nogueira, M.A.Z. Arruda, J.A. Nóbrega, Microchem. J. 82 (2006) 189.

Available online at www.sciencedirect.com
ScienceDirect
Talanta 73 (2007) 831–837
Talanta
www.elsevier.com/locate/talanta

Functionalization of chitosan with 3-nitro-4-amino benzoic acid moiety and its application to the collection/concentration of molybdenum in environmental water samples

Akhmad Sabarudin [a,*], Mitsuko Oshima [b], Osamu Noguchi [b], Shoji Motomizu [b]

[a] *Department of Chemistry, Faculty of Science, Brawijaya University, Jl. Veteran, Malang 65145, East Java, Indonesia*
[b] *Department of Chemistry, Faculty of Science, Okayama University, Tsushimanaka 3-1-1, Okayama City 700-8530, Japan*

Received 7 March 2007; received in revised form 30 April 2007; accepted 30 April 2007
Available online 22 May 2007

Abstract

A chitosan resin functionalized with 3-nitro-4-amino benzoic acid moiety (CCTS-NABA resin) was newly synthesized for the collection/concentration of trace molybdenum by using cross-linked chitosan (CCTS) as base material. The carboxyl group of the moiety was chemically attached to amino group of cross-linked chitosan through amide bond formation. The adsorption behavior of molybdenum as well as other 60 elements on the resin was examined by passing the sample solutions through a mini-column packed with the resin. After the elution of the elements collected on the resin with 1 M HNO_3, the eluates were analyzed by inductively coupled plasma-mass spectrometry (ICP-MS) and atomic emission spectrometry (ICP-AES).

The CCTS-NABA resin can adsorb several metal ions, such as vanadium, gallium, arsenic, selenium, silver, bismuth, thorium, tungsten, tin, tellurium, copper, and molybdenum at appropriate pHs. Among these metal ions, only molybdenum could be adsorbed almost completely on the resin at acidic regions. An excellent selectivity toward molybdenum could be obtained at pH 3–4. The adsorption capacity of CCTS-NABA resin for Mo(VI) was 380 mg g^{-1} resin. Through the column pretreatment, alkali and alkaline earth metals in river water and seawater samples were successfully removed.

The CCTS-NABA resin was applied to the adsorption/collection of molybdenum in river water and seawater samples. The concentrations of molybdenum in river water samples were found in the range of 0.84 and 0.95 ppb (ng g^{-1}), whereas molybdenum in seawater was about 9 ppb. The validation of the proposed method was carried out by determining molybdenum in the certified reference materials of SLRS-4, CASS-4, and NASS-5 after passing through the CCTS-NABA resin; the results showed good agreement with the certified values.

Keywords: Chitosan resin; 3-Nitro-4-amino benzoic acid; Molybdenum; Adsorption behavior; Water and seawater; ICP-MS; ICP-AES; Certified reference materials

1. Introduction

Molybdenum is one of the biologically essential microelements for all classes of organisms, because of its important role in enzymatic processes, and stimulating the synthesis of proteins and nucleic acids. However, over intake of molybdenum will result in molybdenum poisoning [1,2]. Molybdenum is also widely used in industrial processes as substance for metal alloys, pigments, lubricant, and chemical catalysis [3], which can increase the level of molybdenum released to environment. Molybdenum in natural water exists in the form of MoO_4^{2-} (Mo(VI)) and its protonated species, whose concentrations are very low [4]. In Japan, the concentration of molybdenum in environmental waters, such as drinking, river, and seawaters, were reported to be 0.11–6.2, 1, and 10 ppb, respectively [5,6]. Accordingly, precise and accurate, as well as selective separation and sensitive analytical methods for the determination of molybdenum in environmental samples should be developed.

Direct determination of molybdenum in environmental samples by using spectroscopic analytical techniques, such as flame and graphite furnace atomic absorption spectrometry (FAAS and GFAAS), inductively coupled plasma-mass spectrometry (ICP-MS) and atomic emission spectrometry (ICP-AES) are difficult because of its low concentrations and/or matrix interferences. In

* Corresponding author. Tel.: +62 341 575 835; fax: +62 341 575 835.
E-mail address: sabarjpn@gmail.com (A. Sabarudin).

0039-9140/$ – see front matter © 2007 Elsevier B.V. All rights reserved.
doi:10.1016/j.talanta.2007.04.057

order to overcome these problems, the separation and preconcentration procedures are required [7–10].

Santos et al. [11] reported the enrichment of molybdenum in seawater. The method is based on the complexation of Mo(VI) with by calmagite reagent and its sorption onto activated carbon. Molybdenum as calmagite complex could be quantitatively adsorbed (>90%) onto activated carbon. However, the heating of loaded activated carbon with concentrated nitric acid at 120 °C was required for desorption of molybdenum before its measurement by ICP-AES. The separation of molybdenum based on its chelation with quercetin immobilized on silica gel in a slightly acidic medium (pH 5) was reported by Azeredo et al. [12]. Molybdenum could be recovered quantitatively (95–99%). Nevertheless, the use of organic eluent, α-benzoinoxime, for the desorption of molybdenum prior to its determination by ICP-AES, could not be avoided. Octadecyl silica sorbent and silica-based strongly basic anion exchanger-packed in a mini-column have been reported for the separation and preconcentration of molybdenum [13]. In this method, small amount of NO_3^-, SO_4^{2-}, PO_4^{3-}, K^+, Na^+, Mg^{2+}, Ca^{2+}, Al^{3+}, and Fe^{3+} did not interfere with the determination of molybdenum by ICP-AES. The complicated procedures, which include evaporation, elimination of organic solvent (96% ethanol) and removal of excess mineral acid (HNO_3) after elution of molybdenum from mini-column, are the drawback of this method.

The use of chitosan as a solid support for an ion exchange and a chelating resin is increasing due to its advantages, such as easy derivatization of its amino groups and more hydrophilic characteristic than such synthetic base materials as polystyrene-divinylbenzene, polyethylene and polyurethane [14,15]. These advantages provide fast reaction rate in sorption and desorption kinetics of analyte species in aqueous media. However, chitosan itself will easily dissolve in acidic solutions due to the protonation of its amino groups. Therefore, cross-linking agents such as ethyleneglycoldiglycidylether (EGDE) and glutaraldehyde [16,17] were used for improving its chemical stability and mechanical strength. In our previous work [18], the cross-linked chitosan functionalized with leucine moiety was synthesized for the collection/concentration of molybdenum. It was found that molybdenum could be adsorbed quantitatively on the resin from pH 1 to 5, whereas alkaline and alkaline-earth metals could not be retained on the resin. The adsorption capacity of the resin for molybdenum was about 96 mg Mo(VI) g^{-1} resin.

In this work, a new chitosan resin for adsorption/collection of molybdenum was developed. The moiety of 3-nitro-4-amino benzoic acid (NABA) was chemically bonded to the amino group of cross-linked chitosan through the amide bond formation (CCTS-NABA resin). The adsorption capacity of CCTS-NABA resin for molybdenum was 380 mg Mo(VI) g^{-1} resin, which is superior to the leucine-type chitosan resin [18], as well as superior to other molybdenum resins reported so far. The collected molybdenum on the CCTS-NABA resin is easily eluted with 1 M nitric acid. The resin was successfully applied to the adsorption/collection of molybdenum in river water and seawater samples before its measurement by ICP-AES and ICP-MS. The certified reference materials of river water (SLRS-4), nearshore seawater (CASS-4), and open ocean seawater (NASS-5) were also examined. The results obtained by using the proposed method were in good agreement with the certified values. In addition, the matrices commonly existing in river and seawater samples were successfully removed by using this resin.

2. Experimental

2.1. Reagents and materials

Flake-type chitosan and 3-nitro-4-amino benzoic acid (NABA) were purchased from Tokyo Kasei Co. Ltd. (Tokyo, Japan). All other reagents used for the synthesis of CCTS-NABA resin were of analytical reagent grade.

Multielement standard solutions including molybdenum were prepared by diluting several kinds of a single element standard solution for atomic absorption spectrometry (1000 ppm) purchased from Wako Pure Chemicals (Osaka, Japan) and a multi-element standard solution for ICP-MS; XSTC-13 and XSTC-1 (10 ppm) provided by Spex CertiPrep Inc. (Metuchen, NJ, USA).

To examine the adsorption capacity of CCTS-NABA resin toward Mo(VI), ammonium heptamolybdate tetrahydrate ($(NH_4)_6Mo_7O_{24}.4H_2O$) from Wako pure chemicals (Osaka, Japan) was used.

Ultrapure grade nitric acid (60%, density 1.38 g mL^{-1} Kanto Chemicals, Tokyo, Japan) was diluted with ultrapure water to give 1 and 2 M acid solutions for column treatment. Acetic acid (minimum 96%) and ammonia water (29%) used for the preparation of ammonium acetate buffer solution were of an electronic industrial reagent grade (Kanto Chemicals, Tokyo, Japan).

2.2. Instrumentations

The ICP-MS, which was used for the measurement of molybdenum ($m/z = 98$), as well as other 60 elements, was a SPQ 8000H (Seiko Instruments, Chiba, Japan). An ICP-AES system (Vista Pro, Seiko Instruments, Chiba, Japan) was used for the measurement of molybdenum at wavelength of 202.032 nm. The operating conditions of ICP-MS and ICP-AES were almost similar to those reported in the previous work [15,18]. Infrared spectra (4000–400 cm^{-1}) were taken by a KBr pellet method using a FT/IR-4100 spectrometer, JASCO Co. (Tokyo, Japan). An automatic titration system Model AT-510, Kyoto Electronics Manufacturing Co. (Kyoto, Japan), was used for the acid-base titration to estimate the pK_a values of CCTS-NABA resin.

2.3. Preparation of CCTS-NABA resin

Cross-linked chitosan (CCTS) with the cross-linker of ethyleneglycoldiglycidylether (EGDE) was synthesized in a similar manner to the previous work [15,18–20]. Amino group of 3-nitro-4-amino benzoic acid moiety (NABA, 10 g) was protected with benzaldehyde as in the previous work [20] before its reaction with CCTS. Then, the CCTS-NABA resin was synthesized by reacting CCTS with amino-protected NABA moiety through the amide bond formation as shown in Fig. 1. In this step, 16 g of 1-ethyl-3-(3-dimethylaminopropyl)-

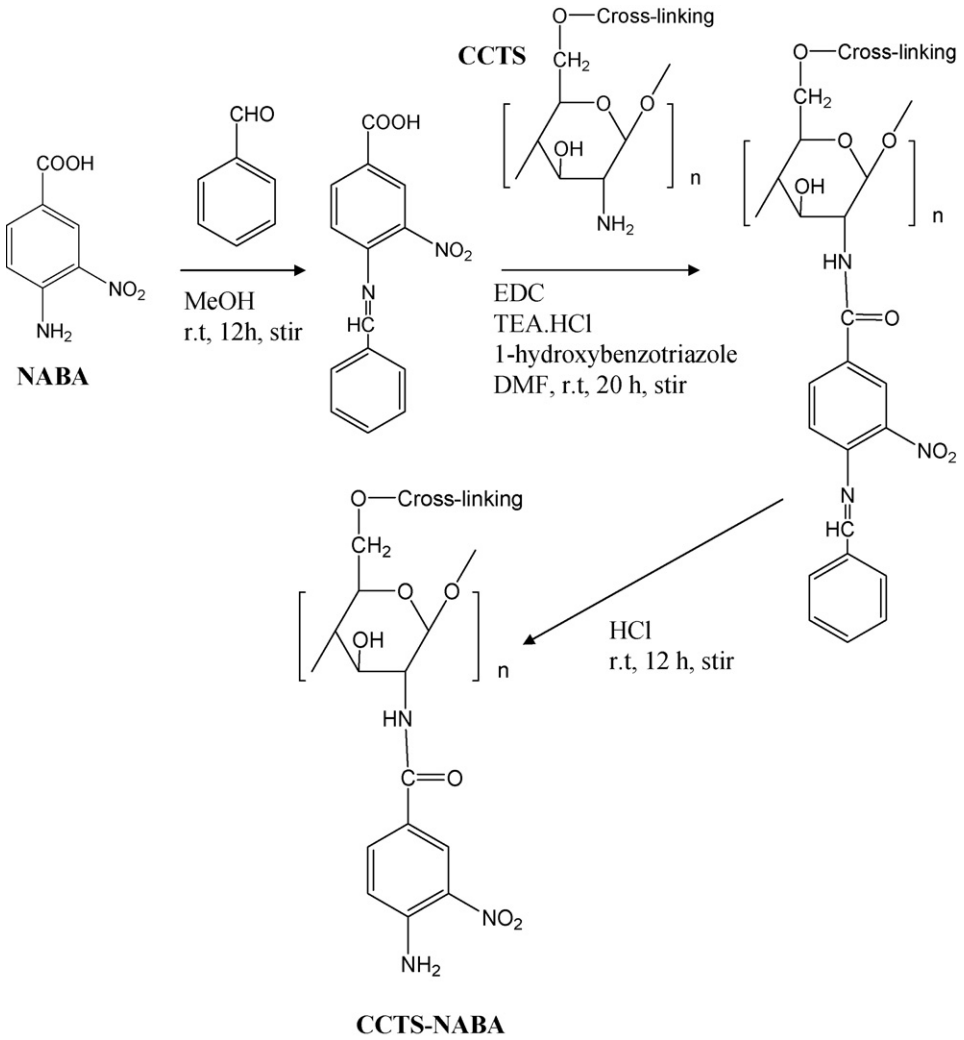

Fig. 1. Synthesis scheme of CCTS-NABA resin cross-linking: NABA: 3-nitro-4-amino benzoic acid; CCTS-NABA: cross-linked chitosan possessing 3-nitro-4-amino benzoic acid moiety; EDC: 1-ethyl-3-(3-dimethylaminopropyl)-carbodiimide; TEA: triethylamine; DMF: dimethyl formamide.

carbodiimide (EDC), 12 g of triethylamine (TEA) and 1 g of 1-hydroxybenzotriazole were mixed with amino-protected NABA in 60 mL of dimethyl formamide (DMF). Then, 5 g of the CCTS was suspended into the solution; the mixture was stirred for 20 h at room temperature. The product was filtered off using a glass filter and washed with methanol and water. In the last step, the protection group (benzaldehyde), which was condensed with amino groups of NABA, was removed by stirring the product in 50 mL of 0.5M HCl for 12 h at room temperature; this procedure was repeated two times. Finally, the product (CCTS-NABA) was filtered on the glass filter and washed with ethanol and water.

2.4. Precedures for column pretreatment of sample solutions

The CCTS-NABA resin synthesized in this work was washed by stirring the resin in 2M HNO_3 for 6 h to remove residual metal impurities during the production of chitosan and the synthesis of CCTS-NABA. Then, the resin was filtered on a filter paper, and rinsed with the ultrapure water. A 1-mL portion of the resin, which corresponds to 0.2 g of dry weight, was packed in polypropylene mini-columns (5 mm i.d. × 50 mm), Muromachi Chemical (Kyoto, Japan) for the examination of the adsorption behavior of the resin toward 61 elements.

The column pretreatment procedures are similar to our previous work [15,18–21]. The resin, packed in the mini-columns, was washed with each 10-mL of 2 M nitric acid and ultrapure water. Then, 5-mL of buffer solution (pH 1–2: nitric acid; pH 3–9: 0.5 M ammonia-acetate solutions) was passed through the column for conditioning. Sample solutions (10 mL), whose pHs were adjusted with the same buffer as the one for the column conditioning, were passed through the column. A 5-mL aliquot of a 0.2 M buffer solution (pH 1–9) was then passed through the column to remove matrix ions remained on the resin, such as alkali and alkaline earth metals. In order to rinse the remaining buffer components in the column, 5-mL of ultrapure water was passed through the column. Finally, 10-mL aliquot of 1 M nitric acid was passed through the column to recover the ele-

ments adsorbed on the resin, and the eluate was measured by ICP-AES and ICP-MS. For the determination of molybdenum with 10-fold preconcentration, 100 mL of the sample solution was used, and was adjusted to pH 4.

2.5. Adsorption capacity

The adsorption capacity of CCTS-NABA resin for Mo(VI) was examined by equilibrating 0.2 g of CCTS-NABA resin in the presence of Mo(VI) solution (100 mL, 1000 ppm). The acidity of the solution was adjusted to pH 4. The solution was stirred, and at certain time interval, 0.1 mL of the solution was transferred to a clean bottle until equilibrium was reached. Then, the concentration of Mo(VI) ion remained in the solution was measured by ICP-AES after 100-fold dilution.

2.6. Sampling and preserving of water samples

River water samples were collected from Zasu and Asahi rivers, which flow through Okayama City. The seawater sample was taken at Shibukawa Sea located at Okayama Prefecture, Japan. The original pHs of the samples were measured; they were in the range of 6.8–7.2. These samples were acidified to about pH 1 by adding a small amount of concentrated nitric acid before filtration with 0.45 μm membrane filter. Before being flowed through the mini-column packed with CCTS-NABA resin, the samples were adjusted to pH 4. The sampling and analysis of the water samples were performed within the same day.

The certified reference materials of the river water (SLRS-4), the nearshore seawater (CASS-4) and the open ocean seawater (NASS-5), which are issued by the National Research Council Canada (NRCC), were used for the validation of the proposed method.

3. Results and discussion

3.1. Characteristics of CCTS-NABA resin

The IR spectrum of CCTS-NABA resin, in comparison with the one of cross-linked chitosan (CCTS), depicted several bands at 1541.81, and 1707.21 cm^{-1}, which are attributed to $–NO_2$ of NABA moiety and C=O of the amide bond, respectively. These bands showed the existence of NABA moiety attached to CCTS in the synthesized resin.

The result of acid-base titration for the synthesized CCTS-NABA resin in an acidic solution with 0.1 M NaOH as a titrant was shown in Fig. 2. It can be expected from the chemical structure of CCTS-NABA resin that there must be seen one pK_a value, which comes from the amino group of NABA moiety. For estimation, the pK_a value of 2-nitroaniline, which is attributed to $–NH_2$ group (pK_a: −0.25) can be referred [22]. As shown in Fig. 2, a pK_a value of 9.0 can be observed clearly in the titration curve. The pK_a of 9.0 in resin seemed to be attributed to the unreacted amino group of cross-linked chitosan (CCTS). The pK_a value of amino group at *para*-position of NABA cannot be observed at the titration curve because it is extremely low. In this experiment, 2 mL of 0.10 M HCl was added to the resin-

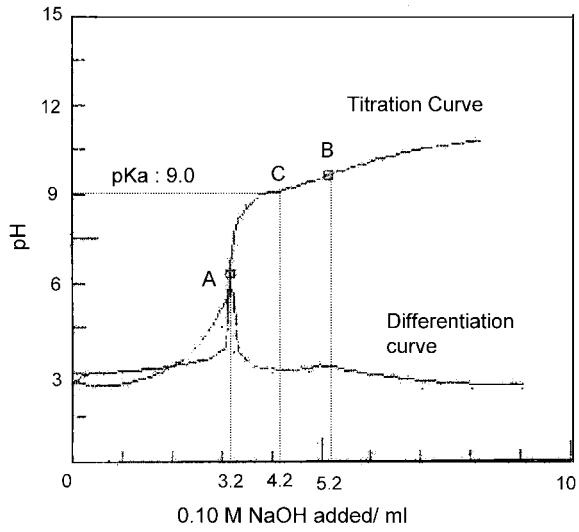

Fig. 2. Acid-base titration of the CCTS-NABA resin. A sample for the titration consists of 0.2 g CCTS-NABA resin, 2 mL of 0.1 M HCl and 28 mL of ultrapure water; A: the inflection point of HCl and partly protonated $–NH_2$ group of the resin; B: the inflection point of remaining $–NH_2$ in CCTS; C: the half point of the equivalent points.

suspended solution (30 mL water) before titration. Therefore, the pH of HCl solution is about 2.2, whereas $–NH_2$ group of NABA is seemed to be about −0.25 of pK_a, which may result in incomplete protonation of $–NH_2$ group.

As shown in the titration curve (Fig. 2), the first end point (A) corresponds to the neutralization of 2 mL of 0.1 M HCl and partly protonated $–NH_2$ group of NABA moiety; that is, 2 mL of 0.1 M NaOH corresponds to 2 mL of 0.1 M HCl, and 1.2 mL of 0.1 M NaOH corresponds to partly protonated of $–NH_2$ group of NABA moiety. The second end point (B) corresponds to the neutralization of the protonation of unreacted amino group of CCTS. A 2.0 mL of 0.1 M NaOH was required, which means that about 0.2 mmol in 0.2 g resin ($\simeq$1.0 mmol g^{-1}) of amino group remains in the resin as $–NH_2$.

Assuming that NABA moiety is attached to all glucamine unit of chitosan, about 2.5 mmol NABA may exist in 1 g of the resin. However, from the titration result, it can be calculated that the amount of NABA moiety chemically bonded to CCTS is about 1.5 mmol g^{-1} (2.5–1.0 mmol g^{-1}). Such result indicated that about 40% of $–NH_2$ of NABA Moiety could be protonated in the first end point of the titration (A). Accordingly, the mole ratio of NABA moiety to glucamine unit of chitosan can be estimated to be 0.6:1.0 (1.5:2.5); that is, 60% of amino group of CCTS is bound to NABA moiety.

The adsorption capacity of CCTS-NABA was obtained by equilibrating the resin with Mo(VI) solution at pH 4. The adsorption capacity of this resin for Mo(VI) was found to be 380 mg g^{-1} resin. The loading half time ($t_{1/2}$), defined as the time necessary for the adsorption of a half of its maximum adsorption capacity, was about 8 min: the sorption kinetics of the resin for molybdenum is very fast. In a similar way, the adsorption capacity of the cross-linked chitosan (CCTS) itself was also examined: it was found that maximum adsorption capacity for Mo(VI) was 200 mg g^{-1}. Guibal et al. [23] reported that the adsorption capac-

ity for Mo(VI) of chitosan (without cross-linking) was about 670 mg g^{-1}. However, in our experiment, when Mo(VI) solution was adjusted to pH 4 using 0.2 M ammonium acetate buffer, chitosan itself dissolved easily and completely. In addition, chitosan was also partially soluble in diluted hydrochloric, nitric, and sulfuric acids at pH 3–4. Therefore, too high adsorption capacity of Mo(VI), 670 mg g^{-1}, with raw chitosan without any cross-linker is unexpected. This feature showed that the use of chitosan in raw form as solid phase extractant is restricted.

The adsorption capacity of cross-linked chitosan functionalized with leucine moiety [18] for Mo(VI) was 96 mg g^{-1}, which is much lower compared with CCTS and CCTS-NABA. This behavior can be explained as follows: the amino group (-NH_2) seems to play an important role for the adsorption of Mo(VI). When the cross-linker of ethyleneglycoldiglycidylether (EGDE) is chemically bonded to chitosan, the accessibility of Mo(VI) to internal site of chitosan is reduced. However, when the moiety possessed –NH_2 group is attached to chitosan, the adsorption capacity increases due to the extension of –NH_2 group, which is easily accessed by Mo(VI). This is why the adsorption capacity of CCTS-NABA is higher than CCTS. On the other hand, in case of the CCTS functionalized with leucine moiety, the extension of –NH_2 is not available, which results in decreasing adsorption capacity due to an increase in steric hindrance.

3.2. Adsorption behavior of metal ions on the CCTS-NABA resin

The adsorption behavior of metal ions on the CCTS-NABA resin was examined by the column method. Fig. 3 shows the results obtained for the adsorption/recovery of 10 ppb of 61 elements in the pH range from 1 to 9. The analytes adsorbed on the resin were quantitatively recovered with 10 mL of 1 M nitric acid as an eluent. The CCTS-NABA resin can adsorb various kinds of elements, such as vanadium, gallium, arsenic, selenium, silver, bismuth, thorium, tungsten, tin, tellurium, etc. However, these elements are adsorbed on the resin less than 80% at all pHs examined. Molybdenum (VI) and copper (II) could be adsorbed almost completely at appropriate pH on the resin. Copper could be adsorbed completely at neutral pH regions, whereas molybdenum could be adsorbed almost completely at acidic regions (pH 3–5). Accordingly, the CCTS-NABA resin is good selectivity for the adsorption of molybdenum at acidic regions and less competitive to other metal ions.

In our previous work [16], the cross-linked chitosan (CCTS) itself could adsorb copper at neutral pH region by the chelation mechanism. Similarly, in the present resin, Cu can form chelate rings with nitrogen atoms of amino groups and oxygen atoms of hydroxyl groups of the resin.

The amounts of molybdenum, which is adsorbed on the CCTS-NABA resin at acidic regions, were higher than 95%, whereas in the CCTS itself was less than 70%. As mentioned in section 3.1, the cross-linker agent (EGDE) attached to chitosan reduced the accessibility of Mo(VI) to internal site of chitosan, which can result in lower adsorption of CCTS, compared with CCTS-NABA. In addition, Mo(VI) exists as oxoanionic species in aqueous solutions, which can be adsorbed on the resin at the acidic region by anion-exchange mechanism. By introducing NABA moiety to the CCTS, the adsorption of Mo(VI) on the CCTS-NABA resin may consist of several combination of interactions including electrostatic attraction, anion exchange and/or chelation mechanism. Compared to the CCTS itself, it can be

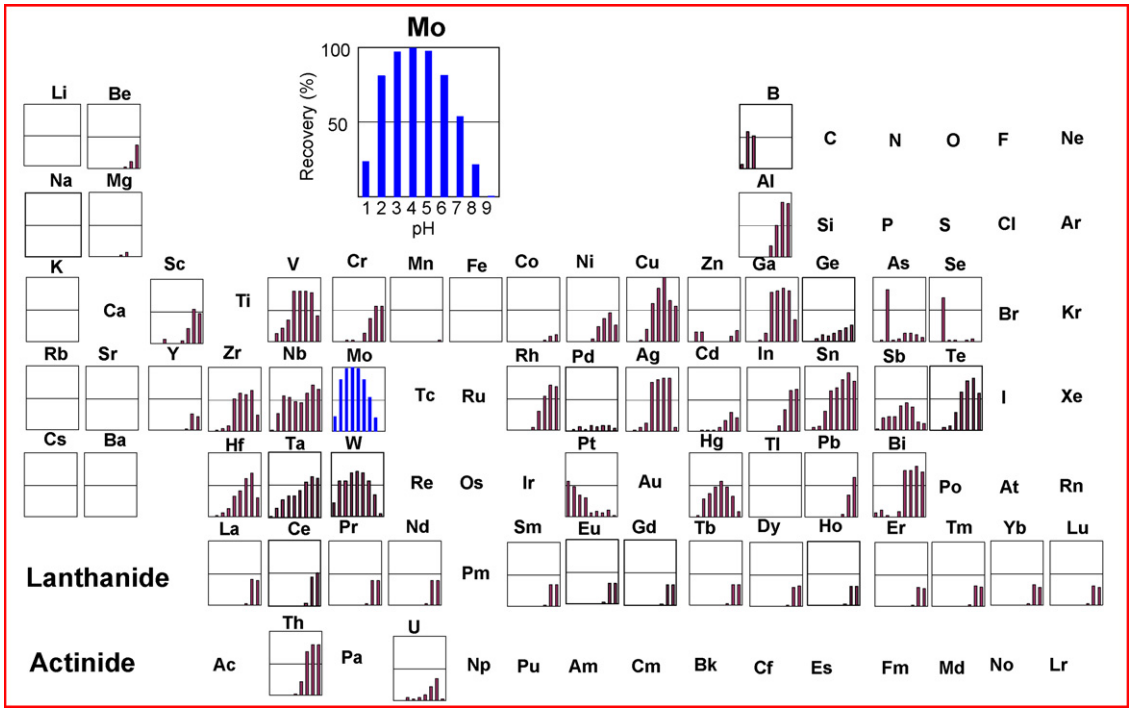

Fig. 3. Adsorption behavior of trace elements at various pHs with CCTS-NABA resin. Sample: 10 mL; concentration of each element in the samples: 10 ppb; column: 1 mL (0.2 g dry weight) of the CCTS-NABA resin; all elements were measured by ICP-MS.

Table 1
Recovery test of molybdenum in the present of matrices

Sample	Mo found/ppb		Recovery (%)	
	ICP-MS	ICP-AES	ICP-MS	ICP-AES
Artificial river water[a]	0.48 ± 0.02	0.46 ± 0.03[c]	96	92
Artificial seawater[b]	9.88 ± 0.12	9.69 ± 0.91	99	97

All samples were adjusted to pH 4; volume of sample: 10 mL; eluent (1M HNO_3): 10 mL.
[a] Artificial river water contains Mo (0.50 ppb), Na (20 ppm), K (15 ppm), Mg (10 ppm), and Ca (50 ppm).
[b] Artificial seawater contains Mo (10 ppb), Na (11,500 ppm), K (1200 ppm), Mg (3900 ppm), and Ca (400 ppm).
[c] Samples were concentrated by 10-fold; volume of samples: 100 mL; eluent (1 M HNO_3): 10 mL.

said that CCTS-NABA resin is more effective for the adsorption/collection of molybdenum (Mo), and less competitive to other ions at acidic region. Then, pH 4 of the adsorption procedure for sample solution was selected for further experiments. Such a result resembles that coupling NABA moiety to CCTS improves selectivity toward Mo(VI).

The chemistry of molybdenum in an aqueous phase is very complex because of its multiple oxidation states and various different species [24]. Molybdenum (VI) is the most stable oxidation state in aqueous solutions. Polymeric species of molybdenum, such as $H_2Mo_7O_{24}^{4-}$, $HMo_7O_{24}^{5-}$, and $Mo_7O_{24}^{6-}$ are successively formed at pH 2.53, 3.54, and 4.40, respectively, when the concentration of Mo(VI) is greater than 96 ppm (≃1 mM). However, when the concentration of Mo(VI) is at several ppb levels or lower, the main species of molybdenum exist as H_2MoO_4 (pK_a: 3.61), $HMoO_4^-$ (pK_a: 3.89) and MoO_4^{2-} [25]. In this work, since the collection/adsorption of molybdenum in environmental water samples was performed at pH 4, and its concentration was lower than 10 ppb, the monomeric species of MoO_4^{2-}, $HMoO_4^-$ and H_2MoO_4 may adsorb on the CCTS-NABA resin.

3.3. Detection limit and quantification limit

The detection limit of the method (LOD) was calculated from the sum of average concentration and 3σ of blank values (LOD: blank value + 3σ, σ: standard deviation of blank value), whereas the quantification limit of the method (LOQ) was calculated from the sum of average concentration and 10σ of blank values (LOQ: blank value + 10σ). The LOD of Mo obtained by coupling the pretreatment with CCTS-NABA resin and measurement by ICP-MS was 0.01 ppb and theLOQ was 0.02 ppb when 10 mL of each sample volume and the eluent was used (without preconcentration).

The LOD of Mo using ICP-AES after pretreatment with CCTS-NABA resin was 0.19 ppb, while the LOQ was 0.40 ppb when 10-fold preconcentration of sample solution was performed.

3.4. Application of CCTS-NABA resin to the collection/concentration of molybdenum in water samples

The applicability of CCTS-NABA resin was examined for the collection/concentration of molybdenum in river water and seawater samples. The major matrices, such as Na, K, Mg and Ca can interfere with the determination of trace elements, as well as can damage the detector of the ICP-MS system. Therefore, the matrices must be removed from the samples prior to the measurement by ICP-MS. Table 1 shows the results obtained for the examination of the effect of cationic matrices, such as Na, K, Mg and Ca on the recovery of molybdenum in artificial river water and seawater samples. The results indicate that the CCTS-NABA resin is capable of adsorbing molybdenum quantitatively because almost complete recoveries (92–99%) were achieved even in the presence of large amounts of matrices. The concentrations of matrices after column pretreatment were also determined by ICP-AES, and it was found that Na, K, Mg, and Ca could be removed in the range of 99–100%. Due to its great ability to remove matrices, the CCTS-NABA resin can be applied effectively to the collection/concentration of molybdenum in natural river water and seawater.

In order to evaluate the accuracy of the proposed method, the certified reference materials of the river water (SLRS-4), the nearshore seawater (CASS-4), and the open ocean seawater (NASS-5), issued by National Research Council Canada, were examined. The pH of the samples was adjusted to 4, followed by the procedure described in the experimental section. The results are shown in Table 2, in which there is no significant difference between the results obtained by the proposed method and the certified values. However, molybdenum in SLRS-4 could not be detected with 10-fold preconcentration by ICP-AES because its concentration is closed to the MDL of ICP-AES.

Table 3 showed the analytical results of molybdenum in river water and seawater samples obtained after the pretreatment with a mini-column packed with CCTS-NABA resin. Molybdenum in seawater can be accurately determined by ICP-AES and ICP-MS. However, 10-fold enrichment factor was required for

Table 2
Analytical results of molybdenum in certified reference materials

Sample	Mo found/ppb		Certified value/ppb
	ICP-MS	ICP-AES	
SLRS-4	0.22 ± 0.00	n.d.[a]	0.21 ± 0.02
CASS-4	8.64 ± 0.11	8.21 ± 0.44	8.78 ± 0.86
NASS-5	9.32 ± 0.18	9.32 ± 0.28	9.6 ± 1.0

All samples were adjusted to pH 4; volume of sample: 10 mL; eluent (1M HNO_3): 10 mL.
[a] Samples were concentrated by 10-fold; volume of samples: 100 mL; eluent (1 M HNO_3): 10 mL; n.d.: not detected.

Table 3
Analytical results of molybdenum in environmental water samples

Sample	Mo found/ppb	
	ICP-MS	ICP-AES
River water (Asahi)	0.94 ± 0.00	0.95 ± 0.08[a]
River water (Zasu)	0.84 ± 0.05	0.84 ± 0.01[a]
Shibukawa seawater	9.04 ± 0.04	9.01 ± 0.20

All samples were adjusted to pH 4; volume of sample: 10 mL; eluent (1M HNO_3): 10 mL.

[a] Samples were concentrated by 10-fold; volume of samples: 100 mL; eluent (1 M HNO_3): 10 mL.

the determination of molybdenum in river water by ICP-AES, though preconcentration procedure is unnecessary for ICP-MS.

4. Conclusions

The CCTS-NABA resin, synthesized by chemically bonding 3-nitro-4-amino benzoic acid (NABA) moiety to amino group of cross-linked chitosan (CCTS) through amide bond formation, provides effective separation and preconcentration of molybdenum in river water and seawater, when it is used as a packing material in the mini-column. The resin has an excellent selectivity toward molybdenum at acidic regions (pH 3–4). The molybdenum collected on the resin was easily eluted with 1M nitric acid. In addition, the CCTS-NABA resin is stable in acidic solution and can be used continuously for at least 20 cycles. Moreover, the resin offers high adsorption capacity for molybdenum (VI), 380 mg g^{-1}, which is better than other molybdenum resins reported so far [8,18].

Acknowledgements

The present work was partially supported by the Grant-in-Aid for Scientific Research No. 17550143 from the Ministry of Education, Culture, Sports, Technology, Japan and DOWA Techno Engineering Co. Ltd., Japan.

References

[1] Y.C. Sun, J. Mierzwa, C.R. Lan, Talanta 52 (2000) 417.
[2] V.M. Ivanov, G.A. Kochelaeva, G.V. Prokhorova, J. Anal. Chem. 57 (2002) 902.
[3] A.R. Ghiasvand, S. Shadabi, E. Mohagheghzadeh, P. Hasemi, Talanta 66 (2005) 912.
[4] J.X. Du, J.J. Li, L.J. Yang, J.R. Lu, Anal. Chim. Acta 481 (2003) 239.
[5] A. Vyskocil, C. Viau, J. Appl. Toxicol. 19 (1999) 185.
[6] T. Koyama, N. Handa, Y. Sugimura, Kosui-kaisui no bunseki, Kodansha-Scientific, Tokyo, 1972, p. 259.
[7] S.L.C. Ferreira, H.C. Santos, R.C. Campos, Talanta 61 (2003) 789.
[8] J.C. Yu, S.M. Chan, Z.L. Chen, Anal. Bioanal. Chem. 376 (2003) 728.
[9] A. Tunçeli, A.R. Türker, Microchim. Acta 144 (2004) 69.
[10] Q. Li, X. Zhao, X. Guan, G. Liu, Anal. Chim. Acta 562 (2006) 44.
[11] H.C. Santos, M.G.A. Korn, S.L.C. Ferreira, Anal. Chim. Acta 426 (2001) 79.
[12] L.C. Azeredo, M.A.A. Azeredo, R.N. Castro, M.F.C. Saldanha, D.V. Perez, Spectrochim. Acta Part B 57 (2002) 2181.
[13] K. Martynkova, R. Komendova, M. Fisera, L. Sommer, Microchim. Acta 147 (2004) 65.
[14] K. Oshita, M. Oshima, Y.H. Gao, K.H. Lee, S. Motomizu, Anal. Sci. 18 (2002) 1121.
[15] Y.H. Gao, K. Oshita, K.H. Lee, M. Oshima, S. Motomizu, Analyst 127 (2002) 1713.
[16] K. Oshita, Y.H. Gao, M. Oshima, S. Motomizu, Anal. Sci. (Suppl.) 17 (2001) a317.
[17] T.Y. Hsien, G.L. Rorrer, Ind. Eng. Chem. Res. 36 (1997) 3631.
[18] K. Oshita, J. Xu, Y.H. Gao, K.H. Lee, M. Oshima, S. Motomizu, Bull. Chem. Soc. Jpn. 76 (2003) 1555.
[19] A. Sabarudin, K. Oshita, M. Oshima, S. Motomizu, Talanta 66 (2005) 136.
[20] A. Sabarudin, K. Oshita, M. Oshima, S. Motomizu, Anal. Chim. Acta 542 (2005) 207.
[21] A. Sabarudin, M. Oshima, T. Takayanagi, L. Hakim, K. Oshita, Y.H. Gao, S. Motomizu, Anal. Chim. Acta 581 (2007) 214.
[22] D.R. Lide, Handbook of Chemistry and Physics, 81st ed., CRC press, New York, 2000, pp. 8–49.
[23] E. Guibal, C. Milot, J.M. Tobi, Ind. Eng. Chem. Res. 37 (1998) 1454.
[24] B.L. Rivas, H.A. Maturana, P. Hauser, J. Appl. Polym. Sci. 73 (1999) 369.
[25] M.T. Pope, Heteropoly and Isopoly Oxometalates, 8, Springer-Verlag, Heidelberg, 1983, pp. 42–43.

Available online at www.sciencedirect.com
ScienceDirect
Talanta 73 (2007) 795–802
Talanta
www.elsevier.com/locate/talanta

Review

Trends in ultrasonic-based equipment for analytical sample treatment

H.M. Santos, J.L. Capelo *

Departamento de Química, Faculdade de Ciências e Tecnologia, Universidade Nova de Lisboa, Quinta da Torre, 2829-516 Monte de Caparica, Portugal

Received 12 February 2007; received in revised form 15 May 2007; accepted 18 May 2007
Available online 26 May 2007

Abstract

The recent developments achieved in ultrasonic equipment urges the need for the revision of its applications in analytical chemistry. In the present work, the last ultrasonic devices are easily presented and their applications for sample treatment are critically discussed. Comments are given on edge areas of research, such as proteomics or polymer science, which are presently taking advantage of ultrasonic sample treatments. Future applications and trends for ultrasonic-based handling approaches are also given and commented.

Keywords: Ultrasound power; Sonication bath; Sonication probe; Ultrasonic energy; Analytical uses

Contents

1. Introduction 796
2. Ultrasonic devices 796
   2.1. The ultrasonic bath 796
   2.2. Advances on ultrasonic bath technology 796
   2.3. The ultrasonic probe 796
   2.4. Advances on ultrasonic probe technology 797
      2.4.1. Silica glass probes 797
      2.4.2. Spiral probes 798
      2.4.3. Multiple probe 798
   2.5. Cup horns/sonoreactors 798
      2.5.1. Microplate horns 798
3. Traditional applications under the perspective of new ultrasonic technology 798
4. New ultrasonic applications 800
   4.1. Application to proteomic research 800
   4.2. Application to polymer research 801
   4.3. Application to pesticide research 801
   4.4. On-line applications 801
5. Future prospects 801
6. Conclusions 802
   References 802

* Corresponding author. Tel.: +351 212 948 386; fax: +351 212 948 550.
E-mail address: jlcapelom@dq.fct.unl.pt (J.L. Capelo).

0039-9140/$ – see front matter © 2007 Elsevier B.V. All rights reserved.
doi:10.1016/j.talanta.2007.05.039

1. Introduction

The use of ultrasonic energy – ultrasonication – for analytical chemistry is nowadays a constant growing area of research. The recent advances in ultrasonic energy performance have led to the development of new and powerful devices, whose many possible applications for sample treatment are still not well known. Although there are recent reviews dealing with ultrasonication and its applications for the analytical laboratory [1–4], none of them is paying attention on the new ultrasonic devices, their characteristics and most important, their applications. Therefore, a manuscript describing what it is new on ultrasonication for analytical chemists and in particular how to use it at the analytical laboratory is mandatory.

The main aim of the present work is not to provide a deep explanation about ultrasonication effects. To get a good knowledge about ultrasonic energy and its applications, the book of Professor Mason is highly recommended [5]. To go further with the reading of this manuscript, it is enough to know that when ultrasonic waves cross through a liquid media, an effect known as cavitation occurs. The name cavitation defines a physical process by which numerous tiny gas bubbles are generated. Those bubbles, grow, oscillate, split and finally implosion, in such a way, that they can be considered as micro-reactors in which temperatures near to 5000 °C and pressures of 1000 atm are reached. Cavitation causes physical phenomena, such as pitting and mechanical erosion of solids, including particle rupture, leading to smaller particle size. In addition, chemical radicals are formed into the liquid media, which produces the oxidation of chemical species. As an example, energy oxidative radicals, such as hydroxyl radical or chemical compounds, such as hydrogen peroxide are formed when ultrasonic power is applied to water.

In this work is given a peer revision of the most recent advances on ultrasonic devices, including their uses for analytical chemistry, as well as their advantages and drawbacks, which are listed and discussed. In addition, future trends and new applications are also commented.

2. Ultrasonic devices

2.1. The ultrasonic bath

The ultrasonic bath is so common in the chemical laboratories that it does not need presentation. It is not a powerful tool; the irradiation power given by a common ultrasonic bath is comprised between 1 and 5 W cm^{-2}. When used for analytical tasks, the ultrasonic bath lacks in reproducibility. Finding the highest intensity place of sonication inside an ultrasonic bath is always a critical issue, as pointed out by Mason in his highly recommendable book about sonochemistry [5]. In the aforementioned book is described in detail the so-called “aluminum foil test”, which is done to find the best place inside the bath in terms of sonication intensity (reference [5], pp. 44–45). As described in detail in previous manuscripts [1,2,6], different variables must be taken into account when sonication is going to be performed with an ultrasonic bath, briefly the following ones:

(i) particle size, if a solid is studied;
(ii) acid and/or oxidant used in the treatment;
(iii) leaching volume;
(iv) sonication time;
(v) water temperature inside the bath;
(vi) frequency of the ultrasonic energy;
(vii) the position in which the sample container is situated inside the bath (vertical and horizontal position);
(viii) the use of detergent in the water, by which the ultrasonic transmission through the liquid achieve better results.

2.2. Advances on ultrasonic bath technology

The Elma Company (www.elma-ultrasonic.com, *disclaimer*: specific company, product and equipment names are given to provide useful information; their mention does not imply recommendation or endorsement by the authors) offers some of the most advanced ultrasonic baths on market. Their remarkable features include the following ones:

(i) Dual frequency of sonication, for choosing of either 25/45 or 35/130 kHz. The baths are designed to work with only one of the two frequencies at a time.
(ii) Power regulation: the ultrasonic power is variable from 10 to 100%.
(iii) Three operation modes:
  (a) Sweep: in this mode the frequency varies permanently within a defined range, shifting the minima and maxima of the sound field within the bath. The ultrasonic efficiency is more homogeneously distributed in the bath than during standard operation.
  (b) Standard: in this mode the frequency is regulated against the mechanical resonance of the ultrasound transducer. This optimizes the performance in the distributed maxima.
  (c) Degas: the set power is interrupted for a short period so that the bubbles are not retained by the ultrasonic forces.
(iv) Heating and timer.

In further sections, it will be shown the important new findings regarding extraction capabilities of ultrasonic baths as a function of sonication frequency.

The Bandelin Company (www.bandelin.com) also offers a novel type of ultrasonic baths, named TwinSonic®. Those devices are multi-frequency units that operate using at the same time ultrasonic transducers with different frequencies, 25 and 40 kHz, on the bottom and the side, respectively. The result is a uniform ultrasonic power distribution.

2.3. The ultrasonic probe

Fig. 1 provides a description of the different components of an ultrasonic probe. Two are the main differences when comparing the ultrasonic probe with the ultrasonic bath. Firstly, the ultrasonic probe is immersed directly into the solution, where the sonication takes place, and secondly, the utrasonic power

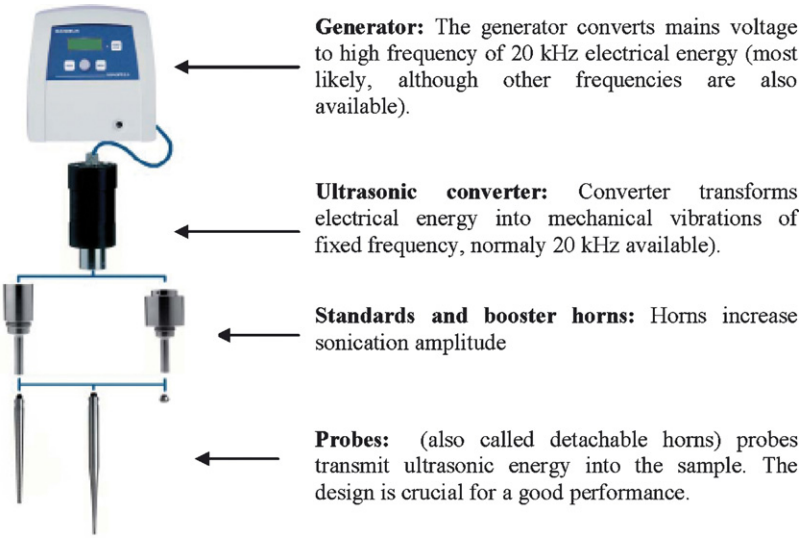

Fig. 1. Comprehensive scheme of an ultrasonic probe (adapted from Bandelin Company with its kind permission).

provided by the probe is at least up to 100 times greater than the one supplied by the bath. Those major differences make each system devoted for a different set of applications. The probe is a powerful system for the solid–liquid extraction of analytes that can be extracted but can also be degraded. There are dedicated probes for a given range of volumes. It should be stressed that the amplitude control of the probes allows the ultrasonic vibrations at the probe tip to be set to any desired level. However, to achieve cavitation, normally it is not necessary to use high amplitude levels; otherwise the probe will deteriorate rapidly. Temperature is another factor that must be controlled. As the ultrasound are delivered into the solution, a slow but constant increase in the bulk temperature is achieved and, at one point, the physical characteristics of the liquid media changes so that a decoupling of the probe can occur and no more cavitation is achieved. At this point the procedure must be stopped and the solution refrigerate. If long sonication times are needed the "pulse" mode is recommended. In this mode, the amplifier switches the power of the probe on and off repeatedly, thus avoiding the build up of reaction temperature. In some instances, when the main cause of sonochemical effects is cavitational collapse, then a bubbled gas should be used to generate large numbers of nucleation sites for cavitation. Mono-atomic gases are preferable to diatomics or polyatomics ones. A critical factor to be considered for a correct ultrasonic probe application, deals with the shape of the reaction vessel, which must be conical-type [7] and with the diameter as small as possible in order to rise up the liquid level. In this way the probe can be inserted more deeply into the processed sample, thus avoiding aerosoling and foaming, which has the effect of "de-coupling" the probe, that is, no more cavitation is obtained. Touching the sides of the vessel with the probe must be always avoided. The most important part of the whole system is the probe or detachable horn, which allows the vibration of the booster horn to be transmitted through a further length of metal in such a way that the power delivered is magnified. Power magnification depends on the shape of the probes, as can be seen in Fig. 2. The stepped probe shape presents the higher amplitude magnification [i.e., power, amplitude gain $(D/d)^2$] from all the probes' shapes. Nevertheless, the exponential probe shape, although difficult to manufacture, offers small diameters in its working end, which makes it particularly suited to micro-applications. Probes are usually made of titanium alloy (titanium probes) and are thermo-resistant, can be treated in autoclaves and are resistant to corrosive media. The sample volume to be treated along with the sample type is crucial to determine the selection of unit and the type of probe. It must be always borne in mind that the higher the amplitude provided by the probe the more intense is the sonication.

2.4. Advances on ultrasonic probe technology

Some companies have presented some interesting advances on probes' performance. Thus, the need for a metal-free probe has been addressed since a long time ago by researchers working in trace analysis. This requirement has been achieved by the called silica glass probes. Other important advances are the spiral probes that can supply power ultrasound in all its length. Both probes are available from the Bandelin Company.

2.4.1. Silica glass probes

This type of probes (Fig. 3a, www.bandelin.com) offers several advantages for applications in food analysis, pharmaceutical

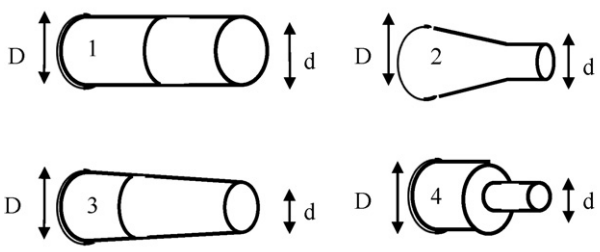

Fig. 2. Probes shapes: (1) uniform cylinder; (2) linear taper or cone; (3) exponential taper; (4) stepped.

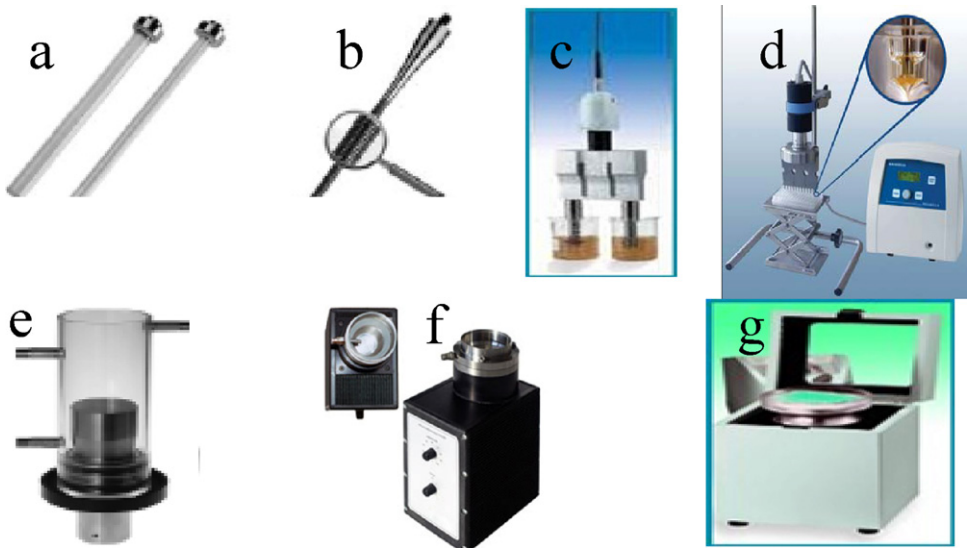

Fig. 3. Advances on ultrasonic probe technology: (a) silica glass probe; (b) spiral probe; (c) dual probe; (d) multi probe; (e) cup horns; (f) sonoreactor; (g) microplate horns. (a–d) are reproduced with permission of Bandelin Company; (e) and (g) are reproduced with permission of Misonix Company; (e) is reproduced with permission of dr. Hielscher Company.

or environmental analysis, such as no intrusion of metal particles or contamination by metals, such as boron or aluminium. The last item makes this tool theoretically ideal for trace analysis. Those probes are high chemical and temperature shock resistance. In addition, silica glass probes do not present electric conductivity. However, several drawbacks must be addressed. For instance, the cavitation strength of silica glass is relatively low and, consequently, the amplitude must be limited. All silica glass probes are designed to be used with a maximum power setting of 50%, which corresponds to maximum amplitude of 12 μm. In addition, this kind of probes are especially fragile during operation, so they must not be put down and/or allowed to make contact with the vessel.

2.4.2. Spiral probes

This type of probe (Fig. 3b, www.bandelin.com) is made of Ti, Al and V and provides gentle ultrasonic treatment of aqueous media in test tubes or other long, thin laboratory containers. As opposed to traditional probes, the ultrasonic power is distributed across the entire surface of the spiral probe.

2.4.3. Multiple probe

Multiples probes (Fig. 3c, www.bandelin.com and Fig. 3d, www.misonix.com) are manufactured allowing the accomplishment of two or more probes at the same time. Those type of sonicators meet the Unites States Environmental Protection Agency, USEPA, requirements specified in Method SW846-3550, which is referenced by the following USEPA analytical test methods: 8040, 8060, 8080, 8090, 8100, 8120, 8140, 8250, 8270, 413.2, 418.1.

2.5. Cup horns/sonoreactors

Cup horns (Fig. 3e, www.bandelin.com) are available from almost all ultrasonic companies, the sonoreactor (Fig. 3f, www.hielscher.com) is provided by the dr. Hielscher Company. Both ultrasonic devices offer indirect sonication. Indirect sonication means that the ultrasonic waves need to cross the wall of the sample container. This does not occur with the ultrasonic probe, which is directly immersed in the sample, giving direct in-sample sonication. Cup horns and sonoreactor can be compared to high intensity ultrasonic water baths. As an example, the sonoreactor is 50 times more intense than an ultrasonic bath. Samples can be processed in sealed tubes or vials eliminating aerosols and cross-contamination. Those devices are ideal for samples, such as sterile or dangerous pathogenic ones. In the cup horn, the titanium probe is held within an acrylic cup filled with water. Samples are placed within the cup, above the probe. The cavitation produced in the immersed samples is higher than the one given by an ultrasonic bath but it is lower than the cavitation produced by direct immersion of the ultrasonic probe into the solution. Both systems allow refrigeration.

2.5.1. Microplate horns

The microplate horn (Fig. 3g, www.misonix.com) is similar to the cup horn, but it allows high throughput applications. Different versions of the same concept can be found in several of the ultrasonic companies cited in Table 1.

3. Traditional applications under the perspective of new ultrasonic technology

The power of ultrasound has been used since decades in analytical chemistry mainly for the following purposes:

(i) Total solid–liquid elemental extraction

From the ultrasonic devices listed in the previous sections, the bath and the probe have been by large the most used to date for solid–liquid elemental extraction, also called ultrasonic-assisted acid leaching. In fact, most of the literature available to date for this purpose deals with both

Table 1
Ultrasonic probe models and their main characteristics available from the most important companies

Company	Model	Amplitude control (%)	Pulsation (%)	Working volume (mL)	Ultrasonic frequency (kHz)	Timer (min)	Power output (W)/T control	LCD/display of energy (kJ)	PC control
(1)	2070/2200	10–100	10–100	(2–50)/(20–900)	20	0.017–99	70/no, 200/no	Yes/no	No
	3100/3200	In % or in W	0.1–600 s	(2–50)/(20–900)	20	0.017–600	100/yes, 200/yes	Yes/yes	Yes
(2)	UP50H/UP100H	20–100	0–100	0.01–500	30	0–100	50/yes[a], 100/yes[a]	No/yes[a]	Yes
	UP200H/UP200S/ UP400S	20–100	0–100	(0.1–1000)/(0.1–1000)/ (5–4000)	24	0–100	200/yes[a], 200/yes[a], 400/yes[a]	No/yes[a]	Yes
(3)	S-150D	10–100	Yes (not specified)	Not specified	20	No	100/no	Yes	No
	S-250D/S-450D	10–100	Yes (not specified)	1–500	20	Not specified	200/yes, 400/yes	Yes/no	Yes
	SLP_f/SLP_e	10–100	Yes (not specified)	Yes (not specified)	40	Yes (not specified)	150/no, 150/no	Yes/no, yes/yes[a]	Yes
(4)	VS100/VS600	10–100	0.1–3600 s	(0.2–60)/(0.2–1000)	20	0.017–6000	100/no, 600/yes	Yes/No, yes/yes	No

(1) www.bandelin.com; (2) www.hielscher.com; (3) www.bransonultrasonics.com; (4) www.equilabcanada.com. Additional webpages from companies offering similar products: www.misonix.com, www.elma-ultrasonic.com.
[a] Through PC control.

systems. It must be stressed that there is some controversy regarding the robustness of the extraction protocols, since date reported in literature is sometimes contradictory. For instance, Pb has been cited as highly or totally extractable from reference sediment material by some authors [8,9], whilst other researchers reported low Pb extractability for the same kind of matrix [10]. Based on our own experience and in data taken from literature [1,2,8], it can be concluded that most of the contradictory results reported to date in literature regarding ultrasonic elemental extraction can be linked to an incorrect application of the ultrasonic procedure rather than to a lack in ultrasonic extraction efficiency. Thus, the most critical factor frequently ignored is sample size, which must be as small as possible, whenever possible. In fact, the percentage of analyte ultrasonically extracted for a given matrix, E, can be related to a constant K through the particle radius [2], assuming that particles are spherical, as follows:

$$K = \pi r^2 E$$

Through this constant, it is possible to know the particle size necessary to achieve total extraction. Obviously, for some matrixes, the particle size should be so small that the effort necessary to attain such sizes makes the ultrasonic procedure useless, requiring other analytical approaches to perform the solubilization of the target analyte, such as high pressure microwave digestion. Sonication time, sonication amplitude, temperature and leaching reagents are variables accounting for a successful extraction procedure. For a detailed description of the aforementioned variables, including a general approach about how to develop an ultrasonic extraction scheme refers to reference [2].

The technological innovations in ultrasonication will affect the metal extractability mainly in two ways, higher throughputs and lower contamination rates. Regarding throughput, the multiple probes (see Section 2.4.3) will allow to handle numerous samples at once, which joint to the cheap prices, will convert this methodology into an even more attractive alternative to microwave irradiation energy. As far as contamination concerns, the new glass probes will help to avoid the introduction into sample of non-desired elements from the titanium probes. In addition, the probe applicability will be expanded to analytical techniques with low limits of detection, such as ICP-MS, for which, avoiding contamination is an issue of primary importance. In terms of extraction rates, the technological advances seem not to present important improvements, since the new ultrasonic probes, such as the spiral probe or the glass probe, cannot deliver more ultrasonic power than the previous titanium ones. In fact, the glass probe has even lower amplitude, i.e., less ultrasonic power density than the titanium probe. This drawback can be related to the long sonication times reported in literature to get an acceptable elemental extraction rate from solid matrices when glass probe was used, as long as 20 min [11].

(ii) Shortening of sequential extraction schemes

Common sequential extraction schemes, such as the Tessier scheme or the BCR protocol, take long sample preparation times (BCR protocol c.a. 50 h). Different tentatives have been presented to date aiming to speed up such time-consuming procedures, using bath [12] or probe [13] sonication. However, those new approaches need to be tested in international trials, in order to get conditions for robust protocols. In this way, the new ultrasonic baths allowing two different frequencies of sonication at the same time or the new baths allowing amplitude and temperature control will help to find out conditions conducting to reproducible results wherever the protocol is applied.

(iii) Elemental speciation

Elemental speciation using ultrasonication has been done in different ways. On one hand, ultrasonication has been used for boosting the enzymatic kinetics [14] in order to degrade organic matter, in such a manner, that elemental organic species are extracted into solution without further degradation and can be easily detected by chromatographic-based techniques. This approach, formerly done with ultrasonic baths, has been recently successfully implemented with ultrasonic probes, for the speciation of Se, Hg and As from different matrices, such as oyster, mussel, yeast, chicken, fish and rice [15–18]. On the other hand, ultrasonication can be also used for distinguishing between elemental fractions, such as organic mercury from inorganic mercury or toxic arsenic [i.e., the sum of As(III) + As(V) + dimethylarsinic acid (DMA) + monomethylarsonic acid (MMA)] from arsenobetaine [19,20]. Although recent findings [21] suggest that probe sonication can be even used for a more selective As species extraction, that is, to differentiate As species, our lab experiences [22] put forward that this approach is non-robust, given to inter-conversion of As species, i.e., As(III) is transformed to As(V), and DMA and MMA are degraded to inorganic arsenic. Therefore, more research is expected in this specific area to find out whether probe sonication can be used for the aforementioned purpose or not. Once again, the silica probe and also the sonoreactor are going to play an interesting role in this approach. Their small energetic profile compared to the one given by titanium probes will probably also led to the extraction of the elemental species but with lower risks of species inter-conversion.

(iv) Extraction of organic species

Ultrasonic baths have been traditionally used for the extraction of organic molecules from solids [1], such as polychlorinated biphenyls (PCBs), nitrophenols, pesticides, alkylbencene sulphonate, additives from polymers and polycyclic aromatic hydrocarbons, PAHs. In addition, natural compounds, such as flavours from seeds, paclitaxel from Taxus tissue, opiates from hair samples and antioxidants from rosemary have been also extracted with baths. The new bath technology will allow the increment of extraction rates, since the ultrasonic energy is distributed more homogeneously inside the bath. In addition, the temperature control will also help to increase the performance of the extraction, by helping to speed up the kinetics involved in the processes. Ultrasonic probes can also be used for the extraction of organics. In fact, the USEPA recommends in its method 3550B for the determination and quantification of its 16 priority PAHs pollutant list, ultrasonication with probe. Nevertheless, it must be bore in mind that organic molecules can be extracted but also can be destroyed or easily volatilized when probe is used [7]. New trends are expected in this area mainly focused in two new devices, the previously referred glass ultrasonic probe and sonoreactor. Both systems are able to deliver ultrasonic energy in an intermediate level, higher than the ultrasonic bath but lower than the titanium ultrasonic probe. In other words, higher extraction rates with lower risks of degradation are anticipated.

(v) Electroanalytical applications

Most of the electro-analytical applications of ultrasonic power are related to ultrasonic probes and are devoted to enhance the mass transport processes involved in the near surface of the electrodes or to take advantage of the oxidation processes produced by the cavitation phenomena [23,24]. In addition, some interesting works dealing with theoretical calculations regarding kinetics involved in the enhancement of electroanalytical signals due to ultrasonic power are described in literature [25,26]. The references given from Professor Compton [23,24] and his related works are highly recommended in this area of application for electrochemistry researchers. Here, the role to be played by the glass probe will be remarkable, since the metal contamination produced by titanium probes has limited the applicability of the method to some metals and to some concentration levels.

4. New ultrasonic applications

4.1. Application to proteomic research

This area of research is growing up quickly. Recent findings have dramatically transformed the way by which sample treatments for protein identification have been traditionally done, reducing the times needed to identify proteins from 12 to 24 h to less than 60 min (the whole procedure). The most time-consuming step from protein identification used to be the trypsin digestion, especially for proteins separated by gel electrophoresis. When sonication with probe or the sonoreactor technology are used [27], the enzymatic kinetics are boosted in such a way that less than 5 min are enough for protein degradation, producing the peptides that are used then to identify the proteins by matrix-assisted laser desorption time of flight mass spectrometry, using a methodology called peptide mass fingerprint, PMF [28–30]. In this way, sample throughput for protein identification will benefit from the new ultrasonic devices accomplishing simultaneous sonication at two different frequencies due to the higher ultrasonic power supplied and homogeneous intensity distribution. Furthermore, the capabilities of ultrasonic baths joint low sonication frequencies (e.g. 35 kHz) with thermostat need to be further explored, bearing in mind that enzymatic

kinetics are also boosted al high temperatures (e.g. 60 °C). In this application, the sonoreactor technology has the advantage over the ultrasonic probes of simplicity for handling and higher throughput [29].

4.2. Application to polymer research

Recent literature stressed the applicability of joint ultrasonic power with imprinted polymers in two different ways. On one hand, the influence of sonication on the preparation of molecularly imprinted polymers, MIPs, toward theophylline showed that MIPs prepared in an ultrasonic bath operating at 35 kHz displayed binding and separation characteristics similar to those of the reference MIPs prepared using more traditional protocols.

In addition, results showed that sonication can be used as a tool for the preparation of MIPs, thus offering the chemist a way of increasing the solubility of troublesome templates [31]. On the other hand, speciation of organotin compounds was possible by a two-step procedure that jointed solid–liquid extraction done with probe sonication with an imprinted polymer designed for tributyltin. The accuracy, precision and limit of detection were improved when comparing with standard protocols [32]. The last procedure was evaluated against reference materials.

4.3. Application to pesticide research

A new finding recently described in literature [33] has opened new trends highlighting the remarkable influence of the frequency of sound for some analytical applications. Thus, a bath with two frequencies, at 35 and 130 kHz, was tested as a way to speed up the kinetics for transfer pesticides from honey to a SPME fiber. The 35 kHz frequency provided worst results since the recoveries were lower, probably because at that frequency the cavitation phenomena interfere with the liquid–solid separation process (the lower the frequency, the higher the cavitation phenomena), doing it difficult. It must be kept in mind that low frequencies are used for solid–liquid extraction processes. On the other hand, at 130 kHz, the separation process was enhanced in such a way that, for the same extraction time, recoveries for four pesticides were higher being the RSDs lower than the ones obtained with magnetic stirring or sonication at 35 kHz. Therefore, an interesting future trend would be to establish if higher frequencies would be used for making liquid–solid extraction processes faster.

4.4. On-line applications

The on-line uses of ultrasound are still involved in some controversy. A detailed description of on-line systems employing sonication with baths can be found in literature [3,4]. Most of the on-line described methods are based on a column immersed into the bath previously filled with a resin or with the sample, in which a liquid–solid or solid–liquid extraction or both processes, one before another, takes place under the ultrasonic field provided by the bath. However, some physical limitations of this approach make it only available for few applications. Thus, the ultrasonic waves need to cross the walls of the column to reach the resin/sample. Taking into account that baths are not a powerful ultrasonic energy source, the effects inside the column are very limited, especially for the resin/sample deep inside the column. Thus, the on-line approach using columns in ultrasonic baths, even with the extra ultrasonic energy provided by an external ultrasonic probe (see Fig. 4) was unsuccessful for back-extracting mercury from a resin in which it was previously pre-concentrated from a liquid sample [34]. Therefore, an on-line approach taking advantage of the high ultrasonic power energy provided by titanium probes was mandatory being recently published, a work that accomplished for the first time (see Fig. 4) a sequential/flow injection system allowing on-line probe sonication [35]. For the on-line applications, the new bath technology is not very promising, since the drawbacks of column walls will always remain. In this sense, the sonoreactor will successfully substitute the ultrasonic bath, since it is 50 times more powerful; however, its real applicability needs further confirmation. In contrast, the glass probe is the most promising device to be used in on-line applications since will not add metal contamination into solution and can be easily adapted to the on-line system described in Fig. 5.

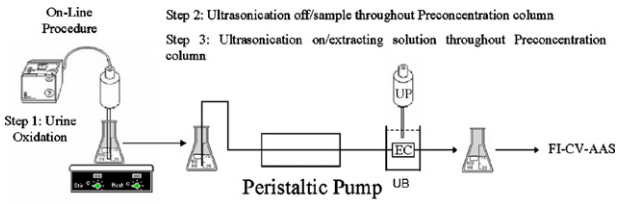

Fig. 4. On-line ultrasonic sample treatment, jointing ultrasonication with bath and probe for on-column Hg solid–liquid extraction. (UP) ultrasonic probe; (UB) ultrasonic bath; (FI-CV-AAS) flow injection cold vapor atomic absorption spectrometry (adapted from reference [34]).

5. Future prospects

Ultrasonic-based sample treatment procedures are going to be in the arena for long. As a matter of fact, it is expected an upcoming of works dealing with analytical applications of the new, powerful and technologically advanced ultrasonic devices described in the first part of this manuscript. Some of the new areas of application, such as proteomics, will open the gates for further new ones. As an example, some of the approaches previously described for proteomics can be easily adapted to the other "-omics" methodologies, such as metabolomics or genomics.

There is also a need to develop some international trials in order to verify if the present state-of-the-art of ultrasonic extraction from solid material for elemental quantification is a robust procedure or, on the contrary, still needs further development. Those trials are even more important if we consider that fast sequential extraction schemes are an alternative of remarkable importance to the traditional, time-consuming ones.

New on-line approaches are also anticipated, specially devoted to the sonoreactor device. Joint ultrasonic bath and probe in the same on-line procedure but taking advantage of

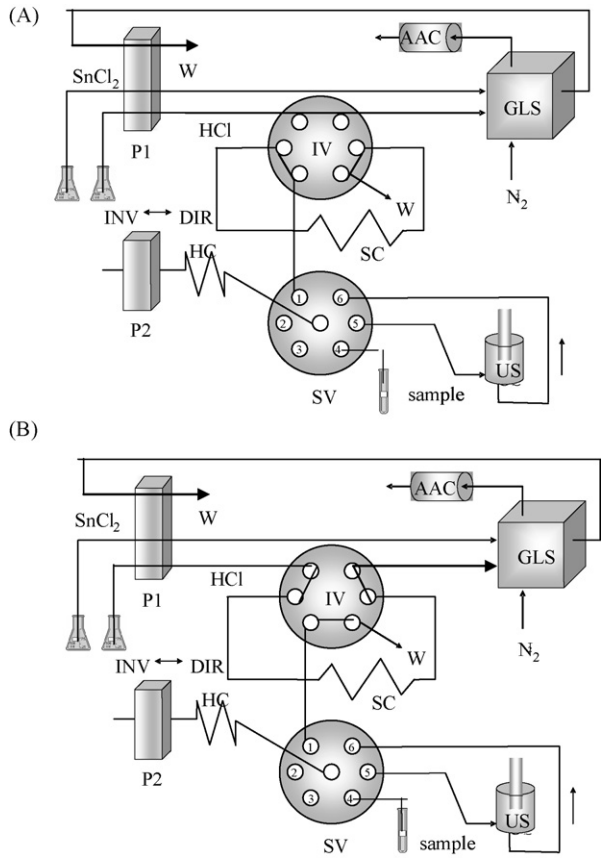

Fig. 5. SIA/HIFU/FIA manifold for on-line determination of mercury by cold vapor atomic absorption spectroscopy. Key: ($SnCl_2$) $SnCl_2$ solution; (HCl) HCl solution; (sample) sample solution mixed with HCl and NaClO; (P1 and P2) peristaltic pumps; (INV) inverse flow; (DIR) direct flow; (HC) holding coil; (IV) injection valve with a 500-μL sample loop; (SV) selection valve; (W) waste; (AAS) atomic absorption spectrometry; (GLS) gas–liquid separator; (N_2) stream of N_2; (US) ultrasonic probe. (A) Injection valve in load position. (B) Injection valve in injection position. (CR) chemical reactor (adapted from reference [35]).

the different properties of each one is also expected as a new promising area.

6. Conclusions

Sonic energy and its applications for the analytical laboratory are old, yet full of life in research area. The novel technological advances in ultrasonic engineering and their recent applications in analytical and bio-analytical chemistry open new and fascinating lines of investigation that deserve the effort of the analytical community in order to find out what is still hidden from human knowledge in aspect so diverse like proteomics or environmental chemistry.

The latest advances in ultrasonic devices along with their most recent applications for analytical chemistry have been described in this work with the aim to aid those researchers involved in this area or those who would like to join this interesting field of research to get a rapid overview about what can be expected from ultrasonic power and how to handle with.

References

[1] J.L. Capelo, A.M. Mota, Curr. Anal. Chem. 1 (2005) 193.
[2] J.L. Capelo, C. Maduro, C. Vilhena, Ultrason. Sonochem. 12 (2005) 225.
[3] F. Priego-Capote, M.D. Luque de Castro, TrAC, Trends Anal. Chem. 23 (2004) 644.
[4] F. Priego-Capote, M.D. Luque de Castro, TrAC, Trends Anal. Chem. 23 (2004) 829.
[5] T.J. Mason, Sonochemistry, Oxford University Press, Oxford, UK, 1999.
[6] J.L. Capelo-Martinez, P. Ximenez-Embun, Y. Madrid-Albarrán, C. Camara, TrAC, Trends Anal. Chem. 23 (2004) 331.
[7] J.L. Capelo, M.M. Galesio, G.M. Felisberto, C. Vaz, J. Costa Pessoa, Talanta 66 (2005) 1272.
[8] K. Ashley, R.N. Andrews, L. Cavazos, M. Demange, J. Anal. At. Spectrom. 16 (2001) 1147.
[9] L. Amoedo, J.L. Capelo, I. Lavilla, C. Bendicho, J. Anal. At. Spectrom. 14 (1999) 1221.
[10] E.C. Lima, F. Barbosa, F.J. Krug, J. Anal. At. Spectrom. 14 (1999) 1913.
[11] D. Hristozov, C.E. Domini, V. Kmetov, V. Stefanova, D. Georgieva, A. Canals, Anal. Chim. Acta 516 (2004) 187.
[12] E. Dabek-Zlotorzynska, M. Kelly, H. Chen, C.L. Chakrabarti, Anal. Chim. Acta 498 (2003) 175.
[13] A.V. Filgueiras, I. Lavilla, C Bendicho, Anal. Bioanal. Chem. 37 (2002) 103.
[14] P. Bermejo, J.L. Capelo, A. Mota, Y. Madrid, C. Cámara, TrAC, Trends Anal. Chem. 23 (2004) 654.
[15] J.L. Capelo, P. Ximenez-Embun, Y. Madrid-Albarran, C. Camara, Anal. Chem. 76 (2004) 233.
[16] E. Sanz, R. Munoz-Olivas, C. Camara, J. Chromatogr. A 1097 (2005) 1.
[17] A.I. Cabanero, Y. Madrid, C. Camara, Anal. Bioanal. Chem. 381 (2005) 373.
[18] C. Pena-Farfal, A. Moreda-Pineiro, A. Bermejo-Barrera, P. Bermejo-Barrera, H. Pinochet-Cancino, I. de Gregori-Henriquez, Anal. Chim. Acta 548 (2005) 183.
[19] J.L. Capelo, I. Lavilla, C. Bendicho, Anal. Chem. 72 (2000) 4979.
[20] J.L. Capelo, I. Lavilla, C. Bendicho, Anal. Chem. 73 (2001) 3732.
[21] A. Huerga, I. Lavilla, C. Bendicho, Anal. Chim. Acta 534 (2005) 121.
[22] A. Correia, M. Galesio, H. Santos, R. Rial-Otero, C. Lodeiro, A. Oehmen, A.C.L. Conceição, J.L. Capelo, Talanta 72 (2007) 968.
[23] J. Davis, D.H. Vaughan, D. Stirling, L. Nei, R.G. Compton, Talanta 57 (2002) 1045.
[24] E.L. Beckett, N.S. Lawerence, R.G. Evans, J. Davis, R.G. Compton, Talanta 54 (2001) 871.
[25] F.M. Matysik, S. Matysik, A.M. Brett, C.M.A. Brett, Anal. Chem. 69 (1997) 1651.
[26] I.C. Stefan, Y. Mo, C.I. Zaneli, D.A. Scherson, Anal. Chem. 73 (2001) 4384.
[27] D. Lopez-Ferrer, J.L. Capelo, J. Vazquez, J. Proteome Res. 4 (2005) 1569.
[28] D. Lopez-Ferrer, B. Canas, J. Vazquez, C. Lodeiro, R. Rial-Otero, I. Moura, J.L. Capelo, TrAC, Trends Anal. Chem. 25 (2006) 996.
[29] R.J. Carreira, F.M. Cordeiro, A.J. Moro, M.G. Rivas, R. Rial-Otero, E.M. Gaspar, I. Moura, J.L. Capelo, J. Chromatogr. A 1153 (2007) 291.
[30] R. Rial-Otero, R.J. Carreira, F.M. Cordeiro, A.J. Moro, M.G. Rivas, L. Fernandez, I. Moura, J.L. Capelo, J. Proteome Res. 6 (2007) 909.
[31] J. Svenson, Anal. Lett. 39 (2006) 2749.
[32] M. Gallego-Gallegos, M. Liva, R.M. Oliva, C. Camara, J. Chromatogr. A 1114 (2006) 8.
[33] R. Rial-Otero, E.M. Gaspar, I. Moura, J.L. Capelo, Talanta 71 (2007) 1906.
[34] A. Patricio, C. Fernandez, A.M. Mota, J.L. Capelo, Talanta 69 (2006) 769.
[35] C. Fernandez, A.C.L. Conceicao, R. Rial-Otero, C. Vaz, J.L. Capelo, Anal. Chem. 78 (2006) 2494.

Available online at www.sciencedirect.com
ScienceDirect
Talanta 73 (2007) 857–861
Talanta
www.elsevier.com/locate/talanta

In situ prepared polypyrrole for low humidity QCM sensor and related theoretical calculation

Yi-Lu Sun [a], Ren-Jang Wu [b], Yu-Ching Huang [b], Pi-Guey Su [c], Murthy Chavali [d], Yi-Zhen Chen [a], Chu-Chieh Lin [a,*]

[a] *Department of Chemistry, National Chung Hsing University, Taichung 402, Taiwan, ROC*
[b] *Department of Applied Chemistry, Providence University, Shalu, Taichung Hsien 433, Taiwan, ROC*
[c] *Department of Chemistry, Chinese Culture University, Taipei 111, Taiwan, ROC*
[d] *Center for Measurement Standards, Industrial Technology Research Institute, Hsinchu 300, Taiwan, ROC*

Received 13 March 2007; received in revised form 1 May 2007; accepted 1 May 2007
Available online 10 May 2007

Abstract

In situ preparation of polypyrrole (Ppy) by photo-polymerization coated on a quartz crystal microbalance (QCM) as a low humidity sensor was reported. Different concentrations of Ppy films say 0 wt.% (as blank), 0.1, 1, and 10 wt.% were investigated to measure humidity concentrations between 14.7 and 5412.5 ppm_v. The adsorption/desorption behavior was also examined at humidity concentration 510.2 ppm_v. The sensitivities of 0, 0.1 and 1 wt.% Ppy films at 51.5 ppm_v were 0.143, 0.219 and 0.427, respectively. For 1 wt.% Ppy, the highest sensitivity was obtained. The slope and correlation coefficients (R^2) for 1 wt.% Ppy at the ranges of 14.7–898.6 ppm_v were 0.0646 and 0.9909, respectively. A series of molecular simulations have been carried out to calculate bond energy for the water molecule interaction with Ppy, which was found to be ∼3 kcal/mol indicating the existence of hydrogen bonding during the sorption process. Based on Langmuir isotherm adsorption assumption, for 0.1 and 1 wt.% Ppy films, the association constants were 2606.30 and 5792.98, respectively. This larger association constant for 1 wt.% Ppy film explains higher sensitivity.

Keywords: Low humidity sensor; Polypyrrole; QCM; Photo-polymerization; Association constant

1. Introduction

Humidity is one of the most commonly measured physical quantities, significant to a wide variety of fields, like environmental, food and agriculture, industrial, clinical and biotechnological fields. In many specialty industries, nowadays low humidity detection becoming mandatory. Whilst measuring low humidity levels, often there has been great amount of confusion about the accuracy in humidity measurement. Notably, several promising technologies has been developed and applied to revolutionize the design of the accurate humidity sensors. However, it still remains demanding to develop a humidity sensor with complete set of characteristics, like, good linearity, high sensitivity, low hysteresis, rapid response time and obviously with low cost. Of the various sensing technologies for humidity detection, a majority are capacitive hygrometers, a conductive layer covered with an organic substance/polymer and a metallic layer thin enough to be porous to water vapor.

The quartz crystal microbalance (QCM) is an extremely sensitive mass sensor in the nanogram scale. The QCM detectors have also been used for a long time to monitor low humidity with wide measuring range contributing to several advantages [1–4]. The quantitative relationship between changes of frequency Δf (Hz) of piezoelectric crystal and the mass change caused by mass loading on the piezoelectric crystal surface have firstly derived by Sauerbrey [5]:

$$\Delta f = \left(-2.3 \times 10^6 \frac{f_o^2}{A}\right) \Delta m \quad (1)$$

where f_o (MHz) is the basic frequency of the unloaded piezoelectric crystal, A (cm^2) the surface area of the electrode, and Δm (g) is the change in mass on the surface of the crystal.

* Corresponding author. Tel.: +886 4 22840411x718; fax: +886 4 22862547.
E-mail address: cchlin@mail.nchu.edu.tw (C.-C. Lin).

0039-9140/$ – see front matter © 2007 Published by Elsevier B.V.
doi:10.1016/j.talanta.2007.05.002

Different sensing materials, such as modified nitrated polystyrene [6], TiO_2 nanowires/PAMPS [7], Nafion-Ag [8], MWCNTs/Nafion [9], SWCNTs/Nafion [10] and polypyrrole [11] were developed as films and are coated on the QCM electrode to detect vapor and humidity. Conducting polymers and their composites were extensively studied for the past two decades for applications like optical electronics [12], solar cell [13,14] and other sensing fields [15–17]. In recent years they have emerged as new type of smart materials for humidity sensing. Several sensors using conducting polymer materials were reported in the literature [11,18–21]. QCM sensors coated with conducting polypyrrole as sensing material for measuring humidity with relative humidity range [11], and hydrogen bonding was mentioned in humidity sensing by Collins and Buckley [19].

In this paper, we prepared Ppy coated over QC electrodes by photo-polymerization instead of complicated synthesis methods, and applied for low humidity sensing between 14.7 and 5412.5 ppm_v. Materials Studio® Version 3.2 (http://www.accelrys.com/products/mstudio/, Accelrys Software Inc.) was used for series of molecular simulations to calculate bond energy, towards water molecule adsorption to the Ppy surface, the bond distance between oxygen and hydrogen was calculated as 2.305 Å and the bond energy is around 3 kcal/mol that attribute to the presence of hydrogen bonding in the sorption process. At lower water vapor concentration, sensitivites are higher and the sorption behaviors were also calculated by the Langmuir isotherm adsorption conditions [8].

2. Experimental

2.1. Material preparation

All the chemicals used are analytical reagent (AR) grade (purity > 99%), purchased from Sigma–Aldrich Co., Inc., USA, unless otherwise mentioned. All the chemicals were used as received. Water was distilled and deionized (DI) using a 'Milli-Q' water purification system (Millipore Corp.).

Different concentrations of 10, 1, 0.1 and 0 wt.% of pyrrole (C_4H_5N) in ethanol (EtOH, 95%) were prepared and to these concentrations of pyrrole in EtOH solution, a 10 mol% of silver nitrate ($AgNO_3$) was added as an electron acceptor during photo-polymerization. The mixtures were sonicated for less than a minute, until the added $AgNO_3$ was completely dissolved. No significant data was obtained for the 10 wt.% Ppy, as the crystal could not oscillate further due to overloading.

2.2. Electrode of QCM fabrication

Planar AT-cut quartz crystals (QC) of 5 mm in diameter with a fundamental resonance frequency of 9 MHz were obtained from Affinity New Technology Co. Ltd., Taiwan. The gold electrode of the QCM was rinsed with DI water and then thoroughly cleaned ultrasonically in acetone. After drying, both sides of the QCM electrode were coated with the mixture solution. Polypyrrole (PPy) was synthesized using a UV-irradiation method [22]. A sensing film was coated onto quartz piezoelectric crystals using a commercial spin coater. The films were left 15 h under UV light (365 nm) to allow polymerization to complete, resulting in slightly black coloured films. The uncoated quartz crystal was used to compare the sensitivity with that of the doubly coated quartz crystal. All experiments were performed at room temperature (23.0 ± 1.5) °C

2.3. Equipment

Quartz crystal microbalance (ANT Inc., Taiwan) used in this study was a modified version from P-Sensor 1000, equipped with an ultra-high frequency counter (custom designed and fabricated for CMS/ITRI, by Affinity New Technology Co. Ltd., Taiwan; Chang, et al., USPTO 6557416, 06th May 2003) for counting the pulse signals and a potentiostat (PE-1000; Model #AA7706061, Affinity New Technology Co. Ltd., Taiwan) and a Spin Coater (PM-490, SWIENCO, YEONG SHIN Co. LTD, Taiwan). A divided humidity generator was used as the principal facility for producing the test gases. Required water vapor concentration was obtained by adjusting the proportion of dry and humid air generated by the divided flow humidity generator. The lowest testing point is limited by the dryness of the gas. A low humidity hygrometer (HYGROCLIP IC-3, Rotronic Inc., USA) and a QCM sensor were connected to an outlet of the divided flow humidity generator. The low humidity hygrometer was used as the reference standard for calibrating the QCM sensor. The volume ratio of the moist air was adjusted according to the reading of the low humidity hygrometer traceable to the National Measurement Laboratory, Taiwan (NML) humidity laboratory. The volume ratio of the moist air was calculated by the following equation:

$$ppm_v = \frac{V_v}{V} \times 10^6 \quad (2)$$

$$ppm_v = \frac{e}{P - e} \times 10^6 \quad \text{(ideal gas)} \quad (3)$$

where V_v is the volume of water vapor, V the total volume, e the partial pressure of water vapor and P is the total pressure. The schematic sketch of the system was shown in Fig. 1. Bond energy was calculated using Materials Studio® Version 3.2 software (Accelrys Software Inc.) evaluating the adsorption behavior of water vapor and Ppy.

3. Results and discussion

3.1. Adsorption simulation studies

Molecular simulations were done for hydrogen bonding energy calculation towards water molecule bonding to the Ppy surface was investigated. The total potential energies of Ppy and water molecules adsorbed Ppy is denoted as Ut(Ppy) and Ut(Ppy + H_2O), respectively. The hydrogen bond energy is the difference of total potential energy to the combined sum of potential energies of Ppy and H_2O, depicted in the form of equation as Ut(Ppy + H_2O) − (Ut(Ppy) + Ut(H_2O)). Thus, calculated adsorption simulation results for 1–50 water molecules were shown in Fig. 2.

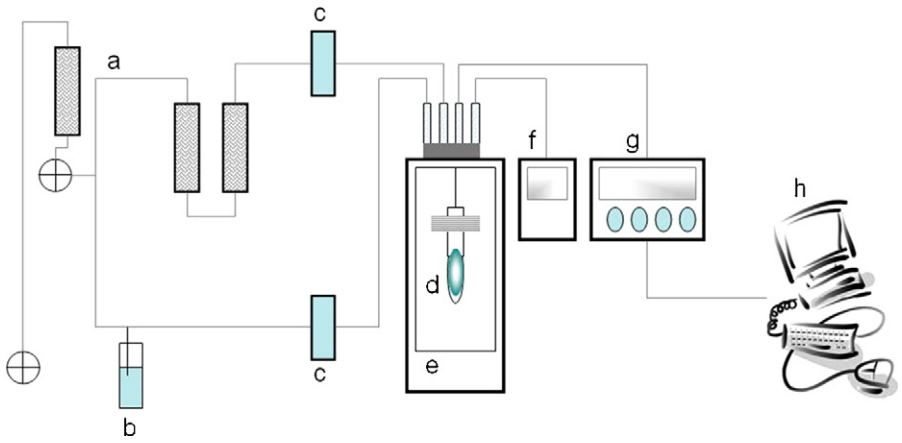

Fig. 1. Scheme of the experimental set-up for the QCM sensor and low humidity atmosphere controller. (a) Molecular sieve and desiccating agent; (b) water; (c) mass flow controller; (d) detecting chamber and QCM; (e) thermostat; (f) low humidity hygrometer; (g) oscillator and frequency counter; (h) PC.

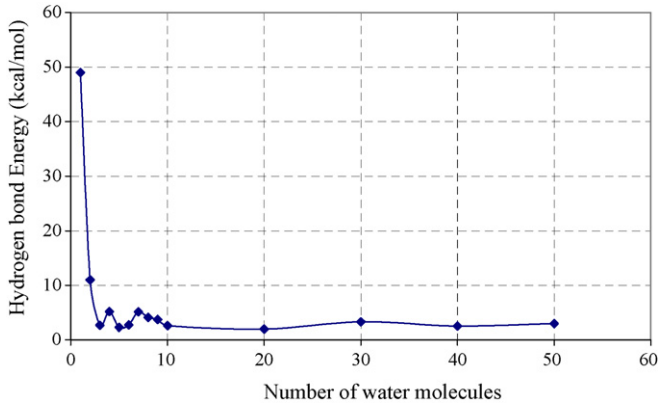

Fig. 2. Number of water molecules vs. hydrogen bond energy.

The local adsorption geometry for the adsorption of 10 water molecules onto the Ppy surface is shown in Fig. 3, which explains the oxygen atom of water vapor was bonded to the H atom of Ppy. The bond distance between the oxygen atom of water molecule and the hydrogen atom from the Ppy is around 2.305 Å, the bond energy is close to 3 kcal/mol with increase in adsorption of water molecules.

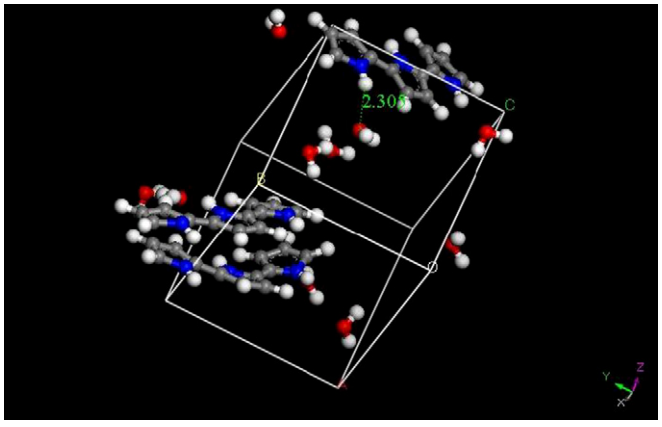

Fig. 3. Local adsorption geometry for the adsorption of 10 water molecules on to the Ppy surface (red: oxygen; white: hydrogen; blue: nitrogen and gray: carbon). (For interpretation of the references to colour in this figure legend, the reader is referred to the web version of the article.)

3.2. Low humidity sensing properties of Ppy films

The response time (T_{90}) and recovery time of the 1 wt.% Ppy films were 48 and 91 s, respectively, at the testing point of 510.2 ppm_v (Fig. 4). The frequency shifts and sensitivity of 1 and 0.1 wt.% Ppy films for different volume ratios of the moist air, 14.7–5412.5 ppm_v, are plotted in Fig. 5. Calibration curves were plotted for 1 and 0.1 wt.% Ppy films for the volume ratio, ranging from 0 to 6000 ppm_v (Fig. 6). Fig. 7 illustrates the calibration plots with frequency change ($-\Delta$Hz) as a function of volume ratio ranging from 0 to 1000 ppm_v for 0.1 and 1 wt.% Ppy films. The correlation coefficient (R^2) for 0.1 and 1 wt.% Ppy films are 0.9909 and 0.9799, respectively.

As shown in Table 1, when the volume ratio of moist air was 51.1 ppm_v, the sensitivity of 0, 0.1 and 1 wt.% Ppy films were 0.143, 0.219, and 0.427, respectively. These results demonstrated that the sensitivity of 1 wt.% Ppy film was higher than that of 0 and 0.1 wt.% Ppy films, especially at humidity lower than 898.6 ppm_v. The calibration curve of 1 wt.% Ppy film showed an acceptable linear behavior with slope and correlation coefficient of 0.0646 and 0.9909 Hz/ppm_v, respectively. The comparative results for low humidity sensing characteristics of 1 and 0.1 wt.% Ppy films are given in Table 2. The sensing characteristics of 1 and 0.1 wt.% Ppy films at the ranges of 14.7–898.6 ppm_v and 898.6–5412.5 ppm_v

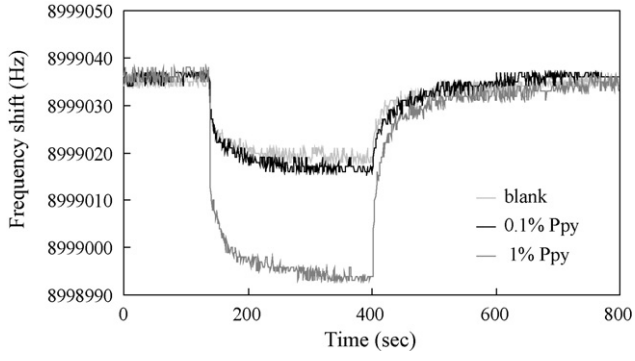

Fig. 4. Reversibility of adsorption of water vapors (510.2 ppm_v) on 0, 0.1 and 1 wt.% Ppy films.

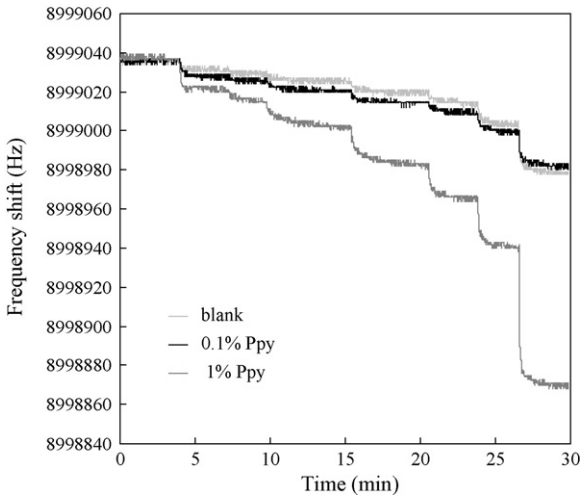

Fig. 5. Frequency shifts (Hz) as a function of time (s) for different volume ratio of the moist air on 0, 0.1 and 1 wt.% Ppy films.

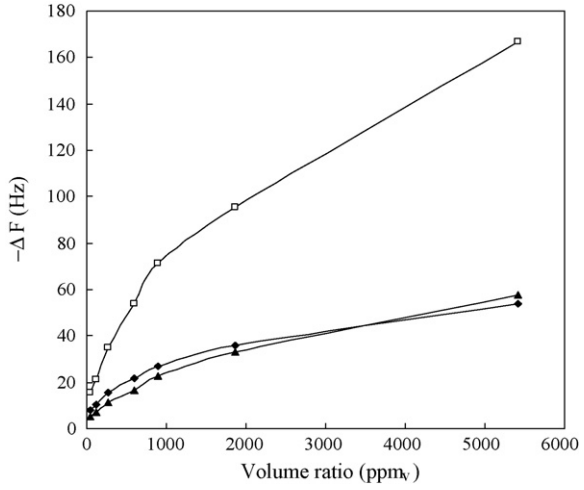

Fig. 6. Frequency change (−ΔHz) as a function of volume ratio (ppm_v) for 0 wt.% (▲), 0.1 wt.% Ppy (♦) and 1 wt.% Ppy (□) films.

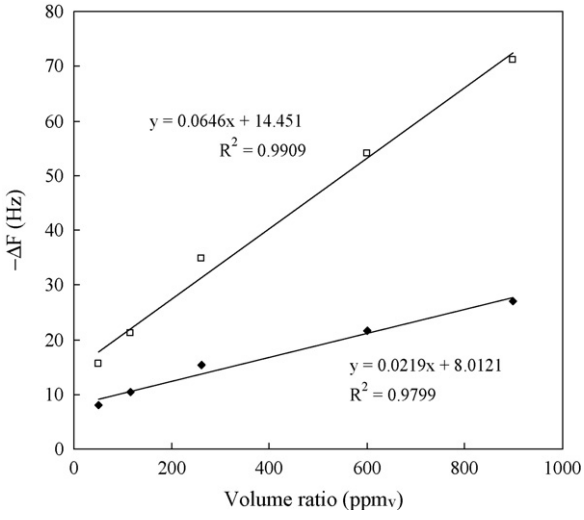

Fig. 7. Frequency change (−ΔHz) as a function of volume ratio (ppm_v) for 0.1 wt.% Ppy (♦) and 1 wt.% Ppy (□) films.

Table 1
The sensitivity of the 0, 0.1 and 1 wt.% Ppy films coated on QCM for different volume ratios of moist air

Volume ratio (ppm_v)	Sensitivity[a]		
	0 wt.%	0.1 wt.% Ppy	1 wt.% Ppy
51.1	0.143	0.219	0.427
116.7	0.067	0.101	0.209
261.6	0.045	0.062	0.141
599.8	0.028	0.037	0.092
898.6	0.025	0.031	0.081
1870.5	0.018	0.019	0.051
5412.5	0.011	0.010	0.031

[a] The sensitivity of the various sensing film was defined as $-\Delta Hz/\Delta ppm_v$ [6].

were shown different performances as expected. The slopes at 14.7–898.6 ppm_v were larger than 898.6–5412.5 ppm_v, underlining that the physical adsorption of the sensing films with water vapor was attaining saturation. They were in the order: 1 wt.% Ppy > 0.1 wt.% Ppy > 0 wt.%. This result explained that the sensitivity of the Ppy films increases with the coated Ppy amount.

3.3. Adsorption properties of 1 and 0.1 wt.% Ppy f ilms

In order to elucidate the effect of Ppy percentages in sensing humidity, the adsorption dynamics of water vapor molecules onto the Ppy films say, 1, 0.1 and 0 wt.% that are coated on QC were investigated. The observed shift in frequency for the 1 wt.% Ppy film was the highest. It was also noted that desorption of water molecule from 1 wt.% Ppy film was relatively slower than 0.1 wt.% film. The process of adsorption and desorption of water on 1 and 0.1 wt.% Ppy thin films was found to be reversible. The results also implied that 1 wt.% Ppy film had larger affinity to water vapor molecules than 0.1 wt.% Ppy film.

Comparing the adsorption behaviors of water vapor molecules onto 1 and 0.1 wt.% Ppy films and explanation increasing the sensitivity of humidity sensing of higher percentage of Ppy, the following reaction was adopted as the following described [8]:

$$\text{Sensing films} + \text{H}_2\text{O vapor molecules} \underset{k_2}{\overset{k_1}{\rightleftarrows}} \text{Sensing films} - \text{H}_2\text{O vapor molecules} \quad (4)$$

where k_1 and k_{-1} are referred to binding rate constant and dissociation rate constant, respectively. The formed amount of water

Table 2
The comparison of low humidity sensing characteristics of 0.1 and 1 wt.% Ppy films

Sensing characteristics		0 wt.%	0.1 wt.% Ppy	1 wt.% Ppy
14.7–898.6 ppm_v	Slope	0.0199	0.0219	0.0646
	Linearity[a]	0.9917	0.9799	0.9909
898.6–5412.5 ppm_v	Slope	0.0076	0.0057	0.0209
	Linearity[a]	0.9913	0.9825	0.9984

[a] Correlation coefficient.

Table 3
Kinetic parameters for binding and dissociation of water vapor molecules onto 0.1 and 1 wt.% Ppy films

Films	Binding rate constant k_1 ($M^{-1}\,s^{-1}$)	Dissociation rate constant k_{-1} ($s^{-1}10^{-2}$)	Association constant K ($M^{-1}10^2$)
0.1 wt.%	405.54	0.1556	2606.30
1 wt.%	586.25	0.1012	5792.98

vapor molecules, Δm_t, on the sensing films at time t, is then given by the following equations under Langmuir isotherm adsorption conditions [8]:

$$\Delta m_t = \Delta m_\infty \left[1 - \exp\left(\frac{-t}{\tau}\right)\right] \quad (5)$$

$$\frac{-t}{\tau} = \ln\left[\frac{\Delta m_\infty - \Delta m_t)}{\Delta m_\infty}\right] \quad (6)$$

$$\tau^{-1} = k_1[\text{water vapor molecules}] + k_{-1} \quad (7)$$

where Δm_∞ is the maximal adsorbed amount of water vapor molecules on sensing films at $t \to \infty$ and τ^{-1} is relaxation time. Utilizing Eqs. (5)–(7), the binding rate constant k_1, dissociation rate constant k_{-1} and association constant K ($K = k_1/k_{-1}$) for water vapor molecules onto the sensing films (1 and 0.1 wt.% Ppy) were calculated and listed in Table 3. The 0.1 wt.% Ppy-water vapor molecules showed a largest k_{-1} value. This agrees with the result that water vapor molecule was easier to dissociate from 0.1 wt.% Ppy than 1 wt.% Ppy film. The association constant, K of water vapor molecules onto the 1 wt.% Ppy sensing films was larger than 0.1 wt.% Ppy film, indicates that 1 wt.% Ppy coated films to water vapor molecules were more sensitive than 0.1 wt.% film at lower humidity range (shown in Tables 1 and 2).

4. Conclusion

Polypyrrole (Ppy) prepared *in situ* by photo-polymerization was used in combination with QCM for low humidity sensing. 10, 1, 0.1 and 0 wt.% Ppy coated QCM electrodes were fabricated, of which 1 wt.% Ppy film showed the highest sensitivity, especially at low humidity with an acceptable linearity, far better than the 0.1 wt.% Ppy. The sensitivity for the 10 wt.% Ppy was not obtained, as the crystal could not oscillate due to overloading. Based on these results so far obtained in this study, the conducting Ppy film coated over the QCM crystal can be considered a reliable technique for the measuring trace humidity. Langmuir isotherm adsorption assumption showed larger association constant, K for water vapor molecules on 1 wt.% Ppy than 0.1 wt.% Ppy films coated on QCM. The results also demonstrate that the water vapor molecules were being adsorbed easily on the 1 wt.% Ppy than on 0.1 wt.% Ppy film, owing to their larger sensitivity. Accelrys Software, Materials Studio modeled the adsorption of water molecule onto the Ppy surface, the calculations indicate the existence of hydrogen bonding as suggested by the earlier researchers.

Acknowledgement

Financial support from the National Science Council of Republic of China is greatly appreciated.

References

[1] Y. Zhang, K. Yu, R. Xu, D. Jiang, L. Luo, Z. Zhu, Sens. Actuators A 120 (2005) 142–146.
[2] F.P. Delannoy, B. Sorli, A. Boyer, Sens. Actuators B 84 (2000) 285–291.
[3] P.R. Story, D.W. Galipeau, R.D. Mileham, Sens. Actuators B 24–25 (1995) 681–685.
[4] C. Lu, A.W. Czanderna, Elsevier, Amsterdam, 1984.
[5] G. Sauerbrey, Z. Phys. 155 (1959) 206–222.
[6] M. Neshkova, R. Petrova, V. Petrov, Anal. Chim. Acta 332 (1996) 93–103.
[7] P.G. Su, Y.L. Sun, C.C. Lin, Talanta 69 (2006) 946–951.
[8] L.X. Sun, T. Okada, Anal. Chim. Acta 421 (2000) 83–92.
[9] P.G. Su, Y.L. Sun, C.C. Lin, Sens. Actuators B 115 (2006) 338–343.
[10] H.W. Chen, R.J. Wu, K.H. Chan, Y.L. Sun, P.G. Su, Sens. Actuators B 104 (2005) 80–84.
[11] V. Syritski, J. Reut, A. Öpik, K. Idla, Synth. Met. 102 (1999) 1326–1327.
[12] K. Yoshino, K. Kaneto, S. Takeda, Synth. Met. 18 (1987) 741–746.
[13] B.J. Landi, R.P. Raffaelle, S.L. Castro, S.G. Bailey, Prog. Photovolt.: Res. Appl. 13 (2005) 165–172.
[14] A.A.R. Watt, D. Blake, J.H. Warner, E.A. Thomsen, E.L. Tavenner, H. Rubinsztein-Dunlop, P. Meredith, J. Phys. D Appl. Phys. 38 (2005) 2006–2012.
[15] A. Riul Jr., R.R. Malmegrim, F.J. Fonseca, L.H.C. Mattoso, Biosens. Bioelec. 18 (2003) 1365–1369.
[16] F. Musio, M.E.H. Amrani, K.C. Persaud, Sens. Actuators B 23 (1995) 223–226.
[17] Q. Pei, O. Inganäs, Synth. Met. 57 (1993) 3730–3735.
[18] A.C. Partridge, M.L. Jansen, W.M. Arnold, Mater. Sci. Eng. C 12 (2000) 37–42.
[19] G.E. Collins, L.J. Buckley, Synth. Met. 78 (1996) 93–101.
[20] Y. Li, M.J. Yang, G. Casalbore-Miceli, N. Camaioni, Synth. Met. 128 (2002) 293–298.
[21] V. Syritski, J. Reut, A. Opik, K. Idla, Synth. Met. 120 (1999) 1326–1327.
[22] P. Poddar, J.L. Wilson, H. Srikanth, S.A. Morrison, E.E. Carpenter, Nanotechnology 15 (2004) S570–S574.

Available online at www.sciencedirect.com
ScienceDirect
Talanta 73 (2007) 913–919
Talanta
www.elsevier.com/locate/talanta

Voltammetric behaviour of bromhexine and its determination in pharmaceuticals

M. Turchán, P. Jara-Ulloa, S. Bollo, L.J. Nuñez-Vergara, J.A. Squella, A. Álvarez-Lueje *

Bioelectrochemistry Laboratory, Chemical and Pharmaceutical Sciences Faculty, University of Chile, P.O. Box 233, Santiago 1, Chile

Received 16 March 2007; received in revised form 3 May 2007; accepted 11 May 2007
Available online 21 May 2007

Abstract

A complete electrochemical study and a novel electroanalytical procedure for bromhexine quantitation are described. Bromhexine in methanol/0.1 mol L^{-1} Britton–Robinson buffer solution (2.5/97.5) shows an anodic response on glassy carbon electrode between pH 2 and 7.5. By DPV and CV, both peak potential and current peak values were pH-dependent in all the pH range studied. A break at pH 5.5 in E_P versus pH plot revealing a protonation–deprotonation (pK_a) equilibrium of bromhexine was observed. Spectrophotometrically, an apparent pK_a value of 4.3 was also determined.

An electrodic mechanism involving the oxidation of bromhexine via two-electrons and two-protons was proposed. Controlled potential electrolysis followed by HPLC–UV and GC–MS permitted the identification of three oxidation products: *N*-methylcyclohexanamine, 2-amino-3,5-dibromobenzaldehyde and 2,4,8,10-tetrabromo dibenzo[*b*,*f*][1,5] diazocine.

DPV at pH 2 was selected as optimal pH for analytical purposes. Repeatability, reproducibility and selectivity parameters were adequate to quantify bromhexine in pharmaceutical forms. The recovery was $94.50 \pm 2.03\%$ and the detection and quantitation limits were 1.4×10^{-5} and 1.6×10^{-5} mol L^{-1}, respectively. Furthermore, the DPV method was applied successfully to individual tablet assay in order to verify the uniformity content of bromhexine. No special treatment of sample were required due to excipients do not interfered with the analytical signal. Finally the method was not time-consuming and less expensive than the HPLC one.

Keywords: Bromhexine; Differential pulse voltammetry; Tablets; Oxidation mechanism

1. Introduction

Bromhexine, 2-amino-3,5-dibromo-*N*-cyclohexyl-*N*-methylbenzenemethanamine (Fig. 1), is a mucolytic agent used in the treatment of respiratory disorders associated with viscid or excessive mucus [1,2]. The drug is well absorbed by oral route and spreads to the tissues, included the bronchial epithelium, where reaches sufficient concentrations to act locally. It undergoes oxidation and conjugation hepatic biotransformation, and the drug and its metabolites are excreted in urine and feces [3]. Its pharmacological effect begins at 24–48 h and reaches its maximum to 5–7 days.

The drug has been quantified using different methods, in pharmaceutical forms [4–18] and in biological fluids [19–22]. For these purposes, UV–vis spectrophotometry [4–9], flow injection analysis with ion-selective electrodes [5], liquid chromatography [10–15,19,20], inductively coupled plasma mass spectrometry [20], capillary isotachophoresis [16], electrokinetic chromatography [17], liquid–gas chromatography [10,18] and gas chromatography with mass detection [22] have been employed.

From the electrochemical point of view, bromhexine has been also assayed by using chromatography with potentiometric detection [11] without an electrochemical characterization. On the other hand, its active metabolite, ambroxol (4-[[(2-amino-3,5-dibromophenyl)methyl]amino]cyclohexanol), has been assayed in human serum using chromatography with amperometric detection [23]. Also, the voltammetric oxidation

* Corresponding author. Fax: +56 7378920.
E-mail address: aalvarez@ciq.uchile.cl (A. Álvarez-Lueje).

0039-9140/$ – see front matter © 2007 Elsevier B.V. All rights reserved.
doi:10.1016/j.talanta.2007.05.010

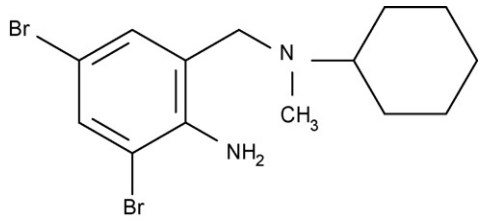

Fig. 1. Chemical structure of bromhexine.

of ambroxol and a differential pulse voltammetric method for its quantification in pharmaceuticals has been carried out [24]. Finally, a bromhexine-selective PVC membrane electrode based on bromhexinium tetraphenylborate has been also described [25].

At the best of our knowledge the electrochemical oxidation of bromhexine has not been previously reported. In this paper, we reveal the electrooxidation of bromhexine at the glassy carbon electrode focused to both clarifying the electrode mechanism and proposing a new method for its determination in pharmaceutical forms.

2. Experimental

2.1. Reagents

Bromhexine (99.89% chromatographically pure) was supplied by Labomed Laboratories (Santiago, Chile). Commercial tablets of Bisolvon® (declared amount per tablet 8.0 mg bromhexine, Boheringer Ingelheim S.A. Laboratories, Santiago, Chile) were obtained commercially.

All others reagents were of analytical grade unless indicated otherwise. Sodium hydrogen phosphate, phosphoric acid and acetonitrile HPLC grade were obtained from Merck. All solutions were prepared with ultrapure water ($\rho = 18\,M\Omega$) from Millipore-MilliQ system.

2.2. Solutions preparation

2.2.1. Buffer solutions

0.1 mol L^{-1} Britton–Robinson buffer (acetic/boric/phosphoric acids mixture) for voltammetric experiments was used, and desired pH was adjusted with concentrate solutions of NaOH or HCl. For HPLC 0.01 mol L^{-1} buffer phosphate solution (di-Sodium hydrogen phosphate anhydrous salt) adjusted at pH 3.0 with phosphoric acid was used.

2.2.2. Stock drug solution

Approximately 154 mg bromhexine was dissolved and diluted up to 10 mL with methanol, to obtain a final concentration around of 4×10^{-2} mol L^{-1} bromhexine. The solution was protected from light by using amber glass material.

2.2.3. Work solution

An aliquot (12.5 μL) of the stock solution was taken and diluted to 10 mL with methanol–Britton–Robinson buffer solution (0.1 mol L^{-1}) (2.5:97.5, v/v), for both UV–vis spectroscopy and electrochemical experiments or with acetonitrile-phosphate buffer solution (pH 3.0; 0.01 mol L^{-1}) (30:70, v/v) for HPLC experiments.

2.3. Apparatus

2.3.1. Voltammetric analyser

Differential pulse voltammetric (DPV) and cyclic voltammetric (CV) experiments were performed with a totally automatized workstation (BAS 100 B/W). A 25-mL thermostated BAS measuring cell with a glassy carbon electrode (GCE) (Ø = 3 mm, BAS) as working electrode were used. A platinum wire and an Ag/AgCl were used as counter and reference electrodes, respectively. The operating conditions were: sensitivity 10–100 μA V^{-1}; potential range 0–1500 mV; sweep rate 100–1000 mV s^{-1} for CV experiments. The working electrode surface was polished with 0.3 and 0.05 μm alumina slurries before each measurement [26].

2.3.2. Controlled potential electrolysis

Assays were carried out using a totally automatized assembly (BAS CV-100W), composed by a 10-mL electrolysis cell, a reticulated vitreous carbon (RVC) as a working electrode, an Ag/AgCl 3 M KCl and Pt as reference and auxiliary electrodes, respectively. The electrolysis potential was set at 1200 mV at pH 2, and the experiments were carried out in triplicate.

2.3.3. HPLC

Measurements were carried out by using a Waters assembly equipped with a model 600 Controller pump and a model 996 Photodiode Array Detector. The acquisition and treatment of data were made with the Millenium version 2.1 software. As chromatographic column a Bondapak/Porasil C18 column of 3.9 mm × 150 mm was used. As column guard a C18 Bondapak (30 mm × 4.6 mm) was employed. The injector was a 20 μL Rheodyne valve. UV detection at 245 nm was employed and the column was kept at constant temperature using a Waters column heater cartridge model 600.

An isocratic elution composed by a solution consisting of acetonitrile-phosphate buffer (pH 3.0; 0.01 mol L^{-1}) (30:70, v/v) mobile phase was used. The flow was 1.0 mL min^{-1} and the working temperature was kept constant at 40 ± 1 °C. Below these conditions, bromhexine exhibited a retention time of 5.996 ± 0.030 min.

2.3.4. Spectrophotometer

Spectrophotometric measurements were carried out with an UV–vis spectrophotometer ATI Unicam model UV3, using 1 cm quartz cell and equipped with a 486 computer with Vision acquisition and treatment program.

2.3.5. Gas chromatography (GC)

GC measurements were carried out in a Hewlett Packard GC 5890 with MSD 5972 mass detector (mode EI) and autosampler Hewlett Packard 7673A. The operating conditions were: injector temperature 250 °C; detector temperature 310 °C; program temperature: initial temperature 90 °C (1 min), 15 °C min^{-1}, final temperature 310 °C (3 min). Run time: 18.67 min.

2.4. Analytical procedure

2.4.1. Calibration curve preparation

2.4.1.1. DPV and UV spectroscopy. By diluting the bromhexine stock solution with methanol–Britton–Robinson buffer ($0.1\,mol\,L^{-1}$) (2.5:97.5, v/v) (pH 2), working solutions ranging between 2×10^{-5} and $1 \times 10^{-4}\,mol\,L^{-1}$ were prepared.

2.4.1.2. HPLC. By diluting the bromhexine stock solution with mobile phase, working solutions ranging between 3×10^{-6} and $3 \times 10^{-5}\,mol\,L^{-1}$ were prepared. The solutions were injected and chromatographed according to the working conditions previously given. UV detector was operated at $\lambda = 245$ nm.

2.4.2. Synthetic samples

Excipients (cornstarch, magnesium stearate, lactose, sodium lauryl sulfate and microcrystalline cellulose) were added to the drug for recovery studies, according to manufacturer's batch formulas for 8.0 mg bromhexine per tablet.

2.4.3. Individual tablet assay procedure

2.4.3.1. DPV. No less than 10 commercial tablets of bromhexine (Bisolvon®, amount declared 8.0 mg bromhexine per tablet) were used. Every tablet was independently suspended in 10 mL methanol with ultrasonic agitation to assure the complete dissolution of the drug and diluted to a final volume of 100 mL with the same solvent. Then, 250 μL were taken and diluted to 10 mL with methanol–Britton–Robinson buffer solution ($0.1\,mol\,L^{-1}$) (2.5:97.5, v/v) pH 2. Finally, the sample solution was transferred to a voltammetric cell and recorded at least twice from 0 to 1500 mV. The amount of bromhexine (mg) in the sample solution was calculated using the standard calibration curve.

2.4.3.2. HPLC. The same procedure above described was applied for HPLC analysis, but the solution was filtered previous to inject on chromatograph. The amount of bromhexine (mg) in the sample solution was calculated from the corresponding prepared standard calibration curve.

2.4.4. Selectivity studies [27]

2.4.4.1. Degradation trials. Hydrolysis. Individually ca. 15 mg bromhexine were dissolved in 10 mL $1\,mol\,L^{-1}$ HCl in a 25 mL-distillation flask or 10 mL water for acid or neutral hydrolysis, respectively. Each solution was boiled for one hour at reflux.

Photolysis. (a) Bromhexine raw material: ca. 15 mg bromhexine were put on a black box and irradiated with UV light (UV Black-Ray long wave ultraviolet lamp, UVP model B 100 AP (50 Hz, 2.0 A) with a 100 W Par 38 Mercury lamp equipped with a 366 nm filter). Fifteen centimeter distance for 8 h (1.2×10^{19} quanta/s, determined by using the potassium ferrioxalate chemical actinometer [28]) were selected as experimental conditions. (b) Bromhexine solution: 10 mL of $1 \times 10^{-3}\,mol\,L^{-1}$ bromhexine solution (methanol–water (30:70, v/v)) was bubbled by 2 min with nitrogen and transferred to a black box and then irradiated with UV light as the raw material.

Thermolysis: ca. 15 mg bromhexine were heated at 105 °C for 5 h.

Appropriates volumes of each obtained solution from degradation trials or the corresponding mg from thermolysis and photolysis in raw material assays were taken and completed to a final volume with methanol–Britton–Robinson buffer solution ($0.1\,mol\,L^{-1}$) (2.5:97.5, v/v) (pH 2) to obtain a theoretical concentration of $5 \times 10^{-5}\,mol\,L^{-1}$ bromhexine. Samples from these studies were stored at −20 °C and protected from light prior to voltammetric and HPLC analysis. Each sample was analyzed by duplicate.

2.4.5. Statistic analysis

Comparison between different techniques, as well as the comparison with standard deviations, was carried out by means of the Student's *t*-test, and using significance limits between 95 and 99% of confidence [29,30].

3. Results and discussion

3.1. Electrochemical characterization

Bromhexine in methanol/$0.1\,mol\,L^{-1}$ Britton–Robinson buffer solution (2.5/97.5) shows an anodic response on glassy carbon electrode in the pH range 2–7.5 (Fig. 2). Above this pH

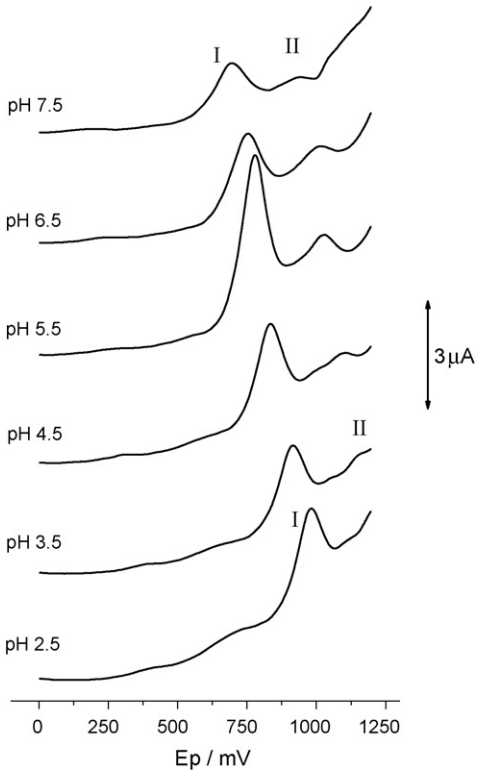

Fig. 2. Differential pulse voltammograms of $5 \times 10^{-5}\,mol\,L^{-1}$ bromhexine solution at different pHs (methanol/$0.1\,mol\,L^{-1}$ Britton–Robinson buffer: 2.5/97.5).

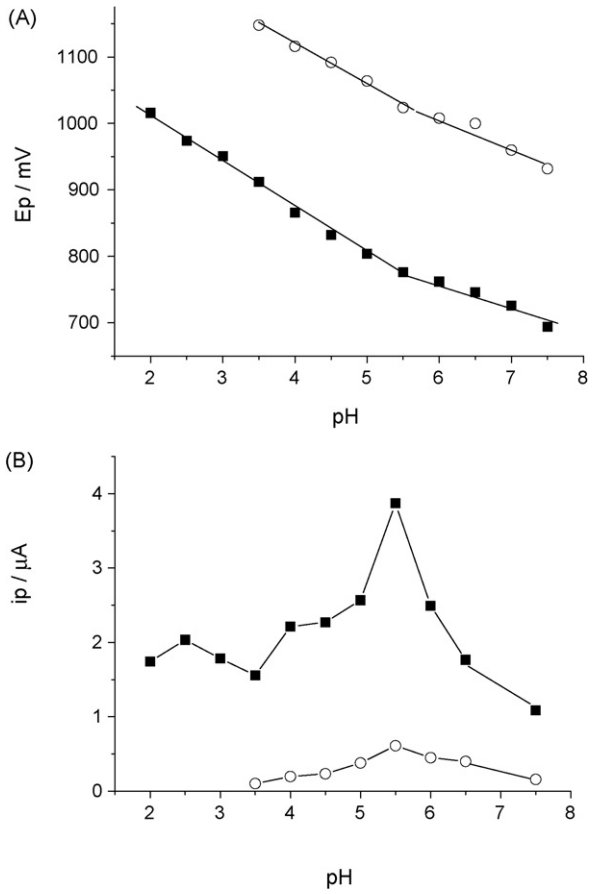

Fig. 3. (A) Peak potential evolution of 5×10^{-5} mol L^{-1} bromhexine solution at different pHs (methanol/0.1 mol L^{-1} Britton–Robinson buffer: 2.5/97.5) and (B) i.p.–pH graph: (■) peak I, (◯) peak II.

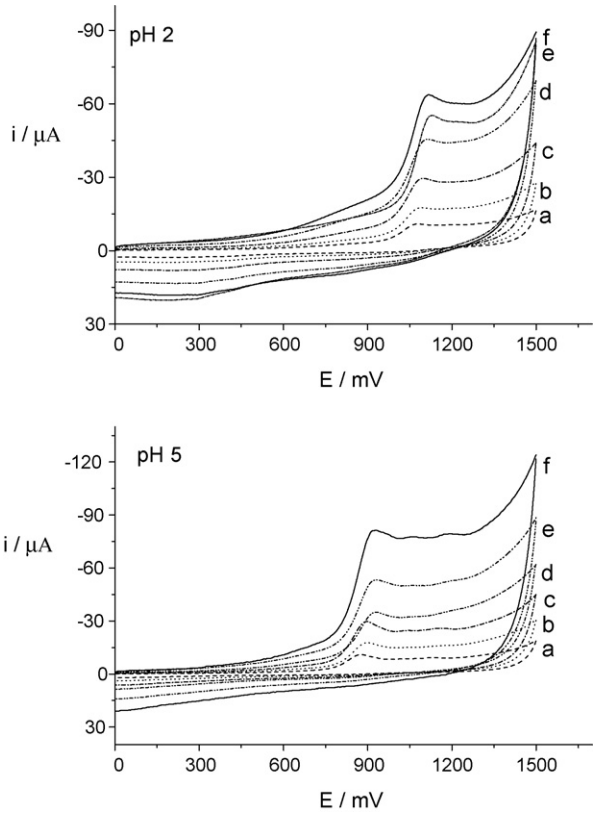

Fig. 4. Cyclic voltammograms of 1×10^{-3} mol L^{-1} bromhexine solution in methanol/0.1 mol L^{-1} Britton–Robinson buffer: 2.5/97.5 at different sweep rate ($a = 100$ mV s^{-1}, $b = 200$ mV s^{-1}, $c = 400$ mV s^{-1}, $d = 600$ mV s^{-1}, $e = 800$ mV s^{-1}, $f = 1000$ mV s^{-1}) at pH 2 and pH 5.

bromhexine precipitated. At pH < 3.5 bromhexine exhibits only one signal (peak I) and above pH 4 a second one appears at higher potentials (peak II). Peak I is pH-dependent in all the pH range studied (Fig. 3A), however a break in the E_P versus pH plot at pH 5.5 is observed, presumably due to a pK_a of bromhexine. To confirm this assumption, the spectrophotometric behaviour of bromhexine was evaluated determining an apparent pK_a value of 4.3 from the absorbance-pH plot (data not shown). On the other hand peak II shows to be pH-dependent between pH 3.5 and 7.5 but its intensity is very low compared with peak I. Fig. 3B shows the peak current dependence with pH for both signals. The peak current intensity of signal I increases up to pH 5.5 and then decreases probably due to the precipitation of bromhexine that it occurs at alkaline pHs. On the other hand, the peak current of signal II follows a similar pattern that signal I but with a lower intensity of current.

The electrooxidation of bromhexine was also studied by cyclic voltammetry (Fig. 4). Experiments were conducted at two pH values (2 and 5) at different sweep rate values (100–1000 mV s^{-1}) and demonstrated that the bromhexine oxidation is irreversible. Furthermore, log i.p. versus log sweep rate plot exhibits a slope value ~0.9 evidencing that bromhexine undergoes an adsorption processes on the electrode surface [31].

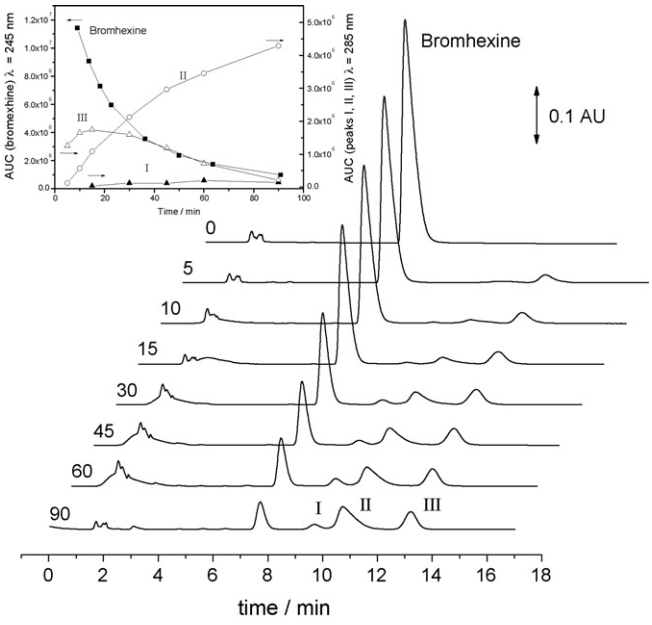

Fig. 5. Time course (min) of bromhexine electrolysis followed by HPLC–UV at λ = 245 nm. Electrolysis potential = 1200 mV. Inset: area under curve (AUC) of each chromatographic signal vs. electrolysis time: (■) Bromhexine$_{245\,nm}$, (▲) peak I$_{285\,nm}$, (◯) peak II$_{285\,nm}$, (△) peak III$_{285\,nm}$.

Controlled potential electrolysis experiments coupled with HPLC–UV were conducted to elucidate the mechanism of bromhexine electrooxidation. Concomitant with this experiment and using a rotating disk electrode a diffusion coefficient value of $1.22 \times 10^{-6}\,cm^2\,s^{-1}$ was calculated for bromhexine solution at pH 2. From the total charge transferred after applied a constant potential of 1200 mV and using the Faraday equation [31], was possible to conclude that two electrons are involved in the electrodic process. Furthermore, at large electrolysis time ($t > 30$ min) the colourless solution turned red. Fig. 5 shows the time course of the electrolysis procedure followed by HPLC–UV at $\lambda = 245$ nm. In this figure, it can be appreciated that the main peak of bromhexine (Rt = 7.4 min) decreases as the electrolysis time increases; and three new peaks at Rt of 9.6 min (peak I), 10.8 min (peak II) and 13.3 min (peak III), appeared. Insert in Fig. 5 shows the electrolysis time evolution, expressed as area under curve at $\lambda = 285$ nm, of each new chromatographic signal (peaks I, II and III). As it can be seen, peak III increases up to 15 min of electrolysis and then decrease until almost disappeared after 90 min of electrolysis. The UV–vis spectra of each product reveals that both products I and II exhibit only one absorption band with a maximum near to $\lambda = 300$ nm. On the other hand, peak III exhibits the higher retention time, presenting an absorption band in the visible region (~400 nm) being coherent with the above mentioned color change in the solution. Obviously this color change suggests that this oxidation product has higher conjugation than the parent bromhexine (data not shown).

On the basis of these experimental evidences and the literature report [32], the following overall electrode mechanism was proposed for the bromhexine oxidation:

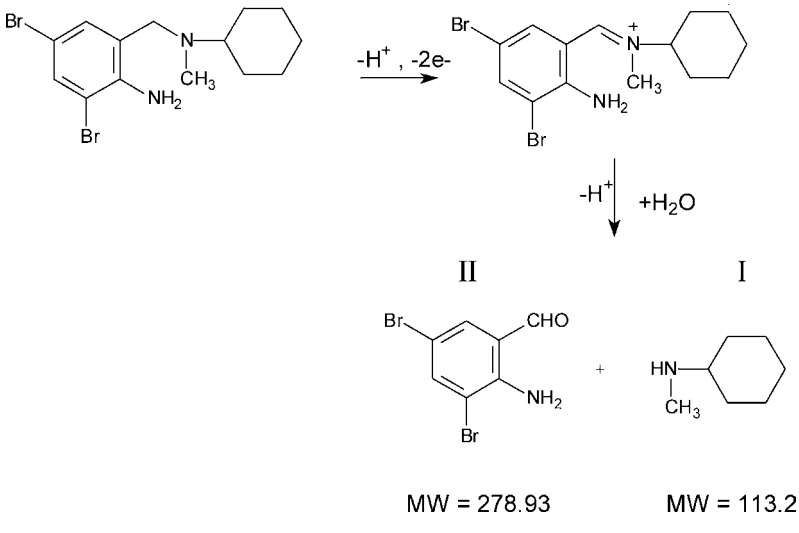

This proposed mechanism explains the appearance of products I and II (*N*-methylcyclohexanamine and 2-amino-3,5-dibromobenzaldehyde, respectively). To elucidate the nature of the product III, we have considered it higher retention time and also it visible absorption band, concluding that the product must be more lipophyllic and conjugated than bromhexine. According to that, we propose that product II reacts itself to form a dimeric structure via a dehydration reaction to generate product III (2,4,8,10-tetrabromodibenzo[*b*,*f*][1,5] diazocine) according to:

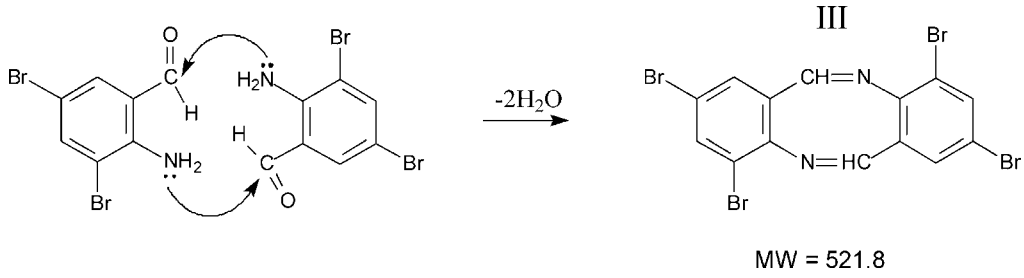

To confirm this mechanism, an identification of the final products by GC–MS was performed. From GC chromatogram, three products were detected at 2.191 min (product I, $M = 113$) and 7.62 min (product II, $M = 279$; $M + H^+ - CHO = 251$; $M - CHO - Br = 170$; $M - CHO - 2Br = 90$). Product II exhibited the typical isotopical relation of a 2Br-containing molecule [33]. Also it was possible to distinguish a signal corresponding to product III at 14.382 min ($M = 522$; $M + H^+ - Br = 443$; $M + H^+ - 2Br = 363$), which exhibited the typical isotopical relation of a 4Br-containing molecule [33]. In conclusion, the three products proposed as final products of the bromhexine electrooxidation were clearly identified by GC–MS, supporting the proposed electrochemical oxidation mechanism.

3.2. Selectivity studies

In order to prove the selectivity of the method, we tested typical excipients used in oral formulations (corn starch, magnesium stearate, lactose, sodium lauryl sulfate and microcrystalline cellulose) and follow classical degradation trials: hydrolysis (acidic and neutral), photolysis and thermolysis

Table 1
Analytical parameters for the developed methods

Parameter	DPV (E_P = 1016 mV)	HPLC–UV (λ = 245 nm)
Repeatability, CV (%)[a]	0.46	0.24
Reproducibility, CV (%)[a]	0.57	0.39
Recovery (%)[b] ± S.D.	94.50 ± 2.03	91.0 ± 0.16
Concentration range (M)	$2.0 \times 10^{-5} - 1.0 \times 10^{-4}$	$2.0 \times 10^{-5} - 1.0 \times 10^{-4}$
Calibration curve	I_p (μA) = 0.03684 C(M) − 4.0923×10^{-7}	AUC = 1.25×10^{10} C(M) − 107801
Detection limit (M)	1.4×10^{-5}	1.1×10^{-6}
Quantitation limit (M)	1.6×10^{-5}	1.5×10^{-6}

[a] Concentration level of 5.0×10^{-5} M.
[b] Average on a concentration level of 5.0×10^{-5} M.

[27]. Results indicate that no new signal appeared in the voltammograms and also the signal of analyte is not disturbed due to neither the excipients nor the degradation trials for bromhexine. According with those results, it can be concluded that the proposed DPV method is sufficiently selective in order to be applied to bromhexine quantification and no previous separation or extractions were necessary.

3.3. Analytical studies

For developing an electroanalytical method to quantify bromhexine in pharmaceuticals we have selected peak I at pH 2 as the optimal analytical signal.

In order to provide a DPV quantitative procedure, the dependence between peak current (I_p) and bromhexine concentration was studied. A linear relation between 2×10^{-5} and 1×10^{-4} mol L^{-1} was found. Above this concentration (1×10^{-4} mol L^{-1}) lost of linearity was observed, probably due to the absorption of bromhexine on electrode surface. The calibration curve was described by the following regression equation: I_p (μA) = 3.684×10^{-3} C (mol L^{-1}) − 4.0923×10^{-7} (r = 0.9996, n = 8). Within-day and inter-day reproducibilities were adequate with R.S.D. values lower than 3%.

For comparative purposes a HPLC method was developed. In Table 1, the analytical parameters achieved using both methodologies are summarized.

Our findings are rather different from those previously obtained using conventional and coated wire ion-selective electrodes [5]. There, the recoveries values were higher than ours. Methodological procedures could explain the differences since in our case bromhexine was tested in presence of typical excipients used in oral formulations and in Reference [5] it was tested in presence of cations, anions and others drugs.

3.4. Determination of bromhexine in tablets

Finally, the developed DPV method was applied successfully to the individual tablet assay in order to verify the uniformity content of bromhexine. For comparative purposes, also HPLC analysis was carried out. Table 2 shows the analytical results obtained by both methods which show a good agreement between them. The content for all assayed tablets fulfill the Pharmacopoeia requirement, i.e., for uniformity content of tablets (average) the content must be in the range of 85.0–115.0% of label claim and none individual value must be out of the range of 75.0–125.0% of label claim [34].

Table 2
Individual tablet assay of bromhexine

	Differential pulse voltammetry (E_P = 1016 mV)	HPLC–UV (λ = 245 nm)
	mg/tablet	mg/tablet
	7.5	7.2
	7.4	7.3
	7.4	7.3
	7.5	7.3
	7.4	7.3
	7.4	7.3
	7.5	7.3
	7.4	7.3
	7.5	7.2
Average	7.4	7.3
S.D.	0.05	0.04
CV (%)	0.7	0.6

Declared amount per tablet: 8.0 mg bromhexine.

Using the Student's t-test; the average of both analytical methods were not significantly different, since the calculated t-test value (DPV: −1.47; HPLC: −1.34) were less than the tabulated value (2.262) at p = 0.05.

4. Conclusions

A two-electron two-proton mechanism for the electrochemical oxidation of bromhexine was revealed. *N*-methylcyclohexanamine, 2-amino-3,5-dibromobenzaldehyde and 2,4,8,10-tetrabromodibenzo[*b*,*f*][1,5] diazocine were identified as the oxidation products from bromhexine.

On the basis of the electrochemical response of bromhexine, a DPV method for its determination was proposed and compared with a HPLC one. The proposed DPV method was successfully applied to the determination of the drug in tablets without excipients' interference. Preparation of the sample was easy and the method is not time consuming and cheap.

Acknowledgements

Financial support from FONDECYT "Lineas Complementarias" (grant no. 8000016) and Chemical and Pharmaceutical

Sciences Faculty, University of Chile is gratefully acknowledged.

References

[1] L. Parvez, M. Vaidya, A. Sakhardande, S. Subburaj, T.G. Rajagopalan, Pulm. Pharmacol. Ther. 9 (1996) 299.
[2] J.M. Grang, N.J. Snell, J. Ethnopharmacol. 50 (1996) 49.
[3] Z. Kopitar, R. Jauch, R. Hankwitz, H. Pelzer, Eur. J. Pharmacol. 21 (1973) 6.
[4] S.V.M.M. Rao, I.N. Rao, T.R.S. Reddy, C.S.P. Sastry, Indian J. Chem. Technol. 12 (2005) 170.
[5] N.T. Abdel-Ghani, Y.M. Issa, H.M. Ahmed, Scientia Pharm. 74 (2006) 121.
[6] H.C. Goicoechea, A.C. Olivieri, Talanta 49 (1999) 793.
[7] A.C.B. Dias, J.L.M. Santos, J.L.F.C. Lima, E.A.G. Zagatto, Anal. Chim. Acta 499 (2003) 107.
[8] I.H. Habib, M.E. Hassouna, G.A. Zaki, Farmaco 60 (2005) 249.
[9] V. Tantishaiyakul, C. Poeaknapo, P. Sribun, K. Sirisuppanon, J. Pharm. Biomed. Anal. 15 (1996) 287.
[10] E.V. Rao, G.R. Rao, S. Raghuveer, P. Khadgapathi, Analyst 112 (1987) 871.
[11] G. Bazylak, L.J. Nagels, J. Pharm. Biomed. Anal. 32 (2003) 887.
[12] J.P. Rauha, H. Salomies, M. Aalto, J. Pharm. Biomed. Anal. 17 (1998) 237.
[13] S.K. Lee, S.H. Choi, H.S. Kwak, Y.S. Kang, K.R. Chae, Eur. J. Pharm. Sci. 23 (2004) S39.
[14] S.J. Liu, L. Zhao, X. Liu, F. Zhou, S.X. Jiang, J. Food Drug Anal. 12 (2004) 306.
[15] J.E. Koundourellis, E.T. Malliou, T.A. Broussali, J. Pharm. Biomed. Anal. 23 (2000) 469.
[16] M. Pospisilova, M. Polasek, V. Jokl, J. Pharm. Biomed. Anal. 24 (2001) 421.
[17] H. Okamoto, T. Nakajima, Y. Ito, T. Aketo, K. Shimada, S. Yamato, J. Pharm. Biomed. Anal. 37 (2005) 517.
[18] O.W. Lau, Y.M. Cheung, Analyst 115 (1990) 1349.
[19] E. Bechgaard, A. Nielsen, J. Chromatogr. 228 (1982) 392.
[20] B.P. Jensen, B. Gammelgaard, S.H. Hansen, J.V. Andersen, J. Anal. At. Spectrom. 20 (2005) 204.
[21] M. Johansson, S. Lenngren, J. Chromatogr. 432 (1988) 243.
[22] C.E. Uboh, J.A. Rudy, L.R. Soma, M. Fennell, L. May, R. Sams, F.A. Railing, J. Shellenberger, M. Kahler, J. Pharm. Biomed. Anal. 9 (1991) 33.
[23] F.J. Flores-Murrieta, C. Hoyo-Vadillo, E. Hong, G. Castañeda-Hernández, J. Chromatogr. 490 (1989) 464.
[24] B.T. Demircigil, B. Uslu, Y. Ozkan, S.A. Ozkan, Z. Senturk, Electroanal. 15 (2003) 230.
[25] S. Khalil, M.M. Elrabiehi, Microchem. J. 62 (1999) 237.
[26] I.F. Hu, D.H. Karweik, T. Kuwana, J. Electroanal. Chem. 188 (1985) 59.
[27] O.A. Quattrochi. S.A. De Andrizzi, R.F. Laba, Introducción a la HPLC, aplicación y práctica, Artes Gráficas Farro, SA, Argentina, 1992.
[28] K. Akimoto, H. Kurosaka, I. Nakagawa, K. Sugimoto, Chem. Pharm. Bull. 36 (1988) 1483.
[29] R.C. Graham, Data Analysis for the Chemical Sciences. A Guide to Statistical Techniques, VHC Publishers, Inc., New York, 1993.
[30] J.K. Taylor, Statistical Techniques for Data Analysis, Lewis Publishers, Inc., New York, 1990.
[31] P. Kissinger, W. Heineman, Laboratory Techniques in Electroanalytical Chemistry, tenth ed., Marcel Dekker, NY, New York, 1984.
[32] H. Lund, P. Hammerich, Organic Electrochemistry, fourth ed., Marcel Dekker, NY, New York, 2001.
[33] F.W. McLafferty, Interpretation of Mass Spectra, third ed., University Science Books, Mill Valley California, USA, 1980.
[34] USP 27-NF 22. United States Pharmacopoeial Convention, Inc., Rockville MD, USA, 2004.

Available online at www.sciencedirect.com
ScienceDirect
Talanta 73 (2007) 812–819
Talanta
www.elsevier.com/locate/talanta

Comparison of extraction techniques of robenidine from poultry feed samples

Joanna Wilga, Agata Kot- Wasik *, Jacek Namieśnik

Department of Analytical Chemistry, Chemical Faculty, Gdańsk University of Technology, G. Narutowicza 11/12 Street, 80-952 Gdańsk, Poland

Received 16 January 2007; received in revised form 17 April 2007; accepted 30 April 2007
Available online 10 May 2007

Abstract

In this paper, effectiveness of six different commonly applied extraction techniques for the determination of robenidine in poultry feed has been compared. The sample preparation techniques included shaking, Soxhlet, Soxtec, ultrasonically assisted extraction, microwave – assisted extraction and accelerated solvent extraction. Comparison of these techniques was done with respect to the recovery extraction, temperature and time, reproducibility and solvent consumption. Every single extract was subjected to clean – up using aluminium oxide column (Pasteur pipette filled with 1 g of aluminium oxide), from which robenidine was eluted with 10 ml of methanol. The eluate from the clean-up column was collected in a volumetric flask, and finally it was analysed by HPLC–DAD–MS. In general, all extraction techniques were capable of isolating of robenidine from poultry feed, but the recovery obtained using modern extraction techniques was higher than that obtained using conventional techniques.

In particular, accelerated solvent extraction was more superior to other techniques, which highlights the advantages of this sample preparation technique. However, in routine analysis, shaking and ultrasonically assisted extraction is still the preferred method for the solution of robenidine and other coccidiostatics.

Keywords: Poultry feed; Sample preparation; Robenidine; Extraction techniques

1. Introduction

Sample preparation is one of the most important steps in the majority of analytical procedures to determine trace constituents in samples with complex matrices. An ideal sample preparation technique should be simple, inexpensive, efficient, selective and compatible with various analytical techniques. It should give as high as possible recovery the supreme samples clean-up, be environmentally friendly and it should use the minimum amount of solvent. In practise it is difficult to fulfil all theses requirements. Usually the sample preparation is the most labour intensive, and it is very often the slowest and most costly step in the whole analytical procedure, especially if multi step procedures are used [1,2]. Over the last ten years, research on sample preparation has been driven to solve these problems and find which will the ideal sample preparation technique.

Due to their state, solid samples cannot be directly analysed. It is necessary to transfer the analytes from the matrix to the liquid phase so that chromatographic techniques can be used to determine the constituents.

Lots of factors can be considered in order to select the proper sample preparation technique, for example the amount of solvents used and amount of wastes products obtained, the time needed for the extraction, the cost and availability of instruments, the cost of each operation, the quantity of sample required for the extraction, whether the process is automated and the number of steps that have to be done (which can be a source of mistake) [1].

The extraction techniques that are currently available can be devided into two groups: classical and modern ones. Generally, for classical extraction techniques, like shaking flask extraction (SFE), Soxhlet extraction, Soxtec extraction, the extraction efficiency depends mainly on the type of solvent applied for the isolation and extraction time [3,4]. In case of modern extraction techniques, such as ultrasonic assisted extraction (UE), microwave assisted extraction (MAE) and accelerated solvent extraction (ASE), the extraction efficiency depends not only on

* Corresponding author. Tel.: +48 58 347 21 10; fax: +48 58 347 26 94.
E-mail addresses: jawil@wp.pl (J. Wilga), agata@pg.gda.pl (A.K. Wasik), chemanal@pg.gda.pl (J. Namieśnik).

0039-9140/$ – see front matter © 2007 Published by Elsevier B.V.
doi:10.1016/j.talanta.2007.04.046

the type of solvent applied for the isolation and extraction time, but also on many different parameters characteristic for every technique used [2,5].

To prove above assumption the determination of coccidiostatic in poultry feed samples has been selected. Feed samples include a lot of substances, which should be strictly controlled during the manufacturing process (for example hormones, enzymes, dye stuff, aromatic and tested substances, antioxidants, herbs, coccidiostatics). Coccidiostatics are compounds that are widely used to prevent and treat coccidiosis, a contagious amoebic disease affecting livestock, agricultural poultry that is associated with warm and humid conditions. EC regulations established minimum and maximum content of coccidostaics in complete feeding stuffs. The typical dosages of required for coccidiostatics inhibition or to improve weight gain are dependent on the kind of theirs and therapeutic effects.

In this paper, the advantages and disadvantages of six different extraction techniques to remove of coccidiostatics from feeding stuff have been discussed. An investigation of numerous sample preparation techniques was carried out, with special attention paid to the conditions needed for efficient isolation of robenidine (1,3-bis[(4-chlorobenzylidene)amino]quanidine-hydrochloride), one of the most popular coccidiostatics in the world. Comparative studies of classical techniques, like Soxhlet extraction, Soxtec extraction, and shaking flask extraction and other modern techniques like ultrasonically assisted extraction, microwave accelerated extraction (MAE), accelerated solvent extraction (ASE) have been performed (Fig. 1). All extraction procedures were compared in terms of extraction time, extraction yields, solvent consumption and reproducibility. Furthermore, the importance of different parameters, on the recovery of robenidine was evaluated.

2. Experimental

2.1. Reagents

Methanol (HPLC grade), molecular sieve 3 Å, as well as acetic and formic acids (chemically pure) were purchased from POCH (Gliwice, Poland). Methanol for mobile phase composition (HPLC grade), aluminium oxide and trifluoroacetic acid (TFAA) were purchased from Merck (Warsaw, Poland). Water was purified in a Super Plus, Millipore, Waters System (Millipore, Milano, Italy). Quartz sand, which was used as the extraction cell filler, was collected at the local beach. Quartz sand was thoroughly washed with hot solution of water and nitric acid (1:1 v/v). After washing, it was rinsed several times with distilled water (until a pH = 7 of was achieved) and dried at 200 °C. After drying it was cleaned up with methanol in Soxhlet, dried and then it sifted with ≤1 mm sieve. Aluminium oxide (activity grade I) was prepared by drying at 170 °C for 10 h, then cooled and wetted with water (1%).

2.2. Standards and samples

Due to difficulties with finding a supplier of pure robenidine, the compound was extracted from "Robenvit", a commercially available premix used in feedstuff manufacturing. This was a kind donation from Cargil (Pruszcz Gdański, Poland). Robenidine was extracted with chloroform and purified by

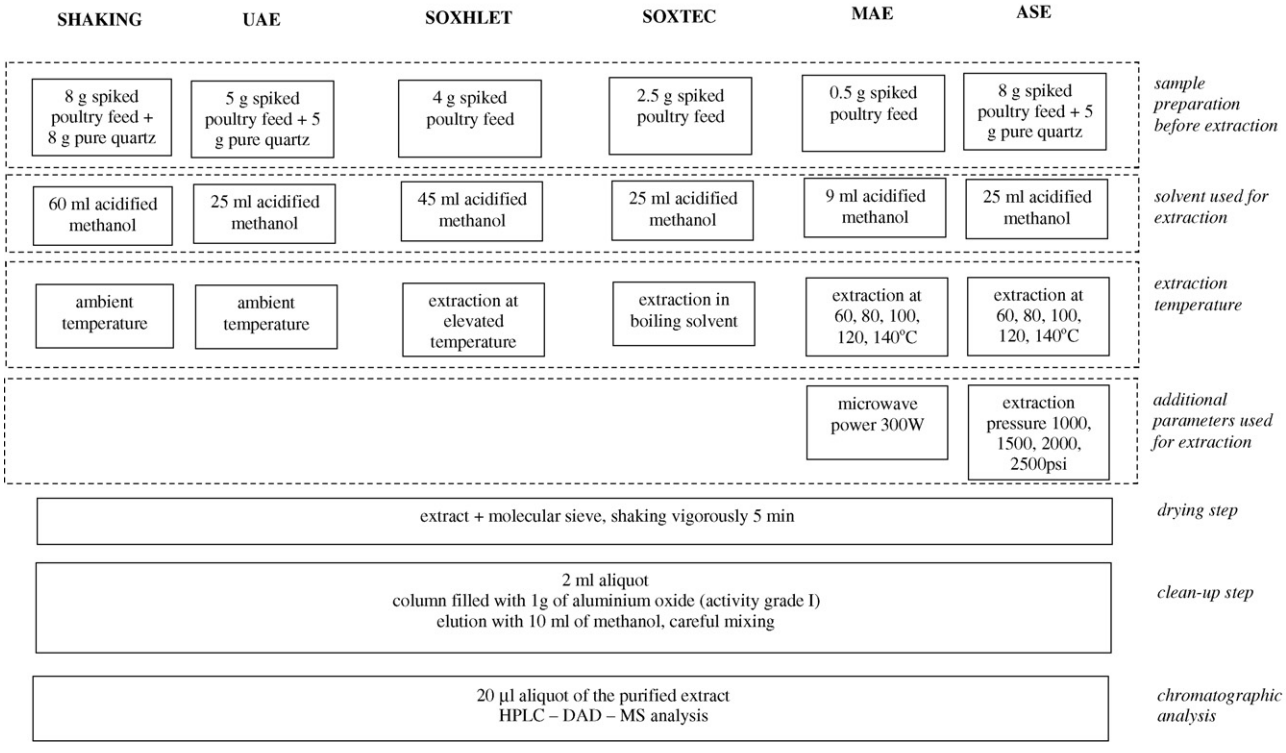

Fig. 1. Scheme of sample preparation and analysis of robenidine by using different techniques of extraction.

recrystallization. The identity and the purity of the substance were confirmed by ^{13}C NMR and HPLC–MS techniques.

Robenidine stock solution (63 μg ml^{-1}), which was used to prepare the calibration curve was obtained by dissolving appropriate amount of robenidine in methanol by using ultra sonic bath.

Standard solutions were prepared by diluting the stock solution with the methanol to obtain concentrations ranging from 0.01 to 4.46 μg ml^{-1}. Since robenidine is sensitive to light, all flasks were wrapped with aluminium foil and stored in a dark place.

Optimisation of the procedure was done using commercially available poultry feeds, with and without robenidine addition. All samples were grounded before the analysis and then processed as described in Section 2.3.

For the isolation of robenidine from poultry samples acidified methanol has been used. For this purpose acidified methanol was prepared by transferring 4.0 ml hydrochloric acid into a 500 ml graduated flask, making up to the mark with methanol and mixing. This solution was freshly prepared before use.

2.3. Chromatographic equipment

The analyses were performed using a Hewlett Packard HP 1100 LC system equipped with a binary pump, an automatic sampler, a diode array detector and mass spectrometer. The separation was carried out on a Purospher (Merck, Poland) C18 analytical column (125 × 3.0 mm, 3 μm particle size) maintained at 10 °C using isocratic elution mode. The mobile phase was a mixture of 70% methanol and 30% water acidified with 0.1% TFAA (v/v), and the flow rate was 0.7 ml min^{-1}. The diode array UV detector (HP 1100 Series) was set to 317 nm. A single quadrupole mass spectrometer (Hewlett-Packard HP 1100) with electrospray ionisation was used with the following parameters: fragmentor 95 eV, spray voltage 5 kV, neublizer pressure 310 kPa (45 psi), drying gas temperature 350 °C, drying flow 12 l min^{-1}. Positive ionisation with selected ion monitoring (SIM) (multiplier gain set to 5, dwell times set to 289 ms) was used for all analyses. Pseudomolecular ion $(M+H)^+$ *m/z* 334 and ions at *m/z* 336 and *m/z* 337 were monitored.

2.4. Shaking flask extraction

An 8 g portion of spiked poultry feed and 8 g of pure quartz were accurately weighed, mixed and shaken with 60 ml of acidified methanol for 30 and 60 min at an ambient temperature of heating, and for this process, a shaker was developed in-house (Department of Analytical Chemistry of Gdańsk University of Technology, Poland). Real poultry feed samples, originally containing robenidine (66 mg kg^{-1}), were extracted within 30 min under optimised conditions. For method development, extractions were repeated eight times per each set of experimental conditions.

2.5. Ultrasonic extraction method

Extractions were performed with a Sonorex ultrasonic instrument (Bandelin Electronic, Berlin, Deutschland), the power of which was set at 80 W. A 5 g portion of the spiked poultry feed (accurately weighed) mixed with 5 g of pure quartz were extracted with 25 ml of acidified methanol at an ambient temperature of heating for 15 and 30 min. Real poultry feed samples, originally containing robenidine (66 mg kg^{-1}), were extracted within 30 min under optimised conditions. For method development, extractions were repeated eight times per each set of experimental conditions.

2.6. Soxhlet

A 4 g portion of spiked poultry feed was accurately weighed and extracted with 45 ml of acidified methanol for 6 and 12 h in heatcoat at 65 °C. Real poultry feed samples, originally containing robenidine (66 mg kg^{-1}), were extracted within 6 h. For method development, extractions were repeated eight times per each set of experimental conditions.

2.7. Soxtec

A Soxtec system, HT6 (Tecator, Höganä, Sweden), was used. A 2.5 g portion of spiked poultry feed was placed in a 33 mm × 80 mm extraction thimble (supplied by the manufacture) and extracted with 25 ml of acidified methanol in boiling solvent for 15, 30, and 45 min. Real poultry feed samples originally containing robenidine (66 mg kg^{-1}) were extracted within 30 min. All procedures were repeated eight times per each set of experimental conditions. Repeated eight times at each of conditions.

2.8. Microwave-assisted extraction

A CEM MARS 5 Microwave Accelerated Reaction System (CEM Corporation, Matthews, NC, USA) was used. The 0.5 g portion of spiked poultry feed was accurately weighed and it was loaded into extraction cylinders containing 10 ml of acidified methanol. The extraction temperature was 110 °C and programmed as follows: ramp to the final temperature in 10 min. Microwave power was set at 300 W (100%). Once the extraction was complete ∼5 g of molecular sieve was added. MAE parameters (temperature, extraction time, watt power) were optimised in order to maximise the amount of robenidine extracted. The extraction temperature was optimised in the range of 60–120 °C, while the time of extraction was set between 1 and 5 min. For method development, extractions were repeated eight times per each set of experimental conditions.

2.9. Accelerated solvent extraction

An ASE 200 system (Dionex, Sunnyvale, CA, USA) was used. The ASE extractor was equipped with an autosampler carousel and a collection tray that allowed up to 24 separate samples to be extracted sequentially. Approximately 8 g of spiked feed sample were thoroughly mixed with ∼8 g quartz and then placed in the 22 ml extraction cell. Extractions were performed with acidified methanol.

ASE parameters (temperature, pressure, extraction time, number of cycles and solvent composition) were optimised in order to maximise the amount of robenidine extracted. Extraction temperature was optimised in the range 60–140 °C, while pressure was kept between 1000 and 3000 bars. Extraction time was evaluated between 1 and 5 min.

For method development, extractions were repeated eight times per each set of experimental conditions.

2.10. Sample clean-up

After extraction, each extract was collected in vials containing ~5 g of molecular sieve (drying agent). The content of the collecting vials was shaken vigorously for 5 min. An aliquot (2 ml) of the extract was then subjected to clean up using a handmade column, which was prepared from Pasteur pipette and filled with 1 g of aluminium oxide (activity grade I). Robenidine was eluted from the clean-up column with 10 ml of methanol. The elute from the clean-up column was collected in a volumetric flask (10 ml). After careful mixing, 20 μl aliquot of the purified extract was analysed by HPLC–DAD–MS technique.

3. Results and discussion

The whole set of results contained 400 analyses results since six extraction methods were applied to 52 different test samples, and each combination of the sample and the extraction method were performed eight times. All data obtained were subjected to statistical analyses in order to establish which of the extraction methods investigated in this study gave significantly higher results than the other methods. The influence of different parameters on the effectiveness of the extraction processes was also checked.

3.1. Solvent

For an efficient extraction, the solvent should be able to dissolve the target analytes while leaving the sample matrix unchanged. The polarity of the extraction solvent should closely match the polarity of the target compounds. For an efficient extraction, the solvent has to create sufficient contact with the analytes. So, the higher the surface area of the sample, the faster the extraction will be. For that reason all samples were grounded before the analysis [5].

For ASE extraction, combinations of two solvents (methanol and acetonitrile) and two organic acids (acetic and formic acid) used as modifiers, were compared in terms of extraction efficiency. Results were obtained for seven different solvents of different composition, which were applied to isolate robenidine from spiked poultry feed (Fig. 2).

Based on the results obtained, methanol containing CH_3COOH (1% v/v), was selected as the solvent with optimal composition used for the extraction of robenidine from feeding stuff. This composition was characterized by the highest recovery of robenidine from poultry samples (85%; R.S.D. = 1.4%).

3.2. Temperature

Temperature plays an important role during the extraction process. As the temperature is increased, the viscosity of the matrix and solubility of the target analytes in the solvent used for the extraction increases. The added thermal energy also helps to break the analyte–matrix surface [2,7]. However, in most techniques, isolation is taking place ether at ambient temperature or at the boiling point of the solvent applied for the extraction. The only exception is ASE and MAE, for which extraction temperature can be evaluated. The effect of temperature on the extraction efficiency for ASE and MAE is shown in Fig. 3.

Generally higher recoveries were obtained in case of MAE extraction (from 86 up to 95%), while for ASE extraction recovery was below 85%. A temperature between 80 and 100 °C assures the best results (in terms of efficiency and R.S.D.) in both types of extraction.

3.3. Time of extraction

Certain sample matrices can retain analytes within pores or other structures. Increasing the static time at elevated temperatures can allow these compounds to diffuse into the extraction solvent. Static time is one of the most important parameters during extraction; even if the other parameters are optimised, static time does not improve the recovery from the sample to the

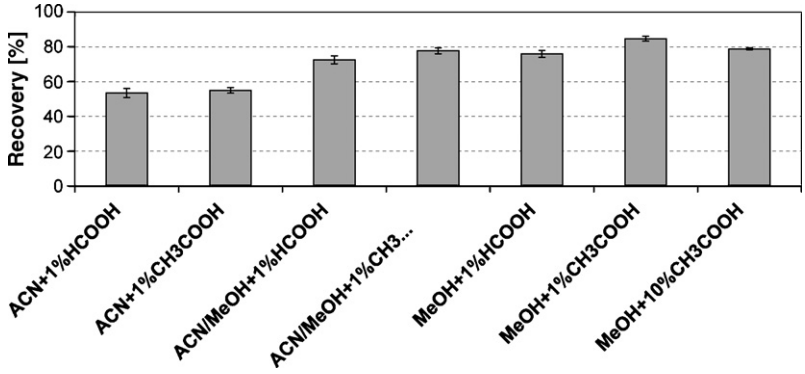

Fig. 2. The effect of different solvents of different composition on the robenidine isolation from spiked poultry samples during ASE extraction.

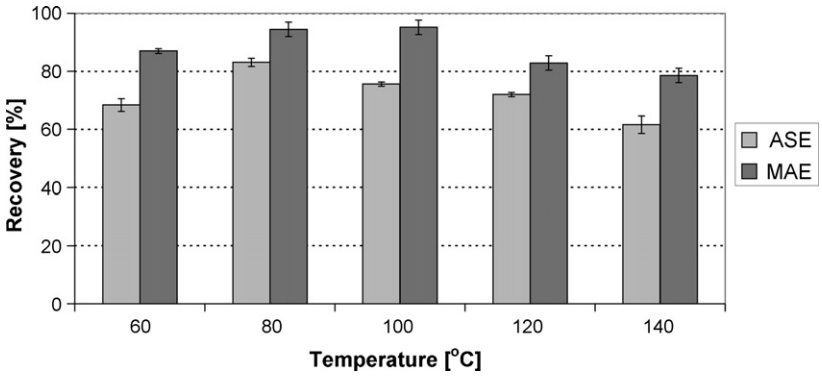

Fig. 3. The effect of temperature on the extraction efficiency for ASE and MAE.

same degree. The time of extraction was evaluated in all extraction techniques that have been applied within the scope of our investigations. All techniques used for the isolation of robenidine from poultry feed have different optimal extraction times. Shortening the extraction time is crucial in chemical analysis, since the sample preparation step is often obligatory and the most time consuming part of the analytical procedure. A comparison of the extraction time for all investigated techniques (Soxhlet, Soxtec, UAE, MAE, ASE) is shown in Fig. 4.

The results showed that extraction time is the shortest in case of MAE and ASE and comparable with that used for Soxtec, however, the time that an analyst must spend until the extract is ready for further treatment differs a lot. Using the ASE technique, the extract is ready immediately, while using the MAE technique it is mandatory to wait nearly half an hour for cooling and even then filtration or centrifugation has to be performed. In case of Soxtec extraction, although the extraction time is comparable with that which is optimised for ASE, two adverse effects can be observed. Cooling of the extract, which is necessary after extraction using Soxtec, takes time; however, evaporation of the excess of the solvent can be performed in this time. In the case of Soxhlet, optimal extraction time is very long in comparison with all the other techniques. Moreover, filtration and clean-up steps are nearly always essential, what causes that Soxhlet extraction is the most time-consuming extraction technique.

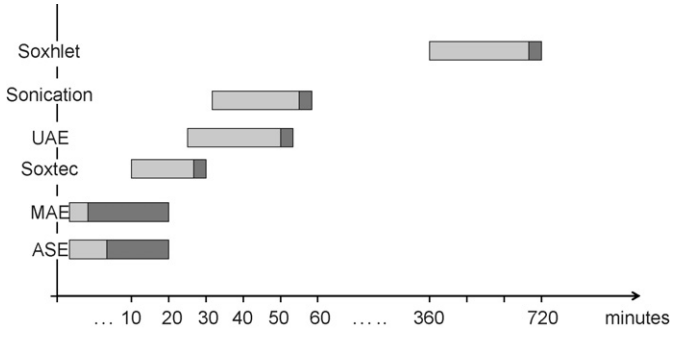

Fig. 4. Comparison of extraction time for Soxhlet, Soxtec, UAE, MAE and ASE (extraction efficiency was optimised to be the highest possible). Light grey box represents time needed for the extraction; dark grey box represents time spent to obtain extract ready for analysis.

3.4. Miscellaneous extraction parameters

For ASE, lots of parameters should be optimised; additionally to the extraction time and temperature, parameters such as pressure, numbers of cycles and volume have to be evaluated.

Elevated pressure is needed to maintain the solvents in liquid phase, even above their atmospheric boiling points. This is because liquids are able to dilute much better than gases. As it is shown in Fig. 5a changes in pressure applied for the extraction have very little impact on robenidine recovery, and thus it was not considered as a critical experimental parameter.

In comparison extraction efficiencies make have obtained at 1500 and 2500 psi are similar (82%), other experiments, had pressure set at 1500 psi (pressure of 2500 psi is the maximum that can be used in ASE, therefore some problems in maintaining of these parameters during extraction can be observed).

For the extract obtained using ASE, the flush volume should be adjusted in the method development so that the volume of the extract is equal and at a certain level. In our method, the flush volume was set at 100% and gave better results (higher recoveries of robenidine from the feeding stuff material) in comparison with the results obtained for 60 and 80% flush volume (Fig. 5b), so this flush volume (100%) was applied in all the investigations. When more than one cycle was applied in a method, the flush volume was divided by that number.

The use of static cycles was developed in order to introduce fresh solvent during the extraction process, which helps to maintain favourable extraction equilibrium. This effectively approximates dynamic extraction conditions without the need for troublesome flow restrictors to maintain pressure. Up to 5 static cycles were chosen to be evaluated during our experiments and data obtained are presented in Fig. 6a.

More that one static cycle has proven to be useful for such matrices such stuff (quite high concentration of analyte clogged in the sample difficult for any penetration). No significant difference was observed between one and five extraction static cycles. However in the case of MAE and UAE, some differences where observed between one, two and three extraction repetitions (from the same sample) – Fig. 5b. During the ASE extraction, nearly negligible amount of analyte was obtained after the second and third extraction. In the MAE extraction, up to 5% of robenidine was obtained after the second extraction, while in the UAE

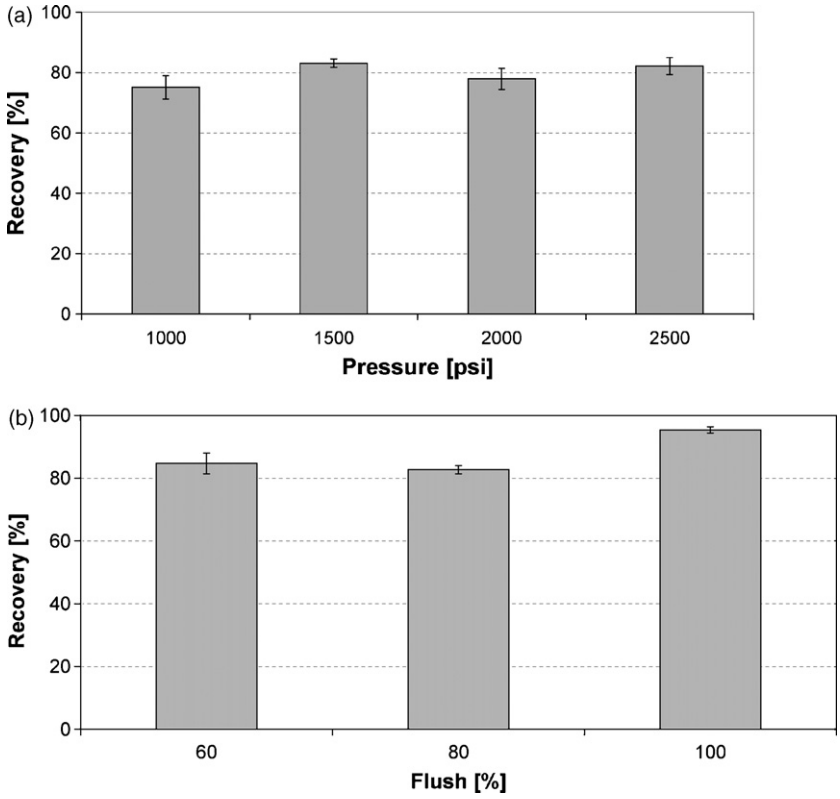

Fig. 5. (a) The effect of pressure on the robenidine extraction efficiency during ASE extraction. (b) The effect of flush volume on the robenidine extraction efficiency during ASE extraction.

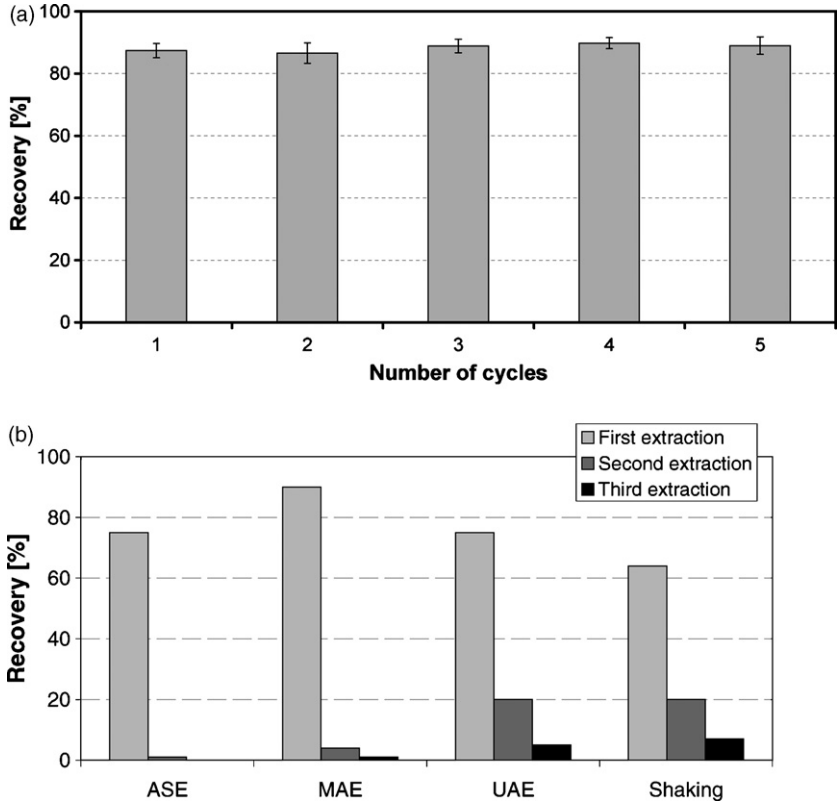

Fig. 6. (a) The effect of number of extraction static cycles on the extaction efficiency during ASE. (b) Influence of extraction repetitions from the same sample on the robenidine recoveries using ASE, MAE, shaking and UAE extraction techniques.

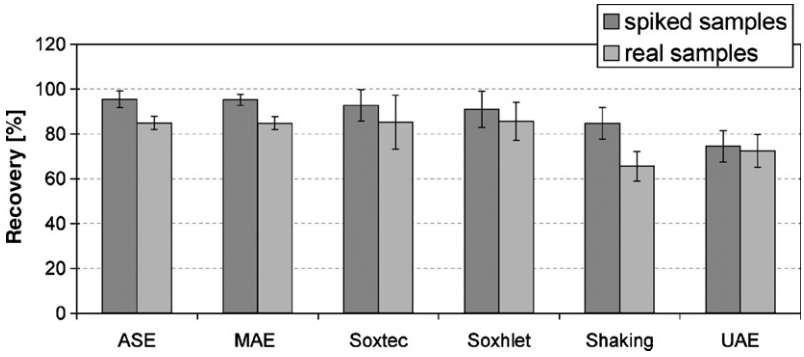

Fig. 7. Compaison of robenidine recovery obtained for ASE, MAE, Soxtec, Soxhlet, Shaking and UAE extraction. Real samples were obtained from manufacturer and contained certaine value of robenidine (according to the producer: 66 mg kg^{-1}).

extraction even 15% of the analyte was still isolated during the second repetition and nearly 5% during the third repetition of the extraction of the same spiked sample. The worst situation was observed using shaking, because a repetition of the extraction from the same sample gave nearly 20% of analyte recovered and the third one up to 10%.

3.5. Analyses of real-world samples

An overall comparison of the recoveries obtained for all the different extraction techniques applied within the scope of this paper (namely Soxhlet extraction, Soxtec, UAE, MAE, ASE, shaking) is shown in Fig. 7.

Interestingly, four from six checked techniques using acidified methanol (1% CH_3COOH) and sound choices of extraction time and temperature nearly identical data. Parameters which give the best results in terms of efficiency and extraction time are shown in Table 1.

The results have shown that the best extraction efficiency was achieved using the MAE and ASE techniques. The outcome of the statistical assessment also revealed that the relative standard deviations (R.S.D.) of these methods were very comparable, particularly 2.9% for ASE and 3.0% for MAE. The use of microwave energy enables rapid heating of the solvent mixture, accelerating the speed of the heating and consequently reducing the extraction time required. The extraction time is extremely short (2 min!), with the advantage of enabling the simultaneous extraction of even 12 samples. But cooling of the extract takes 20 min, so the final extraction time in case of MAE is usually established at 20–25 min. Alternatively, ASE combines high temperature with high pressure and dynamic extraction lead to slightly better extraction efficiency than conventional techniques. Although this technique required a little more time for packing of the thimbles, it has the great advantages of being fully automatic, samples could be easily extracted overnight, extra handling is not needed to separate the matrix from the solvent (as it is in case of all the others techniques), and reduced manpower is required.

The results showed that very good efficiency can be achieved for Soxtec and Soxhlet extractions. In general, data obtained

Table 1
Optimal parameters of investigated extraction techniques: ASE, MAE, Soxtec, Soxlet, shaking and UE

Technique of extraction	Conditions
ASE	Temperature: 80 °C
	Time of extraction: 4 min
	Flush: 100%
	Pressure: 1500 psi
	Number of cycles: 3
MAE	Temperature: 100 °C
	Time of extraction: 2 min
	Power: 150 W
Soxtec	Time of extraction: 30 min
Soxhlet	Time of extraction: 6 h
Shaking	Time of extraction: 30 min
UE	Time of extraction: 15 min

Table 2
Characteristic features of investigated extraction techniques

	Shaking	UAE	ASE	MAE	Soxhlet	Soxtec
Full time of extraction per one sample (include heating and cooling and filtration)	40 min	30 min	20 min	45 min	6.5 h	45 min
Volume of solvent used	60 ml	25 ml	30 ml	10 ml	45	25 ml
Parameters assisted of extraction	Shaking	Ultrasonic	Temperature pressure	Microwave	Temperature	Temperature
Level of difficulty	Low	Low	Medium	Medium	Low	Medium
Number of sample, which can be extracted simultaneously	One sample or series	One sample or series	One sample or series	One sample or series	One	6
Level of automatisation	Low	Low	High	High	Low	Medium
Cost of instruments	Low	Low	High	High	Low	Medium

using Soxtec are very similar to data achieved using Soxhlet, and robenidine was isolated from the feeding material with an efficiency reaching 90%. Even so, a relatively high R.S.D. is the largest disadvantage observed for both methods.

The lowest recovery was obtained for shaking and ultrasonic assisted extraction. Nevertheless shaking is the most frequently used extraction technique. The instrumentation required is not expensive and is frequently available at all analytical laboratories. UAE is also often applied. In case of isolation of robenidine from poultry samples using UAE and shaking R.S.D. varied a lot (7–9%).

The most important points concluded from this study of extraction techniques are summarised in Table 2.

4. Conclusions

Sample preparation is an essential part of every solvent based extraction procedure. While many types of samples can be efficiently extracted without any pre-treatment, lots of them will require some manipulation to achieve an efficient extraction. This study demonstrates, that for the determination of robenidine from feeding stuff, six different extraction techniques are in principle interchangeable. Although ASE and MAE have previously been considered as alternative methods, the results clearly classify ASE and MAE as methods with similar performance to the Shaking method, recommended by EU. The results have revealed that two alternative extraction methods, ASE and MAE, were more efficient than other conventional methods.

References

[1] G. Theodoridis, I.N. Papadoyannis, Microchim. Acta 136 (2001) 199–204.
[2] L. Pallaroni, C. von Holst, Anal. Bioanal. Chem. 376 (2003) 908–912.
[3] S. Babić, M. Petrović, M. Kaštelan - Macan, J. Chromatogr. A 823 (1998) 3–9.
[4] S. Sporring, S. Bøwadt, B. Svensmark, E. Björklund, J. Chromatogr. A 1090 (2005) 1–9.
[5] J. Shen, X. Shao, Anal. Bioanal. Chem. 383 (2005) 1003–1008.
[7] Commission Decision of 14 August 2002 implementing Council Directive 96/23/EC concerning the performance of analytical methods and the interpretation of results (notified under document number C (2002) 3044) (text with EEA relevance) (2002/657/EC).

Further reading

[6] J. Wilga, A. Kot-Wasik, Bromat. Chem. Toksykol. 38 (2005) 405–416.
[8] A. Kot-Wasik, A. Wasik, Anal. Chim. Acta 543 (2005) 46–51.
[9] Application Note 208, Methods Optimization in Accelerated Solvent Extraction (ASE®), Dionex.
[10] Application Note 326, Extraction of Drugs from Animal Feeds Using Accelerated Solvent Extraction (ASE®), Dionex.

Available online at www.sciencedirect.com
ScienceDirect
Talanta 73 (2007) 932–937
Talanta
www.elsevier.com/locate/talanta

Carbon nanotube/polystyrene composite electrode for microchip electrophoretic determination of rutin and quercetin in Flos Sophorae Immaturus

Jingjing Xu [a], Haiying Zhang [b], Gang Chen [a,*]

[a] School of Pharmacy, Fudan University, Shanghai 200032, China
[b] Department of Biology, Dezhou University, Dezhou 253023, China

Received 25 March 2007; received in revised form 13 May 2007; accepted 14 May 2007
Available online 21 May 2007

Abstract

In this report, carbon nanotube/polystyrene (CNT/PS) composite electrodes have been fabricated as sensitive amperometric detectors of microchip capillary electrophoresis (CE) for the determination of rutin and quercetin in Flos Sophorae Immaturus. The composite electrode was fabricated on the basis of the in situ polymerization of a mixture of CNT and styrene in the microchannel of a piece of fused silica capillary under heat. The surface morphologies of the composite in the electrodes were observed by using a scanning electron microscope. The performance of this unique system has been demonstrated by separating and detecting rutin and quercetin. The new CNT-based CE detector offered significantly lower detection potentials, yielded substantially enhanced signal-to-noise characteristics, and exhibited resistance to surface fouling and hence enhanced stability. It demonstrated long-term stability and reproducibility with a relative standard deviation of less than 5% for the peak current ($n = 20$) and should also find a wide range of applications in conventional CE, flowing injection analysis, and other microfluidic analysis systems.

Keywords: Carbon nanotube; Polystyrene; Composite; Capillary electrophoresis; Rutin; Quercetin; Flos Sophorae Immaturus

1. Introduction

Carbon nanotube (CNT) has attracted more and more attention since Iijima reported its existence in 1991 because of their high electrical conductivity, mechanical strength, and chemical stability [1–3]. The unique properties of CNT make it extremely attractive for electrochemical sensors and biosensors [4–6]. It has been found that CNT shows strong electrocatalytic activity and minimization of surface fouling when it was employed to improve the electrochemical response of some important bioactive substances [7–10]. Various CNT-based electrodes have been fabricated for electrochemical sensing, including CNT modified screen-printed carbon electrode [11], CNT powder microelectrode [12], CNT/PMMA composite electrode [13], magnetic CNT electrode [14], CNT/epoxy composite electrode [15], CNT/copper composite electrode [16], etc. Surface modification is the commonly used approach for fabricating CNT modified electrode. Recently, methods based on electrochemical deposition [17] and electrochemical polymerization [18,19] have been employed for loading CNT on electrodes. CNT-based electrodes have been demonstrated to reduce the overpotential and to promote the electron-transfer reactions significantly [4,17].

Nowadays, more and more attention has been paid to capillary electrophoresis (CE) microchips owing to their advantages of high performance, design flexibility, reagent economy, high throughput, miniaturization, and automation [11,20–23]. These microchip analysis systems hold considerable promise for biomedical and pharmaceutical analysis, clinical diagnostics, environmental monitoring, and forensic investigations [11,20–23]. Electrochemical detection (ECD) mainly in the mode of amperometric detection (AD) offers great promise for CE microchips, with features that include high sensitivity, inherent miniaturization of both the detector and the control instrumentation, low cost, low-power demands, and high compatibility with micromachining technologies [24–26]. The performance of microchip CE-AD is strongly influenced by the detection-electrode material. The detection electrode should

* Corresponding author. Tel.: +86 21 5423 7313; fax: +86 21 6418 7117.
E-mail address: gangchen@fudan.edu.cn (G. Chen).

0039-9140/$ – see front matter © 2007 Elsevier B.V. All rights reserved.
doi:10.1016/j.talanta.2007.05.019

provide favorable signal-to-background characteristics, as well as a reproducible response. A range of materials, including platinum, gold, and various forms of carbon, have thus been found useful for chip-based electrochemical detection [27–30].

Rutin and some related flavones are found widely presented in plants. It usually coexists with its aglycone, quercetin. Chinese traditional herbal medicine, Flos Sophorae Immaturus is the dried flower bud of *Sophora japonica* L. It possesses the function of cleaning away heat, preventing and treating blood capillary and hypertension diseases and can also be used as a haemostat [31]. Some related investigations show that rutin has a broad range of physiological activities such as anti-inflammatory [32], anti-tumor [33] and anti-bacteria [34]. It is thought to improve capillary function by reducing abnormal leakage and has been given to reduce capillary impairment and venous insufficiency of the low limb [35]. Quercetin has the similar effects such as anti-tumor [36], anti-bacteria [37] and inhibition of human platelet aggregation [38]. Rutin has been isolated from plants and used clinically as a therapeutic medicine [35]. The Pharmacopoeia of China requires the content of rutin in Flos Sophorae Immaturus should not be less than 20% [31]. Hence, it is necessary to develop some simple, economical and efficient methods for the determination of rutin and other flavones in herbal drugs or plants. Liquid chromatography, as a common analytical technique, has been widely used to determine rutin and coexistent flavones in plants [39–42]. Because both rutin and quercetin (their molecular structures are shown in Fig. 1) contain phenolic hydroxyl groups that are electroactive at modest oxidation potential on carbon electrodes, microchip CE-AD should be an assistant, alternative, and complement technique for the constituent investigation of Flos Sophorae Immaturus.

Polystyrene (PS) is a versatile polymer with the features of low price, good optic transparency, and excellent electric and mechanical properties. CNT/PS composites have been prepared by solvent evaporation [43] solution polymerization [44], emulsion polymerization [45], etc. The existing investigations mainly focus on its electrical prosperities. The prepared CNT composites cannot be used as electrode materials because the content of CNT in the composites was in the range of 0.1–2% (w/w) resulting in low conductivity [43–45]. In this work, CNT/PS composite microdisc electrode has been fabricated by in situ polymerization and employed as the end-column amperometric detector of a microchip CE system for the rapid determination of rutin and quercetin in Flos Sophorae Immaturus. The content of CNT in the composite was increased to 40% (w/w). The fabrication details, characterization, feasibility, and performance of the novel CNT/PS composite electrode have been demonstrated by monitoring flavones in connection with microchip CE in the following sections.

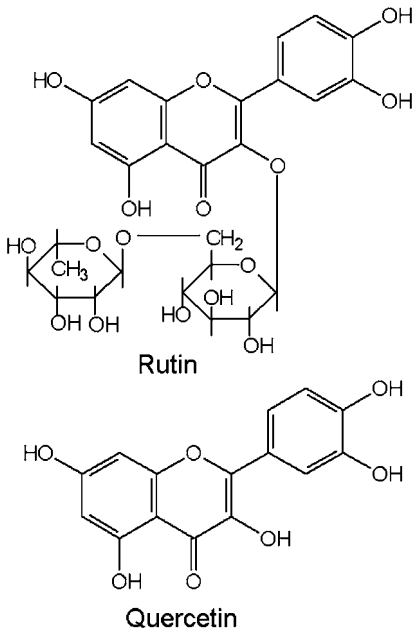

Fig. 1. Molecular structures of rutin and quercetin.

2. Experimental

2.1. Reagent and solutions

Both rutin and quercetin were obtained from Aldrich (Milwaukee, WI, USA). Multiwall carbon nanotube (MWCNT, 40–60 nM diameter, 5–15 μm long), with a purity of more than 95%, were provided by Shenzhen Nanoport Company (Shenzhen, China). Styrene, benzoyl peroxide (BPO), and borax were all purchased from SinoPharm (Shanghai, China). Before use, styrene needs to be purified by washing with 10% sodium hydroxide aqueous solution and distilled under vacuum. The graphite powder was supplied by Aldrich (Wilwaukee, WI, USA). All aqueous solutions were made up in doubly distilled water. Other chemicals were of analytical grade.

Stock solutions of rutin and quercetin (10 mM) were prepared in methanol and were kept in a 4 °C refrigerator. They were stable for at least 1 month. The running buffer was 50 mM borate buffer (pH 9.2). The stock solutions were diluted to the desired concentration with the running buffer just prior to use.

2.2. Apparatus

Details of the three-dimensionally (3D) adjustable microchip capillary electrophoresis-amperometric detection (CE-AD) system and its operation procedures have been described previously [26,46]. Briefly, a homemade ±4000 V high-voltage dc power supply provided a voltage for the electrophoretic separation and the electrokinetic sample introduction. The simple-cross single-separation channel glass microchip was obtained from Micralyne (model MC-BF4-001, Edmonton, Canada). The original detection cell was cut off; leaving the channel outlet at the end side of the chip, thus facilitate the end-column AD. The 88 mm × 16 mm chip shown consisted of a four-way injection cross with a 74 mm long separation channel and 5 mm long each injection channels. The channels had a maximum depth of 20 μm and a width of 50 μm at the top. Short pipet tips were inserted into the holes of the various reservoirs. A 3-D adjustable Plexiglass device for microchip CE-AD was fabricated for housing the separation chip and the detector, allowing

their convenient replacement, and facilitating the precise 3D alignment between the outlet of the separation channel and a capillary-based microdisc electrode for end-column AD [46]. Platinum wires, inserted into the individual reservoirs on the holder, served as contacts to the high voltage power supply. An YS73-4A-3KVA alternate constant-voltage power supply (Shanghai Keyi Instrumental Factory, Shanghai, China) was employed to suppress the voltage fluctuation of the power line. In order to improve the repeatability of the peak current and migration time, the whole CE system was assembled in a room that was air-conditioned at 25 °C to reduce the temperature fluctuation.

2.3. Electrode fabrication

Fig. 2 illustrates the schematic of the fabrication process for the composite electrodes. Prior to the fabrication of the electrode by in situ polymerization, 0.2 g of BPO was dissolved in 20 mL of styrene and the clear mixture solution in a conical flask was allowed to prepolymerize to generate a dense prepolymer solution in an 85 °C water bath for ~60 min. The CNT powder and the viscous prepolymerized styrene solution were hand-mixed at a ratio of 2:3 (w/w). Subsequently, a piece of copper wire (b, 10 cm long, 150 μm diameter) was inserted into a 3.0 cm long fused silica capillary (a, 320 μm i.d. × 450 μm o.d., Hebei Yongnian Ruipu Chromatogram Equipment Co., Ltd., Hebei, China) and a 2 mm opening was left in the capillary for the subsequent filling of the mixture (c) of the prepolymerized styrene and CNT powder. The mixture (c) was then packed into the capillary by pressing the opening end of the capillary (to a depth of ~3 mm) into a sample of the composite. The CNT-containing mixture should touch the end of the copper wire inside the capillary tightly for the electric contact and was then allowed to polymerize completely in a 50 °C oven for 12 h. Finally, hot melt adhesive (e) was applied to glue copper wire (b) in place.

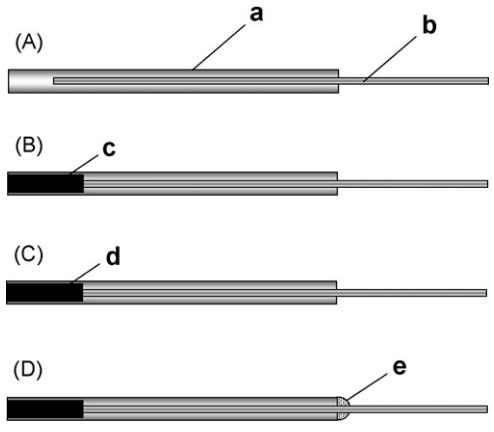

Fig. 2. Schematic of the fabrication process for the composite electrode. (A) Inserting a piece of copper wire (b, 10 cm long, 150 μm diameter) into a 3.0 cm long fused-silica capillary (a, 320 μm i.d. × 450 μm o.d.); (B) filling the other end of (a) with prepolymerized styrene solutions containing graphite or CNT (c); (C) polymerizing under heat to form CNT/PS or graphite/PS composite (d); (D) applying hot melt adhesive (e) to glue (b) in place.

The filled end of the electrode was successively polished with emery paper to form a CNT/polystyrene (PS) composite disc electrode. The graphite/polystyrene (graphite:PS = 2:3 (w/w)) composite electrode, used for comparison, was prepared in the same procedures. The morphology of graphite/PS and CNT/PS composites was observed by a PHILIPS XL 30 scanning electron microscope (SEM, Netherlands).

2.4. Sample preparation

Flos Sophorae Immaturus (i.e. Japanese Pagodatree flower bud, a traditional Chinese medicine) was obtained from Sun-Tian-Tang Traditional Chinese Medicine Store (Shanghai, China). It was dried at 60 °C for 2 h and then was pulverized. About 2 g of the powder was weighed accurately and dispersed in 100 mL of methanol. The mixture was kept in a 60 °C water bath for 3 h. After cooling, it was sonicated for 30 min and filtered through a filter paper. The extract was diluted using 50 mM borate buffer (pH 9.2) at a ratio of 10 (1–10) just prior to CE analysis.

2.5. Electrophoretic procedure

Before use, the composite microdisc electrode was successively polished with emery paper and alumina powder, sonicated in doubly distilled water, and finally the surface of the detection electrode was positioned carefully opposite the channel outlet of the separation channel through the guiding metal tube. The gap distance between the disc electrode and the channel outlet was adjusted to 50 μm approximately by comparison with the channel width (50 μm) while being viewed under a microscope. Amperometric detection for microchip CE was performed with a CHI 830B electrochemical analyzer (Shanghai Chen-Hua Instruments Co., Shanghai, China) in combination with a three-electrode electrochemical cell consisting of a laboratory-made disc detection electrode, an auxiliary electrode, and an Ag/AgCl wire reference electrode. The electropherograms were recorded with a time resolution of 0.1 s (without any software filtration) using the "amperometric *i–t* curve" mode while applying the detection potential. Sample injections were performed after stabilization of the baseline. All experiments were performed at room temperature.

The channels of the glass chip were treated before use by rinsing with 0.1 M NaOH and doubly distilled water for 10 min each. The running buffer reservoir and the unused reservoir were filled with running buffer solution, while the sample reservoir was filled with a sample solution. The detection cell was filled with the running buffer solution. A high voltage was applied for 20 s to the sample reservoir to facilitate the filling of the injection channel, while the detection cell was grounded and all the other reservoirs were floating. The sample solution was loaded into the separation channel by applying an injection voltage to the sample reservoir for 3 s, while the detection cell grounded and other reservoirs were kept floating. The separation was performed by applying a separation voltage to the running buffer reservoir with the detection cell grounded and other reservoirs floating.

3. Results and discussion

The graphite/PS and the CNT/PS composite electrode were directly fabricated in the bore of a 320 μm i.d. and 450 μm o.d. fused silica capillary due to the size compatibility of the electrode and the channel outlet (20 μm deep, 50 μm wide), providing an simple way to prepare the detection electrodes for microchip CE. Fig. 3 shows the SEM images of the surface of the 40% (w/w) graphite/PS (A) and the 40% (w/w) CNT/PS (B) composites. It can be seen clearly from Fig. 3B that the carbon nanotubes are dispersed and embedded throughout the PS matrix and an interconnected CNT network has formed. This conductive nanotube network may establish electrical conduction pathways throughout the whole system, which is responsible for the electric conductivity and electrochemical sensing. Fig. 3A indicates that the sheet-like structure of graphite still exists in the graphite/PS composite.

In the present work, the CNT/PS composite microdisc electrode was coupled with microchip CE system as an end-column amperometric detector. The attractive performance of the detector is indicated from the detection of two flavones offering enhanced sensitivity, lower noise levels, and well-resolved peaks. Shown in Fig. 4 are representative electropherograms for a mixture containing rutin and quercetin at the graphite/PS (A) and CNT/PS (B) composite electrode detectors. The two flavones can be separated resulting in well-defined and resolved peaks with the CNT/PS composite electrode within 150 s. Fig. 5A depicts the typical hydrodynamic voltammograms (HDVs) for the oxidation of 0.5 mM rutin on the graphite/PS and

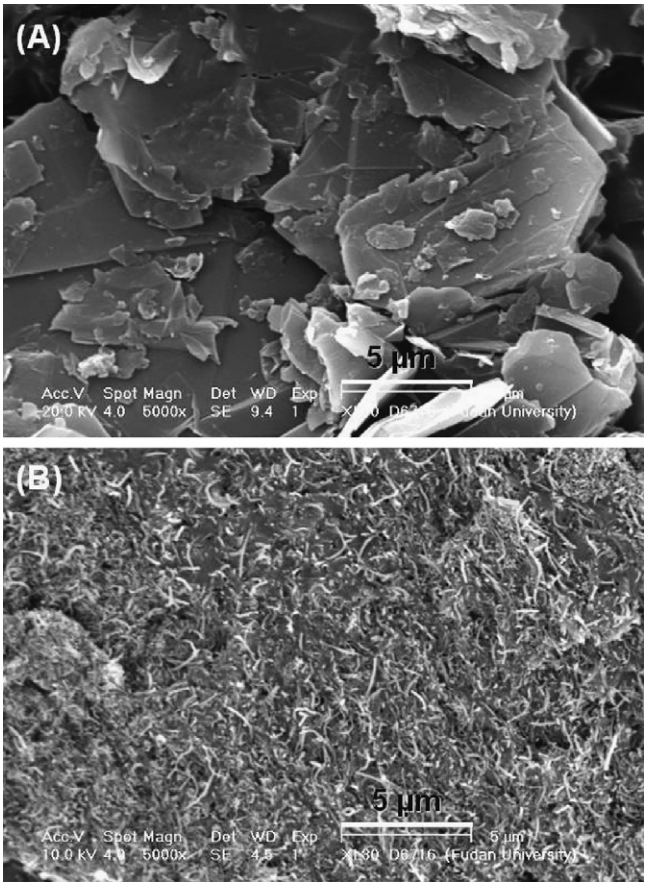

Fig. 3. Scanning electron micrograph (SEM) images of the cross section of the graphite/PS composite (A) and the CNT/PS (B) composite. Conditions: accelerating voltage, 20 kV; magnification, 5000×.

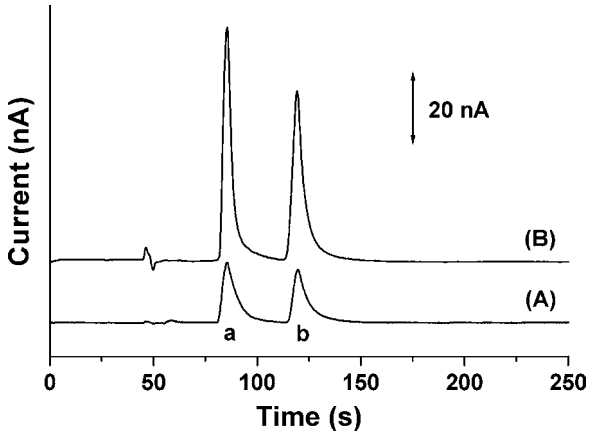

Fig. 4. Electropherograms for a mixture containing 0.5 mM of rutin (a) and quercetin (b) at the graphite/PS (A) and the CNT/PS (B) composite microdisc electrodes. The separation channel in the glass CE microchip, 50 μm wide × 20 μm deep × 74 mm long; separation and injection voltage, +2000 V; injection time, 3 s; running buffer, 50 mM borate buffer (pH 9.2); detection potential, +0.8 V (vs. Ag/AgCl electrode).

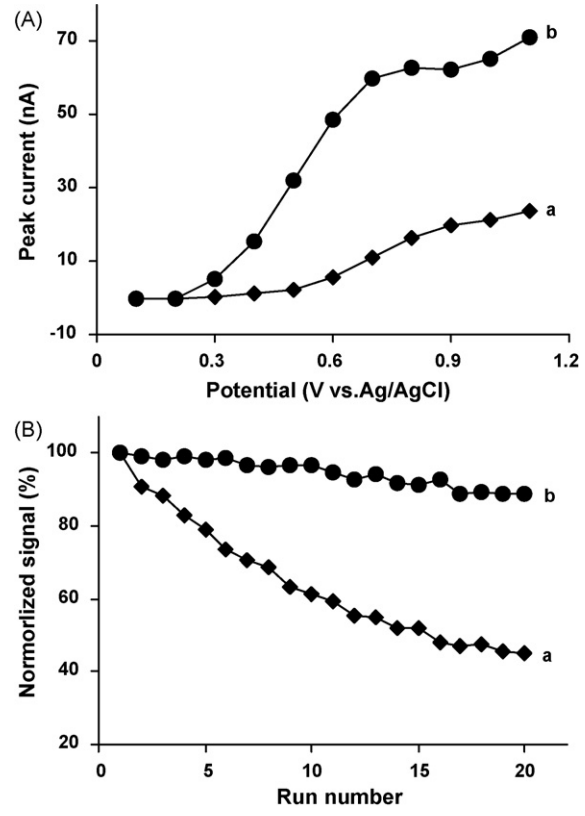

Fig. 5. (A) Hydrodynamic voltammograms (HDVs) for 0.5 mM rutin at the graphite/PS (a) and the CNT/PS (b) composite electrodes and (B) stability of the response for repetitive measurements of 100 μM rutin at the graphite/PS (a) and the CNT/PS (b) composite microdisc electrodes. Other conditions, as in Fig. 4.

CNT/PS composite microelectrodes. The curves were recorded point-wise over the +0.1 to +1.1 V (versus Ag/AgCl electrode) range by changing the applied potential by 0.1 V. The current response of the CNT/PS composite electrode is higher than that of the graphite-based electrode at the same potential although the geometric areas of both electrodes are the same. When the applied potential exceeds +0.50 V for the graphite/PS and +0.30 V for the CNT/PS composite electrodes, the peak current of both electrodes raises rapidly. However, the current response increases much slowly upon increasing the potential above +0.90 V and +0.70 V for the graphite/PS and the CNT/PS composite electrodes, respectively. The applied potential of the CNT-based electrode was, therefore, maintained at +0.80 V, under which condition the background current was not too high and the signal-to-noise ratio was the highest. The half-wave potentials at the graphite/PS and CNT/PS composite disc electrode are +0.67 and +0.49 V for rutin. The electrocatalytic activity toward the investigated analyte is pronounced as the half-wave potential on the CNT/PS composite electrode has decreased by 180 mV in comparison with that on the graphite/PS composite electrode, indicating that the CNT-based electrode allows amperometric detection with higher sensitivity and at significantly lower detection potentials.

The ability of CNT to promote electron-transfer reactions on the electrode has been attributed to their special electronic structure and high electrical conductivity [11]. As shown in Fig. 4A and B, the peak currents of rutin and quercetin at the CNT/PS composite electrodes are much higher than those at the graphite/PS detector. The sensitivities of rutin and quercetin were 126.3 and 91.54 nA mM^{-1} at the CNT/PS composite electrode and 32.68 and 28.62 nA mM^{-1} at the graphite/PS composite electrode, respectively. The higher sensitivity of the CNT/PS composite detector is well in agreement with the HDV data and leads to lower detection limits compared to the graphite/PS composite electrode [0.48 μM versus 7.34 μM (rutin) and 0.66 μM versus 8.39 μM (quercetin), respectively (based on S/N = 3)]. Overall, the CNT/PS composite is a promising material for electrochemical sensing. The present CNT/PS composite electrode shows low-noise characteristics and stable baseline, which is not always a case of other CNT electrodes in conventional CE and microchip CE, such as CNT coated electrodes [11,47] and CNT paste electrodes [16,48]. The typical detection limits of the CNT coated and the CNT paste electrodes employed as microchip CE detectors were in the ranges of 6.9–7.9 and 20–25 μM for catecholamines [11] and carbohydrates [16], respectively. This CNT/PS electrode has a significant advantage over other CNT electrodes mentioned above because it is rigid and stable and is not prone to wearing over time. Its low-noise level may be attributed to the stable and rigid conductive network of the CNT/PS composite. The enhanced current response of the present CNT/PS composite electrode can be ascribed to not only the electrocatalytic activity of CNT, but also the higher surface area of the CNT composite.

In this work, the performances of the CNT/PS and graphite/PS composite electrodes were compared to demonstrate the advantages of CNT for electrochemical sensing in combination with CE microchip. Recently, Compton's group has significantly demonstrated that both CNT-based electrode and edge-plane pyrolytic graphite electrode showed similar electrocatalytic activity toward a range of redox systems while basal plane pyrolytic graphite electrode displayed low activity, indicating the edge plane sites of edge plane pyrolytic graphite electrode were electroactive sites [6,49,50]. In this work, the graphite/PS composite electrode was made from a mixture of graphite powder and prepolymerized styrene. A great deal of edge plane sites of graphite were embedded in the composite so that the electrocatalytic activity of the graphite/PS composite electrode was poor, resulting in lower current response. As shown in Fig. 3B, the CNTs (40–60 nM diameter) on the surface of the composite work like thousands upon thousands nanoelectrodes. The mass transfer on the CNT electrode network is much faster than that on the micro-size graphite on the surface of the graphite/PS composite so that the current response was enhanced to some extent.

During the amperometric detection of microchip and conventional CE, some analytes tend to be adsorbed on the surface of the detection electrode. Sometimes, nonconducting polymers may form on the electrode. Such surface fouling usually results in decreased signal. The electrocatalytic detection on the CNT/PS composite electrode is coupled to resistance to surface fouling and hence good stability. Such improvements were illustrated by the microchip CE measurements of rutin that is known to promote surface passivation [51]. Fig. 5B displays the response of the graphite/PS (a) and CNT/PS (b) detectors to 20 repetitive CE measurements of 0.1 mM rutin. The initial response was found to drop off gradually at the graphite-based detector, with a decrease of 55% (R.S.D. 26%, $n = 20$). In contrast, a stable response (R.S.D. of 4.1%, $n = 20$), with a very slow decrease of the response (up to 11%) is observed over the entire operation for the CNT-based detector. The good stability is coupled to a reproducible response. The higher anti-passivation capability of the CNT/PS composite can be attributed to the electrocatalytic activity of CNT.

The CNT/PS composite electrode detector offers a well-defined concentration dependence. The calibration curves exhibit satisfactory linear relationship between the peak cur-

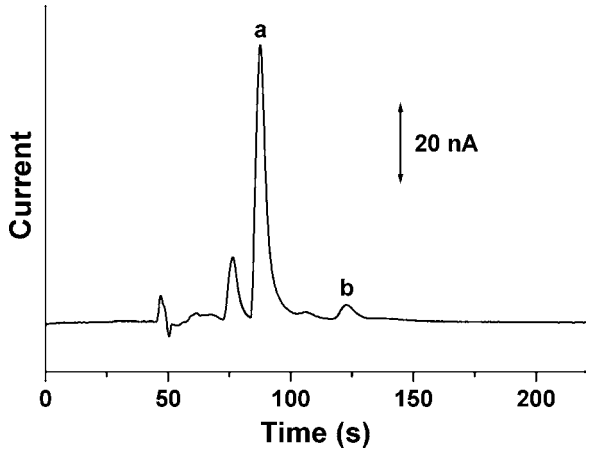

Fig. 6. Typical electropherogram for the diluted extract from a sample of Flos Sophorae Immaturus in 50 mM borate buffer (pH 9.2). Other conditions, as in Fig. 4.

Table 1
Results from assay of rutin and quercetin in Flos Sophorae Immaturus ($n = 3$, mg/g)[a]

Sample	Rutin	Quercetin
1	164.4 (2.8)[b]	5.402 (3.3)
2	204.7 (2.4)	6.214 (2.9)
3	211.0 (3.1)	4.857 (3.7)

[a] Conditions are the same as in Fig. 4.
[b] The data in the parentheses are the R.S.D.s (%).

rent and the concentration for both rutin and quercetin over the concentration range from 1 μM to 1 mM. The linear equations were $y = 0.1033 + 126.7x$ ($R = 0.9995$, rutin), $y = 0.1142 + 91.85x$ ($R = 0.9991$, quercetin), where y is the peak current (nA), x the concentration of the analytes (mM), and R is the correlation coefficient.

The suitability of the CNT/PS composite electrode for measuring rutin and quercetin in herbal drug can be demonstrated in Fig. 6 that illustrates the typical electropherogram of a diluted extract from a sample of Flos Sophorae Immaturus in 50 mM borate buffer (pH 9.2). Peak identification was performed by the standard addition method. The assay results are summarized in Table 1. The determined contents of rutin and quercetin in the three samples of Flos Sophorae Immaturus are well in agreement with the data in a previous report [51].

4. Conclusions

In summary, we have developed a new approach based on the in situ polymerization of styrene for the fabrication of CNT/PS composite electrode as the end-column amperometric detector of microchip CE. The performance, the utility, and the advantages of the novel set-up have been demonstrated in combination with the separation and detection of two naturally occurring flavones in traditional Chinese medicine. It is characterized by its higher resolution and sensitivity, lower expense of operation, and less amount of sample. The new CNT-based CE detector offers favorable signal-to-background characteristics, good resistance to surface fouling, strong electrocatalytic activity, sharp peaks for the analytes, and simple design and fabrication. It is concluded that microchip CE coupled with CNT/PS composite amperometric detector is an efficient approach for the constituent and fingerprint study of herbal drugs due to its special attributes.

Acknowledgments

This work was supported by Shanghai Science Committee (051107089), NSFC (20675017 and 20405002), and State Education Ministry of China.

References

[1] S. Iijima, Nature 354 (1991) 56.
[2] R.H. Baughman, A. Zakhidov, W.A. de Heer, Science 297 (2002) 787.
[3] P.M. Ajayan, Chem. Rev. 99 (1999) 1787.
[4] J. Wang, Electroanalysis 17 (2005) 7.
[5] R.S. Chen, W.H. Huang, H. Tong, Z.L. Wang, J.K. Cheng, Anal. Chem. 75 (2003) 6341.
[6] C.E. Banks, T.J. Davies, G.G. Wildgoose, R.G. Compton, Chem. Commun. 7 (2005) 829.
[7] Z.H. Wang, J. Liu, Q.L. Liang, Y.M. Wang, G. Luo, Analyst 127 (2002) 653.
[8] G. Zhao, S.Q. Zang, K.Z. Liu, S. Lin, J. Liang, X.Y. Guo, Z.J. Zhang, Anal. Lett. 35 (2002) 2233.
[9] J. Wang, M. Musameh, Analyst 128 (2003) 1382.
[10] M. Musameh, J. Wang, A. Merkoci, Y.H. Lin, Electrochem. Commun. 4 (2002) 743.
[11] J. Wang, G. Chen, M.P. Chatrathi, M. Musameh, Anal. Chem. 76 (2004) 298.
[12] Y.D. Zhao, W.D. Zhang, H. Chen, Q.M. Luo, Talanta 58 (2002) 529.
[13] X. Yao, X.J. Xu, P.Y. Yang, G. Chen, Electrophoresis 27 (2006) 3233.
[14] S. Qu, J. Wang, J.L. Kong, P.Y. Yang, G. Chen, Talanta 71 (2007) 1096.
[15] G. Chen, L.Y. Zhang, W. Wang, Talanta 64 (2004) 1018.
[16] J. Wang, G. Chen, M. Wang, M.P. Chatrathi, Analyst 129 (2004) 512.
[17] X.L. Luo, J.J. Xu, J.L. Wang, H.Y. Chen, Chem. Commun. 16 (2005) 2169.
[18] M.L. Guo, J.H. Chen, J. Li, B. Tao, S.Z. Yao, Anal. Chim. Acta 532 (2005) 71.
[19] M. Gao, S. Huang, L. Dai, G. Wallace, R. Gao, Z. Wang, Angew. Chem. Int. Ed. 39 (2000) 3664.
[20] D.R. Reyes, D. Iossifidis, P.A. Auroux, A. Manz, Anal. Chem. 74 (2002) 2623.
[21] P.A. Auroux, D. Iossifidis, D.R. Reyes, A. Manz, Anal. Chem. 74 (2002) 2637.
[22] G. Chen, J.H. Li, S. Qu, D. Chen, P.Y. Yang, J. Chromatogr. A 1094 (2005) 138.
[23] G. Chen, Y.H. Lin, J. Wang, Talanta 68 (2006) 497.
[24] W.R. Vandaveer, S.A. Pasas, R.S. Martin, S.M. Lunte, Electrophoresis 23 (2002) 3667.
[25] J. Wang, Talanta 56 (2002) 223.
[26] G. Chen, H.M. Bao, P.Y. Yang, Electrophoresis 26 (2005) 4632.
[27] J. Wang, M.P. Chatrathi, B.M. Tian, Anal. Chim. Acta 416 (2000) 9.
[28] R.S. Martin, K.L. Ratzlaff, B.H. Huynh, S.M. Lunte, Anal. Chem. 74 (2002) 1136.
[29] W.R. Vandaveer, S.A. Pasas-Farmer, D.J. Fischer, C.N. Frankenfeld, S.M. Lunte, Electrophoresis 25 (2004) 3528.
[30] L. Nyholm, Analyst 130 (2005) 599.
[31] Committee of National Pharmacopoeia, Pharmacopoeia of People's Republic of China, vol. 1, Press of Chemical Industry, Beijing, 2005, pp. 246–247.
[32] R.M. Gene, C. Cartana, T. Adzet, E. Marin, T. Panella, S. Canigueral, Planta Med. 62 (1996) 232.
[33] R. Ramanathan, W.P. Das, C.H. Tan, Int. J. Oncol. 3 (1993) 115.
[34] A. Hasan, I. Ahmad, Fetoterapia 67 (1996) 182.
[35] J.E.F. Reynolds, MARTINDALE, the Extra Pharmacopoeia, 31st ed., The Royal Pharmaceutical Society, Council of the Royal Pharmaceutical Society of Great Britain, London, 1996, pp. 1.679–1.680.
[36] J.F.M. Post, R.S. Varma, Cancer Lett. 67 (1992) 207.
[37] M. Liu, S. Matsuzaki, Dokkyo, J. Med. Sci. 22 (1995) 253.
[38] A. Bertz, A. Stierle, R. Anton, Biochem. Pharmacol. 31 (3) (1982) 597.
[39] A. Hasler, O. Sticher, J. Chromatogr. 508 (1990) 236.
[40] L. Nancy, R.A. Dixon, P.W. Geno, J. Mass Spectrum. 31 (1996) 472.
[41] A. Rehmald, B. Meier, D. Sticher, J. Chromatogr. A 677 (1994) 25.
[42] E. Conde, E. Cadahia, M.C. Garcia-Vallejo, Chromatographia 41 (1995) 657.
[43] T.E. Chang, A. Kisliuk, S.M. Rhodes, W.J. Brittain, A.P. Sokolov, Polymer 47 (2006) 7740.
[44] Z. Wang, M. Lu, H.L. Li, X.Y. Guo, Mater. Chem. Phys. 100 (2006) 77.
[45] H.S. Xia, G.H. Qiu, Q. Wang, J. Appl. Polym. Sci. 100 (2006) 3123.
[46] X. Yao, J. Wang, L.Y. Zhang, P.Y. Yang, G. Chen, Talanta 69 (2006) 1285.
[47] M. Pumera, X. Llopis, A. Merkoci, S. Alegret, Microchim. Acta 152 (2006) 261.
[48] M. Chicharro, A.E. Sanchez, Bermejo, A. Zapardiel, M.D. Rubianes, G.A. Rivas, Anal. Chim. Acta 543 (2005) 84.
[49] R.R. Moore, C.E. Banks, R.G. Compton, Anal. Chem. 76 (2004) 2677.
[50] C.E. Banks, R.G. Compton, Analyst 130 (2005) 1232.
[51] G. Chen, H.W. Zhang, J.N. Ye, Anal. Chim. Acta 423 (2000) 69.

Available online at www.sciencedirect.com
ScienceDirect
Talanta 73 (2007) 820–830
Talanta
www.elsevier.com/locate/talanta

Influence of extractant on quality and trace elements content of peat humic acids

C. Zaccone [a,*], C. Cocozza [a], V. D'Orazio [a], C. Plaza [b], A. Cheburkin [c], T.M. Miano [a]

[a] *Dipartimento di Biologia e Chimica Agro-Forestale ed Ambientale, Università degli Studi di Bari, Via Amendola 165/A, 70126 Bari, Italy*
[b] *Centro de Ciencias Medioambientales, Consejo Superior de Investigaciones Cientificas, Serrano 115 dpdo., 28006 Madrid, Spain*
[c] *Institute of Environmental Geochemistry, University of Heidelberg, Im Neuenheimer Feld 236, 69120 Heidelberg, Germany*

Received 21 February 2007; received in revised form 26 April 2007; accepted 30 April 2007
Available online 10 May 2007

Abstract

Among several extractants used to isolate humic acids (HA) from terrestrial environments, sodium hydroxide (NaOH) and sodium pyrophosphate ($Na_4P_2O_7$) are the most utilized. In order to evaluate the influence of these different extractant solutions on the HA quality and on their trace elements content, HA were isolated from five *Sphagnum*-peat samples using three different solutions: (a) 0.5 M NaOH; (b) 0.1 M $Na_4P_2O_7$; (c) 0.5 M NaOH + 0.1 M $Na_4P_2O_7$. The obtained HA have been analyzed with respect to ash content, elemental composition, main atomic ratios and characterized by FT-IR and total luminescence (TL) spectroscopies. In addition, both raw peat and HA have been analyzed using X-ray fluorescence in order to determine the Br, Cu, Fe, Ni, Pb and Zn contents.

Results showed that HA extracted with NaOH and NaOH + $Na_4P_2O_7$ are quite similar with respect to ash, elemental contents and spectroscopic characteristics, while $Na_4P_2O_7$ solution, which in general reduces the extraction yield, seems to affect the nature of HA, featuring a more complex and aromatic character. With respect to the contents in the corresponding raw peat samples, the HA fractions were richer in Br, Cu and Ni, regardless of the extractant used, and poorer in Fe, Pb and Zn. Further, Br, Cu, Ni and Zn were more concentrated in HA extracted with $Na_4P_2O_7$ than in those extracted with NaOH and NaOH + $Na_4P_2O_7$, probably because of the greater affinity of these elements for these more aromatic humic molecules.

Keywords: Humic acids; *Sphagnum*-peat; Extractant; Trace elements; Spectroscopy

1. Introduction

Humic substances (HS) are refractory, dark coloured, heterogeneous organic compounds produced as by-products of microbial metabolism. These materials, widespread in all terrestrial and aquatic environment, can be isolated according to a fractionation scheme based on their water solubility under acidic or alkaline conditions. Briefly, humin is the insoluble fraction of humic substances; humic acids (HA) are the fraction soluble under alkaline conditions; and fulvic acids (FA) are the fraction soluble in all pH range [1].

Different models have been proposed for HA structure in the literature. Commonly, HA are believed to consist of large polymers presenting newly formed molecular structures scarcely resembling those of the original precursor [1]. A more recent theory views HS as supra-molecular associations in which several relatively small and chemically diverse organic molecules form clusters linked by hydrogen bonds (H-bonds) and hydrophobic interactions [2,3].

More renowned isolation methods should take into account that soil organic matter (OM) occurs as: (a) insoluble macromolecular complex; (b) macromolecular complexes bound together by di- and trivalent cations (i.e. Ca^{2+}, Fe^{3+} and Al^{3+}); (c) in combination with clay minerals, through polyvalent cations bridges (clay-metal-humus) and H-bonding; (d) organic substances held within the inter-layers of expanding-type clay minerals [1].

Numerous extractants (e.g. NaOH, Na_2CO_3, $Na_4P_2O_7$, NaF, organic acid salts) have been employed, depending upon the nature of the material to be examined [4].

Sodium hydroxide (NaOH) and sodium pyrophosphate ($Na_4P_2O_7$) have been widely used in HA extraction. Several authors [1,5,6] showed that, in general, the HA extraction yield using NaOH (from 0.1 to 0.5 M) is greater than the $Na_4P_2O_7$

* Corresponding author. Fax: +39 080 5442850.
E-mail address: zaccone@agr.uniba.it (C. Zaccone).

0039-9140/$ – see front matter © 2007 Elsevier B.V. All rights reserved.
doi:10.1016/j.talanta.2007.04.052

one, even though the use of $Na_4P_2O_7$ (at 0.1–0.15 M) produces reduced chemical alterations. Neutral salts, in fact, are thought to extract OM by forming insoluble precipitates or soluble complexes with Ca, Fe and Al and other polyvalent cations to which soil OM is linked. As a result, soil OM is converted to water-soluble Na-salts [7].

In general, a solution of 0.1 M $Na_4P_2O_7$ extracts less than 30% of the OM removed by a solution of 0.1 M NaOH [1], even if the latter seems to extract more high-molecular weight OM [8,9].

Previous investigations on the influence of various extractants on the yields and structural properties of HA have been focused mainly on soil HA [1,5,6,8,9]. In contrast, relatively little attention has been devoted to HA isolated from peat. In addition, no data are available in the literature on the effects of the extractants on trace elements contents in HA. Thus, the objective of this work was to investigate the structural features and trace element contents of HA extracted from different layers of an ombrotrophic bog profile as affected by three different extractants including NaOH, $Na_4P_2O_7$ and NaOH + $Na_4P_2O_7$.

2. Materials and methods

Etang de la Gruère is a small ombrotrophic peat bog located in the Jura Mountains, NW Switzerland. A peat core, 2T (13 cm × 13 cm × 105 cm), was collected in 2005 using a Wardenaar peat profile sampler [10]. The core was sliced into 1 ± 0.15 cm sections using a stainless steel band saw with stainless steel blades. Humic acids were extracted from five peat samples from this core using three different solutions, i.e. (i) 0.5 M NaOH; (ii) 0.1 M $Na_4P_2O_7$; (iii) 0.5 M NaOH + 0.1 M $Na_4P_2O_7$. The sampling site and procedure as well as the main properties of the peat profile are described more in detail elsewhere [11].

After stirring for 12 h under N_2 atmosphere at room temperature, centrifugation, and filtration through Whatman GF/C filter, the alkaline extract was acidified with HCl to pH 1 and allowed to precipitate for 24 h. The sediment was separated from the supernatant by centrifugation, washed with a solution of Milli-Q water + HCl (pH = 3), manually shaken, and centrifuged. Milli-Q water was added to the sediment and stirring was carried out for 3 h. Finally, the HA were transferred to a dialysis membrane (Spectra/Por membrane, MWCO 6-8000) and dialyzed against Milli-Q water, successively replaced at frequent intervals (6–7 h) in order to remove Cl^- until the EC of discharged water decreased below 10^{-2} dS m^{-1}. Following these treatments, the HA were freeze-dried. All solutions were prepared with high purity water (18.2 MΩ cm) from a Milli-Q Element system (Millipore, Molsheim, France) and high purity grade reagents.

The ash content, expressed as a percentage of the initial dry weight, was determined by combustion at 550 °C for 12 h; all samples were analyzed in triplicate.

Carbon, hydrogen, nitrogen, and sulphur concentrations were determined using a combustion-gas chromatography technique (Fisons EA 1108 Elemental Analyzer, Milan, Italy). Oxygen content was calculated by difference: O% = 100−(C + H + N + S)%. The instrument was calibrated by BBOT [2,5-bis-(5-*tert*-butyl-benzoxazol-2-yl)-thiophen] standard (ThermoQuest Italia s.p.a.). The obtained data were corrected for moisture and ash contents. All HA samples were analyzed in triplicate.

The FT-IR spectra were acquired in transmittance mode using a Thermo Nicolet Nexus FT-IR Spectrophotometer equipped with a Nicolet Omnic 6.0 software. Potassium bromide pellets were obtained by pressing, under vacuum, a homogenized mixture of 400 mg of infrared-grade KBr and 1 mg of sample. Spectra were recorded under a N_2 atmosphere in the range of 4000–400 cm^{-1}, with 2 cm^{-1} resolution and 64 scans per each acquisition.

Total luminescence spectra (TL) in the form of excitation–emission matrix (EEM, contour maps) were obtained on aqueous solutions of HA at a concentration of 100 mg L^{-1} equilibrated overnight at room temperature, and adjusted to pH 8 with 0.05 M NaOH. All spectra were recorded using a Perkin-Elmer (Norwalk, CT) LS 55 luminescence spectrophotometer equipped with the WinLab 4.00.02 software (Perkin-Elmer Inc., 2001, Norwalk, CT) for data processing. Emission and excitation slits were set at a 5 nm band width, and a scan speed of 500 nm min^{-1} was selected for both monochromators. The fluorescence EEM spectra were recorded over the emission wavelength range from 350 to 550 nm, increasing sequentially by 5 mm step the excitation wavelength from 300 to 500 nm. The EEM plots were generated as contour maps from fluorescence data by using the Surfer 8.01 software (Golden Software Inc., 2002, Golden, CO).

The EMMA-XRF analyses were carried out on powered samples with no further preparation. Selected trace elements (Br, Cu, Fe, Ni, Pb, and Zn) were measured directly on dried, milled peat and related humic acids with a 600 s analysis time. Calibration, lower limits of detection (LLD), accuracy and precision of this method are given elsewhere [12,13].

3. Results and discussion

Obtained data show that the extraction yield ($EY = g_{HA}/g_{dry\ peat} \times 100$) is affected by the extractant used for HA isolation. In particular, it ranges between 7.6% (2T 13) and 22.8% (2T 41) with 0.5 M NaOH, between 0.3% (2T 21) and 2.0% (2T 41) with 0.1 M $Na_4P_2O_7$, and between 8.0% (2T 21) and 18.0% (2T 41) with the mixture of both solutions. Regardless of the extractant utilized, the EYs generally increase with depth following homogeneous and highly correlated trends ($R^2 > 0.9$) (Fig. 1).

According to Choudhri and Stevenson [14], the variability in EY could be ascribed to the different pH values, ranging between ca. 12.5 with 0.5 M NaOH and/or the mixture, and ca. 9.0 with 0.1 M $Na_4P_2O_7$ (Fig. 2).

3.1. Elemental analysis, main atomic ratios and ash content

Data reported in Table 1 shows that the elemental composition of HA extracted with NaOH and NaOH + $Na_4P_2O_7$ is quite similar, whereas it appears slightly different in $Na_4P_2O_7$ extracted HA. In general, the latter exhibits, in agreement with the litera-

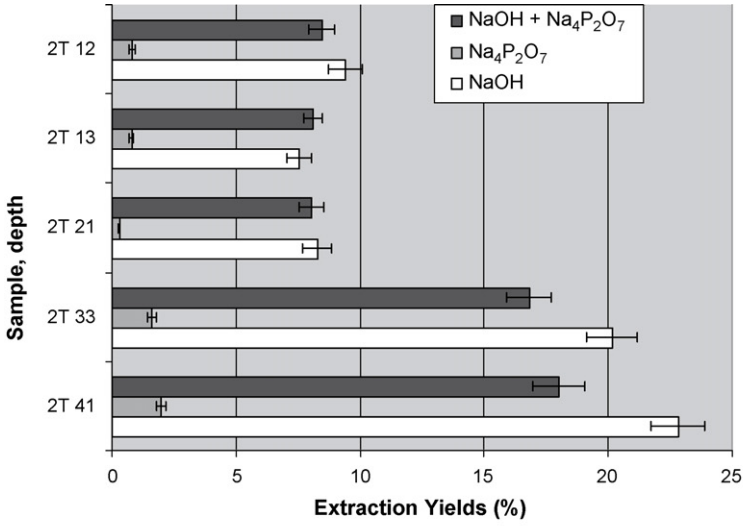

Sample	Depth (cm)	Average depth (cm)	Extraction Yields (%)		
			NaOH	$Na_4P_2O_7$	NaOH + $Na_4P_2O_7$
2T 12	9.4 – 10.5	9.9	9.4±0.7	0.8±0.1	8.5±0.5
2T 13	10.5 – 11.6	11.0	7.6±0.5	0.8±0.1	8.1±0.4
2T 21	18.8 – 19.9	19.3	8.3±0.6	0.3±0.0	8.0±0.5
2T 33	32.7 – 34.0	33.4	20.1±1.0	1.6±0.2	16.8±0.9
2T 41	42.7 – 43.9	43.3	22.8±1.1	2.0±0.2	18.0±1.0

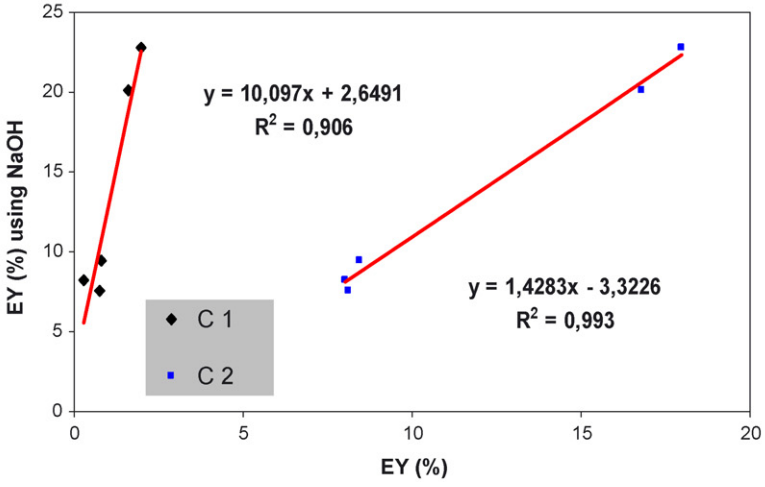

Fig. 1. Humic acids extraction yields (EYs) along the profile and correlations among EYs obtained with different solutions. C1: NaOH EY correlated to $Na_4P_2O_7$ EY; C2: NaOH EY correlated to NaOH + $Na_4P_2O_7$ EY.

ture [7], lower C and H contents and greater S and O ones with respect to the others. Similar N content is measured for all HA extracted.

Humic acids extracted with $Na_4P_2O_7$ show, with respect to those extracted with the other extractants, an higher C/H ratio suggesting the occurrence of humic macromolecules with extended molecular complexity and aromatic character. These samples present simultaneously also highest O/C ratios, commonly inversely related to the C/H ratio and due to the degree of oxidation, thus suggesting the possible formation of insoluble phosphate compounds with polyvalent cations occurring onto the humic molecule surfaces (Fig. 3), as reported elsewhere [15]. The much higher ash content seems to confirm this hypothesis.

The C/N ratio is rather similar in all HA extracted from deep samples (i.e. 2T 33 and 2T 41), while, in samples from the upper layers, $Na_4P_2O_7$ extracted HA show lower values of this ratio.

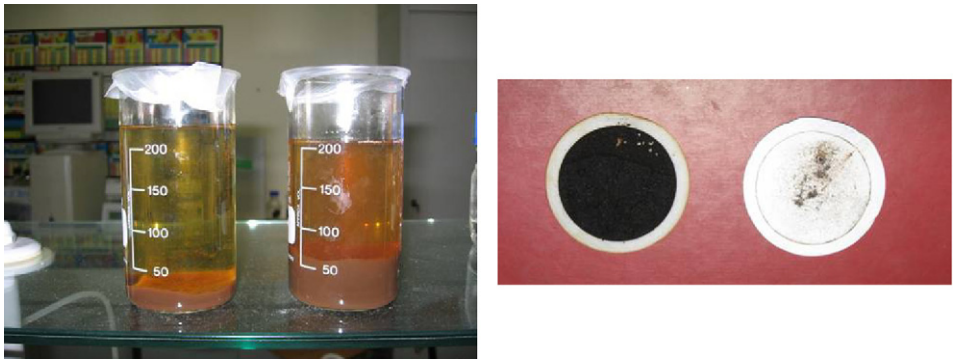

Fig. 2. Comparison between the flocculated amounts and between the material collected on the Whatman GF/C filter after centrifugation. In both cases, the sample on the left was extracted with $Na_4P_2O_7$, while the one on the right with NaOH.

Anyway, regardless of the extractant used, the C/N ratio and the O/C one decrease with depth, whereas C/H shows an opposite trend. According to Stevenson [1], data suggest an increasing peat decomposition with depth, as well as reported elsewhere [11].

3.2. FT-IR spectroscopy

FT-IR spectra of some representative HA samples extracted with different solutions are reported in Fig. 4.

All spectra are characterized by a number of absorption bands, exhibiting variable relative intensities, typical of humic-like materials [1,16,17]: (1) a broad band at about 3420–3400 cm^{-1}, generally ascribed to O–H stretching of hydrogen bonded O–H groups; (2) twin peaks at 2925 and 2855 cm^{-1}, due to asymmetric and symmetric C–H stretching of CH_2 and CH_3 groups, respectively; (3) a distinct peak at 1720 cm^{-1}, typically associated to the C=O stretching of carbonyl functions, particularly aldehydes, ketones, and carboxyl groups; (4) a wide absorption band at about 1620 cm^{-1}, ascribed to aromatic and olefinic vibrations and COO^- groups; (5) a discrete peak at about 1520–1515 cm^{-1}, possibly ascribed to aromatic skeletal vibrations, to conjugated C=N systems and amino functionalities; (6) two peaks at 1450 and 1420 cm^{-1}, ascribed to the C–H bending of CH_2 and CH_3 groups; (7) a peak at 1380 cm^{-1}, ascribed to asymmetric stretching of COO^- groups and C–H bending of CH_2 and CH_3 groups; (8) a broad band at 1220 cm^{-1}, probably due to C–O stretching and OH bending of carboxyl groups; (9) a peak at about 1156 cm^{-1}, probably due to O–H stretching of alcoholic groups; (10) a band at 1080–1070 cm^{-1}, probably due to phosphono-group stretching and/or mineral impurities; (11) a band at 1040–1030 cm^{-1}, ascribed to OH stretching of polysaccharides.

FT-IR spectra of HA extracted with NaOH and NaOH + $Na_4P_2O_7$ do not show significant differences throughout the profile. On the contrary, $Na_4P_2O_7$ extracted HA spectra show some important differences. In particular, peaks located at 2920–2855 and 1420 cm^{-1} are less intense and defined, confirming a minor aliphatic character of these HA in comparison to the others. In addition, the $Na_4P_2O_7$ extracted HA features inversely a decreased aliphaticity (1040 cm^{-1}) and an increase of phosphono-group signals (1080 cm^{-1}) on the HA surfaces, also in agreement with the elemental analysis data and ash content.

Table 1
Elemental analysis, main atomic ratios and ash content of differently extracted humic acids

	Average depth (cm)	C (%)	H (%)	N (%)	S (%)	O (%)	C/N	C/H	O/C	Ash (%)
2T 12 HA_{NaOH}	−9.9	54.91 ± 0.29	5.82 ± 0.11	2.12 ± 0.01	0.08 ± 0.02	37.07	30.2	0.79	0.51	2.44
2T 12 $HA_{Na_4P_2O_7}$	−9.9	49.50 ± 1.14	5.08 ± 0.06	2.15 ± 0.12	0.33 ± 0.02	42.93	26.8	0.81	0.65	9.70
2T 12 $HA_{NaOH+Na_4P_2O_7}$	−9.9	52.95 ± 1.47	5.51 ± 0.44	1.91 ± 0.06	0.11 ± 0.04	39.53	32.4	0.80	0.56	5.14
2T 13 HA_{NaOH}	−11.0	56.12 ± 0.63	6.11 ± 0.16	2.18 ± 0.04	0.13 ± 0.02	35.46	30.0	0.77	0.47	2.34
2T 13 $HA_{Na_4P_2O_7}$	−11.0	50.52 ± 0.99	5.02 ± 0.01	2.22 ± 0.01	0.32 ± 0.00	41.92	26.6	0.84	0.62	6.67
2T 13 $HA_{NaOH+Na_4P_2O_7}$	−11.0	55.84 ± 0.19	5.89 ± 0.13	1.98 ± 0.06	0.08 ± 0.02	36.20	32.9	0.79	0.49	4.82
2T 33 HA_{NaOH}	−33.4	58.55 ± 0.34	5.94 ± 0.10	2.61 ± 0.01	0.10 ± 0.02	32.81	26.2	0.82	0.42	1.59
2T 33 $HA_{Na_4P_2O_7}$	−33.4	55.62 ± 0.72	4.88 ± 0.25	2.52 ± 0.02	0.28 ± 0.04	36.70	25.7	0.95	0.49	7.77
2T 33 $HA_{NaOH+Na_4P_2O_7}$	−33.4	57.73 ± 0.81	5.95 ± 0.32	2.60 ± 0.10	0.15 ± 0.05	33.57	25.9	0.81	0.44	3.96
2T 41 HA_{NaOH}	−43.3	58.94 ± 0.75	5.93 ± 0.30	3.39 ± 0.07	0.09 ± 0.03	31.65	20.3	0.83	0.40	1.91
2T 41 $HA_{Na_4P_2O_7}$	−43.3	55.93 ± 0.31	4.80 ± 0.02	3.21 ± 0.02	0.19 ± 0.02	35.86	20.3	0.97	0.48	8.63
2T 41 $HA_{NaOH+Na_4P_2O_7}$	−43.3	58.91 ± 0.34	5.96 ± 0.11	3.41 ± 0.06	0.14 ± 0.04	31.58	20.2	0.82	0.40	4.06

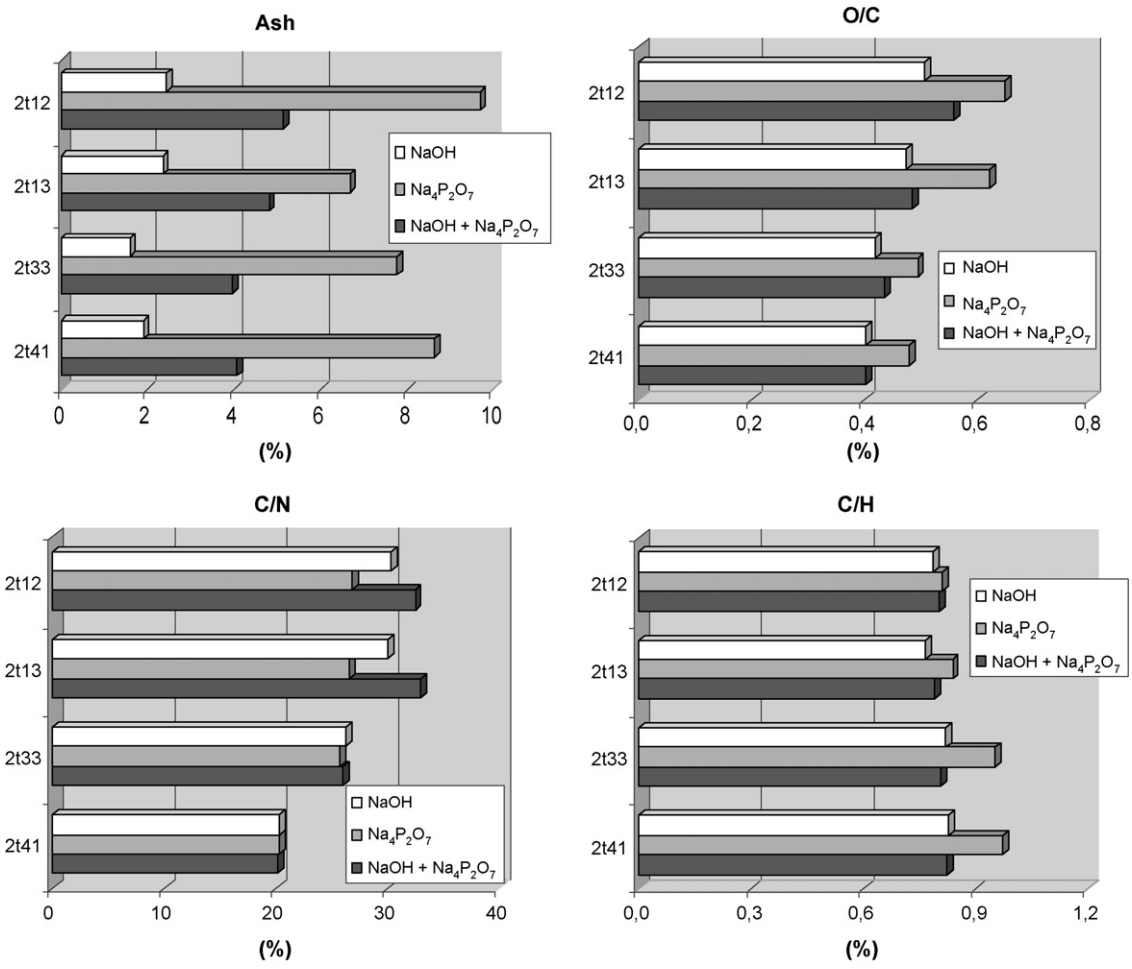

Fig. 3. Ash content and atomic ratios of differently extracted humic acids.

3.3. Fluorescence spectroscopy

In general, EEM spectra (Fig. 5) of $Na_4P_2O_7$ extracted HA feature the highest fluorescence intensity (FI) values, both for the main and the secondary (shoulder) fluorophore, with respect to the others. Further, they also show the main fluorophore centered at higher excitation/emission wavelengths pairs (EEWP) with respect to the other HA and a shoulder, absent in the other HA samples, located in the top high hand side of the contour map (470 exc/528 em nm). With increasing depth, FI values of the shoulder increase, whereas those of the main peak initially tend to decrease (Table 2). The EEM spectra of HA extracted with NaOH + $Na_4P_2O_7$ and NaOH are characterized by the appearance, in the high wavelengths region, of a shoulder which, similarly to the previous HA, shows increasing FI values with depth. Moreover, the spectra of these HA also exhibit slight variations both of the wavelength pairs localization and the FI values of the main fluorophore (Fig. 5).

In general, fluorescence data suggest that the HA isolated with NaOH + $Na_4P_2O_7$ and especially NaOH, as compared to the $Na_4P_2O_7$ isolated HA, are characterized by a larger occurrence of aliphatic components of wider molecular heterogeneity

Table 2
Excitation/emission wavelength pairs (EEWP, nm/nm) and relative fluorescence intensities (RFI, arbitrary units) in the fluorescence excitation–emission matrix spectra of selected HA samples

HA samples	EEWP	RFI	
		Main peak	Secondary peaks and/or shoulders
2T 13 HA_{NaOH}	375/468	15.4	
2T 13 $HA_{Na_4P_2O_7}$	395/484	18.4	
	470/528		11.9
2T 13 $HA_{NaOH+Na_4P_2O_7}$	370/483	16.9	
2T 33 HA_{NaOH}	385/499	14.0	
	370/482		13.6
	470/525		10.8
2T 33 $HA_{Na_4P_2O_7}$	470/525	19.4	
	385/471		14.5
2T 33 $HA_{NaOH+Na_4P_2O_7}$	380/486	14.0	
	470/526		10.8
2T 41 HA_{NaOH}	375/479	15.0	
	470/525		12.2
2T 41 $HA_{Na_4P_2O_7}$	475/526	22.6	
	385/482		19.5
2T 41 $HA_{NaOH+Na_4P_2O_7}$	379/468	13.6	

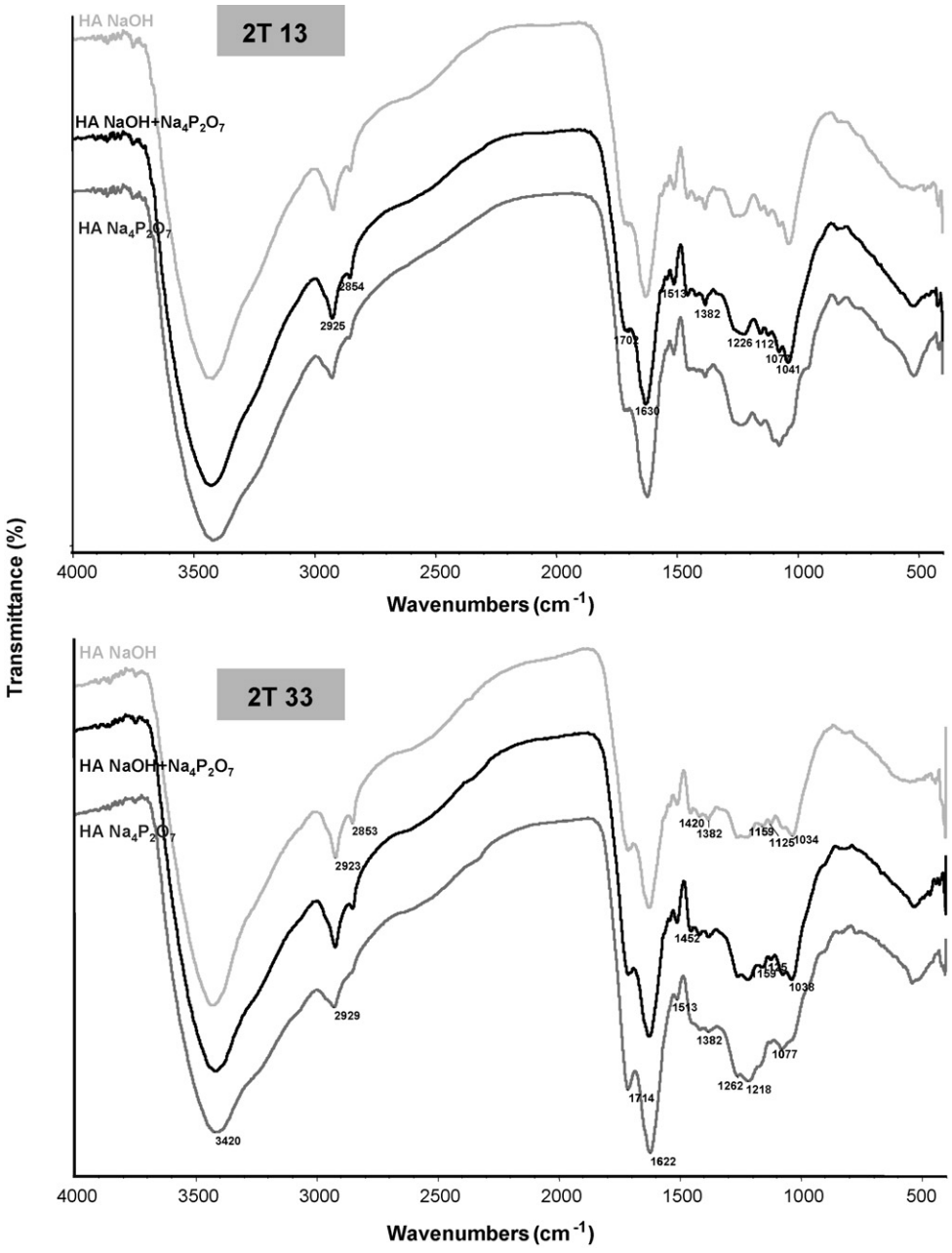

Fig. 4. FT-IR spectra relative to two HA samples (2T 13 and 2T 33) extracted with NaOH, NaOH + $Na_4P_2O_7$, and $Na_4P_2O_7$, respectively.

and lower molecular weight and aromaticity features. With increasing depth, molecular units of higher structural complexity seem to appear. On the contrary, $Na_4P_2O_7$ extracted HA seem to closely resemble linearly/condensed aromatic ring systems and/or unsaturated bond systems capable of a high degree of conjugation.

3.4. X-ray fluorescence

Fig. 6 shows the percentage content of each studied element in HA, considered 100 the correspondent one in the peat. In Fig. 7 and in Table 3, instead, the elemental concentrations in raw peat and HA are compared.

3.4.1. Bromine

At least 32.0% of the Br in peat is recovered in HA extracted with NaOH and with the mixture of both extractants, while Br reaches 6.6% by using $Na_4P_2O_7$.

Bromine concentration in HA is always higher than the one in the peat, regardless of the extractant used. In particular, Br seems to be more concentrated in $Na_4P_2O_7$ extracted HA showing a greater affinity for the more aromatic and complex fraction of organic matter.

However, even though the metabolic pathway is still not clear, data show that Br could be stably incorporated into HA molecules, as already reported by Zaccone [18] who presented similar results analyzing HA from two different ombrotrophic peat cores.

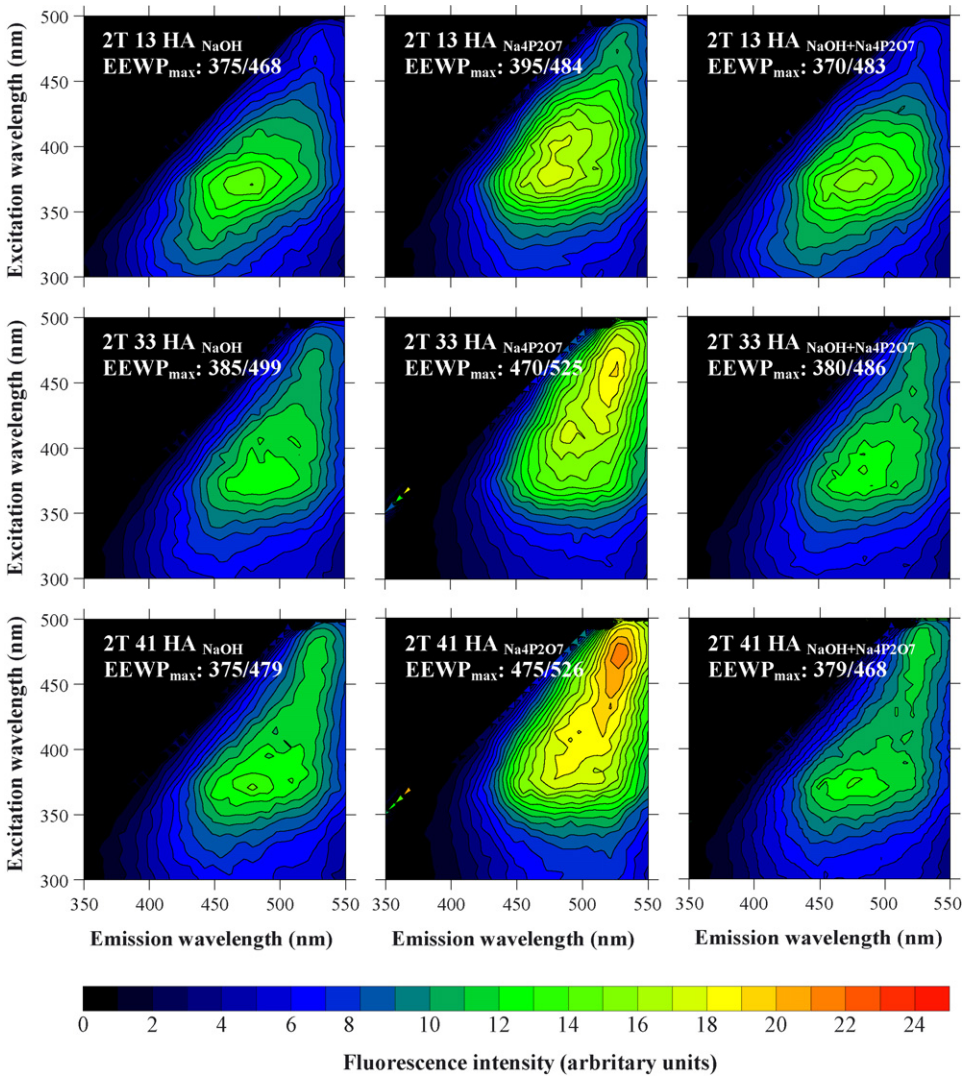

Fig. 5. Fluorescence excitation–emission matrix spectra of humic acids (HA) of representative *Sphagnum*-peat samples extracted using NaOH, $Na_4P_2O_7$ and NaOH + $Na_4P_2O_7$. $EEWP_{max}$: excitation/emission wavelength pairs at the maximum fluorescence intensity.

3.4.2. Copper

The total Cu content varies from 66.6% in NaOH extracted HA, 48.8% in HA extracted with the mixture of both extraents, to 27.9% in $Na_4P_2O_7$ extracted HA.

Copper concentrates dramatically in HA, especially in the $Na_4P_2O_7$ extracted HA, thus confirming its great affinity for the organic matter in general, and the humified fraction in particular [19], behaving as a soft cation and therefore forming inner-sphere complexes.

3.4.3. Iron

The total Fe content decreases from 4.6% in NaOH extracted HA to less than 0.5% in the other two cases. Although the apparent influence of $Na_4P_2O_7$, the limited occurrence of Fe also in NaOH extracted HA suggests a rather weak Fe affinity with humic molecules.

Iron concentration in HA is always lower than the one in raw peat, regardless of the extractant used, possibly because Fe, prevalently occurring as Fe^{2+} in the anoxic conditions characterizing the bog [20], is rapidly oxidized to Fe^{3+} during the oven drying procedure and finally precipitated as insoluble chemical forms prior the extraction.

3.4.4. Nickel

The total Ni average content ranges from 35.9% in NaOH extracted HA, 18.1% in HA extracted with the mixture of both extraents, to 10.4% in $Na_4P_2O_7$ extracted HA. With respect to raw peat, Ni concentration is always higher in HA, especially considering the HA extracted with $Na_4P_2O_7$.

Nickel shows a behaviour very similar to Cu, suggesting its possible involvement in inner-sphere complexes with the organic matter.

3.4.5. Lead

Although the total Pb average content is very low in HA extracted both with $Na_4P_2O_7$ (0.1%) and the mixture of both

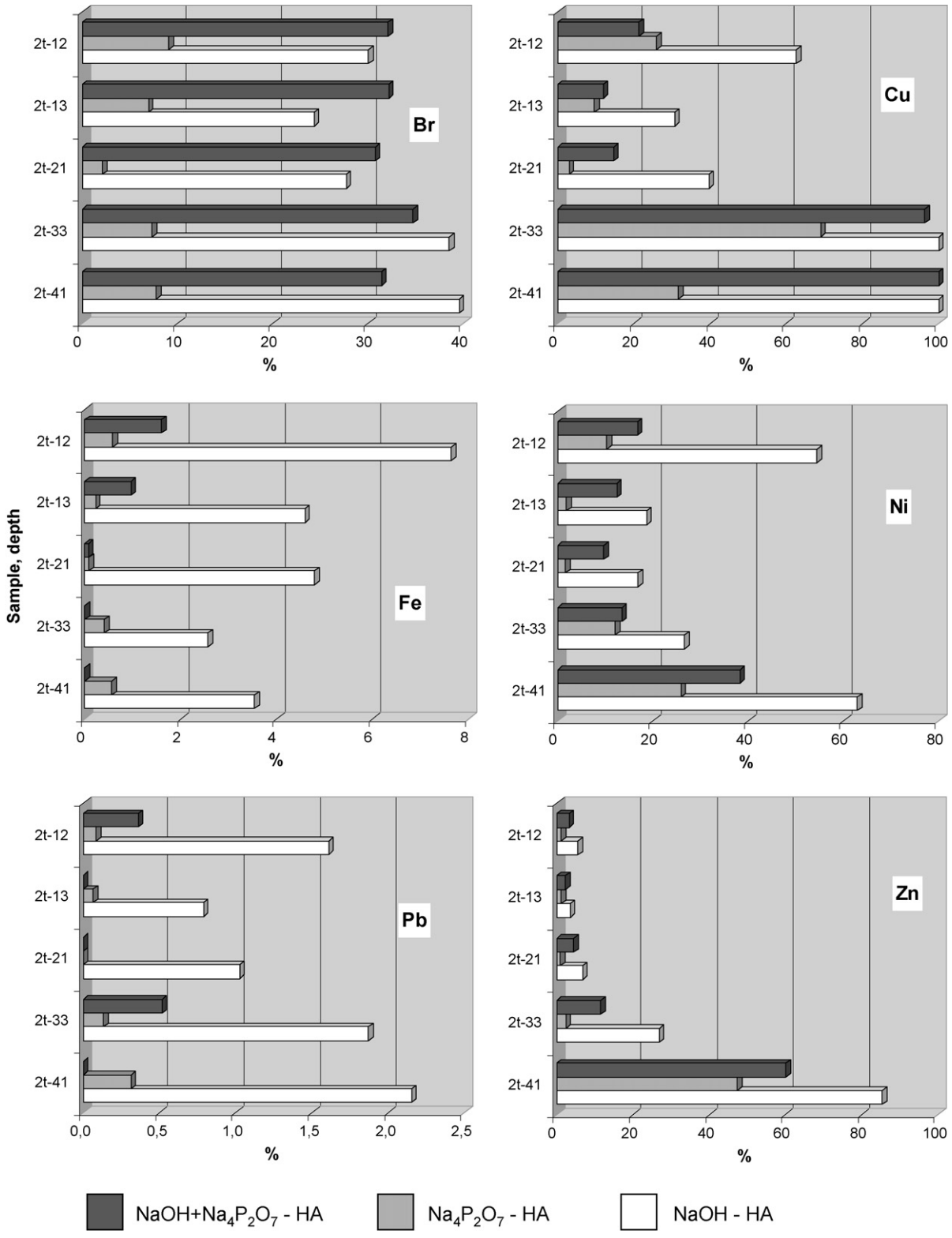

Fig. 6. Content of each element in differently extracted HA, considered 100 the total content in peat.

extractants (0.2%), and taking into account the possible formation of insoluble Pb-phosphates during the HA extraction, the very limited amount of Pb in NaOH extracted HA (1.5%) seems to suggest the extremely weak interaction of this element with humic molecules.

3.4.6. Zinc

Zinc concentration in HA is generally lower than the one in the peat, except for HA extracted with $Na_4P_2O_7$; thus, also this element seems to show a greater affinity for the more aromatic and complex fraction of organic matter. Zinc content in HA is

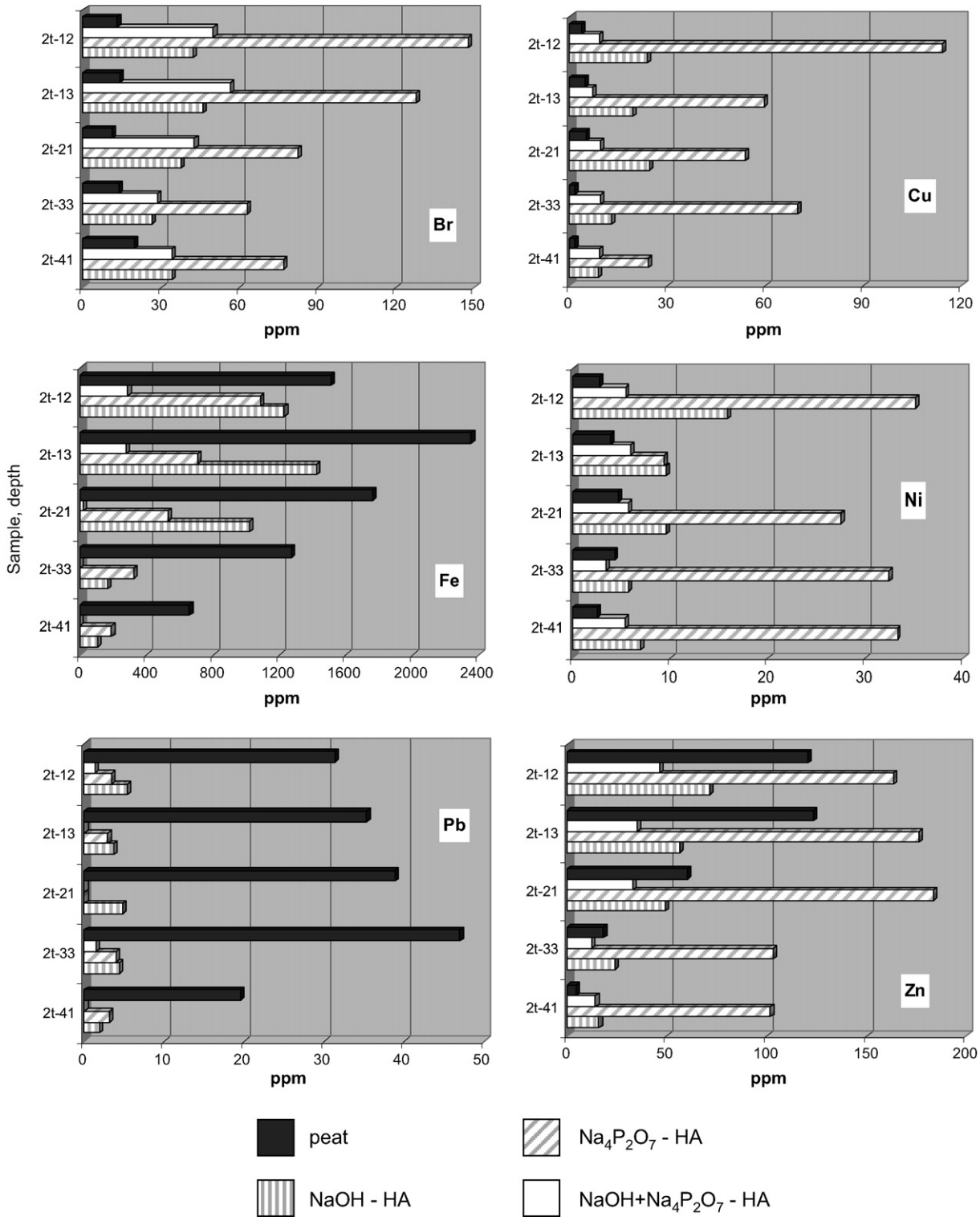

Fig. 7. Elemental concentrations both in raw peat and in differently extracted HA.

very low in the upper samples (from 2T 12 to 2T 21), where the total average content is less than 5.5%, while it increases in the bottom samples, reaching a maximum value of 85.6%. Although several authors demonstrated that Zn is relatively weakly complexed by HA [21–24], our data suggest that at high metal concentration, most of Zn is bound as an outer-sphere complex, whereas, at low concentrations, Zn^{2+} tend to form inner-sphere complexes with HA.

Table 3
Trace element contents ($\mu g\,g^{-1}$) in raw peat and related HA differently extracted

	Trace elements					
	Br ($\mu g\,g^{-1}$)	Cu ($\mu g\,g^{-1}$)	Fe ($\mu g\,g^{-1}$)	Ni ($\mu g\,g^{-1}$)	Pb ($\mu g\,g^{-1}$)	Zn ($\mu g\,g^{-1}$)
LDD	0.6	1.5	10.0	2.0	0.6	2.0
2T 12 raw peat	13.2 ± 1.3	3.6 ± 0.7	1509.6 ± 75.5	2.5 ± 1.0	31.3 ± 3.1	120.4 ± 6.0
2T 12 HA_{NaOH}	42.1 ± 4.2	23.7 ± 2.4	1226.4 ± 61.3	15.8 ± 1.6	5.4 ± 1.1	71.5 ± 7.1
2T 12 $HA_{Na_4P_2O_7}$	147.6 ± 44.3	114.1 ± 34.2	1084.2 ± 325.3	35.1 ± 10.5	3.4 ± 1.2	163.2 ± 48.9
2T 12 $HA_{NaOH+Na_4P_2O_7}$	50.0 ± 5.0	9.0 ± 0.9	286.2 ± 14.3	5.4 ± 1.1	1.3 ± 0.3	46.2 ± 4.6
2T 13 raw peat	14.3 ± 1.4	4.8 ± 1.0	2351.5 ± 117.6	3.9 ± 1.2	35.3 ± 3.5	123.3 ± 6.2
2T 13 HA_{NaOH}	45.9 ± 4.6	19.4 ± 1.9	1423.7 ± 71.2	9.6 ± 1.4	3.7 ± 0.7	56.4 ± 5.6
2T 13 $HA_{Na_4P_2O_7}$	127.6 ± 38.3	59.5 ± 17.9	705.9 ± 211.8	9.4 ± 2.8	2.9 ± 1.0	176.1 ± 52.8
2T 13 $HA_{NaOH+Na_4P_2O_7}$	56.7 ± 5.7	7.0 ± 0.7	278.7 ± 13.9	6.0 ± 0.9	<LLD	35.2 ± 3.5
2T 21 raw peat	11.2 ± 1.1	5.1 ± 0.8	1759.5 ± 88.0	4.7 ± 1.4	38.9 ± 3.9	60.2 ± 6.0
2T 21 HA_{NaOH}	37.5 ± 3.7	24.5 ± 2.4	1019.1 ± 51.0	9.6 ± 1.4	4.8 ± 1.0	49.2 ± 4.9
2T 21 $HA_{Na_4P_2O_7}$	82.5 ± 24.8	53.7 ± 16.1	528.2 ± 158.5	27.5 ± 8.2	<LLD	183.4 ± 55.0
2T 21 $HA_{NaOH+Na_4P_2O_7}$	42.8 ± 4.3	9.3 ± 0.9	17.8 ± 3.6	5.7 ± 1.1	<LLD	32.9 ± 3.3
2T 33 raw peat	13.8 ± 1.4	1.6 ± 0.6	1271.8 ± 63.6	4.3 ± 1.3	47.0 ± 4.7	18.0 ± 1.8
2T 33 HA_{NaOH}	26.3 ± 2.6	13.0 ± 1.3	161.8 ± 8.1	5.7 ± 1.1	4.4 ± 0.9	23.9 ± 2.4
2T 33 $HA_{Na_4P_2O_7}$	62.8 ± 18.8	69.6 ± 20.9	323.9 ± 97.2	32.4 ± 9.7	3.9 ± 1.4	102.9 ± 30.9
2T 33 $HA_{NaOH+Na_4P_2O_7}$	28.5 ± 2.8	9.3 ± 0.9	<LLD	3.4 ± 1.0	1.4 ± 0.3	12.3 ± 1.2
2T 41 raw peat	19.6 ± 2.0	1.5 ± 0.5	658.0 ± 32.9	2.5 ± 0.9	19.5 ± 2.0	4.2 ± 0.8
2T 41 HA_{NaOH}	34.0 ± 3.4	8.8 ± 0.9	102.2 ± 10.2	7.0 ± 1.0	1.8 ± 0.4	15.8 ± 1.6
2T 41 $HA_{Na_4P_2O_7}$	77.0 ± 23.1	24.2 ± 7.2	187.2 ± 56.2	33.2 ± 10.0	3.1 ± 1.1	101.7 ± 30.5
2T 41 $HA_{NaOH+Na_4P_2O_7}$	34.2 ± 3.4	8.9 ± 0.9	<LLD	5.4 ± 0.8	<LLD	14.1 ± 1.4

Lower detection limits (LDD) and standard deviations are also reported.

4. Conclusions

In the present paper, authors isolated HA from several samples along a peat profile using three different extractants in order to verify their influence both on HA quality and on the content of selected trace elements (Br, Cu, Fe, Ni, Pb and Zn).

Elemental composition, main atomic ratios, FT-IR and fluorescence data indicate that HA extracted with NaOH and $NaOH + Na_4P_2O_7$ are quite similar and differ markedly from the $Na_4P_2O_7$ extracted ones.

All analytical results confirm the role of $Na_4P_2O_7$ in selectively extracting high molecular weight organic materials, rich in aromatic features but poor in aliphatic compounds. In particular, FT-IR spectra and atomic ratios strongly support the dominant role of pyrophosphate in solubilizing preferentially more aromatic compounds from the raw material and in adding phosphono-groups on the HA surface. At the same time, total luminescence spectra indicate the occurrence of linearly/condensed aromatic ring systems and a high degree of unsaturated bond systems in these HA with respect to the ones isolated with NaOH.

Furthermore, the EMMA X-ray fluorescence underlines on one hand that HA get rich in Br, Cu and Ni, regardless of the extraent used, while a depletion of Fe, Pb and, partially, Zn is observed; on the other hand, that Br, Cu, Ni and Zn are more concentrated in $Na_4P_2O_7$ extracted HA probably because of their greater affinity for this more aromatic and complex humic material. The higher elemental concentration in $Na_4P_2O_7$ extracted HA is consistent with a higher ash content compared to NaOH and $NaOH + Na_4P_2O_7$ extracted HA.

Further studies are needed to investigate more closely the chemical mechanisms and the complexation behaviour of different trace elements in natural organic soils in order to better understand the environmental fate of this chemical species and to provide more clear indications on the practical application of these organic materials in the agriculture and industrial field.

Acknowledgement

A special thank goes to Prof. William Shotyk, University of Heidelberg, for providing peat samples and allowing XRF analysis in his institute.

References

[1] F.J. Stevenson, Humus Chemistry. Genesis, Composition, Reactions, 2nd ed., Wiley & Sons, New York, 1994.
[2] A. Piccolo, Soil Sci. 166 (2001) 810–832.
[3] R. Sutton, G. Sposito, Environ. Sci. Technol. 39 (2005) 9009–9015.
[4] N. Senesi, E. Loffredo, in: D.L. Sparks (Ed.), Soil Physical Chemistry, CRC Press LLC, 1999, pp. 239–370.
[5] M.M. Kononova, Soil Organic Matter, Pergamon, Elmsford, NY, 1966.
[6] M. Schnitzer, S.U. Khan, Soil Organic Matter, Elsevier Science Publishers, New York, 1978.
[7] M. Schnitzer, P. Schuppli, Can. J. Soil Sci. 69 (1989) 253–262.
[8] R.S. Cameron, B.K. Thornton, R.S. Swift, A.M. Posner, J. Soil Sci. 23 (1972) 394–408.
[9] A. Piccolo, A. Mirabella, Sci. Total Environ. 62 (1987) 39–46.
[10] E.C.P. Wardenaar, Can. J. Bot. 65 (1987) 1772–1773.
[11] C. Zaccone, T.M. Miano, W. Shotyk, Org. Geochem. 38 (2007) 151–160.
[12] A.K. Cheburkin, W. Shotyk, Fresen. J. Anal. Chem. 354 (1996) 688–691.
[13] W. Shotyk, P. Blaser, A. Grünig, A.K. Cheburkin, Sci. Total Environ. 249 (2000) 281–295.

[14] M.B. Choudhri, F.J. Stevenson, Soil Sci. Soc. Am. Proc. 21 (1957) 508–513.
[15] O. Francioso, C. Ciavatta, V. Tugnoli, S. Sànchez-Cortés, G. Gessa, Soil Sci. Soc. Am. J. 1 (1998) 181–187.
[16] N. Senesi, T.M. Miano, M.R. Provenzano, G. Brunetti, Sci. Total Environ. 81/82 (1989) 143–156.
[17] N. Senesi, T.M. Miano, G. Sposito, Proceedings of the International Conference on Peat Production and Use-Peat 90, Jyväskylä, 11–15 June 1990, The Association of Finnish Peat Industries, Jyväskylä, 1990, pp. 412–421.
[18] C. Zaccone, PhD Thesis, University of Bari, Italy, 2007, pp. 135.
[19] N. Senesi, E. Loffredo, Chemical Processes in Soils, Soil Science Society of America Inc., Madison, Wisconsin, 2005, pp. 564–617.
[20] P. Steinmann, W. Shotyk, Geochim. Cosmochim. Acta 61 (1997) 1143–1163.
[21] F.J. Stevenson, Soil Sci. 123 (1977) 10–17.
[22] H. Kerndorff, M. Schnitzer, Geochim. Cosmochim. Acta 44 (1980) 1701–1708.
[23] X.-H. Chen, T. Gossett, D.R. Thevenot, Water Res. 24 (1990) 1463–1471.
[24] E.J. Smith, C. Rey-Castro, H. Longworth, S. Lofts, A.J. Lawlor, E. Tipping, Eur. J. Soil Sci. 55 (2004) 433–447.

Available online at www.sciencedirect.com
ScienceDirect
Talanta 73 (2007) 938–942
Talanta
www.elsevier.com/locate/talanta

Chiral discrimination of quinine and quinidine based on notable room temperature phosphorescence lifetime differences with γ-cyclodextrin as chiral selector

Xiao Hua Zhang [a], Yu Wang [a,*], Wei Jun Jin [a,b,*]

[a] *School of Chemistry and Chemical Engineering, Shanxi University, Taiyuan 030006, PR China*
[b] *College of Chemistry, Beijing Normal University, Beijing 100875, PR China*

Received 8 December 2006; received in revised form 10 May 2007; accepted 15 May 2007
Available online 21 May 2007

Abstract

Upon addition of small amount of bromocyclohexane (BrCH), quinine (QN) and quinidine (QD) display strong room temperature phosphorescence (RTP) in γ-cyclodextrin (γ-CD) solution without deoxygenation. The associated phosphorescence decay curves can be best fitted to biexponential patterns and quite different RTP lifetimes are obtained for QN (86.9 and 12.5 ms) and QD (12.1 and 4.17 ms), indicating a distinct chiral discrimination of γ-CD toward this pair of pseudo-enantiomers. The corresponding association constants evaluated for QN/γ-CD/BrCH and QD/γ-CD/BrCH are 3.47×10^5 and 4.67×10^4 L mol^{-1}, respectively. It can be inferred that their different ability to form complexes with the chiral γ-CD is accounted for the notable difference in RTP lifetimes between QN and QD.

Keywords: Quinine; Quinidine; Room temperature phosphorescence; Chiral discrimination; Lifetime

1. Introduction

The chiral recognition is of great importance in many different fields including chemistry, biology, pharmaceutical, medical and life science, etc. Various methods such as capillary electrophoresis, chromatographic (HPLC and thin-layer chromatography) and spectroscopic techniques have been used for chiral separation and recognition [1–6]. In the spectroscopic detection methods, fluorescence lifetime resolution based on either time-domain or frequency-domain has been demonstrated to be a powerful technique for the analysis of chiral molecules. Based on phase modulation fluorescence lifetime measurement, quinine and quinidine can be resolved without chemical separation [7]. As an important complementary method of fluorescence sensing, room temperature phosphorimetry (RTP) gives much more advantages, e.g., large Stokes shift, good selectivity and especially longer and easily measurable triplet lifetimes. However, only recent RTP technique has been employed for chiral analysis [8,9]. In deoxygenated aqueous solutions [8], the complexes of two camphorquinone (CQ) enantiomers with α-cyclodextrin exhibited strong and different RTP signals. And the phosphorescence lifetime of (+)-CQ was about four times longer than that of (−)-CQ, which enabled the determination of the two enantiomers in a mixture without involving a separation procedure. Wei et al. [9] also reported the alteration of phosphorescence lifetimes of QN and QD by adding chiral modifiers. The lifetime difference, however, was less than 15% and not large enough. In addition, the observation of RTP required deoxygenation in the above-mentioned reports.

As a highly organized host media, cyclodextrins (CDs) have been used to induce RTP under aerated conditions with a third component as a space regulator [10–16]. Owing to their chiral cavities, CDs have also been widely used as chiral selector in chiral separation and recognition [1–3,17–20]. In the present paper, we investigated the RTP of QN and QD in γ-CD aqueous solution without deoxygenation and demonstrated that γ-CD can

* Corresponding authors.
E-mail addresses: wangyu1168@163.com (Y. Wang), wjjin@bnu.edu.cn (W.J. Jin).

0039-9140/$ – see front matter © 2007 Elsevier B.V. All rights reserved.
doi:10.1016/j.talanta.2007.05.014

be used as a chiral selector to increase RTP lifetime differences between QN and QD by altering their photophysical properties.

2. Experimental

2.1. Reagents

Quinine (QN) and quinidine (QD) were purchased from Alfa Aesar Reagent Company. α-CD, HP-β-CD, Me-β-CD and γ-CD were kindly presented by Wacker Co. and used as received. Absolute ethyl alcohol (≥99.7%) and bromocyclohexane (BrCH, ≥98.0%) were purchased from Beijing Chemicals Factory. Stock solutions of QD and QN were prepared in ethanol at 1×10^{-2} M. Double distilled water was used throughout.

2.2. Apparatus

Phosphorescence measurements were performed on Cary Eclipse Fluorescence Spectrophotometer (Varian Co.) equipped with a pulse xenon lamp. The samples were excited at 330 nm and the phosphorescence signal was monitored at 503 nm. The excitation and emission slit widths were set at 10 and 20 nm, respectively.

The delay time of 0.10 ms was used in order to remove interfering fluorescence and scattering light from the phosphorescence spectrum, and the gate time was selected as 5.0 ms. For the lifetime measurements the initial delay time was set at 0.06 ms while the gate time is typically set at 7.0 ms. The phosphorescence lifetime values were obtained by fitting the RTP decay curves to a mono- or bi-exponential curve.

2.3. Procedures

Typically, appropriate amount of stock solutions of QN or QD was transferred into a 10 mL comparison tube and then proper volumes of γ-CD and BrCH solution were added. The mixed solution was diluted to the final 5 ml with double distilled water and shaken thoroughly. The working solutions were left to equilibrate for 40 min at room temperature and then were transferred into a 1 cm standard quartz cell with a cover to measure the phosphorescence spectra and phosphorescence lifetimes.

3. Results and discussion

3.1. Phosphorescence spectra of QN and QD

No RTP signals were observed in individual γ-CD solutions in the presence of oxygen. Upon addition of BrCH, both QN and QD produced strong RTP in γ-CD solution under nondeoxygenated conditions, indicating the formation of a three-component inclusion complex, namely, γ-CD/QN (QD)/BrCH. Fig. 1 shows RTP excitation and emission spectra of QN and QD. As expected, they exhibited very similar spectrum profiles, with maximum emission at 503 nm and excitation peak was at 231, 276 and 330 nm. 330 nm was used for all the lifetime and intensity measurements. Furthermore, the RTP intensity was linear with the concentration of QN or QD in the range of 2.00×10^{-6} to 8.00×10^{-5} M ($R^2 = 0.9969$) and 8.00×10^{-6} to 1.00×10^{-4} M ($R^2 = 0.9811$). The limits of detection are 1.93×10^{-6} M for QN and 6.69×10^{-7} M for QD, respectively.

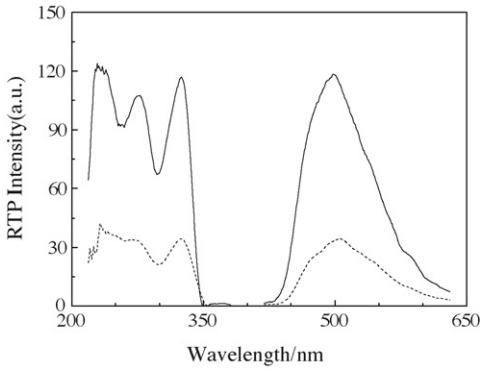

Fig. 1. Phosphorescence excitation and emission spectra of QN (—) and QD (···) ([QN] = [QD] = 8×10^{-5} M; [γ-CD] = 18 mM; V_{BrCH} = 4 μL in 5 mL).

As comparative investigations, the experiments were also performed in other CDs systems including α-CD, β-CD, HP-β-CD and Me-β-CD, but no RTP of QD or QN was observed, indicating the sizes of these CDs are too small to include QN or QD while γ-CD can easily form inclusion complexes with QN or QD.

3.2. Effect of pH on RTP intensity

It is well known that the spectroscopic properties of cinchona alkaloid are pH-sensitive. As can be seen in Fig. 2, in the presence of BrCH and γ-CD, the RTP intensity of QN increased gradually with increasing pH and leveled off at pH 6.5. RTP intensity of QD, however, was relatively insensitive to pH and reached a plateau at pH 6. The following experiments were performed at the pH of the working solution, namely pH 7.6.

3.3. Selection of both γ-CD and BrCH concentrations.

The influences of γ-CD concentration and BrCH concentration on the phosphorescence intensity of QN and QD were investigated. In the presence of BrCH, RTP intensity increased

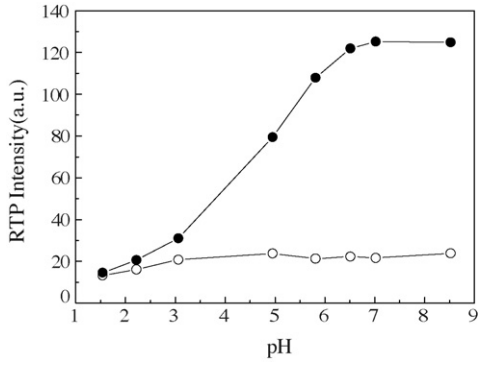

Fig. 2. Effect of pH on the phosphorescence intensity of QN (●) and QD (○) ([QN] = [QD] = 8×10^{-5} M; V_{BrCH} = 4 μL in 5 mL).

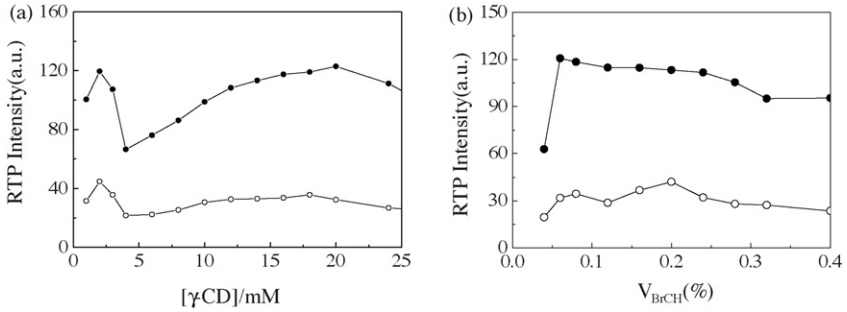

Fig. 3. (a) Effect of γ-CD concentration on the phosphorescence intensity of QN (●) and QD (◯) ([QN] = [QD] = 8×10^{-5} M; V_{BrCH} = 4 μL in 5 mL). (b) The volume of BrCH on the phosphorescence intensity of QN (●) and QD (◯) ([QN] = [QD] = 8×10^{-5} M; [γ-CD] = 18 mM) (*V* (%): the ratio of the volume of BrCH to the total volume of the solution).

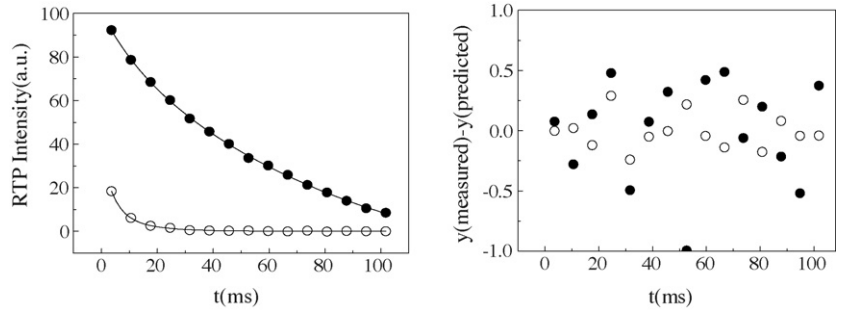

Fig. 4. (Left) Phosphorescence decay curves of QN (●) and QD (◯) ([QN] = [QD] = 8×10^{-5} M; [γ-CD] = 18 mM; V_{BrCH} = 4 μL in 5 mL). (Right) Residual analysis of phosphorescence decay fitting of QN (●) and QD (◯) ([QN] = [QD] = 8×10^{-5} M; [γ-CD] = 18 mM; V_{BrCH} = 4 μL in 5 mL).

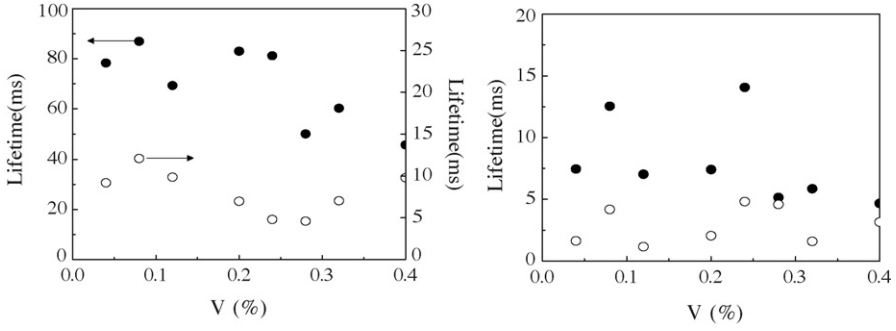

Fig. 5. (Left) Effect of the volume of BrCH on the long lifetime of QN (●) and QD (◯) ([QN] = [QD] = 8×10^{-5} M; [γ-CD] = 18 mM); *V* (%): the ratio of the volume of BrCH to the total volume of the solution. (Right) Effect of the volume of BrCH the short lifetime of QN (●) and QD (◯) ([QN] = [QD] = 8×10^{-5} M; [γ-CD] = 18 mM); *V* (%): the ratio of the volume of BrCH to the total volume of the solution.

with the addition of γ-CD, followed by a sharp decrease, and then increased with further increase of γ-CD. The exact reason for this change is still not clear. Different inclusion mechanism might be involved and much work remains to be done to elucidate it. As shown in Fig. 3a, a plateau was reached in the concentration range of γ-CD from 12.0 to 20.0 mM, indicating that the complex formation was complete. Eighteen millimolar γ-CD was used in the experiments.

From Fig. 3b, it can be seen that RTP intensities sharply increased with the increase of BrCH, and then leveled off when the volume proportion of BrCH concentration in the working solution was more than 0.08% (the ratio of the volume of BrCH to the total volume of the sample solution). Further increase of BrCH concentration, however, resulted in the decrease of RTP intensity. A suitable BrCH volume of 0.08%

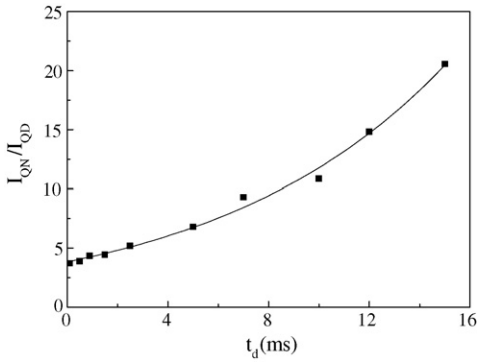

Fig. 6. Effect of different delay time (t_d) on the ratio of phosphorescence intensity of QN to QD ([QN] = [QD] = 8×10^{-5} M; [γ-CD] = 18 mM; V_{BrCH} = 4 μL in 5 mL).

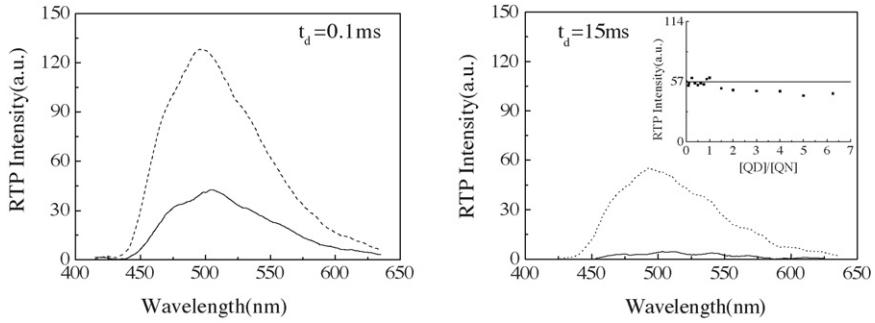

Fig. 7. Phosphorescence emission spectra of QN (···) and QD (—) with different delay time (t_d) ([QN] = [QD] = 8×10^{-5} M; [γ-CD] = 18 mM; V_{BrCH} = 4 μL in 5 mL). (Inset) RTP intensities of QN with increasing concentration of QD ([QN] = 8×10^{-5} M; [γ-CD] = 18 mM; V_{BrCH} = 4 μL in 5 mL).

was selected in this work. Herein bromocyclohexane (BrCH) acts as space-regulator, heavy atom perturber, and emulsion reagent. As space-regulator, BrCH inserts into the cavity of CD and contributes to the formation of a tight ternary complex (QD or QN/γ-CD/BrCH), which protects the excited triplet states of QN or QD and reduces the effects of quenching. As heavy atom perturber, BrCH can enhance the $S_1 \rightarrow T_1$ intersystem crossing probability and induce strong phosphorescence. But excess of BrCH may decrease the solubility of the phosphor in the solution and weaken the RTP signals.

3.4. Measurements of phosphorescence lifetime

Due to the chiral circumstances of CDs cavity, they can form diastereoisomeric complexes with optically active organic compounds so that luminescence characteristics of the organic molecules may be altered.

Using 18 mM γ-CD, the lifetimes of both QN and QD were determined by plotting the phosphorescence intensity against the delay time. Fig. 4 shows the phosphorescence decay curves and the residual analysis for QN and QD, respectively. The decay curves could be best fitted to bi-exponential functions, i.e., two different lifetimes of the excited QD and QN residues could be observed. The two lifetimes obtained can be assigned to two complex configurations, namely, the binary complex γ-CD/QN(QD) and the ternary complex γ-CD/QN(QD)/BrCH, in which the triplet state of QN(QD) is somewhat better protected in case of the ternary complex with the result of longer lifetime. The association constants of QN/γ-CD/BrCH and QD/γ-CD/BrCH evaluated according to the references [21,22] were 3.47×10^5 and 4.67×10^4 L mol^{-1}, respectively. It can be inferred that the different stereochemical structures of QN and QD lead to their different ability to form complexes with the chiral γ-CD. It is clear that QN/γ-CD/BrCH complex is more stable so that its triplet lifetime is much longer.

The triplet lifetimes indicated a distinct chiral discrimination of γ-CD toward this pair of pseudo-enantiomers, with lifetimes of 86.9 and 12.5 ms ($R^2 = 0.9997$) for QN, 12.1 and 4.17 ms ($R^2 = 0.9989$) for QD, the difference being 151 and 99.9%, respectively. Because of so large lifetime difference observed for QN and QD, time-resolved phosphorescence technique can be used for the recognition of QN and QD.

The concentration of BrCH significantly affected the lifetimes of QN and QD (Fig. 5). As space-regulator and emulsion reagent, BrCH can increase the triplet lifetime of phosphor. As a heavy atom perturber, however, BrCH always decreases the triplet lifetime of phosphor. So there was a trade-off between these two effects with the change of BrCH concentration.

3.5. Effect of delay time on RTP intensities of QN and QD

As shown in Fig. 6, the phosphorescence intensities of QN and QD in the γ-CD inclusion complex are different and the differences are affected by delay time setting. At the delay time of 15 ms, the phosphorescence intensity of QD was 8.85% less than that of QN (Fig. 7). Fig. 7 also shows that RTP intensities of QN stayed almost constant with increasing of QD until the mole ratio of QD concentration to QN concentration reached 1.0, and then slightly decreased with further increase of QD. Thus, time-resolved RTP technique can be used for the chiral discrimination of QN and QD below a [QD]/[QN] ratio of 1.0, without the need of separation.

4. Conclusions

In conclusion, intense RTP of QN and QD in aqueous γ-CD solution have been observed under aerated conditions in the presence of BrCH. Dramatic differences in their lifetimes were obtained with lifetimes of 86.9 and 12.5 ms ($R^2 = 0.9997$) for QN, 12.1 and 4.17 ms ($R^2 = 0.9989$) for QD, the difference being 151 and 99.9%, respectively. Such a large difference in phosphorescence lifetime enabled easy spectroscopic discrimination between this pair of pseudo-enantiomers based on simple time-resolved detection without chemical separation.

Acknowledgment

Authors thank the National Natural Science Foundation of China (No. 20475035) for the support.

References

[1] J. Chromatogr. A 875 (2000) 1–492 (a special issue for chiral separation).
[2] T.J. Ward, Anal. Chem. 78 (2006) 3947–3956.

[3] J. Ruta, C. Ravelet, C. Grosset, J. Fize, A. Ravel, A. Villet, E. Peyrin, Anal. Chem. 78 (2006) 3032–3039.
[4] Y. Liu, G.S. Chen, Y. Chen, F. Ding, J. Chen, Org. Biomol. Chem. 3 (2005) 2519–2523.
[5] Y. Liu, Y.W. Y, H.Y. Zhang, B.W. Hu, F. Ding, C.J. Li, Chem. & Biodivers. 1 (2004) 481–488.
[6] Y. Liu, L. Li, H.Y. Zhang, Z. Fan, X.D. Guan, Bioorg. Chem. 31 (2003) 11–23.
[7] A. Navas Díaz, F. García Sánchez, M.C. Torijas, Anal. Chim. Acta 381 (1999) 11–16.
[8] C. Garcia-Ruiz, M.J. Scholtes, F. Ariese, C. Gooijer, Talanta 66 (2005) 641–645.
[9] Y.L. Wei, W.H. Chan, A.W.M. Lee, C.W. Huie, Chem. Comm. (2004) 288–289.
[10] J.J. Wu, Y. Wang, J.B. Chao, L.N. Wang, W.J. Jin, J. Phys. Chem. B 108 (2004) 8915–8919.
[11] Y.L. Peng, Y.T. Wang, Y. Wang, W.J. Jin, J. Photochem. Photobiol. A: Chem. 173 (2005) 301–308.
[12] R.H. Zhu, W.J. Jin, Room Temperature Phosphorimetry: Principle and Applications, Science Press, Beijing, 2006.
[13] W.J. Jin, in: A. Duhal (Ed.), Cyclodextrin Inclusion Complexes: Triplet States and Phosphorescence in Cyclodextrin Materials: Photochemistry, Photophysics and Photobiology, Elsevier, 2006.
[14] Y. Wang, J.J. Wu, Y.F. Wang, L.P. Qin, W.J. Jin, Chem. Comm. (2005) 1090–1091.
[15] L.H. Liu, J.W. Xie, S.Z. Zhang, W.J. Jin, Chem. J. Chin. Univ. 23 (2002) 219–221.
[16] G.R. Li, J.J. Wu, W.J. Jin, J.W. Xie, Talanta 60 (2003) 555–562.
[17] W.L. Hinze, T.E. Riehl, D.W. Armstrong, W. DeMond, A. Alak, T. Ward, Anal. Chem. 57 (1985) 237–242.
[18] T.J. Ward, Anal. Chem. 72 (2000) 4521–4528.
[19] S. Li, W.C. Purdy, Chem. Rev. 92 (1992) 1457–1470.
[20] D. Wistuba, V. Schurig, J. Chromatogr. A 875 (2000) 255–276.
[21] J.W. Xie, J.G. Xu, G.Z. Chen, C.S. Liu, Sci. Chin. B 39 (1996) 416–424.
[22] H.A. Benesi, J.H. Hildebrand, J. Am. Chem. Soc. 71 (1949) 2703–2707.

Available online at www.sciencedirect.com
ScienceDirect
Talanta 73 (2007) 920–925
Talanta
www.elsevier.com/locate/talanta

An ionic liquid-type carbon paste electrode for electrochemical investigation and determination of calcium dobesilate

Jianbin Zheng [a,*], Ya Zhang [a,b], Pingping Yang [a]

[a] *Institute of Analytical Science, Shaanxi Provincial Key Lab of Electroanalytical Chemistry, Northwest University, Xi'an, Shaanxi 710069, China*
[b] *Department of Chemistry and Chemical Engineering, Yulin College, Yulin, Shaanxi 719000, China*

Received 12 January 2007; received in revised form 14 May 2007; accepted 14 May 2007
Available online 21 May 2007

Abstract

An ionic liquid-type carbon paste electrode (IL-CPE) had been fabricated by replacing non-conductive organic binders with a conductive room temperature ionic liquid, 1-pentyl-3-methylimidazolium hexafluorophosphate ($PMIMPF_6$). The electrochemical responses of calcium dobesilate were investigated at the IL-CPE and the traditional carbon paste electrode (T-CPE) in 0.05 mol L^{-1} H_2SO_4, respectively. The results showed the superiority of IL-CPE to T-CPE in terms of provision of higher sensitivity, faster electron transfer and better reversibility. A novel method for determination of calcium dobesilate was proposed. The oxidation peak current was rectilinear with calcium dobesilate concentration in the range of 8.0×10^{-7} to 1.0×10^{-4} mol L^{-1}, with a detection limit of 4.0×10^{-7} mol L^{-1} (S/N = 3) by differential pulse voltammetry. The proposed method was applied to directly determine calcium dobesilate in capsule and urine samples.

Keywords: Voltammetry; Ionic liquid; Ionic liquid-type carbon paste electrode; Carbon paste electrode; Calcium dobesilate

1. Introduction

Calcium dobesilate (CD, doxium) is an angioprotective agent, which acted on capillary vessel selectively. It not only modulated osmose and crispness of patients of the capillary vessel, also inhibited active substance such as hormonal peptide. As CD was principally used to cure disease of capillary vessel, it was necessary to develop a simple, sensitive and rapid method for the determination of it. Several methods had been recommended for the determination of CD such as HPLC [1,2], spectrophotometry [3], thin-layer chromatography and UV spectroscopy [4], flow-injection biamperometric method [5], electrochemical method [6] and flow injection chemiluninescence [7]. Fig. 1 is the molecule structure of CD.

Adams reported the first example of a carbon paste electrode for use in anodic polarography showing the concept of a paste prepared from carbon and organic liquid [8]. Up to now, the T-CPE has been widely applied in electrochemical realm due to its simplicity of fabrication, low background current, renewable surface, low cost and inherent sensitivity [9–14]. Generally, the organic liquid as a binder component of paste is a non-conductive mineral oil such as nujol, paraffin or alike.

Room temperature ionic liquids (RTILs, ILs), also called room temperature molten salts are molten at temperatures lower than 373 K [15]. In the past years, RTILs have emerged as a frontier and novel area of research because of their excellent chemical and physical properties such as high chemical and thermal stability, almost negligible vapor pressure, high conductivity and wide electrochemical windows [15–20]. They have been used in electrochemistry [21], organic synthesis [22], catalysis [23], extraction [24,25], etc. Recently, RTILs have been proposed to be very interesting and efficient pasting binders in place of non-conductive organic binders for the preparation of carbon composite electrodes [26,27]. To our knowledge, there was no report about the fabrication of IL-CPE with $PMIMPF_6$.

In this paper, we present a new IL-CPE, which utilizes $PMIMPF_6$ as a binder. The electrochemical behavior of CD at the proposed electrode and the T-CPE was investigated in detail. The results showed the superiority of IL-CPE to T-CPE in terms of both provision of better reversibility and higher sensitivity. In addition, a novel method for the determination of CD with simple, sensitive and rapid characteristics was developed.

* Corresponding author. Tel.: +86 29 88302077; fax: +86 29 88303448.
E-mail address: zhengjb@nwu.edu.cn (J. Zheng).

0039-9140/$ – see front matter © 2007 Elsevier B.V. All rights reserved.
doi:10.1016/j.talanta.2007.05.016

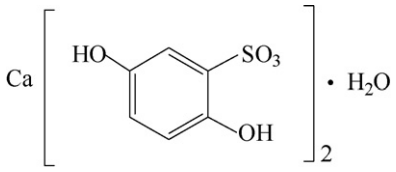

Fig. 1. Molecule structure of calcium dobesilate.

2. Experimental

2.1. Reagents and solution

Pentyl chloride (Shanghai Shiyan Reagent Corporation, Shanghai, China) and ethyl acetate (Tianjin Chemical Reagent Corporation, Tianjin, China) were of analytical reagent grade. The concentration of hexafluorophosphate acid is 65% (w/w, Hongyan Chemical Reagent Corporation, Jiangsu, China), and purity of 1-methylimidazole is 99% (w/w, Kaile Chemical Reagent Factory, Zhejiang, China). High purity graphite powder (Shanghai Carbon Plant, Shanghai, China) and paraffin liquid (AR, Kermel Center of chemical reagent, Tianjin, China) were used without further treatment. Other chemicals were all analytical grade. Ionic liquid $PMIMPF_6$ was prepared following the similar procedures described in the literature [28].

All solutions were prepared with ultrapure water from a Milli-Q water purification system. 0.05 mol L^{-1} H_2SO_4 was employed as supporting electrolyte. CD capsules (Batch no. 0201002-6, Xi'an Rejoy Pharmaceutical Co., Ltd., Xi'an, China) were purchased from the local drugstore. Stock solution of CD (1.0×10^{-3} mol L^{-1}) was prepared daily by dissolving CD (Xi'an Rejoy Pharmaceutical Co., Ltd., Xi'an, China) in water. Diluted working standard solutions were prepared from the stock solution by appropriated dilutions with water.

2.2. Apparatus

Cyclic voltammetry (CV), linear sweep voltammetry (LSV) and DPV experiments were performed on a CHI660A electrochemical workstation (Shanghai Chenhua Co., China) controlled by a microcomputer with CHI660 software. The measurements were carried out in a conventional electrochemical cell with T-CPE or IL-CPE as working electrode, a Pt wire counter electrode and a saturated calomel reference electrode (SCE). All potentials reported were versus the SCE. The surface morphologies of the prepared electrodes were observed through scanning electron microscopy (SEM) on JEOL JSM-6700F at an accelerating voltage of 20 kV.

The HPLC system is Agilent 1100 series (Agilent Technologies, USA), including a quaternary solvent delivery pump, a thermostat column compartment, a diode array detector (DAD) and a manual sample injection valve with a 20 μL loop. Chromatographic separation was carried out using a Zorbax Eclipse XDB-C_8 (150 mm × 4.6 mm i.d., 5 μm) column. All the experiments were conducted at room temperature.

2.3. Electrode preparation

The T-CPE was prepared as follows. 1.0 g graphite powder and 0.5 mL paraffin liquid were mixed in a mortar by hand until a homogeneous paste was obtained. The prepared carbon paste was tightly packed into a PVC tube (3 mm internal diameter) and a cope wire was introduced into the other end for electrical contact. The preparation process of the IL-CPE was similar to that of the T-CPE but a replacement of paraffin liquid with $PMIMPF_6$. Prior to use, the surface of the well-prepared electrode was smoothed with a weighing paper.

2.4. Voltammetric procedure

About 10 mL of the electrolyte solution containing appropriate amount of CD standard solution or sample were added to the electrolytic cell. Then the electrodes were immersed and CV, LSV or DPV experiments were performed between 0.0 and 1.0 V. The peak currents and potentials of CD were recorded by CHI660A workstation. The CD content in the samples was obtained by using the calibration curve method.

2.5. Chromatographic procedure

Standard samples of CD were made by taking an appropriate volume of stock solution and dissolving in a suitable quantity of the mobile phase. The HPLC separation was carried out by isocratic elution with a mobile phase of CH_3OH–H_2O (60:40, v/v) at a flow rate of 1.0 mL min^{-1}. Detection by diode array was performed at 295.8 nm. Each sample was injected and the height of peak was used for quantitative determination.

3. Results and discussion

3.1. The surface morphologies of T-CPE and IL-CPE

The morphological features of the two electrodes were studies using SEM, as shown in Fig. 2. The T-CPE is characterized by a surface formed by irregularly shaped flakes of graphite that were isolated and each layer could be clearly distinguished (Fig. 2a). Fig. 2b shows a SEM image of IL-CPE with more uniform surface topography and no separated carbon layers could be observed. The uniformity of the surface shows the good adherence of $PMIMPF_6$ to graphite due to the high viscousness of IL. A layer of $PMIMPF_6$ is formed on the graphite particles even with the addition of small amount of $PMIMPF_6$ to the graphite. With further addition of $PMIMPF_6$, the void spaces between the graphite particles are filled with excess $PMIMPF_6$. Significant improvement in the surface structure of IL-CPE is observed. This phenomenon is consistent with literatures [26,27].

3.2. Voltammetric behavior of CD at T-CPE and IL-CPE

Fig. 3 showed electrochemical responses of 8.0×10^{-5} mol L^{-1} CD in 0.05 mol L^{-1} H_2SO_4 solution at the IL-CPE and the T-CPE, respectively.

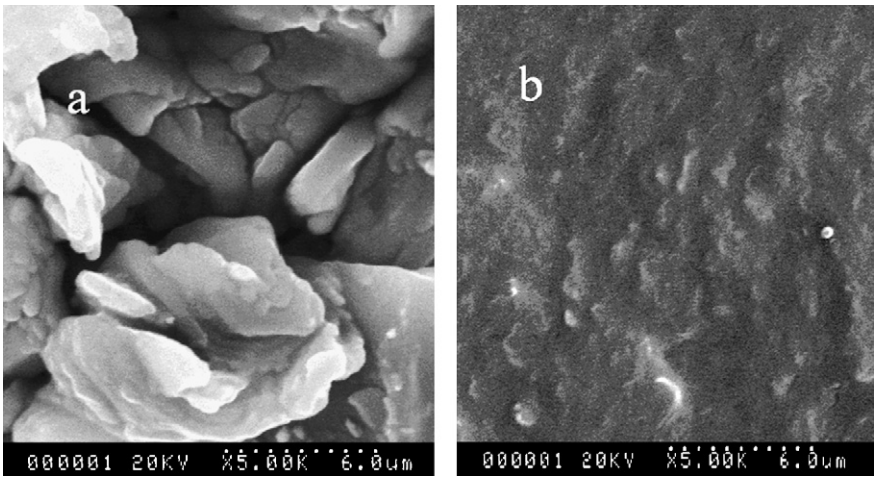

Fig. 2. SEM images of (a) T-CPE and (b) IL-CPE.

CD showed a pair of redox peaks at the T-CPE (Fig. 3A(a)), with oxidation potential (E_{pa}) of +0.614 V, reduction potential (E_{pc}) of +0.192 V and the peak-to-peak potential separation (ΔE_p) of 0.422 V. A pair of redox peaks is also observed for the same concentration of CD at IL-CPE (Fig. 3A(b)). But a negative shift for E_{pa} and a positive shift for E_{pc} were observed and the ΔE_p is decreased to 0.100 V. Furthermore, the current response at the IL-CPE was much larger than at the T-CPE, by DPV it was 70 times of that at the T-CPE (Fig. 3B). A remarkably background response at the IL-CPE is due to the accessible capacitance of the IL at the carbon surface [29]. The results show the superiority of IL-CPE to T-CPE in terms of both provision of better reversibility and higher sensitivity, indicating the IL-CPE facilitates electron transfer between CD and electrode. This is surely due to the use of the RTIL as agglutinant.

3.3. Kinetics of CD at T-CPE and IL-CPE

The influence of potential scan rate (v) on the peak currents (I_p) of CD was studied at two electrodes by LSV and different kinetics processes were obtained. At CPE, when $v > 0.7\,V\,s^{-1}$, the linear relationship of I_p versus v was presented, which illustrated a adsorption-controlled redox process (Fig. 4(a)). With an increase of $v(v > 0.7\,V\,s^{-1})$, an linear relation of I_p versus the square root of the potential scan rate $(v)^{1/2}$ was obtained, which revealed a diffusion-controlled mechanism (Fig. 4(b)). While at the IL-CPE, I_p varied linearly with v, which indicated the redox process of CD was a adsorption-controlled mechanism, as shown in Fig. 4(c). A further evidence of the adsorption of CD at the surface of the IL-CPE is the restraint effect of surfactant on the peak current because competitive adsorption would happen at the surface of electrode [30]. In $0.05\,mol\,L^{-1}$ H_2SO_4 solution containing $8.0 \times 10^{-5}\,mol\,L^{-1}$ CD, a small quantity of polyvinyl alcohol (PVA), diphenylguanidine, sodium dodecyl sulfonate (SDS), hexadecyl pyridine bromide (HPB), cetyl trimethyl ammonium bromide (CTAB), were added into the solution, respectively. As expected for an adsorption-controlled process, all these surfactants decreased the peak current of CD in different degree.

In an effort to gain further insight into the kinetics, cyclic voltammograms of CD on T-CPE and IL-CPE were measured at different sweep rate, as shown in Fig. 5.

The oxidation peak current and reduction peak current increased with increasing of sweep rate, meantime, the oxidation peak potential is positively shifted and the reduction peak potential is negatively shifted, indicating that the redox reversibility of CD was impaired with increasing sweep rate. According to above results, the electron transfer kinetics of CD at the two electrodes can be obtained by using the approach developed by Laviron [31], when peak-to-peak separation is higher than

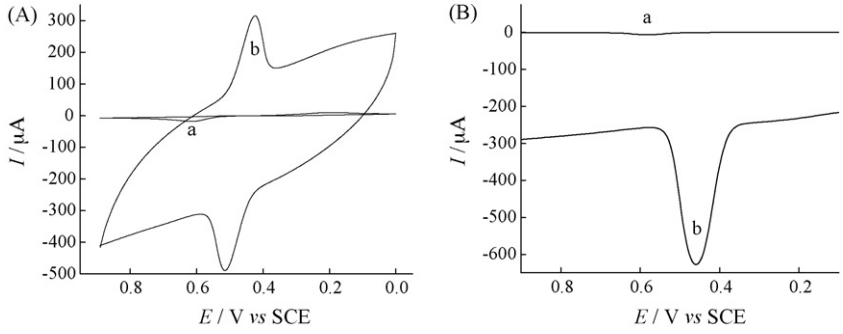

Fig. 3. CV (A) and DPV (B) curves of $8.0 \times 10^{-5}\,mol\,L^{-1}$ CD in $0.05\,mol\,L^{-1}$ H_2SO_4 at (a) T-CPE and (b) IL-CPE. In Fig. 2A: scan rate $0.05\,V\,s^{-1}$, in Fig. 2B: amplitude 0.05 V, pulse width 0.05 s, pulse period 0.2 s and potential step width 0.004 V.

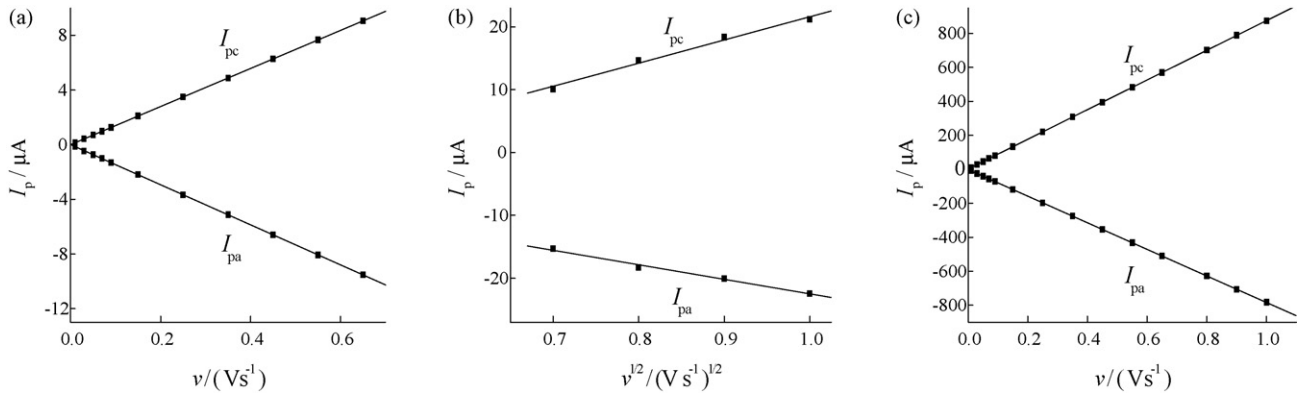

Fig. 4. Linear relationship of (a) I_p vs. $v(v < 0.7\,V\,s^{-1})$, (b) I_p vs. $v^{1/2}(v > 0.7\,V\,s^{-1})$ at T-CPE and (c) I_p vs. v at IL-CPE in a solution of 8.0×10^{-5} mol L^{-1} CD + 0.05 mol L^{-1} H_2SO_4.

0.20 V/n, the relationship between the peak potential E_p and the scan rate can be expressed in the following equation:

$$E_p = f(\log \upsilon) \quad (1)$$

where for cathode peak, the slope value is $-2.3RT/\alpha nF$, and for anode peak, $2.3RT/(1-\alpha)nF$. And k_s, the electron transfer rate constant of reaction, is expressed in the following equation:

$$\log k_s = \alpha \log(1-\alpha) + (1-\alpha)\log\alpha - \log(RT/nF\upsilon) - \frac{\left[\alpha(1-\alpha)nf\Delta E_p\right]}{2.3RT} \quad (2)$$

where α is the electron transfer coefficient, n the number of electrons involved in the reaction and ΔE_p is the peak-to-peak separation. The number of electrons involved in the reaction of CD is 2 [6]. From the slope of $E_p - \log \upsilon$, the value of α at T-CPE and IL-CPE is calculated to be 0.59 and 0.48, respectively. Based on Eq. (2), the calculating results showed that the k_s of CD at T-CPE and IL-CPE was 0.000625 and 0.259 s^{-1}, indicating that the IL-CPE dramatically enhanced the electron transfer rate constant of CD. This was surely attributed to the use of RTIL as binder, revealing the high conductibility of RTIL plays a key in promoting the electron transfer.

4. Determination of CD

4.1. Optimization of analytical conditions

As illustrated in Fig. 2, the oxidation peak current (I_{pa}) of CD at the IL-CPE was much larger than that at the T-CPE. Therefore, the IL-CPE was chosen as working electrode to determine CD. To further enhance the sensitivity, DPV was investigated.

The types of supporting electrolyte played a key role in the voltammetric responses of CD. The current responses of 8.0×10^{-5} mol L^{-1} CD were estimated in different supporting electrolytes such as Na_2HPO_4–KH_2PO_4, NaAc–HAc, tartaric acid–sodium tartrate, HAc and H_2SO_4. The results showed that higher peak current and better peak shape could be obtained in H_2SO_4.

The effect of H_2SO_4 concentration, which ranged from 0.001 to 0.8 mol L^{-1}, on the response of 8.0×10^{-5} mol L^{-1} CD was investigated. With the increasing of H_2SO_4 concentration, its peak current increased slightly but peak shape became ill-defined. These indicated the ionic strength and pH value of H_2SO_4 had influence on the determination of CD. The best performance was obtained in 0.05 mol L^{-1} H_2SO_4. Therefore, 0.05 mol L^{-1} H_2SO_4 (pH 1.3) was selected as supporting electrolyte. At the same time, the oxidation peak potential of CD was found to be dependent on pH and linear shifted to negative potential with increasing of pH. The peak potential shows

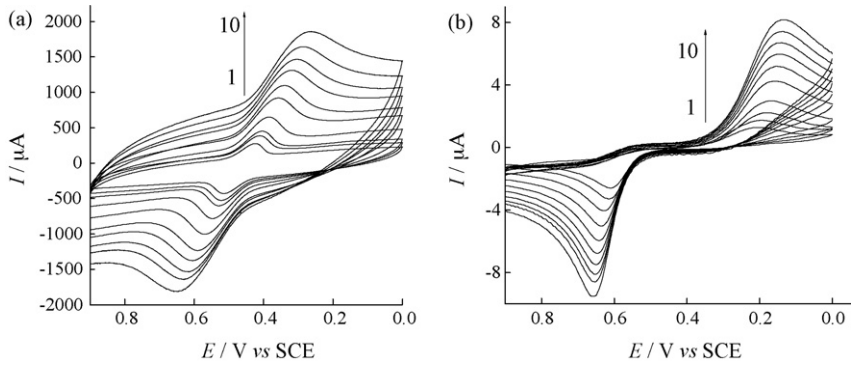

Fig. 5. Cyclic voltammograms of 8.0×10^{-5} mol L^{-1} CD + 0.05 mol L^{-1} H_2SO_4 at different scan rate on (a) IL-CPE and (b) T-CPE. Scan rate 1–10: 0.03; 0.05; 0.07; 0.09; 0.15; 0.25; 0.35; 0.45; 0.55; 0.65 V s^{-1}.

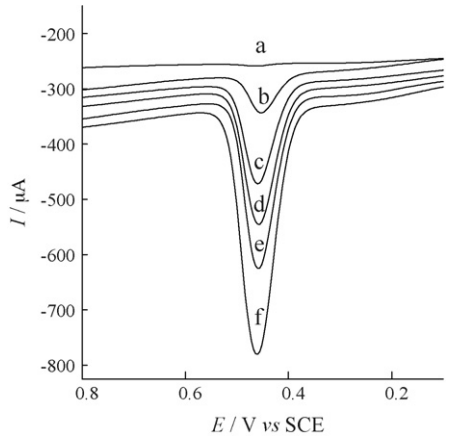

Fig. 6. DPV curves of different concentrations of CD in 0.05 mol L^{-1} H_2SO_4 at IL-CPE: (a) 0.8; (b) 15;(c) 40; (d) 50; (e) 70; (f) 100×10^{-6} mol L^{-1}. Amplitude 0.05 V, pulse width 0.05 s, pulse period 0.2 s and accumulation time 120 s.

a slope of −0.053 V/pH for CD oxidation, indicating that the number of electrons and protons involved in the reaction mechanisms is the same. It has been known that CD oxidation is a two electron process. Thus, the oxidation mechanism of CD may be tentatively assigned to:

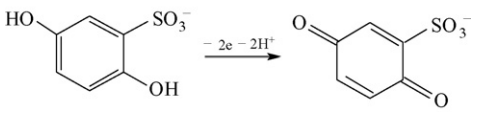

This conclusion is consistent with literature [6].

DPV was used to determine CD, and corresponding parameters were optimized. The effects of accumulation time and potential on the peak current were investigated. The peak current of 8.0×10^{-5} mol L^{-1} CD increased with the increasing of accumulation time and then reached a maximum when accumulation time is above 120 s. So the accumulation time of 120 s was used for further studies. The accumulation potential has little effect on peak current of 8.0×10^{-5} mol L^{-1} CD in the range of −0.3 to +0.1 V. To reduce scanning time, 0.1 V was selected as the accumulation potential in this experiment.

The influence of DPV parameters such as pulse amplitude, pulse width and pulse period on the peak current was also investigated. The optimum parameters were found to be amplitude of 0.05 V, pulse width of 0.05 s and pulse period of 0.2 s.

4.2. Calibration curves, stability and repeatability

Fig. 6 is DPV curves of six different concentrations of CD at IL-CPE under the optimum conditions. A linear relationship could be established between the oxidation peak current and the concentration of CD in the range of 8.0×10^{-7}–1.0×10^{-4} mol L^{-1}. The linear regression equation was $I_{ap} = 4.192 \times 10^{6}\ c_{CD} + 0.5815$, $r = 0.9984$, where I_{pa} is the oxidation peak current in μA and c_{CD} is the CD concentration in mol L^{-1}, the detection limit of CD was found to be 4.0×10^{-7} mol L^{-1} (S/N = 3).

Table 1
The determination results of calcium dobesilate in capsules by DPV and HPLC

DPV ($n = 5$)	
CD content (mg/capsule)	493.9
RSD (%)	1.3
Added (mg L^{-1})	6.362
Found (mg L^{-1})	6.526
Recovery (%)	102.6
RSD of Recovery (%)	1.7
HPLC ($n = 5$)	
CD content (mg/capsule)	493.3
RSD (%)	0.6

Label amount: 500 mg/capsule.

To estimate the repeatability of the proposed method, the RSD of six times successful measurement of peak current of 5.0×10^{-5} mol L^{-1} CD at a IL-CPE was calculated to be 1.2%, which demonstrate the good repeatability of the method. The electrode-to-electrode reproducibility of the DPV method was examined on five IL-CPEs constructed individually, the RSD of the five average peak current of 5.0×10^{-5} mol L^{-1} CD was calculated to be 2.7%.

4.3. Interferences study

The effects of inorganic ions and organic compounds commonly existed in pharmaceuticals and biological samples on the determination of 5.0×10^{-5} mol L^{-1} CD was studied. The tolerance limit was defined as the concentration ratio of additive/CD causing less than ±5.0% relative error. The tolerance limit of additives to 5.0×10^{-5} mol L^{-1} CD was 100-fold of Ni^{2+}, Al^{3+}, Co^{2+}, Ca^{2+}, Fe^{3+}, Bi^{3+}, Cr^{3+}, Na^{+}, K^{+}, CO_3^{2-}, PO_4^{3-}, Cl^{-}, NO_3^{-}, 50-fold of ascorbic acid, lactic acid, urea, thein, glucose, starch and sucrose.

4.4. Determination of calcium dobesilate in calcium dobesilate capsules

Ten CD capsules (label amount: 500 mg/capsule) were weighed then grinded to a fine powder and mixed adequately. The sample solutions were prepared by accurately weighing a certain amount of the powder and dissolving it in water. The determination of CD was conducted by DPV method and the HPLC method, respectively. As shown in Table 1, the results obtained by both methods showed excellent agreement with label amount. The DPV results agreed with the results obtained by HPLC method within 95% of confidence level. Because the proposed method was more simple and time-saving than the HPLC method, it can be recommended for the CD analysis in pharmaceutical preparations. The recovery of DPV method was also conducted to evaluate the accuracy of the method, and the results were also listed in Table 1. From Table 1, the average recovery of five independent experiments was calculated to be 102.6%.

4.5. Determination of CD in urine samples

The investigations showed that calcium dobesilate did not have any significant decomposition in human plasma [32], and

Table 2
Application of the DPV method to determination of calcium dobesilate in urine sample

Samples	CD added (10^{-5} mol L^{-1})	CD found (10^{-5} mol L^{-1})[a]	Average recovery (%)	RSD of recovery (%)
1	0.50	0.481	96.2	2.1
2	1.20	1.183	98.6	2.6
3	1.50	1.482	98.8	2.0
4	3.50	3.524	100.7	2.1
5	5.00	5.095	101.9	1.8

[a] Average of five determinations.

the urinary elimination of calcium dobesilate in the first 24 h reached 75% after intravenous medication and 50% after oral medication [1]. Accordingly, in present work, recovery tests were carried out by adding certain amount of CD standard solutions into the five diluted urine samples of healthy specimen. Each 1.5 mL of fresh sample was taken and diluted to 20 mL with 0.05 mol L^{-1} H_2SO_4. The results obtained were listed in Table 2. As can be seen, the recovery for the determination of CD added to urine samples was good. It showed the proposed method was available for the determination of CD in urine samples too.

5. Conclusions

An IL-CPE had been fabricated by using $PMIMPF_6$ as binder. At T-CPE, CD showed a pair of redox peaks with ΔE_p of 0.422 V, while at the proposed electrode the ΔE_p was decreased to 0.105 V. Furthermore, the current response and the electron transfer rate constant of CD at the IL-CPE were much larger than that at the T-CPE. Compared with the poor response at T-CPE, the electrochemical reversibility and sensitivity of CD at the proposed electrode was improved dramatically, revealing some advantages of IL-CPE over T-CPE such as high conductivity and fast electron transfer. A sensitive, rapid and simple method for the determination of CD was established. Under the optimized conditions, this method has been successfully applied to the determination of CD in capsule samples and urine samples.

Acknowledgments

This work was supported by the National Natural Science Foundation of China (No. 20675062) and the Natural Science Foundation of Shaanxi Province in China (No. 2004B20).

References

[1] K. Rona, K. Ary, J. Chromatogr. B 755 (2001) 245.
[2] Lj. Zivanovic, M. Zecevic, S. Markovic, S. Petrovic, I. Ivanovic, J. Chromatogr. A 1088 (2005) 182.
[3] J. Kracmar, J. Kracmavova, A. Kovarova, Z. Stejskal, Pharmazie 43 (1988) 681.
[4] S. Negritescu, D. Belu, R. Dragoi, E. Sisman, A. Cosmin, A. Candidatu, D. Georgescu, Rev. Chim. 30 (1979) 912.
[5] J.F. Song, J.Q. Chen, J. Pharm. Biomed. Anal. 33 (2003) 789.
[6] S.H. Yan, Y.F. Hei, S.P. Wu, J.B. Zheng, Chin. J. Anal. Lab. 23 (2004) 4.
[7] Z.H. Song, Q.L. Yue, C.N. Wang, Spectrochim. Acta A 60 (2004) 2377.
[8] R.N. Adams, Anal. Chem. 30 (1958) 1576.
[9] J. Wang, J. Liu, G. Cepra, Anal. Chem. 69 (1997) 3124.
[10] P. Tomcik, C.E. Banks, T.J. Davies, R.G. Compton, Anal. Chem. 76 (2004) 161.
[11] C.M.V.B. Almeida, B.F. Giannetti, Electrochem. Commun. 4 (2002) 985.
[12] D. Moscone, D. D'Ottavi, D. Compagnone, G. Palleschi, A. Amine, Anal. Chem. 73 (2001) 2529.
[13] N.S. Lawrence, R.P. Deo, J. Wang, Anal. Chem. 76 (2004) 3735.
[14] A. Abbaspour, M.A. Mehrgardi, Anal. Chem. 76 (2004) 5690.
[15] T. Welton, Chem. Rev. 99 (1999) 2071.
[16] G. Maciej, L. Andrzej, S. Izabela, Electrochim Acta 51 (2006) 5567.
[17] H. Rika, I. Yasuhiko, J. Fluorine Chem. 105 (2000) 221.
[18] N. Nishi, S. Imakura, T. Kakiuchi, Anal. Chem. 78 (2006) 2726.
[19] C.M. Lang, K. Kim, L. Guerra, P.A. Kohl, J. Phys. Chem. B 109 (2005) 19454.
[20] C.A. Brooks, A.P. Doherty, Electrochem. Commun. 6 (2004) 867.
[21] K. Tian, Y.S. Wang, Y.L. Chen, X.G. Chen, Z.D. Hu, Talanta 72 (2007) 587.
[22] P. Kubisa, Prog. Polym. Sci. 29 (2004) 3.
[23] M.Ch. Law, K. Wong, T.H. Chan, J. Org. Chem. 70 (2005) 10434.
[24] Z.J. Li, Q. Wei, R. Yuan, X. Zhou, H.Z. Liu, H.X. Shan, Q.J. Song, Talanta 71 (2007) 68.
[25] H. Heitzman, B.A. Young, D.J. Rausch, P. Rickert, D.C. Stepinski, M.L. Dietz, Talanta 69 (2006) 527.
[26] N. Maleki, A. Safavi, F. Tajabadi, Anal. Chem. 78 (2006) 3820.
[27] H.T. Liu, P. He, Z.Y. Li, C.Y. Sun, L.H. Shi, Y. Liu, G.Y. Zhu, J.H. Li, Electrochem. Commun. 7 (2005) 1357.
[28] A.B. Pereiro, E. Tojo, A. Rodrı′guez, J. Canosa, J. Tojo, J. Chem. Thermodyn. 38 (2006) 651.
[29] E. Rozniecka, G. Shul, J. Sirieix-Plenet, L. Gaillon, M. Opallo, Electrochem. Commun. 7 (2005) 299.
[30] A.P. dos Reis, C.R.T. Tarley, N. Maniasso, L.T. Kubota, Talanta 67 (2005) 829.
[31] E. Laviron, J. Electroanal. Chem. 101 (1979) 19.
[32] T. Tejerina, E. Ruiz, Gen. Pharmacol. 31 (1998) 357.

Available online at www.sciencedirect.com
ScienceDirect
Talanta 73 (2007) 943–947
Talanta
www.elsevier.com/locate/talanta

Voltammetric behavior of urapidil and its determination at multi-wall carbon nanotube paste electrode

Zheng Li [a,b], Song Junfeng [a,*]

[a] *Institute of Analytical Science, Northwest University, 710069, PR China*
[b] *College of Chemistry and Chemical Engineering, Xi'an Shiyou University, 710065, PR China*

Received 12 December 2006; received in revised form 11 May 2007; accepted 15 May 2007
Available online 21 May 2007

Abstract

The voltammetric behavior of urapidil was investigated. In pH 6.8 Britton-Robinson buffer, an irreversible oxidation peak of urapidil at 0.62 V (versus SCE) at a multi-wall carbon nanotube paste electrode (MWNT-PE) was observed, which was more sensitive with lower potential than that at the carbon paste electrode (CPE). The oxidation of urapidil was a two-electron and two-proton process with adsorption character. A differential pulse voltammetric method was proposed for the determination of urapidil. The peak current of the oxidation peak of urapidil was linearly with its concentration in a range from 5.0×10^{-8} to 2.0×10^{-6} mol/L at open-circuit accumulation for 60 s, with a detection limit of 3.8×10^{-8} mol/L. The proposed method was employed to determine urapidil in urapidil tablets.

Keywords: Urapidil; Multi-wall carbon nanotubes; Chemically modified electrode; Voltammetry

1. Introduction

Urapidil (structure shown in Scheme 1) is a potent antihypertensive compound without serious side effects. Its action is mainly due to a postsynaptic α-receptor antagonism that inhibits the vasoconstrictive action of catecholamines and reduces blood pressure by decreasing peripheral vascular resistance. Urapidil also has an agonistic effect on central 5-HT_{1A} receptors and lowers blood pressure by preventing the stimulation of baroreceptors [1]. Since urapidil is a widely used drug, an effective method for its analysis is highly desirable. Current methods include high-performance liquid chromatography (HPLC) [2–4], chemiluminescence (CL) [5] and fluorescence spectrophotometry [6]. These methods are either too complicated, or of low sensitivity.

Voltammetric techniques have been widespread used in pharmaceutical analysis, which possess many advantages such as high sensitivity, rapid response and simplicity in operation procedure. Recent development in electrode materials such as carbon nanotubes (CNTs) has further enhanced the applications of voltammetric techniques in pharmaceutical and biological analysis [7–14]. However, no attempts have been made to determine urapidil by any voltammetric techniques.

In this work, the voltammetric behavior of urapidil has been studied for the first time at a multi-wall carbon nanotube-paraffin oil paste electrode (MWNT-PE), and electrocatalytic activity of MWNT for the oxidation of urapidil has been explored by comparing voltammetric responses at MWNT-PE with that at CPE. A differential pulse voltammetric method for the determination of urapidil in urapidil tablets is proposed. This method is convenient and affordable because of its high sensitivity and low cost.

2. Experimental

2.1. Apparatus

All the electrochemical measurements were performed on a CHI 660 electrochemical workstation (CH Instrument Inc., USA) with a three-electrode system. The working electrode was a home-made MWNT-PE. The reference and counter electrode were a saturated calomel electrode (SCE) and a Pt wire, respectively. All the potentials in this work were referred to the SCE.

* Corresponding author. Tel.: +86 29 8830 3448; fax: +86 29 8830 3448.
E-mail address: songjunf@nwu.edu.cn (J. Song).

0039-9140/$ – see front matter © 2007 Elsevier B.V. All rights reserved.
doi:10.1016/j.talanta.2007.05.015

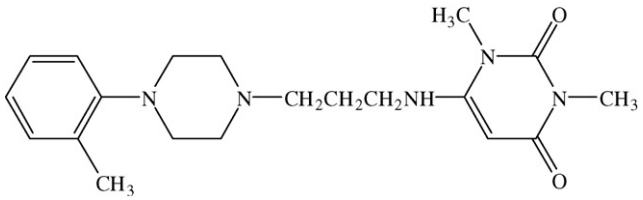

Scheme 1. Structural formula of urapidil.

The MWNT-PE was prepared by mixing multi-wall carbon nanotube powder (diameter 10–20 nm, length 1–2 μm, purity > 95%, Shenzhen Nanotech Port Co., Ltd., China) and paraffin oil (chemical pure, Tianjin Chemical Reagent Factory, Tianjin, China) in a ratio of 60.0% nanotube powder to 40.0% paraffin oil (w/w) in a mortar [13]. The conventional carbon paste electrode (CPE) was prepared in a similar way by mixing graphite powder (chemical pure, Beijing Chemical Reagent Factory, Beijing, China) with paraffin oil. A portion of the resulting paste was packed firmly into the cavity (1.6 mm diameter) of a polytetrafluoro ethylene tube (PTFE). The electric contact was established via a copper wire. The surface of the electrode was smoothed on a weighing paper and rinsed with water.

2.2. Reagents

All chemicals used were of analytical reagent grade. Twice-distilled water was used throughout the experiments. The 1.0×10^{-3} mol/L standard stock solution of urapidil was prepared by dissolving 0.0387 g urapidil (reference standard, Xi'an Lijun Pharmaceutical Co., China) in 2.0 mL 0.1 mol/L HCl solution and diluted with water to 100 mL. The standard working solutions were freshly prepared by diluting the standard stock solution with water for each experiment.

2.3. Procedure

A 5 mL pH 6.8 Britton-Robinson buffer containing appropriate urapidil was transferred into a voltammetric cell. The cyclic voltammograms or the linear sweep voltammograms were recorded between 0.0 and 1.2 V. After each measurement, the electrode was refreshed by successive cyclic voltammetric sweeps from 0.0 to 1.2 V in pH 6.8 Britton-Robinson buffer until the voltammogram became stable. If necessary, the surface was renewed by pushing an excess MWNT paste out of the tube (a thickness of 2–3 mm), followed by polishing and washing with water. All experiments were performed at room temperature.

2.4. Tablets analysis

Ten pieces of urapidil tablet (Xi'an Lijun Pharmaceutical Co., China) were powdered in a mortar, a portion of the powder equivalent to one tablet was accurately weighted and dissolved in 1.5 mL 0.1 mol/L HCl solution and diluted with water to 100 mL. Then microliters of the supernatant liquid was added into 5 mL pH 6.8 Britton-Robinson buffer. The differential pulse voltammograms were recorded between 0.45 and 0.75 V after open-circuit accumulation for 60 s. The oxidation peak current of urapidil was measured. The parameters of differential pulse voltammetry (DPV) were pulse width of 0.05 s, pulse increment of 4 mV and pulse amplitude of 50 mV. The concentration of urapidil was calculated using standard addition method.

3. Results and discussion

3.1. Voltammetric behavior of urapidil

The voltammetric behavior of urapidil at the MWNT-PE was examined. Fig. 1 shows the cyclic voltammograms of urapidil in pH 6.8 Britton-Robinson buffer. A well-defined oxidation peak was observed at 0.62 V on the first anodic scan from 0.0 to 1.2 V. On the reversal scan, no corresponding reduction peak was detected. The oxidation peak current showed a large decrease on the second cyclic scanning. After the second scan, the peak current decreased slightly and finally reached a constant level. The oxidation peak current i_p was found to increase linearly with the scan rate v in the range of 20–600 mV/s (Fig. 2), the linear regression equation was $i_p\,(\mu A) = 0.134 + 2.25v\,(V/s)$ ($R = 0.998$). The oxidation peak potential E_p shifted to positive direction with increasing scan rate v, the linear regression equation was $E_p\,(V) = 0.538 + 0.050 \log v\,(mV/s)$ ($R = 0.996$). These results indicated that the oxidation of urapidil was an irreversible process with adsorption character.

In order to demonstrate the oxidation mechanism of urapidil, potential-controlled coulometry was used to determine the number of electrons transferred in the oxidation of urapidil. Five milliliters 5.0×10^{-6} mol/L urapidil in pH 6.8 Britton-Robinson buffer was exhaustively electrolyzed at 0.70 V. The average value of the consumed net charge ΔQ for three duplicate measurements was 4.61 mC. According to the coulomb's law, the

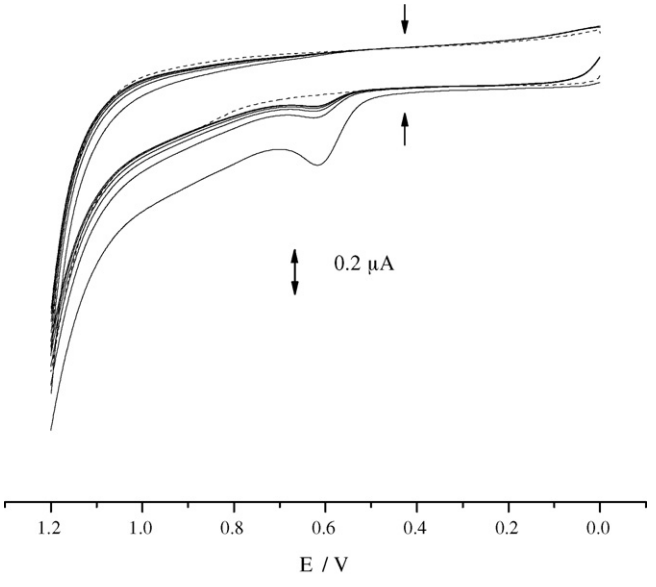

Fig. 1. Cyclic voltammograms of urapidil in pH 6.8 Britton-Robinson buffer at MWNT-PE in the absence (dashed line) and the presence (solid line) of 5.0×10^{-6} mol/L urapidil. Scan cycles: 1–5 from the outer to the inner. Scan rate: 100 mV/s.

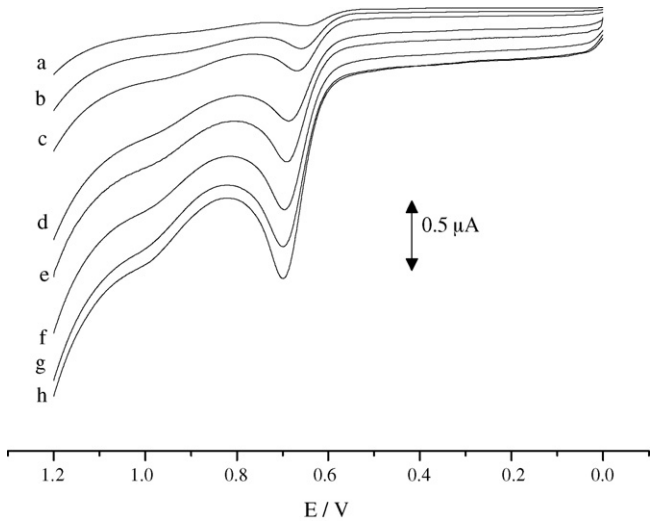

Fig. 2. Linear sweep voltammograms of 5.0×10^{-6} mol/L urapidil in pH 6.8 Britton-Robinson buffer at scan rate of (from a to h): 20, 50, 100, 200, 300, 400, 500 and 600 mV/s.

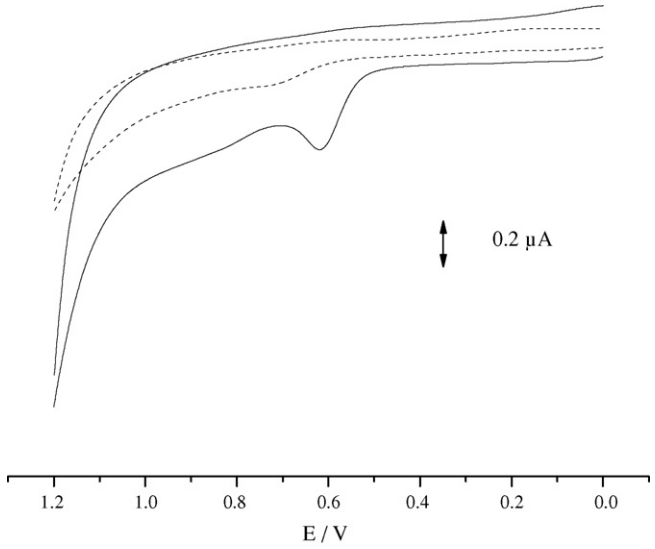

Fig. 3. Cyclic voltammograms of 5.0×10^{-6} mol/L urapidil at CPE (dashed line) and MWNT-PE (solid line) in pH 6.8 Britton-Robinson buffer. Scan rate: 100 mV/s.

number of electrons n transferred in the oxidation of urapidil was 1.91, which approximated to 2.

Additionally, the oxidation peak potential shifted negatively with the increase of pH value and obeyed the following equation: $E_p = 0.917 - 0.046\text{pH}$ ($R = 0.987$). The slope of 0.046 V/pH indicated that the number of protons involved in the oxidation of urapidil was equal to that of electrons transferred.

Urapidil was a derivative of uracil with the addition of a phenylpiperazinyl group. The phenylpiperazinyl group was known to be electroinactive, uracil also had no voltammetric response within the studied potential window. Therefore, the possible reaction group was the secondary amino group at C-6 of uracil and the electrode reaction of urapidil was suggested as follows [15]:

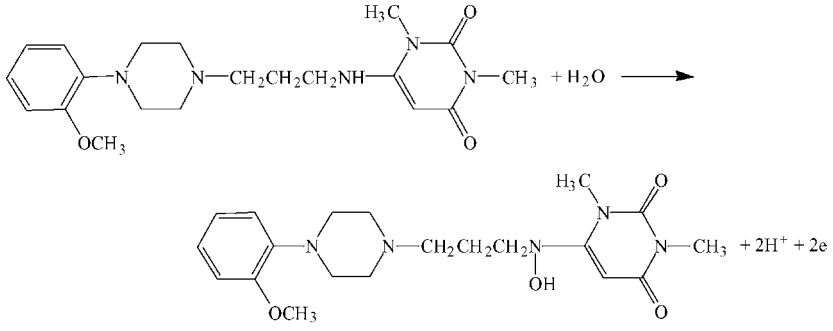

3.2. Electrocatalysis of MCNTs for the oxidation of urapidil

The voltammetric responses of 5.0×10^{-6} mol/L urapidil at CPE and MWNT-PE with the same geometric surface were compared, and the results were shown in Fig. 3. At CPE, a poorly defined oxidation peak was observed. The peak current was smaller. The peak potential was at 0.71 V. Under identical conditions, the oxidation peak current of urapidil at MWNT-PE was much higher, and its oxidation peak potential lowered to 0.62 V. Both the enhancement of peak current and the negative shift of the peak potential demonstrated that MWNT-PE exhibited electrocatalytic activity for the oxidation of urapidil.

In order to explore the cause of the electrocatalytic action of MWNTs, the efficient areas of the MWNT-PE and the CPE with the same geometric surface were compared. This was achieved by comparing voltammetric responses of 1.0×10^{-3} mol/L $K_3Fe(CN)_6$ at different scan rates in pH 6.8 Britton-Robinson buffer. The linear regression equations of the anodic peak current i_{pa} of $K_3Fe(CN)_6$ with scan rate v (from 20 to 500 mV/s) were $i_{pa}\,(\mu A) = 0.124 + 0.339v^{1/2}\,(\text{mV/s})^{1/2}$ ($R = 0.996$) for the MWNT-PE, $i_{pa}\,(\mu A) = 0.0143 + 0.173v^{1/2}\,(\text{mV/s})^{1/2}$ ($R = 0.998$) for the CPE, respectively. The ratio of slopes of the two equations was 1.96. Assuming a constant diffusion coefficient D_R, the efficient area of the MWNT-PE was about two times as large as that of the CPE according to the Randles–Sevcik equation [16].

In addition, the chronocoulometry was used to determine the Faradaic charge Q_{ads} of urapidil, according to the formula given by Anson [17]:

$$Q = 2nFAc_0 D_R^{1/2} \pi^{-1/2} t^{1/2} + Q_{dl} + Q_{ads}$$

When the double-layer charge Q_{dl} was assumed unchanged, Q_{ads} could be obtained by the intercepts of the plot of Q versus $t^{1/2}$ after background was subtracted. The adsorptive amount

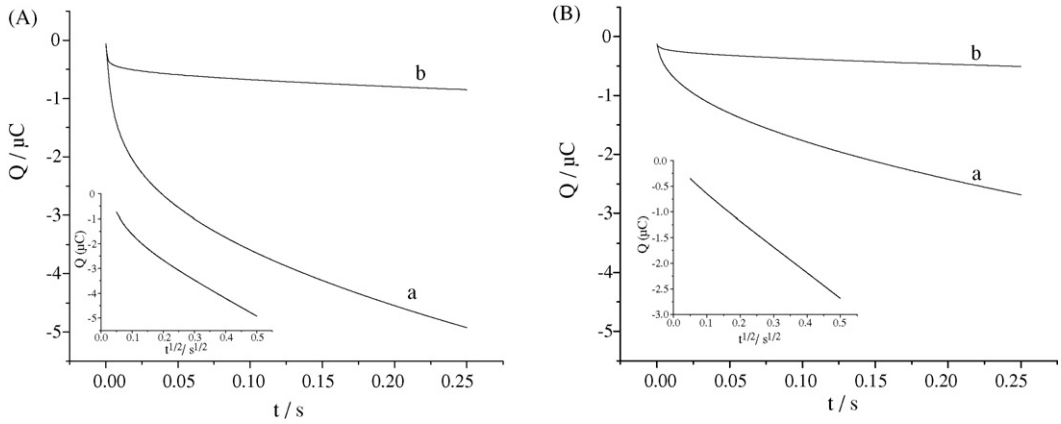

Fig. 4. Q–t plots of 5×10^{-4} mol/L urapidil at MWNT-PE (A, curve a) and CPE (B, curve a). Corresponding plots of the blank solution are shown by curve b. Inset: plots of Q–$t^{1/2}$ curve (background subtracted). Measurement conditions: initial potential 0.4 V, final potential 0.9 V, pulse width 0.25 s.

Γ of urapidil could be evaluated from the following equation: $Q_{ads} = nFA\Gamma$.

The Q_{ads} at CPE and MWNT-PE determined was 1.61×10^{-7} and 1.09×10^{-6} C, respectively (Fig. 4). From the number of electron transferred in the oxidation of urapidil and the geometric area of the electrode, it was calculated that Γ was 4.15×10^{-11} mol/cm^2 at CPE and 2.81×10^{-10} mol/cm^2 at MWNT-PE, respectively. Therefore, the adsorptive amount Γ of urapidil at the MWNT-PE was 6.8 times as large as that of the CPE.

Combining the above quantitative analysis, the larger effective surface area of MWNTs and the stronger adsorption of urapidil at MWNT-PE were responsible for the electrocatalytic oxidation of urapidil at the MWNT-PE.

3.3. Optimization of experimental conditions

The oxidation peak current of urapidil can be used to quantify urapidil concentration. Differential pulse voltammetry was used in the voltammetric measurement owing to its good sensitivity and resolving power. The experimental conditions were optimized.

The voltammetric responses of 5.0×10^{-6} mol/L urapidil at the MWNT-PE in such supporting electrolytes as hydrochloric acid, sulphuric acid and sodium hydroxide solutions, sodium acetate–acetic acid, ammonia–ammonium chloride, and Britton-Robinson buffers were examined. It was found that the oxidation peak of urapidil was well-defined and more sensitive in the Britton-Robinson buffer than in other solutions. Moreover, the oxidation peak currents increased with the increase of the pH value when pH value was below 6.8. And the peak current reached the maximum value at pH 6.8. When pH value was above 6.8, the peak current began to decrease. Thus, pH 6.8 Britton-Robinson buffer was chosen as supporting electrolyte.

Additionally, the oxidation peak potential and the peak currents of urapidil kept almost unchanged when the accumulation potential changed from 0.50 to − 0.50 V. The oxidation peak current increased greatly within the first 60 s of accumulation and then reached maximum value. So an open-circuit accumulation for 60 s was used in the determination of urapidil.

3.4. Analytical determination of urapidil

3.4.1. Calibration curve

Under optimized conditions, differential pulse voltammograms of urapidil were showed (Fig. 5). The linear region was from 5.0×10^{-8} to 2.0×10^{-6} mol/L with a regression equation of i_p (nA) $= 9.90 \times 10^7 c$ (mol/L) $+ 4.88$ ($R = 0.999$). The detection limit ($3\sigma/s$, where σ is the standard deviation of the intercept and s is the slope of the calibration curve) was 3.8×10^{-8} mol/L.

The relative standard deviation (R.S.D.) for 10 replicate measurements of 5.0×10^{-6} mol/L urapidil at a MWNT-PE was 2.93%. Seven pieces of MWNT-PE with the same surface area were fabricated and the R.S.D. for the individual determination of 5.0×10^{-6} mol/L urapidil was 2.48%. These results demonstrated the good reproducibility of the proposed method.

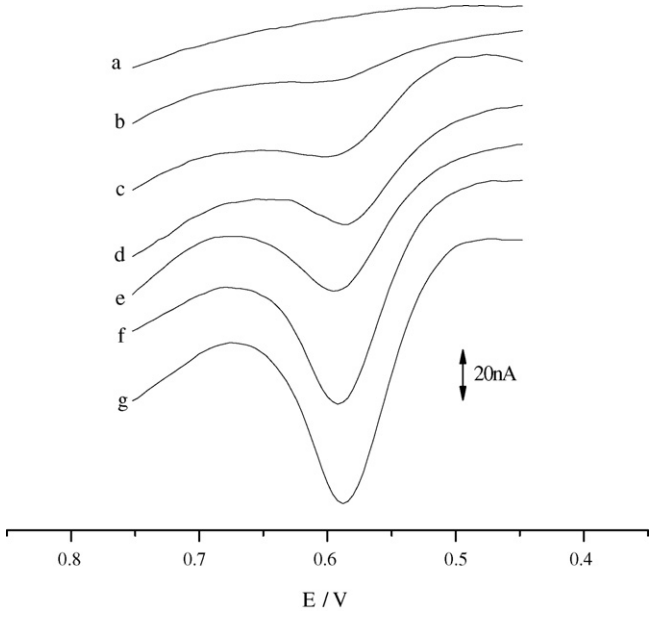

Fig. 5. Differential pulse voltammograms of urapidil in pH 6.8 Britton-Robinson buffer. The concentration of urapidil from a to g: 0.00, 0.05, 0.10, 0.20, 0.40, 0.80 and 1.00 μmol/L.

Table 1
Determination of urapidil content and recovery in urapidil tablets[a]

Sample	Content[b] (mg/tablet)	Added (10^{-7} mol/L)	Measured (10^{-7} mol/L)	Average[c] recovery (%)
1	29.5 ± 0.4	0.5	0.51 ± 0.01	102
		5.0	4.92 ± 0.14	98.4
		10.0	9.93 ± 0.19	99.3
2	30.1 ± 0.7	0.5	0.49 ± 0.01	98.0
		5.0	5.05 ± 0.09	101
		10.0	10.02 ± 0.20	100

[a] Label amount 30 mg/tablet.
[b] Mean value ± S.D. ($n = 7$).
[c] The urapidil concentration taken in the sample: 5.0×10^{-7} mol/L.

3.4.2. Interferences

In order to evaluate the selectivity of the proposed method, some common interferences were tested under optimized conditions. The tolerable limit was defined as the concentrations of foreign substances, which gave an error less than ±5.0% in the determination of 5.0×10^{-6} mol/L urapidil. The results showed that 400-fold starch, urea, theophylline; 200-fold dextrine, Co^{2+}, Zn^{2+}, Cu^{2+}, Mg^{2+}, Ca^{2+}; 100-fold glucose, sucrose; 50-fold pyridine, inosine did not interfere with the determination. The results proved that the proposed method had acceptable selectivity.

3.4.3. Analytical applications

The proposed method was applied to the determination of urapidil in urapidil tablets. The measured values (shown in Table 1) were in accordance with those of the labeled. The relative standard deviation of each sample for seven replicate determinations was less than 3.0%. In addition, the recovery of this method was estimated and the average recovery (also shown in Table 1) was between 98.0 and 102%. These results demonstrated that the proposed method had good accuracy in urapidil measurement.

4. Conclusion

The voltammetric behavior and oxidation mechanism of urapidil were investigated at a multi-wall carbon nanotube-paraffin oil paste electrode (MWNT-PE) by using cyclic voltammetry and coulometry. The oxidation of urapidil was found to be an irreversible two-electron and two-proton process with adsorption character. The secondary amino group at C-6 of uracil was the possible reaction group. MWNTs showed electrocatalytic action for the oxidation of urapidil, characterizing by the enhancement of the peak current and the reduction of peak potential, which was probably due to the larger effective surface area of MWNTs and the stronger adsorption of urapidil at MWNT-PE. Differential pulse voltammetric method for the determination of urapidil was proposed. The process was simple, rapid and high sensitive.

Acknowledgement

The authors would like to acknowledge financial support from the National Natural Science Foundation of China (Grant No. 20475043).

References

[1] R.L. Wang, Z.P. Yuan, The Handbook of Chemical Products, Pharmaceutical Part, Chemical Industry Press, Beijing, 1993, pp. 329–330.
[2] K. Zech, R. Huber, J. Chromatogr. 353 (1986) 351–360.
[3] R. Baker, J. Chromatogr. 393 (1987) 447–453.
[4] L. Huber, K. Zech, J. Pharm. Biomed. Anal. 6 (1988) 1039–1043.
[5] H.Y. Lang, Y.R. Li, W.P. Zhang, X.J. Zhang, Y.H. Sheng, Chem. J. Chin. Univ. 24 (2003) 618–620.
[6] Y.F. Wei, D.M. Ma, X.H. Li, Chin. J. Anal. Lab. 23 (2004) 42–44.
[7] J.J. Davis, R.J. Coles, H. Allen, O.J. Hill, Electroanal. Chem. 440 (1997) 279–282.
[8] M. Musameh, J. Wang, A. Merkoci, Y. Lin, Electrochem. Commun. 4 (2002) 743–746.
[9] R.R. Moore, C.E. Banks, R.G. Compton, Anal. Chem. 76 (2004) 2677–2682.
[10] M. Trojanowicz, Trends Anal. Chem. 25 (2006) 480–489.
[11] L. Qian, X.R. Yang, Talanta 68 (2006) 721–727.
[12] D. Vega, L. Agüí, A. González-Cortés, P. Yáñez-Sedeño, J.M. Pingarrón, Talanta 71 (2007) 1031–1038.
[13] M.D. Rubianes, G.A. Rivas, Electrochem. Commun. 5 (2003) 689–694.
[14] N.S. Lawrence, R.P. Deo, J. Wang, Talanta 63 (2004) 443–449.
[15] H.B. Gao, Organic Chemistry, Higher Education Press, Beijing, 1999, p. 446.
[16] A.J. Bard, L.R. Faulkner, Electrochemical Methods, Fundamentals and Applications, John Wiley & Sons, Inc., 1980, pp. 213–248.
[17] F.C. Anson, Anal. Chem. 36 (1964), 932-334.

Available online at www.sciencedirect.com
ScienceDirect
Talanta 73 (2007) 870–877
Talanta
www.elsevier.com/locate/talanta

Headspace solid-phase microextraction with novel sol–gel permethylated-β-cyclodextrin/hydroxyl-termination silicone oil fiber for determination of polybrominated diphenyl ethers by gas chromatography–mass spectrometry in soil

Jingjing Zhou [a], Fangxing Yang [b], Dongmei Cha [a,c], Zhaorui Zeng [a,*], Ying Xu [b]

[a] *Department of Chemistry, Wuhan University, Wuhan 430072, China*
[b] *State Key Laboratory of Freshwater Ecology and Biotechnology, Institute of Hydrobiology, Chinese Academy of Sciences, Wuhan 430072, China*
[c] *Key Laboratory for Analytical Chemistry of the State Ethnic Affairs Commission, College of Chemistry and Material Science, South-Central University for Nationalities, Wuhan 430074, China*

Received 10 January 2007; received in revised form 9 May 2007; accepted 9 May 2007
Available online 18 May 2007

Abstract

A simple, sensitive, and accurate method for determination of polybrominated diphenyl ethers (PBDEs) in soil has been developed based on headspace solid-phase microextraction (HS-SPME) followed by gas chromatography–mass spectrometry (GC–MS). Permethylated-β-cyclodextrin/hydroxyl-termination silicone oil (PM-β-CD/OH-TSO) fiber was first prepared by sol–gel technology and employed in SPME procedure. By exploiting the superiorities of sol–gel coating technique and the advantages of the high hydrophobic doughnut-shaped cavity of PM-β-CD, the novel fiber showed desirable operational stability and extraction ability. After optimization on extraction conditions like water addition, extraction temperature, extraction time, salts effect, and solvents addition, the method was validated in soil samples, achieving good linearity ($r > 0.999$), precision (R.S.D. < 10%), accuracy (recovery > 78%), and detection limits (S/N = 3) raging from 13.0 to 78.3 pg/g.

Keywords: Solid-phase microextraction; Polybrominated diphenyl ethers; β-Cyclodextrin; Soil

1. Introduction

Polybrominated diphenyl ethers (PBDEs) are a group of brominated flame retardants (BFRs) that are widely used in polymers, especially in the manufacture of a great variety of electrical appliances, building materials, and textiles. As additive (noncovalently bound) BFRs, PBDEs are merely blended physically with the polymer and are therefore more likely to leach out of products and enter the environment during their production, delivery, use, and disposal and through the recycling of materials containing PBDEs [1]. Although little is still known about their toxic effects on humans, recent reports indicate serious concerns regarding possible developmental neurotoxicity and endocrine disruption [2]. In addition, the combustion of PBDEs could generate highly toxic substances such as polybrominated dibenzofurans and polybrominated dibenzo-*p*-dioxins [3]. Hence, environmental PBDE analysis has becoming a problem of great social and scientific concern.

With rising use of BFRs over the last 20 years, PBDEs have been detected in nearly all environmental compartments (air, water, soil, sediment, and biota) [4–6]. According to the detection methods reported, sample preparation served as a crucial step before determination conventionally conducted using gas chromatography (GC) with electron capture detection (ECD) or mass spectrometry (MS) due to the complexity of the environmental matrices and the low concentrations of the analytes. Routine sample pretreatments involved extraction with organic solvents or supercritical fluid extraction and further clean-up by adsorption chromatography or by solid-phase extraction (SPE) [7,8]. These traditional procedures are often time-consuming and labor-intensive, and require large volumes of sample and solvent, suffering great risks of contamination and analytes loss.

* Corresponding author. Fax: +86 27 8764 7617.
E-mail address: zrzeng@whu.edu.cn (Z. Zeng).

0039-9140/$ – see front matter © 2007 Published by Elsevier B.V.
doi:10.1016/j.talanta.2007.05.006

Solid-phase microextraction (SPME) is a technique that provides simple, time-saving, and solvent-free analyses, achieving extraction and concentration in the same analytical step with very low or no sample manipulation [9]. Headspace-SPME (HS-SPME) with sampling from the headspace above the sample was especially recommended in complex matrices analysis, for producing neat spectra and protecting the fiber from damages by concomitants present in the matrix [10]. SPME has been successfully applied to the determination of trace levels of many other organic pollutants in environmental matrices [11–13]. As for PBDEs, only a few SPME applications with commercially available fibers have been reported [14–16]. Considering PBDEs' high hydrophobicity and low volatility, comparatively high extraction temperature and long extraction time are quite needed, which hence demands extremely good thermal stability and long lifespan of SPME fibers. This somehow suggests high challenges to commercial fibers due to their preparation usually by mere physical deposition of the polymer coating on the surface of the fibers. In addition, the present commercial fibers are limited and restrict the choice of fibers with more targeted extraction ability towards analytes, which is especially important to complex environmental PBDEs analysis. Therefore, new SPME fibers with better operational stability and extraction efficiency to conform to PBDEs analysis are expected.

Sol–gel coating technology, established by Malik and coworkers [17,18], has been proved excellent to develop novel SPME fibers with high operational stability and good extraction capability by chemically bonding the porous sol–gel network to fused-silica surface of the fiber. Cyclodextrins (CDs), the second generation of supermolecules next to crown ether, are well known to readily form inclusion compounds with a wide variety of organic compounds for possessing a hydrophobic doughnut-shaped cavity [19]. More recently, CDs have been used to prepare SPME fibers by sol–gel technology. The fibers were reported to demonstrate nice extraction ability to phenols, amines, and amphetamine-like drugs [20,21]. Here, novel permethylated-β-cyclodextrin/hydroxyl-termination silicone oil (PM-β-CD/OH-TSO) fiber was first prepared, expected to realize desirable SPME efficiency to hydrophobic PBDEs.

Employing the novel PM-β-CD/OH-TSO fiber, HS-SPME coupled to GC–MS analysis without a further clean-up step is developed for determination of PBDEs in soil samples. The novel fiber's extraction efficiency, operational stability, and preparation reproducibility were investigated in detail. After SPME conditions were systematically optimized, the method was validated in red clay and applied to analysis other different soil samples, including those from Taizhou, Zhejiang, one the largest electronic waste disassembling areas in China.

2. Experimental

2.1. Instrumentation

Chromatography analysis was performed using a 6890 series gas chromatograph and 5973 quadrapole mass selective detector (Agilent Technologies, USA). In order to mix the various ingredients in solution thoroughly, a model KQ-50DE ultrasonator (Kunshan Ultrasonator Instrument Corporation, Kunshan, China) was used. A centrifuge model TGL-16C (Shanghai Anting Instrument Factory, Shanghai, China) was used to separate the sol solution from the precipitate during fiber preparation. A magnetic stirrer DF-101B (Leqing, China) was employed for stirring the sample during extraction. The fused-silica fiber (120 μm, o.d.) with protective polyimide coating was obtained from the Academy of Post and Telecommunication, Wuhan, China. A microscope BA22031 (Guangdian, Chongqing, China) was used for the evaluation of fiber thickness. SPME devices equipped with PM-β-CD/OH-TSO fibers (65–70 μm) were laboratory-made. Commercial SPME assemblies and poly(dimethylsiloxane) (PDMS) fiber (100 μm) were purchased from Supelco (Bellefonte, PA). IR spectra were done on IR instrument of model FTIR-8201PC (Shimadzu, Japan).

2.2. Chemicals and samples

PM-β-CD was synthesized by referring the reported method [22]. OH-TSO was purchased from Chengdu Center for Applied Research of Silicone (Chengdu, China). Tetraethoxysilane (TEOS) was obtained from the chemical plant of Wuhan University, China. Trifluoroacetic acid (TFA) was purchased from Merck, Germany. 2,4,4′-Tribromodiphenyl ether (BDE-17), 2,2′,4,4′-tetrabromodiphenylether (BDE-47), 2,3′,4,4′-tetrabromodiphenylether (BDE-66), 2,2′,3,4,4′-pentabromodiphenyl ether (BDE-85), 2,2′,4,4′,5-pentabromodiphenyl ether (BDE-99), 2,2′,4,4′,6-pentabromodiphenyl ether (BDE-100), 2,2′,3,4,4′,5′-hexabromodiphenyl ether (BDE-138), 2,2′,4,4′,5,5′-hexabromodiphenyl ether (BDE-153), and 2,2′,4,4′,5,6′-hexabromodiphenyl ether (BDE-154) were purchased from Accu Standards (New Haven, CT). Isooctane stock solution of PBDEs was prepared at a concentration of 1.0 μg/mL. Working solutions were obtained by subsequent dilutions in isooctane. Both stock and working solutions were stored at −4 °C. All other chemicals used were obtained from the Chemical Plant of Wuhan University and of analytical grade.

Three types of soils, namely red clay, sandy soil, and garden soil were collected from suburb of Wuhan City (China). They were all air-dried to constant weight at room temperature, pulverized and sieved to a grain size of 2 mm. After homogenization, the soil samples were stored at 4 °C. Red clay was taken as standard soil to perform extraction parameter optimization and method validation. Blank analysis of the standard soil was carried out before spiking. Three sandy soil samples (soil 1, 2, and 3) for method application were collected in the vicinity of an open electronic waste disposal and recycling facility located in Taizhou, Zhejiang, China. They were air-dried, pounded, and stored at 4 °C.

2.3. Fiber preparation

Prior to sol–gel coating, 6-cm-long fused-silica fibers were dipped in acetone for 3 h to remove the protective polyimide layer and 1 mol/L NaOH solution for 1 h to expose the maximum number of silanol groups on the surface. Then they were cleaned with water before dipping in 0.1 mol/L HCl solution for 30 min

to neutralize the excess NaOH. Finally, they were cleaned again with water and air-dried at room temperature.

The mass of PM-β-CD and the corresponding proportion of other ingredients in sol–gel solution were optimized to gain desirable coating effect and extraction capacity. The sol–gel solution was finally prepared as follows: about 28.0 mg of PM-β-CD was dissolved in 150 μL of methylene chloride, and then 90 mg of OH-TSO, 100 μL of TEOS, and 80 μL TFA aqueous solution (95%) were added and mixed thoroughly by ultrasonic agitation in a plastic tube. The mixture was centrifuged at 12,000 rpm for 5 min. The top clear sol solution was collected for fiber coating. After the fibers were dipped vertically into the solution for about 30–45 min, sol–gel coating was formed on the outer surface of the fibers' end (about 1 cm). This coating process was repeated several times until the desired thickness of the coating was obtained. The fibers were then placed in a desiccator at room temperature for 12 h and then conditioned under nitrogen at 300 °C for 2 h in the GC injection port. The final thickness of the PM-β-CD/OH-TSO fiber was 65–70 μm. For comparison, a sol–gel-derived OH-TSO fiber with no PM-β-CD blended was also prepared in similar way.

2.4. IR experiment

After being conditioned, the PM-β-CD/OH-TSO and OH-TSO fibers were dipped in methylene chloride for 2 h before the IR experiment. Afterwards, coating of the pretreated fiber was harvested with a razor blade, finely ground, and then blended with potassium bromide (KBr). The KBr pellet spectra of the coatings were acquired with air as background at a resolution of 4 cm^{-1} over the full mid-IR range (4000–400 cm^{-1}).

2.5. Headspace solid-phase microextraction procedure

Spiked soil sample was prepared by adding 10 μL of stock/working solution to 1 g of standard soil, shaking carefully for homogenization, and finally leaving the sample for 24 h for drying and aging. To the 10-mL clean silanized glassware containing spiked soil, were added 5 μL of methanol, 5 mL deionized water, and a magnetic rotator. Then the vial was rapidly sealed with a cap wrapped with PTFE sealing tape and put on a magnetic stirrer for heating and stirring. The septum piecing needle of the SPME device was introduced into the vial and the fiber was exposed in headspace to begin SPME at 95 °C for 60 min with constant stirring (1000 rpm). Finally, the fiber was withdrawn into the needle and immediately transferred to the GC injector for desorption.

2.6. GC–MS analysis

The SPME samples were analyzed immediately by GC–MS. A HP-1MS fused-silica capillary column (30 m × 0.25 mm × 0.25 μm; Agilent Technologies, USA) was used, with helium carrier gas at 1.1 mL/min (constant flow mode). The spectrometer was operated in the electron impact (70 eV) selected ion monitoring (SIM) mode at 1.75 kV. Ion masses 248, 246 were selected for PBDE-17, and masses 486, 488 for PBDE-47 and -66, and masses 565, 566 for PBDE-85, -99, and -100, and masses 643, 641 for PBDE-138, -153, and 154. The GC oven was programmed to increase from 80 to 240 °C at 10 °C/min and then until 280 °C (hold for 3 min) at 5 °C/min. The injector temperature and the mass spectrometer transfer line were all kept at 300 °C. Desorption of the SPME fiber samples was accomplished in the splitless injection mode for 12 min.

3. Results and discussion

3.1. Characteristics of PM-β-CD/OH-TSO fiber

3.1.1. Possible mechanism of the coating process

Table 1 lists the names and chemical structures of the principal ingredients of the sol–gel coating solution in this work. The sol–gel process involves mainly hydrolysis and polycondensation of TEOS and OH-TSO, generating a three-dimensional (3D) network and extending it further. At the same time as the network is growing, the loose network anchors the PM-β-CD in and produces an integral matrix together with PM-β-CD. When growing near the fused-silica fiber, the network gets chemical bonded to the outer surface of the fiber. Fig. 1 represents the probable chemical structure of the PM-β-CD/OH-TSO fiber coating. Though it seems different from the conventional incorporation mechanism for sol–gel SPME fiber coating [21], similar mechanism description has actually appeared and applied successfully in the preparation of sol–gel peralkylated-β-CD stationary phases for GC capillary column [23].

Fig. 2 shows the IR spectra of sol–gel-derived OH-TSO stationary phase, sol–gel-derived PM-β-CD/OH-TSO stationary phase and pure PM-β-CD. The feature identified for PM-β-CD [24]: 1458.44 cm^{-1} (φOCHφHCH), 1366.32 cm^{-1} (φOCHφCCH), and 564.34 cm^{-1} (ring vibration) also appeared in sol–gel-derived PM-β-CD/OH-TSO coating. It revealed the successful and firm encapsulation of PM-β-CD into the sol–gel matrix. Moreover, fine qualities of the fiber proved in the follow-

Table 1
Names and chemical structures of coating ingredients for sol–gel-derived PM-β-CD/OH-TSO fiber

Name	Chemical structure
TEOS	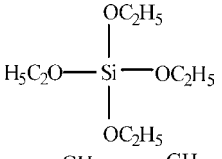
OH-TSO	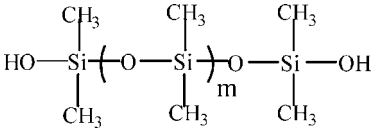
PM-β-CD	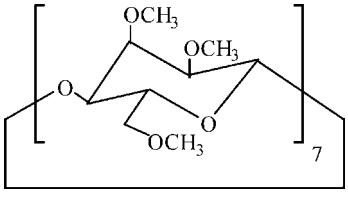

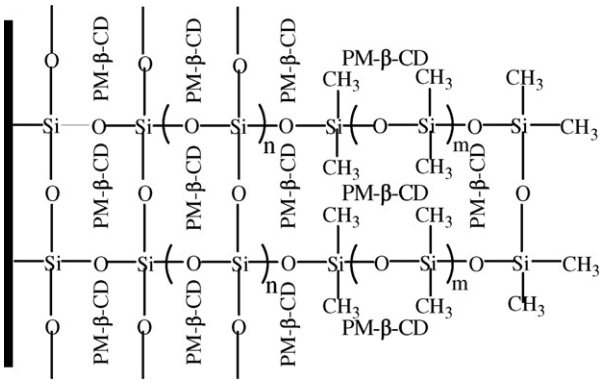

Fig. 1. Chemical structure of PM-β-CD/OH-TSO fiber coating.

ing section imply also the strong immobilization and structural integrity of the coating.

3.1.2. Extraction efficiency

To explore the extraction superiority of the novel fiber, comparison of extraction efficiencies of sol–gel PM-β-CD/OH-TSO, OH-TSO fibers and commercial PDMS fiber, was made under the same experimental conditions (Fig. 3), except that the desorption temperature was lowered to 280 °C when using PDMS fiber. The extraction efficiencies were evaluated by comparison of the peak areas per microliter from HS-SPME with the peak areas per microliter from direct injection of stand solution with the same concentration. As demonstrated clearly in the figure, the two sol–gel fibers both showed better extraction

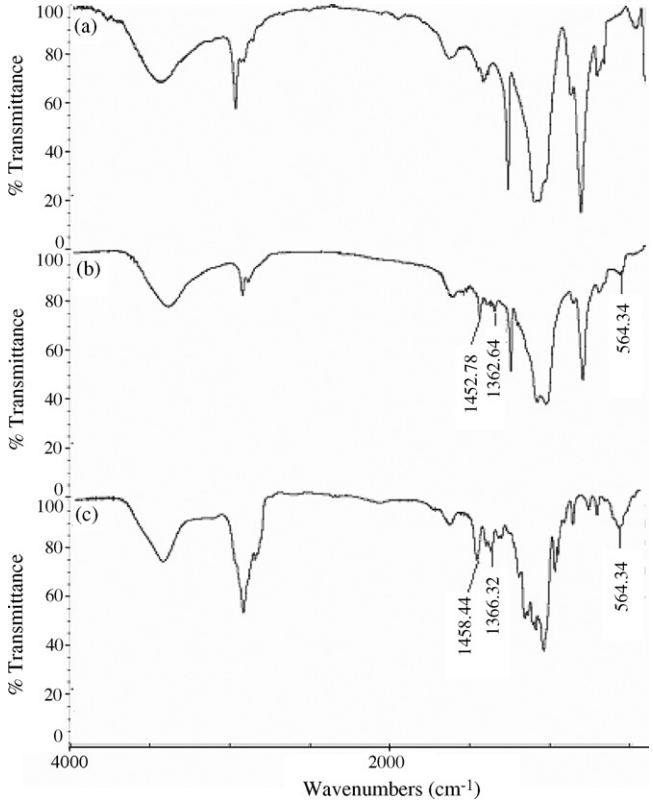

Fig. 2. IR spectra of sol–gel OH-TSO fiber coating (a), sol–gel PM-β-CD/OH-TSO fiber coating (b), and pure PM-β-CD (c).

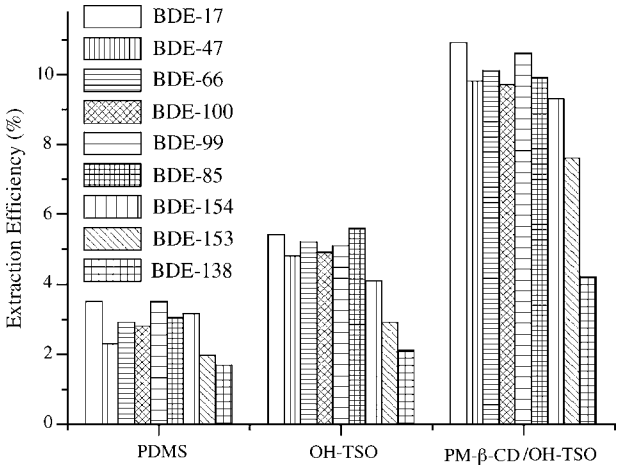

Fig. 3. Comparison of extraction efficiencies of PM-β-CD/OH-TSO fiber (70 μm) with OH-TSO fiber (70 μm) and commercial PDMS fiber (100 μm) for analysis of PBDEs in soil. SPME conditions: sampling mode, headspace; water added, 5 mL; extraction temperature, 95 °C; extraction time, 60 min; solvent (methanol) added, 10 μL.

efficiency than PDMS fiber; it was sol–gel process that generated 3D network onto the fibers enabling the enhanced area and hence sample capacity. As for the PM-β-CD/OH-TSO fiber, which gave the highest extraction response to PBDEs among the three, not only sol–gel coating technology worked, but also the hydrophobic interactions between hydrophobic doughnut-shaped cavity of PM-β-CD and PBDEs played great part to impart desirable extraction efficiency to the fiber.

3.1.3. Operational stability

The fiber's thermal stability was investigated by performing extraction after its being exposed at the GC injector for 1 h at 280, 300, 320, 340, and 360 °C, successively. Results showed that the fiber exhibits excellent thermal stability (>340 °C) like other sol–gel fibers. This character could undoubtedly contribute to better extraction performance in this work, because PBDEs are all high-boiling-point compounds and need comparatively high extraction temperature. Under the high temperature along with long extraction time, the fiber's extraction efficiency was monitored during its use and no obvious decline was observed after it had been used for about 220 runs.

3.1.4. Preparation reproducibility

Four PM-β-CD/OH-TSO fibers prepared within batch and three ones in different batches (fiber thickness was about 65 μm) were used to evaluate the fibers' preparation reproducibility. Table 2 gives the relative standard deviation (R.S.D.) when using these fibers perform SPME on the analytes, which nicely illustrates that the sol–gel PM-β-CD/OH-TSO fibers have good reproducibility not only within batch but also between batches.

3.2. HS-SPME optimization

The proposed HS-SPME procedure was optimized on the variables related to extraction steps, including the volume of water added to the soil, extraction temperature, extraction time,

Table 2
Preparation reproducibility of PM-β-CD/OH-TSO fiber with same thickness (65 μm)

Compound	R.S.D.[a] (%)	
	Fiber-to-fiber ($n=4$)	Batch-to-batch ($n=3$)
BDE-17	1.49	3.68
BDE-47	1.68	3.78
BDE-66	3.28	8.30
BDE-100	5.64	5.10
BDE-99	4.94	6.46
BDE-85	6.68	9.35
BDE-154	2.57	9.64
BDE-153	5.34	5.89
BDE-138	5.54	6.48

[a] Calculated from the samples spiked at 1.0 ng/g level.

salt effect, and solvent addition. The optimization experiments were performed on four representative PBDEs: BDE-17, BDE-47, BDE-99, and BDE-153.

Adding water to soils was effective in improving the release of analytes from solid substrate, thereby increasing sensitivity of SPME [25,26]. Effect of the volume of water added to 1.0 g soil was studied by varying the volume from 1 to 5 mL (extraction need at least 5 mL for headspace sampling). As shown in Fig. 4a, the increasing water volume augmented response apparently. Hence, 5 mL was chosen as the optimal amount of water added.

The temperature effect on extraction was investigated within 65–95 °C as demonstrated in Fig. 4b. The increasing temperature heavily favored the extraction amounts, and this phenomenon is in accord with HS-SPME optimization performed in water samples [14]. PBDEs' high boiling points of 310–425 °C could

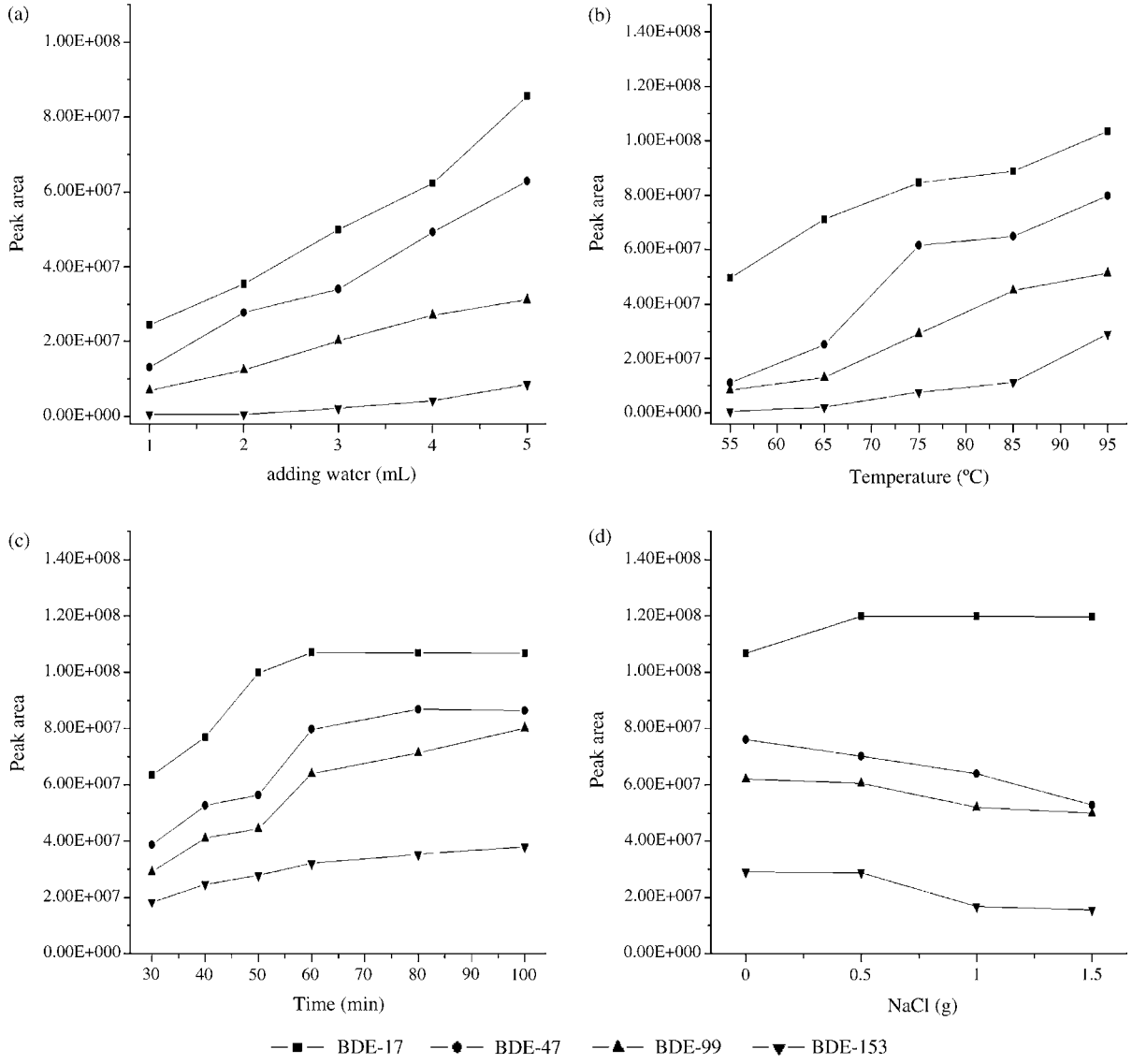

Fig. 4. Effect of extraction conditions on HS-SPME of representative PBDEs (1 ng/g of each analyte). (a) Effect of the water volume adding in 1.0 g of soil. Conditions: extraction temperature, 80 °C; extraction time, 60 min; NaCl, 0 g. (b) Extraction temperature profile. Conditions: water added, 5 mL; extraction time, 60 min; NaCl, 0 g. (c) Extraction time profile. Conditions: water added, 5 mL; extraction temperature, 95 °C; NaCl, 0 g. (d) Effect of the amount of NaCl added. Conditions: water added, 5 mL; extraction temperature, 95 °C; extraction time, 60 min.

Table 3
Effect of solvents addition on SPME of PBDEs

Compound	Mean relative response to ethanol ($n=3$)						
	Ethanol	Methanol	Isopropylalcohol	Acetonitrile	Hexane	Dichloromethane	Acetone
BDE-17	100	101	97.3	90.5	76.2	87.3	92.0
BDE-47	100	102	93.4	97.7	46.0	67.3	86.9
BDE-99	100	121	103	113	46.7	70.8	90.1
BDE-153	100	109	99.0	84.3	40.9	62.9	77.2

Table 4
Linear ranges, correlation coefficients (r), limit of detection (LOD), and precisions (R.S.D.) of the proposed method

Compound	Linear range (ng/g)	r	LOD[a] (pg/g)	R.S.D.[b] (%, $n=5$)	Recovery[b] (%)
BDE-17	0.1–10	0.9999	13.0	8.97	96.0
BDE-47	0.1–10	0.9996	25.1	7.91	99.2
BDE-66	0.1–10	0.9995	27.6	8.83	82.4
BDE-100	0.1–10	0.9992	28.3	8.26	80.7
BDE-99	0.1–10	0.9992	26.7	7.63	99.3
BDE-85	0.1–10	0.9993	27.9	7.74	89.5
BDE-154	0.5–10	0.9993	44.6	8.99	87.2
BDE-153	0.5–10	0.9997	51.7	9.93	78.2
BDE-138	0.5–10	0.9997	78.3	6.90	80.7

[a] Calculated from the lowest concentrations of calibration curves with a signal-to-noise ratio of 3.
[b] Calculated from the samples spiked at 1.0 ng/g level.

explain this easily. Considering the pressure limits of the glass vials, higher temperatures were not been explored and 95 °C was chosen to proceed to next optimizations.

Study of extraction time was carried out employing sampling time varying from 40 to 100 min (Fig. 4c). It seemed that the system could not reached equilibrium within 100 min to all analytes except BDE-17 and the equilibrium time increased with the number of bromine substituents in the compounds, which has also been reported to appear in HS-SPME optimization of PBDEs water analysis [14]. Finally, 60 min was chosen to avoid a protracted extraction method.

Fig. 4d illustrates the effect of salt (NaCl) on the extraction from soil sample. After salts adding, the extraction amounts of BDE-47, BDE-99, and BDE-153 were all decreased and only a slight increase of response on BDE-17 was observed. Some inorganic salts existed already in the soil could maybe responsible for this phenomenon. Salt adding was consequently considered unnecessary.

Effect of solvents addition was also evaluated. Seven solvents differed in polarity were involved: methanol, ethanol, isopropylalcohol, acetonitrile, hexane, dichloromethane, and acetone. Considering high concentration of organic solvents would somehow cause decrease on the extraction efficiency [25,27], 20 μL of each solvent was added first. Table 3 lists the analytes' response to different solvent addition; responses to ethanol were set as references (100). Apparently, polar solvents gave better favorable effect, among which methanol worked best. The methanol volume was adjusted further for the optimal by changing the volume from 5 to 30 μL, and 10 μL was finally selected with increase of 5.79, 23.1, 37.9, and 26.3% on BDE-17, BDE-47, BDE-99, and BDE-153, respectively. This increase can be explained by the solvent molecules helping to liberate the analytes from active sites in the soil and hence to drag them from the matrix into the gas phase. However, too much solvent will generate extraction competition with the target analytes, and result in decrease of extraction efficiency.

3.3. Method validation

A series of experiments with regard to the linearity, limit of detection, precision, and accuracy were performed to validate

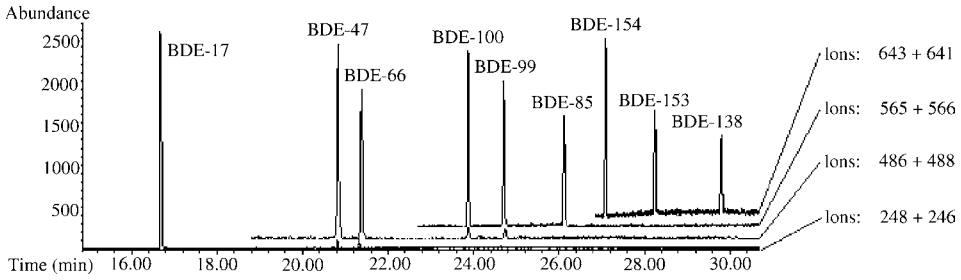

Fig. 5. Typical GC–MS selected ion chromatograms obtained from the soil sample spiked with 1.0 ng/g of each analyte.

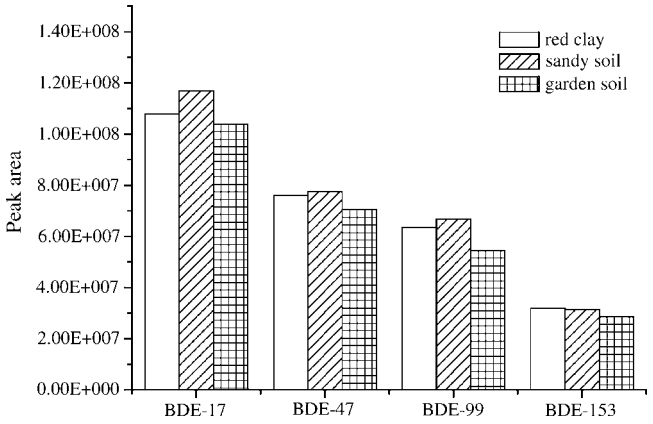

Fig. 6. Extraction responses of different environmental soil samples. HS-SPME conditions are the same as in Fig. 3.

the proposed HS-SPME-GC–MS method. Results obtained are listed in Table 4.

Linearity of the method was tested over a range between 0.1 and 10 ng/g and analyzed each level (i.e. 0.1, 0.5, 1, 5, and 10 ng/g) in triplicate. After plotting the mean peak areas versus sample concentration to generate the calibration curves, a statistical regression model was applied and square regression coefficients (r) were higher than 0.999 for all compounds. Limit of detection (LOD), calculating from the lowest concentration of calibration curves with a signal-to-noise ratio of 3, ranged from 13.0 to 78.3 pg/g. Fig. 5 shows typical GC–MS selected ion chromatograms obtained from the soil sample spiked with 1.0 ng/g of each analyte.

The precision of the method was determined by analysis of five spiked soil samples. For all the congeners, the R.S.D. were all below 10%, illustrating the good reproducibility of this method.

To evaluate the accuracy of the method, recovery tests were performed by analysis of spiked soil samples at 1.0 ng/g level. The recoveries were satisfactory (>78%) in all cases.

Table 5
Concentrations of PBDEs detected in contaminated soil samples (ng/g, dried weight)

Compound	Soil 1	Soil 2	Soil 3	$\bar{C} \pm$ Std. (%)
BDE-47	0.38	0.37	0.32	0.36 ± 3.2
BDE-99	0.22	0.19	0.21	0.21 ± 1.5
BDE-100	0.30	0.26	0.29	0.28 ± 2.1

3.4. Environmental soil samples analysis

Soils of diverse origins differ on composition and may generate different SPME behaviors. Fig. 6 shows the SPME responses of three types of environmental soil samples from different sampling location: sandy soil, red clay, and garden soil. All samples were previously analyzed for the presence of the target analytes, and no detectable concentrations were obtained. After spiking with the analytes (1 ng/g of each PBDEs congener), they were extracted using the PM-β-CD/OH-TSO fiber under the same HS-SPME conditions. As revealed in Fig. 6 evidently, sandy soil and red clay gave nearly the same high extraction response; response from garden soil decreased a little due probably to the increase of organic matters existed in the matrix. In conclusion, no significant difference was observed in when the method was applied to three different environmental soil samples, confirming that the matrix effect in these soils is very small using this method established in red clay.

Finally, sandy soils collected in the vicinity of open electronic waste treatment sites located in Taizhou, Zhejiang (China) were analyzed using the proposed HS-SPME-GC–MS method. PBDE congeners with tetra- and penta-brominated substitutions (i.e. BDE-47, -100, and-99) were detected. Results listed in Table 5 revealed that the congeners concentrations varied from 0.19 to 0.38 ng/g. Fig. 7 shows typical GC/MS chromatograms of contaminated samples.

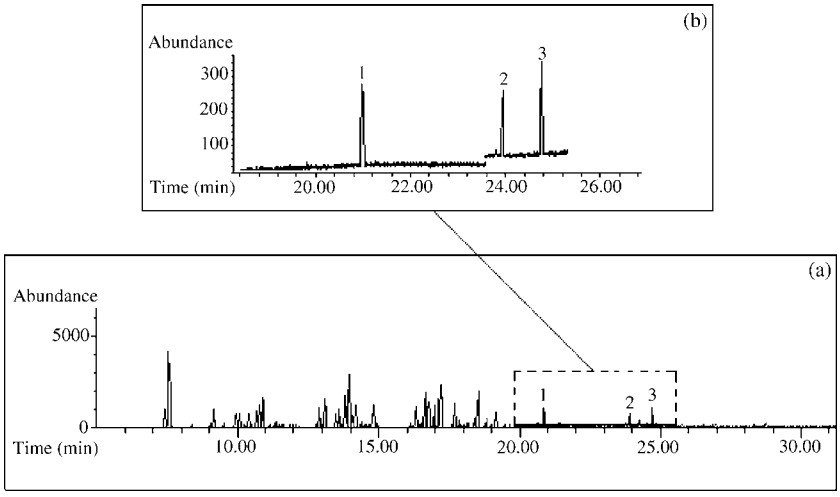

Fig. 7. Typical GC–MS total ion (a) and selected ion (b) chromatograms of a contaminated soil sample (1 = BDE-47, 2 = BDE-100, 3 = BDE-99).

4. Conclusions

In this work, a simple, sensitive and accurate method for determination of PBDEs in soils has been developed based on HS-SPME followed by GC–MS. Novel PM-β-CD/OH-TSO fiber was firstly prepared by sol–gel technology and applied in HS-SPME procedure. The fiber exhibits not only high operational stability under comparatively harsh extraction conditions, but also desired extraction efficiencies towards PBDEs due mainly to the presence of hydrophobic cavity-shaped cavity possessed by PM-β-CD. Fine fiber qualities thus assured good linearity ($r > 0.999$), precision (R.S.D. < 10%), accuracy (recovery > 78%), and detection limits (13.0–78.3 pg/g, S/N = 3) of the method as well as its application to other soil samples.

Acknowledgements

This work was kindly supported by the National Natural Science Foundation of China (Grant No. 20375028), the National Basic Research Program of China (2003CB415005), and Chinese Academy of Sciences (KSCX2-SW-128).

References

[1] F. Rahman, K.H. Langford, M.D. Scrimshaw, J.N. Lester, Sci. Total Environ. 275 (2001) 1.
[2] T.A. McDonald, Chemosphere 46 (2002) 745.
[3] L.S. Birnbaum, D.F. Staskal, Environ. Health Perspect. 112 (2004) 9.
[4] S. Harrad, Environ. Sci. Technol. 40 (2006) 4548.
[5] C. Sanchez-Brunete, E. Miguel, J.L. Tadeo, Talanta 70 (2006) 1051.
[6] Y. Ashizuka, R. Nakagawa, K. Tobiishi, T. Hori, T. Ida, J. Agric. Food Chem. 53 (2005) 3807.
[7] J.F. Focant, C. Pirard, E. De Pauw, Talanta 63 (2004) 1101.
[8] E. Eljarrat, D. Barcelo, Trends Anal. Chem. 23 (2004) 727.
[9] C.L. Arthur, J. Pawliszyn, Anal. Chem. 62 (1990) 2145.
[10] S. Ulrich, J. Chromatogr. A 902 (2000) 167.
[11] A. Penalver, E. Pocurull, F. Borrull, R.M. Marce, Trends Anal. Chem. 18 (1999) 557.
[12] B. Zygmunt, A. Jastrzebska, J. Namiesnik, Crit. Rev. Anal. Chem. 31 (2001) 1.
[13] J. Ji, C.H. Deng, W.W. Shen, X.M. Zhang, Talanta 69 (2006) 894.
[14] M. Polo, G. Gomez-Noya, J.B. Quintana, M. Llompart, C. Garcia-Jares, R. Cela, Anal. Chem. 76 (2004) 1054.
[15] C. Salgado-Petinal, M. Garcia-Chao, M. Llompart, C. Garcia-Jares, R. Cela, Anal. Bioanal. Chem. 385 (2006) 637.
[16] A. Gago-Martinez, M.J. Nogueiras, S. Rellan, J. Prado, M.F. Alpendurada, W. Vetter, J. AOAC Int. 87 (2004) 1021.
[17] D. Wang, S.L. Chong, A. Malik, Anal. Chem. 69 (1997) 4566.
[18] S. Bigham, J. Medlar, A. Kabir, C. Shende, A. Alli, A. Malik, Anal. Chem. 74 (2002) 752.
[19] W. Saenger, Angew. Chem. Int. Ed. 19 (1980) 344.
[20] Y.L. Fu, Y.L. Hu, Y.J. Zheng, G.K. Li, J. Sep. Sci. 29 (2006) 2684.
[21] J.J. Zhou, Z.R. Zeng, Anal. Chim. Acta 56 (2006) 400.
[22] R.J. Boger, R.J. Corcoran, J.-M. Lehn, Helv. Chim. Acta 61 (1978) 2190.
[23] M.M. Liang, M.L. Qi, C.B. Zhang, R.N. Fu, J. Chromatogr. A 1059 (2004) 111.
[24] B. Casu, M. Reggiani, J. Polym. Sci. Pt. C 7 (1964) 171.
[25] M. Llompart, K. Li, M. Fingas, Talanta 48 (1999) 451.
[26] R.A. Doong, P.L. Liao, J. Chromatogr. A 918 (2001) 177.
[27] R. Batlle, C. Sanchez, C. Nerin, Anal. Chem. 71 (1999) 2417.